



Universiteit  
Leiden

The Netherlands

## New chemical tools to illuminate N-acylphosphatidylethanolamine biosynthesis

Wendel, T.J.

### Citation

Wendel, T. J. (2023, March 23). *New chemical tools to illuminate N-acylphosphatidylethanolamine biosynthesis*. Retrieved from <https://hdl.handle.net/1887/3576707>

Version: Publisher's Version

License: [Licence agreement concerning inclusion of doctoral thesis in the Institutional Repository of the University of Leiden](#)

Downloaded from: <https://hdl.handle.net/1887/3576707>

**Note:** To cite this publication please use the final published version (if applicable).

# **New chemical tools to illuminate *N*-acylphosphatidylethanolamine biosynthesis**

Proefschrift

ter verkrijging van  
de graad van doctor aan de Universiteit Leiden,  
op gezag van rector magnificus prof.dr.ir. H. Bijl,  
volgens besluit van het college voor promoties  
te verdedigen op donderdag 23 maart 2023  
klokke 15.00 uur

door

**Tiemen Josse Wendel**

geboren te Delft  
in 1993

Promotores: Prof.dr. M. van der Stelt  
Prof.dr. C.A.A. van Boeckel

Co-promotor: Dr. R.J.B.H.N. van den Berg

Promotiecommissie: Prof.dr. J.M.F.G. Aerts  
Prof.dr. H.S. Overkleeft  
Dr. M.E. Artola Pérez de Azanza  
Dr. R. Zimmermann (KFU Graz)  
Dr. S.H.L. Verhelst (KU Leuven)

Cover design: Natascha Kwee, Timo Wendel

ISBN: 978-94-6473-060-9

Printing: Ipskamp Printing

Publication was financially supported by the Leiden University Library.

All rights reserved. No parts of this thesis may be reproduced, stored in a retrieval system or transmitted in any form or by any means without prior written permission from the author.





## **Table of contents**

<b>Chapter 1</b>	<b>7</b>
Introduction	
<b>Chapter 2</b>	<b>47</b>
Identification of triazole ureas as potent PLA2G4E inhibitors	
<b>Chapter 3</b>	<b>91</b>
Biochemical profiling of the novel PLA2G4E inhibitor WEN091	
<b>Chapter 4</b>	<b>119</b>
Optimization of WEN091 towards selective PLA2G4E inhibitors	
<b>Chapter 5</b>	<b>173</b>
Development of an activity-based probe that visualizes cellular PLA2G4E activity	
<b>Chapter 6</b>	<b>191</b>
Development of potent and selective ABHD6 inhibitors based on caged hydrocarbon structures	
<b>Chapter 7</b>	<b>217</b>
Summary and future prospects	
<b>Nederlandse samenvatting</b>	<b>231</b>
<b>List of Publications</b>	<b>246</b>
<b>Curriculum vitae</b>	<b>247</b>
<b>Dankwoord</b>	<b>248</b>



# 1

## General introduction



Lipids are a major type of biomolecules that are defined as small, hydrophobic or amphipathic molecules that (partially) originate from the condensations of ketoacyl thioesters and/or isoprene units.<sup>1</sup> This definition gives rise to a chemically diverse set of compounds, in which eight classes are distinguished: fatty acyls, glycerolipids, glycerophospholipids, sphingolipids, saccharolipids, polyketides, sterol lipids and prenol lipids. These molecules exert a wide array of biological functions, including membrane building blocks, energy storage, vitamins, hormones, immunomodulatory agents and toxins.<sup>1,2</sup> Many signaling lipids are low-abundant, short-lived and chemically unstable, which has complicated efforts to elucidate their physiological activities.<sup>2</sup>

*N*-acylphosphatidylethanolamines (NAPEs) are a family of glycerophospholipids with both structural and signaling activities (Figure 1.1). They are low-abundant, making up only 0.01% of the membrane phospholipids in animal brains under physiological conditions, corresponding to low nanomoles per gram tissue.<sup>3</sup> Nevertheless, they are widespread across different tissues, being found in mammalian central nervous system, gut, spleen, testes and plasma.<sup>3,4</sup> NAPEs are more abundant in plasma membranes than intracellular compartments and were found in erythrocytes, which do not have intracellular membranes.<sup>5,6</sup> They were first discovered in 1965<sup>7</sup>, and until the 1990s they were regarded as nothing more than short-lived intermediates in the biosynthesis of phosphatidic acid (PA) or *N*-acylethanolamines (NAEs).<sup>8–10</sup> Only recently their specific biochemical and biophysical properties are being appreciated.<sup>3,4</sup> These properties include regulation of membrane dynamics, feeding and tissue degeneration (Figure 1.2).

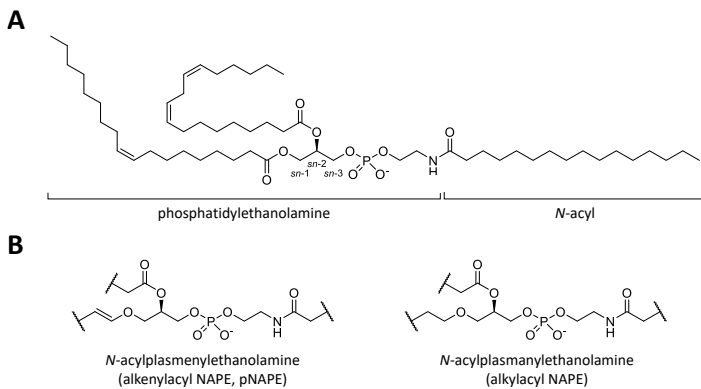


**Figure 1.1. General structure of NAPE-type lipids.** A) Structure of *N*-palmitoyl-1-oleoyl-2-linoleoyl-*sn*-glycero-3-phosphoethanolamine, a typical NAPE. Indicated are the phosphatidylethanolamine (PE) and *N*-acyl building blocks and the stereospecific numbering (*sn*) of the glycerol backbone. B) Structures of alternative NAPE-like species, with an *sn*-1 ether-linked substituent.

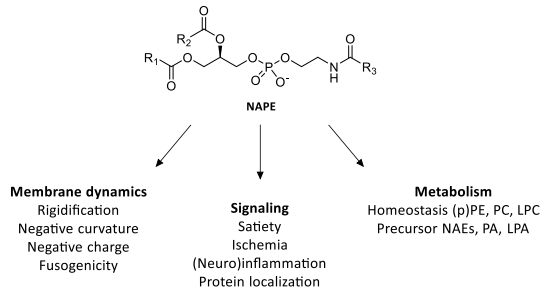


**Figure 12. Overview of most important reported activities of NAPes.** Structural and signaling functions of NAPes have been reported. In addition, they may exert functionalities through maintaining levels of up- or downstream bioactive metabolites. Functions are not mutually exclusive and may not be restricted to one classification.

## Structural properties of NAPes

NAPes are triacylated glycerophospholipids synthesized from phosphatidylethanolamine (PE). In plants, NAPes are formed by direct acylation of the PE amine with free fatty acids (FFAs)<sup>11,12</sup>, whereas in mammals the acyl is transferred from a fatty acid donor.<sup>13,14</sup> This *N*-acyl transfer converts the zwitterionic PE into a negatively charged phospholipid (Figure 1.3). The composition of the three tails is highly diverse, but in general the *sn*-1 position is occupied by saturated or monounsaturated chains and the *sn*-2 position by (poly)unsaturated acyl groups, reflecting the composition of the PE precursor (Figure 1.1).<sup>15,16</sup> In rat brain, the *sn*-2 substituent was found to often be an oleoyl (18:1) ester, suggesting an enzymatic preference for 2-oleoyl-PE substrates.<sup>17</sup> The *N*-substituent composition appears to be dictated by acyl donor availability, as it mirrors the *sn*-1 composition of PC.<sup>3,18</sup> *N*-palmitoyl (16:0)-PE (NPPE) was the most abundant NAPE species found in human plasma, rat brain, rat testes (over 50%) and rat heart (~20%), with lower levels of *N*-stearoyl (18:0), *N*-oleoyl (18:1) and *N*-linoleoyl (18:2)-PE. Reported levels of polyunsaturated species such as *N*-arachidonoyl (20:4), *N*-docosapentaenoyl (22:5) and *N*-docosahexaenoyl (DHA, 22:6)-PE range from 0.6% to 11%.<sup>16,18–21</sup> NAPE concentrations are highly dependent on cell type and developmental state. For example, the concentration of *N*-arachidonoyl-PE (NArPE) in rat brainstem and striatum is two to three times higher than in hippocampus, hypothalamus or diencephalon and six times higher than in cortex.<sup>22</sup> In adult rats, brain NArPE levels are increased over three-fold compared to neonatals.<sup>23</sup>

Important NAPE-like classes include *N*-acylplasmalyethanolamines, in which the *sn*-1 substituent is an alkyl ether, and *N*-acylplasmenyethanolamines or plasmalogen NAPes (pNAPes), in which the *sn*-1 substituent is a vinyl ether (Figure 1.1). Compared to canonical NAPes, they can be relatively high-abundant. For example, in dog heart and rat brain, levels of *sn*-1 vinyl ether NArPEs were found to be equal to or higher than their *sn*-1 acyl counterpart, respectively.<sup>24,25</sup> Rat intestinal mucosa, however, does not contain *sn*-1 alkyl nor alkenyl NAPes, whereas serosa contains all classes.<sup>26</sup> Nevertheless, (vinyl) ether-linked NAPes are underappreciated as a separate class and plasmalogen species are often neglected in studies on NAPes.<sup>27–29</sup>

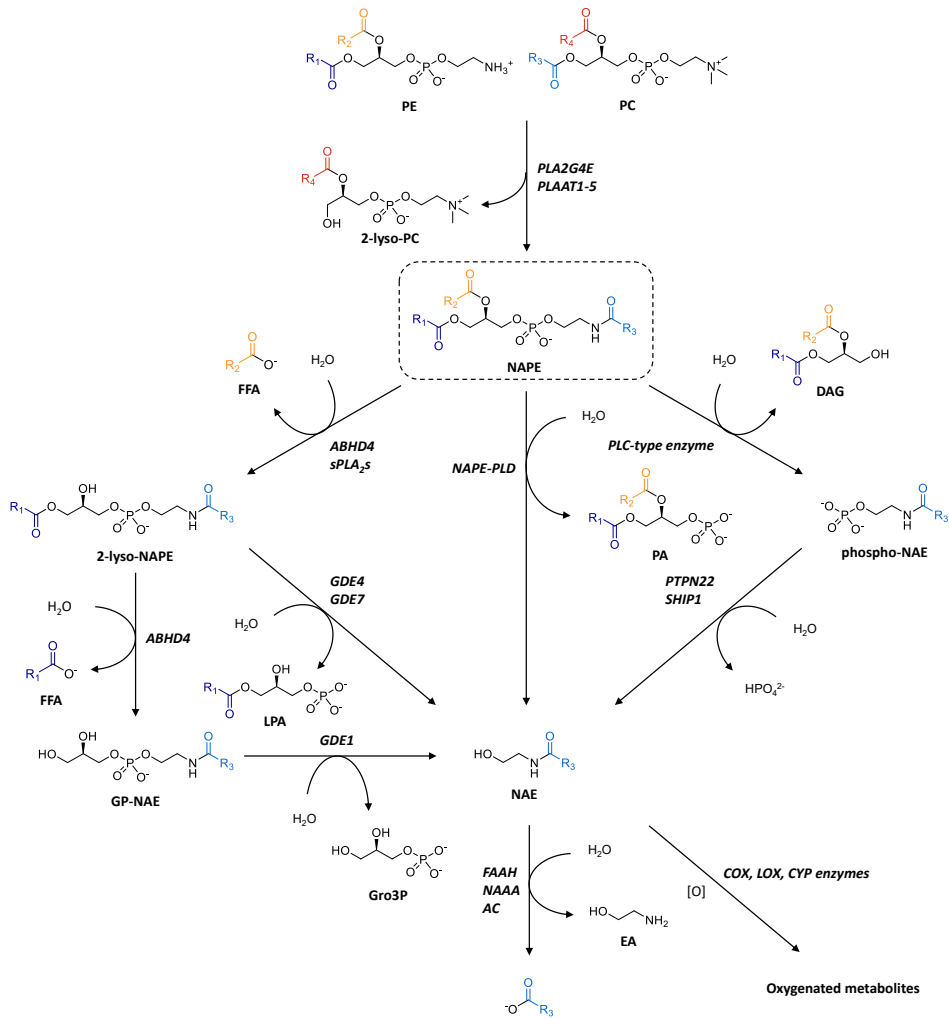


**Figure 13. Metabolic pathways involved in biosynthesis and degradation of NAPEs.** Shown are the transacylation reaction from canonical acyl donor phosphatidylcholine (PC) to phosphatidylethanolamine (PE), the direct hydrolysis of *N*-acylphosphatidylethanolamine (NAPE) to *N*-acylethanolamine (NAE) by NAPE-specific phospholipase D (NAPE-PLD), the three multistep pathways leading to NAE and the metabolism of NAE. Indicated are the responsible enzymes and secondary products formed. Ether-type NAPEs and alternative acyl donors are not explicitized. PLA2G4E: phospholipase A<sub>2</sub> group IV E, PLAAT: phospholipase A/acyltransferase, ABHD4:  $\alpha/\beta$  hydrolase domain-containing protein 4, sPLA<sub>2</sub>: secreted phospholipase A<sub>2</sub>, GDE: glycerophosphodiesterase, PLC: phospholipase C, PTPN22: protein tyrosine phosphatase non-receptor type 22, SHIP1: Src homology 2 domain-containing inositol 5' phosphatase 1, FAAH: fatty acid amide hydrolase, NAAA: NAE-hydrolyzing acid amidase, AC: acid ceramidase, PA: phosphatidic acid, LPA: lysophosphatidic acid, GP-NAE: glycerophospho-NAE, Gro3P: glycerol-3-phosphate, DAG: diacylglycerol, EA: ethanolamine, FFA: free fatty acid.

The three tails of NAPEs give it extraordinary interactions in lipid membranes. Similar to other phospholipids, the *sn*-1 and *sn*-2 acyl groups are embedded in the lipid bilayer, but the conformation of the *N*-acyl chain depends on the number of carbons. Short-chain substituents (<10 carbons) appeared to be randomly oriented or to reside at the membrane interface, whereas longer-chain substituents ( $\geq 10$  carbons) are oriented parallel to the other two substituents (Figure 1.4A, B).<sup>30,31</sup> Penetration of a third fatty acid chain into the membrane leaflet leads to increased steric bulk and consequently promotes a negative membrane curvature<sup>32,33</sup> and rigidifies the membrane.<sup>34</sup> In addition, acylation of the ethanolamine disrupts intermolecular hydrogen bonds between the amine and phosphate groups. However, this is probably compensated for by intermolecular hydrogen bonds between the N-H and carbonyls of the acylamide (Figure 1.4C).<sup>34,35</sup> The membrane-stabilizing effect of NAPEs has been exploited in liposome formulations. Liposomes with increased NAPE content were larger and less permeable, as determined by measuring leakage of its fluorescent cargo.<sup>32</sup> In a similar experiment, NPPE was shown to increase the stability of vesicles in the presence of human serum, an effect that was attributed to a combination of increased membrane rigidity, altered surface charge and reduced lipid exchange with serum lipoproteins.<sup>36</sup> In addition to a stabilizing function, *N*-dodecanoyl (12:0)-PE and NPPE-containing liposomes showed increased cation-dependent fusogenicity with each other, erythrocyte ghosts and U-937 cells.<sup>37,38</sup> The negative surface charge of NAPEs probably played a role, as low pH also stimulated fusion. However, no fusion was observed with phosphatidylglycerol (PG) or phosphatidylserine (PS)-containing liposomes, indicating a NAPE-specific effect.<sup>37</sup> In line with these results, NAPEs were enriched around division sites in mutant *Escherichia coli* lacking PG and cardiolipin, possibly fulfilling the natural role of these lipids in budding and cell division through their effects on membrane curvature and surface charge.<sup>39</sup> The combination of increased liposome stability in serum and fusogenicity make the incorporation of NAPEs into liposomal formulations interesting for drug delivery purposes.

## NAPEs as feeding hormones

In fasted rats, plasma and lymph NAPE levels were found to increase following a high-fat diet.<sup>20,40</sup> These NAPEs are synthesized in the small intestine from the ingested lipids and their general composition reflects that of those. Of note, NARPE levels did not respond to feeding, but increased upon starvation.<sup>41</sup> *N*-palmitoyl-1,2-dioleoyl-*sn*-PE (*N*-palmitoyl-DOPE) administration was shown to have an anorectic effect, whereas DOPE and *N*-palmitoylethanolamine (PEA) did not.<sup>20</sup> The same effect was observed in *N*-acylphosphatidylethanolamine-specific phospholipase D (NAPE-PLD) KO mice and with non-hydrolyzable *N*-palmitoyl-dialkyl-PE, indicating it was not mediated by NAPE metabolites.<sup>42</sup> Since administration of *N*-<sup>14</sup>C-palmitoyl-DOPE led to an accumulation of the radiolabel in the hypothalamus and modulation of activity of hypothalamic neural networks involved in feeding behavior, it was suggested that NAPEs function as gut-

derived hormones sending satiety signals to the brain.<sup>20</sup> However, this view later was contested as other mechanisms could not be ruled out. For example, high concentrations of dipalmitoyl-PE and phosphatidic acid were shown to have a similar hypophagic effect, suggesting the satiety signaling is not specific for NAPEs.<sup>42</sup> Also, expression of NAPE-PLD, the enzyme responsible for the direct conversion of NAPEs to NAEs, in rat jejunum is postprandially increased, while expression of NAE-degrading enzyme fatty acid amide hydrolase (FAAH) is decreased, suggesting an important role for NAEs rather than NAPEs.<sup>26</sup> Indeed, NAPE-PLD activity was found to be required for the anorectic effects of NAPEs when they were administered orally instead of intraperitoneally.<sup>43</sup>

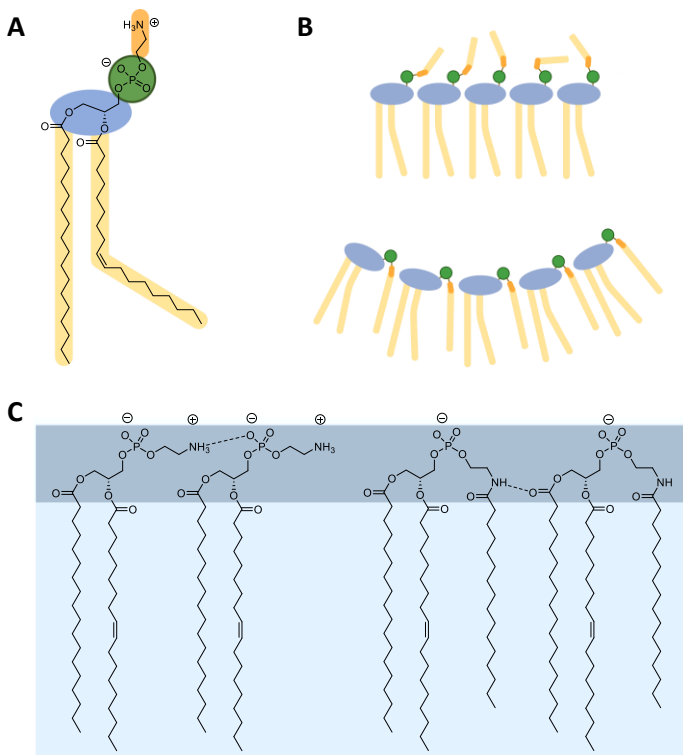


**Figure 1.4. Schematic representation of NAPE conformations in lipid membranes.** A) Cartoon representation of phosphatidylethanolamine (PE) as used in (B). B) Short-chain *N*-acyl substituents (top) are positioned randomly across the membrane interface and do not influence membrane curvature. Longer-chain *N*-acyls (bottom) are positioned parallel to the other two substituents and induce negative membrane curvature. C) PEs (left) make intermolecular hydrogen bonds between the amine and phosphate groups, whereas NAPEs (right) make hydrogen bonds between the carbonyl and NH of the amide.

## NAPes in degenerating tissue

### Ischemia

One of the earliest recognized features of NAPE biology is their increased levels in degenerating tissue. In the 1980s, several studies reported an accumulation following ischemia. In myocardium of dogs, levels of diacyl NAPes, their plasmalogens and *N*-acylplasmalylethanolamines were increased in central and peripheral infarcted areas to 4–6% of the phospholipid content, accompanied by a relative decrease in PE levels.<sup>44</sup> pNAPes accounted for approximately 50% of the total NAPE-like species, the *sn*-2 *O*-acyls of which were highly enriched in arachidonoyl (75%). In contrast, diacyl NAPes consisted for only 33% of 2-arachidonoyl species in central infarcted areas and were enriched in *sn*-2 linoleoyl esters instead.<sup>44</sup> Elevated levels of NAPes were also found in infarcted myocardium of cats, but not of rabbits and humans.<sup>9</sup> In addition, NAPE accumulation was reported in ischemic rat brains following decapitation<sup>8</sup> or artery occlusion.<sup>45,46</sup> Here, diacyl NAPes formed the majority (77%).<sup>8</sup> In striatum and cortex, the 2–3-fold NAPE accumulation was accompanied by a 30-fold increase in NAEs.<sup>46</sup> Models of chemical-induced anoxic toxicity were also shown to increase NAPE levels. During anoxia or NaN<sub>3</sub>-induced anoxic stress, NAPes accumulated in potato cells and cultured rat neocortical neurons.<sup>47,48</sup>

In general, the composition of the three lipids of the elevated NAPE species does not significantly differ between healthy and diseased tissue, with *sn*-1 *O*-acyl and *N*-acyl consisting mainly of palmitoyl, stearoyl or linoleoyl groups.<sup>8,44–46,49</sup> However, on the *sn*-2 position, NAPes in ischemic tissue appeared to be enriched in linoleoyl or docosahexaenoyl esters.<sup>8,44,47</sup>

### Neurodegeneration

Accumulation of NAPes in neuronal cells has been observed in response to other stimuli than anoxic stress. Stimulation of cultured mouse neocortical neurons with *N*-methyl-D-aspartate (NMDA) or NMDA receptor agonist glutamate resulted in increased NAPE and NAE levels, preceding neuronal death.<sup>50,51</sup> In line, *in vivo* necrotic brain damage, induced by concussive traumatic injury or intrastriatal injection of NMDA in infant rats, provoked a 19- to 44-fold increase in NAPE levels within 24 h, respectively.<sup>49</sup> In contrast to other studies showing an ischemia-localized effect<sup>44,46</sup>, NAPE levels were also elevated in the unaffected tissue of the contralateral cortex. Similarly, ethanol-induced neuronal apoptosis in infant mice led to an 4–6-fold accumulation of NAPes, most notably in cortex, hippocampus and inferior colliculus.<sup>52,53</sup>

The neurotoxin 6-hydroxydopamine (6-OHDA), which is used in Parkinson's disease (PD) models for its ability to cause dopaminergic neuronal death<sup>54–56</sup>, increased levels of specific NAPE species in the striatum, but not in the substantia nigra (SN).<sup>29,57</sup> (p)NAPes with *sn*-2 *O*-arachidonoyl or docosahexaenoyl substituents and saturated *N*-acyls were significantly elevated, while *N*-arachidonoyl species were not affected. In mice lacking NAPE-PLD, NAPE levels were increased even further. In these mice, neuronal damage due to 6-OHDA was less pronounced, suggesting a protective role of NAPes against 6-OHDA-

induced neurotoxicity.<sup>29</sup> 6-OHDA treatment led to an increase in activated Rac1 in the SN of wildtype mice, but not in NAPE-PLD KO mice. Rac1 is a GTPase implicated in dopaminergic neuronal survival and PD<sup>58,59</sup> that can be activated through interactions with membrane-bound leucine-rich repeat kinase 2 (LRRK2), also known as PARK8 and associated with both familial and sporadic PD.<sup>60,61</sup> LRRK2 was found to dissociate from the plasma membrane in NAPE-PLD KO mice.<sup>62</sup> It is tempting to speculate that elevated levels of NAEs would exert a neuroprotective activity through alteration the plasma membrane architecture, leading to LRRK2 dissociation and subsequent reduced activation of Rac1, which has an anti-inflammatory effect. In line, *N*-palmitoyl-DOPE was shown to decrease Rac1 activation in macrophages, inhibiting phagocytosis.<sup>63</sup>

Moreover, (p)NAPE biosynthesis may provide an important means to maintain homeostasis of precursors PE and PC. These are important structural lipids in the brain, and deregulation of their levels is related to neurodegenerative diseases.<sup>64</sup> Both PE and PC are synthesized in the ER membrane from diacylglycerol (DAG) by specialized cytidyltransferases. Expression of these enzymes was found to be increased in SN of PD patients.<sup>65</sup> PE can also be synthesized by decarboxylation of PS. Downregulation of this second pathway has been shown to cause accumulation of  $\alpha$ -synuclein, a hallmark symptom of PD.<sup>66</sup> Plasmenylethanolamine composes over 50% of the PE content in neurons and even 80–90% of all phospholipids in myelin sheaths, where it provides structural rigidity.<sup>67,68</sup> Levels of pPE were found to drop dramatically during Alzheimer's disease (AD) onset and the decrease was correlated to the severity of the patient's dementia.<sup>68</sup>

Effects on NAPE levels were also observed in other forms of tissue degeneration. In a model system for inflammation, CdCl<sub>2</sub>-treated rat testes showed increased NAPE levels enriched in saturated *N*-acyls. The NAEs levels were even more drastically increased.<sup>69</sup> Furthermore, NAEs were able to activate lysosomal  $\beta$ -glucosidases from healthy individuals *in vitro*, but not those from Gaucher's disease patients, suggesting a possible link to the molecular basis of this disease.<sup>70</sup>

## Metabolism of NAEs

### NAEs

Despite having physiological functions themselves, NAEs are primarily known as the precursors to NAEs. NAEs have long been appreciated as a diverse class of signaling lipids, which exert a plethora of biological activities.<sup>71–73</sup> *N*-palmitoylethanolamine (PEA) was the first NAE to be identified.<sup>71</sup> It has anti-inflammatory<sup>74</sup>, analgesic<sup>75</sup>, retinoprotective<sup>76,77</sup>, satietal<sup>78</sup> and anti-addictive<sup>79,80</sup> effects, which are mediated through activation of the peroxisome proliferator-activated receptor  $\alpha$  (PPAR $\alpha$ ).<sup>81,82</sup> PEA levels are elevated in tissue surrounding stroke or ischemia<sup>83</sup>, where it reduces infarct size through inhibiting astrocyte activation,<sup>84</sup> and it plays a neuroprotective role in Alzheimer's disease.<sup>85–88</sup> Affinity for

orphan receptors GPR55 and GPR119 and transient receptor potential cation channel V1 (TRPV1) has been reported, but the physiological relevance is unclear.<sup>89–92</sup>

*N*-oleoylethanolamine (OEA) is well-studied as a satiety factor produced intestinally from food.<sup>26,93,94</sup> It stimulates lipolysis<sup>95</sup> and reduces feeding<sup>96,97</sup> through its activation of peripheral PPAR $\alpha$  and GPR119, and works as a satiety hormone in the brain.<sup>98,99</sup> Therefore it is considered an anti-obesity nutraceutical.<sup>100</sup> Like PEA, it has anti-addictive<sup>101</sup> and neuroprotective effects.<sup>83</sup> Furthermore, OEA is an antagonist of TRPV1 that alleviated L-DOPA-induced dyskinetic symptoms in a mouse model of PD.<sup>102,103</sup>

The most extensively studied NAE is *N*-arachidonylethanolamine (AEA, or anandamide), because it targets the cannabinoid receptors CB<sub>1</sub> and CB<sub>2</sub>.<sup>104,105</sup> It is relatively low-abundant (up to 100-times lower than PEA and OEA), but found in most tissues including the central nervous system (CNS).<sup>106</sup> Because CB<sub>1</sub> is activated by (-)- $\Delta^9$ -tetrahydrocannabinol (THC), the psychoactive component of marijuana, anandamide has gained much attention for its ability to function as an endogenous cannabinoid, or endocannabinoid. As such, it modulates emotional behavior, including stress<sup>107,108</sup>, anxiety<sup>109,110</sup> and depression.<sup>111</sup> Indeed, anandamide was shown to reduce stress-induced corticosterone release<sup>112</sup>, although a seemingly opposite effect was also reported.<sup>113</sup> Other cannabimimetic activities of AEA include orexigenia<sup>114,115</sup>, anticonvulsion<sup>116–118</sup>, hypotension<sup>119</sup>, analgesia<sup>107,120,121</sup> and memory formation.<sup>122,123</sup> Furthermore, it is involved in neuroprotection<sup>124–127</sup>, fertility<sup>128,129</sup>, inflammation<sup>130–133</sup> and cancer.<sup>134–136</sup> Beside the cannabinoid receptors, AEA also activates the TRPV1 receptor and this way regulates vasodilation<sup>137,138</sup>, nociception<sup>139,140</sup> and mood.<sup>141,142</sup>

Other NAEs have received less attention, despite their similar activities. *N*-stearoylethanolamine (SEA) has anti-inflammatory<sup>143</sup>, anorexic<sup>78,144</sup> and pro-apoptotic<sup>145</sup> properties. *N*-linoleoylethanolamine (LEA) is the most abundant NAE in the jejunum, but has very low levels in the brain.<sup>146</sup> It was found to play a role in inflammatory bowel disease, stimulating bacterial growth.<sup>147</sup> *N*-docosahexaenoylethanolamine (DHEA, or synaptamide) stimulates neurogenesis, neuritogenesis and synaptogenesis through activation of GPR110<sup>148,149</sup> and also has anti-(neuro)inflammatory activity.<sup>150,151</sup> Some of the physiological roles of different NAEs are likely related to the function of their respective NAE metabolites.

### Metabolic pathways

Four metabolic pathways have been described for the conversion of NAEs into NAEs. Of these four pathways, three go via one or more intermediate lipids, which have biological relevance on their own (Figure 1.3). The direct conversion of NAEs and pNAEs into NAEs is performed by NAPE-PLD.<sup>10</sup> NAPE-PLD is a metallo- $\beta$ -lactamase, structurally unrelated to other human PLDs, that uses two active site Zn<sup>2+</sup>-ions to hydrolyze the NAPE phosphate.<sup>152,153</sup> In its active conformation, it is a membrane-associated dimer that has a membrane-facing hydrophobic cavity to extract NAEs from the membrane and allosteric pockets that accommodate activating bile acids and polyamines.<sup>152,154–156</sup> It is expressed in



several organs, most abundantly in brain, kidney and testes.<sup>157</sup> *In vitro*, NAPE-PLD is specific for (p)NAPEs (with modest lyso-NAPE-PLD activity), but has no selectivity for the *N*-acyl substituents, suggesting it is capable of synthesizing all NAEs.<sup>157,158</sup> Independent KO studies, however, have described conflicting results on AEA and DHEA levels, which might be attributed to compensatory effects.<sup>159–161</sup> Recently, the first *in vivo* active NAPE-PLD inhibitor was described, which decreased the levels of saturated, monounsaturated and  $\omega$ -6-polyunsaturated NAEs, including AEA.<sup>162</sup> Beside NAEs, NAPE-PLD produces phosphatidic acid (PA). PA is a central precursor in the biosynthesis of many glycerolipids, including PE, PC and PS.<sup>163</sup> In addition, it has pH-dependent interactions with proteins involved in membrane component biosynthesis.<sup>164</sup>

The second pathway of NAPE degradation involves the sequential actions of  $\alpha/\beta$  hydrolase domain containing protein 4 (ABHD4) and glycerophosphodiesterase 4 or 7 (GDE4, GDE7). First, the *sn*-2 ester is saponified by ABHD4, producing 2-lyso-NAPE, which is then hydrolyzed to NAE by lyso-NAPE-PLD activity of GDE4 or GDE7.<sup>14</sup> ABHD4 is a serine hydrolase that hydrolyzes NAPEs and *N*-acylphosphatidylserine (NAPS).<sup>165</sup> It is expressed in several tissues, most abundantly in CNS and testes.<sup>166</sup> GDE4 and GDE7 are lyso-PLDs that accept lyso-NAPEs, lyso-PE and lyso-PC and convert these to lysophosphatidic acid (LPA).<sup>167,168</sup> Little is known about the physiological importance of lyso-NAPEs, but LPA is regarded an important signaling lipid in (neuro)development, tissue regeneration and cancer.<sup>169–172</sup> Both GDE4 and GDE7 are ubiquitously expressed, but GDE4 is more abundant in brain and testes, whereas GDE7 is more abundant in kidney.<sup>168</sup> Both ABHD4 and GDE4 have a preference for plasmalogen substrates<sup>165,167</sup>, suggesting this second pathway is used mainly for the degradation of pNAPEs. Alternatively, three secretory phospholipases, sPLA<sub>2</sub>B, sPLA<sub>2</sub>IIA and sPLA<sub>2</sub>V, were shown to be able to hydrolyze the *sn*-2 ester of NAPEs.<sup>173</sup> As these enzymes are mainly present in the gastrointestinal system, they might be important for the local metabolism of NAPEs from food.

In the third metabolic pathway, ABHD4 sequentially hydrolyzes both NAPE *O*-acyls, producing glycerophospho-NAEs (GP-NAEs).<sup>166</sup> These intermediates are then converted to NAEs by GDE1 (also known as MIR16).<sup>174</sup> Like GDE4, GDE1 is a magnesium-dependent PLD predominantly expressed in CNS, kidney and testes.<sup>174</sup> It has shown activity on several glycerophospho metabolites, including GP-serine, GP-glycerate and GP-inositol.<sup>175,176</sup> Of note, GP-DHEA was found to be one of the most abundant peripheral GP-NAEs<sup>161</sup>, while its levels in the brain were very low<sup>174</sup>, suggesting distinct regulation of this pathway in different tissues. ABHD4 was recently shown to play a crucial role in anoikis in prostate cancer cells and embryonic brain development, but it is unclear which metabolites are involved in this process.<sup>177,178</sup> Because of the non-hydrolyzable *sn*-1 ether linkage in plasmanyl and plasmenyl NAPEs, these lipids cannot be metabolized via this third pathway.

The fourth NAPE metabolic pathway is the least characterized, and includes PLC-type hydrolysis to phospho-NAEs by an unknown enzyme followed by dephosphorylation to NAEs. Protein tyrosine phosphatase non-receptor type 22 (PTPN22) and Src homology 2 (SH2) domain-containing inositol 5' phosphatase (SHIP1) have been identified to be able

to catalyze this final reaction. This pathway was discovered in macrophages and is responsive to lipopolysaccharide (LPS) stimulation.<sup>179,180</sup> Of note, PLC-type hydrolysis of NAPes produces DAG, a key intermediate in the biosynthesis of many phospholipids.<sup>67</sup> It is unclear whether this pathway is used for the degradation of plasmanyl and plasmenyl NAPes.

Bioactivity of NAEs is terminated by FAAH and *N*-acylethanolamine-hydrolyzing acid amidase (NAAA), that hydrolyze the amide bond to produce ethanolamine and FFAs. FAAH is a widely-expressed serine hydrolase that has been extensively studied for its central role in NAE metabolism, and specifically for AEA.<sup>120,181,182</sup> In higher mammals, including humans, but not rodents, a second enzyme named FAAH-2 was discovered that also hydrolyzes fatty acid amides, but without preference for NAEs.<sup>183</sup> Its physiological importance to NAE homeostasis has not been established. NAAA is a lysosomal cysteine hydrolase that belongs to the cholyglycine hydrolase family and is unrelated to FAAH.<sup>184</sup> It preferentially hydrolyses PEA and inhibition of NAAA was shown to have immunosuppressive effects.<sup>185,186</sup> Recently, the lysosomal cysteine hydrolase acid ceramidase (AC) was found to possess NAE hydrolytic activity.<sup>187</sup> AC is well-studied for its degradation of sphingolipids, and its concomitant role in lysosomal storage diseases.<sup>188</sup> The physiological relevance of its ability to hydrolyze NAEs remains unclear.

Polyunsaturated NAEs, such as AEA and DHEA, can additionally be converted to eicosanoid-type signaling lipids through oxygenation of their double bonds. Cyclooxygenases (COX), lipoxygenases (LOX) and cytochrome P450 (CYP) enzymes form different types of eicosanoid-ethanolamines for which bioactivities have been reported, for example in immunomodulation and cytoprotection.<sup>189,190</sup> A detailed description of these functions is outside the scope of this thesis.

## **NAPE biosynthesis**

In mammals, NAPes are synthesized by transacylation reaction between PE and a fatty acid donor catalyzed by calcium-dependent or -independent *N*-acyltransferases (Figure 1.3). Phosphatidylcholine (PC) is considered the canonical donor, but PE and cardiolipin can also be used.<sup>13,191,192</sup> Calcium-dependent *N*-acyltransferase (Ca-NAT) activity was first described in ischemic dog heart in 1982<sup>13</sup>, but the responsible enzyme remained elusive until in 2016, phospholipase A<sub>2</sub> Group IV E (PLA2G4E) was reported to be able to produce NAPes from PE and PC (see below).<sup>193</sup>

### **PLAAT family**

The second pathway of NAPE biosynthesis does not require calcium and is catalyzed by members of the phospholipase/acyltransferase (PLAAT) family.<sup>194–196</sup> PLAAT1–5 are small (162–279 amino acids) cysteine hydrolases encoded by the HRASLS1–5 genes that exert phospholipase A<sub>1</sub> (PLA<sub>1</sub>), PLA<sub>2</sub> and acyltransferase activity.<sup>17,197</sup> They are structurally similar to lecithin-retinol acyl transferase (LRAT), but they cannot use retinol as an acyl acceptor.<sup>196</sup>

They are characterized by a conserved NCEHFV sequence, which contains the catalytic cysteine which is part of a Cys-His-His triad (except in PLAAT1), and a C-terminal hydrophobic domain (except in PLAAT5).<sup>198</sup> Whereas calcium-dependent NAT activity is regarded the canonical pathway of NAPE biosynthesis, the physiological importance of the PLAAT enzymes has not been fully elucidated.<sup>14</sup>

PLAAT1 (also known as A-C1) is highly expressed in testes and skeletal muscle and also in brain and heart, which is similar to the expression profile of PLA2G4E.<sup>199</sup> It has a Cys-His catalytic dyad and an N-terminal enrichment of basic residues, which is involved in its localization to the nucleus.<sup>200</sup> It displays higher *N*- and *O*-acyltransferase activity than PLA<sub>1/2</sub>, with preferential cleavage of the *sn*-1 ester.<sup>199</sup> Its expression has been correlated to several forms of cancer, suggesting a role as tumor suppressor.<sup>201,202</sup> Recently, PLAAT1 was found to be responsible for developmental organelle degradation in the lens of zebrafish.<sup>203</sup> It is recruited to damaged organelle membranes dependent on its C-terminal hydrophobic domain.

PLAAT2 is expressed in gastrointestinal tissues, most abundantly in the small intestine and liver, and in kidney and trachea, but not in rodents.<sup>195,204</sup> Its C-terminal domain is important for its perinuclear localization.<sup>204</sup> PLAAT2 has the highest NAT activity of all PLAAT enzymes and also significant *O*-acyltransferase activity to 2-lysophospholipid acceptors.<sup>27,195</sup> Its anti-proliferative effect on several cancer cell lines may suggest a tumor suppressor function.<sup>204</sup>

PLAAT3 (also known as AdPLA, H-Rev107 or PLA2G16) is the most well-studied PLAAT. Its expression was found in many peripheral tissues, particularly in adipocytes.<sup>195,205,206</sup> It has a perinuclear localization, partially co-localizing with the endoplasmic reticulum (ER).<sup>205</sup> Of all PLAATs, PLAAT3 was found to have the highest phospholipase activity, with much lower transferase activity.<sup>27</sup> Contradictory results have been reported regarding preference towards the *sn*-1 or 2 position, as well as activation by calcium.<sup>195,196,205</sup> PLAAT3 has most extensively been studied as a tumor suppressor<sup>207–213</sup>, but oncogenic activity has also been reported.<sup>214,215</sup> Similar to the activity of PLAAT1 in zebrafish, PLAAT3 is responsible for organelle degradation in the lens of mice.<sup>203</sup> Recently, it was found to be a host factor used by picornaviridae to prevent clearance.<sup>216</sup> In addition, overexpression of both PLAAT2 and PLAAT3 was found to cause peroxisomal dysfunction through their depletion of plasmenylethanolamines<sup>27,217</sup>, which is known to be related to demyelinating diseases such as multiple sclerosis (MS).<sup>67,218</sup> PLAAT3 KO mice are resistant to diet-induced obesity due to increased lipolytic activity in adipocytes. It was suggested that PGE<sub>2</sub> derived from PLAAT3-produced AA inhibits lipolysis, implying PLAAT3 as an anti-obesity drug target.<sup>206</sup>

PLAAT4 (also referred to as RIG1, TIG3 or RARRES3) is ubiquitously found in human tissues, but not in rodents.<sup>195</sup> It has higher PLA<sub>1/2</sub> activity than NAT activity, but when it was overexpressed, NAPEs were shown to accumulate.<sup>27,195</sup> PLAAT4 expression is downregulated in several cancers<sup>219–222</sup>, and its anti-proliferative effect was found to be dependent on its localization to the Golgi apparatus, mediated by the C-terminal hydrophobic segment.<sup>223</sup> In the epidermis it is involved in regulation of keratinocyte

proliferation and differentiation<sup>224,225</sup>, and reduced expression is related to psoriasis and squamous cell carcinoma.<sup>226</sup>

PLAAT5 (also known as iNAT or RLP-1) is the largest of the PLAAT family.<sup>14</sup> It has low expression in brain and several peripheral organs, but is highly expressed in testes.<sup>227,228</sup> It is localized to the cytosol, possibly owing to the lack of a C-terminal hydrophobic domain.<sup>227</sup> PLAAT5 has higher NAT activity than PLA<sub>1/2</sub>, and does not discriminate between *sn*-1 and *sn*-2 *O*-acyl cleavage.<sup>227</sup> No physiological function of PLAAT5 has been established yet.

Recently, the first PLAAT inhibitors have been published.<sup>229,230</sup> LEI-110 was able to inhibit PLAAT3-dependent arachidonic acid (AA) production in an overexpression system.<sup>229</sup> LEI-301 inhibited the accumulation of several NAEs by overexpressed PLAAT2 or PLAAT5.<sup>230</sup> These chemical tools will aid in elucidating the physiological role of these enzymes, including their relative importance in NAPE biosynthesis compared to Ca-NAT.

### PLA<sub>2</sub>G<sub>4</sub>E

PLA<sub>2</sub>G<sub>4</sub>E is a serine hydrolase that belongs to the family of cytosolic phospholipases A<sub>2</sub> (cPLA<sub>2</sub>), also known as the Group IV PLA<sub>2</sub>s. This family of phospholipid-metabolizing enzymes consists of six known members (PLA<sub>2</sub>G<sub>4</sub>A–F, cPLA<sub>2</sub>α–ζ), which share low amino acid sequence identity (<40% on average).<sup>231</sup> They are, however, highly conserved throughout evolution, with human and mouse PLA<sub>2</sub>G<sub>4</sub>A sharing over 95% amino acid identity.<sup>232</sup> In both mice and humans, PLA<sub>2</sub>G<sub>4</sub>B, D, E and F form a gene cluster, suggesting evolutionary paralogy.<sup>233</sup> The PLA<sub>2</sub>G<sub>4</sub> family is characterized by a catalytic Ser-Asp dyad. In PLA<sub>2</sub>G<sub>4</sub>A–C, an additional arginine residue is required for catalytic activity, and this Arg is conserved among all PLA<sub>2</sub>G<sub>4</sub> enzymes.<sup>234</sup> All members except PLA<sub>2</sub>G<sub>4</sub>C have an N-terminal C2 lipid-binding domain with conserved residues involved in Ca<sup>2+</sup> binding.<sup>233</sup> Each member has different preferential PLA<sub>1/2</sub>, lyso-PLA and acyltransferase activity and expression pattern, suggesting different roles in phospholipid homeostasis.<sup>231</sup> For more information about PLA<sub>2</sub>G<sub>4</sub>A–D and PLA<sub>2</sub>G<sub>4</sub>F, see Box 1.

Early on it was recognized that PLA<sub>2</sub>G<sub>4</sub>E (cPLA<sub>2</sub>ε) had only low PLA<sub>1</sub>, PLA<sub>2</sub> and lyso-PLA activity, and in 2016 it was shown to be a principal *N*-acyltransferase that is strongly stimulated by calcium.<sup>193,233</sup> It was confirmed that this enzyme has the characteristics of the elusive Ca-NAT. The enzyme specifically transfers the *sn*-1 *O*-acyl from the acyl donor, which can be PC or PE, to the amine of (p)PE, but shows no preference for *sn*-1 lipid composition.<sup>18,192,193</sup> As such, PLA<sub>2</sub>G<sub>4</sub>E might be involved in the downstream production of NAEs.<sup>192,235</sup> When overexpressed, cellular *sn*-2-oleoyl-NAPE levels were increased most prominently, which is in line with the notion that these are the most abundant NAPE species in the brain.<sup>17,192</sup> Beside calcium, activity is stimulated by several anionic lipids, including PS, PA and PG, but not phosphatidylinositol-4,5-bisphosphate (PI(4,5)P<sub>2</sub>).<sup>235,236</sup>

**Box 1 – PLA2G4 family**

PLA2G4A is the first characterized and most-studied member of the PLA2G4 family.<sup>257</sup> It is a ubiquitously expressed cytosolic protein that translocates to intracellular membranes upon  $\text{Ca}^{2+}$  binding. From the elucidated X-ray crystal structure it was concluded that it possesses an N-terminal C2 domain featuring three calcium-binding loops (CBLs).<sup>258</sup> Upon calcium binding the negative charge of these is shielded, increasing the lipid binding properties of the domain.<sup>259</sup> Depending on the  $\text{Ca}^{2+}$  concentration, the C2 domain directs the enzyme to the membranes of the Golgi, ER or nuclear envelope.<sup>243,260,261</sup> The catalytic domain does not adopt a classical  $\alpha/\beta$  hydrolase fold. Instead, the catalytic dyad is located in a deep funnel covered with a flexible, amphipathic lid that may confer substrate specificity, and a 'cap' region rich in basic residues that could interact with membrane phospholipids.<sup>258</sup> Translocation to intracellular membranes is required for catalytic activity, which can be enhanced through phosphorylation by various kinases.<sup>262–264</sup> A putative binding site for phosphatidylinositol phosphates (PIPs) is suggested to regulate intracellular localization as well as catalytic activity, but this has not been proven *in vivo*.<sup>265–268</sup> PLA2G4A has preferential PLA<sub>2</sub> activity and showed a strong preference for hydrolysis of *sn*-2 arachidonoyl esters from PC (regardless of the *sn*-1 linkage type), PE, PA and PS.<sup>232,269</sup> Indeed, it plays a central role in the production of arachidonic acid and its physiological importance has been established in mediating the release of immunomodulatory eicosanoids, which are oxidative products of arachidonic acid.<sup>270–272</sup> This way, PLA2G4A was found to be involved in the immune responses related to injury<sup>271–274</sup>, ischemia<sup>275</sup>, neurodegenerative diseases<sup>276,277</sup> and (auto)immune diseases<sup>277–280</sup>, as well as in fertility<sup>275</sup> and cancer.<sup>281,282</sup> It contributes to trafficking of proteins within the Golgi apparatus and from the Golgi to the plasma membrane through the formation of membrane tubules.<sup>244,283</sup> This function appeared to require catalytic activity of PLA2G4A, but was independent of downstream production of eicosanoids, suggesting an additional function of PLA2G4A in mediating membrane dynamics.<sup>244</sup>

Less is known about the other members of the PLA2G4 family. In humans, three splicing isoforms of PLA2G4B (cPLA<sub>2</sub> $\beta$ ) exist, of which only one (PLA2G4B3) was found to be endogenously translated.<sup>284</sup> It is found in most tissues, most abundantly in pancreas, liver and brain<sup>234</sup>, and is constitutively localized to early endosomal and mitochondrial membranes.<sup>284</sup> It predominantly hydrolyzes 2-lysophospholipids in a calcium-independent manner.<sup>284,285</sup> The enzyme has an N-terminal truncated jumonji C (JmjC) domain upstream of the C2 domain, which lacks several conserved elements for histone lysine demethylation and therefore is of unknown relevance.<sup>284,286</sup> Recently, a read-through fusion gene formed by splicing of PLA2G4B with neighboring JmjD-containing protein 7 (JMJD7) was shown to play a role in cancer cell proliferation.<sup>287</sup>

PLA2G4B also has a C-terminal polybasic (PB) domain (-RRRQRR-) with unknown functionality.<sup>284</sup>

PLA2G4C (cPLA<sub>2</sub>γ) is the smallest member of the family, as it lacks a C2 domain.<sup>234</sup> Consequently, its catalytic activity is calcium-independent.<sup>234</sup> PLA2G4C has low PLA<sub>1</sub> and PLA<sub>2</sub> activity, but higher lyso-PLA activity.<sup>285,288</sup> It has a preference for polyunsaturated *sn*-2 *O*-acyls, and overexpression increases arachidonic acid release.<sup>289,290</sup> In addition, it is able to transfer fatty acids from 1-lyso-PC and 1-lyso-PE to 2-lyso-PC and 2-lyso-PE.<sup>291</sup> Recently, it was shown to accept NAPes as substrate for sequential *sn*-1 and *sn*-2 hydrolysis to GP-NAEs *in vitro*, similar to ABHD4.<sup>292</sup> It is highly expressed in human heart and skeletal muscle<sup>290</sup>, and is tightly associated with the ER membrane and possibly the outer mitochondrial leaflet.<sup>291,293–295</sup> N- and C-terminal protein lipidation sites are potentially involved in the subcellular localization.<sup>289–291,294,296</sup> PLA2G4C is involved in lipid droplet formation and translocates to these upon formation.<sup>295</sup> Here, it plays a role as a host factor in hepatitis C viral genome replication and virion assembly.<sup>297</sup> The similarity of this function to that of PLAAT3 makes PLA2G4C an interesting subject for investigation.

PLA2G4D (cPLA<sub>2</sub>δ) is predominantly a PLA<sub>1</sub>, but also has relatively high PLA<sub>2</sub> activity, which can be slightly stimulated by calcium.<sup>285</sup> It has preference for PC and 2-lyso-PC over other phospholipids and preferentially cleaves linoleoyl esters.<sup>298</sup> After PLA2G4A, it is the only PLA2G4 for which the crystal structure was elucidated, which showed a remarkable tandem C2 domain.<sup>240</sup> The N-terminal of these was homologous to the C2 of PLA2G4A and showed conserved CBLs, whereas the second had similar overall topology but no CBLs. Of note, the second C2 showed significant sequence similarity with PLA2G4B, E and F, suggesting these might also have a double C2 domain.<sup>240</sup> Similar to PLA2G4A, PLA2G4D calcium-dependently translocates from the cytosol to ER/Golgi membranes.<sup>233</sup> In humans, it is found exclusively in stratified squamous epithelia of skin and cervix.<sup>298</sup> Its expression is increased in mast cells and keratinocytes in psoriatic lesions and atopic dermatitis, and the enzyme was found in mast cell-derived exosomes that could be taken up by antigen-presenting cells.<sup>298,299</sup>

Similar to PLA2G4B and C, mouse PLA2G4F (cPLA<sub>2</sub>ζ) preferentially hydrolyzes 2-lyso-PLA esters, but it also contains PLA<sub>1</sub> and PLA<sub>2</sub> activity.<sup>233,285</sup> Its PLA<sub>1</sub> and PLA<sub>2</sub> activity were found to be stimulated by calcium, while lyso-PLA activity was not.<sup>285</sup> High expression was found in thyroid, and also some in stomach and intestinal tissue.<sup>233</sup> When overexpressed, mPLA2G4F localized to the cytosol and did not respond to calcium.<sup>233</sup> It appeared to be involved in arachidonic acid production in mouse lung fibroblasts.<sup>300</sup> Human PLA2G4F was reported to be the main phospholipase responsible for mitochondrial arachidonic acid production in healthy myocardium, providing the precursor for production of protective epoxyeicosatrienoic acids (EETs).<sup>301</sup>

Activity was increased most notably by PS, which also increased PLA2G4E's affinity for  $\text{Ca}^{2+}$ .<sup>235</sup> However, since these experiments were carried out on purified enzyme, the physiological relevance is not clear. The enzyme is expressed in brain, heart, testes, skeletal muscle and skin. Within the brain, only neuronal cells were found to express PLA2G4E.<sup>193,237</sup> Of note, the tissue distribution is highly similar to PLAAT1 and PLAAT5, both of which also have high acyltransferase activity.<sup>199,227</sup>

In humans, two isoforms of PLA2G4E exist, which differ in their N-terminal sequence. *In vitro*, these isoforms, consisting of 834 and 868 amino acids (97 and 100 kDa, respectively), showed similar activity and substrate preference.<sup>235</sup> Google's AlphaFold 2 predicts the N-terminus to be disordered (Figure 1.5)<sup>238,239</sup>, and no physiological relevance for the two isoforms is known.<sup>235</sup> PLA2G4E has a C2 domain with three calcium-binding loops (CBLs), followed by a region with high sequence similarity to PLA2G4D's second C2 domain.<sup>240</sup> AlphaFold 2 predicts a C2-like topology for this region, but lacking CBLs, similar to PLA2G4D (Figure 1.5 and Box 1).<sup>238</sup> The lipase domain contains the conserved Arg<sup>384</sup> and Ser<sup>412</sup>-Asp<sup>700</sup> catalytic dyad. How the topology of this domain prevents hydrolysis of substrate in favor of transacylation is not known.<sup>241</sup> Additionally, it has a C-terminal polybasic (PB) domain (-KKKRLK-), similar to PLA2G4B.<sup>235</sup> Removal of any of these domains was found to be detrimental for catalytic activity, but the mechanism through which the C2 and PB domains cooperate in substrate conversion was not elucidated.<sup>236</sup>

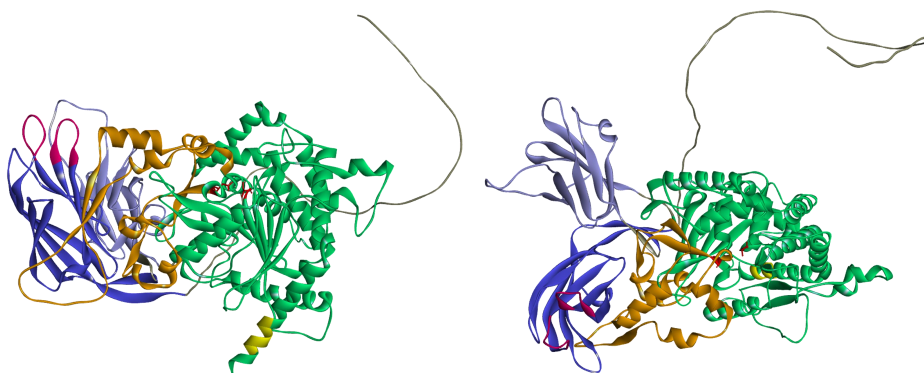


**Figure 1.5. AlphaFold2 prediction of human PLA2G4E structure.** Domains are color-coded based on sequence similarity with hPLA2G4A and hPLA2G4D. The disordered N-terminus (grey) is followed by the C2 domain (blue), which contains two calcium-binding loops (red). A second domain with C2 topology (purple) is predicted, but does not contain calcium-binding loops. The central lipase domain (green) contains the catalytic dyad (red, stick representation), a putative cap domain (orange) and the C-terminal polybasic stretch (yellow).

PLA2G4E is constitutively localized to perinuclear membranes.<sup>233</sup> In RAW264.7 macrophages, human PLA2G4E localized to lysosomes, which are rich in PS.<sup>235</sup> In HeLa cells, mouse PLA2G4E localized to vesicles and tubules associated with the clathrin-independent endocytic machinery. It was specifically present in early endosomes, but not in late endosomes, lysosomes or the Golgi apparatus. This localization appeared to be mediated

by interactions of the PB domain with PIPs, predominantly PI(4,5)P<sub>2</sub>, which are enriched in clathrin-independent endocytic vesicles.<sup>242</sup> Removal of either the PB or the C2 domain abrogated the specific localization.<sup>236</sup> Additionally, in contrast to PLA2G4A and D<sup>233,243</sup>, treatment with ionomycin was also shown to release the protein into the cytosol, which was suggested to be a consequence of calcium-dependent PIP degradation.<sup>242</sup> At these vesicles, PLA2G4E is involved in recycling internalized cargo, including MHC-I, CD55 and CD147, back to the plasma membrane. Tubule formation and trafficking were dependent on catalytic activity, but which metabolites are involved is not known.<sup>242</sup> As noted above, NAPEs have membrane- and vesicle-stabilizing properties, stimulate liposome fusion and might be involved in cellular division.<sup>3,4</sup> In addition, they can regulate the membrane association of intracellular proteins.<sup>62</sup> Lysophospholipids, which are a side product of NAPE production, can induce positive membrane curvature needed for vesicle formation and budding. PLA2G4A's regulation of Golgi trafficking might be mediated by lysophospholipids<sup>244</sup>, suggesting that PLA2G4E could regulate endosomal recycling through production of either or both NAPEs and lysophospholipids (Figure 1.6).

One interesting class of clathrin-independent endocytic vesicles are caveolae. These vesicles, formed by assembly of caveolin and cavin, are thought to invaginate from the plasma membrane depending on the local lipid composition, particularly PS.<sup>67,245</sup> They are enriched in PS and PI(4,5)P<sub>2</sub><sup>246</sup>, and have been shown to colocalize with Rac<sup>247</sup> and AEA.<sup>248,249</sup> Caveolae are not found in neurons, but high levels are present in endothelial and muscle cells.<sup>250</sup> It is tempting to speculate about the role of NAPEs and PLA2G4E in caveolae, but PLA2G4E depletion in cervical cells was shown to have no effect on caveolin-1.<sup>242</sup> However, a possible link in other cell types cannot be ruled out.

Recently, expression of PLA2G4E was linked to memory retention in Alzheimer's disease.<sup>251</sup> AD patients with clinical symptoms of cognitive deficits appeared to have lower brain PLA2G4E expression than early-stage AD patients and healthy controls. In a mouse model for AD, animals with impaired spatial memory showed downregulated cortical and hippocampal PLA2G4E compared to wild type mice. Resilient transgenic animals with intact memory, however, had significantly higher brain PLA2G4E expression than the impaired mice. Importantly, overexpression of PLA2G4E in the hippocampus of symptomatic mice restored their memory and increased neurogenesis, suggesting an important role for PLA2G4E in memory formation and retention.<sup>251</sup> Whether catalytic activity of PLA2G4E is required and which metabolites are involved in this process is not known. Furthermore, gene variants of PLA2G4E have been correlated to AD<sup>252,253</sup> and panic disorder<sup>254</sup>, supporting a role in neurological diseases.



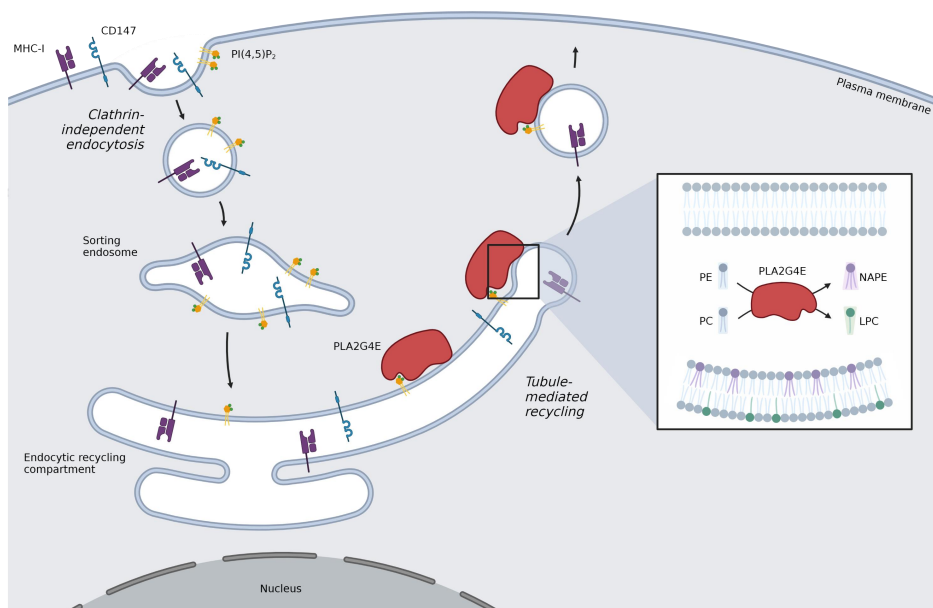


**Figure 1.6. Schematic overview of the putative role of PLA2G4E in clathrin-independent endocytic recycling.** Cargo internalized via clathrin-independent endocytosis (e.g. MHC-I and CD147) is transported to a sorting endosome to determine its fate. One pathway of recycling the cargo back to the plasma membrane involves tubular elements produced from the endocytic recycling compartment. Catalytic activity of PLA2G4E, recruited via interactions with PI(4,5)P<sub>2</sub>, is necessary for tubule formation and transport to the plasma membrane. This may be dependent on modification of the membrane architecture by either or both NAPEs and lyso-PC (LPC) produced by PLA2G4E (see inset). Other possible endocytic pathways are omitted for clarity.

## Aim and outline of this thesis

NAPEs are an underexplored class of phospholipids with diverse functionalities within the cell. Understanding their roles in membrane dynamics, signaling and metabolism and the regulation thereof will help to understand the molecular mechanisms underlying cellular (patho)physiology. The ability to selectively modulate the biosynthesis and degradation of NAPEs is pivotal to study their biology, and might lead to the development of drugs for the treatment of (neuro)degenerative diseases. So far, no potent and selective inhibitors of the calcium-dependent route of NAPE biosynthesis have been reported. The aim of this thesis, therefore, was to develop PLA2G4E inhibitors that could potently and selectively decrease cellular NAPE levels (see also Box 2).

**Chapter 2** describes the optimization of the first PLA2G4E inhibitors previously identified.<sup>255</sup> Organic synthesis and activity-based protein profiling (ABPP) were applied to build a library of compounds and determine their structure-activity relationships on PLA2G4E. This led to the identification of **WEN091** as potent PLA2G4E inhibitor (Figure 1.8).

## Box 2 – Inhibitors of PLA2G4 enzymes

The central role of PLA2G4A in immunomodulatory lipid production has stimulated the development of several inhibitors for this enzyme. The first inhibitor discovered was arachidonyl trifluoromethylketone (AACOCF<sub>3</sub>), a reversible covalent derivative of arachidonic acid (Figure 1.7).<sup>302</sup> It showed some selectivity over the sPLA<sub>2</sub> family, but does inhibit cyclooxygenases and is not regarded a selective inhibitor.<sup>303</sup> Nevertheless, it has been applied in many studies as a selective PLA2G4A inhibitor.<sup>304,305</sup> Several pyrrolidine-based inhibitors were developed, which were reported to be more selective.<sup>306,307</sup> These compounds showed efficacy in suppressing cellular arachidonic acid and lysophospholipid production.<sup>307–309</sup> Pyrrolidine-2 was reported to also be an inhibitor of PLA2G4F, but not PLA2G4B.<sup>300</sup> Pharmaceutical companies, including AstraZeneca<sup>310</sup>, Asubio Pharma<sup>311,312</sup> and Avexin<sup>313–315</sup> have developed nanomolar potent PLA2G4A inhibitors that showed *in vivo* efficacy in lowering levels of pro-inflammatory lipids and alleviating symptoms of inflammation. Ziaco Pharma's ZPL-5212372 (previously Pfizer) was proceeded into Phase II human trials for the treatment of atopic dermatitis.<sup>316</sup> Wyeth (now Pfizer) has developed ecopladib, which was orally efficacious in reducing inflammatory edema in rats<sup>317</sup>, and giripladib, which was tested in Phase II for the treatment of osteoarthritis, but failed due to adverse gastrointestinal events.<sup>318</sup> These compounds displayed selectivity over PLA2G4B, C and F and cyclooxygenases.<sup>317,319</sup> Whether the adverse side effects were due to PLA2G4A inhibition or an unidentified off-target is not known. Recently, AK106-001616, a PLA2G4A inhibitor based on a different scaffold, showed less gastrointestinal problems than generic anti-inflammatory drug naproxen.<sup>320</sup> These examples indicate the therapeutic potential of PLA2G4A inhibition, but knowledge about the selectivity profile of the compounds is limited. No selective inhibitors of the other members of the PLA2G4 family have been reported.

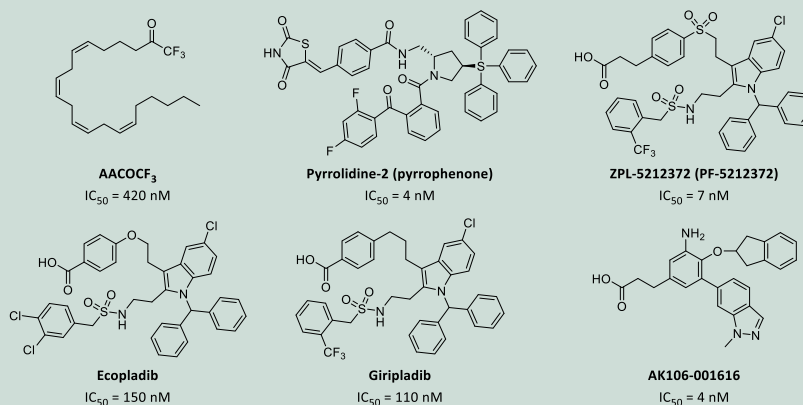


**Figure 1.7. Structures of published inhibitors of PLA2G4 enzymes.** Names and reported activities on PLA2G4A are indicated. Inhibitory values were determined in similar phospholipase assays measuring arachidonic acid release from PC-containing vesicles.<sup>307,315,317,320</sup>

**Chapter 3** describes the biological evaluation of **WEN091**. Using ABPP and biochemical assays, the selectivity profile of **WEN091** was determined across PLA2G4 family members, NAPE-metabolic enzymes and other brain serine hydrolases. **WEN091** was found to be a potent and selective inhibitor of PLA2G4E *in vitro*, with important off-targets in Neuro-2a cells. Lipidomics analysis of PLA2G4E-overexpressing Neuro-2a cells showed that cellular NAPE levels can be decreased by treatment with **WEN091**.

Further optimization of the inhibitors is described in **Chapter 4**. Structural analogs of **WEN091** were synthesized with the aim of improving the cellular selectivity of the PLA2G4E inhibitors. ABPP and biochemical assays were used for the biological profiling of these inhibitors regarding their potency and selectivity. **IK015** and **WEN222** were identified as potent inhibitors of PLA2G4E *in vitro* with an improved selectivity profile in Neuro-2a cells. In addition, **WEN258** was identified as an inactive structural analog, which can be used as a control compound to distinguish on-target from off-target effects of the inhibitors (Figure 1.8).

In **Chapter 5** the development of a cellular target engagement assay for PLA2G4E is described. **WEN175**, an alkynylated inhibitor based on **IK015**, was synthesized, and was shown to activity-dependently label PLA2G4E (Figure 1.8). Using **WEN175**, the cellular activity of PLA2G4E was visualized and *in situ* target engagement of **WEN091** was confirmed. In addition, ABPP with **WEN175** confirmed PLA2G4E's requirement for both the C2 and PB domain for catalytic activity.

**Chapter 6** describes the incorporation of caged hydrocarbons into novel inhibitors of lipid metabolic enzymes ABHD6, ABHD16a and diacylglycerol lipase (DAGL). These structures were combined with known chemical elements for target recognition, leading to the identification of **RED353** as a highly potent and selective ABHD6 inhibitor (Figure 1.8). In Neuro-2a cells, **RED353** showed better selectivity over AEA hydrolysis than widely-used ABHD6 inhibitor KT182, as determined using ABPP and targeted lipidomics. Furthermore, ABHD6 inhibition by **RED353** was shown to decrease basal levels of 2-arachidonoylglycerol, supporting previous reports that ABHD6 possesses DAGL activity.<sup>256</sup>

The findings of this thesis are summarized in **Chapter 7**. Here, concluding remarks are made and limitations of this study are noted. Suggestions are included for further research based on this thesis.

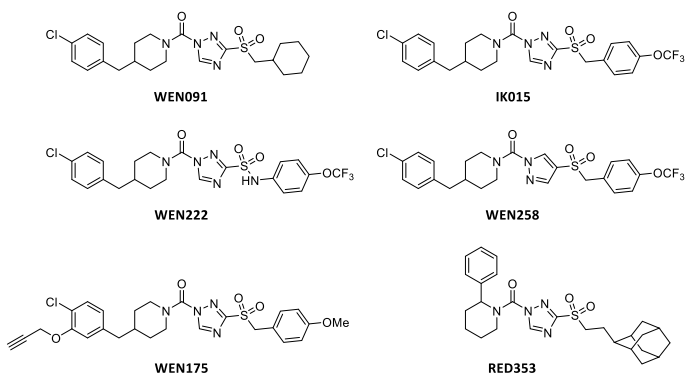


**Figure 1.8. Structures of key inhibitors identified in this thesis.** PLA2G4E inhibitor **WEN091** is identified in Chapter 2, PLA2G4E inhibitors **IK015**, **WEN222** and control compound **WEN258** are identified in Chapter 4, PLA2G4E ABP **WEN175** is identified in Chapter 5, and ABHD6 inhibitor **RED353** is identified in Chapter 6.

## References

1. Fahy, E., Cotter, D., Sud, M. & Subramaniam, S. Lipid classification, structures and tools. *Biochim. Biophys. Acta - Mol. Cell Biol. Lipids* **1811**, 637–647 (2011).
2. Koenders, S. T. A., Gagestein, B. & van der Stelt, M. Opportunities for Lipid-Based Probes in the Field of Immunology. in *Current Topics in Microbiology and Immunology* **420**, 283–319 (Springer Verlag, 2018).
3. Coulon, D., Faure, L., Salmon, M., Wattelet, V. & Bessoule, J. J. Occurrence, biosynthesis and functions of N-acylphosphatidylethanolamines (NAPE): Not just precursors of N-acylethanolamines (NAE). *Biochimie* **94**, 75–85 (2012).
4. Wellner, N., Diep, T. A., Janfelt, C. & Hansen, H. S. N-acylation of phosphatidylethanolamine and its biological functions in mammals. *Biochim. Biophys. Acta - Mol. Cell Biol. Lipids* **1831**, 652–662 (2013).
5. Matsumoto, M. & Miwa, M. Study on the new phospholipid, N-acyl-1-alkyl glycerophosphoryl-ethanolamine, from bovine erythrocytes. *Biochim. Biophys. Acta - Lipids Lipid Metab.* **296**, 350–364 (1973).
6. Cadas, H., Schinelli, S. & Piomelli, D. Membrane localization of N-acylphosphatidylethanolamine in central neurons: Studies with exogenous phospholipases. *J. Lipid Mediat. Cell Signal.* **14**, 63–70 (1996).
7. Bomstein, R. A. A new class of phosphatides isolated from soft wheat flour. *Biochem. Biophys. Res. Commun.* **21**, 49–54 (1965).
8. Natarajan, V., Schmid, P. C. & Schmid, H. H. O. N-Acylethanolamine phospholipid metabolism in normal and ischemic rat brain. *Biochim. Biophys. Acta - Lipids Lipid Metab.* **878**, 32–41 (1986).
9. Hack, M. H. & Helmy, F. M. A reappraisal of the dog-heart infarct plasmalogen, its conception as a bis-phosphatidic acid and current recognition as an N-acyl phosphatidyl ethanolamine. *Comp. Biochem. Physiol. Part B Biochem.* **73**, 873–879 (1982).
10. Schmid, P. C., Reddy, P. V., Natarajan, V. & Schmid, H. H. Metabolism of N-acylethanolamine phospholipids by a mammalian phosphodiesterase of the phospholipase D type. *J. Biol. Chem.* **258**, 9302–9306 (1983).
11. Chapman, K. D. & Moore, T. S. Catalytic properties of a newly discovered acyltransferase that synthesizes N-acylphosphatidylethanolamine in cottonseed (*Gossypium hirsutum* L.) microsomes. *Plant Physiol.* **102**, 761–769 (1993).
12. Faure, L. *et al.* Discovery and Characterization of an *Arabidopsis thaliana* N-Acylphosphatidylethanolamine Synthase. *J. Biol. Chem.* **284**, 18734–18741 (2009).
13. Natarajan, V., Reddy, P. V., Schmid, P. C. & Schmid, H. H. O. N-acylation of ethanolamine phospholipids in canine myocardium. *Biochim. Biophys. Acta - Lipids Lipid Metab.* **712**, 342–355 (1982).
14. Hussain, Z., Uyama, T., Tsuboi, K. & Ueda, N. Mammalian enzymes responsible for the biosynthesis of N-acylethanolamines. *Biochim. Biophys. Acta - Mol. Cell Biol. Lipids* **1862**, 1546–1561 (2017).
15. Romano, A., Tempesta, B., Provensi, G., Passani, M. B. & Gaetani, S. Central mechanisms mediating the hypophagic effects of oleoylethanolamide and N-acylphosphatidylethanolamines: Different lipid signals? *Front. Pharmacol.* **6**, 1–8 (2015).
16. Kilaru, A. *et al.* Lipid Profiling Reveals Tissue-Specific Differences for Ethanolamide Lipids in Mice Lacking Fatty Acid Amide Hydrolase. *Lipids* **45**, 863–875 (2010).

17. Tsuboi, K. *et al.* Enzymatic formation of N-acylethanolamines from N-acylethanolamine plasmalogen through N-acylphosphatidylethanolamine-hydrolyzing phospholipase D-dependent and -independent pathways. *Biochim. Biophys. Acta - Mol. Cell Biol. Lipids* **1811**, 565–577 (2011).
18. Sugiura, T. *et al.* Enzymatic synthesis of anandamide, an endogenous cannabinoid receptor ligand, through N-Acylphosphatidylethanolamine pathway in testis: Involvement of Ca<sup>2+</sup>-dependent transacylase and phosphodiesterase activities. *Biochem. Biophys. Res. Commun.* **218**, 113–117 (1996).
19. Petersen, G. *et al.* Endocannabinoid metabolism in human glioblastomas and meningiomas compared to human non-tumour brain tissue. *J. Neurochem.* **93**, 299–309 (2005).
20. Gillum, M. P. *et al.* N-acylphosphatidylethanolamine, a Gut-Derived Circulating Factor Induced by Fat Ingestion, Inhibits Food Intake. *Cell* **135**, 813–824 (2008).
21. Cadas, H., Di Tomaso, E. & Piomelli, D. Occurrence and biosynthesis of endogenous cannabinoid precursor, N-arachidonoyl phosphatidylethanolamine, in rat brain. *J. Neurosci.* **17**, 1226–1242 (1997).
22. Bisogno, T. *et al.* Brain Regional Distribution of Endocannabinoids: Implications for Their Biosynthesis and Biological Function. *Biochem. Biophys. Res. Commun.* **256**, 377–380 (1999).
23. Berrendero, F., Sepe, N., Ramos, J. A., Di Marzo, V. & Fernández-Ruiz, J. J. Analysis of cannabinoid receptor binding and mRNA expression and endogenous cannabinoid contents in the developing rat brain during late gestation and early postnatal period. *Synapse* **33**, 181–191 (1999).
24. Reddy, P. V., Natarajan, V., Schmid, P. C. & Schmid, H. H. O. N-acylation of dog heart ethanolamine phospholipids by transacylase activity. *Biochim. Biophys. Acta - Lipids Lipid Metab.* **750**, 472–480 (1983).
25. Astarita, G., Ahmed, F. & Piomelli, D. Identification of biosynthetic precursors for the endocannabinoid anandamide in the rat brain. *J. Lipid Res.* **49**, 48–57 (2008).
26. Fu, J. *et al.* Food intake regulates oleoylethanolamide formation and degradation in the proximal small intestine. *J. Biol. Chem.* **282**, 1518–1528 (2007).
27. Uyama, T. *et al.* Generation of N-acylphosphatidylethanolamine by members of the phospholipase A/acyltransferase (PLA/AT) family. *J. Biol. Chem.* **287**, 31905–31919 (2012).
28. Moesgaard, B., Petersen, G., Jaroszewski, J. W. & Hansen, H. S. Age dependent accumulation of N-acyl-ethanolamine phospholipids in ischemic rat brain: A <sup>31</sup>P NMR and enzyme activity study. *J. Lipid Res.* **41**, 985–990 (2000).
29. Palese, F., Pontis, S., Realini, N. & Piomelli, D. A protective role for N-acylphosphatidylethanolamine phospholipase D in 6-OHDA-induced neurodegeneration. *Sci. Rep.* **9**, 1–16 (2019).
30. Lafrance, D., Marion, D. & Pérolet, M. Study of the structure of N-Acyldipalmitoylphosphatidylethanolamines in aqueous dispersion by infrared and Raman spectroscopies. *Biochemistry* **29**, 4592–4599 (1990).
31. Swamy, M. J., Ramakrishnan, M., Angerstein, B. & Marsh, D. Spin-label electron spin resonance studies on the mode of anchoring and vertical location of the N-acyl chain in N-acylphosphatidylethanolamines. *Biochemistry* **39**, 12476–12484 (2000).
32. Domingo, J. C., Mora, M. & Africa de Madariaga, M. Incorporation of N-acylethanolamine phospholipids into egg phosphatidylcholine vesicles: characterization and permeability properties of the binary systems. *Biochim. Biophys. Acta - Biomembr.* **1148**, 308–316 (1993).

33. Lee, Y. C., Zheng, Y. O., Taraschi, T. F. & Janes, N. Hydrophobic alkyl headgroups strongly promote membrane curvature and violate the headgroup volume correlation due to 'headgroup' insertion. *Biochemistry* **35**, 3677–3684 (1996).
34. Domingo, J. C., Mora, M. & de Madariaga, M. A. The influence of *N*-acyl chain length on the phase behaviour of natural and synthetic *N*-acylethanolamine phospholipids. *Chem. Phys. Lipids* **75**, 15–25 (1995).
35. Lafrance, C. P., Blochet, J. É. & Pézolet, M. *N*-acylphosphatidylethanolamines: Effect of the *N*-acyl chain length on its orientation. *Biophys. J.* **72**, 2559–2568 (1997).
36. Mercadal, M., Domingo, J. C., Bermudez, M., Mora, M. & De Madariaga, M. A. *N*-Palmitoyl-phosphatidylethanolamine stabilizes liposomes in the presence of human serum: effect of lipidic composition and system characterization. *Biochim. Biophys. Acta - Biomembr.* **1235**, 281–288 (1995).
37. Shangguan, T., Pak, C. C., Ali, S., Janoff, A. S. & Meers, P. Cation-dependent fusogenicity of an *N*-acyl phosphatidylethanolamine. *Biochim. Biophys. Acta* **1368**, 171–183 (1998).
38. Mora, M., Mir, F., Madariaga, M. A. de & Sagrista, M. L. Aggregation and fusion of vesicles composed of *N*-palmitoyl derivatives of membrane phospholipids. *Lipids* **35**, 513–524 (2000).
39. Mileykovskaya, E. *et al.* Phosphatidic Acid and *N*-Acylphosphatidylethanolamine Form Membrane Domains in *Escherichia coli* Mutant Lacking Cardiolipin and Phosphatidylglycerol. *J. Biol. Chem.* **284**, 2990–3000 (2009).
40. Fu, J. *et al.* Sympathetic activity controls fat-induced oleoylethanolamide signaling in small intestine. *J. Neurosci.* **31**, 5730–5736 (2011).
41. Petersen, G. *et al.* Intestinal levels of anandamide and oleoylethanolamide in food-deprived rats are regulated through their precursors. *Biochim. Biophys. Acta - Mol. Cell Biol. Lipids* **1761**, 143–150 (2006).
42. Wellner, N. *et al.* Studies on the anorectic effect of *N*-acylphosphatidylethanolamine and phosphatidylethanolamine in mice. *Biochim. Biophys. Acta - Mol. Cell Biol. Lipids* **1811**, 508–512 (2011).
43. Chen, Z. *et al.* Leptogenic effects of NAPE require activity of NAPE-hydrolyzing phospholipase D. *J. Lipid Res.* **58**, 1624–1635 (2017).
44. Epps, D. E., Natarajan, V., Schmid, P. C. & Schmid, H. H. O. Accumulation of *N*-acylethanolamine glycerophospholipids in infarcted myocardium. *Biochim. Biophys. Acta - Lipids Lipid Metab.* **618**, 420–430 (1980).
45. Janfelt, C. *et al.* Visualization by mass spectrometry of 2-dimensional changes in rat brain lipids, including *N*-acylphosphatidylethanolamines, during neonatal brain ischemia. *FASEB J.* **26**, 2667–2673 (2012).
46. Berger, C. *et al.* Massive accumulation of *N*-acylethanolamines after stroke. Cell signalling in acute cerebral ischemia? *J. Neurochem.* **88**, 1159–1167 (2004).
47. Rawlyer, A. J. & Braendle, R. A. *N*-Acylphosphatidylethanolamine Accumulation in Potato Cells upon Energy Shortage Caused by Anoxia or Respiratory Inhibitors. *Plant Physiol.* **127**, 240–251 (2001).
48. Hansen, H. H., Hansen, S. H., Schousboe, A. & Hansen, H. S. Determination of the phospholipid precursor of anandamide and other *N*-acylethanolamine phospholipids before and after sodium azide-induced toxicity in cultured neocortical neurons. *J. Neurochem.* **75**, 861–871 (2000).
49. Hansen, H. H., Ikonomidou, C., Bittigau, P., Hansen, S. H. & Hansen, H. S. Accumulation of the anandamide precursor and other *N*-acylethanolamine phospholipids in infant rat models of *in vivo* necrotic and apoptotic neuronal death. *J. Neurochem.* **76**, 39–46 (2001).

50. Hansen, H. S. *et al.* Characterization of glutamate-induced formation of *N*- acylphosphatidyl-ethanolamine and *N*-acylethanolamine in cultured neocortical neurons. *J. Neurochem.* **69**, 753–761 (1997).
51. Hansen, H. S., Lauritzen, L., Strand, A. M., Moesgaard, B. & Frandsen, A. Glutamate stimulates the formation of *N*-acylphosphatidylethanolamine and *N*-acylphosphatidylethanolamine in cortical neurons in culture. *Biochim. Biophys. Acta - Lipids Lipid Metab.* **1258**, 303–308 (1995).
52. Saito, M. *et al.* Ethanol alters lipid profiles and phosphorylation status of AMP-activated protein kinase in the neonatal mouse brain. *J. Neurochem.* **103**, 1208–1218 (2007).
53. Saito, M. *et al.* Involvement of ceramide in ethanol-induced apoptotic neurodegeneration in the neonatal mouse brain. *J. Neurochem.* **115**, 168–177 (2010).
54. Greenamyre, J. T. & Hastings, T. G. Parkinson's - Divergent causes, convergent mechanisms. *Science* **304**, 1120–1122 (2004).
55. Jeon, B. S., Jackson-Lewis, V. & Burke, R. E. 6-Hydroxydopamine Lesion of the Rat Substantia Nigra: Time Course and Morphology of Cell Death. *Neurodegeneration* **4**, 131–137 (1995).
56. Morales, I., Sanchez, A., Rodriguez-Sabate, C. & Rodriguez, M. The degeneration of dopaminergic synapses in Parkinson's disease: A selective animal model. *Behav. Brain Res.* **289**, 19–28 (2015).
57. Basit, A., Pontis, S., Piomelli, D. & Armirotti, A. Ion mobility mass spectrometry enhances low-abundance species detection in untargeted lipidomics. *Metabolomics* **12**, 1–10 (2016).
58. Kim, H. *et al.* The Small GTPase RAC1/CED-10 Is Essential in Maintaining Dopaminergic Neuron Function and Survival Against  $\alpha$ -Synuclein-Induced Toxicity. *Mol. Neurobiol.* **55**, 7533–7552 (2018).
59. Stankiewicz, T. R. & Linseman, D. A. Rho family GTPases: Key players in neuronal development, neuronal survival, and neurodegeneration. *Frontiers in Cellular Neuroscience* **8**, 314 (2014).
60. Sarkar, S. *et al.* Oligomerization of Lrrk controls actin severing and  $\alpha$ -synuclein neurotoxicity *in vivo*. *Mol. Neurodegener.* **16**, 1–18 (2021).
61. Helton, L. G. *et al.* Allosteric Inhibition of Parkinson's-Linked LRRK2 by Constrained Peptides. *ACS Chem. Biol.* acschembio.1c00487 (2021). doi:10.1021/ACSCHEMBIO.1C00487
62. Palese, F., Pontis, S., Realini, N. & Piomelli, D. NAPE-specific phospholipase D regulates LRRK2 association with neuronal membranes. in *Advances in Pharmacology* **90**, 217–238 (Academic Press Inc., 2021).
63. Shiratsuchi, A. *et al.* Inhibitory effect of *N*-palmitoylphosphatidylethanolamine on macrophage phagocytosis through inhibition of Rac1 and Cdc42. *J. Biochem.* **145**, 43–50 (2008).
64. Vaz, F. M. *et al.* Mutations in PCYT2 disrupt etherlipid biosynthesis and cause a complex hereditary spastic paraplegia. *Brain* **142**, 3382–3397 (2019).
65. Ross, B. M., Mamalias, N., Moszczynska, A., Rajput, A. H. & Kish, S. J. Elevated activity of phospholipid biosynthetic enzymes in substantia nigra of patients with Parkinson's disease. *Neuroscience* **102**, 899–904 (2001).
66. Wang, S. *et al.* Phosphatidylethanolamine deficiency disrupts  $\alpha$ -synuclein homeostasis in yeast and worm models of Parkinson disease. *Proc. Natl. Acad. Sci. U. S. A.* **111**, E3976–E3985 (2014).
67. Alberts, B. *et al.* *Molecular Biology of the Cell.* (Garland Science, 2008).
68. Han, X., Holtzman, D. M. & McKeel, D. W. Plasmalogen deficiency in early Alzheimer's disease subjects and in animal models: molecular characterization using electrospray ionization mass spectrometry. *J. Neurochem.* **77**, 1168–1180 (2001).



69. Kondo, S. *et al.* Accumulation of various *N*-acylethanolamines including *N*-arachidonoyl-ethanolamine (anandamide) in cadmium chloride-administered rat testis. *Arch. Biochem. Biophys.* **354**, 303–310 (1998).
70. Basu, A., Prence, E., Garrett, K., Glew, R. H. & Ellingson, J. S. Comparison of *N*-acyl phosphatidylethanolamines with different *N*-acyl groups as activators of glucocerebrosidase in various forms of Gaucher's disease. *Arch. Biochem. Biophys.* **243**, 28–34 (1985).
71. Kuehl, F. A., Jacob, T. A., Ganley, O. H., Ormond, R. E. & Meisinger, M. A. P. The identification of *N*-(2-hydroxyethyl)-palmitamide as a naturally occurring anti-inflammatory agent. *J. Am. Chem. Soc.* **79**, 5577–5578 (1957).
72. Ganley, O. H., Graessle, O. E. & Robinson, H. J. Anti-inflammatory activity of compounds obtained from egg yolk, peanut oil, and soybean lecithin. *J. Lab. Clin. Med.* **51**, 709–714 (1958).
73. Ganley, O. H. & Robinson, H. J. Antianaphylactic and antiserotonin activity of a compound obtained from egg yolk, peanut oil, and soybean lecithin. *J. Allergy* **30**, 415–419 (1959).
74. Alhouayek, M. & Muccioli, G. G. Harnessing the anti-inflammatory potential of palmitoylethanolamide. *Drug Discov. Today* **19**, 1632–1639 (2014).
75. Gabrielsson, L., Mattsson, S. & Fowler, C. J. Palmitoylethanolamide for the treatment of pain: pharmacokinetics, safety and efficacy. *Br. J. Clin. Pharmacol.* **82**, 932–942 (2016).
76. Keppel Hesselink, J. M., Costagliola, C., Fakhry, J. & Kopsky, D. J. Palmitoylethanolamide, a Natural Retinoprotectant: Its Putative Relevance for the Treatment of Glaucoma and Diabetic Retinopathy. *J. Ophthalmol.* **2015**, 9 (2015).
77. Paterniti, I. *et al.* Palmitoylethanolamide treatment reduces retinal inflammation in streptozotocin-induced diabetic rats. *Eur. J. Pharmacol.* **769**, 313–323 (2015).
78. Gómez-Boronat, M. *et al.* Diurnal Profiles of *N*-Acylethanolamines in goldfish brain and gastrointestinal tract: Possible role of feeding. *Front. Neurosci.* **13**, 450 (2019).
79. Fotio, Y., Ciccocioppo, R. & Piomelli, D. *N*-acylethanolamine acid amidase (NAAA) inhibition decreases the motivation for alcohol in Marchigian Sardinian alcohol-preferring rats. *Psychopharmacology* **238**, 249–258 (2021).
80. Melis, M. *et al.* Endogenous Fatty Acid Ethanolamides Suppress Nicotine-Induced Activation of Mesolimbic Dopamine Neurons through Nuclear Receptors. *J. Neurosci.* **28**, 13985–13994 (2008).
81. Petrosino, S., Iuvone, T. & Di Marzo, V. *N*-palmitoyl-ethanolamine: Biochemistry and new therapeutic opportunities. *Biochimie* **92**, 724–727 (2010).
82. Petrosino, S. & Di Marzo, V. The pharmacology of palmitoylethanolamide and first data on the therapeutic efficacy of some of its new formulations. *Br. J. Pharmacol.* **174**, 1349–1365 (2017).
83. Schäbitz, W. R. *et al.* Release of fatty acid amides in a patient with hemispheric stroke: A microdialysis study. *Stroke* **33**, 2112–2114 (2002).
84. Ahmad, A. *et al.* Reduction of ischemic brain injury by administration of palmitoylethanolamide after transient middle cerebral artery occlusion in rats. *Brain Res.* **1477**, 45–58 (2012).
85. D'Agostino, G. *et al.* Palmitoylethanolamide protects against the amyloid-B25-35-induced learning and memory impairment in mice, an experimental model of Alzheimer disease. *Neuropsychopharmacology* **37**, 1784–1792 (2012).
86. Beggiato, S., Tomasini, M. C. & Ferraro, L. Palmitoylethanolamide (PEA) as a potential therapeutic agent in Alzheimer's disease. *Front. Pharmacol.* **10**, (2019).
87. Scuderì, C. *et al.* Palmitoylethanolamide controls reactive gliosis and exerts neuroprotective functions in a rat model of Alzheimer's disease. *Cell Death Dis.* **5**, e1419 (2014).
88. Mattace Raso, G., Russo, R., Calignano, A. & Meli, R. Palmitoylethanolamide in CNS health and disease. *Pharmacol. Res.* **86**, 32–41 (2014).

89. Ambrosino, P., Soldovieri, M. V., Russo, C. & Tagliatalata, M. Activation and desensitization of TRPV1 channels in sensory neurons by the PPAR $\alpha$  agonist palmitoylethanolamide. *Br. J. Pharmacol.* **168**, 1430–1444 (2013).
90. Ambrosino, P., Soldovieri, M. V., De Maria, M., Russo, C. & Tagliatalata, M. Functional and biochemical interaction between PPAR $\alpha$  receptors and TRPV1 channels: Potential role in PPAR $\alpha$  agonists-mediated analgesia. *Pharmacol. Res.* **87**, 113–122 (2014).
91. Ryberg, E. *et al.* The orphan receptor GPR55 is a novel cannabinoid receptor. *Br. J. Pharmacol.* **152**, 1092–1101 (2007).
92. Overton, H. A. *et al.* Deorphanization of a G protein-coupled receptor for oleoylethanolamide and its use in the discovery of small-molecule hypophagic agents. *Cell Metab.* **3**, 167–175 (2006).
93. Piomelli, D. A fatty gut feeling. *Trends Endocrinol. Metab.* **24**, 332–341 (2013).
94. Fu, J., Kim, J., Oveisi, F., Astarita, G. & Piomelli, D. Targeted enhancement of oleoylethanolamide production in proximal small intestine induces across-meal satiety in rats. *Am. J. Physiol. - Regul. Integr. Comp. Physiol.* **295**, 45–50 (2008).
95. Guzmán, M. *et al.* Oleoylethanolamide Stimulates Lipolysis by Activating the Nuclear Receptor Peroxisome Proliferator-activated Receptor  $\alpha$  (PPAR- $\alpha$ ). *J. Biol. Chem.* **279**, 27849–27854 (2004).
96. Lauffer, L. M., Iakubov, R. & Brubaker, P. L. GPR119 Is Essential for Oleoylethanolamide-Induced Glucagon-Like Peptide-1 Secretion From the Intestinal Enteroendocrine L-Cell. *Diabetes* **58**, 1058–1066 (2009).
97. Brown, J. D., Karimian Azari, E. & Ayala, J. E. Oleoylethanolamide: A fat ally in the fight against obesity. *Physiol. Behav.* **176**, 50–58 (2017).
98. Provensi, G. *et al.* Satiety factor oleoylethanolamide recruits the brain histaminergic system to inhibit food intake. *Proc. Natl. Acad. Sci. U. S. A.* **111**, 11527–11532 (2014).
99. Gaetani, S. *et al.* The Fat-Induced Satiety Factor Oleoylethanolamide Suppresses Feeding through Central Release of Oxytocin. *J. Neurosci.* **30**, 8096–8101 (2010).
100. Bowen, K. J. *et al.* Oleic acid-derived oleoylethanolamide: A nutritional science perspective. *Prog. Lipid Res.* **67**, 1–15 (2017).
101. Bilbao, A. *et al.* Role of the satiety factor oleoylethanolamide in alcoholism. *Addict. Biol.* **21**, 859–872 (2016).
102. Ahern, G. P. Activation of TRPV1 by the Satiety Factor Oleoylethanolamide. *J. Biol. Chem.* **278**, 30429–30434 (2003).
103. González-Aparicio, R. & Moratalla, R. Oleoylethanolamide reduces L-DOPA-induced dyskinesia via TRPV1 receptor in a mouse model of Parkinson's disease. *Neurobiol. Dis.* **62**, 416–425 (2014).
104. Devane, W. A. *et al.* Isolation and structure of a brain constituent that binds to the cannabinoid receptor. *Science* **258**, 1946–1949 (1992).
105. Felder, C. C. *et al.* Anandamide, an endogenous cannabimimetic eicosanoid, binds to the cloned human cannabinoid receptor and stimulates receptor-mediated signal transduction. *Proc. Natl. Acad. Sci. U. S. A.* **90**, 7656–7660 (1993).
106. Gouveia-Figueira, S. & Nording, M. L. Validation of a tandem mass spectrometry method using combined extraction of 37 oxylipins and 14 endocannabinoid-related compounds including prostamides from biological matrices. *Prostaglandins Other Lipid Mediat.* **121**, 110–121 (2015).
107. Hohmann, A. G. *et al.* An endocannabinoid mechanism for stress-induced analgesia. *Nature* **435**, 1108–1112 (2005).
108. Morena, M., Patel, S., Bains, J. S. & Hill, M. N. Neurobiological Interactions Between Stress and the Endocannabinoid System. *Neuropsychopharmacology* **41**, 80–102 (2016).

109. Kathuria, S. *et al.* Modulation of anxiety through blockade of anandamide hydrolysis. *Nat. Med.* **9**, 76–81 (2003).
110. Lutz, B., Marsicano, G., Maldonado, R. & Hillard, C. J. The endocannabinoid system in guarding against fear, anxiety and stress. *Nat. Rev. Neurosci.* **16**, 705–718 (2015).
111. Gobbi, G. *et al.* Antidepressant-like activity and modulation of brain monoaminergic transmission by blockade of anandamide hydrolysis. *Proc. Natl. Acad. Sci. U. S. A.* **102**, 18620–18625 (2005).
112. Hill, M. N. *et al.* Endogenous cannabinoid signaling is essential for stress adaptation. *Proc. Natl. Acad. Sci. U. S. A.* **107**, 9406–9411 (2010).
113. Morena, M. *et al.* Upregulation of anandamide hydrolysis in the basolateral complex of amygdala reduces fear memory expression and indices of stress and anxiety. *J. Neurosci.* **39**, 1275–1292 (2019).
114. Jamshidi, N. & Taylor, D. A. Anandamide administration into the ventromedial hypothalamus stimulates appetite in rats. *Br. J. Pharmacol.* **134**, 1151–1154 (2001).
115. Hansen, H. S. & Diep, T. A. *N*-acylethanolamines, anandamide and food intake. *Biochem. Pharmacol.* **78**, 553–560 (2009).
116. Alger, B. E. Endocannabinoids and Their Implications for Epilepsy. *Epilepsy Curr.* **4**, 169–173 (2004).
117. Grillo, A. *et al.* Selective Fatty Acid Amide Hydrolase Inhibitors as Potential Novel Antiepileptic Agents. *ACS Chem. Neurosci.* **12**, 1716–1736 (2021).
118. Romigi, A. *et al.* Cerebrospinal fluid levels of the endocannabinoid anandamide are reduced in patients with untreated newly diagnosed temporal lobe epilepsy. *Epilepsia* **51**, 768–772 (2010).
119. Tsuboi, K., Uyama, T., Okamoto, Y. & Ueda, N. Endocannabinoids and related *N*-acylethanolamines: biological activities and metabolism. *Inflamm. Regen.* **38**, (2018).
120. Cravatt, B. F. *et al.* Supersensitivity to anandamide and enhanced endogenous cannabinoid signaling in mice lacking fatty acid amide hydrolase. *Proc. Natl. Acad. Sci. U. S. A.* **98**, 9371–9376 (2001).
121. Clapper, J. R. *et al.* Anandamide suppresses pain initiation through a peripheral endocannabinoid mechanism. *Nat. Neurosci.* **13**, 1265–1270 (2010).
122. Morena, M. *et al.* Endogenous cannabinoid release within prefrontal-limbic pathways affects memory consolidation of emotional training. *Proc. Natl. Acad. Sci. U. S. A.* **111**, 18333–18338 (2014).
123. Di Marzo, V. Targeting the endocannabinoid system: To enhance or reduce? *Nature Reviews Drug Discovery* **7**, 438–455 (2008).
124. Hansen, H. S., Moesgaard, B., Petersen, G. & Hansen, H. H. Putative neuroprotective actions of *N*-acyl-ethanolamines. *Pharmacol. Ther.* **95**, 119–126 (2002).
125. Marsicano, G. *et al.* CB1 cannabinoid receptors and on-demand defense against excitotoxicity. *Science* **302**, 84–88 (2003).
126. Milton, N. G. N. Anandamide and noladin ether prevent neurotoxicity of the human amyloid- $\beta$  peptide. *Neurosci. Lett.* **332**, 127–130 (2002).
127. Van der Stelt, M. *et al.* Exogenous Anandamide Protects Rat Brain against Acute Neuronal Injury *In Vivo*. *J. Neurosci.* **21**, 8765–8771 (2001).
128. Maccarrone, M. Endocannabinoids: Friends and foes of reproduction. *Prog. Lipid Res.* **48**, 344–354 (2009).
129. Schuel, H. *et al.* Evidence that anandamide-signaling regulates human sperm functions required for fertilization. *Mol. Reprod. Dev.* **63**, 376–387 (2002).

130. Walter, L. & Stella, N. Cannabinoids and neuroinflammation. *Br. J. Pharmacol.* **141**, 775–785 (2004).
131. Eljaschewitsch, E. *et al.* The endocannabinoid anandamide protects neurons during CNS inflammation by induction of MKP-1 in microglial cells. *Neuron* **49**, 67–79 (2006).
132. Pacher, P., Bátkai, S. & Kunos, G. The Endocannabinoid System as an Emerging Target of Pharmacotherapy. *Pharmacol. Rev.* **58**, 389–462 (2006).
133. Maccarrone, M. *et al.* Endocannabinoid signaling at the periphery: 50 years after THC. *Trends in Pharmacological Sciences* **36**, 277–296 (2015).
134. Bifulco, M. & Di Marzo, V. Targeting the endocannabinoid system in cancer therapy: A call for further research. *Nature Medicine* **8**, 547–550 (2002).
135. De Petrocellis, L. *et al.* The endogenous cannabinoid anandamide inhibits human breast cancer cell proliferation. *Proc. Natl. Acad. Sci. U. S. A.* **95**, 8375–8380 (1998).
136. Joseph, J., Niggemann, B., Zaenker, K. S. & Entschladen, F. Anandamide is an endogenous inhibitor for the migration of tumor cells and T lymphocytes. *Cancer Immunol. Immunother.* **53**, 723–728 (2004).
137. Smart, D. *et al.* The endogenous lipid anandamide is a full agonist at the human vanilloid receptor (hVR1). *Br. J. Pharmacol.* **129**, 227–230 (2000).
138. Zygmunt, P. M. *et al.* Vanilloid receptors on sensory nerves mediate the vasodilator action of anandamide. *Nature* **400**, 452–457 (1999).
139. Dinis, P. *et al.* Anandamide-evoked activation of vanilloid receptor 1 contributes to the development of bladder hyperreflexia and nociceptive transmission to spinal dorsal horn neurons in cystitis. *J. Neurosci.* **24**, 11253–11263 (2004).
140. Singh Tahim, A., Sántha, P. & Nagy, I. Inflammatory mediators convert anandamide into a potent activator of the vanilloid type 1 transient receptor potential receptor in nociceptive primary sensory neurons. *Neuroscience* **136**, 539–548 (2005).
141. Van Der Stelt, M. *et al.* Anandamide acts as an intracellular messenger amplifying Ca<sup>2+</sup> influx via TRPV1 channels. *EMBO J.* **24**, 3026–3037 (2005).
142. Chávez, A. E., Chiu, C. Q. & Castillo, P. E. TRPV1 activation by endogenous anandamide triggers postsynaptic long-term depression in dentate gyrus. *Nat. Neurosci.* **13**, 1511–1519 (2010).
143. Dalle Carbonare, M. *et al.* A saturated *N*-acylethanolamine other than *N*-palmitoyl ethanolamine with anti-inflammatory properties: A neglected story... *J. Neuroendocrinol.* **20**, 26–34 (2008).
144. Terrazzino, S. *et al.* Stearoylethanolamide exerts anorexic effects in mice via downregulation of liver stearyl-coenzyme A desaturase-1 mRNA expression. *FASEB J.* **18**, 1580–1582 (2004).
145. Maccarrone, M., Pauselli, R., Di Rienzo, M. & Finazzi-Agrò, A. Binding, degradation and apoptotic activity of stearoylethanolamide in rat C6 glioma cells. *Biochem. J.* **366**, 137–144 (2002).
146. Artmann, A. *et al.* Influence of dietary fatty acids on endocannabinoid and *N*-acylethanolamine levels in rat brain, liver and small intestine. *Biochim. Biophys. Acta - Mol. Cell Biol. Lipids* **1781**, 200–212 (2008).
147. Fornelos, N. *et al.* Growth effects of *N*-acylethanolamines on gut bacteria reflect altered bacterial abundances in inflammatory bowel disease. *Nat. Microbiol.* **5**, 486–497 (2020).
148. Kim, H.-Y. *et al.* *N*-Docosahexaenoylethanolamide promotes development of hippocampal neurons. *Biochem. J.* **435**, 327–336 (2011).
149. Lee, J. W. *et al.* Orphan GPR110 (ADGRF1) targeted by *N*-docosahexaenoylethanolamine in development of neurons and cognitive function. *Nat. Commun.* **7**, (2016).

150. Park, T., Chen, H., Kevala, K., Lee, J. W. & Kim, H. Y. *N*-Docosahexaenoylethanolamine ameliorates LPS-induced neuroinflammation via cAMP/PKA-dependent signaling. *J. Neuroinflammation* **13**, 1–15 (2016).
151. Meijerink, J. *et al.* Inhibition of COX-2-mediated eicosanoid production plays a major role in the anti-inflammatory effects of the endocannabinoid *N*-docosahexaenoylethanolamine (DHEA) in macrophages. *Br. J. Pharmacol.* **172**, 24–37 (2015).
152. Magotti, P. *et al.* Structure of human *N*-acylphosphatidylethanolamine-hydrolyzing phospholipase D: Regulation of fatty acid ethanolamide biosynthesis by bile acids. *Structure* **23**, 598–604 (2015).
153. Stuckey, J. A. & Dixon, J. E. Crystal structure of a phospholipase D family member. *Nat. Struct. Biol.* **6**, 278–284 (1999).
154. Margheritis, E. *et al.* Bile Acid Recognition by NAPE-PLD. *ACS Chem. Biol.* **11**, 2908–2914 (2016).
155. Liu, Q., Tonai, T. & Ueda, N. Activation of *N*-acylethanolamine-releasing phospholipase D by polyamines. *Chem. Phys. Lipids* **115**, 77–84 (2002).
156. Wang, J., Okamoto, Y., Tsuboi, K. & Ueda, N. The stimulatory effect of phosphatidylethanolamine on *N*-acylphosphatidylethanolamine-hydrolyzing phospholipase D (NAPE-PLD). *Neuropharmacology* **54**, 8–15 (2008).
157. Wang, J. *et al.* Functional analysis of the purified anandamide-generating phospholipase D as a member of the metallo- $\beta$ -lactamase family. *J. Biol. Chem.* **281**, 12325–12335 (2006).
158. Okamoto, Y., Morishita, J., Tsuboi, K., Tonai, T. & Ueda, N. Molecular Characterization of a Phospholipase D Generating Anandamide and Its Congeners. *J. Biol. Chem.* **279**, 5298–5305 (2004).
159. Leung, D., Saghatelian, A., Simon, G. M. & Cravatt, B. F. Inactivation of *N*-Acyl phosphatidylethanolamine phospholipase D reveals multiple mechanisms for the biosynthesis of endocannabinoids. *Biochemistry* **45**, 4720–4726 (2006).
160. Leishman, E., Mackie, K., Luquet, S. & Bradshaw, H. B. Lipidomics profile of a NAPE-PLD KO mouse provides evidence of a broader role of this enzyme in lipid metabolism in the brain. *Biochim. Biophys. Acta - Mol. Cell Biol. Lipids* **1861**, 491–500 (2016).
161. Inoue, M. *et al.* Peripheral tissue levels and molecular species compositions of *N*-acyl-phosphatidylethanolamine and its metabolites in mice lacking *N*-acyl-phosphatidylethanolamine-specific phospholipase D. *J. Biochem.* **162**, 449–458 (2017).
162. Mock, E. D. *et al.* Discovery of a NAPE-PLD inhibitor that modulates emotional behavior in mice. *Nat. Chem. Biol.* **16**, 667–675 (2020).
163. Athenstaedt, K. & Daum, G. Phosphatidic acid, a key intermediate in lipid metabolism. *Eur. J. Biochem.* **266**, 1–16 (1999).
164. Young, B. P. *et al.* Phosphatidic acid is a pH biosensor that links membrane biogenesis to metabolism. *Science* **329**, 1085–1088 (2010).
165. Lee, H. C., Simon, G. M. & Cravatt, B. F. ABHD4 regulates multiple classes of *N*-acyl phospholipids in the mammalian central nervous system. *Biochemistry* **54**, 2539–2549 (2015).
166. Simon, G. M. & Cravatt, B. F. Endocannabinoid biosynthesis proceeding through glycerophospho-*N*-acyl ethanolamine and a role for  $\alpha/\beta$ -hydrolase 4 in this pathway. *J. Biol. Chem.* **281**, 26465–26472 (2006).
167. Tsuboi, K. *et al.* Glycerophosphodiesterase GDE4 as a novel lysophospholipase D: A possible involvement in bioactive *N*-acylethanolamine biosynthesis. *Biochim. Biophys. Acta - Mol. Cell Biol. Lipids* **1851**, 537–548 (2015).

168. Rahman, I. A. S. *et al.* Calcium-dependent generation of *N*-acylethanolamines and lysophosphatidic acids by glycerophosphodiesterase GDE7. *Biochim. Biophys. Acta - Mol. Cell Biol. Lipids* **1861**, 1881–1892 (2016).
169. Moolenaar, W. H. Lysophosphatidic acid, a multifunctional phospholipid messenger. *J. Biol. Chem.* **270**, 12949–12952 (1995).
170. Mills, G. B. & Moolenaar, W. H. The emerging role of lysophosphatidic acid in cancer. *Nat. Rev. Cancer* **3**, 582–591 (2003).
171. Sheng, X., Yung, Y. C., Chen, A. & Chun, J. Lysophosphatidic acid signalling in development. *Development* **142**, 1390–1395 (2015).
172. Yung, Y. C., Stoddard, N. C., Mirendil, H. & Chun, J. Lysophosphatidic Acid Signaling in the Nervous System. *Neuron* **85**, 669–682 (2015).
173. Sun, Y. X. *et al.* Biosynthesis of anandamide and *N*-palmitoylethanolamine by sequential actions of phospholipase A<sub>2</sub> and lysophospholipase D. *Biochem. J.* **380**, 749–756 (2004).
174. Simon, G. M. & Cravatt, B. F. Anandamide biosynthesis catalyzed by the phosphodiesterase GDE1 and detection of glycerophospho-*N*-acyl ethanolamine precursors in mouse brain. *J. Biol. Chem.* **283**, 9341–9349 (2008).
175. Kopp, F. *et al.* The glycerophospho metabolome and its influence on amino acid homeostasis revealed by brain metabolomics of GDE1(-/-) mice. *Chem. Biol.* **17**, 831–840 (2010).
176. Zheng, B., Chen, D. & Farquhar, M. G. MIR16, a putative membrane glycerophosphodiester phosphodiesterase, interacts with RGS16. *Proc. Natl. Acad. Sci. U. S. A.* **97**, 3999–4004 (2000).
177. Simpson, C. D. *et al.* A genome wide shRNA screen identifies  $\alpha/\beta$  hydrolase domain containing 4 (ABHD4) as a novel regulator of anoikis resistance. *Apoptosis* **17**, 666–678 (2012).
178. László, Z. I. *et al.* ABHD4-dependent developmental anoikis safeguards the embryonic brain. *Nat. Commun.* **11**, 1–16 (2020).
179. Liu, J. *et al.* A biosynthetic pathway for anandamide. *Proc. Natl. Acad. Sci. U. S. A.* **103**, 13345–13350 (2006).
180. Liu, J. *et al.* Multiple pathways involved in the biosynthesis of anandamide. *Neuropharmacology* **54**, 1–7 (2008).
181. Cravatt, B. F. *et al.* Molecular characterization of an enzyme that degrades neuromodulatory fatty-acid amides. *Nature* **384**, 83–87 (1996).
182. Johnson, D. S. *et al.* Discovery of PF-04457845: A Highly Potent, Orally Bioavailable, and Selective Urea FAAH Inhibitor. *ACS Med. Chem. Lett.* **2**, 91–96 (2011).
183. Wei, B. Q., Mikkelsen, T. S., McKinney, M. K., Lander, E. S. & Cravatt, B. F. A second fatty acid amide hydrolase with variable distribution among placental mammals. *J. Biol. Chem.* **281**, 36569–36578 (2006).
184. Tsuboi, K. *et al.* Molecular characterization of *N*-acylethanolamine-hydrolyzing acid amidase, a novel member of the choloylglycine hydrolase family with structural and functional similarity to acid ceramidase. *J. Biol. Chem.* **280**, 11082–11092 (2005).
185. Solorzano, C. *et al.* Selective *N*-acylethanolamine-hydrolyzing acid amidase inhibition reveals a key role for endogenous palmitoylethanolamide in inflammation. *Proc. Natl. Acad. Sci. U. S. A.* **106**, 20966–20971 (2009).
186. Migliore, M. *et al.* Second-Generation Non-Covalent NAAA Inhibitors are Protective in a Model of Multiple Sclerosis. *Angew. Chemie - Int. Ed.* **128**, 11359–11363 (2016).
187. Tsuboi, K. *et al.* Involvement of acid ceramidase in the degradation of bioactive *N*-acylethanolamines. *Biochim. Biophys. Acta - Mol. Cell Biol. Lipids* **1866**, 158972 (2021).

188. Park, J. H. & Schuchman, E. H. Acid ceramidase and human disease. *Biochim. Biophys. Acta - Biomembr.* **1758**, 2133–2138 (2006).
189. Urquhart, P., Nicolaou, A. & Woodward, D. F. Endocannabinoids and their oxygenation by cyclooxygenases, lipoxygenases and other oxygenases. *Biochim. Biophys. Acta - Mol. Cell Biol. Lipids* **1851**, 366–376 (2015).
190. McDougale, D. R. *et al.* Anti-inflammatory  $\omega$ -3 endocannabinoid epoxides. *Proc. Natl. Acad. Sci. U. S. A.* **114**, E6034–E6043 (2017).
191. Reddy, P. V., Schmid, P. C., Natarajan, V. & Schmid, H. H. O. The role of cardiolipin as an acyl donor in dog heart *N*-acylethanolamine phospholipid biosynthesis. *Biochim. Biophys. Acta - Lipids Lipid Metab.* **751**, 241–246 (1983).
192. Binte Mustafiz, S. S. *et al.* Intracellular  $\text{Ca}^{2+}$ -dependent formation of *N*-acyl-phosphatidylethanolamines by human cytosolic phospholipase  $\text{A}_2\epsilon$ . *Biochim. Biophys. Acta - Mol. Cell Biol. Lipids* **1864**, 158515 (2019).
193. Ogura, Y., Parsons, W. H., Kamat, S. S. & Cravatt, B. F. A calcium-dependent acyltransferase that produces *N*-Acyl phosphatidylethanolamines. *Nat. Chem. Biol.* **12**, 669–671 (2016).
194. Jin, X. H. *et al.* cDNA cloning and characterization of human and mouse  $\text{Ca}^{2+}$ -independent phosphatidylethanolamine *N*-acyltransferases. *Biochim. Biophys. Acta - Mol. Cell Biol. Lipids* **1791**, 32–38 (2009).
195. Uyama, T., Jin, X. H., Tsuboi, K., Tonai, T. & Ueda, N. Characterization of the human tumor suppressors TIG3 and HRASLS2 as phospholipid-metabolizing enzymes. *Biochim. Biophys. Acta - Mol. Cell Biol. Lipids* **1791**, 1114–1124 (2009).
196. Uyama, T. *et al.* The tumor suppressor gene H-Rev107 functions as a novel  $\text{Ca}^{2+}$ -independent cytosolic phospholipase A1/2 of the thiol hydrolase type. *J. Lipid Res.* **50**, 685–693 (2009).
197. Mardian, E. B., Bradley, R. M. & Duncan, R. E. The HRASLS (PLA/AT) subfamily of enzymes. *J. Biomed. Sci.* **22**, 1–11 (2015).
198. Golczak, M. *et al.* Structural basis for the acyltransferase activity of lecithin:retinol acyltransferase-like proteins. *J. Biol. Chem.* **287**, 23790–23807 (2012).
199. Shinohara, N. *et al.* Enzymological analysis of the tumor suppressor A-C1 reveals a novel group of phospholipid-metabolizing enzymes. *J. Lipid Res.* **52**, 1927–1935 (2011).
200. Hussain, Z. *et al.* Comparative analyses of isoforms of the calcium-independent phosphatidylethanolamine *N*-acyltransferase PLAAT-1 in humans and mice. *J. Lipid Res.* **57**, 2051–2060 (2016).
201. Akiyama, H. *et al.* Molecular cloning and biological activity of a novel Ha-Ras suppressor gene predominantly expressed in skeletal muscle, heart, brain, and bone marrow by differential display using clonal mouse EC cells, ATDC5. *J. Biol. Chem.* **274**, 32192–32197 (1999).
202. Kaneda, A., Kaminishi, M., Yanagihara, K., Sugimura, T. & Ushijima, T. Identification of silencing of nine genes in human gastric cancers. *Cancer Res.* **62**, 6645–6650 (2002).
203. Morishita, H. *et al.* Organelle degradation in the lens by PLAAT phospholipases. *Nature* **592**, 634–638 (2021).
204. Shyu, R. Y., Hsieh, Y. C., Tsai, F. M., Wu, C. C. & Jiang, S. Y. Cloning and functional characterization of the HRASLS2 gene. *Amino Acids* **35**, 129–137 (2008).
205. Duncan, R. E., Sarkadi-Nagy, E., Jaworski, K., Ahmadian, M. & Hei, S. S. Identification and functional characterization of adipose-specific phospholipase  $\text{A}_2$  (AdPLA). *J. Biol. Chem.* **283**, 25428–25436 (2008).
206. Jaworski, K. *et al.* AdPLA ablation increases lipolysis and prevents obesity induced by high-fat feeding or leptin deficiency. *Nat. Med.* **15**, 159–168 (2009).

207. Hajnal, A., Klemenz, R. & Schäfer, R. Subtraction cloning of H-rev107, a gene specifically expressed in H-ras resistant fibroblasts. *Oncogene* **9**, 479–490 (1994).
208. Sers, C. *et al.* Growth-inhibitory activity and downregulation of the class II tumor-suppressor gene H-rev107 in tumor cell lines and experimental tumors. *J. Cell Biol.* **136**, 935–944 (1997).
209. Sers, C. *et al.* The class II tumour suppressor gene H-REV107-1 is a target of interferon-regulatory factor-1 and is involved in IFN $\gamma$ -induced cell death in human ovarian carcinoma cells. *Oncogene* **21**, 2829–2839 (2002).
210. Nazarenko, I., Schäfer, R. & Sers, C. Mechanisms of the HRSL3 tumor suppressor function in ovarian carcinoma cells. *J. Cell Sci.* **120**, 1393–1404 (2007).
211. Roder, K., Latasa, M. J. & Sul, H. S. Silencing of the mouse H-rev107 gene encoding a class II tumor suppressor by CpG methylation. *J. Biol. Chem.* **277**, 30543–30550 (2002).
212. Yanatsanejit, P. *et al.* Promoter hypermethylation of CCNA1, RARRES1, and HRASLS3 in nasopharyngeal carcinoma. *Oral Oncol.* **44**, 400–406 (2008).
213. Shyu, R. Y. *et al.* H-rev107 regulates prostaglandin D2 synthase-mediated suppression of cellular invasion in testicular cancer cells. *J. Biomed. Sci.* **20**, 1–12 (2013).
214. Nazarenko, I. *et al.* H-REV107-1 stimulates growth in non-small cell lung carcinomas via the activation of mitogenic signaling. *Am. J. Pathol.* **169**, 1427–1439 (2006).
215. Xiong, S. *et al.* Pla2g16 phospholipase mediates gain-of-function activities of mutant p53. *Proc. Natl. Acad. Sci. U. S. A.* **111**, 11145–11150 (2014).
216. Staring, J. *et al.* PLA2G16 represents a switch between entry and clearance of Picornaviridae. *Nature* **541**, 412–416 (2017).
217. Uyama, T. *et al.* Regulation of peroxisomal lipid metabolism by catalytic activity of tumor suppressor H-rev107. *J. Biol. Chem.* **287**, 2706–2718 (2012).
218. Kassmann, C. M. *et al.* Axonal loss and neuroinflammation caused by peroxisome-deficient oligodendrocytes. *Nat. Genet.* **39**, 969–976 (2007).
219. DiSepio, D. *et al.* Identification and characterization of a retinoid-induced class II tumor suppressor/growth regulatory gene. *Proc. Natl. Acad. Sci. U. S. A.* **95**, 14811–14815 (1998).
220. Casanova, B. *et al.* The class II tumor-suppressor gene RARRES3 is expressed in B cell lymphocytic leukemias and down-regulated with disease progression. *Leukemia* **15**, 1521–1526 (2001).
221. Hsu, T. H. *et al.* Expression of the class II tumor suppressor gene RIG1 is directly regulated by p53 tumor suppressor in cancer cell lines. *FEBS Lett.* **586**, 1287–1293 (2012).
222. Morales, M. *et al.* RARRES 3 suppresses breast cancer lung metastasis by regulating adhesion and differentiation. *EMBO Mol. Med.* **6**, 865–881 (2014).
223. Tsai, F. M., Shyu, R. Y. & Jiang, S. Y. RIG1 suppresses Ras activation and induces cellular apoptosis at the Golgi apparatus. *Cell. Signal.* **19**, 989–999 (2007).
224. Jans, R., Sturniolo, M. T. & Eckert, R. L. Localization of the TIG3 transglutaminase interaction domain and demonstration that the amino-terminal region is required for TIG3 function as a keratinocyte differentiation regulator. *J. Invest. Dermatol.* **128**, 517–529 (2008).
225. Sturniolo, M. T. *et al.* A Novel Tumor Suppressor Protein Promotes Keratinocyte Terminal Differentiation via Activation of Type I Transglutaminase. *J. Biol. Chem.* **278**, 48066–48073 (2003).
226. Duvic, M. *et al.* Expression of a retinoid-inducible tumor suppressor, Tazarotene-inducible gene-3, is decreased in psoriasis and skin cancer. *Clin. Cancer Res.* **6**, 3249–3259 (2000).
227. Jin, X. H. *et al.* Discovery and characterization of a Ca<sup>2+</sup>-independent phosphatidylethanolamine N-acyltransferase generating the anandamide precursor and its congeners. *J. Biol. Chem.* **282**, 3614–3623 (2007).



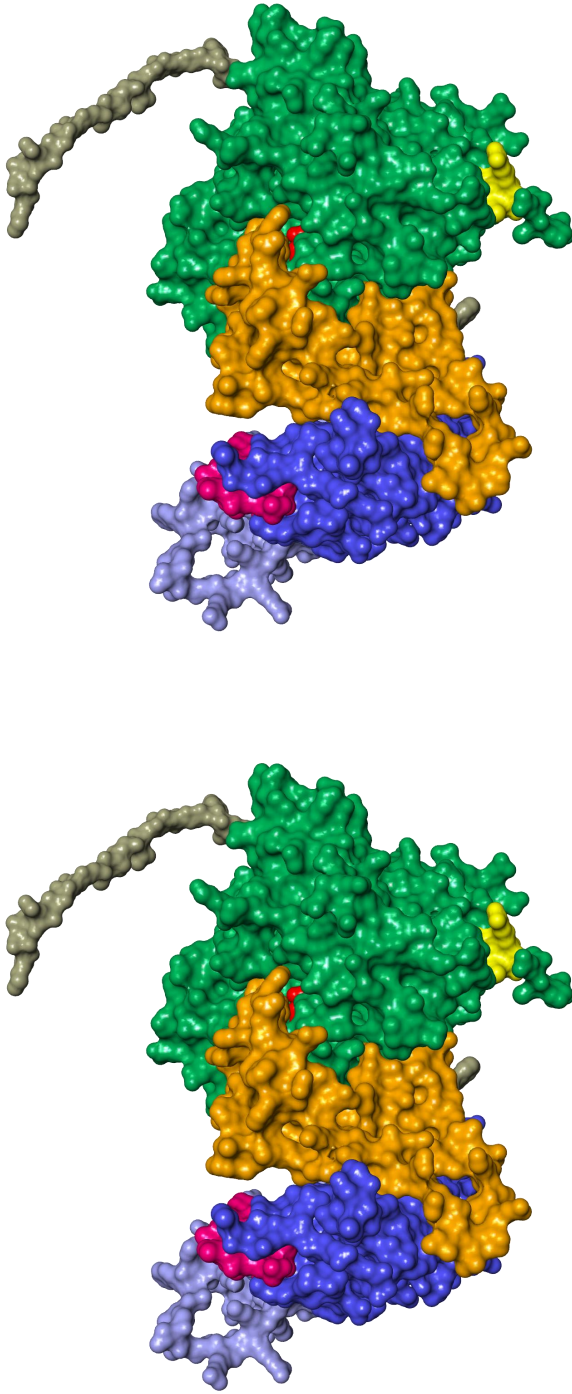
228. Yamano, Y. *et al.* Expression of the Ha-ras suppressor family member 5 gene in the maturing rat testis. *Biosci. Biotechnol. Biochem.* **72**, 1360–1363 (2008).
229. Zhou, J. *et al.* Activity-Based Protein Profiling Identifies  $\alpha$ -Ketoamides as Inhibitors for Phospholipase A<sub>2</sub> Group XVI. *ACS Chem. Biol.* **14**, 164–169 (2019).
230. Zhou, J. *et al.* Structure-Activity Relationship Studies of  $\alpha$ -Ketoamides as Inhibitors of the Phospholipase A and Acyltransferase Enzyme Family. *J. Med. Chem.* **63**, 9340–9359 (2020).
231. Ghosh, M., Tucker, D. E., Burchett, S. A. & Leslie, C. C. Properties of the Group IV phospholipase A<sub>2</sub> family. *Prog. Lipid Res.* **45**, 487–510 (2006).
232. Clark, J. D. *et al.* A novel arachidonic acid-selective cytosolic PL<sub>A2</sub> contains a Ca<sup>2+</sup>-dependent translocation domain with homology to PKC and GAP. *Cell* **65**, 1043–1051 (1991).
233. Ohto, T., Uozumi, N., Hirabayashi, T. & Shimizu, T. Identification of novel cytosolic phospholipase A<sub>2s</sub>, murine cPLA<sub>2</sub> $\delta$ ,  $\epsilon$ , and  $\zeta$ , which form a gene cluster with cPLA<sub>2</sub> $\beta$ . *J. Biol. Chem.* **280**, 24576–24583 (2005).
234. Pickard, R. T., Striffler, B. A., Kramer, R. M. & Sharp, J. D. Molecular cloning of two new human paralogs of 85-kDa cytosolic phospholipase A<sub>2</sub>. *J. Biol. Chem.* **274**, 8823–8831 (1999).
235. Hussain, Z. *et al.* Phosphatidylserine-stimulated production of *N*-acyl-phosphatidylethanolamines by Ca<sup>2+</sup>-dependent *N*-acyltransferase. *Biochim. Biophys. Acta - Mol. Cell Biol. Lipids* **1863**, 493–502 (2018).
236. Binte Mustafiz, S. S. *et al.* The role of intracellular anionic phospholipids in the production of *N*-acyl-phosphatidylethanolamines by cytosolic phospholipase A<sub>2</sub> $\epsilon$ . *J. Biochem.* **165**, 343–352 (2019).
237. Cadas, H., Gaillet, S., Beltramo, M., Venance, L. & Piomelli, D. Biosynthesis of an endogenous cannabinoid precursor in neurons and its control by calcium and cAMP. *J. Neurosci.* **16**, 3934–3942 (1996).
238. Cytosolic phospholipase A2 epsilon (human). (2021). Available at: <https://alphafold.ebi.ac.uk/entry/Q3MJ16>. (Accessed: 8th March 2021)
239. Jumper, J. *et al.* Highly accurate protein structure prediction with AlphaFold. *Nature* **596**, 583–589 (2021).
240. Wang, H. *et al.* Structure of Human GIVD Cytosolic Phospholipase A<sub>2</sub> Reveals Insights into Substrate Recognition. *J. Mol. Biol.* **428**, 2769–2779 (2016).
241. Schmid, P. C. & Schmid, H. H. O. *N*-Acylation of ethanolamine phospholipids by acyl transfer does not involve hydrolysis. *Biochim. Biophys. Acta - Lipids Lipid Metab.* **922**, 398–400 (1987).
242. Capestrano, M. *et al.* Cytosolic phospholipase A<sub>2</sub> $\epsilon$  drives recycling through the clathrin-independent endocytic route. *J. Cell Sci.* **127**, 977–993 (2014).
243. Evans, J. H., Spencer, D. M., Zweifach, A. & Leslie, C. C. Intracellular Calcium Signals Regulating Cytosolic Phospholipase A<sub>2</sub> Translocation to Internal Membranes. *J. Biol. Chem.* **276**, 30150–30160 (2001).
244. Regan-Klapisz, E. *et al.* Golgi-associated cPLA<sub>2</sub> $\alpha$  regulates endothelial cell-cell junction integrity by controlling the trafficking of transmembrane junction proteins. *Mol. Biol. Cell* **20**, 4225–4234 (2009).
245. Hirama, T. *et al.* Phosphatidylserine dictates the assembly and dynamics of caveolae in the plasma membrane. *J. Biol. Chem.* **292**, 14292–14307 (2017).
246. Zoncu, R. *et al.* Loss of endocytic clathrin-coated pits upon acute depletion of phosphatidylinositol 4,5-bisphosphate. *Proc. Natl. Acad. Sci. U. S. A.* **104**, 3793–3798 (2007).
247. Sathe, M. *et al.* Small GTPases and BAR domain proteins regulate branched actin polymerisation for clathrin and dynamin-independent endocytosis. *Nat. Commun.* **9**, 1–16 (2018).

248. McFarland, M. J. *et al.* A role for caveolae/lipid rafts in the uptake and recycling of the endogenous cannabinoid anandamide. *J. Biol. Chem.* **279**, 41991–41997 (2004).
249. Rimmerman, N. *et al.* Compartmentalization of endocannabinoids into lipid rafts in a microglial cell line devoid of caveolin-1. *Br. J. Pharmacol.* **165**, 2436–2449 (2012).
250. Lamaze, C., Tardif, N., Dewulf, M., Vassilopoulos, S. & Blouin, C. M. The caveolae dress code: structure and signaling. *Curr. Opin. Cell Biol.* **47**, 117–125 (2017).
251. Pérez-González, M. *et al.* PLA2G4E, a candidate gene for resilience in Alzheimer's disease and a new target for dementia treatment. *Prog. Neurobiol.* **191**, (2020).
252. Cruchaga, C. *et al.* Cerebrospinal fluid APOE levels: An endophenotype for genetic studies for Alzheimer's disease. *Hum. Mol. Genet.* **21**, 4558–4571 (2012).
253. Piccio, L. *et al.* Cerebrospinal fluid soluble TREM2 is higher in Alzheimer disease and associated with mutation status. *Acta Neuropathol.* **131**, 925–933 (2016).
254. Morimoto, Y. *et al.* Whole-exome sequencing and gene-based rare variant association tests suggest that PLA2G4E might be a risk gene for panic disorder. *Transl. Psychiatry* **8**, (2018).
255. Zhou, J. Development of a PLA2G4E Assay and Subsequent Application in Hit Identification. *Inhibitor Discovery of Phospholipase and N-Acyltransferase* (Leiden University, 2020).
256. van Esbroeck, A. C. M. *et al.* Identification of  $\alpha$ , $\beta$ -Hydrolase Domain Containing Protein 6 as a Diacylglycerol Lipase in Neuro-2a Cells. *Front. Mol. Neurosci.* **12**, (2019).
257. Clark, J. D., Milona, N. & Knopf, J. L. Purification of a 110-kilodalton cytosolic phospholipase A<sub>2</sub> from the human monocytic cell line U937. *Proc. Natl. Acad. Sci. U. S. A.* **87**, 7708–7712 (1990).
258. Dessen, A. *et al.* Crystal structure of human cytosolic phospholipase A<sub>2</sub> reveals a novel topology and catalytic mechanism. *Cell* **97**, 349–360 (1999).
259. Perisic, O., Fong, S., Lynch, D. E., Bycroft, M. & Williams, R. L. Crystal structure of a calcium-phospholipid binding domain from cytosolic phospholipase A<sub>2</sub>. *J. Biol. Chem.* **273**, 1596–1604 (1998).
260. Glover, S., Bayburt, T., Jonas, M., Chi, E. & Gelb, M. H. Translocation of the 85-kDa phospholipase A<sub>2</sub> from cytosol to the nuclear envelope in rat basophilic leukemia cells stimulated with calcium ionophore or IgE/antigen. *J. Biol. Chem.* **270**, 15359–15367 (1995).
261. Schievella, A. R., Regier, M. K., Smith, W. L. & Lin, L. L. Calcium-mediated translocation of cytosolic phospholipase A<sub>2</sub> to the nuclear envelope and endoplasmic reticulum. *J. Biol. Chem.* **270**, 30749–30754 (1995).
262. Lin, L. L. *et al.* cPLA<sub>2</sub> is phosphorylated and activated by MAP kinase. *Cell* **72**, 269–278 (1993).
263. Hefner, Y. *et al.* Serine 727 phosphorylation and activation of cytosolic phospholipase A<sub>2</sub> by MNK1-related protein kinases. *J. Biol. Chem.* **275**, 37542–37551 (2000).
264. Muthalif, M. M. *et al.* Functional Interaction of Calcium-/Calmodulin-dependent Protein Kinase II and Cytosolic Phospholipase A<sub>2</sub>. *J. Biol. Chem.* **276**, 39653–39660 (2001).
265. Mosior, M., Six, D. A. & Dennis, E. A. Group IV cytosolic phospholipase A<sub>2</sub> binds with high affinity and specificity to phosphatidylinositol 4,5-bisphosphate resulting in dramatic increases in activity. *J. Biol. Chem.* **273**, 2184–2191 (1998).
266. Das, S. & Cho, W. Roles of catalytic domain residues in interfacial binding and activation of group IV cytosolic phospholipase A<sub>2</sub>. *J. Biol. Chem.* **277**, 23838–23846 (2002).
267. Six, D. A. & Dennis, E. A. Essential Ca<sup>2+</sup>-independent role of the group IVA cytosolic phospholipase A<sub>2</sub> C2 domain for interfacial activity. *J. Biol. Chem.* **278**, 23842–23850 (2003).
268. Casas, J., Valdearcos, M., Pindado, J., Balsinde, J. & Balboa, M. A. The cationic cluster of group IVA phospholipase A<sub>2</sub> (Lys<sup>488</sup>/Lys<sup>541</sup>/Lys<sup>543</sup>/Lys<sup>544</sup>) is involved in translocation of the enzyme to phagosomes in human macrophages. *J. Lipid Res.* **51**, 388–399 (2010).

269. Hanel, A. M., Schüttel, S. & Gelb, M. H. Processive Interfacial Catalysis by Mammalian 85-Kilodalton Phospholipase  $A_2$  Enzymes on Product-Containing Vesicles: Application to the Determination of Substrate Preferences. *Biochemistry* **32**, 5949–5958 (1993).
270. Leslie, C. C. Regulation of the specific release of arachidonic acid by cytosolic phospholipase  $A_2$ . *Prostaglandins, Leukot. Essent. Fat. Acids* **70**, 373–376 (2004).
271. Nagase, T. *et al.* Acute lung injury by sepsis and acid aspiration: A key role for cytosolic phospholipase  $A_2$ . *Nat. Immunol.* **1**, 42–45 (2000).
272. Nagase, T. *et al.* A pivotal role of cytosolic phospholipase  $A_2$  in bleomycin-induced pulmonary fibrosis. *Nat. Med.* **8**, 480–484 (2002).
273. Brooke, M. A. *et al.* Cryptogenic multifocal ulcerating stenosing enteritis associated with homozygous deletion mutations in cytosolic phospholipase  $A_2$ - $\alpha$ . *Gut* **63**, 96–104 (2014).
274. Faioni, E. M. *et al.* Bleeding diathesis and gastro-duodenal ulcers in inherited cytosolic phospholipase- $A_2$  alpha deficiency. *Thromb. Haemost.* **112**, 1182–1189 (2014).
275. Bonventre, J. V. *et al.* Reduced fertility and postischemic brain injury in mice deficient in cytosolic phospholipase  $A_2$ . *Nature* **390**, 622–625 (1997).
276. Sanchez-Mejia, R. O. *et al.* Phospholipase  $A_2$  reduction ameliorates cognitive deficits in a mouse model of Alzheimer's disease. *Nat. Neurosci.* **11**, 1311–1318 (2008).
277. Marusic, S. *et al.* Cytosolic phospholipase  $A_2\alpha$ -deficient mice are resistant to experimental autoimmune encephalomyelitis. *J. Exp. Med.* **202**, 841–851 (2005).
278. Uozumi, H. *et al.* Role of cytosolic phospholipase  $A_2$  in allergic response and parturition. *Nature* **390**, 618–622 (1997).
279. Oikawa, Y. *et al.* Protective role for cytosolic phospholipase  $A_2\alpha$  in autoimmune diabetes of mice. *FEBS Lett.* **579**, 3975–3978 (2005).
280. Hegen, M. *et al.* Cytosolic phospholipase  $A_2\alpha$ -deficient mice are resistant to collagen-induced arthritis. *J. Exp. Med.* **197**, 1297–1302 (2003).
281. Hong, K. H., Bonventre, J. C., O'Leary, E., Bonventre, J. V. & Lander, E. S. Deletion of cytosolic phospholipase  $A_2$  suppresses ApcMin-induced tumorigenesis. *Proc. Natl. Acad. Sci. U. S. A.* **98**, 3935–3939 (2001).
282. Ilesley, J. N. M. *et al.* Cytoplasmic phospholipase  $A_2$  deletion enhances colon tumorigenesis. *Cancer Res.* **65**, 2636–2643 (2005).
283. Choukroun, G. J. *et al.* Cytosolic phospholipase  $A_2$  regulates Golgi structure and modulates intracellular trafficking of membrane proteins. *J. Clin. Invest.* **106**, 983–993 (2000).
284. Ghosh, M., Loper, R., Gelb, M. H. & Leslie, C. C. Identification of the expressed form of human cytosolic phospholipase  $A_2\beta$  (cPLA $_2\beta$ ): cPLA $_2\beta$ 3 is a novel variant localized to mitochondria and early endosomes. *J. Biol. Chem.* **281**, 16615–16624 (2006).
285. Ghomashchi, F. *et al.* Interfacial kinetic and binding properties of mammalian group IVB phospholipase  $A_2$  (cPLA $_2\beta$ ) and comparison with the other cPLA $_2$  isoforms. *J. Biol. Chem.* **285**, 36100–36111 (2010).
286. Klose, R. J., Kallin, E. M. & Zhang, Y. JmJc-domain-containing proteins and histone demethylation. *Nat. Rev. Genet.* **7**, 715–727 (2006).
287. Cheng, Y., Wang, Y., Li, J., Chang, I. & Wang, C. Y. A novel read-through transcript JMJD7-PLA $_2$ G4B regulates head and neck squamous cell carcinoma cell proliferation and survival. *Oncotarget* **8**, 1972–1982 (2017).
288. Stewart, A., Ghosh, M., Spencer, D. M. & Leslie, C. C. Enzymatic properties of human cytosolic phospholipase  $A_2\gamma$ . *J. Biol. Chem.* **277**, 29526–29536 (2002).

289. Murakami, M., Masuda, S. & Kudo, I. Arachidonate release and prostaglandin production by group IVC phospholipase A<sub>2</sub> (cytosolic phospholipase A<sub>2</sub> $\gamma$ ). *Biochem. J.* **372**, 695–702 (2003).
290. Underwood, K. W. *et al.* A novel calcium-independent phospholipase A<sub>2</sub>, cPLA<sub>2</sub> $\gamma$ , that is prenylated and contains homology to cPLA<sub>2</sub>. *J. Biol. Chem.* **273**, 21926–21932 (1998).
291. Yamashita, A. *et al.* Subcellular localization and lysophospholipase/transacylation activities of human group IVC phospholipase A<sub>2</sub> (cPLA<sub>2</sub> $\gamma$ ). *Biochim. Biophys. Acta - Mol. Cell Biol. Lipids* **1791**, 1011–1022 (2009).
292. Guo, Y. *et al.* Involvement of the  $\gamma$  Isoform of cPLA<sub>2</sub> in the Biosynthesis of Bioactive N-Acylethanolamines. *Molecules* **26**, 5213 (2021).
293. Asai, K. *et al.* Human group IVC phospholipase A<sub>2</sub> (cPLA<sub>2</sub> $\gamma$ ): Roles in the membrane remodeling and activation induced by oxidative stress. *J. Biol. Chem.* **278**, 8809–8814 (2003).
294. Tucker, D. E. *et al.* Group IVC cytosolic phospholipase A<sub>2</sub> $\gamma$  is farnesylated and palmitoylated in mammalian cells. *J. Lipid Res.* **46**, 2122–2133 (2005).
295. Su, X. *et al.* Requirement of cytosolic phospholipase A<sub>2</sub> gamma in lipid droplet formation. *Biochim. Biophys. Acta - Mol. Cell Biol. Lipids* **1862**, 692–705 (2017).
296. Jenkins, C. M. *et al.* Purification of recombinant human cPLA<sub>2</sub> $\gamma$  and identification of C-terminal farnesylation, proteolytic processing, and carboxymethylation by MALDI-TOF-TOF analysis. *Biochemistry* **42**, 11798–11807 (2003).
297. Xu, S. *et al.* Cytosolic Phospholipase A<sub>2</sub> Gamma Is Involved in Hepatitis C Virus Replication and Assembly. *J. Virol.* **86**, 13025–13037 (2012).
298. Chiba, H. *et al.* Cloning of a Gene for a Novel Epithelium-specific Cytosolic Phospholipase A<sub>2</sub>, cPLA<sub>2</sub> $\delta$ , Induced in Psoriatic Skin. *J. Biol. Chem.* **279**, 12890–12897 (2004).
299. Cheung, K. L. *et al.* Psoriatic T cells recognize neolipid antigens generated by mast cell phospholipase delivered by exosomes and presented by CD1a. *J. Exp. Med.* **213**, 2399–2412 (2016).
300. Ghosh, M. *et al.* Function, activity, and membrane targeting of cytosolic phospholipase A<sub>2</sub> $\zeta$  in mouse lung fibroblasts. *J. Biol. Chem.* **282**, 11676–11686 (2007).
301. Moon, S. H. *et al.* Heart failure-induced activation of phospholipase iPLA<sub>2</sub> $\gamma$  generates hydroxyeicosatetraenoic acids opening the mitochondrial permeability transition pore. *J. Biol. Chem.* **293**, 115–129 (2018).
302. Trimble, L. A. *et al.* NMR Structural Studies of the Tight Complex between a Trifluoromethyl Ketone Inhibitor and the 85-kDa Human Phospholipase A<sub>2</sub>. *Biochemistry* **32**, 12560–12565 (1993).
303. Ong, W. Y., Farooqui, T., Kokotos, G. & Farooqui, A. A. Synthetic and Natural Inhibitors of Phospholipases A<sub>2</sub>: Their Importance for Understanding and Treatment of Neurological Disorders. *ACS Chem. Neurosci.* **6**, 814–831 (2015).
304. Kalyvas, A. & David, S. Cytosolic Phospholipase A<sub>2</sub> Plays a Key Role in the Pathogenesis of Multiple Sclerosis-like Disease. *Neuron* **41**, 323–335 (2004).
305. Su, H. *et al.* Activation of Raf/MEK/ERK/cPLA<sub>2</sub> Signaling Pathway Is Essential for Chlamydial Acquisition of Host Glycerophospholipids. *J. Biol. Chem.* **279**, 9409–9416 (2004).
306. Ghomashchi, F. *et al.* A pyrrolidine-based specific inhibitor of cytosolic phospholipase A<sub>2</sub> $\alpha$  blocks arachidonic acid release in a variety of mammalian cells. *Biochim. Biophys. Acta - Biomembr.* **1513**, 160–166 (2001).
307. Seno, K. *et al.* Pyrrolidine inhibitors of human cytosolic phospholipase A<sub>2</sub>. *J. Med. Chem.* **43**, 1041–1044 (2000).
308. Rubin, B. B. *et al.* Cytosolic phospholipase A<sub>2</sub> $\alpha$  is necessary for platelet-activating factor biosynthesis, efficient neutrophil-mediated bacterial killing, and the innate immune response to

- pulmonary infection: cPLA<sub>2</sub>- $\alpha$  does not regulate neutrophil NADPH oxidase activity. *J. Biol. Chem.* **280**, 7519–7529 (2005).
309. Müller, C. *et al.* Inhibition of cytosolic phospholipase A<sub>2</sub> $\alpha$  impairs an early step of coronavirus replication in cell culture. *J. Virol.* **92** e01463-17 (2017).
310. Connolly, S. *et al.* Design and synthesis of a novel and potent series of inhibitors of cytosolic phospholipase A<sub>2</sub> based on a 1,3-disubstituted propan-2-one skeleton. *J. Med. Chem.* **45**, 1348–1362 (2002).
311. Kanai, S. *et al.* ASB14780, an orally active inhibitor of group IVA phospholipase A<sub>2</sub>, is a pharmacotherapeutic candidate for nonalcoholic fatty liver disease. *J. Pharmacol. Exp. Ther.* **356**, 604–614 (2016).
312. Tomoo, T. *et al.* Design, synthesis, and biological evaluation of 3-(1-aryl-1*H*-indol-5-yl)propanoic acids as new indole-based cytosolic phospholipase A<sub>2</sub> $\alpha$  inhibitors. *J. Med. Chem.* **57**, 7244–7262 (2014).
313. Kokotos, G. *et al.* Inhibition of group IVA cytosolic phospholipase A<sub>2</sub> by thiazolyl ketones *in vitro*, *ex vivo*, and *in vivo*. *J. Med. Chem.* **57**, 7523–7535 (2014).
314. Kim, E. *et al.* Anti-vascular effects of the cytosolic phospholipase A<sub>2</sub> inhibitor AVX235 in a patient-derived basal-like breast cancer model. *BMC Cancer* **16**, 1–11 (2016).
315. Kokotou, M. G., Limnios, D., Nikolaou, A., Psarra, A. & Kokotos, G. Inhibitors of phospholipase A<sub>2</sub> and their therapeutic potential: an update on patents (2012-2016). *Expert Opin. Ther. Pat.* **27**, 217–225 (2017).
316. Ziarc Pharma Ltd. NCT02795832. (2016). Available at: <https://clinicaltrials.gov/ct2/show/study/NCT02795832>. (Accessed: 20th September 2021)
317. Lee, K. L. *et al.* Discovery of ecopladib, an indole inhibitor of cytosolic phospholipase A<sub>2</sub> $\alpha$ . *J. Med. Chem.* **50**, 1380–1400 (2007).
318. Pfizer Inc. NCT00396955. (2006). Available at: <https://clinicaltrials.gov/ct2/show/NCT00396955>. (Accessed: 20th September 2021)
319. Thakker, P. *et al.* Cytosolic phospholipase A<sub>2</sub> $\alpha$  blockade abrogates disease during the tissue-damage effector phase of experimental autoimmune encephalomyelitis by its action on APCs. *J. Immunol.* **187**, 1986–1997 (2011).
320. Shimizu, H. *et al.* AK106-001616, a potent and selective inhibitor of cytosolic phospholipase A<sub>2</sub>: *In vivo* efficacy for inflammation, neuropathic pain, and pulmonary fibrosis. *J. Pharmacol. Exp. Ther.* **369**, 511–522 (2019).



**Stereoscopic image of the predicted structure of PLA2G4E (AlphaFold2).** To see the 3D image, hold the paper close to your face while looking cross-eyed. Slowly move the paper away from you. You should see a third image appearing in the middle. Try to get this one into focus by moving the paper further away or closer to your eyes. Grey: disordered N-terminus, blue: C2 domain with calcium-binding loops (magenta), purple: lipase domain with active site residues (red), orange: putative cap region, yellow: polybasic domain.



# 2

**Identification of triazole ureas as  
potent PLA<sub>2</sub>G<sub>4</sub>E inhibitors**



Phospholipase A2 $\epsilon$  (PLA2G4E) is a serine hydrolase that belongs to the Group IV cytosolic phospholipases. This subfamily consists of six intracellular phospholipases (PLA2G4A–F or cPLA2 $\alpha$ – $\zeta$ ) with low sequence homology that metabolize phospholipids.<sup>1–3</sup> PLA2G4A has an important role in the production of arachidonic acid (AA) and proinflammatory eicosanoids<sup>4–6</sup>, but much less is known about the physiological function of PLA2G4E and the other members. In 2016, Cravatt and coworkers discovered that PLA2G4E exerted high *N*-acyltransferase activity and produced *N*-acylphosphatidylethanolamines (NAPEs) from phosphatidylcholine (PC) and phosphatidylethanolamine (PE) in a calcium-dependent manner.<sup>7</sup>

Two PLA2G4E isoforms, consisting of either 834 or 868 amino acids (97 or 100 kDa, respectively), have been detected in the human proteome.<sup>8</sup> They differ in their N-terminal sequence, but it is unknown whether they have different biological roles. PLA2G4E is mainly expressed in neurons, skeletal muscle, heart and testes.<sup>7,9,10</sup> The enzyme has a central catalytic lipase domain, preceded by a C2 domain, which functions as a Ca<sup>2+</sup>-dependent lipid binding site.<sup>1–3</sup> While the translocation of PLA2G4A to intracellular membranes upon a Ca<sup>2+</sup> stimulus is needed for its activity<sup>11–13</sup>, PLA2G4E may be directly activated by Ca<sup>2+</sup>

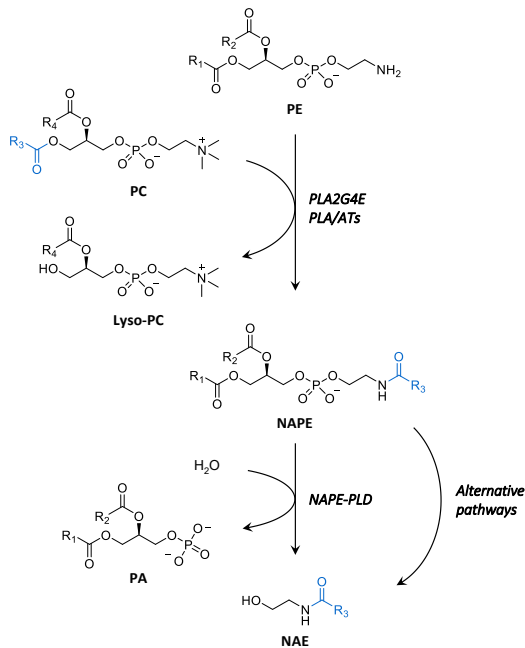


**Figure 2.1. Biosynthetic pathways of NAPEs and NAEs.** The *sn*-1 *O*-acyl chain of PC (blue) is transferred by PLA2G4E or PLA/ATs to PE to form NAPE. NAEs are synthesized either through direct hydrolysis by NAPE-PLD releasing phosphatidic acid (PA) or through alternative multistep pathways. R<sub>1</sub>, R<sub>2</sub> and R<sub>3</sub> indicate saturated, mono- or poly-unsaturated fatty acid. For anandamide synthesis R<sub>3</sub> = arachidonyl.

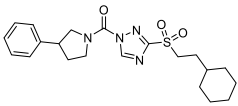
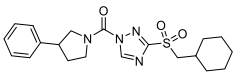
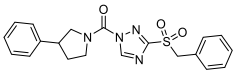
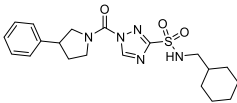
ions, independent of its translocation.<sup>7</sup> Instead, PLA2G4E has a KKKRLK polybasic domain at the C-terminus, that interacts with anionic lipids and is important for the subcellular localization of the enzyme to tubules and vesicles of the endocytic machinery.<sup>8,14,15</sup> Both the C2 and polybasic domain are necessary for catalytic activity.<sup>14,15</sup> PLA2G4E is an atypical serine hydrolase, because it uses a Ser-Asp catalytic dyad opposed to the canonical triad and most likely does not adopt a classical  $\alpha/\beta$ -hydrolase fold.<sup>1,2,16</sup> It accepts various PCs as acyl donor, and has a preference for cleavage of the ester at the *sn*-1 position by the nucleophilic serine.<sup>7</sup> The acyl chain is subsequently transferred to the free amine of PE, thereby producing NAPEs and lyso-PC (Figure 2.1). However, a more detailed understanding of its *N*-acyltransferase activity mechanism is currently lacking.

NAPEs are an understudied class of bioactive lipids. They are important modulators of membrane dynamics via various mechanisms, including stabilization of membranes and lipid raft structures<sup>17–19</sup>, induction of membrane fusion<sup>20</sup> and interaction with intracellular proteins.<sup>21</sup> Furthermore, they might regulate feeding by inhibiting food intake<sup>22,23</sup> and have anti-inflammatory activities.<sup>24</sup> Following ischemia, cellular NAPE levels are highly elevated, an effect most studied in neuronal tissue, which is suggested to represent a cytoprotective mechanism.<sup>25–31</sup> NAPEs also serve as substrates for NAPE-specific phospholipase D (NAPE-PLD) that generates *N*-acylethanolamines (NAEs) (Figure 2.1).<sup>32–38</sup> NAEs are a diverse family of signaling lipids, including the endocannabinoid anandamide (*N*-arachidonoyl-ethanolamine, AEA).<sup>39,40</sup> Anandamide exerts its physiological functions through activation of the cannabinoid receptors (CB) 1 and 2 and is involved in inflammation, neurotransmission, appetite and mood.<sup>41–43</sup>

PLA2G4E is not the only enzyme that produces NAPEs. Phospholipases A<sub>1/2</sub>/acyltransferases (PLAAT) 1–5 synthesize NAPEs in a calcium-independent manner.<sup>44,45</sup> Recently, pan-PLAAT inhibitors have been developed and were shown to reduce NAE levels in cells overexpressing PLAAT 2 or 5.<sup>46</sup> However, Ca<sup>2+</sup>-dependent *N*-acyltransferase activity is presumed to be the rate-limiting step in the on-demand biosynthesis of anandamide in the brain.<sup>47–50</sup> Whether PLA2G4E is the main enzyme driving NAPE and anandamide production in neuronal cells and the brain has not been established. PLA2G4E inhibitors would be valuable chemical tools to answer this question and to investigate the (patho)physiological role of PLA2G4E and NAPEs, but are currently lacking.

Recently, a competitive activity-based protein profiling (cABPP) assay was developed using membrane preparations of PLA2G4E-overexpressing HEK293T cells to screen a focused lipase inhibitor library containing 208 compounds.<sup>51</sup> Compounds **1–4** were identified as inhibitors with apparent half-maximal inhibitory concentration (IC<sub>50</sub>) values of around 1  $\mu$ M (Table 2.1). In this chapter, the synthesis and testing of novel analogues based on hits **1–4** is described.

**Table 2.1. Hits from in-house library screening.** Structure, activity and physicochemical properties of the four most potent molecules on PLA2G4E identified with gel-based cABPP ( $N \geq 2$ ). <sup>a</sup>Molecular weight (MW) was calculated using ChemDraw Professional 16.0; <sup>b</sup>Partition coefficient (clogP) was calculated using DataWarrior 5.0.0; <sup>c</sup>HAC = number of heavy atoms; <sup>d</sup>Lipophilic efficiency LipE =  $pIC_{50} - clogP$ ; <sup>e</sup>Ligand efficiency LE =  $1.4pIC_{50}/HAC$ .

ID	Structure	$pIC_{50} \pm SEM$	MW (Da) <sup>a</sup>	clogP <sup>b</sup>	HAC <sup>c</sup>	LipE <sup>d</sup>	LE <sup>e</sup>
1		$6.00 \pm 0.02$	417	3.78	29	2.22	0.29
2		$5.93 \pm 0.03$	403	3.33	28	2.60	0.30
3		$5.66 \pm 0.04$	396	2.97	28	2.69	0.28
4		$5.56 \pm 0.03$	418	3.36	29	2.20	0.27

## Results

### Structure activity relationship analysis of the screening hits

Hits **1–4** belong to the class of triazole ureas, which is a commonly used scaffold in serine hydrolase inhibitor design.<sup>52–55</sup> **1–4** have a 3-phenylpyrrolidine urea, which forms a stable carbamate adduct with the enzyme, and a lipophilic triazole sulfone that functions as a leaving group (Figure 2.2). Lipophilicity is a key parameter for binding affinity in many protein ligand interactions. Here, only a slight drop in activity was observed when the cyclohexyl group in **2** (clogP = 3.33, DataWarrior 5.0.0) was replaced by a phenyl in **3** (clogP = 2.97). This may suggest that new (electronic) interactions with the phenyl ring may compensate for the loss in lipophilicity. Sulfone **1** was more active than sulfonamide **4** ( $pIC_{50}$  = 6.0 and 5.6, respectively), which might be attributed to more favorable lipophilic

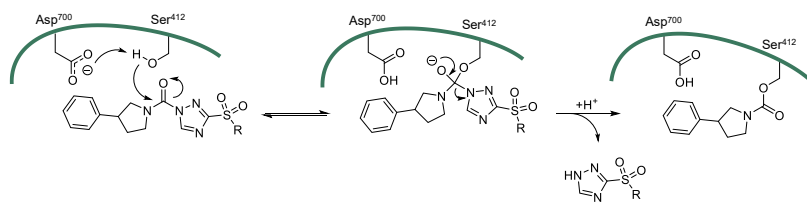


**Figure 2.2. Schematic mechanism of enzyme inactivation.** The nucleophilic serine of PLA2G4E, activated by Asp<sup>700</sup>, attacks the carbonyl of the inhibitor (indicated as general structure of the hit molecules **1–4**). The triazole leaving group is expelled, leading to irreversible carbamylation of Ser<sup>412</sup>, inactivating the catalytic activity of the enzyme.

interactions of **1** or to increased reactivity of the warhead due to the stronger electron-withdrawing effect of the sulfone. No substantial difference in activity was observed between a one or two-carbon spacer between the sulfone and cyclohexane (**1**, **2**). Of interest, four close analogs of the hits (**5–8**) were also previously tested in the focused screen, but they did not show any significant inhibition of PLA2G4E labeling (<50% at 10  $\mu$ M, Table 2.2). Compound **5** lacks the alkyl spacer between the cyclohexyl group and the sulfone, whereas compound **6**, **7** and **8** have a 2-substituted piperidine or pyrrolidine or a diethylamine substituent, respectively. This indicated that the 3-phenylpyrrolidine and the cyclohexyl group in hits **1–4** access specific subpockets of the active site and that the activity of the hits is not only due to reactivity of the warhead.

**Table 2.2. Inactive compounds identified from in-house library screening.** Structure and activity of four compounds structurally related to hits **1–4** that showed <50% inhibition of PLA2G4E at 10  $\mu$ M, as determined with gel-based cABPP (N = 2).

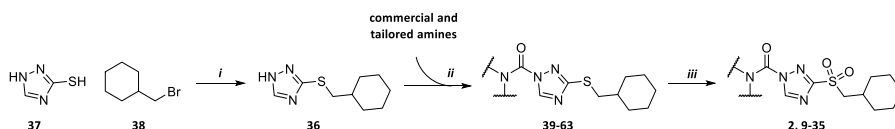
ID	Structure	Inhibition at 10 $\mu$ M (%)	ID	Structure	Inhibition at 10 $\mu$ M (%)
5		8	7		37
6		26	8		5

### Synthesis of PLA2G4E inhibitors 9–35

The design of inhibitors **9–35** was based on the structure of hit **2**, because this compound had higher lipophilic efficiency (LipE) and ligand efficiency (LE) than hit **1** (Table 2.1). Different amine substituents on the triazole urea scaffold were introduced to explore the size and properties of the binding pocket. To this end, building block **36** was synthesized at large scale via alkylation of 1,2,4-triazole-3-thiol (**37**) with (cyclohexylmethyl)bromide (**38**) (88%, Scheme 2.1). A two-step reaction sequence was used to obtain the final compounds. First, the amines were coupled to building block **36** with triphosgene to afford urea compounds **39–63** (Scheme 2.1), which were then oxidized to the final inhibitors (**2**, **9–35**). Of note, for the synthesis of inhibitors **20**, **27** and **31** the sulfide in building block **36** was oxidized before the urea formation (Supplementary Scheme S2.1).

The amine substituents used in inhibitors **2**, **9**, **10** and **14–19** were commercially available, whereas those for compounds **11** and **13** were synthesized as previously described<sup>56</sup> (Table 2.3). To synthesize compound **12**, phenethylamine (**64**, Supplementary Scheme S2.2) was methylated via formation of a methyl carbamate intermediate (**65**) using methyl chloroformate (84%), followed by a reduction using LiAlH<sub>4</sub> to compound **66** (62%). The benzylpiperidine derivatives in compounds **21–28**, **30** and **33–35** were synthesized via Suzuki-Miyaura coupling (Supplementary Scheme S2.3).<sup>57</sup> To this end, 4-methylene-

piperidine (**67**) was hydroborated with 9-BBN, immediately followed by Pd(dppf)Cl<sub>2</sub>-catalyzed cross-coupling to desired organohalide **68–78**, yielding compounds **79–89** (44%–quant.). Subsequent Boc deprotection afforded amines **90–100** (71%–quant.). Benzoylation of piperazine under reflux conditions efficiently yielded benzylpiperazine **101** (85%). 4-(4-Chlorobenzyl)piperidine (**102**) was synthesized by catalytic hydrogenation of 4-(4-chlorobenzyl)pyridine over PtO<sub>2</sub> (87%). Suzuki coupling of 4-(4-chlorobenzyl)pyridine to phenylboronic acid provided compound **103** (58%), which was hydrogenated to afford 4-(4-phenylbenzyl)piperidine **104**. The protected building block for inhibitors **31** and **32** was synthesized as described earlier<sup>58</sup>, which then was deprotected to yield the free amine (**105**).



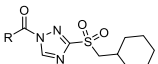
**Scheme 2.1.** General synthetic route for PLA2G4E inhibitors. Reagents and conditions: *i*) K<sub>2</sub>CO<sub>3</sub>, DMF, 6 h RT; *ii*) 1. Appropriate amine, triphosgene, DIPEA or Et<sub>3</sub>N, THF, 3 h 0°C → RT, then 2. **36**, K<sub>2</sub>CO<sub>3</sub>, DMF, o/n RT; *iii*) AcOOH, DCM, 6 h 0°C → RT.

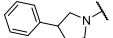
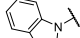
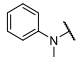
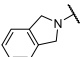
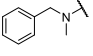
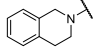
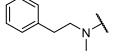
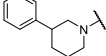
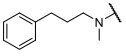
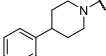
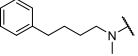
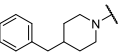
## Hit confirmation and optimization of triazole urea derivatives as PLA2G4E inhibitors

First, the activity of resynthesized compound **2** was tested using a competitive, gel-based ABPP assay. This assay relies on fluorophosphonate-tetramethylrhodamine (FP-TAMRA) as a broad-spectrum activity-based probe (ABP). The fluorophosphonate moiety covalently binds to the catalytic serine of PLA2G4E and the TAMRA functions as a fluorescent reporter to visualize the enzyme activity in a biological setting.<sup>51,59</sup> Briefly, lysates of human embryonic kidney (HEK293T) cells that transiently expressed recombinant human PLA2G4E were treated with inhibitor or vehicle (DMSO) for 30 min at room temperature, followed by a 5-min incubation with FP-TAMRA to label residual PLA2G4E activity. Subsequently, protein resolution on molecular weight by sodium dodecyl sulfate–polyacrylamide gel electrophoresis (SDS-PAGE) and in-gel fluorescence scanning allowed quantitation of enzyme inhibition by the compounds. The activity of hit **2** was confirmed, albeit slightly lower than the compound from the screening deck (pIC<sub>50</sub> = 5.70 ± 0.03, Table 2.3). To study the influence of the spacer between the urea and the phenyl on the inhibitory activity, compounds **9–13** were tested (Table 2.3). Compound **9**, in which the phenyl ring was directly coupled to the urea, was inactive, but by introducing various alkyl linkers with increasing length (**10–13**) the inhibitory activity was regained and up to 10-fold improved compared to the original hit. Compounds with propyl (**12**) and butyl (**13**) linkers showed similar activity, indicating that there was some flexibility in the binding pocket. In line with the results obtained with compound **9**, inhibitors with small fused bicyclic amines indoline (**14**) and isoindoline (**15**) displayed reduced activity. Tetrahydroquinoline **16**, however, was

10-fold more potent than hit **(2)**. Compound **17** with a 3-phenylpiperidine was not active, but compound **18** with a 4-phenylpiperidine was tolerated and inhibitor **19** with a 4-benzylpiperidine moiety was the most potent compound identified so far ( $pIC_{50} = 6.9$ ). These findings indicated that this subpocket of the PLA2G4E active site can accommodate rather large substituents.

**Table 2.3. Structure-activity relationships of PLA2G4E inhibitors 9–19.** Potency determined with gel-based cABPP on PLA2G4E-overexpressing HEK293T membranes ( $N \geq 2$ ).



ID	R	$pIC_{50} \pm SEM$	ID	R	$pIC_{50} \pm SEM$
2		$5.70 \pm 0.03$	14		$< 5.0$
9		$< 5.0$	15		$< 5.0$
10		$6.28 \pm 0.17$	16		$6.79 \pm 0.15$
11		$< 5.0$	17		$< 5.0$
12		$6.70 \pm 0.15$	18		$6.58 \pm 0.03$
13		$6.73 \pm 0.14$	19		$6.86 \pm 0.05$

Next, 13 derivatives of the 4-benzylpiperidine of compound **19** were synthesized and their potency on PLA2G4E was determined (Table 2.4). A synthetically more convenient benzylpiperazine scaffold was not active (**20**). Compound **21** with an *ortho*-methoxy had a slightly decreased potency, whereas compound **22** with a *para*-methoxy showed increased potency. This suggested that steric effects, rather than electronic, were important. Accordingly, compounds with other small *para*-substituents, both electron donating (**23**) and electron withdrawing (**24–26**), showed similarly improved activity ( $pIC_{50}$ 's 7.5–8.0). Of note, compound **27** with an acetylene substituent showed similar potency, but inhibitors **28** and **29** with a larger *tert*-butyl or phenyl substituent, respectively, had a reduced activity. Variants with a large substituent on the *meta* (**30–32**) and *ortho* (**33**) position were also less active, but they did not completely lose activity. Compound **24** with a 4-chloro substituent was the most potent compound identified in this study with  $pIC_{50} = 8.01 \pm 0.02$  (Figure 2.3, Table 2.5). Introducing an additional nitrogen in the aromatic ring decreased potency (**34, 35**).

**Table 2.4. Structure-activity relationships of PLA2G4E inhibitors 20–35.** Potency determined with gel-based cABPP on PLA2G4E-overexpressing HEK293T membranes ( $N \geq 2$ ).

ID	R	$pIC_{50} \pm SEM$	ID	R	$pIC_{50} \pm SEM$
19		$6.86 \pm 0.05$	28		$6.83 \pm 0.06$
20		$< 5.0$	29		$6.60 \pm 0.06$
21		$6.33 \pm 0.08$	30		$6.41 \pm 0.12$
22		$7.50 \pm 0.11$	31		$7.30 \pm 0.09$
23		$7.46 \pm 0.17$	32		$6.58 \pm 0.03$
24 (WEN091)		$8.01 \pm 0.02$	33		$6.86 \pm 0.05$
25		$7.00 \pm 0.07$	34		$6.62 \pm 0.19$
26		$7.53 \pm 0.39$	35		$7.42 \pm 0.10$
27		$7.36 \pm 0.03$			

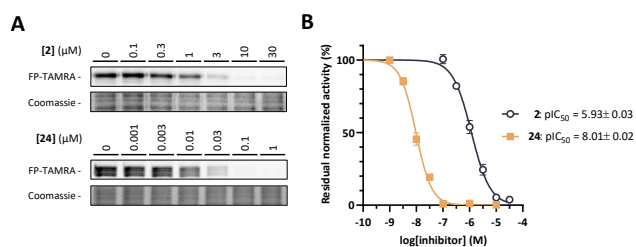


**Figure 2.3. Activity of compounds 2 and 24 on PLA2G4E.** A) Representative gel excerpts of cABPP experiments with 2 and 24 on PLA2G4E overexpression lysates. B) Corresponding inhibition curves and  $pIC_{50}$  values. Data presented as mean  $\pm$  SEM ( $N \geq 2$ ).

## Discussion and conclusion

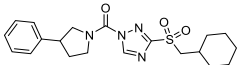
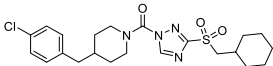
The PLA2G4 proteins have previously been exploited for the discovery and development of molecular therapeutics. Several classes of *in vivo* active inhibitors have been reported.<sup>60-66</sup> For example, PLA2G4A inhibitor WAY-196025 was able to fully protect mice from developing clinical symptoms of multiple sclerosis in the experimental autoimmune encephalomyelitis (EAE) model.<sup>67</sup> Ecopladib, ZPL-5212372 and giripladib have even advanced into phase I and phase II clinical trials for the treatment of atopic dermatitis or rheumatoid arthritis.<sup>68,69</sup> To date, no potent inhibitors for PLA2G4E have been described. These inhibitors are required to further our understanding of the biological role of PLA2G4E and may help the development of drugs for the treatment of neurodegeneration, metabolic syndrome or inflammatory pain.<sup>41,70-73</sup>

Here, the identification and ABPP-guided optimization of the first potent inhibitors of PLA2G4E is reported. Compound **24** ((4-(4-chlorobenzyl)piperidin-1-yl)(3-((cyclohexylmethyl)sulfonyl)-1H-1,2,4-triazol-1-yl)methanone, **WEN091**) is a covalent, irreversible potent inhibitor of PLA2G4E with an IC<sub>50</sub> of 10 nM, which is 100-fold more potent than the original hit (**2**). Of note, the IC<sub>50</sub> of an irreversible inhibitor is dependent on its incubation time with the enzyme. The values reported in this thesis, therefore, are apparent IC<sub>50</sub> values that only apply to the assay conditions described here. These values can only be reliably compared between compounds tested under identical conditions. Both LipE and LE of **24** were increased compared to **2** (Table 2.5) and with MW < 500 Da, HBA < 10, HBD < 5, RB < 10, clogP < 5 and tPSA < 90 Å<sup>2</sup>, **24** has favorable physicochemical properties for a lead compound in the development of a CNS-active enzyme inhibitor, according to Lipinski's and Veber's rules for druglikeness.<sup>74,75</sup>

Triazole urea-based inhibitors have been previously applied as valuable tool compounds to study the biology of serine hydrolases.<sup>54,76</sup> ABPP assays, substrate-based assays and lipid analysis platforms have been set up to measure their activity and selectivity in complex proteomes.<sup>77-79</sup> In addition, they have shown efficacy in both cellular and *in vivo* systems, demonstrating good brain penetration and low toxicity.<sup>52-54,80</sup> The identification of triazole ureas as inhibitors of PLA2G4E therefore holds promise for the development of valuable tool compounds with therapeutic potential. The activity of compound **24** in biological systems and its selectivity over other PLA2G4 family members, ECS-related enzymes and other serine hydrolases will be described in the next chapter.



**Table 2.5. Physicochemical properties of hit 2 and most potent molecule 24.** Potency on PLA2G4E determined using gel-based cABPP ( $N \geq 2$ ) <sup>a</sup>Molecular weight (MW) and topological polar surface area (tPSA) calculated using ChemDraw Professional 16.0; <sup>b</sup>Partition coefficient (clogP) using DataWarrior 5.0.0; <sup>c</sup>HAC = number of heavy atoms; <sup>d</sup>HBA = number of hydrogen bond acceptors; <sup>e</sup>HBD = number of hydrogen bond donors; <sup>f</sup>RB = number of rotatable bonds; <sup>g</sup>Lipophilic efficiency LipE =  $pIC_{50} - clogP$ ; <sup>h</sup>Ligand efficiency LE =  $1.4pIC_{50}/HAC$ .

ID	Structure	$pIC_{50}$ $\pm$ SEM	MW (Da) <sup>a</sup>	tPSA (Å <sup>2</sup> ) <sup>a</sup>	clogP <sup>b</sup>	HAC <sup>c</sup>	HBA <sup>d</sup>	HBD <sup>e</sup>	RB <sup>f</sup>	LipE <sup>g</sup>	LE <sup>h</sup>
2		5.93 $\pm$ 0.03	403	82.4	3.33	28	7	0	5	2.60	0.30
24		8.01 $\pm$ 0.02	465	82.4	4.24	31	7	0	6	3.77	0.36

## Acknowledgements

Paul ten Bras is kindly acknowledged for performing organic synthesis and cABPP, Francisca Schutter and Juan Zhou for cABPP on the hits, Hans van den Elst for HRMS analysis. Hans den Dulk and Tom van der Wel are acknowledged for plasmid cloning and purification.

## Experimental procedures

### General remarks

All chemicals and reagents for biochemical experiments were purchased from Thermo Fisher Scientific or Bio-Rad, unless noted otherwise. Inhibitors were synthesized in-house as described below.

### Plasmids

The full-length wild-type human PLA2G4E cDNA was obtained from GenScript Biotech and cloned into a pcDNA3.1(+) expression vector in-frame with a C-terminal FLAG tag. Plasmids were isolated from transformed *Escherichia coli* XL-10 using a Qiagen Plasmid Midi kit and stored at 4°C in TE buffer (10 mM Tris, 0.1 mM EDTA, pH 8.0). The sequence was determined (Macrogen) and verified using CLC Main Workbench.

### Cell culture

HEK293T (human embryonic kidney, ATCC) cells were cultured in DMEM (Sigma-Aldrich, D6546) with additional heat-inactivated new-born calf serum (10% (v/v), Avantor Seradigm), L-Ala-L-Gln (2 mM, Sigma-Aldrich), penicillin and streptomycin (both 200 µg/mL, Duchefa Biochemie) at 37°C, 7% CO<sub>2</sub>. Medium was refreshed every 2–3 days and cells were passaged twice a week at 70–80% confluence by aspirating the medium, thorough pipetting in fresh medium and seeding to appropriate density. Cell cultures were regularly tested for mycoplasma and discarded after 2–3 months.

### Transient transfection

One day prior to transfection, 10<sup>7</sup> HEK293T cells were seeded to a 15 cm dish. Upon transfection, medium was aspirated and replaced by 13 mL fresh medium. Plasmid DNA (20 µg per 15 cm dish) and PEI (60 µg per 15 cm dish) were separately dissolved in 1 mL DMEM without serum, mixed, incubated for 15 min and added dropwise to the cells. 24 h p.t. medium was replaced by 25 mL fresh medium. 72 h p.t. medium was aspirated and the cells were washed with RT Dulbecco's PBS, harvested in PBS and centrifuged (3000 × g, 15 min, RT). Cell pellets were flash-frozen in liquid N<sub>2</sub> and stored at –80°C until use.

### HEK293T membrane preparation

HEK293T cell pellets were thawed on ice and homogenized in 2 mL ice-cold lysis buffer (50 mM Tris-HCl, 2 mM DTT, 3 mM CaCl<sub>2</sub>, 1 mM MgCl<sub>2</sub>, 5 U/mL Benzonase® (Santa Cruz Biotechnology, Inc.), pH 8.0) per 15 cm cell culture dish using a Sonics® Vibra-Cell VCX 130 probe sonicator equipped with a 2 mm microtip (3 × 10 s on/10 s off, 20% amplitude). After incubation on ice for 30 min, the insoluble ("membrane") fraction was separated from the soluble ("cytosol") fraction by ultracentrifugation (10<sup>5</sup> × g, 35 min, 4°C, Beckman-Coulter ultracentrifuge, Ti70.1 rotor). The pellet was resuspended in 1 mL ice-cold storage buffer (50 mM Tris-HCl, 2 mM DTT, pH 8.0) per 15 cm plate and homogenized by passing through an insulin needle. After determination of the protein concentration using a Quick Start™ Bradford Protein Assay (Bio-Rad), the samples were diluted to 1.0 mg/mL in ice-cold storage buffer, aliquoted to single-use volumes, flash-frozen in liquid N<sub>2</sub> and stored at –80°C until further use.

### Activity-based protein profiling

Membrane preparations were thawed on ice. 19.5 µL lysate was incubated with 0.5 µL inhibitor in DMSO (30 min, RT), followed by 0.5 µL FP-TAMRA in DMSO (50 nM, 5 min, RT, final DMSO concentration 5%). The reactions were quenched by addition of 7 µL 4× Laemmli buffer (240 mM Tris, 8% (w/v) SDS, 40% (v/v) glycerol, 5% (v/v) β-mercaptoethanol (Sigma-Aldrich), 0.04% bromophenol

blue). 10  $\mu\text{L}$  sample was resolved on 8% acrylamide SDS-PAGE gel (180 V, 70 min) and afterwards imaged on a Bio-Rad Chemidoc MP using Cy3/TAMRA settings (ex. 532/12 nm, em. 602/50 nm). Coomassie Brilliant Blue R250 staining was used for total protein loading correction. Images were analyzed using Bio-Rad Image Lab 6.  $\text{IC}_{50}$  calculations were performed in GraphPad Prism 8.

## Organic synthesis

### General remarks

All reagents were purchased from Sigma-Aldrich, Fluorochem, Fisher Scientific, Combi-Blocks or Alfa Aesar and used without further purification. Solvents were purchased from Sigma-Aldrich, VWR Chemicals or Honeywell Riedel-de Haën, common salts from Sigma-Aldrich or Chem-Lab and used without further purification. Moisture-sensitive reactions were carried out in solvents dried over heat-activated molecular sieves (4 Å, Sigma-Aldrich), using flame-dried glassware under an atmosphere of  $\text{N}_2$ . TLC analysis was performed on Merck silica gel 60  $\text{F}_{254}$  aluminum TLC plates, on which compounds were visualized under 254 or 366 nm UV light and using  $\text{KMnO}_4$  (30 mM  $\text{KMnO}_4$ , 180 mM  $\text{K}_2\text{CO}_3$  in water) or ninhydrin (7.5 mM ninhydrin, 10% (v/v)  $\text{AcOH}$  in  $\text{EtOH}$ ) stain. Flash column chromatography was performed using  $\text{SiO}_2$  (Macherey-Nagel, 60 M) as stationary phase.

NMR spectra were recorded on a Bruker AV-400 MHz or AV-500 MHz spectrometer at 400 MHz ( $^1\text{H}$ ) and 101 MHz ( $^{13}\text{C}$ ) or 500 MHz ( $^1\text{H}$ ) and 126 MHz ( $^{13}\text{C}$ ) respectively, using  $\text{CDCl}_3$  or  $\text{MeOD}$  (Eurisotop) as solvent. Chemical shifts are reported in ppm with TMS ( $^1\text{H}$   $\text{CHCl}_3$ ,  $\delta$  0.00) or solvent resonance ( $^1\text{H}$   $\text{MeOD}$ ,  $\delta$  3.31;  $^{13}\text{C}$   $\text{MeOD}$ ,  $\delta$  49.00;  $^{13}\text{C}$   $\text{CHCl}_3$ ,  $\delta$  77.16) as internal standard. Data are reported as follows: chemical shift  $\delta$  (ppm), multiplicity (s = singlet, d = doublet, t = triplet, p = pentet, dd = doublet of doublets, td = triplet of doublets, qd = quartet of doublets, dt = doublet of triplets, bs = broad singlet ( $^1\text{H}$ ), br = broad ( $^{13}\text{C}$ ), m = multiplet), coupling constants  $J$  (Hz) and integration. HPLC-MS analysis was performed on a Finnigan Surveyor HPLC system equipped with a Macherey-Nagel NUCLEODUR  $\text{C}_{18}$  Gravity, 5  $\mu\text{m}$ , 50  $\times$  4.6 mm column followed by a Thermo Scientific LTQ Orbitrap XL spectrometer, using  $\text{H}_2\text{O}/\text{CH}_3\text{CN}$  + 1% TFA as mobile phase. All compounds used for biological experiments were  $\geq 95\%$  pure based on LC-MS UV absorbance.

### General procedure A

Triazole urea thioether or sulfoxide (1 eq) was dissolved in dry DCM (40–50 mL/mmol) and cooled on ice. Peracetic acid (5–10 eq, 36–40% solution in  $\text{AcOH}$ ) was added dropwise, after which the mixture was allowed to warm to RT and stirred for at least 6 h. When full conversion was confirmed using TLC analysis, the mixture was washed once with water, dried over  $\text{MgSO}_4$ , filtrated and concentrated *in vacuo*.

### General procedure B

*N*-Boc 4-methylenepiperidine (1 eq) was dissolved in dry THF (7 mL/mmol) which had been degassed by three cycles of reduced pressure and  $\text{N}_2$  purging. The solution was cooled on ice before 9-BBN (1.5 eq, 0.5 M in THF) was added dropwise. The ice bath was removed and the reaction mixture was stirred for 6 h. In the meantime, desired halobenzene (1.5 eq) and  $\text{K}_2\text{CO}_3$  (1.5 eq) were added to a three-neck flask equipped with a reflux cooler which was then flushed with  $\text{N}_2$ . DMF (7 mL/mmol) and water (0.7 mL/mmol) were degassed, added to the flask and purged with  $\text{N}_2$ . When full consumption of *N*-Boc 4-methylenepiperidine was confirmed using TLC analysis, the reaction mixture was added to the three-neck flask and purging was continued.  $\text{Pd}(\text{dppf})\text{Cl}_2$  (1 mol%) was added and the mixture was heated to 60°C and stirred overnight. The mixture was cooled to RT, diluted with  $\text{Et}_2\text{O}$  and washed with 1 M aq.  $\text{NaOH}$ . The pH of the aqueous layer was set to 7 with 12 M  $\text{HCl}$ , after which the aqueous

layer was extracted with Et<sub>2</sub>O. The combined organic layers were washed with brine, dried over MgSO<sub>4</sub>, filtrated and concentrated *in vacuo*.

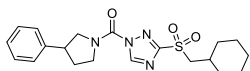
### General procedure C

Desired amine intermediate (1 eq) was dissolved in dry THF (10–15 mL/mmol of amine intermediate) and added dropwise (< 0.5 mL/min) to an ice-cold solution of triphosgene (3 eq) and Et<sub>3</sub>N or DIPEA (3 eq) in dry THF (10–15 mL/mmol of amine intermediate). The cloudy mixture was stirred on ice for 1 h, followed by 2 h at RT. When full conversion was confirmed using TLC analysis, the mixture was diluted with EtOAc and washed with 1 M aqueous HCl and brine, dried over MgSO<sub>4</sub>, filtrated and concentrated *in vacuo*. Water was removed by co-evaporation with toluene, after which the oily residue was dissolved in dry DMF (5–10 mL/mmol of amine intermediate). Desired triazole or pyrazole intermediate (1 eq) and K<sub>2</sub>CO<sub>3</sub> (3 eq) were added and the mixture was stirred overnight. The mixture was diluted with EtOAc and washed with water and brine, dried over MgSO<sub>4</sub>, filtrated and concentrated *in vacuo*.

### General procedure D

Triazole urea thioether (1 eq) was dissolved in dry DCM (5 mL) and cooled on ice. Peracetic acid (1–3 eq, 36–40% solution in AcOH) was added dropwise, after which the mixture was allowed to warm to RT and stirred for at least 6 h. When full conversion was confirmed using TLC analysis, the mixture was washed once with water, dried over MgSO<sub>4</sub>, filtrated and concentrated *in vacuo*.

### (3-((Cyclohexylmethyl)sulfonyl)-1H-1,2,4-triazol-1-yl)(3-phenylpyrrolidin-1-yl)methanone (2)



**39** (51 mg, 0.138 mmol) was oxidized according General procedure A. Flash column chromatography (20 → 30% EtOAc in pentane) afforded the title compound (55 mg, 0.137 mmol, quant.). HPLC showed presence of a single product (rt = 8.15 min). NMR showed two products which are probably conformationally restricted isomers (ratio ~1:1), as reported before for similar compounds (data not published).

Conformer 1:

<sup>1</sup>H NMR (400 MHz, CDCl<sub>3</sub>) δ 9.02 (s, 1H), 7.41 – 7.32 (m, 2H), 7.32 – 7.21 (m, 3H), 4.42 (dd, *J* = 11.8, 7.6 Hz, 1H), 4.24 (ddd, *J* = 11.3, 8.1, 2.8 Hz, 1H), 4.13 – 4.04 (m, 1H), 3.92 (dd, *J* = 11.8, 9.8 Hz, 1H), 3.56 – 3.43 (m, 1H), 3.32 (d, *J* = 6.4 Hz, 2H), 2.50 – 2.33 (m, 1H), 2.23 – 2.10 (m, 1H), 2.12 – 1.97 (m, 1H), 1.96 – 1.82 (m, 2H), 1.75 – 1.51 (m, 2H), 1.38 – 1.00 (m, 6H).

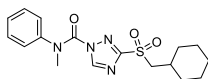
<sup>13</sup>C NMR (101 MHz, CDCl<sub>3</sub>) δ 162.73, 147.66, 146.11, 139.70, 128.94, 127.49, 127.17, 60.68, 55.86, 50.00, 45.04, 33.73, 32.98, 32.53, 25.71, 25.66.

Conformer 2:

<sup>1</sup>H NMR (400 MHz, CDCl<sub>3</sub>) δ 9.00 (s, 1H), 7.41 – 7.32 (m, 2H), 7.32 – 7.21 (m, 3H), 4.17 (dd, *J* = 12.0, 7.6 Hz, 1H), 3.99 (ddd, *J* = 11.3, 8.3, 2.6 Hz, 1H), 3.79 (ddd, *J* = 12.1, 10.2, 6.8 Hz, 1H), 3.71 (dd, *J* = 12.0, 9.6 Hz, 1H), 3.56 – 3.43 (m, 1H), 3.28 (d, *J* = 6.4 Hz, 2H), 2.50 – 2.33 (m, 1H), 2.23 – 2.10 (m, 1H), 2.12 – 1.97 (m, 1H), 1.96 – 1.82 (m, 2H), 1.75 – 1.51 (m, 2H), 1.38 – 1.00 (m, 6H).

<sup>13</sup>C NMR (101 MHz, CDCl<sub>3</sub>) δ 162.70, 147.59, 146.11, 139.34, 128.92, 127.37, 127.02, 60.68, 54.85, 49.07, 42.06, 32.93, 32.50, 31.11, 25.69, 25.66.

HRMS: [M+H]<sup>+</sup> calculated for C<sub>20</sub>H<sub>26</sub>N<sub>4</sub>O<sub>3</sub>S+H<sup>+</sup> 403.17984, found 403.17950.

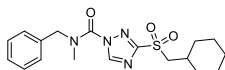
**3-((Cyclohexylmethyl)sulfonyl)-*N*-methyl-*N*-phenyl-1*H*-1,2,4-triazole-1-carboxamide (9)**

**107** (24 mg, 0.069 mmol) was oxidized according General procedure A. Flash column chromatography (25 → 35% EtOAc in pentane) afforded the title compound (yield not determined).

$^1\text{H}$  NMR (400 MHz,  $\text{CDCl}_3$ )  $\delta$  8.74 (s, 1H), 7.43 – 7.29 (m, 3H), 7.19 – 7.12 (m, 2H), 3.56 (s, 3H), 2.97 – 2.93 (m, 2H), 2.02 – 1.87 (m, 1H), 1.83 – 1.75 (m, 2H), 1.72 – 1.59 (m, 4H), 1.36 – 1.08 (m, 2H), 0.99 (qd,  $J$  = 11.6, 3.6 Hz, 2H).

$^{13}\text{C}$  NMR (101 MHz,  $\text{CDCl}_3$ )  $\delta$  162.38, 147.65, 142.43, 129.91, 128.46, 126.28, 60.45, 40.91, 32.94, 32.16, 25.78, 25.68.

HRMS:  $[\text{M}+\text{H}]^+$  calculated for  $\text{C}_{17}\text{H}_{22}\text{N}_4\text{O}_3\text{S}+\text{H}^+$  363.14854, found 363.14808.

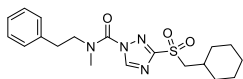
***N*-Benzyl-3-((cyclohexylmethyl)sulfonyl)-*N*-methyl-1*H*-1,2,4-triazole-1-carboxamide (10)**

**41** (37 mg, 0.107 mmol) was oxidized according General procedure A. Flash column chromatography (15 → 30% EtOAc in pentane) afforded the title compound as blue-grayish oil (25 mg, 0.066 mmol, 62%).

$^1\text{H}$  NMR (500 MHz,  $\text{CDCl}_3$ )  $\delta$  8.94 (s, 1H), 7.43 – 7.29 (m, 5H), 5.02 – 4.66 (m, 2H), 3.36 – 3.09 (m, 5H), 2.13 – 1.99 (m, 1H), 1.96 – 1.78 (m, 2H), 1.72 – 1.60 (m, 4H), 1.34 – 1.20 (m, 2H), 1.19 – 1.01 (m, 2H).

$^{13}\text{C}$  NMR (126 MHz,  $\text{CDCl}_3$ )  $\delta$  162.45, 148.36, 134.94, 129.12, 128.50, 60.75, 54.74, 37.26, 33.04, 32.52, 29.82, 25.77, 25.74.

HRMS:  $[\text{M}+\text{Na}]^+$  calculated for  $\text{C}_{18}\text{H}_{24}\text{N}_4\text{O}_3\text{S}+\text{Na}^+$  399.14613, found 399.14614.

**3-((Cyclohexylmethyl)sulfonyl)-*N*-methyl-*N*-phenethyl-1*H*-1,2,4-triazole-1-carboxamide (11)**

**42** (17 mg, 0.047 mmol) was oxidized according General procedure A. Flash column chromatography (20 → 30% EtOAc in pentane) afforded the title compound as white crystalline solid (16 mg, 0.040 mmol, 84%). HPLC

showed presence of a single product ( $r_t$  = 4.64 min). NMR showed two products which are probably conformationally restricted isomers (ratio ~1:2), as reported before for similar compounds (data not published).

Conformer 1:

$^1\text{H}$  NMR (400 MHz,  $\text{CDCl}_3$ )  $\delta$  8.88 (s, 1H), 7.44 – 7.03 (m, 5H), 3.81 – 3.68 (m, 2H), 3.35 – 3.17 (m, 5H), 3.05 – 2.94 (m, 2H), 2.14 – 2.02 (m, 1H), 1.95 – 1.85 (m, 2H), 1.74 – 1.59 (m, 3H), 1.35 – 1.14 (m, 3H), 1.18 – 1.03 (m, 2H).

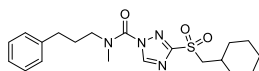
$^{13}\text{C}$  NMR (101 MHz,  $\text{CDCl}_3$ )  $\delta$  147.69, 137.32, 128.93, 127.09, 60.81, 53.04, 34.44, 33.03, 32.53, 25.76, 25.74.

Conformer 2:

$^1\text{H}$  NMR (400 MHz,  $\text{CDCl}_3$ )  $\delta$  8.35 (s, 1H), 7.44 – 7.03 (m, 5H), 4.01 – 3.87 (m, 2H), 3.35 – 3.17 (m, 5H), 3.05 – 2.94 (m, 2H), 2.14 – 2.02 (m, 1H), 1.95 – 1.85 (m, 2H), 1.74 – 1.59 (m, 3H), 1.35 – 1.14 (m, 3H), 1.18 – 1.03 (m, 2H).

$^{13}\text{C}$  NMR (101 MHz,  $\text{CDCl}_3$ )  $\delta$  147.69, 137.32, 128.93, 127.09, 60.81, 53.36, 34.44, 33.03, 32.53, 25.76, 25.74.

HRMS:  $[\text{M}+\text{Na}]^+$  calculated for  $\text{C}_{19}\text{H}_{26}\text{N}_4\text{O}_3\text{S}+\text{Na}^+$  413.16178, found 413.16131.

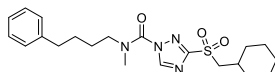
**3-((Cyclohexylmethyl)sulfonyl)-*N*-methyl-*N*-(3-phenylpropyl)-1*H*-1,2,4-triazole-1-carboxamide (12)**

**43** (9.8 mg, 0.026 mmol) was oxidized according General procedure A. Flash column chromatography (15 → 25% EtOAc in pentane) afforded the title compound (7.4 mg, 0.018 mmol, 70%).

<sup>1</sup>H NMR (400 MHz, CDCl<sub>3</sub>) δ 8.87 (s, 1H), 7.34 – 7.26 (m, 2H), 7.24 – 7.15 (m, 3H), 3.69 – 3.52 (m, 2H), 3.33 – 3.26 (m, 4H), 3.15 (s, 1H), 2.76 – 2.63 (m, 2H), 2.16 – 2.00 (m, 3H), 1.96 – 1.86 (m, 2H), 1.75 – 1.59 (m, 3H), 1.36 – 1.21 (m, 3H), 1.18 – 1.03 (m, 2H).

<sup>13</sup>C NMR (101 MHz, CDCl<sub>3</sub>) δ 148.54, 128.71, 128.38, 126.39, 60.83, 51.31, 33.07, 32.55, 29.84, 25.79, 25.77.

HRMS: [M+H]<sup>+</sup> calculated for C<sub>20</sub>H<sub>28</sub>N<sub>4</sub>O<sub>3</sub>S+H<sup>+</sup> 405.19549, found 405.19542.

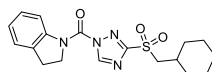
**3-((Cyclohexylmethyl)sulfonyl)-*N*-methyl-*N*-(4-phenylbutyl)-1*H*-1,2,4-triazole-1-carboxamide (13)**

**44** (17 mg, 0.044 mmol) was oxidized according General procedure A. Flash column chromatography (15 → 30% EtOAc in pentane) afforded the title compound as white crystalline solid (17 mg, 0.041 mmol, 92%).

<sup>1</sup>H NMR (500 MHz, CDCl<sub>3</sub>) δ 8.87 (s, 1H), 7.32 – 7.25 (m, 2H), 7.23 – 7.11 (m, 3H), 3.72 – 3.49 (m, 2H), 3.32 – 3.08 (m, 5H), 2.71 – 2.60 (m, 2H), 2.14 – 2.03 (m, 1H), 1.94 – 1.86 (m, 2H), 1.80 – 1.56 (m, 6H), 1.35 – 1.21 (m, 2H), 1.21 – 1.05 (m, 4H).

<sup>13</sup>C NMR (126 MHz, CDCl<sub>3</sub>) δ 148.28, 148.17, 141.76, 128.56, 128.51, 126.11, 60.82, 51.47, 37.69, 36.76, 35.55, 33.06, 32.55, 29.83, 29.79, 28.45, 25.79, 25.76.

HRMS: [M+Na]<sup>+</sup> calculated for C<sub>21</sub>H<sub>30</sub>N<sub>4</sub>O<sub>3</sub>S+Na<sup>+</sup> 441.19308, found 441.19293.

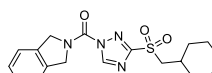
**(3-((Cyclohexylmethyl)sulfonyl)-1*H*-1,2,4-triazol-1-yl)(indolin-1-yl)methanone (14)**

**45** (50 mg, 0.146 mmol) was oxidized according General procedure A. Flash column chromatography (0 → 20% EtOAc in pentane) afforded the title compound as off-white crystalline solid (45 mg, 0.120 mmol, 82%).

<sup>1</sup>H NMR (400 MHz, CDCl<sub>3</sub>) δ 9.06 (s, 1H), 8.06 (d, *J* = 8.1 Hz, 1H), 7.34 – 7.26 (m, 2H), 7.22 – 7.12 (m, 1H), 4.61 (t, *J* = 8.3 Hz, 2H), 3.33 (d, *J* = 6.4 Hz, 2H), 3.26 (t, *J* = 8.3 Hz, 2H), 2.19 – 2.02 (m, 1H), 1.98 – 1.87 (m, 2H), 1.76 – 1.60 (m, 2H), 1.36 – 1.15 (m, 4H), 1.12 (qd, *J* = 12.1, 10.6, 4.6 Hz, 2H).

<sup>13</sup>C NMR (101 MHz, CDCl<sub>3</sub>) δ 162.74, 148.09, 145.03, 141.49, 132.26, 127.89, 125.99, 125.22, 117.65, 60.74, 51.43, 33.02, 32.52, 28.62, 25.74, 25.73.

HRMS: [M+Na]<sup>+</sup> calculated for C<sub>18</sub>H<sub>22</sub>N<sub>4</sub>O<sub>3</sub>S+Na<sup>+</sup> 397.13048, found 397.13035.

**(3-((Cyclohexylmethyl)sulfonyl)-1*H*-1,2,4-triazol-1-yl)(isoindolin-2-yl)methanone (15)**

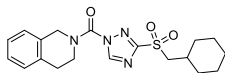
**46** (61 mg, 0.178 mmol) was oxidized according General procedure A. Flash column chromatography (15 → 25% EtOAc in pentane) afforded the title compound as white crystalline solid (66 mg, 0.176 mmol, quant.).

<sup>1</sup>H NMR (500 MHz, CDCl<sub>3</sub>) δ 9.08 (s, 1H), 7.37 – 7.30 (m, 4H), 5.38 (s, 2H), 5.08 (s, 2H), 3.35 (d, *J* = 6.4 Hz, 2H), 2.18 – 2.06 (m, 1H), 1.98 – 1.89 (m, 2H), 1.75 – 1.61 (m, 2H), 1.40 – 1.23 (m, 4H), 1.13 (qd, *J* = 12.1, 3.6 Hz, 2H).

<sup>13</sup>C NMR (126 MHz, CDCl<sub>3</sub>) δ 163.03, 147.79, 146.28, 135.95, 133.75, 128.26, 128.19, 122.85, 122.63, 60.73, 55.61, 55.28, 33.00, 32.57, 25.74, 25.68.

HRMS: [M+H]<sup>+</sup> calculated for C<sub>18</sub>H<sub>22</sub>N<sub>4</sub>O<sub>3</sub>S+H<sup>+</sup> 375.14845, found 375.14828.

**(3-((Cyclohexylmethyl)sulfonyl)-1*H*-1,2,4-triazol-1-yl)(3,4-dihydroisoquinolin-2(1*H*)-yl)methanone (16)**



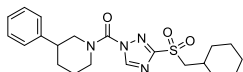
**47** (58 mg, 0.163 mmol) was oxidized according General procedure A. Flash column chromatography (15 → 30% EtOAc in pentane) afforded the title compound (46 mg, 0.12 mmol, 73%).

<sup>1</sup>H NMR (500 MHz, CDCl<sub>3</sub>) δ 8.91 (s, 1H), 7.28 – 7.14 (m, 4H), 5.09 – 4.79 (m, 2H), 4.13 – 3.89 (m, 2H), 3.32 (d, *J* = 6.3 Hz, 2H), 3.06 (t, *J* = 5.9 Hz, 2H), 2.15 – 2.05 (m, 1H), 1.95 – 1.88 (m, 2H), 1.76 – 1.61 (m, 2H), 1.35 – 1.23 (m, 2H), 1.22 – 1.06 (m, 4H).

<sup>13</sup>C NMR (126 MHz, CDCl<sub>3</sub>) δ 162.68, 148.23, 147.67, 133.91, 131.57, 128.79, 127.47, 126.93, 126.43, 60.74, 49.29, 47.79, 45.79, 44.11, 33.00, 32.54, 29.10, 25.74, 25.72.

HRMS: [M+Na]<sup>+</sup> calculated for C<sub>19</sub>H<sub>24</sub>N<sub>4</sub>O<sub>3</sub>S+Na<sup>+</sup> 411.14613, found 411.14584.

**(3-((Cyclohexylmethyl)sulfonyl)-1*H*-1,2,4-triazol-1-yl)(3-phenylpiperidin-1-yl)methanone (17)**



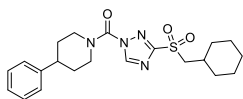
**48** (50 mg, 0.130 mmol) was oxidized according General procedure A. Flash column chromatography (0 → 30% EtOAc in pentane) afforded the title compound as colorless oil (22 mg, 0.053 mmol, 41%).

<sup>1</sup>H NMR (400 MHz, CDCl<sub>3</sub>) δ 8.91 (s, 1H), 7.44 – 7.36 (m, 2H), 7.34 – 7.27 (m, 3H), 5.87 – 5.72 (m, 1H), 4.33 – 4.23 (m, 1H), 3.27 (d, *J* = 6.4 Hz, 2H), 3.15 (td, *J* = 13.2, 12.4, 3.4 Hz, 1H), 2.55 – 2.45 (m, 1H), 2.17 – 1.99 (m, 2H), 1.93 – 1.85 (m, 2H), 1.84 – 1.59 (m, 6H), 1.35 – 1.20 (m, 4H), 1.20 – 1.01 (m, 2H).

<sup>13</sup>C NMR (101 MHz, CDCl<sub>3</sub>) δ 162.62, 148.59, 148.32, 137.63, 129.17, 127.52, 126.56, 60.64, 56.42 (br), 44.19, 33.03, 32.52, 30.42, 29.81, 25.78, 25.76, 19.20.

HRMS: [M+Na]<sup>+</sup> calculated for C<sub>21</sub>H<sub>28</sub>N<sub>4</sub>O<sub>3</sub>S+Na<sup>+</sup> 439.17743, found 439.17742.

**(3-((Cyclohexylmethyl)sulfonyl)-1*H*-1,2,4-triazol-1-yl)(4-phenylpiperidin-1-yl)methanone (18)**



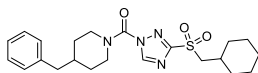
**108** (19 mg, 0.047 mmol) was oxidized according General procedure A. Flash column chromatography (25 → 35% EtOAc in pentane) afforded the title compound (12 mg, 0.029 mmol, 61%).

<sup>1</sup>H NMR (400 MHz, CDCl<sub>3</sub>) δ 8.89 (s, 1H), 7.38 – 7.30 (m, 2H), 7.26 – 7.19 (m, 3H), 4.72 – 4.48 (m, 2H), 3.32 (d, *J* = 6.3 Hz, 2H), 3.40 – 3.04 (m, 2H), 2.85 (tt, *J* = 12.2, 3.8 Hz, 1H), 2.20 – 2.02 (m, 1H), 1.97 – 1.75 (m, 4H), 1.75 – 1.53 (m, 4H), 1.42 – 1.13 (m, 4H), 1.11 (qd, *J* = 12.2, 3.3 Hz, 2H).

<sup>13</sup>C NMR (101 MHz, CDCl<sub>3</sub>) δ 162.61, 148.28, 147.37, 144.35, 128.85, 126.96, 126.82, 60.77, 48.09 (br), 47.05 (br), 42.37, 33.07, 32.57, 29.83, 25.78.

HRMS: [M+H]<sup>+</sup> calculated for C<sub>21</sub>H<sub>28</sub>N<sub>4</sub>O<sub>2</sub>S+H<sup>+</sup> 401.20057, found 401.20033.

**(4-Benzylpiperidin-1-yl)(3-((cyclohexylmethyl)sulfonyl)-1*H*-1,2,4-triazol-1-yl)methanone (19)**

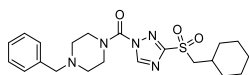


**109** (26 mg, 0.063 mmol) was oxidized according General procedure A. Flash column chromatography (25 → 35%) afforded the title compound (18 mg, 0.042 mmol, 67%).

<sup>1</sup>H NMR (400 MHz, CDCl<sub>3</sub>) δ 8.84 (s, 1H), 7.33 – 7.25 (m, 2H), 7.25 – 7.19 (m, 1H), 7.16 – 7.12 (m, 2H), 4.53 – 4.32 (m, 2H), 3.30 (d, *J* = 6.4 Hz, 2H), 3.18 – 2.89 (m, 2H), 2.59 (d, *J* = 6.9 Hz, 2H), 2.16 – 2.02 (m, 1H), 1.96 – 1.86 (m, 2H), 1.90 – 1.74 (m, 1H), 1.75 – 1.59 (m, 2H), 1.38 (qd, *J* = 12.7, 2.9 Hz, 2H), 1.35 – 1.11 (m, 6H), 1.11 (qd, *J* = 12.5, 3.2 Hz, 2H).

<sup>13</sup>C NMR (101 MHz, CDCl<sub>3</sub>) δ 162.50, 148.17, 147.28, 139.56, 129.18, 128.54, 126.38, 60.76, 47.57 (br), 46.53 (br), 42.77, 37.96, 33.06, 32.54, 29.83, 25.78, 25.77.

HRMS: [M+Na]<sup>+</sup> calculated for C<sub>22</sub>H<sub>30</sub>N<sub>4</sub>O<sub>3</sub>S+Na<sup>+</sup> 453.19308, found 453.19268.

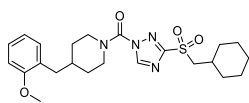
**(4-Benzylpiperazin-1-yl)(3-((cyclohexylmethyl)sulfonyl)-1H-1,2,4-triazol-1-yl)methanone (20)**

**101** (1.5 eq, 65 mg, 0.37 mmol) dissolved in 5 mL dry DCM was added dropwise to an ice-cold solution of triphosgene (3.5 eq, 219 mg, 0.74 mmol) and  $\text{Na}_2\text{CO}_3$  (5.5 eq, 122 mg, 1.15 mmol) in dry DCM. The mixture was stirred on ice for 1 h, after which it was allowed to warm to RT. 1 h later solids were removed by filtration and volatiles by reduced pressure. Traces of water were removed by co-evaporation with toluene, after which the resulting white powder was dissolved in 5 mL dry DMF. **106** (1 eq, 48 mg, 0.21 mmol) and  $\text{K}_2\text{CO}_3$  (3.5 eq, 102 mg, 0.74 mmol) were added and the mixture was stirred overnight. Solids were removed by filtration and volatiles by reduced pressure. Flash column chromatography afforded the title compound as off-white crystalline solid (74 mg, 0.171 mmol, 82%).

$^1\text{H}$  NMR (400 MHz,  $\text{CDCl}_3$ )  $\delta$  8.87 (s, 1H), 7.37 – 7.24 (m, 5H), 4.04 – 3.67 (m, 4H), 3.57 (s, 2H), 3.29 (d,  $J$  = 6.4 Hz, 2H), 2.65 – 2.50 (m, 4H), 2.16 – 2.01 (m, 1H), 1.94 – 1.86 (m, 2H), 1.74 – 1.59 (m, 3H), 1.36 – 1.21 (m, 2H), 1.21 – 1.05 (m, 3H).

$^{13}\text{C}$  NMR (101 MHz,  $\text{CDCl}_3$ )  $\delta$  162.50, 148.28, 147.10, 137.15, 129.17, 128.47, 127.52, 62.64, 60.65, 52.82, 52.19, 47.63, 45.74, 32.96, 32.43, 25.69, 25.68.

HRMS:  $[\text{M}+\text{H}]^+$  calculated for  $\text{C}_{21}\text{H}_{29}\text{N}_5\text{O}_3\text{S}+\text{H}^+$  432.20639, found 432.20613.

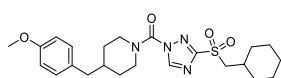
**(3-((Cyclohexylmethyl)sulfonyl)-1H-1,2,4-triazol-1-yl)(4-(2-methoxybenzyl)piperidin-1-yl)-methanone (21)**

**51** (69 mg, 0.16 mmol) was oxidized according General procedure A. Flash column chromatography (20 → 70% EtOAc in pentane) afforded the title compound as gray gum (74 mg, 0.16 mmol, quant.).

$^1\text{H}$  NMR (400 MHz,  $\text{CDCl}_3$ )  $\delta$  8.84 (s, 1H), 7.20 (td,  $J$  = 7.8, 1.8 Hz, 1H), 7.06 (dd,  $J$  = 7.3, 1.7 Hz, 1H), 6.92 – 6.83 (m, 2H), 4.44 – 4.33 (m, 2H), 3.82 (s, 3H), 3.30 (d,  $J$  = 6.4 Hz, 2H), 3.19 – 2.87 (m, 2H), 2.60 (d,  $J$  = 7.1 Hz, 2H), 2.15 – 2.02 (m, 1H), 1.97 – 1.83 (m, 3H), 1.77 (s, 2H), 1.75 – 1.59 (m, 3H), 1.46 – 1.31 (m, 2H), 1.32 – 1.14 (m, 3H), 1.18 – 1.03 (m, 2H).

$^{13}\text{C}$  NMR (101 MHz,  $\text{CDCl}_3$ )  $\delta$  162.36, 157.59, 148.09, 147.21, 130.95, 127.95, 127.59, 120.31, 110.40, 60.69, 55.29, 47.97, 46.42, 36.73, 36.25, 32.98, 32.48, 31.36, 25.72, 25.70.

HRMS:  $[\text{M}+\text{H}]^+$  calculated for  $\text{C}_{23}\text{H}_{32}\text{N}_4\text{O}_4\text{S}+\text{H}^+$  461.22170, found 461.22158.

**(3-((Cyclohexylmethyl)sulfonyl)-1H-1,2,4-triazol-1-yl)(4-(4-methoxybenzyl)piperidin-1-yl)-methanone (22)**

**52** (61 mg, 0.14 mmol) was oxidized according General procedure A. Flash column chromatography (20 → 80% EtOAc in pentane) afforded the title compound as gray gum (65 mg, 0.14 mmol, quant.).

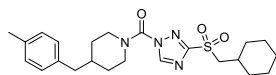
$^1\text{H}$  NMR (400 MHz,  $\text{CDCl}_3$ )  $\delta$  8.83 (s, 1H), 7.09 – 7.01 (m, 2H), 6.88 – 6.79 (m, 2H), 4.46 – 4.38 (m, 2H), 3.79 (s, 3H), 3.30 (d,  $J$  = 6.3 Hz, 2H), 3.17 – 2.85 (m, 2H), 2.53 (d,  $J$  = 6.7 Hz, 2H), 2.17 – 2.02 (m, 1H), 1.97 – 1.87 (m, 2H), 1.87 – 1.74 (m, 3H), 1.74 – 1.59 (m, 3H), 1.43 – 1.27 (m, 2H), 1.32 – 1.14 (m, 3H), 1.18 – 1.04 (m, 2H).

$^{13}\text{C}$  NMR (101 MHz,  $\text{CDCl}_3$ )  $\delta$  162.47, 158.16, 148.13, 147.25, 131.56, 130.05, 113.89, 60.74, 55.35, 47.96 (br), 46.44 (br), 41.80, 38.07, 33.02, 32.52, 32.02 (br), 31.46 (br), 25.76, 25.74.

HRMS:  $[\text{M}+\text{Na}]^+$  calculated for  $\text{C}_{23}\text{H}_{32}\text{N}_4\text{O}_4\text{S}+\text{Na}^+$  483.2036, found 483.2038.



**(3-((Cyclohexylmethyl)sulfonyl)-1*H*-1,2,4-triazol-1-yl)(4-(4-methylbenzyl)piperidin-1-yl)-methanone (23)**



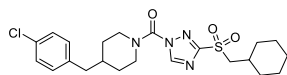
**53** (100 mg, 0.24 mmol) was oxidized according General procedure A. Flash column chromatography (20 → 80% EtOAc in pentane) afforded the title compound as gray gum (100 mg, 0.23 mmol, 93%).

<sup>1</sup>H NMR (400 MHz, CDCl<sub>3</sub>) δ 8.84 (s, 1H), 7.13 – 7.07 (m, 2H), 7.06 – 6.99 (m, 2H), 4.50 – 4.31 (m, 2H), 3.30 (d, *J* = 6.3 Hz, 2H), 3.18 – 2.84 (m, 2H), 2.55 (d, *J* = 6.7 Hz, 2H), 2.32 (s, 3H), 2.14 – 2.02 (m, 1H), 1.95 – 1.86 (m, 2H), 1.86 – 1.74 (m, 3H), 1.74 – 1.57 (m, 3H), 1.43 – 1.31 (m, 2H), 1.32 – 1.16 (m, 3H), 1.10 (qd, *J* = 12.1, 10.7, 3.2 Hz, 2H).

<sup>13</sup>C NMR (101 MHz, CDCl<sub>3</sub>) δ 162.38, 148.11, 147.19, 136.38, 135.73, 129.10, 128.97, 60.67, 47.88, 46.35, 42.20, 37.88, 32.94, 32.45, 32.13, 31.39, 25.69, 25.67, 21.04.

HRMS: [M+Na]<sup>+</sup> calculated for C<sub>23</sub>H<sub>32</sub>N<sub>4</sub>O<sub>3</sub>S+Na<sup>+</sup> 467.2087, found 467.2072.

**(4-(4-Chlorobenzyl)piperidin-1-yl)(3-((cyclohexylmethyl)sulfonyl)-1*H*-1,2,4-triazol-1-yl)-methanone (24, WEN091)**



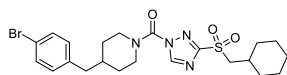
**54** (20 mg, 0.046 mmol) was oxidized according General procedure D. Flash column chromatography (0 → 100% Et<sub>2</sub>O in pentane) afforded the title compound as white gum (5 mg, 0.011 mmol, 23%).

<sup>1</sup>H NMR (500 MHz, CDCl<sub>3</sub>) δ 8.83 (s, 1H), 7.30 – 7.24 (m, 2H), 7.10 – 7.05 (m, 2H), 4.54 – 4.33 (m, 2H), 3.30 (d, *J* = 6.4 Hz, 2H), 3.20 – 2.84 (m, 2H), 2.57 (d, *J* = 6.8 Hz, 2H), 2.09 (m, 1H), 1.95 – 1.88 (m, 2H), 1.88 – 1.74 (m, 3H), 1.74 – 1.61 (m, 2H), 1.37 (qd, *J* = 12.7, 4.0, 3.2 Hz, 2H), 1.33 – 1.20 (m, 3H), 1.22 – 1.13 (m, 1H), 1.11 (qd, *J* = 12.2, 11.3, 3.4 Hz, 2H).

<sup>13</sup>C NMR (126 MHz, CDCl<sub>3</sub>) δ 162.61, 148.19, 147.30, 137.98, 132.24, 130.50, 128.70, 60.79, 42.11, 37.91, 33.09, 32.57, 25.81, 25.79.

HRMS: [M+H]<sup>+</sup> calculated for C<sub>22</sub>H<sub>29</sub>ClN<sub>4</sub>O<sub>3</sub>S+H<sup>+</sup> 465.17217, found 465.17183.

**(4-(4-Bromobenzyl)piperidin-1-yl)(3-((cyclohexylmethyl)sulfonyl)-1*H*-1,2,4-triazol-1-yl)-methanone (25)**



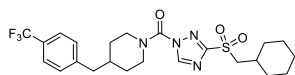
**55** (47 mg, 0.098 mmol) was oxidized according General procedure A. Flash column chromatography (20 → 80% EtOAc in pentane) afforded the title compound as gray gum (43 mg, 0.084 mmol, 86%).

<sup>1</sup>H NMR (400 MHz, CDCl<sub>3</sub>) δ 8.84 (s, 1H), 7.44 – 7.38 (m, 2H), 7.06 – 6.98 (m, 2H), 4.51 – 4.35 (m, 2H), 3.30 (d, *J* = 6.4 Hz, 2H), 3.17 – 2.87 (m, 2H), 2.55 (d, *J* = 6.8 Hz, 2H), 2.17 – 2.03 (m, 1H), 1.96 – 1.86 (m, 2H), 1.88 – 1.74 (m, 3H), 1.74 – 1.60 (m, 3H), 1.45 – 1.32 (m, 2H), 1.33 – 1.13 (m, 3H), 1.15 – 1.05 (m, 2H).

<sup>13</sup>C NMR (101 MHz, CDCl<sub>3</sub>) δ 162.49, 148.16, 147.23, 138.47, 131.58, 130.87, 120.15, 60.72, 47.85 (br), 46.44 (br), 42.09, 37.77, 33.01, 32.50, 32.07 (br), 25.74, 25.73.

HRMS: [M+Na]<sup>+</sup> calculated for C<sub>22</sub>H<sub>29</sub>BrN<sub>4</sub>O<sub>3</sub>S+Na<sup>+</sup> 531.1036 and 533.1015, found 531.1033 and 533.1017.

**(3-((Cyclohexylmethyl)sulfonyl)-1*H*-1,2,4-triazol-1-yl)(4-(4-(trifluoromethyl)benzyl)piperidin-1-yl)methanone (26)**



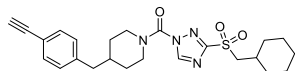
**56** (42 mg, 0.090 mmol) was oxidized according General procedure A. Flash column chromatography (20 → 60% EtOAc in pentane) afforded the title compound as gray gum (38 mg, 0.076 mmol, 85%).

$^1\text{H}$  NMR (400 MHz,  $\text{CDCl}_3$ )  $\delta$  8.85 (s, 1H), 7.56 (d,  $J$  = 7.9 Hz, 2H), 7.27 (d,  $J$  = 8.2 Hz, 2H), 4.53 – 4.35 (m, 2H), 3.31 (d,  $J$  = 6.3 Hz, 2H), 3.19 – 2.86 (m, 2H), 2.66 (d,  $J$  = 7.0 Hz, 2H), 2.16 – 2.02 (m, 1H), 1.95 – 1.84 (m, 3H), 1.84 – 1.74 (m, 2H), 1.75 – 1.59 (m, 3H), 1.40 (qd,  $J$  = 12.7, 4.0 Hz, 2H), 1.36 – 1.14 (m, 3H), 1.16 – 1.04 (m, 2H).

$^{13}\text{C}$  NMR (101 MHz,  $\text{CDCl}_3$ )  $\delta$  162.54, 148.20, 147.26, 143.68 (q,  $J$  = 1.2 Hz), 129.46, 128.78 (q,  $J$  = 32.4 Hz), 125.47 (q,  $J$  = 3.8 Hz), 124.33 (q,  $J$  = 272.1 Hz), 60.73, 42.52, 37.74, 33.03, 32.52, 25.74.

HRMS:  $[\text{M}+\text{H}]^+$  calculated for  $\text{C}_{23}\text{H}_{29}\text{F}_3\text{N}_4\text{O}_3\text{S}+\text{H}^+$  calculated 499.1985, found 499.2000

**(3-((Cyclohexylmethyl)sulfonyl)-1H-1,2,4-triazol-1-yl)(4-(4-ethynylbenzyl)piperidin-1-yl)-methanone (27)**

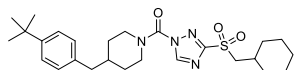


**95** (1 eq, 20 mg, 0.064 mmol) dissolved in 5 mL dry THF was added dropwise over the course of 15 min to an ice-cold solution of triphosgene (4.8 eq, 91 mg, 0.31 mmol) and  $\text{Na}_2\text{CO}_3$  (4.8 eq, 33 mg, 0.31 mmol) in 6 mL dry THF. The mixture was stirred on ice for 1.5 h, after which it was allowed to warm to RT. When TLC analysis showed full conversion ( $\sim$ 1.5 h) the mixture was dissolved with EtOAc, washed with water and brine, dried over  $\text{MgSO}_4$ , filtrated and concentrated *in vacuo*. Traces of water were removed by co-evaporation with toluene, after which the residue was dissolved in 5 mL dry DMF. **106** (1.6 eq, 23 mg, 0.10 mmol) and  $\text{K}_2\text{CO}_3$  (5.0 eq, 44 mg, 0.32 mmol) were added and the mixture was stirred overnight. Water and EtOAc were added and the layers were separated. The aqueous layer was extracted with EtOAc, after which the combined organic layers were washed with brine, dried over  $\text{MgSO}_4$ , filtrated and concentrated *in vacuo*. Flash column chromatography (30  $\rightarrow$  50%  $\text{Et}_2\text{O}$  in pentane) afforded the title compound (9 mg, 0.020 mmol, 31%).

$^1\text{H}$  NMR (500 MHz,  $\text{CDCl}_3$ )  $\delta$  8.83 (s, 1H), 7.43 (d,  $J$  = 8.1 Hz, 2H), 7.10 (d,  $J$  = 8.1 Hz, 2H), 4.49 – 4.39 (m, 2H), 3.30 (d,  $J$  = 6.4 Hz, 2H), 3.06 (s, 1H), 3.17 – 2.86 (m, 2H), 2.60 (d,  $J$  = 5.8 Hz, 2H), 2.15 – 2.04 (m, 1H), 1.95 – 1.88 (m, 2H), 1.88 – 1.77 (m, 3H), 1.70 – 1.59 (m, 2H), 1.43 – 1.38 (m, 4H), 1.33 – 1.26 (m, 2H), 1.11 (qd,  $J$  = 12.4, 2.9 Hz, 2H).

$^{13}\text{C}$  NMR (126 MHz,  $\text{CDCl}_3$ )  $\delta$  162.71, 147.31, 140.53, 132.36, 129.20, 120.23, 83.63, 77.13, 60.80, 42.69, 37.84, 33.10, 32.57, 29.85, 24.13, 23.11.

**(4-(4-(tert-Butyl)benzyl)piperidin-1-yl)(3-((cyclohexylmethyl)sulfonyl)-1H-1,2,4-triazol-1-yl)-methanone (28)**

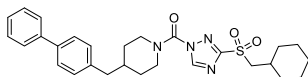


**58** (48 mg, 0.11 mmol) was oxidized according General procedure A. Flash column chromatography (20  $\rightarrow$  80% EtOAc in pentane) afforded the title compound as gray gum (38 mg, 0.078 mmol, 74%).

$^1\text{H}$  NMR (400 MHz,  $\text{CDCl}_3$ )  $\delta$  8.84 (s, 1H), 7.35 – 7.27 (m, 2H), 7.11 – 7.03 (m, 2H), 4.46 – 4.38 (m, 2H), 3.30 (d,  $J$  = 6.4 Hz, 2H), 3.16 – 2.87 (m, 2H), 2.56 (d,  $J$  = 6.9 Hz, 2H), 2.16 – 2.02 (m, 1H), 1.96 – 1.88 (m, 2H), 1.88 – 1.74 (m, 3H), 1.74 – 1.59 (m, 3H), 1.45 – 1.31 (m, 2H), 1.31 (s, 9H), 1.29 – 1.14 (m, 3H), 1.17 – 1.04 (m, 2H).

$^{13}\text{C}$  NMR (101 MHz,  $\text{CDCl}_3$ )  $\delta$  162.45, 149.15, 148.14, 147.25, 136.44, 128.81, 125.37, 60.74, 53.56, 47.96 (br), 46.49 (br), 42.17, 37.87, 34.48, 33.02, 32.51, 32.13, 31.48 (br), 25.76, 25.74.

HRMS:  $[\text{M}+\text{Na}]^+$  calculated for  $\text{C}_{26}\text{H}_{38}\text{N}_4\text{O}_3\text{S}+\text{Na}^+$  calculated 509.2557, found 509.2553.

**(4-([1,1'-Biphenyl]-4-ylmethyl)piperidin-1-yl)(3-((cyclohexylmethyl)sulfonyl)-1*H*-1,2,4-triazol-1-yl)methanone (29)**

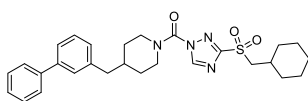
**110** (12 mg, 0.024 mmol) was oxidized according to General procedure A. Flash column chromatography (50 → 100% Et<sub>2</sub>O in pentane) afforded the title compound as white powder (8 mg,

0.016 mmol, 65%).

<sup>1</sup>H NMR (500 MHz, CDCl<sub>3</sub>) δ 8.84 (s, 1H), 7.61 – 7.55 (m, 2H), 7.56 – 7.50 (m, 2H), 7.47 – 7.40 (m, 2H), 7.34 (tt, *J* = 7.3, 1.9, 1.3 Hz, 1H), 7.25 – 7.19 (m, 2H), 4.45 (s, 2H), 3.31 (d, *J* = 6.4 Hz, 1H), 3.21 – 2.90 (m, 2H), 2.64 (d, *J* = 6.5 Hz, 2H), 2.15 – 2.03 (m, 1H), 1.95 – 1.77 (m, 4H), 1.74 – 1.60 (m, 4H), 1.41 (qd, *J* = 12.3, 4.1 Hz, 2H), 1.36 – 1.27 (m, 3H), 1.20 – 1.14 (m, 1H), 1.11 (qd, *J* = 12.5, 4.6 Hz, 2H).

<sup>13</sup>C NMR (126 MHz, CDCl<sub>3</sub>) δ 162.58, 148.17, 147.32, 140.99, 139.39, 138.66, 129.63, 128.91, 127.31, 127.28, 127.12, 60.80, 42.42, 37.99, 33.09, 32.57, 25.81, 25.79.

HRMS: [M+H]<sup>+</sup> calculated for C<sub>28</sub>H<sub>34</sub>N<sub>4</sub>O<sub>3</sub>S+H<sup>+</sup> 507.2424, found 507.2424.

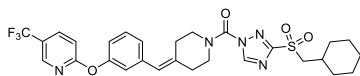
**(4-([1,1'-Biphenyl]-3-ylmethyl)piperidin-1-yl)(3-((cyclohexylmethyl)sulfonyl)-1*H*-1,2,4-triazol-1-yl)methanone (30)**

**59** (75 mg, 0.16 mmol) was oxidized according General procedure A. Flash column chromatography (20 → 80% EtOAc in pentane) afforded the title compound as colorless oil (64 mg, 0.13 mmol, 80%).

<sup>1</sup>H NMR (400 MHz, CDCl<sub>3</sub>) δ 8.83 (s, 1H), 7.62 – 7.54 (m, 2H), 7.48 – 7.40 (m, 3H), 7.39 – 7.31 (m, 3H), 7.12 (dt, *J* = 7.5, 1.3 Hz, 1H), 4.51 – 4.35 (m, 2H), 3.30 (d, *J* = 6.3 Hz, 2H), 3.17 – 2.88 (m, 2H), 2.65 (d, *J* = 6.9 Hz, 2H), 2.16 – 2.01 (m, 1H), 1.95 – 1.86 (m, 3H), 1.87 – 1.77 (m, 2H), 1.74 – 1.58 (m, 3H), 1.40 (qd, *J* = 12.7, 4.2 Hz, 2H), 1.33 – 1.12 (m, 3H), 1.10 (qd, *J* = 12.3, 3.2 Hz, 2H).

<sup>13</sup>C NMR (101 MHz, CDCl<sub>3</sub>) δ 162.41, 148.12, 147.21, 141.44, 141.10, 140.02, 128.89, 128.83, 128.06, 127.93, 127.40, 127.19, 125.18, 60.69, 47.88 (br), 46.33 (br), 42.77, 37.89, 32.96, 32.47, 32.07 (br), 31.51 (br), 25.70, 25.69.

HRMS: [M+Na]<sup>+</sup> calculated for C<sub>28</sub>H<sub>24</sub>N<sub>4</sub>O<sub>3</sub>S+Na<sup>+</sup> 529.22438, found 529.22330.

**(3-((Cyclohexylmethyl)sulfonyl)-1*H*-1,2,4-triazol-1-yl)(4-(3-((5-(trifluoromethyl)pyridin-2-yl)oxy)benzylidene)piperidin-1-yl)methanone (31)**

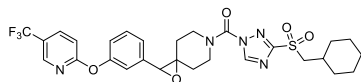
**106** (23 mg, 0.10 mmol) was reacted with **105** (1.7 eq, 56 mg, 0.17 mmol) according to General procedure C. The residue was purified by flash column chromatography (10 → 30%

EtOAc in pentane) yielding the title compound (11 mg, 0.019 mmol, 19%).

<sup>1</sup>H NMR (500 MHz, CDCl<sub>3</sub>) δ 8.88 (s, 1H), 8.46 – 8.42 (m, 1H), 7.92 (dd, *J* = 8.7, 2.3 Hz, 1H), 7.41 (t, *J* = 7.9 Hz, 1H), 7.10 (d, *J* = 7.5 Hz, 1H), 7.04 (d, *J* = 8.6 Hz, 2H), 7.01 – 6.98 (m, 1H), 6.46 (s, 1H), 4.04 – 3.63 (m, 3H), 3.31 (d, *J* = 6.1 Hz, 2H), 2.73 – 2.67 (m, 3H), 2.60 – 2.49 (m, 2H), 2.16 – 2.04 (m, 1H), 1.95 – 1.88 (m, 2H), 1.74 – 1.66 (m, 2H), 1.65 – 1.54 (m, 1H), 1.35 – 1.24 (m, 2H), 1.22 – 1.16 (m, 1H), 1.12 (qd, *J* = 11.9, 3.0 Hz, 2H).

<sup>13</sup>C NMR (126 MHz, CDCl<sub>3</sub>) δ 165.81, 162.74, 153.25, 147.36, 145.63, 138.75, 136.93, 136.90, 136.54, 129.83, 126.14, 125.66, 121.90, 119.98, 111.63, 60.78, 47.36 (br), 33.09, 32.56, 29.84, 25.80, 25.78.

HRMS: [M+H]<sup>+</sup> calculated for C<sub>28</sub>H<sub>30</sub>F<sub>3</sub>N<sub>5</sub>O<sub>4</sub>S+H<sup>+</sup> 590.20434, found 590.20368.

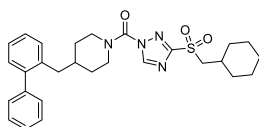
**(3-((Cyclohexylmethyl)sulfonyl)-1*H*-1,2,4-triazol-1-yl)(2-((5-(trifluoromethyl)pyridin-2-yl)oxy)phenyl)-1-oxa-6-azaspiro[2.5]octan-6-yl)methanone (32)**

**60** (9 mg, 0.016 mmol) was oxidized according General procedure A. Flash column chromatography (20 → 50% EtOAc in pentane) afforded the title compound (6 mg, 9.9 μmol, 61%).

<sup>1</sup>H NMR (500 MHz, CDCl<sub>3</sub>) δ 8.87 (s, 1H), 8.45 – 8.41 (m, 1H), 7.92 (dd, *J* = 8.7, 2.4 Hz, 1H), 7.44 (t, *J* = 7.8 Hz, 1H), 7.21 (d, *J* = 7.7 Hz, 1H), 7.13 – 7.09 (m, 2H), 7.04 (d, *J* = 8.7 Hz, 1H), 4.07 (s, 1H), 4.31 – 3.54 (m, 4H), 3.36 – 3.20 (m, 2H), 2.14 – 2.03 (m, 1H), 1.93 – 1.87 (m, 2H), 1.80 – 1.60 (m, 4H), 1.61 – 1.51 (m, 3H), 1.31 – 1.23 (m, 3H), 1.21 – 1.04 (m, 2H).

<sup>13</sup>C NMR (126 MHz, CDCl<sub>3</sub>) δ 165.47, 162.83, 153.45, 147.40, 145.61, 136.98, 130.00, 123.44, 121.20, 119.55, 111.73, 63.73, 60.77, 33.09, 32.55, 25.79, 25.77.

HRMS: [M+H]<sup>+</sup> calculated for C<sub>28</sub>H<sub>30</sub>F<sub>3</sub>N<sub>5</sub>O<sub>5</sub>S+H<sup>+</sup> 606.19925, found 606.19882.

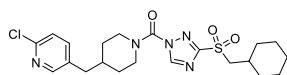
**(4-([1,1'-Biphenyl]-2-ylmethyl)piperidin-1-yl)(3-((cyclohexylmethyl)sulfonyl)-1*H*-1,2,4-triazol-1-yl)methanone (33)**

**61** (75 mg, 0.16 mmol) was oxidized according General procedure A. Flash column chromatography (20 → 80% EtOAc in pentane) afforded the title compound as colorless oil (77 mg, 0.15 mmol, 96%).

<sup>1</sup>H NMR (400 MHz, CDCl<sub>3</sub>) δ 8.79 (s, 1H), 7.44 – 7.38 (m, 2H), 7.38 – 7.30 (m, 1H), 7.31 – 7.24 (m, 5H), 7.24 – 7.18 (m, 1H), 4.31 – 4.19 (m, 2H), 3.28 (d, *J* = 6.4 Hz, 2H), 3.07 – 2.74 (m, 2H), 2.63 (d, *J* = 6.9 Hz, 2H), 2.13 – 2.00 (m, 1H), 1.95 – 1.84 (m, 2H), 1.74 – 1.49 (m, 6H), 1.35 – 1.09 (m, 3H), 1.18 – 1.02 (m, 4H).

<sup>13</sup>C NMR (101 MHz, CDCl<sub>3</sub>) δ 162.28, 148.03, 147.04, 142.36, 141.75, 137.01, 130.27, 129.87, 129.27, 128.22, 127.37, 126.97, 126.20, 60.62, 47.78 (br), 46.18 (br), 39.15, 37.26, 32.92, 32.42, 32.09 (br), 31.18 (br), 25.68, 25.65.

HRMS: [M+Na]<sup>+</sup> calculated for C<sub>28</sub>H<sub>24</sub>N<sub>4</sub>O<sub>3</sub>S+Na<sup>+</sup> 529.22438, found 529.22325.

**(4-((6-Chloropyridin-3-yl)methyl)piperidin-1-yl)(3-((cyclohexylmethyl)sulfonyl)-1*H*-1,2,4-triazol-1-yl)methanone (34)**

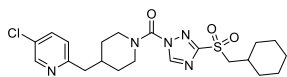
**62** (50 mg, 0.12 mmol) was oxidized according General procedure A. Flash column chromatography (20 → 80% EtOAc in pentane) afforded the title compound as white solid (13 mg, 0.028 mmol, 24%).

<sup>1</sup>H NMR (400 MHz, CDCl<sub>3</sub>) δ 8.85 (s, 1H), 8.52 (dd, *J* = 2.5, 0.7 Hz, 1H), 7.61 (dd, *J* = 8.3, 2.5 Hz, 1H), 7.09 (dd, *J* = 8.2, 0.7 Hz, 1H), 4.51 – 4.37 (m, 2H), 3.31 (d, *J* = 6.4 Hz, 2H), 3.23 – 2.92 (m, 2H), 2.75 (d, *J* = 7.2 Hz, 2H), 2.23 – 2.05 (m, 2H), 1.95 – 1.86 (m, 2H), 1.86 – 1.75 (m, 2H), 1.74 – 1.59 (m, 3H), 1.43 (qd, *J* = 12.7, 4.2 Hz, 2H), 1.36 – 1.22 (m, 3H), 1.20 – 1.04 (m, 2H).

<sup>13</sup>C NMR (101 MHz, CDCl<sub>3</sub>) δ 162.53, 157.75, 148.44, 147.64, 147.29, 136.38, 130.06, 124.65, 60.80, 43.94, 36.36, 33.08, 32.55, 25.78, 25.74.

HRMS: [M+H]<sup>+</sup> calculated for C<sub>21</sub>H<sub>28</sub>ClN<sub>5</sub>O<sub>3</sub>S+H<sup>+</sup> 466.16741, found 466.16649.

**(4-((5-Chloropyridin-2-yl)methyl)piperidin-1-yl)(3-((cyclohexylmethyl)sulfonyl)-1H-1,2,4-triazol-1-yl)methanone (35)**



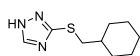
**63** (100 mg, 0.23 mmol) was oxidized according General procedure A. Flash column chromatography (20 → 80% EtOAc in pentane) afforded the title compound as white solid (100 mg, 0.22 mmol, 93%).

$^1\text{H}$  NMR (400 MHz,  $\text{CDCl}_3$ )  $\delta$  8.85 (s, 1H), 8.20 (dd,  $J = 2.4, 0.6$  Hz, 1H), 7.46 (dd,  $J = 8.1, 2.5$  Hz, 1H), 7.29 (dd,  $J = 8.1, 0.7$  Hz, 1H), 4.58 – 4.36 (m, 2H), 3.31 (d,  $J = 6.4$  Hz, 2H), 3.21 – 2.87 (m, 2H), 2.60 (d,  $J = 7.0$  Hz, 2H), 2.17 – 2.03 (m, 1H), 1.96 – 1.87 (m, 2H), 1.87 – 1.75 (m, 3H), 1.76 – 1.60 (m, 3H), 1.39 (qd,  $J = 12.8, 3.4$  Hz, 2H), 1.37 – 1.14 (m, 3H), 1.11 (qd,  $J = 11.6, 3.3$  Hz, 2H).

$^{13}\text{C}$  NMR (101 MHz,  $\text{CDCl}_3$ )  $\delta$  162.60, 150.09, 149.74, 148.23, 147.27, 139.46, 133.76, 124.16, 60.74, 38.97, 37.61, 33.05, 32.53, 25.76.

HRMS:  $[\text{M}+\text{H}]^+$  calculated for  $\text{C}_{21}\text{H}_{28}\text{ClN}_5\text{O}_3\text{S}+\text{H}^+$  466.16741, found 466.16652.

**3-((Cyclohexylmethyl)thio)-1H-1,2,4-triazole (36)**



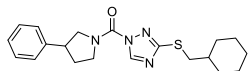
1H-1,2,4-triazole-3-thiol (1 eq, 2.00 g, 19.8 mmol) was dissolved in 70 mL dry DMF and (bromomethyl)cyclohexane (1 eq, 2.76 mL, 19.8 mmol) was added carefully.

$\text{K}_2\text{CO}_3$  (0.73 eq, 2.00 g, 14.4 mmol) was added and the mixture was stirred for 6 h, during which it turned light purple and finally white and cloudy. The mixture was diluted with EtOAc and washed with water. The aqueous layer was extracted with EtOAc, after which the combined organic layers were washed with brine, dried over  $\text{MgSO}_4$ , filtrated and concentrated *in vacuo*. Flash column chromatography (20 → 40% EtOAc in pentane) afforded the title compound as white crystalline solid (3.43 g, 17.4 mmol, 88%).

$^1\text{H}$  NMR (400 MHz,  $\text{CDCl}_3$ )  $\delta$  13.13 (s, 1H), 8.20 (s, 1H), 3.08 (d,  $J = 7.0$  Hz, 2H), 1.91 – 1.80 (m, 2H), 1.76 – 1.61 (m, 3H), 1.69 – 1.52 (m, 1H), 1.31 – 1.05 (m, 3H), 0.98 (qd,  $J = 11.7, 3.4$  Hz, 2H).

$^{13}\text{C}$  NMR (101 MHz,  $\text{CDCl}_3$ )  $\delta$  157.29, 147.61, 39.96, 37.84, 32.49, 26.22, 25.95.

**(3-((Cyclohexylmethyl)thio)-1H-1,2,4-triazol-1-yl)(3-phenylpyrrolidin-1-yl)methanone (39)**



**36** (51 mg, 0.26 mmol) was reacted with 3-phenylpyrrolidine (1.4 eq, 55  $\mu\text{L}$ , 0.37 mmol) according to General procedure C. The residue was purified by flash column chromatography (0 → 25% EtOAc in pentane)

yielding the title compound as a white crystalline solid (79 mg, 0.21 mmol, 82%). HPLC showed presence of a single product ( $t_r = 6.81$  min). NMR showed two products which are probably conformationally restricted isomers (ratio ~1:1), as reported before for similar compounds (data not published).

## Conformer 1:

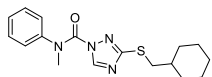
$^1\text{H}$  NMR (500 MHz,  $\text{CDCl}_3$ )  $\delta$  8.83 (s, 1H), 7.38 – 7.31 (m, 2H), 7.30 – 7.23 (m, 3H), 4.44 (dd,  $J$  = 11.9, 7.6 Hz, 1H), 4.24 (ddd,  $J$  = 11.5, 8.1, 2.9 Hz, 1H), 4.09 – 3.99 (m, 1H), 3.98 – 3.86 (m, 1H), 3.50 – 3.39 (m, 1H), 3.05 (d,  $J$  = 6.8 Hz, 2H), 2.45 – 2.30 (m, 1H), 2.17 – 2.00 (m, 1H), 1.92 – 1.86 (m, 2H), 1.78 – 1.70 (m, 2H), 1.70 – 1.56 (m, 2H), 1.35 – 0.96 (m, 3H), 0.96 – 0.85 (m, 2H).

$^{13}\text{C}$  NMR (126 MHz,  $\text{CDCl}_3$ )  $\delta$  163.51, 147.17, 147.09, 140.22, 128.82, 127.27, 127.08, 55.99, 49.73, 45.05, 38.82, 37.91, 33.90, 32.64, 26.26, 26.07.

## Conformer 2:

$^1\text{H}$  NMR (500 MHz,  $\text{CDCl}_3$ )  $\delta$  8.82 (s, 1H), 7.38 – 7.31 (m, 2H), 7.30 – 7.23 (m, 3H), 4.13 (dd,  $J$  = 12.0, 7.6 Hz, 1H), 3.98 – 3.86 (m, 1H), 3.78 – 3.71 (m, 1H), 3.68 (dd,  $J$  = 11.9, 9.5 Hz, 1H), 3.50 – 3.39 (m, 1H), 3.02 – 2.89 (m, 2H), 2.45 – 2.30 (m, 1H), 2.17 – 2.00 (m, 1H), 1.84 – 1.78 (m, 2H), 1.70 – 1.56 (m, 4H), 1.35 – 0.96 (m, 5H).

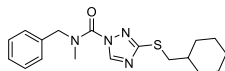
$^{13}\text{C}$  NMR (126 MHz,  $\text{CDCl}_3$ )  $\delta$  163.51, 147.17, 147.09, 139.92, 128.82, 127.18, 127.03, 54.43, 48.66, 42.05, 38.82, 37.83, 32.55, 31.07, 26.28, 25.98.

**3-((Cyclohexylmethyl)thio)-*N*-methyl-*N*-phenyl-1*H*-1,2,4-triazole-1-carboxamide (40)**

**36** (50 mg, 0.25 mmol) was reacted with *N*-methylaniline (1.5 eq, 41  $\mu\text{L}$ , 0.38 mmol) according to General procedure C. The residue was purified by flash column chromatography (0  $\rightarrow$  20% EtOAc in pentane) yielding the title compound as a white crystalline solid (65 mg, 0.20 mmol, 78%).

$^1\text{H}$  NMR (400 MHz,  $\text{CDCl}_3$ )  $\delta$  8.62 (s, 1H), 7.40 – 7.28 (m, 2H), 7.32 – 7.24 (m, 1H), 7.16 – 7.09 (m, 2H), 3.51 (s, 3H), 2.56 (d,  $J$  = 7.0 Hz, 2H), 1.78 – 1.59 (m, 5H), 1.45 – 1.30 (m, 1H), 1.30 – 1.05 (m, 3H), 0.85 (qd,  $J$  = 13.6, 12.8, 4.0 Hz, 2H).

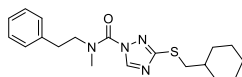
$^{13}\text{C}$  NMR (101 MHz,  $\text{CDCl}_3$ )  $\delta$  163.21, 152.91, 148.62, 146.71, 143.58, 129.53, 127.56, 126.18, 40.62, 38.41, 37.32, 32.48, 26.30, 25.95.

***N*-Benzyl-3-((cyclohexylmethyl)thio)-*N*-methyl-1*H*-1,2,4-triazole-1-carboxamide (41)**

**36** (50 mg, 0.25 mmol) was reacted with *N*-methylbenzylamine (1.5 eq, 51  $\mu\text{L}$ , 0.38 mmol) according to General procedure C. The residue was purified by flash column chromatography (10  $\rightarrow$  20% EtOAc in pentane) yielding the title compound as gray oil (74 mg, 0.22 mmol, 85%).

$^1\text{H}$  NMR (500 MHz,  $\text{CDCl}_3$ )  $\delta$  8.78 (s, 1H), 7.40 – 7.26 (m, 5H), 5.23 – 4.48 (m, 2H), 3.49 – 2.60 (m, 5H), 2.11 – 1.39 (m, 5H), 1.33 – 1.04 (m, 4H), 1.03 – 0.64 (m, 2H).

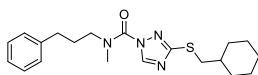
$^{13}\text{C}$  NMR (126 MHz,  $\text{CDCl}_3$ )  $\delta$  163.60, 149.72, 135.91, 128.84, 127.98, 54.46, 38.67, 37.79, 32.54, 26.28, 26.04.

**3-((Cyclohexylmethyl)thio)-*N*-methyl-*N*-phenethyl-1*H*-1,2,4-triazole-1-carboxamide (42)**

**36** (51 mg, 0.26 mmol) was reacted with *N*-methylphenethylamine (1.4 eq, 50 mg, 0.37 mmol) according to General procedure C. The residue was purified by flash column chromatography (15  $\rightarrow$  20% EtOAc in pentane) yielding the title compound as a yellowish oil (41 mg, 0.11 mmol, 44%).

$^1\text{H}$  NMR (500 MHz,  $\text{CDCl}_3$ )  $\delta$  8.80 – 8.30 (m, 1H), 7.32 – 7.25 (m, 2H), 7.25 – 7.20 (m, 1H), 7.25 – 7.07 (m, 2H), 4.11 – 3.57 (m, 2H), 3.37 – 3.06 (m, 3H), 3.04 (d,  $J$  = 6.9 Hz, 2H), 2.99 (t,  $J$  = 7.6 Hz, 2H), 1.91 – 1.84 (m, 2H), 1.76 – 1.69 (m, 2H), 1.69 – 1.57 (m, 2H), 1.33 – 1.06 (m, 3H), 1.00 (qd,  $J$  = 12.1, 3.4 Hz, 2H).

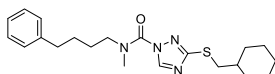
$^{13}\text{C}$  NMR (126 MHz,  $\text{CDCl}_3$ )  $\delta$  163.30, 149.38, 138.07, 128.86, 128.80, 126.85, 52.81 (br), 38.89, 37.97, 36.76 (br), 33.81 (br), 32.67, 26.35, 26.11.

**3-((Cyclohexylmethyl)thio)-*N*-methyl-*N*-(3-phenylpropyl)-1*H*-1,2,4-triazole-1-carboxamide (43)**

**36** (20 mg, 0.10 mmol) was reacted with **66** (1.5 eq, 32 mg, 0.15 mmol) according to General procedure C. The residue was purified by flash column chromatography (15 → 20% EtOAc in pentane) yielding the title compound as a colorless oil (16 mg, 0.043 mmol, 43%).

<sup>1</sup>H NMR (500 MHz, CDCl<sub>3</sub>) δ 8.71 (s, 1H), 7.32 – 7.25 (m, 2H), 7.23 – 7.16 (m, 3H), 3.87 – 3.41 (m, 2H), 3.38 – 3.06 (m, 3H), 3.04 (d, *J* = 6.8 Hz, 2H), 2.70 – 2.63 (m, 2H), 2.09 – 2.00 (m, 2H), 1.92 – 1.84 (m, 2H), 1.77 – 1.69 (m, 2H), 1.69 – 1.62 (m, 1H), 1.65 – 1.57 (m, 1H), 1.25 – 1.09 (m, 3H), 1.00 (qd, *J* = 12.4, 3.4 Hz, 2H).

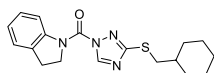
<sup>13</sup>C NMR (126 MHz, CDCl<sub>3</sub>) δ 149.39, 136.02, 128.65, 128.35, 126.30, 50.93, 38.90, 37.98, 36.65, 32.99, 32.73, 30.45, 29.83, 26.37, 26.14.

**3-((Cyclohexylmethyl)thio)-*N*-methyl-*N*-(4-phenylbutyl)-1*H*-1,2,4-triazole-1-carboxamide (44)**

**36** (30 mg, 0.15 mmol) was reacted with *N*-methyl-4-phenylbutylamine (1.5 eq, 36 mg, 0.22 mmol) according to General procedure C. The residue was purified by flash column chromatography (10 → 20% EtOAc in pentane) yielding the title compound as a gray oil (30 mg, 0.078 mmol, 51%).

<sup>1</sup>H NMR (400 MHz, CDCl<sub>3</sub>) δ 8.71 (s, 1H), 7.33 – 7.24 (m, 2H), 7.23 – 7.14 (m, 3H), 3.81 – 3.44 (m, 2H), 3.28 – 3.06 (m, 3H), 3.04 (d, *J* = 6.8 Hz, 2H), 2.66 (t, *J* = 7.3 Hz, 2H), 1.93 – 1.84 (m, 2H), 1.77 – 1.65 (m, 5H), 1.69 – 1.56 (m, 1H), 1.31 – 1.08 (m, 5H), 1.00 (qd, *J* = 11.7, 3.3 Hz, 2H).

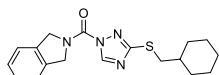
<sup>13</sup>C NMR (101 MHz, CDCl<sub>3</sub>) δ 149.31, 141.88, 128.50, 128.46, 126.04, 51.07, 38.85, 37.92, 35.61, 32.70, 29.81, 28.42, 26.34, 26.10.

**(3-((Cyclohexylmethyl)thio)-1*H*-1,2,4-triazol-1-yl)(indolin-1-yl)methanone (45)**

**36** (55 mg, 0.28 mmol) was reacted with indoline (1.4 eq, 43 μL, 0.38 mmol) according to General procedure C. The residue was purified by flash column chromatography (0 → 10% EtOAc in pentane) yielding the title compound (yield not determined).

<sup>1</sup>H NMR (400 MHz, CDCl<sub>3</sub>) δ 8.86 (s, 1H), 8.02 (d, *J* = 8.1 Hz, 1H), 7.30 – 7.20 (m, 2H), 7.16 – 7.07 (m, 1H), 4.57 (t, *J* = 8.3 Hz, 2H), 3.21 (t, *J* = 8.3 Hz, 2H), 3.06 (d, *J* = 6.8 Hz, 2H), 1.96 – 1.85 (m, 2H), 1.80 – 1.59 (m, 4H), 1.31 – 1.10 (m, 3H), 1.02 (qd, *J* = 12.0, 3.3 Hz, 2H).

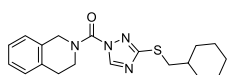
<sup>13</sup>C NMR (101 MHz, CDCl<sub>3</sub>) δ 163.70, 147.09, 146.19, 142.16, 132.05, 127.70, 125.19, 124.97, 117.56, 51.29, 38.88, 37.94, 32.69, 28.73, 26.31, 26.10.

**(3-((Cyclohexylmethyl)thio)-1*H*-1,2,4-triazol-1-yl)(isoindolin-2-yl)methanone (46)**

**36** (50 mg, 0.25 mmol) was reacted with isoindoline (1.5 eq, 43 μL, 0.38 mmol) according to General procedure C. The residue was purified by flash column chromatography (0 → 20% EtOAc in pentane) yielding the title compound as a white crystalline solid (76 mg, 0.22 mmol, 88%).

<sup>1</sup>H NMR (400 MHz, CDCl<sub>3</sub>) δ 8.88 (s, 1H), 7.35 – 7.21 (m, 4H), 5.34 (s, 2H), 5.02 (s, 2H), 3.08 (d, *J* = 6.8 Hz, 2H), 1.99 – 1.90 (m, 2H), 1.82 – 1.73 (m, 2H), 1.77 – 1.64 (m, 2H), 1.36 – 1.12 (m, 3H), 1.04 (qd, *J* = 12.0, 3.3 Hz, 2H).

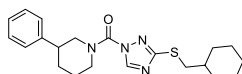
<sup>13</sup>C NMR (75 MHz, CDCl<sub>3</sub>) δ 163.84, 147.23, 146.73, 136.55, 134.29, 127.94, 122.63, 122.53, 55.55, 54.87, 38.92, 38.00, 32.72, 26.32, 26.14.

**(3-((Cyclohexylmethyl)thio)-1H-1,2,4-triazol-1-yl)(3,4-dihydroisoquinolin-2(1H)-yl)-methanone (47)**

**36** (50 mg, 0.25 mmol) was reacted with 1,2,3,4-tetrahydroisoquinoline (1.5 eq, 50  $\mu$ L, 0.38 mmol) according to General procedure C. The residue was purified by flash column chromatography (10  $\rightarrow$  20% EtOAc in pentane) yielding the title compound as a gray oil (83 mg, 0.23 mmol, 92%).

$^1\text{H}$  NMR (400 MHz,  $\text{CDCl}_3$ )  $\delta$  8.73 (s, 1H), 7.26 – 7.02 (m, 4H), 5.28 – 4.64 (m, 2H), 4.29 – 3.73 (m, 2H), 3.09 – 2.99 (m, 4H), 1.96 – 1.87 (m, 2H), 1.80 – 1.60 (m, 3H), 1.33 – 1.09 (m, 4H), 1.02 (qd,  $J$  = 12.0, 3.3 Hz, 2H).

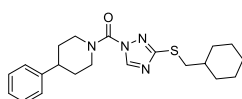
$^{13}\text{C}$  NMR (101 MHz,  $\text{CDCl}_3$ )  $\delta$  163.59, 148.60, 147.37, 147.36, 147.34, 134.07, 132.27, 128.83, 127.10, 126.66, 126.34, 38.81, 37.88, 32.66, 29.74, 26.30, 26.07.

**(3-((Cyclohexylmethyl)thio)-1H-1,2,4-triazol-1-yl)(3-phenylpiperidin-1-yl)methanone (48)**

**36** (51 mg, 0.26 mmol) was reacted with 3-phenylpiperidine (1.2 eq, 50  $\mu$ L, 0.30 mmol) according to General procedure C. The residue was purified by flash column chromatography (0  $\rightarrow$  100% EtOAc in pentane) yielding the title compound (59 mg, 0.15 mmol, 59%).

$^1\text{H}$  NMR (400 MHz,  $\text{CDCl}_3$ )  $\delta$  8.76 (s, 1H), 7.43 – 7.35 (m, 2H), 7.38 – 7.31 (m, 2H), 7.35 – 7.24 (m, 1H), 5.94 (s, 1H), 4.44 – 4.32 (m, 1H), 3.72 – 3.45 (m, 2H), 3.08 – 2.95 (m, 1H), 2.90 (d,  $J$  = 6.8 Hz, 2H), 2.53 – 2.44 (m, 1H), 2.11 – 1.97 (m, 1H), 1.95 – 1.86 (m, 1H), 1.84 – 1.75 (m, 1H), 1.78 – 1.60 (m, 5H), 1.59 – 1.49 (m, 1H), 1.36 – 1.06 (m, 4H), 1.00 (qd,  $J$  = 11.7, 3.2 Hz, 1H).

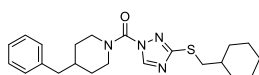
$^{13}\text{C}$  NMR (101 MHz,  $\text{CDCl}_3$ )  $\delta$  163.48, 163.34, 149.53, 147.61, 147.37, 138.14, 128.91, 127.12, 126.74, 56.23, 43.67, 42.94, 38.77, 38.64, 37.77, 37.75, 32.68, 32.57, 32.55, 27.95, 26.35, 26.32, 26.11, 26.08, 25.73, 19.44.

**(3-((Cyclohexylmethyl)thio)-1H-1,2,4-triazol-1-yl)(4-phenylpiperidin-1-yl)methanone (49)**

**36** (50 mg, 0.25 mmol) was reacted with 4-phenylpiperidine (1.5 eq, 61 mg, 0.38 mmol) according to General procedure C. The residue was purified by flash column chromatography (0  $\rightarrow$  20% EtOAc in pentane) yielding the title compound as a white crystalline solid (50 mg, 0.13 mmol, 51%).

$^1\text{H}$  NMR (400 MHz,  $\text{CDCl}_3$ )  $\delta$  8.72 (s, 1H), 7.37 – 7.29 (m, 2H), 7.28 – 7.19 (m, 3H), 5.02 – 4.45 (m, 2H), 3.19 – 3.06 (m, 2H), 3.03 (d,  $J$  = 6.8 Hz, 2H), 2.83 (tt,  $J$  = 12.1, 3.9 Hz, 1H), 2.01 – 1.77 (m, 5H), 1.80 – 1.58 (m, 4H), 1.31 – 1.08 (m, 4H), 0.99 (qd,  $J$  = 11.8, 3.4 Hz, 2H).

$^{13}\text{C}$  NMR (101 MHz,  $\text{CDCl}_3$ )  $\delta$  163.46, 148.42, 147.45, 144.82, 128.75, 126.82, 126.78, 47.12 (br), 42.61, 38.84, 37.91, 33.27, 32.69, 26.33, 26.10.

**(4-Benzylpiperidin-1-yl)(3-((cyclohexylmethyl)thio)-1H-1,2,4-triazol-1-yl)methanone (50)**

**36** (50 mg, 0.25 mmol) was reacted with 4-benzylpiperidine (1.5 eq, 67  $\mu$ L, 0.38 mmol) according to General procedure C. The residue was purified by flash column chromatography (0  $\rightarrow$  20% EtOAc in pentane) yielding the title compound as a white crystalline solid (76 mg, 0.19 mmol, 75%).

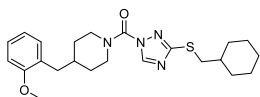
*Analytical data on next page.*



$^1\text{H}$  NMR (400 MHz,  $\text{CDCl}_3$ )  $\delta$  8.67 (s, 1H), 7.32 – 7.25 (m, 2H), 7.24 – 7.18 (m, 1H), 7.16 – 7.12 (m, 2H), 4.80 – 4.25 (m, 2H), 3.02 (d,  $J = 6.8$  Hz, 2H), 2.99 – 2.88 (m, 2H), 2.58 (d,  $J = 7.1$  Hz, 2H), 1.93 – 1.86 (m, 2H), 1.86 – 1.79 (m, 1H), 1.79 – 1.57 (m, 5H), 1.37 (qd,  $J = 12.9, 4.2$  Hz, 2H), 1.30 – 1.09 (m, 4H), 0.99 (qd,  $J = 12.1, 3.4$  Hz, 2H).

$^{13}\text{C}$  NMR (101 MHz,  $\text{CDCl}_3$ )  $\delta$  163.28, 148.31, 147.32, 139.76, 129.12, 128.42, 126.22, 46.71 (br), 42.91, 38.80, 38.09, 37.84, 32.65, 32.01, 29.75, 26.32, 26.08.

**3-((Cyclohexylmethyl)thio)-1*H*-1,2,4-triazol-1-yl)(4-(2-methoxybenzyl)piperidin-1-yl)-methanone (51)**

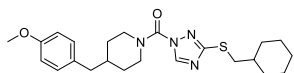


**36** (1.7 eq, 461 mg, 2.34 mmol) was reacted with **90** (1 eq, 275 mg, 1.34 mmol) according to General procedure C. The residue was purified by flash column chromatography (0 → 20% EtOAc in pentane) yielding the title compound as a colorless oil (417 mg, 0.97 mmol, 72%).

$^1\text{H}$  NMR (400 MHz,  $\text{CDCl}_3$ )  $\delta$  8.67 (s, 1H), 7.20 (td,  $J = 7.8, 1.8$  Hz, 1H), 7.06 (dd,  $J = 7.4, 1.8$  Hz, 1H), 6.92 – 6.83 (m, 2H), 4.71 – 4.30 (m, 2H), 3.82 (s, 3H), 3.02 (d,  $J = 6.8$  Hz, 2H), 3.00 – 2.86 (m, 2H), 2.59 (d,  $J = 7.1$  Hz, 2H), 1.94 – 1.80 (m, 3H), 1.77 – 1.70 (m, 4H), 1.70 – 1.58 (m, 2H), 1.37 (qd,  $J = 12.4, 4.2$  Hz, 2H), 1.30 – 1.09 (m, 3H), 1.00 (qd,  $J = 12.0, 3.4$  Hz, 2H).

$^{13}\text{C}$  NMR (101 MHz,  $\text{CDCl}_3$ )  $\delta$  163.24, 157.64, 148.35, 147.33, 130.98, 128.23, 127.53, 120.30, 110.41, 55.32, 38.83, 37.88, 37.00, 36.44, 32.68, 32.16, 26.36, 26.11.

**3-((Cyclohexylmethyl)thio)-1*H*-1,2,4-triazol-1-yl)(4-(4-methoxybenzyl)piperidin-1-yl)-methanone (52)**



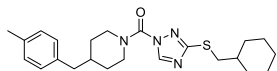
**36** (1.5 eq, 264 mg, 1.34 mmol) was reacted with **91** (1 eq, 183 mg, 0.89 mmol) according to General procedure C. The residue was purified by flash column chromatography (20% EtOAc in pentane)

yielding the title compound as a gray oil (157 mg, 0.37 mmol, 41%).

$^1\text{H}$  NMR (400 MHz,  $\text{CDCl}_3$ )  $\delta$  8.67 (s, 1H), 7.09 – 7.01 (m, 2H), 6.87 – 6.79 (m, 2H), 4.71 – 4.36 (m, 2H), 3.79 (s, 3H), 3.02 (d,  $J = 6.8$  Hz, 2H), 2.99 – 2.86 (m, 2H), 2.52 (d,  $J = 6.9$  Hz, 2H), 1.94 – 1.85 (m, 2H), 1.85 – 1.69 (m, 6H), 1.69 – 1.59 (m, 1H), 1.41 – 1.27 (m, 2H), 1.30 – 1.09 (m, 3H), 1.00 (qd,  $J = 12.0, 3.2$  Hz, 2H).

$^{13}\text{C}$  NMR (101 MHz,  $\text{CDCl}_3$ )  $\delta$  163.27, 158.06, 148.31, 147.32, 131.78, 130.01, 113.80, 55.30, 47.31, 41.98, 38.81, 38.24, 37.84, 32.65, 31.97, 26.33, 26.08.

**3-((Cyclohexylmethyl)thio)-1*H*-1,2,4-triazol-1-yl)(4-(4-methylbenzyl)piperidin-1-yl)-methanone (53)**

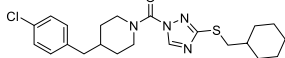


**36** (1.5 eq, 680 mg, 3.45 mmol) was reacted with **92** (1 eq, 435 mg, 2.30 mmol) according to General procedure C. The residue was purified by flash column chromatography (0 → 20% EtOAc in pentane)

yielding the title compound as a yellow oil (305 mg, 0.74 mmol, 32%).

$^1\text{H}$  NMR (400 MHz,  $\text{CDCl}_3$ )  $\delta$  8.67 (s, 1H), 7.15 – 7.07 (m, 2H), 7.06 – 6.99 (m, 2H), 4.73 – 4.29 (m, 2H), 3.01 (d,  $J = 6.8$  Hz, 2H), 2.99 – 2.88 (m, 2H), 2.54 (d,  $J = 6.9$  Hz, 2H), 2.32 (s, 3H), 1.95 – 1.85 (m, 2H), 1.85 – 1.79 (m, 1H), 1.79 – 1.69 (m, 4H), 1.69 – 1.58 (m, 2H), 1.36 (qd,  $J = 12.5, 4.7$  Hz, 2H), 1.29 – 1.09 (m, 3H), 0.99 (qd,  $J = 11.9, 3.4$  Hz, 2H).

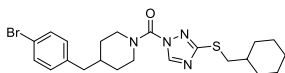
$^{13}\text{C}$  NMR (101 MHz,  $\text{CDCl}_3$ )  $\delta$  163.24, 148.27, 147.30, 136.62, 135.63, 129.06, 128.98, 47.27 (br), 42.43, 38.78, 38.12, 37.82, 32.62, 31.99, 26.30, 26.06, 21.05.

**(4-(4-Chlorobenzyl)piperidin-1-yl)(3-((cyclohexylmethyl)thio)-1H-1,2,4-triazol-1-yl)-methanone (54)**

**36** (17 mg, 0.086 mmol) was reacted with **102** (1.1 eq, 20 mg, 0.095 mmol) according to General procedure C. The residue was purified by flash column chromatography (0 → 30% EtOAc in pentane) yielding the title compound as a white gum (29 mg, 0.067 mmol, 78%).

<sup>1</sup>H NMR (400 MHz, CDCl<sub>3</sub>) δ 8.67 (s, 1H), 7.30 – 7.22 (m, 2H), 7.11 – 7.03 (m, 2H), 4.85 – 4.27 (m, 2H), 3.02 (d, *J* = 6.9 Hz, 2H), 2.99 – 2.89 (m, 2H), 2.56 (d, *J* = 7.0 Hz, 2H), 1.94 – 1.86 (m, 2H), 1.86 – 1.76 (m, 1H), 1.81 – 1.70 (m, 6H), 1.69 – 1.57 (m, 1H), 1.35 (qd, *J* = 12.5, 4.1 Hz, 2H), 1.24 – 1.08 (m, 2H), 1.00 (qd, *J* = 12.0, 3.4 Hz, 2H).

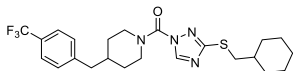
<sup>13</sup>C NMR (101 MHz, CDCl<sub>3</sub>) δ 163.40, 148.36, 147.39, 138.22, 132.08, 130.48, 128.61, 42.28, 38.87, 38.08, 37.90, 32.71, 31.98, 29.82, 26.37, 26.13.

**(4-(4-Bromobenzyl)piperidin-1-yl)(3-((cyclohexylmethyl)thio)-1H-1,2,4-triazol-1-yl)-methanone (55)**

**36** (1.7 eq, 233 mg, 1.18 mmol) was reacted with **93** (1 eq, 200 mg, 0.69 mmol) according to General procedure C. The residue was purified by flash column chromatography (20% EtOAc in pentane) yielding the title compound as a colorless oil (140 mg, 0.29 mmol, 43%).

<sup>1</sup>H NMR (400 MHz, CDCl<sub>3</sub>) δ 8.67 (s, 1H), 7.44 – 7.37 (m, 2H), 7.06 – 6.97 (m, 2H), 4.86 – 4.26 (m, 2H), 3.02 (d, *J* = 6.8 Hz, 2H), 2.99 – 2.88 (m, 2H), 2.54 (d, *J* = 7.0 Hz, 2H), 1.93 – 1.85 (m, 2H), 1.86 – 1.75 (m, 1H), 1.79 – 1.69 (m, 4H), 1.69 – 1.57 (m, 2H), 1.35 (qd, *J* = 13.1, 4.3 Hz, 2H), 1.21 (tdd, *J* = 19.3, 13.7, 10.3 Hz, 3H), 1.00 (qd, *J* = 12.1, 3.4 Hz, 2H).

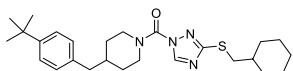
<sup>13</sup>C NMR (101 MHz, CDCl<sub>3</sub>) δ 163.38, 148.33, 147.36, 138.72, 131.54, 130.86, 120.07, 42.31, 38.85, 37.99, 37.88, 32.68, 31.96, 26.35, 26.11.

**(3-((Cyclohexylmethyl)thio)-1H-1,2,4-triazol-1-yl)(4-(4-(trifluoromethyl)benzyl)piperidin-1-yl)methanone (56)**

**36** (1.5 eq, 153 mg, 0.78 mmol) was reacted with **94** (1 eq, 126 mg, 0.52 mmol) according to General procedure C. The residue was purified by flash column chromatography (20% EtOAc in pentane) yielding the title compound as a yellowish oil (150 mg, 0.32 mmol, 62%).

<sup>1</sup>H NMR (400 MHz, CDCl<sub>3</sub>) δ 8.67 (s, 1H), 7.55 (d, *J* = 7.9 Hz, 2H), 7.30 – 7.24 (m, 2H), 4.85 – 4.26 (m, 2H), 3.02 (d, *J* = 6.8 Hz, 2H), 3.00 – 2.89 (m, 2H), 2.65 (d, *J* = 7.2 Hz, 2H), 1.94 – 1.79 (m, 3H), 1.79 – 1.57 (m, 6H), 1.38 (qd, *J* = 12.7, 4.0 Hz, 2H), 1.26 – 1.07 (m, 3H), 1.00 (qd, *J* = 12.0, 3.4 Hz, 2H).

<sup>13</sup>C NMR (101 MHz, CDCl<sub>3</sub>) δ 163.43, 148.34, 147.38, 143.92 (q, *J* = 1.2 Hz), 129.44, 128.95 (q, *J* = 32.3 Hz), 125.42 (q, *J* = 3.8 Hz), 124.36 (q, *J* = 271.7 Hz), 42.73, 38.85, 37.95, 37.89, 32.68, 31.98, 26.34, 26.11.

**(4-(4-(tert-Butyl)benzyl)piperidin-1-yl)(3-((cyclohexylmethyl)thio)-1H-1,2,4-triazol-1-yl)-methanone (57)**

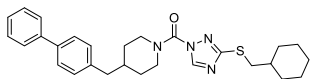
**36** (1.5 eq, 320 mg, 1.62 mmol) was reacted with **96** (1 eq, 250 mg, 1.08 mmol) according to General procedure C. The residue was purified by flash column chromatography (0 → 20% EtOAc in pentane) yielding the title compound as a yellowish oil (132 mg, 0.29 mmol, 27%).

*Analytical data on next page.*

$^1\text{H}$  NMR (400 MHz,  $\text{CDCl}_3$ )  $\delta$  8.67 (s, 1H), 7.35 – 7.26 (m, 2H), 7.11 – 7.03 (m, 2H), 4.69 – 4.33 (m, 2H), 3.73 – 3.45 (m, 2H), 3.02 (d,  $J$  = 6.9 Hz, 2H), 2.99 – 2.89 (m, 2H), 2.55 (d,  $J$  = 7.0 Hz, 2H), 1.95 – 1.86 (m, 2H), 1.86 – 1.77 (m, 2H), 1.77 – 1.69 (m, 2H), 1.69 – 1.57 (m, 2H), 1.37 (qd,  $J$  = 12.4, 3.7 Hz, 2H), 1.31 (s, 9H), 1.25 – 1.09 (m, 2H), 1.00 (qd,  $J$  = 11.9, 3.1 Hz, 2H).

$^{13}\text{C}$  NMR (101 MHz,  $\text{CDCl}_3$ )  $\delta$  163.28, 149.01, 148.33, 147.32, 136.67, 128.79, 125.29, 47.34 (br), 43.66, 42.37, 38.82, 38.05, 37.86, 32.67, 32.06 (br), 31.47, 26.34, 26.10.

**4-([1,1'-Biphenyl]-4-ylmethyl)piperidin-1-yl(3-((cyclohexylmethyl)thio)-1H-1,2,4-triazol-1-yl)methanone (58)**

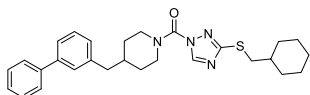


**36** (1 eq, 50 mg, 0.24 mmol) was reacted with **104** (1.2 eq, 79 mg, 0.31 mmol) according to General procedure C. The residue was purified by flash column chromatography (0 → 40%  $\text{Et}_2\text{O}$  in pentane) afforded the title compound (20 mg, 0.042 mmol, 17%).

$^1\text{H}$  NMR (400 MHz,  $\text{CDCl}_3$ )  $\delta$  8.68 (s, 1H), 7.62 – 7.56 (m, 2H), 7.56 – 7.50 (m, 2H), 7.48 – 7.39 (m, 2H), 7.39 – 7.29 (m, 1H), 7.26 – 7.17 (m, 2H), 4.78 – 4.31 (m, 2H), 3.02 (d,  $J$  = 6.8 Hz, 2H), 3.07 – 2.89 (m, 2H), 2.63 (d,  $J$  = 7.0 Hz, 2H), 1.93 – 1.86 (m, 3H), 1.86 – 1.77 (m, 2H), 1.77 – 1.70 (m, 2H), 1.69 – 1.58 (m, 1H), 1.40 (qd,  $J$  = 12.8, 4.2 Hz, 2H), 1.17 (m, 4H), 1.00 (qd,  $J$  = 12.2, 3.0 Hz, 2H).

$^{13}\text{C}$  NMR (101 MHz,  $\text{CDCl}_3$ )  $\delta$  163.37, 148.39, 147.39, 140.99, 139.25, 138.92, 129.61, 128.88, 127.27, 127.20, 127.09, 42.60, 38.88, 38.16, 37.90, 32.71, 32.10, 26.38, 26.14.

**4-([1,1'-Biphenyl]-3-ylmethyl)piperidin-1-yl(3-((cyclohexylmethyl)thio)-1H-1,2,4-triazol-1-yl)methanone (59)**

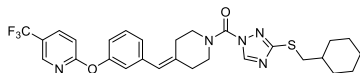


**36** (1.5 eq, 206 mg, 1.04 mmol) was reacted with **97** (1 eq, 175 mg, 0.70 mmol) according to General procedure C. The residue was purified by flash column chromatography (10 → 30%  $\text{EtOAc}$  in pentane) yielding the title compound as a gray oil (280 mg, 0.59 mmol, 85%).

$^1\text{H}$  NMR (400 MHz,  $\text{CDCl}_3$ )  $\delta$  8.67 (s, 1H), 7.61 – 7.54 (m, 2H), 7.48 – 7.39 (m, 3H), 7.38 – 7.30 (m, 2H), 7.18 – 7.13 (m, 1H), 7.13 – 7.08 (m, 1H), 4.76 – 4.29 (m, 2H), 3.01 (d,  $J$  = 6.8 Hz, 2H), 2.98 – 2.87 (m, 2H), 2.63 (d,  $J$  = 7.0 Hz, 2H), 1.92 – 1.82 (m, 3H), 1.82 – 1.74 (m, 2H), 1.74 – 1.67 (m, 2H), 1.68 – 1.57 (m, 2H), 1.38 (qd,  $J$  = 12.6, 4.1 Hz, 2H), 1.28 – 1.08 (m, 3H), 0.98 (qd,  $J$  = 12.0, 3.4 Hz, 2H).

$^{13}\text{C}$  NMR (101 MHz,  $\text{CDCl}_3$ )  $\delta$  163.26, 148.26, 147.30, 141.36, 141.12, 140.24, 128.81, 128.79, 128.04, 127.91, 127.35, 127.16, 125.06, 42.97, 38.76, 38.09, 37.81, 32.60, 32.01, 26.28, 26.04.

**(3-((Cyclohexylmethyl)thio)-1H-1,2,4-triazol-1-yl)(4-(3-((5-(trifluoromethyl)pyridin-2-yl)oxy)-benzylidene)piperidin-1-yl)methanone (60)**

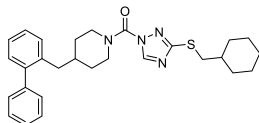


**36** (21 mg, 0.11 mmol) was reacted with **105** (1.3 eq, 46 mg, 0.14 mmol) according to General procedure C. The residue was purified by flash column chromatography (10 → 40%) yielding the title compound as gray oil (38 mg, 0.068 mmol, 64%).

$^1\text{H}$  NMR (400 MHz,  $\text{CDCl}_3$ )  $\delta$  8.71 (s, 1H), 8.44 (m, 1H), 7.92 (dd,  $J = 8.7, 2.5$  Hz, 1H), 7.40 (t,  $J = 7.9$  Hz, 1H), 7.14 – 7.07 (m, 1H), 7.07 – 6.97 (m, 3H), 6.44 (s, 1H), 4.11 – 3.54 (m, 4H), 3.03 (d,  $J = 6.8$  Hz, 2H), 2.71 – 2.63 (m, 2H), 2.52 (t,  $J = 5.9$  Hz, 2H), 1.94 – 1.82 (m, 2H), 1.73 (dt,  $J = 11.7, 3.0$  Hz, 2H), 1.71 – 1.58 (m, 2H), 1.34 – 1.17 (m, 2H), 1.21 – 1.10 (m, 1H), 1.00 (qd,  $J = 11.9, 3.3$  Hz, 2H).

$^{13}\text{C}$  NMR (101 MHz,  $\text{CDCl}_3$ )  $\delta$  165.80, 163.61, 153.16, 148.36, 147.47, 145.59 (q,  $J = 4.5$  Hz), 138.96, 137.51, 136.86 (q,  $J = 3.2$  Hz), 129.74, 126.17, 125.08, 121.93 (q,  $J = 87.1$  Hz), 121.91, 119.79, 111.56, 38.85, 37.90, 32.70, 26.34, 26.11.

**(4-([1,1'-Biphenyl]-2-ylmethyl)piperidin-1-yl)(3-((cyclohexylmethyl)thio)-1H-1,2,4-triazol-1-yl)methanone (61)**

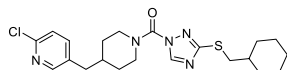


**36** (1.5 eq, 206 mg, 1.04 mmol) was reacted with **98** (1 eq, 175 mg, 0.70 mmol) according to General procedure C. The residue was purified by flash column chromatography (10 → 30% EtOAc in pentane) yielding the title compound as a gray oil (220 mg, 0.46 mmol, 67%).

$^1\text{H}$  NMR (400 MHz,  $\text{CDCl}_3$ )  $\delta$  8.63 (s, 1H), 7.44 – 7.37 (m, 2H), 7.37 – 7.32 (m, 1H), 7.32 – 7.23 (m, 5H), 7.23 – 7.19 (m, 1H), 4.58 – 4.19 (m, 2H), 3.00 (d,  $J = 6.7$  Hz, 2H), 2.91 – 2.73 (m, 2H), 2.62 (d,  $J = 7.0$  Hz, 2H), 1.93 – 1.82 (m, 2H), 1.76 – 1.68 (m, 2H), 1.69 – 1.59 (m, 3H), 1.59 – 1.51 (m, 2H), 1.25 – 1.07 (m, 5H), 0.99 (qd,  $J = 12.4, 3.4$  Hz, 2H).

$^{13}\text{C}$  NMR (101 MHz,  $\text{CDCl}_3$ )  $\delta$  163.22, 148.22, 147.31, 142.44, 141.86, 137.27, 130.33, 129.95, 129.32, 128.23, 127.37, 127.00, 126.17, 39.43, 38.79, 37.86, 37.48, 32.66, 31.90 (br), 26.33, 26.09.

**(4-((6-Chloropyridin-3-yl)methyl)piperidin-1-yl)(3-((cyclohexylmethyl)thio)-1H-1,2,4-triazol-1-yl)methanone (62)**

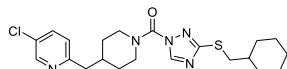


**36** (1.5 eq, 155 mg, 0.78 mmol) was reacted with **99** (1 eq, 110 mg, 0.52 mmol) according to General procedure C. The residue was purified by flash column chromatography (20 → 40% EtOAc in pentane) yielding the title compound as a colorless oil (150 mg, 0.35 mmol, 66%).

$^1\text{H}$  NMR (400 MHz,  $\text{CDCl}_3$ )  $\delta$  8.76 – 8.71 (m, 1H), 8.54 (q,  $J = 2.5$  Hz, 1H), 7.62 (dt,  $J = 8.0, 2.2$  Hz, 1H), 7.12 (dt,  $J = 8.3, 1.8$  Hz, 1H), 4.74 – 4.33 (m, 2H), 3.04 – 2.99 (m, 2H), 3.12 – 2.92 (m, 2H), 2.77 (d,  $J = 7.2$  Hz, 2H), 2.20 – 2.09 (m, 1H), 1.92 – 1.82 (m, 2H), 1.80 – 1.54 (m, 6H), 1.49 – 1.34 (m, 2H), 1.31 – 1.09 (m, 3H), 1.06 – 0.91 (m, 2H).

$^{13}\text{C}$  NMR (101 MHz,  $\text{CDCl}_3$ )  $\delta$  163.13, 156.86, 148.12, 147.56, 147.25, 136.26, 129.84, 124.52, 43.80, 38.67, 37.63, 36.38, 32.46, 31.73 (br), 26.13, 26.11.

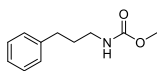
**(4-((5-Chloropyridin-2-yl)methyl)piperidin-1-yl)(3-((cyclohexylmethyl)thio)-1H-1,2,4-triazol-1-yl)methanone (63)**



**36** (1.5 eq, 155 mg, 0.78 mmol) was reacted with **100** (1 eq, 110 mg, 0.52 mmol) according to General procedure C. The residue was purified by flash column chromatography (20 → 40% EtOAc in pentane) yielding the title compound as a colorless oil (175 mg, 0.40 mmol, 77%).

$^1\text{H}$  NMR (400 MHz,  $\text{CDCl}_3$ )  $\delta$  8.74 (d,  $J = 1.8$  Hz, 1H), 8.26 – 8.21 (m, 1H), 7.50 (dt,  $J = 8.2, 2.1$  Hz, 1H), 7.30 (dd,  $J = 8.3, 2.5$  Hz, 1H), 4.73 – 4.44 (m, 2H), 3.02 (d,  $J = 6.9$  Hz, 2H), 3.05 – 2.89 (m, 2H), 2.60 (d,  $J = 7.1$  Hz, 2H), 1.93 – 1.81 (m, 3H), 1.80 – 1.54 (m, 6H), 1.46 – 1.32 (m, 2H), 1.31 – 1.09 (m, 3H), 1.05 – 0.90 (m, 2H).

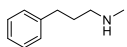
$^{13}\text{C}$  NMR (101 MHz,  $\text{CDCl}_3$ )  $\delta$  163.27, 149.72, 149.29, 148.15, 147.31, 139.59, 134.05, 124.09, 38.91, 38.71, 37.66, 37.51, 32.50, 31.63 (br), 26.14, 26.12.

**Methyl (3-phenylpropyl)carbamate (65)**

To an ice-cold solution of 3-phenylpropylamine (**64**, 84  $\mu\text{L}$ , 0.59 mmol) and DIPEA (2 eq, 206  $\mu\text{L}$ , 1.19 mmol) in DCM (5 mL), methyl chloroformate (1.5 eq, 84  $\mu\text{L}$ , 0.89 mmol) was added. The mixture was allowed to warm to RT and stirred for 2 h. After full reaction conversion the mixture was washed with sat. aq.  $\text{NaHCO}_3$  and brine, dried over  $\text{MgSO}_4$ , filtrated and concentrated *in vacuo*. Flash column chromatography (0-30% EtOAc in pentane) afforded the title compound (96 mg, 0.50 mmol, 84%).

$^1\text{H}$  NMR (400 MHz,  $\text{CDCl}_3$ )  $\delta$  7.32 – 7.21 (m, 3H), 7.21 – 7.11 (m, 2H), 4.73 (s, 1H), 3.65 (s, 3H), 3.20 (q,  $J$  = 6.7 Hz, 2H), 2.63 (t,  $J$  = 7.7 Hz, 2H), 1.82 (p,  $J$  = 7.3 Hz, 2H).

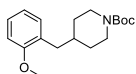
$^{13}\text{C}$  NMR (101 MHz,  $\text{CDCl}_3$ )  $\delta$  157.25, 141.51, 128.54, 128.45, 126.07, 52.10, 40.73, 33.11, 31.71.

**N-methyl-3-phenylpropylamine (66)**

To an ice-cold solution of **65** (96 mg, 0.50 mmol) in dry THF (10 mL),  $\text{LiAlH}_4$  (3 eq, 1.5 mL 1 M in THF, 1.50 mmol) was added dropwise, after which the reaction mixture was heated to reflux for 72 h. The mixture was cooled on ice, diluted with  $\text{Et}_2\text{O}$  and quenched with water and 15% aq.  $\text{NaOH}$ . It was then warmed to RT, dried over  $\text{MgSO}_4$ , filtrated and concentrated *in vacuo*. For flash column chromatography a solution of 10% sat. aq.  $\text{NH}_4\text{OH}$  in MeOH was prepared. Elution with 10% of this solution in DCM afforded the title compound as yellow oil (46 mg, 0.31 mmol, 62%).

$^1\text{H}$  NMR (400 MHz, MeOD)  $\delta$  7.32 – 7.22 (m, 2H), 7.22 – 7.11 (m, 3H), 2.70 – 2.54 (m, 4H), 2.39 (s, 3H), 1.88 – 1.78 (m, 2H).

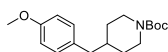
$^{13}\text{C}$  NMR (101 MHz, MeOD)  $\delta$  143.16, 129.41, 129.36, 126.94, 51.89, 35.72, 34.40, 31.74.

**tert-Butyl 4-(2-methoxybenzyl)piperidine-1-carboxylate (79)**

*N*-Boc 4-methylenepiperidine (**67**, 1 eq, 300  $\mu\text{L}$ , 1.48 mmol) was coupled to 2-bromoanisole (**68**, 2 eq, 381  $\mu\text{L}$ , 3.06 mmol) according to General procedure B. Flash column chromatography (2% EtOAc in pentane) afforded the title compound as colorless oil (410 mg, 1.34 mmol, 91%).

$^1\text{H}$  NMR (400 MHz,  $\text{CDCl}_3$ )  $\delta$  7.18 (td,  $J$  = 7.9, 1.8 Hz, 1H), 7.06 (dd,  $J$  = 7.3, 1.8 Hz, 1H), 6.91 – 6.81 (m, 2H), 4.10 – 4.00 (m, 2H), 3.81 (s, 3H), 2.63 (td,  $J$  = 12.9, 2.6 Hz, 2H), 2.54 (d,  $J$  = 7.1 Hz, 2H), 1.78 – 1.62 (m, 1H), 1.63 – 1.55 (m, 2H), 1.45 (s, 9H), 1.16 (qd,  $J$  = 12.3, 4.3 Hz, 2H).

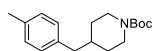
$^{13}\text{C}$  NMR (101 MHz,  $\text{CDCl}_3$ )  $\delta$  157.73, 155.05, 131.05, 128.83, 127.32, 120.25, 110.40, 79.26, 55.36, 44.15, 37.27, 36.69, 32.24, 28.62.

**tert-Butyl 4-(4-methoxybenzyl)piperidine-1-carboxylate (80)**

*N*-Boc 4-methylenepiperidine (**67**, 1.5 eq, 700  $\mu\text{L}$ , 3.44 mmol) was coupled to 4-bromoanisole (**69**, 1 eq, 286  $\mu\text{L}$ , 2.30 mmol) according to General procedure B. Flash column chromatography (2% EtOAc in pentane) afforded the title compound as colorless oil (701 mg, 2.30 mmol, quant.).

$^1\text{H}$  NMR (400 MHz,  $\text{CDCl}_3$ )  $\delta$  7.05 – 6.97 (m, 2H), 6.83 – 6.75 (m, 2H), 4.20 – 3.93 (m, 2H), 3.73 (s, 3H), 2.65 – 2.54 (m, 2H), 2.43 (d,  $J$  = 6.8 Hz, 2H), 1.63 – 1.53 (m, 3H), 1.44 (s, 9H), 1.09 (qd,  $J$  = 12.1, 4.2 Hz, 2H).

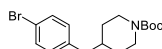
$^{13}\text{C}$  NMR (101 MHz,  $\text{CDCl}_3$ )  $\delta$  157.66, 154.48, 131.87, 129.71, 113.38, 78.77, 54.81, 41.95, 38.06, 31.69, 28.22.

**tert-Butyl 4-(4-methylbenzyl)piperidine-1-carboxylate (81)**

*N*-Boc 4-methylenepiperidine (**67**, 1.3 eq, 700  $\mu$ L, 3.44 mmol) was coupled to 4-iodotoluene (**70**, 1 eq, 293  $\mu$ L, 2.25 mmol) according to General procedure B. Flash column chromatography (2% EtOAc in pentane) afforded the title compound as orange oil (500 mg, 1.73 mmol, 77%).

$^1\text{H}$  NMR (400 MHz,  $\text{CDCl}_3$ )  $\delta$  7.12 – 7.05 (m, 2H), 7.05 – 6.98 (m, 2H), 4.19 – 3.94 (m, 2H), 2.68 – 2.56 (m, 2H), 2.49 (d,  $J$  = 6.8 Hz, 2H), 2.31 (s, 3H), 1.93 – 1.77 (m, 1H), 1.72 – 1.56 (m, 2H), 1.45 (s, 9H), 1.13 (qd,  $J$  = 12.8, 5.9 Hz, 2H).

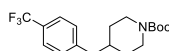
$^{13}\text{C}$  NMR (101 MHz,  $\text{CDCl}_3$ )  $\delta$  154.93, 137.17, 135.40, 129.04, 128.97, 79.25, 42.75, 38.30, 32.11, 28.52, 21.06.

**tert-Butyl 4-(4-bromobenzyl)piperidine-1-carboxylate (82)**

*N*-Boc 4-methylenepiperidine (**67**, 1 eq, 300  $\mu$ L, 1.48 mmol) was coupled to 1-bromo-4-iodobenzene (**71**, 3.3 eq, 2.10 g, 7.42 mmol) according to General procedure B. Flash column chromatography (2% EtOAc in pentane) afforded the title compound as brown wax (230 mg, 0.65 mmol, 44%).

$^1\text{H}$  NMR (400 MHz,  $\text{CDCl}_3$ )  $\delta$  7.41 – 7.37 (m, 2H), 7.03 – 6.98 (m, 2H), 4.07 (dt,  $J$  = 13.7, 3.0 Hz, 2H), 2.62 (td,  $J$  = 13.2, 2.6 Hz, 2H), 2.48 (d,  $J$  = 6.9 Hz, 2H), 1.73 – 1.54 (m, 3H), 1.45 (s, 9H), 1.13 (qd,  $J$  = 12.3, 4.3 Hz, 2H).

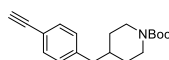
$^{13}\text{C}$  NMR (101 MHz,  $\text{CDCl}_3$ )  $\delta$  154.95, 139.26, 131.42, 130.94, 119.84, 79.41, 44.00 (br), 42.61, 38.17, 31.98, 28.57.

**tert-Butyl 4-(4-(trifluoromethyl)benzyl)piperidine-1-carboxylate (83)**

*N*-Boc 4-methylenepiperidine (**67**, 1 eq, 303  $\mu$ L, 1.49 mmol) was coupled to 1-iodo-4-(trifluoromethyl)benzene (**72**, 1.5 eq, 332  $\mu$ L, 2.26 mmol) according to General procedure B. Flash column chromatography (2  $\rightarrow$  5% EtOAc in pentane) afforded the title compound as brown wax (510 mg, 1.49 mmol, quant.).

$^1\text{H}$  NMR (400 MHz,  $\text{CDCl}_3$ )  $\delta$  7.53 (d,  $J$  = 7.9 Hz, 2H), 7.25 (d,  $J$  = 7.9 Hz, 2H), 4.24 – 3.91 (m, 2H), 2.72 – 2.54 (m, 2H), 2.59 (d,  $J$  = 7.2 Hz, 2H), 1.72 – 1.63 (m, 1H), 1.64 – 1.55 (m, 2H), 1.45 (s, 9H), 1.15 (qd,  $J$  = 12.3, 4.3 Hz, 2H).

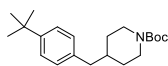
$^{13}\text{C}$  NMR (101 MHz,  $\text{CDCl}_3$ )  $\delta$  154.92, 144.46 (q,  $J$  = 1.5 Hz), 129.47, 128.44 (q,  $J$  = 32.3 Hz), 125.26 (q,  $J$  = 3.8 Hz), 124.42 (q,  $J$  = 271.7 Hz), 79.41, 43.00, 38.10, 31.97, 28.53.

**tert-Butyl 4-(4-ethynylbenzyl)piperidine-1-carboxylate (84)**

*N*-Boc 4-methylenepiperidine (**67**, 1 eq, 300  $\mu$ L, 1.48 mmol) was coupled to 1-bromo-4-ethynylbenzene (**73**, 1.1 eq, 410 mg, 2.27 mmol) according to General procedure B. Flash column chromatography (1  $\rightarrow$  3% EtOAc in pentane) afforded the title compound as colorless oil (95 mg, 0.32 mmol, 22%).

$^1\text{H}$  NMR (400 MHz,  $\text{CDCl}_3$ )  $\delta$  7.43 – 7.37 (m, 2H), 7.11 – 7.05 (m, 2H), 4.17 – 3.96 (m, 2H), 3.04 (s, 1H), 2.62 (td,  $J$  = 12.4, 12.4, 2.8 Hz, 2H), 2.52 (d,  $J$  = 7.0 Hz, 2H), 1.72 – 1.57 (m, 1H), 1.62 – 1.54 (m, 2H), 1.45 (s, 9H), 1.13 (qd,  $J$  = 12.5, 4.3 Hz, 2H).

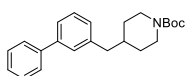
$^{13}\text{C}$  NMR (101 MHz,  $\text{CDCl}_3$ )  $\delta$  154.87, 141.28, 132.08, 129.16, 119.76, 83.71, 79.31, 76.88, 43.97 (br), 43.08, 38.08, 31.97, 28.52.

**tert-Butyl 4-(4-(tert-butyl)benzyl)piperidine-1-carboxylate (85)**

*N*-Boc 4-methylenepiperidine (**67**, 1 eq, 300  $\mu$ L, 1.48 mmol) was coupled to 4-*tert*-butyliodobenzene (**74**, 1.2 eq, 320  $\mu$ L, 1.81 mmol) according to General procedure B. Flash column chromatography (1  $\rightarrow$  2% EtOAc in pentane) afforded the title compound as colorless oil (285 mg, 0.86 mmol, 58%).

$^1\text{H}$  NMR (400 MHz,  $\text{CDCl}_3$ )  $\delta$  7.33 – 7.26 (m, 2H), 7.10 – 7.03 (m, 2H), 4.11 – 4.02 (m, 2H), 2.63 (td,  $J$  = 13.2, 2.5 Hz, 2H), 2.50 (d,  $J$  = 6.8 Hz, 2H), 1.72 – 1.58 (m, 3H), 1.45 (s, 9H), 1.31 (s, 9H), 1.14 (qd,  $J$  = 12.4, 4.4 Hz, 2H).

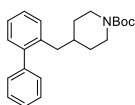
$^{13}\text{C}$  NMR (101 MHz,  $\text{CDCl}_3$ )  $\delta$  155.04, 148.84, 137.28, 128.90, 125.23, 79.33, 44.13, 42.73, 38.24, 34.50, 32.14, 31.55, 28.61.

**tert-Butyl 4-([1,1'-biphenyl]-3-ylmethyl)piperidine-1-carboxylate (86)**

*N*-Boc 4-methylenepiperidine (**67**, 1 eq, 300  $\mu$ L, 1.48 mmol) was coupled to 3-bromo-1,1'-biphenyl (**75**, 1.5 eq, 376  $\mu$ L, 2.25 mmol) according to General procedure B. Flash column chromatography (2  $\rightarrow$  3% EtOAc in pentane) afforded the title compound as yellow oil (450 mg, 1.28 mmol, 87%).

$^1\text{H}$  NMR (400 MHz,  $\text{CDCl}_3$ )  $\delta$  7.58 – 7.51 (m, 2H), 7.42 – 7.34 (m, 3H), 7.34 – 7.32 (m, 1H), 7.32 – 7.23 (m, 2H), 7.10 – 7.02 (m, 1H), 4.19 – 3.92 (m, 2H), 2.65 – 2.49 (m, 2H), 2.53 (d,  $J$  = 7.2 Hz, 2H), 1.70 – 1.55 (m, 3H), 1.44 (s, 9H), 1.17 – 1.04 (m, 2H).

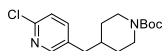
$^{13}\text{C}$  NMR (101 MHz,  $\text{CDCl}_3$ )  $\delta$  154.50, 140.97, 140.95, 140.44, 128.51, 128.46, 127.85, 127.69, 127.01, 126.90, 124.59, 78.83, 43.01, 37.96, 31.79, 28.24.

**tert-Butyl 4-([1,1'-biphenyl]-2-ylmethyl)piperidine-1-carboxylate (87)**

*N*-Boc 4-methylenepiperidine (**67**, 1 eq, 348  $\mu$ L, 1.71 mmol) was coupled to 2-iodo-1,1'-biphenyl (**76**, 1.3 eq, 396  $\mu$ L, 2.25 mmol) according to General procedure B. Flash column chromatography (0  $\rightarrow$  4% EtOAc in pentane) afforded the title compound as colorless oil (600 mg, 1.71 mmol, quant.).

$^1\text{H}$  NMR (400 MHz,  $\text{CDCl}_3$ )  $\delta$  7.40 – 7.33 (m, 2H), 7.32 – 7.28 (m, 1H), 7.28 – 7.21 (m, 4H), 7.21 – 7.12 (m, 2H), 3.97 – 3.92 (m, 2H), 2.54 (d,  $J$  = 6.9 Hz, 2H), 2.51 – 2.44 (m, 2H), 1.89 – 1.79 (m, 1H), 1.56 – 1.44 (m, 2H), 1.41 (s, 9H), 0.92 (qd,  $J$  = 12.4, 4.1 Hz, 2H).

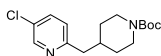
$^{13}\text{C}$  NMR (101 MHz,  $\text{CDCl}_3$ )  $\delta$  154.62, 142.26, 141.84, 137.55, 130.02, 129.81, 129.18, 127.95, 127.08, 126.69, 125.77, 78.95, 41.79, 39.55, 37.54, 31.77, 28.35.

**tert-Butyl 4-((6-chloropyridin-3-yl)methyl)piperidine-1-carboxylate (88)**

*N*-Boc 4-methylenepiperidine (**67**, 1 eq, 315  $\mu$ L, 1.55 mmol) was coupled to 2-chloro-5-iodopyridine (**77**, 1.2 eq, 433 mg, 1.81 mmol) according to General procedure B. Flash column chromatography (5  $\rightarrow$  10% EtOAc in pentane) afforded the title compound as white solid (482 mg, 1.55 mmol, quant.).

$^1\text{H}$  NMR (400 MHz,  $\text{CDCl}_3$ )  $\delta$  8.18 (t,  $J$  = 2.2 Hz, 1H), 7.45 (dd,  $J$  = 8.2, 2.5 Hz, 1H), 7.26 (dd,  $J$  = 8.1, 1.7 Hz, 1H), 4.19 – 3.97 (m, 2H), 2.70 – 2.58 (m, 2H), 2.53 (d,  $J$  = 6.9 Hz, 2H), 1.93 – 1.75 (m, 1H), 1.64 – 1.56 (m, 2H), 1.48 – 1.40 (m, 9H), 1.19 – 1.08 (m, 2H).

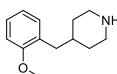
$^{13}\text{C}$  NMR (101 MHz,  $\text{CDCl}_3$ )  $\delta$  154.72, 149.98, 149.17, 139.38, 134.35, 123.85, 79.37, 39.21, 37.78, 31.68, 28.40.

**tert-Butyl 4-((5-chloropyridin-2-yl)methyl)piperidine-1-carboxylate (89)**

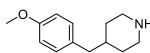
*N*-Boc 4-methylenepiperidine (**68**, 1 eq, 300  $\mu$ L, 1.48 mmol) was coupled to 2-bromo-5-chloropyridine (**78**, 1.5 eq, 439  $\mu$ L, 2.28 mmol) according to General procedure B. Flash column chromatography (0  $\rightarrow$  20% EtOAc in pentane) afforded the title compound as colorless oil (400 mg, 1.29 mmol, 87%).

$^1\text{H}$  NMR (400 MHz, Chloroform-*d*)  $\delta$  8.50 (s, 1H), 7.58 (d,  $J$  = 8.7 Hz, 1H), 7.07 (d,  $J$  = 8.7 Hz, 1H), 4.15 – 4.00 (m, 2H), 2.68 (d,  $J$  = 6.4 Hz, 2H), 2.00 – 1.86 (m, 1H), 1.59 (d,  $J$  = 13.1 Hz, 2H), 1.45 (s, 9H), 1.26 – 1.13 (m, 2H).

$^{13}\text{C}$  NMR (101 MHz,  $\text{CDCl}_3$ )  $\delta$  158.33, 154.72, 148.05, 135.87, 129.47, 124.34, 79.15, 43.29, 42.39, 36.68, 31.81, 28.38.

**4-(2-Methoxybenzyl)piperidine (90)**

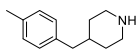
**79** (410 mg, 1.34 mmol) was dissolved in 1,4-dioxane containing 4 M HCl (10 mL) and the mixture was stirred for 16 h. All volatiles were removed *in vacuo*. The residue was dissolved in 5 M aq. KOH and extracted with DCM and  $\text{CHCl}_3$ . The combined organic layers were concentrated *in vacuo*, affording the title compound as yellowish wax (275 mg, 1.34 mmol, quant.), which was used immediately in the next reaction.

**4-(4-Methoxybenzyl)piperidine (91)**

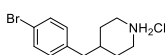
**80** (273 mg, 0.89 mmol) was dissolved in 1,4-dioxane containing 4 M HCl (5 mL) and the mixture was stirred for 18 h. All volatiles were removed *in vacuo*. The residue was dissolved in 5 M aq. KOH and extracted with DCM. The combined organic layers were concentrated *in vacuo*, affording the title compound as yellow wax (183 mg, 0.89 mmol, quant.).

$^1\text{H}$  NMR (400 MHz, MeOD)  $\delta$  7.09 – 7.00 (m, 2H), 6.86 – 6.77 (m, 2H), 3.76 (s, 3H), 3.11 – 3.02 (m, 2H), 2.58 (td,  $J$  = 12.5, 2.5 Hz, 2H), 2.48 (d,  $J$  = 6.8 Hz, 2H), 1.73 – 1.65 (m, 2H), 1.65 – 1.55 (m, 1H), 1.26 – 1.12 (m, 2H).

$^{13}\text{C}$  NMR (101 MHz, MeOD)  $\delta$  158.75, 132.80, 130.65, 114.30, 55.55, 46.31, 43.07, 38.52, 32.48.

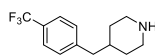
**4-(4-Methylbenzyl)piperidine (92)**

**81** (500 mg, 1.73 mmol) was dissolved in 1,4-dioxane containing 4 M HCl (5 mL) and the mixture was stirred for 16 h. All volatiles were removed *in vacuo*. The residue was dissolved in 5 M aq. KOH and extracted with DCM. The combined organic layers were concentrated *in vacuo*, affording the title compound as orange oil (327 mg, 1.73 mmol, quant.), which was used immediately in the next reaction.

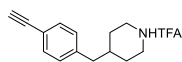
**4-(4-Bromobenzyl)piperidin-1-ium chloride (93)**

**82** (230 mg, 0.65 mmol) was dissolved in 1,4-dioxane containing 4 M HCl (5 mL) and the mixture was stirred for 3 h. All volatiles were removed *in vacuo*. The resulting off-white solid was used immediately in the next reaction.

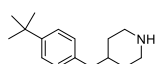


**4-(4-(Trifluoromethyl)benzyl)piperidine (94)**

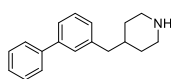
**83** (250 mg, 0.73 mmol) was dissolved in 1,4-dioxane (8 mL). To this HCl (20 eq, 3.64 mL 4 M in 1,4-dioxane) was added and the mixture was stirred for 28 h. All volatiles were removed *in vacuo*. The resulting off-white solid was dissolved in EtOAc and extracted with 1 M aq. HCl. The pH of the aqueous layer was set to 14 with 5 M aq. NaOH, after which the aqueous layer was extracted with EtOAc. The combined organic layers were dried over MgSO<sub>4</sub>, filtrated and concentrated *in vacuo*, affording the title compound as off-white oil (126 mg, 0.52 mmol, 71%), which was used immediately in the next reaction.

**4-(4-Ethynylbenzyl)piperidin-1-ium 2,2,2-trifluoroacetate (95)**

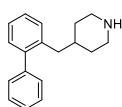
**84** (20 mg, 0.067 mmol) was dissolved in dry DCM (2 mL) and cooled on ice. TFA (10 eq, 51 μL, 0.67 mmol) was added dropwise, after which the mixture was allowed to warm to RT and stirred overnight. When TLC showed full conversion all volatiles were removed *in vacuo*. The residue was used immediately in the next reaction

**4-(4-(tert-Butyl)benzyl)piperidine (96)**

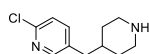
**85** (270 mg, 0.81 mmol) was dissolved in 1,4-dioxane (8 mL). To this HCl (10 eq, 2.0 mL 4 M in 1,4-dioxane, 8.1 mmol) was added and the mixture was stirred for 5 h. All volatiles were removed *in vacuo*. CHCl<sub>3</sub> (5 mL) and 5 M aq. KOH (5 mL) were added to the resulting white solid and the layers were separated. The aqueous layer was extracted with CHCl<sub>3</sub>. The combined organic layers were concentrated *in vacuo*, affording the title compound as yellow oil (188 mg, 0.76 mmol, 93%), which was used immediately in the next reaction.

**4-([1,1'-Biphenyl]-3-ylmethyl)piperidine (97)**

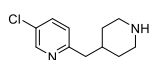
**86** (450 mg, 1.28 mmol) was dissolved in 1,4-dioxane containing 4 M HCl (5 mL) and the mixture was stirred for 21 h. All volatiles were removed *in vacuo*. The residue was dissolved in 1 M aq. HCl and washed with CHCl<sub>3</sub>. The pH of the aqueous layer was set to 14 with 5 M aq. KOH, after which the aqueous layer was extracted with CHCl<sub>3</sub>. The combined organic layers were concentrated *in vacuo*, affording the title compound as yellow oil (247 mg, 0.98 mmol, 77%), which was used immediately in the next reaction.

**4-([1,1'-Biphenyl]-2-ylmethyl)piperidine (98)**

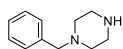
**87** (600 mg, 1.71 mmol) was dissolved in 1,4-dioxane containing 4 M HCl (5 mL) and the mixture was stirred for 16 h. All volatiles were removed *in vacuo*. The residue was dissolved in 1 M aq. HCl and washed with CHCl<sub>3</sub>. The pH of the aqueous layer was set to 14 with 5 M aq. KOH, after which the aqueous layer was extracted with CHCl<sub>3</sub>. The combined organic layers were concentrated *in vacuo*, affording the title compound as yellow oil (350 mg, 1.39 mmol, 82%), which was used immediately in the next reaction.

**2-Chloro-5-(piperidin-4-ylmethyl)pyridine (99)**

**88** (482 mg, 1.55 mmol) was dissolved in 1,4-dioxane containing 4 M HCl (5 mL) and the mixture was stirred for 21 h. All volatiles were removed *in vacuo*. The residue was dissolved in 1 M aq. HCl and washed with CHCl<sub>3</sub>. The pH of the aqueous layer was set to 14 with 5 M aq. KOH, after which the aqueous layer was extracted with CHCl<sub>3</sub>. The combined organic layers were concentrated *in vacuo*, affording the title compound as yellow oil (247 mg, 1.17 mmol, 76%), which was used immediately in the next reaction.

**5-Chloro-2-(piperidin-4-ylmethyl)pyridine (100)**

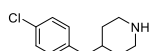
**89** (279 mg, 0.90 mmol) was dissolved in 1,4-dioxane containing 4 M HCl (5 mL) and the mixture was stirred for 16 h. All volatiles were removed *in vacuo*. The residue was dissolved in 1 M aq. HCl and washed with CHCl<sub>3</sub>. The pH of the aqueous layer was set to 14 with 5 M aq. KOH, after which the aqueous layer was extracted with CHCl<sub>3</sub>. The combined organic layers were concentrated *in vacuo*, affording the title compound as colorless oil (190 mg, 0.90 mmol, quant.), which was used immediately in the next reaction.

**1-Benzylpiperazine (101)**

Piperazine (6 eq, 500 mg, 5.80 mmol) was dissolved in dry THF (10 mL) and heated to reflux. To this benzyl chloride (1 eq, 0.11 mL, 0.97 mmol) was added dropwise, leading to formation of white precipitate. After refluxing for 2.5 h full conversion was confirmed using TLC and the mixture was cooled and filtrated. Solids were washed with THF (5 mL) and EtOAc (5 mL) after which the combined filtrates were concentrated *in vacuo*. The resulting white crystalline solid was suspended in 8 mL 1 M aq. KOH + 5% brine and extracted with DCM and EtOAc until the aqueous layer was clear. The combined organic layers were dried over MgSO<sub>4</sub>, filtrated and concentrated *in vacuo*. For flash column chromatography a 10% sat. aq. NH<sub>4</sub>OH solution in MeOH was used. Elution with 0 → 20% of this solution in EtOAc afforded the title compound as colorless oil (145 mg, 0.82 mmol, 85%).

<sup>1</sup>H NMR (400 MHz, MeOD) δ 7.35 – 7.26 (m, 4H), 7.29 – 7.22 (m, 1H), 3.47 (s, 2H), 2.80 (app. t, *J* = 5.0 Hz, 4H), 2.53 – 2.29 (m, 4H).

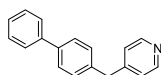
<sup>13</sup>C NMR (101 MHz, MeOD) δ 138.35, 130.63, 129.30, 128.38, 64.48, 54.59, 46.08.

**4-(4-Chlorobenzyl)piperidine (102)**

4-(4-Chlorobenzyl)pyridine (1 eq, 1.71 mL, 9.82 mmol), PtO<sub>2</sub> (0.04 eq, 89 mg, 0.39 mmol) and hydrochloric acid (1 eq, 818 μL 12 M, 9.82 mmol) were added to EtOH (30 mL) and shaken for 24 h under 3 bar H<sub>2</sub> in a Parr reaction vessel. Catalyst was removed by filtration and volatiles under reduced pressure. Flash column chromatography (5 → 15% 7 M methanolic ammonia in EtOAc) afforded the title compound as yellow oil (1.79 g, 8.53 mmol, 87%).

<sup>1</sup>H NMR (400 MHz, CDCl<sub>3</sub>) δ 7.27 – 7.19 (m, 2H), 7.10 – 7.02 (m, 2H), 3.03 (dt, *J* = 12.6, 3.0 Hz, 2H), 2.54 (td, *J* = 12.3, 2.1 Hz, 2H), 2.49 (d, *J* = 6.5 Hz, 2H), 1.66 (bs, 1H), 1.64 – 1.55 (m, 2H), 1.58 – 1.51 (m, 1H), 1.13 (qd, *J* = 13.8, 13.3, 3.8 Hz, 2H).

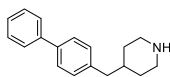
<sup>13</sup>C NMR (101 MHz, CDCl<sub>3</sub>) δ 139.09, 131.58, 130.55, 128.31, 46.80, 43.22, 38.48, 33.44.

**4-([1,1'-Biphenyl]-4-ylmethyl)pyridine (103)**

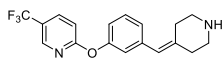
In a MW vial, a solution of 4-(4-chlorobenzyl)pyridine (1 eq, 172 μL, 0.97 mmol) in dry 1,4-dioxane (1.5 mL) was purged with N<sub>2</sub>, to which then CsCO<sub>3</sub> (1.7 eq, 550 mg, 1.69 mmol), phenylboronic acid (1.6 eq, 193 mg, 1.58 mmol), Pd<sub>2</sub>(dba)<sub>3</sub> (0.04 eq, 34 mg, 0.037 mmol) and tricyclohexylphosphane (0.09 eq, 24 mg, 0.086 mmol) were sequentially added. The vial was sealed and heated to 100°C overnight. When product formation was confirmed with LC/MS analysis, the mixture was cooled to RT and diluted with EtOAc. Catalyst was removed by filtration and volatiles under reduced pressure. Flash column chromatography (30 → 60% Et<sub>2</sub>O in pentane) afforded the title compound (140 mg, 0.57 mmol, 59%).

<sup>1</sup>H NMR (400 MHz, CDCl<sub>3</sub>) δ 8.54 – 8.48 (m, 2H), 7.60 – 7.48 (m, 4H), 7.47 – 7.38 (m, 2H), 7.37 – 7.29 (m, 1H), 7.27 – 7.19 (m, 2H), 7.16 – 7.10 (m, 2H), 3.99 (s, 2H).

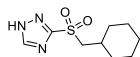
<sup>13</sup>C NMR (101 MHz, CDCl<sub>3</sub>) δ 167.86, 150.04, 149.93, 140.76, 139.73, 138.00, 129.54, 128.87, 127.53, 127.37, 127.10, 124.31, 40.94.

**4-([1,1'-Biphenyl]-4-ylmethyl)piperidine (104)**

A solution of **103** (1 eq, 89 mg, 0.36 mmol) in EtOH (3 mL) was purged with N<sub>2</sub>, to which then PtO<sub>2</sub> (0.05 eq, 4 mg, 0.018 mmol) and hydrochloric acid (1 eq, 30 μL 12 M, 0.36 mmol) were added. The mixture was then purged with H<sub>2</sub> (1 atm) and stirred for 24 h. Catalyst was removed by filtration and volatiles under reduced pressure, affording the title compound which was used immediately in the next reaction.

**2-(3-(Piperidin-4-ylidenemethyl)phenoxy)-5-(trifluoromethyl)pyridine (105)**

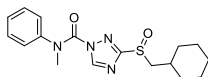
To a solution of *tert*-butyl 4-(3-((5-(trifluoromethyl)pyridin-2-yl)oxy)benzylidene)piperidine-1-carboxylate<sup>58</sup> (98 mg, 0.23 mmol) in 1.5 mL EtOAc, hydrochloric acid (30 eq, 572 μL 12 M, 6.86 mmol) was added dropwise and the mixture was stirred for two days. When TLC analysis showed full conversion the mixture was washed with sat. aq. NaHCO<sub>3</sub> followed by extraction with DCM. The combined organic layers were dried over MgSO<sub>4</sub>, filtrated and concentrated *in vacuo* to afford the title compound which was used immediately in the next reaction.

**3-((Cyclohexylmethyl)sulfonyl)-1H-1,2,4-triazole (106)**

**36** (1.20 g, 6.08 mmol) was dissolved in 20 mL dry DCM and cooled on ice. Peracetic acid (5 eq, 30 mmol, 5.8 mL 35% in AcOH) was added dropwise, after which the mixture was allowed to warm to RT and stirred for 72 h. The mixture was diluted with DCM and washed with water. The aqueous layer was extracted with CHCl<sub>3</sub> with a little MeOH, after which the combined organic layers were dried over MgSO<sub>4</sub>, filtrated and concentrated *in vacuo*. Flash column chromatography (0 → 6% MeOH in DCM) afforded the title compound as white crystalline solid (1.08 g, 4.72 mmol, 78%).

<sup>1</sup>H NMR (400 MHz, MeOD) δ 8.70 (s, 1H), 3.31 (d, *J* = 6.1 Hz, 2H), 2.02 – 1.87 (m, 1H), 1.90 – 1.79 (m, 2H), 1.75 – 1.58 (m, 3H), 1.36 – 1.12 (m, 3H), 1.11 (qd, *J* = 11.8, 3.4 Hz, 2H).

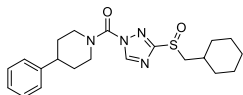
<sup>13</sup>C NMR (101 MHz, MeOD) δ 162.97, 146.97, 61.81, 33.98, 33.82, 26.83.

**3-((Cyclohexylmethyl)sulfinyl)-*N*-methyl-*N*-phenyl-1H-1,2,4-triazole-1-carboxamide (107)**

**40** (53 mg, 0.16 mmol) was oxidized according to General procedure D. Flash column chromatography (0 → 50% EtOAc in pentane) afforded the title compound as gray gum (42 mg, 0.12 mmol, 76%).

<sup>1</sup>H NMR (300 MHz, CDCl<sub>3</sub>) δ 8.74 (s, 1H), 7.44 – 7.26 (m, 3H), 7.19 – 7.10 (m, 2H), 3.56 (s, 3H), 2.99 – 2.84 (m, 1H), 2.65 – 2.50 (m, 1H), 1.98 – 1.87 (m, 2H), 1.87 – 1.77 (m, 1H), 1.77 – 1.69 (m, 2H), 1.38 – 1.13 (m, 4H), 1.12 – 0.87 (m, 2H).

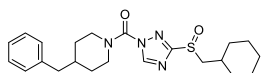
<sup>13</sup>C NMR (75 MHz, CDCl<sub>3</sub>) δ 166.23, 148.06, 147.35, 142.62, 129.72, 128.11, 126.10, 61.01, 40.60, 32.24, 32.01, 25.92, 25.81.

**(3-((Cyclohexylmethyl)sulfinyl)-1H-1,2,4-triazol-1-yl)(4-phenylpiperidin-1-yl)methanone (108)**

**49** (38 mg, 0.099 mmol) was oxidized according General procedure D. Flash column chromatography (0 → 50% EtOAc in pentane) afforded the title compound as white powder (33 mg, 0.082 mmol, 83%).

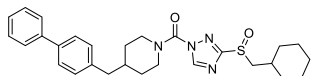
<sup>1</sup>H NMR (300 MHz, CDCl<sub>3</sub>) δ 8.89 (s, 1H), 7.41 – 7.29 (m, 2H), 7.28 – 7.18 (m, 3H), 4.87 – 4.43 (m, 2H), 3.30 (dd, *J* = 13.0, 5.1 Hz, 1H), 3.37 – 3.05 (m, 2H), 2.99 (dd, *J* = 13.0, 8.7 Hz, 1H), 2.84 (tt, *J* = 12.1, 3.9 Hz, 1H), 2.11 – 1.64 (m, 9H), 1.46 – 1.03 (m, 6H).

<sup>13</sup>C NMR (75 MHz, CDCl<sub>3</sub>) δ 166.72, 148.29, 147.75, 144.48, 128.79, 126.86, 126.80, 61.33, 47.22 (br), 42.41, 33.37, 32.60, 32.27, 29.78, 26.02, 25.97, 25.69.

**(4-Benzylpiperidin-1-yl)(3-((cyclohexylmethyl)sulfinyl)-1H-1,2,4-triazol-1-yl)methanone (109)**

**50** (51 mg, 0.128 mmol) was oxidized according General procedure D. Flash column chromatography (0 → 50% EtOAc in pentane) afforded the title compound as gray gum (42 mg, 0.101 mmol, 79%).

$^1\text{H}$  NMR (500 MHz,  $\text{CDCl}_3$ )  $\delta$  8.84 (s, 1H), 7.34 – 7.26 (m, 2H), 7.25 – 7.18 (m, 1H), 7.17 – 7.11 (m, 2H), 4.64 – 4.30 (m, 2H), 3.28 (dd,  $J$  = 13.1, 5.2 Hz, 1H), 2.97 (dd,  $J$  = 13.0, 8.8 Hz, 1H), 3.16 – 2.89 (m, 1H), 2.59 (d,  $J$  = 7.1 Hz, 2H), 2.08 – 2.01 (m, 2H), 2.01 – 1.92 (m, 1H), 1.91 – 1.64 (m, 7H), 1.45 – 1.06 (m, 7H).  $^{13}\text{C}$  NMR (126 MHz,  $\text{CDCl}_3$ )  $\delta$  166.56, 148.15, 147.62, 139.57, 129.12, 128.45, 126.27, 61.30, 46.38 (br), 42.75, 37.93, 33.32, 32.55, 32.22, 25.99, 25.93, 25.65.

**(4-([1,1'-Biphenyl]-4-ylmethyl)piperidin-1-yl)(3-((cyclohexylmethyl)sulfinyl)-1H-1,2,4-triazol-1-yl)methanone (110)**

**58** (20 mg, 0.042 mmol) was oxidized according to General procedure D. Flash column chromatography (40 → 60% EtOAc in pentane) afforded the title compound as white powder (17 mg,

0.035 mmol, 82%).

$^1\text{H}$  NMR (500 MHz,  $\text{CDCl}_3$ )  $\delta$  8.85 (s, 1H), 7.61 – 7.56 (m, 2H), 7.56 – 7.50 (m, 2H), 7.47 – 7.40 (m, 2H), 7.34 (tt,  $J$  = 6.8, 1.2 Hz, 1H), 7.25 – 7.19 (m, 2H), 4.65 – 4.35 (m, 2H), 3.28 (app. dd,  $J$  = 13.0, 5.2 Hz, 1H), 3.17 – 2.90 (m, 2H), 2.97 (app. dd,  $J$  = 13.0, 8.8 Hz, 1H), 2.64 (d,  $J$  = 6.9 Hz, 2H), 2.09 – 2.01 (m, 1H), 2.01 – 1.93 (m, 1H), 1.92 – 1.79 (m, 3H), 1.78 – 1.64 (m, 2H), 1.48 – 1.36 (m, 2H), 1.36 – 1.20 (m, 4H), 1.21 – 1.06 (m, 3H).

$^{13}\text{C}$  NMR (126 MHz,  $\text{CDCl}_3$ )  $\delta$  166.64, 147.72, 140.99, 139.33, 138.74, 129.63, 128.89, 127.29, 127.25, 127.11, 61.40, 42.46, 38.03, 33.41, 32.62, 32.29, 26.06, 26.01, 25.73.

## References

1. Leslie, C. C. Cytosolic phospholipase A<sub>2</sub>: Physiological function and role in disease. *J. Lipid Res.* **56**, 1386–1402 (2015).
2. Ghosh, M., Tucker, D. E., Burchett, S. A. & Leslie, C. C. Properties of the Group IV phospholipase A<sub>2</sub> family. *Prog. Lipid Res.* **45**, 487–510 (2006).
3. Murakami, M. *et al.* Recent progress in phospholipase A<sub>2</sub> research: From cells to animals to humans. *Prog. Lipid Res.* **50**, 152–192 (2011).
4. Leslie, C. C. Regulation of arachidonic acid availability for eicosanoid production. *Biochem. Cell Biol.* **82**, 1–17 (2004).
5. Linkous, A. & Yazlovitskaya, E. Cytosolic phospholipase A<sub>2</sub> as a mediator of disease pathogenesis. *Cell. Microbiol.* **12**, 1369–1377 (2010).
6. Rubin, B. B. *et al.* Cytosolic phospholipase A<sub>2</sub>- $\alpha$  is necessary for platelet-activating factor biosynthesis, efficient neutrophil-mediated bacterial killing, and the innate immune response to pulmonary infection: cPLA<sub>2</sub>- $\alpha$  does not regulate neutrophil NADPH oxidase activity. *J. Biol. Chem.* **280**, 7519–7529 (2005).
7. Ogura, Y., Parsons, W. H., Kamat, S. S. & Cravatt, B. F. A calcium-dependent acyltransferase that produces *N*-Acyl phosphatidylethanolamines. *Nat. Chem. Biol.* **12**, 669–671 (2016).
8. Hussain, Z. *et al.* Phosphatidylserine-stimulated production of *N*-acyl-phosphatidylethanolamines by Ca<sup>2+</sup>-dependent *N*-acyltransferase. *Biochim. Biophys. Acta - Mol. Cell Biol. Lipids* **1863**, 493–502 (2018).
9. Ohto, T., Uozumi, N., Hirabayashi, T. & Shimizu, T. Identification of novel cytosolic phospholipase A<sub>2</sub>s, murine cPLA<sub>2</sub> $\delta$ ,  $\epsilon$ , and  $\zeta$ , which form a gene cluster with cPLA<sub>2</sub> $\beta$ . *J. Biol. Chem.* **280**, 24576–24583 (2005).
10. Prunonosa Cervera, I., Gabriel, B. M., Aldiss, P. & Morton, N. M. The phospholipase A<sub>2</sub> family's role in metabolic diseases: Focus on skeletal muscle. *Physiol. Rep.* **9**, (2021).
11. Schievella, A. R., Regier, M. K., Smith, W. L. & Lin, L. L. Calcium-mediated translocation of cytosolic phospholipase A<sub>2</sub> to the nuclear envelope and endoplasmic reticulum. *J. Biol. Chem.* **270**, 30749–30754 (1995).
12. Glover, S., Bayburt, T., Jonas, M., Chi, E. & Gelb, M. H. Translocation of the 85-kDa phospholipase A<sub>2</sub> from cytosol to the nuclear envelope in rat basophilic leukemia cells stimulated with calcium ionophore or IgE/antigen. *J. Biol. Chem.* **270**, 15359–15367 (1995).
13. Evans, J. H., Spencer, D. M., Zweifach, A. & Leslie, C. C. Intracellular Calcium Signals Regulating Cytosolic Phospholipase A<sub>2</sub> Translocation to Internal Membranes. *J. Biol. Chem.* **276**, 30150–30160 (2001).
14. Binte Mustafiz, S. S. *et al.* The role of intracellular anionic phospholipids in the production of *N*-acyl-phosphatidylethanolamines by cytosolic phospholipase A<sub>2</sub> $\epsilon$ . *J. Biochem.* **165**, 343–352 (2019).
15. Capestrano, M. *et al.* Cytosolic phospholipase A<sub>2</sub> $\epsilon$  drives recycling through the clathrin-independent endocytic route. *J. Cell Sci.* **127**, 977–993 (2014).
16. Dessen, A. *et al.* Crystal structure of human cytosolic phospholipase A<sub>2</sub> reveals a novel topology and catalytic mechanism. *Cell* **97**, 349–360 (1999).
17. Swamy, M. J., Tarafdar, P. K. & Kamlekar, R. K. Structure, phase behaviour and membrane interactions of *N*-acylethanolamines and *N*-acylphosphatidylethanolamines. *Chem. Phys. Lipids* **163**, 266–279 (2010).

18. Domingo, J. C., Mora, M. & Africa de Madariaga, M. Incorporation of *N*-acylethanolamine phospholipids into egg phosphatidylcholine vesicles: characterization and permeability properties of the binary systems. *Biochim. Biophys. Acta - Biomembr.* **1148**, 308–316 (1993).
19. Térová, B., Petersen, G., Hansen, H. S. & Slotte, J. P. *N*-acyl phosphatidylethanolamines affect the lateral distribution of cholesterol in membranes. *Biochim. Biophys. Acta - Biomembr.* **1715**, 49–56 (2005).
20. Shangquan, T., Pak, C. C., Ali, S., Janoff, A. S. & Meers, P. Cation-dependent fusogenicity of an *N*-acyl phosphatidylethanolamine. *Biochim. Biophys. Acta* **1368**, 171–183 (1998).
21. Palese, F., Pontis, S., Realini, N. & Piomelli, D. NAPE-specific phospholipase D regulates LRRK2 association with neuronal membranes. in *Advances in Pharmacology* **90**, 217–238 (Academic Press Inc., 2021).
22. Gillum, M. P. *et al.* *N*-acylphosphatidylethanolamine, a Gut-Derived Circulating Factor Induced by Fat Ingestion, Inhibits Food Intake. *Cell* **135**, 813–824 (2008).
23. Romano, A., Tempesta, B., Provensi, G., Passani, M. B. & Gaetani, S. Central mechanisms mediating the hypophagic effects of oleoylethanolamide and *N*-acylphosphatidylethanolamines: Different lipid signals? *Front. Pharmacol.* **6**, 1–8 (2015).
24. Shiratsuchi, A. *et al.* Inhibitory effect of *N*-palmitoylphosphatidylethanolamine on macrophage phagocytosis through inhibition of Rac1 and Cdc42. *J. Biochem.* **145**, 43–50 (2008).
25. Epps, D. E., Natarajan, V., Schmid, P. C. & Schmid, H. H. O. Accumulation of *N*-acylethanolamine glycerophospholipids in infarcted myocardium. *Biochim. Biophys. Acta - Lipids Lipid Metab.* **618**, 420–430 (1980).
26. Kondo, S. *et al.* Accumulation of various *N*-acylethanolamines including *N*-arachidonylethanolamine (anandamide) in cadmium chloride-administered rat testis. *Arch. Biochem. Biophys.* **354**, 303–310 (1998).
27. Hansen, H. H., Ikonomidou, C., Bittigau, P., Hansen, S. H. & Hansen, H. S. Accumulation of the anandamide precursor and other *N*-acylethanolamine phospholipids in infant rat models of *in vivo* necrotic and apoptotic neuronal death. *J. Neurochem.* **76**, 39–46 (2001).
28. Natarajan, V., Schmid, P. C. & Schmid, H. H. O. *N*-Acylethanolamine phospholipid metabolism in normal and ischemic rat brain. *Biochim. Biophys. Acta - Lipids Lipid Metab.* **878**, 32–41 (1986).
29. Hansen, H. S., Moesgaard, B., Hansen, H. H., Schousboe, A. & Petersen, G. Formation of *N*-acylphosphatidylethanolamine and *N*-acylethanolamine (including anandamide) during glutamate-induced neurotoxicity. *Lipids* **34**, S327–S330 (1999).
30. Moesgaard, B., Petersen, G., Jaroszewski, J. W. & Hansen, H. S. Age dependent accumulation of *N*-acyl-ethanolamine phospholipids in ischemic rat brain: A <sup>31</sup>P NMR and enzyme activity study. *J. Lipid Res.* **41**, 985–990 (2000).
31. Palese, F., Pontis, S., Realini, N. & Piomelli, D. A protective role for *N*-acylphosphatidylethanolamine phospholipase D in 6-OHDA-induced neurodegeneration. *Sci. Rep.* **9**, 1–16 (2019).
32. Okamoto, Y., Morishita, J., Tsuboi, K., Tonai, T. & Ueda, N. Molecular Characterization of a Phospholipase D Generating Anandamide and Its Congeners. *J. Biol. Chem.* **279**, 5298–5305 (2004).
33. Tsuboi, K. *et al.* Enzymatic formation of *N*-acylethanolamines from *N*-acylethanolamine plasmalogen through *N*-acylphosphatidylethanolamine-hydrolyzing phospholipase D-dependent and -independent pathways. *Biochim. Biophys. Acta - Mol. Cell Biol. Lipids* **1811**, 565–577 (2011).

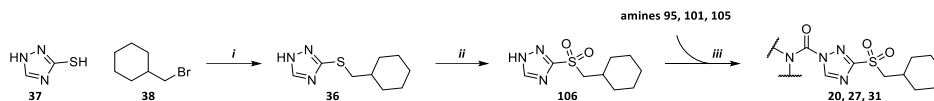
34. Leung, D., Saghatelian, A., Simon, G. M. & Cravatt, B. F. Inactivation of *N*-Acyl phosphatidylethanolamine phospholipase D reveals multiple mechanisms for the biosynthesis of endocannabinoids. *Biochemistry* **45**, 4720–4726 (2006).
35. Sun, Y. X. *et al.* Biosynthesis of anandamide and *N*-palmitoylethanolamine by sequential actions of phospholipase A2 and lysophospholipase D. *Biochem. J.* **380**, 749–756 (2004).
36. Simon, G. M. & Cravatt, B. F. Endocannabinoid biosynthesis proceeding through glycerophospho-*N*-acyl ethanolamine and a role for  $\alpha/\beta$ -hydrolase 4 in this pathway. *J. Biol. Chem.* **281**, 26465–26472 (2006).
37. Simon, G. M. & Cravatt, B. F. Anandamide biosynthesis catalyzed by the phosphodiesterase GDE1 and detection of glycerophospho-*N*-acyl ethanolamine precursors in mouse brain. *J. Biol. Chem.* **283**, 9341–9349 (2008).
38. Tsuboi, K. *et al.* Glycerophosphodiesterase GDE4 as a novel lysophospholipase D: A possible involvement in bioactive *N*-acylethanolamine biosynthesis. *Biochim. Biophys. Acta - Mol. Cell Biol. Lipids* **1851**, 537–548 (2015).
39. Tsuboi, K., Uyama, T., Okamoto, Y. & Ueda, N. Endocannabinoids and related *N*-acylethanolamines: biological activities and metabolism. *Inflamm. Regen.* **38**, (2018).
40. Hansen, H. S. & Vana, V. Non-endocannabinoid *N*-acylethanolamines and 2-monoacylglycerols in the intestine. *Br. J. Pharmacol.* **176**, 1443–1454 (2019).
41. Katona, I. & Freund, T. F. Multiple Functions of Endocannabinoid Signaling in the Brain. *Annu. Rev. Neurosci.* **35**, 529–558 (2012).
42. Cristino, L., Bisogno, T. & Di Marzo, V. Cannabinoids and the expanded endocannabinoid system in neurological disorders. *Nat. Rev. Neurol.* **16**, 9–29 (2020).
43. Lutz, B., Marsicano, G., Maldonado, R. & Hillard, C. J. The endocannabinoid system in guarding against fear, anxiety and stress. *Nat. Rev. Neurosci.* **16**, 705–718 (2015).
44. Uyama, T. *et al.* Generation of *N*-acylphosphatidylethanolamine by members of the phospholipase A/acyltransferase (PLA/AT) family. *J. Biol. Chem.* **287**, 31905–31919 (2012).
45. Golczak, M. *et al.* Structural basis for the acyltransferase activity of lecithin:retinol acyltransferase-like proteins. *J. Biol. Chem.* **287**, 23790–23807 (2012).
46. Zhou, J. *et al.* Structure-Activity Relationship Studies of  $\alpha$ -Ketoamides as Inhibitors of the Phospholipase A and Acyltransferase Enzyme Family. *J. Med. Chem.* **63**, 9340–9359 (2020).
47. Cadas, H., Gaillet, S., Beltramo, M., Venance, L. & Piomelli, D. Biosynthesis of an endogenous cannabinoid precursor in neurons and its control by calcium and cAMP. *J. Neurosci.* **16**, 3934–3942 (1996).
48. Cadas, H., Di Tomaso, E. & Piomelli, D. Occurrence and biosynthesis of endogenous cannabinoid precursor, *N*-arachidonoyl phosphatidylethanolamine, in rat brain. *J. Neurosci.* **17**, 1226–1242 (1997).
49. Reddy, P. V., Natarajan, V., Schmid, P. C. & Schmid, H. H. O. *N*-acylation of dog heart ethanolamine phospholipids by transacylase activity. *Biochim. Biophys. Acta - Lipids Lipid Metab.* **750**, 472–480 (1983).
50. Hussain, Z., Uyama, T., Tsuboi, K. & Ueda, N. Mammalian enzymes responsible for the biosynthesis of *N*-acylethanolamines. *Biochim. Biophys. Acta - Mol. Cell Biol. Lipids* **1862**, 1546–1561 (2017).
51. Zhou, J. Development of a PLA2G4E Assay and Subsequent Application in Hit Identification. *Inhibitor Discovery of Phospholipase and N-Acyltransferase* (Leiden University, 2020).

52. Hsu, K. L. *et al.* Discovery and optimization of piperidyl-1,2,3-triazole ureas as potent, selective, and *in vivo*-active inhibitors of  $\alpha/\beta$ -hydrolase domain containing 6 (ABHD6). *J. Med. Chem.* **56**, 8270–8279 (2013).
53. Deng, H. *et al.* Triazole Ureas Act as Diacylglycerol Lipase Inhibitors and Prevent Fasting-Induced Refeeding. *J. Med. Chem.* **60**, 428–440 (2017).
54. Ogasawara, D. *et al.* Rapid and profound rewiring of brain lipid signaling networks by acute diacylglycerol lipase inhibition. *Proc. Natl. Acad. Sci. U. S. A.* **113**, 26–33 (2016).
55. Adibekian, A. *et al.* Click-generated triazole ureas as ultrapotent *in vivo*-active serine hydrolase inhibitors. *Nat. Chem. Biol.* **7**, 469–478 (2011).
56. Mock, E. D. *et al.* Structure–Activity Relationship Studies of Pyrimidine-4-Carboxamides as Inhibitors of *N*-Acylphosphatidylethanolamine Phospholipase D. *J. Med. Chem.* **64**, 481–515 (2021).
57. Miyaura, N. *et al.* Palladium-Catalyzed Inter- and Intramolecular Cross-Coupling Reactions of *B*-Alkyl-9-Borabicyclo[3.3.1]nonane Derivatives with 1-Halo-1-alkenes or Haloarenes. Syntheses of Functionalized Alkenes, Arenes, and Cycloalkenes via a Hydroboration–Coupling Sequence. *J. Am. Chem. Soc.* **111**, 314–321 (1989).
58. Johnson, D. S. *et al.* Discovery of PF-04457845: A Highly Potent, Orally Bioavailable, and Selective Urea FAAH Inhibitor. *ACS Med. Chem. Lett.* **2**, 91–96 (2011).
59. Liu, Y., Patricelli, M. P. & Cravatt, B. F. Activity-based protein profiling: The serine hydrolases. *Proc. Natl. Acad. Sci. U. S. A.* **96**, 14694–14699 (1999).
60. Ghomashchi, F. *et al.* A pyrrolidine-based specific inhibitor of cytosolic phospholipase A2 $\alpha$  blocks arachidonic acid release in a variety of mammalian cells. *Biochim. Biophys. Acta - Biomembr.* **1513**, 160–166 (2001).
61. McKew, J. C. *et al.* Inhibition of cytosolic phospholipase A2 $\alpha$ : Hit to lead optimization. *J. Med. Chem.* **49**, 135–158 (2006).
62. Ng, C. Y. *et al.* A New Generation of Arachidonic Acid Analogues as Potential Neurological Agent Targeting Cytosolic Phospholipase A2. *Sci. Rep.* **7**, 1–12 (2017).
63. Connolly, S. *et al.* Design and synthesis of a novel and potent series of inhibitors of cytosolic phospholipase A2 based on a 1,3-disubstituted propan-2-one skeleton. *J. Med. Chem.* **45**, 1348–1362 (2002).
64. Seno, K. *et al.* Pyrrolidine inhibitors of human cytosolic phospholipase A2. Part 2: Synthesis of potent and crystallized 4-triphenylmethylthio derivative ‘pyrrophenone’. *Bioorganic Med. Chem. Lett.* **11**, 587–590 (2001).
65. Shimizu, H. *et al.* AK106-001616, a potent and selective inhibitor of cytosolic phospholipase A2: *In vivo* efficacy for inflammation, neuropathic pain, and pulmonary fibrosis. *J. Pharmacol. Exp. Ther.* **369**, 511–522 (2019).
66. Ghomashchi, F. *et al.* Interfacial kinetic and binding properties of mammalian group IVB phospholipase A2 (cPLA2 $\beta$ ) and comparison with the other cPLA2 isoforms. *J. Biol. Chem.* **285**, 36100–36111 (2010).
67. Thakker, P. *et al.* Cytosolic phospholipase A2 $\alpha$  blockade abrogates disease during the tissue-damage effector phase of experimental autoimmune encephalomyelitis by its action on APCs. *J. Immunol.* **187**, 1986–1997 (2011).
68. Ong, W. Y., Farooqui, T., Kokotos, G. & Farooqui, A. A. Synthetic and Natural Inhibitors of Phospholipases A2: Their Importance for Understanding and Treatment of Neurological Disorders. *ACS Chem. Neurosci.* **6**, 814–831 (2015).

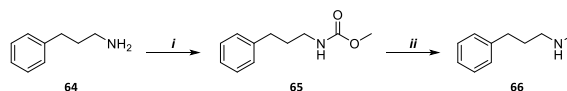


69. Kokotou, M. G., Limnios, D., Nikolaou, A., Psarra, A. & Kokotos, G. Inhibitors of phospholipase A<sub>2</sub> and their therapeutic potential: an update on patents (2012-2016). *Expert Opin. Ther. Pat.* **27**, 217–225 (2017).
70. Donvito, G. *et al.* The Endogenous Cannabinoid System: A Budding Source of Targets for Treating Inflammatory and Neuropathic Pain. *Neuropsychopharmacology* **43**, 52–79 (2018).
71. Ahn, K. *et al.* Mechanistic and pharmacological characterization of PF-04457845: A highly potent and selective fatty acid amide hydrolase inhibitor that reduces inflammatory and noninflammatory pain. *J. Pharmacol. Exp. Ther.* **338**, 114–124 (2011).
72. Coulon, D., Faure, L., Salmon, M., Wattelet, V. & Bessoule, J. J. Occurrence, biosynthesis and functions of *N*-acylphosphatidylethanolamines (NAPE): Not just precursors of *N*-acylethanolamines (NAE). *Biochimie* **94**, 75–85 (2012).
73. Mock, E. D. *et al.* Discovery of a NAPE-PLD inhibitor that modulates emotional behavior in mice. *Nat. Chem. Biol.* **16**, 667–675 (2020).
74. Lipinski, C. A., Lombardo, F., Dominy, B. W. & Feeney, P. J. Experimental and computational approaches to estimate solubility and permeability in drug discovery and development settings. *Adv. Drug Deliv. Rev.* **46**, 3–26 (2001).
75. Veber, D. F. *et al.* Molecular properties that influence the oral bioavailability of drug candidates. *J. Med. Chem.* **45**, 2615–2623 (2002).
76. Hsu, K. L. *et al.* Development and optimization of piperidyl-1,2,3-triazole ureas as selective chemical probes of endocannabinoid biosynthesis. *J. Med. Chem.* **56**, 8257–8269 (2013).
77. Hsu, K. L. *et al.* DAGL $\beta$  inhibition perturbs a lipid network involved in macrophage inflammatory responses. *Nat. Chem. Biol.* **8**, 999–1007 (2012).
78. Van Rooden, E. J. *et al.* Mapping *in vivo* target interaction profiles of covalent inhibitors using chemical proteomics with label-free quantification. *Nat. Protoc.* **13**, 752–767 (2018).
79. van der Wel, T. *et al.* A natural substrate-based fluorescence assay for inhibitor screening on diacylglycerol lipase  $\alpha$ . *J. Lipid Res.* **56**, 927–935 (2015).
80. Manterola, A. *et al.* Re-examining the potential of targeting ABHD6 in multiple sclerosis: Efficacy of systemic and peripherally restricted inhibitors in experimental autoimmune encephalomyelitis. *Neuropharmacology* **141**, 181–191 (2018).

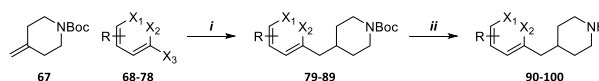
## Supplementary Information



**Supplementary Scheme S2.1. Alternative synthetic route for PLA2G4E inhibitors.** Reagents and conditions: *i*)  $K_2CO_3$ , DMF, 6 h RT; *ii*)  $AcOOH$ , DCM, 6 h  $0^\circ C \rightarrow RT$ ; *iii*) 1. **95**, **101** or **105**, triphosgene,  $Et_3N$  or DIPEA, THF, 3 h  $0^\circ C \rightarrow RT$ , then 2. **106**,  $K_2CO_3$ , DMF, o/n RT.



**Supplementary Scheme S2.2. Methylation of 3-phenylpropylamine.** Reagents and conditions: *i*) Methyl chloroformate, DIPEA, DCM, 2 h  $0^\circ C \rightarrow RT$ ; *ii*)  $LiAlH_4$ , THF,  $0^\circ C \rightarrow$  reflux, 72 h.



**Supplementary Scheme S2.3. Synthesis of 4-benzylpiperidine derivatives.** Reagents and conditions: *i*) 1. **67**, 9-BBN, THF, 6 h  $0^\circ C \rightarrow RT$ , then 2. **68-78**,  $Pd(dppf)Cl_2$ ,  $K_2CO_3$ , THF/DMF/ $H_2O$ , o/n reflux. *ii*) HCl, 1,4-dioxane, o/n RT.  $X_1, X_2 = CH$  or N,  $X_3 = I$  or Br.



# 3

**Biochemical profiling of the novel  
PLA<sub>2</sub>G<sub>4</sub>E inhibitor WEN091**

Phospholipase A<sub>2</sub>ε (PLA<sub>2</sub>G4E) is a serine hydrolase that belongs to Group IV of the phospholipase A<sub>2</sub> family. It has five closely related family members (A–D and F), which share structural similarity despite their relatively low amino acid homology (30% on average).<sup>1</sup> These isozymes have PLA<sub>1</sub>, PLA<sub>2</sub>, lysophospholipase and acyltransferase activity *in vitro*, but have distinct preferences and calcium-dependencies.<sup>2,3</sup> They are characterized by the presence of an N-terminal calcium-binding C2 domain (apart from PLA<sub>2</sub>G4C) and an unconventional Ser-Asp catalytic dyad in their lipase domain.<sup>4,5</sup> PLA<sub>2</sub>G4E was recently proposed to be the enzyme responsible for the Ca<sup>2+</sup>-dependent biosynthesis of *N*-acylphosphatidylethanolamines (NAPEs) in the brain.<sup>6</sup> It acts as an *N*-acyltransferase (NAT) transferring the *sn*-1 *O*-acyl substituent from phosphatidylcholine (PC) to the free amine of phosphatidylethanolamine (PE) (Figure 3.1).<sup>6,7</sup>

NAPEs are an underexplored class of lipids with both structural and signaling functionalities. NAPEs are low-abundant but widely found across species and tissues.<sup>8,9</sup> They provide rigidity to cellular membranes<sup>10,11</sup>, are involved in cation-dependent membrane fusion<sup>12</sup> and influence the localization of membrane-interacting proteins.<sup>13,14</sup> In addition, NAPEs have anorectic and anti-inflammatory signaling functions.<sup>15–17</sup> Beside the Ca<sup>2+</sup>-dependent pathway, Ca<sup>2+</sup>-independent NAPE biosynthesis is performed by NAT activity of phospholipase A<sub>1/2</sub>/acyltransferase (PLAAT) enzymes 1–5.<sup>18,19</sup> NAPEs are converted into *N*-acylethanolamines (NAEs) either directly by NAPE-specific phospholipase D (NAPE-PLD) or via one of several multistep pathways (Figure 3.1).<sup>20–23</sup> The first of these alternative pathways includes *sn*-2 ester hydrolysis to lyso-NAPEs by α/β hydrolase domain-containing protein 4 (ABHD4) or other PLA<sub>2</sub>-type enzymes.<sup>24</sup> Lyso-NAPEs are then converted to NAEs by PLD-type activity of glycerophosphodiesterase 4 (GDE4) or GDE7.<sup>21,25</sup> Alternatively, ABHD4 hydrolyzes the *sn*-1 ester producing glycerophospho-NAEs (GP-NAEs), which are then converted to NAEs by GDE1.<sup>26</sup> Third, NAEs can be biosynthesized via PLC-type hydrolysis of NAPEs to phospho-NAEs and sequential dephosphorylation.<sup>24,27</sup> Of note, plasmalogen-type NAPEs (pNAPEs) bear an *sn*-1 ether, which cannot be hydrolyzed by ABHD4. Metabolism of pNAPEs to NAEs is therefore restricted to the other three pathways (Figure 3.1B).<sup>23</sup> NAEs are a diverse family of signaling lipids that are involved in a plethora of physiological functions, depending on their *N*-acyl substituent, including inflammation, nociception and satiety.<sup>28–32</sup> *N*-Arachidonylethanolamine (AEA or anandamide) is an endocannabinoid, regulating neurotransmission, memory formation, fertility and stress, among others, via activation of cannabinoid receptor 1 (CB<sub>1</sub>).<sup>32–36</sup> The activity of NAEs is terminated by fatty acid amide hydrolase (FAAH) or *N*-acylethanolamine acid amidase (NAAA).<sup>37,38</sup> Following acute brain ischemia both NAPEs and NAEs are dramatically increased, which is suggested to have a neuroprotective effect.<sup>39–41</sup> Since elevated intracellular calcium concentrations are a hallmark of ischemia<sup>42</sup>, PLA<sub>2</sub>G4E activity might be pivotal in this response. Potent and selective inhibitors of PLA<sub>2</sub>G4E would therefore be valuable tools to elucidate the role of PLA<sub>2</sub>G4E in both basal and pathophysiological NAPE production.

In Chapter 2, compound screening and a hit optimization program led to the identification of **WEN091** as an inhibitor of PLA2G4E. In this chapter, the biochemical profile of **WEN091** was further explored in both *in vitro* and cellular assays.

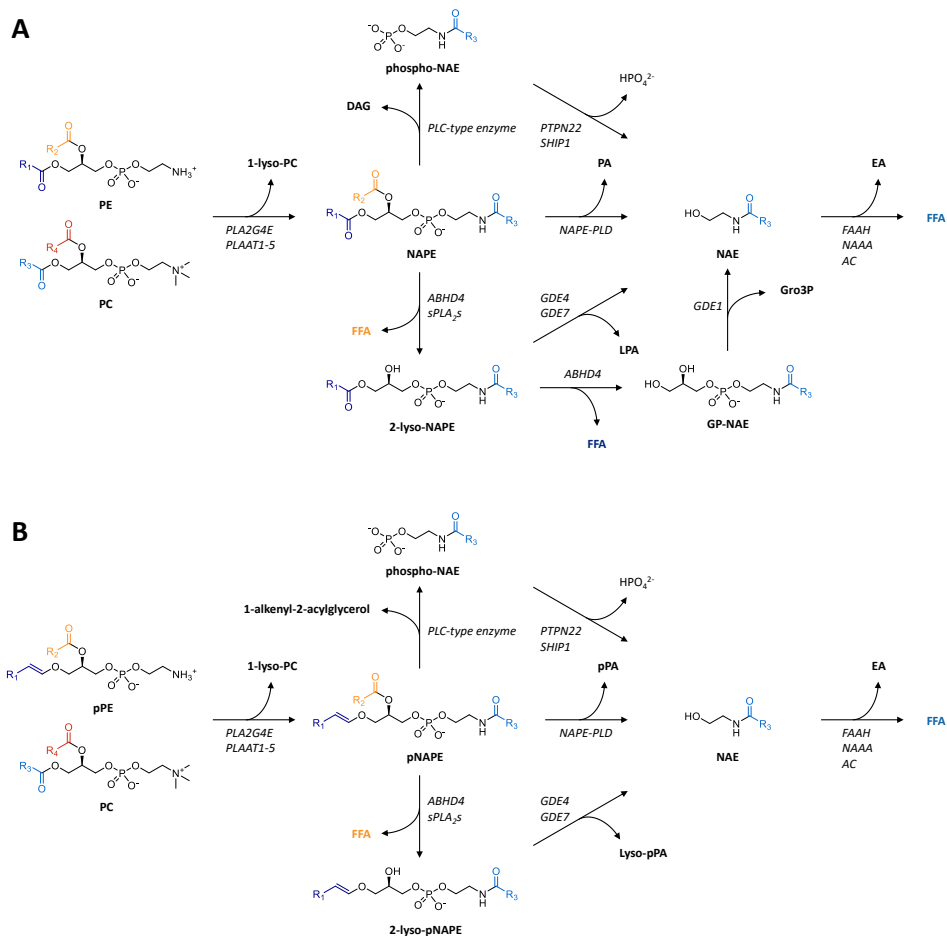


**Figure 3.1. Pathways of NAPE and pNAPE metabolism.** A) Acyl transfer from a donor lipid such as phosphatidylcholine (PC) to phosphatidylethanolamine (PE) by PLA2G4E or phospholipase/acyltransferase (PLAAT) 1–5 produces *N*-acyl-PE (NAPE), which is metabolized to *N*-acylethanolamine (NAE) either via direct phospholipase D (PLD) activity by NAPE-specific PLD (NAPE-PLD) or one of three multistep pathways involving sequential PLA<sub>1</sub>, PLA<sub>2</sub>, PLC, PLD and dephosphorylation reactions. B) Plasmalogen-type NAPE (pNAPE) are produced from plasmenylethanolamine (pPE). Metabolism of pNAPE is restricted to three possible pathways. ABHD4:  $\alpha/\beta$  hydrolase domain-containing protein 4, PLA<sub>2</sub>s: PLA<sub>2</sub>-type enzymes, GDE: glycerophosphodiesterase, PTPN22: protein tyrosine phosphatase non-receptor type 22, SHIP1: Src homology 2 domain-containing inositol 5' phosphatase 1, FAAH: fatty acid amide hydrolase, NAAA: NAE-hydrolyzing acid amidase, AC: acid ceramidase, PA: phosphatidic acid, LPA: lysophosphatidic acid, GP-NAE: glycerophospho-NAE, Gro3P: glycerol-3-phosphate, DAG: diacylglycerol, EA: ethanolamine, FFA: free fatty acid, pPA: plasmalomic acid. R = saturated, mono- or polyunsaturated fatty acyl.

## Results

### Activity on human and mouse PLA2G4E and related enzymes

Competitive activity-based protein profiling (cABPP) is a powerful chemical biology technique to assess the activity and selectivity of enzyme inhibitors in complex proteomes. Competitive ABPP makes use of fluorescently tagged activity-based probes (ABPs), such as fluorophosphonate-tetramethylrhodamine (FP-TAMRA) that reacts in a covalent manner with the nucleophilic serine in the active site of serine hydrolases. Here, cABPP was used to determine the activity of **WEN091** on recombinant human PLA2G4E expressed in human embryonic kidney 293 (HEK293T) cells. In brief, lysates from HEK293T cells overexpressing recombinant human or mouse PLA2G4E were preincubated with various concentrations of **WEN091** or vehicle for 30 min at room temperature followed by 50 nM FP-TAMRA for 5 min. Proteins were resolved by molecular weight using sodium dodecyl sulfate–polyacrylamide gel electrophoresis (SDS-PAGE) and subsequent in-gel fluorescence scanning allowed quantification of enzyme labeling and inhibition thereof by **WEN091**. **WEN091** inhibited hPLA2G4E, with an apparent half maximal inhibitory concentration (IC<sub>50</sub>) of 10 nM (pIC<sub>50</sub> ± SEM = 8.01 ± 0.02) (Figure 3.2A–C). Preliminary experiments indicated that **WEN091** was also active on mouse PLA2G4E (pIC<sub>50</sub> = 6.87 ± 0.07) (Supplementary Figure S3.1). Next, the inhibitory activity of **WEN091** was investigated using a liquid chromatography–mass spectrometry (LC-MS)-based natural

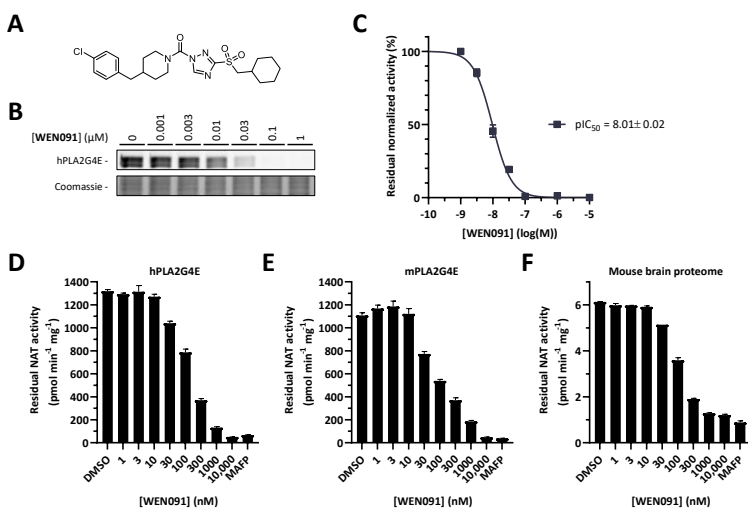


**Figure 3.2. WEN091 is a potent inhibitor of PLA2G4E.** A) Chemical structure of WEN091. B) Representative gel excerpts of cABPP experiments on hPLA2G4E overexpression lysate, using FP-TAMRA. C) Inhibition curve and pIC<sub>50</sub> value corresponding to the cABPP experiment in B. Data presented as mean ± SEM (N = 2). D–F) Dose-dependent inhibition by **WEN091** of NAPE formation from 1,2-dipalmitoyl-PC and 1,2-dioleoyl-PE in human (D) or murine (E) PLA2G4E-overexpression lysate or mouse brain proteome (F). Methyl arachidonoyl-FP (MAFP) was used as control. Bars represent mean ± SEM of conversion rate determined using LC-MS/MS (N = 2).

substrate assay. In line with the gel-based cABPP assay results, **WEN091** dose-dependently inhibited *N*-palmitoyl-*sn*-1,2-dioleoylphosphatidylethanolamine biosynthesis by recombinant human and mouse PLA2G4E and mouse brain homogenate, with  $pIC_{50}$  values of  $6.87 \pm 0.02$  (hPLA2G4E),  $7.09 \pm 0.08$  (mPLA2G4E) and  $7.02 \pm 0.01$  (mouse brain proteome) (Figure 3.2D–F and Supplementary Figure S3.2). Altogether, these data indicate that **WEN091** is a potent inhibitor of PLA2G4E.

To determine **WEN091**'s selectivity over the other Group IV phospholipase members, a gel-based competitive ABPP assay was deployed (Figure 3.3A, B). Of note, the inhibition values determined using this approach are apparent  $IC_{50}$  and apparent selectivity values that can only be used to compare compounds that have been tested under identical conditions. **WEN091** showed inhibitory activity on mouse PLA2G4B ( $pIC_{50} = 6.65 \pm 0.11$ ) and mPLA2G4D ( $pIC_{50} = 5.85 \pm 0.06$ ), but no activity on human PLA2G4C ( $pIC_{50} < 5.0$ ). Activity on PLA2G4A and F could not be determined due to lack of expression in the

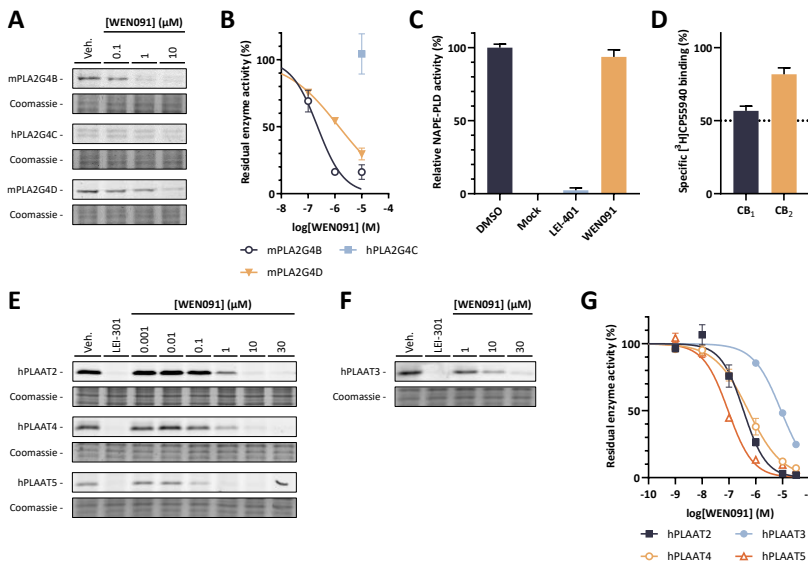


**Figure 3.3. WEN091 is selective over other PLA2G4 enzymes and enzymes involved in NAPE metabolism.** A) Representative gel excerpts of cABPP experiments on mPLA2G4B, hPLA2G4C or mPLA2G4D overexpression lysate, using FP-TAMRA. B) Inhibition curves of **WEN091** on PLA2G4B–D corresponding to the cABPP experiments in A). Data presented as mean  $\pm$  SEM (N = 3). C) Activity of **WEN091** (10  $\mu$ M) on NAPE-PLD in a fluorogenic substrate (PED6) assay on overexpression lysate. NAPE-PLD inhibitor LEI-401 (10  $\mu$ M) was used as control.<sup>43</sup> Data presented as mean  $\pm$  SEM (N = 2, n = 2). D) Displacement of radiolabeled ligand [ $^3$ H]CP55940 from CB<sub>1</sub> and CB<sub>2</sub> receptors by **WEN091** (10  $\mu$ M) in overexpression lysate. Data presented as relative mean of DMSO control (100%)  $\pm$  SEM (N = 3, n = 3). E–F) Representative gel excerpts of cABPP experiments on hPLAAT2, hPLAAT4, hPLAAT5 (E) or hPLAAT3 (F) overexpression lysate, using MB064 as ABP and pan-PLAAT inhibitor LEI-301 (10  $\mu$ M) as control.<sup>44</sup> G) Inhibition curves of **WEN091** on hPLAAT2–5 corresponding to the cABPP experiments in E–F). Data presented as mean  $\pm$  SEM (N = 2).



**Table 3.1. Inhibition values of WEN091 on PLA2G4 enzymes and enzymes involved in NAPE metabolism.** Inhibition values determined using gel-based cABPP (PLA2G4B–D, N = 3, PLAAT2–5, N = 2), PED6 assay (NAPE-PLD, N = 2, n = 2) or [<sup>3</sup>H]CP55,940 displacement assay (CB<sub>1/2</sub>, N = 3, n = 3) on overexpression lysate. Data reported as pIC<sub>50</sub> ± SEM. When <50% inhibition or displacement was observed at 10 μM, % residual activity is reported.

Enzyme	PLA2G4B	PLA2G4C	PLA2G4D	PLAAT2	PLAAT3	PLAAT4	PLAAT5	NAPE-PLD	CB <sub>1</sub>	CB <sub>2</sub>
Inhibition value	6.65 ± 0.11	104 ± 26%	5.85 ± 0.06	6.46 ± 0.07	5.05 ± 0.02	6.28 ± 0.05	7.03 ± 0.07	94 ± 10%	57 ± 3%	82 ± 4%

HEK293T cells. **WEN091** showed no activity on NAPE-hydrolyzing enzyme NAPE-PLD in a biochemical fluorescence-based assay<sup>45</sup> and did not potently bind to cannabinoid CB<sub>1</sub> and CB<sub>2</sub> receptors in a radiometric displacement assay<sup>46</sup> (Figure 3.3C–D, Table 3.1). In addition, activity on the PLAAT enzymes was assessed in a competitive gel-based ABPP assay.<sup>44</sup> At 10 nM (the hPLA2G4E IC<sub>50</sub>), **WEN091** showed no significant inhibitory activity on PLAAT2–5, but at higher concentrations these enzymes were inhibited (Figure 3.3E–G, Table 3.1). The activity on PLAAT1 could not be determined due to lack of expression in the HEK293T cells. Thus, **WEN091** is a potent inhibitor of NAPE biosynthesis with a >10-fold preference for inhibition of the Ca<sup>2+</sup>-dependent pathway of NAPE formation.

The selectivity of **WEN091** over other serine hydrolases in mouse brain proteome was determined using gel-based cABPP (Figure 3.4). **WEN091** appeared to be a selective PLA2G4E inhibitor at 10 and 100 nM (Figure 3.4), but inhibited several enzymes at higher concentrations, including α/β hydrolase domain-containing protein 6 (ABHD6), diacylglycerol lipase α (DAGLα), FAAH, acyl protein thioesterases 1 and 2 (LyPLA1/2) and carboxylesterases (CES) (Table 3.2). Using competitive chemical proteomics, which makes use of LC-MS/MS to accurately identify probe targets, the identity of the serine hydrolase off-targets was confirmed (Table 3.2, Supplementary Figure S3.3).

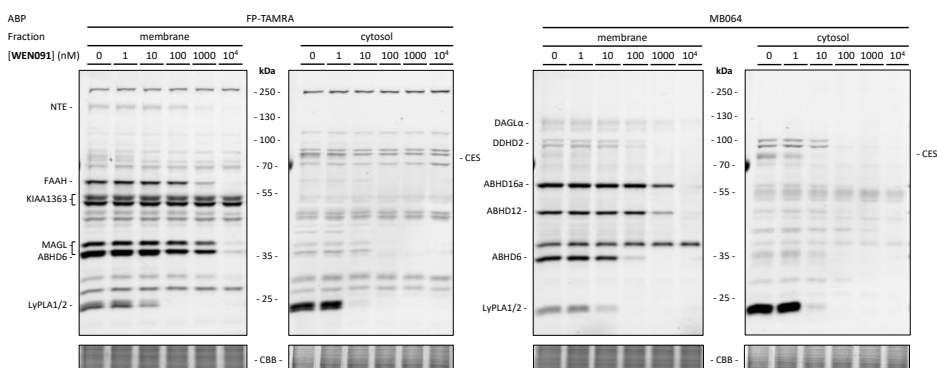


**Figure 3.4. *In vitro* activity of WEN091 on mouse brain enzymes.** Representative gel images of cABPP experiments on mouse brain membrane or cytosol proteome using FP-TAMRA or MB064. Several labeled serine hydrolases are indicated.

**Table 3.2. Inhibition values of WEN091 on mouse brain enzymes.** pIC<sub>50</sub> values determined by cABPP experiments on mouse brain membrane or cytosol proteome (30 min, RT) using FP-TAMRA or MB064 (20 min, RT). Data presented as mean ± SEM (N = 3). The third column shows inhibition of these enzymes by **WEN091** (1 μM, 30 min, 37°C) as determined in a chemical proteomics experiment with FP-biotin (4 μM, 60 min, RT). Data presented as ratios of quantified peptides between **WEN091** and DMSO-treated samples (preliminary, N = 1). Minimal ratio was manually set to 0.05.

Enzyme	pIC <sub>50</sub> ± SEM	Ratio
		WEN091/DMSO
ABHD6	7.89 ± 0.02	≤ 0.05
ABHD12	6.53 ± 0.04	≤ 0.05
ABHD16a	6.33 ± 0.04	0.12
CES	9.06 ± 0.03	≤ 0.05
DAGLα	6.51 ± 0.04	≤ 0.05
DDHD2	7.34 ± 0.04	0.07
FAAH	6.52 ± 0.04	≤ 0.05
KIAA1363	< 5.0	1.38
LyPLA1/2	8.27 ± 0.04	≤ 0.05
MAGL	5.89 ± 0.07	0.08
NTE	6.48 ± 0.06	0.31

### Profiling the cellular activity of WEN091

Next, the cellular activity profile of **WEN091** was determined in mouse Neuro-2a cells using gel-based cABPP.<sup>43,47–49</sup> At 10 and 100 nM, **WEN091** inhibited ABHD6 (pIC<sub>50</sub> = 8.56 ± 0.05), FAAH (pIC<sub>50</sub> = 8.17 ± 0.07) and LyPLA1/2 (pIC<sub>50</sub> = 7.83 ± 0.08, Figure 3.5 and Table 3.3). In addition, **WEN091** partially inhibited DDHD domain-containing protein 2 (DDHD2) and neuropathy target esterase (NTE) (pIC<sub>50</sub> = 7.14 ± 0.08 and 7.13 ± 0.10, respectively). These results indicated that **WEN091** was able to cross the plasma membrane and inhibit intracellular enzymes. Compared to the mouse brain *in vitro* assay, the activity on FAAH was increased approximately 50 times, whereas the activity on DDHD2 and LyPLA1/2 was slightly reduced (approximately 2 and 3 times, respectively, Table 3.2 and Table 3.3). In line with the chemical proteomics results, **WEN091** inhibited several other serine hydrolases at higher concentrations, including ABHD12, ABHD16a and DAGLβ. PLA2G4E activity could not be detected in this assay. Thus, **WEN091** is a cellular active inhibitor, but has several serine hydrolase off-targets in living cells.

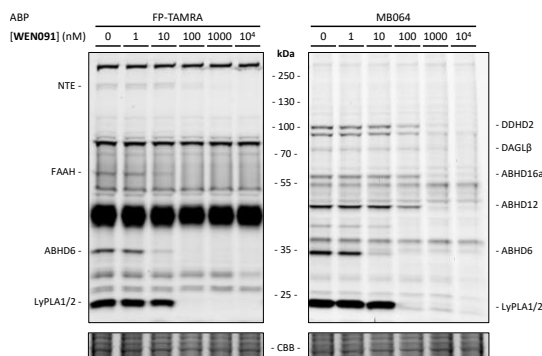


**Figure 3.5. Cellular activity of WEN091 on Neuro-2a enzymes.** Representative gel images of cABPP experiments on Neuro-2a cells using FP-TAMRA or MB064. Several labeled serine hydrolases are indicated.

**Table 3.3. Inhibition values of WEN091 on Neuro-2a enzymes.** Values determined by cABPP experiments on Neuro-2a cells using FP-TAMRA or MB064. Data presented as mean  $\pm$  SEM (N = 3).

Enzyme	ABHD6	ABHD12	ABHD16a	DAGLB	DDHD2	FAAH	LyPLA1/2	NTE
pIC <sub>50</sub>	8.56	7.01	6.62	6.72	7.14	8.17	7.83	7.13
$\pm$ SEM	$\pm$ 0.05	$\pm$ 0.04	$\pm$ 0.07	$\pm$ 0.25	$\pm$ 0.08	$\pm$ 0.07	$\pm$ 0.08	$\pm$ 0.10

To determine the functional effect of **WEN091** in living cells, recombinant hPLA2G4E was transiently overexpressed in Neuro-2a cells. Cells were harvested 24 h after transfection, lysed and the lipids were extracted. Targeted LC-MS/MS analysis revealed increased levels of NAPEs, lyso-NAPEs and NAEs, and to a lesser extent of plasmalogen-type NAPEs (pNAPEs) compared to mock-transfected cells (Figure 3.6A and Supplementary Figure S3.4). All analyzed NAPE levels were increased at least 4-fold, with *N*-palmitoyl (16:0) and *N*-oleoyl (18:1) species showing the largest increase up to 50-fold. NAE levels were all increased at least 2-fold, except *N*-docosahexaenoylethanolamine (DHEA, 22:6), which was not changed. *N*-stearoylethanolamine (SEA, 18:0) and *N*-docosatetraenoylethanolamine (DEA, 22:4) showed the largest accumulation of over 10-fold. Overexpression did not affect levels of lyso-pNAPEs, free fatty acids (FFAs) and glycerides. These results demonstrated that overexpressed PLA2G4E and NAPE-metabolizing enzymes are present and catalytically active in the Neuro-2a cells.

Next, the cells were treated with **WEN091** or **WEN258** (8 h, starting 24 h after transfection). **WEN258** is a structural analog of **WEN091** with a similar cellular selectivity profile but no activity on PLA2G4E (Figure 3.7, see also Chapter 4) and was used as a control-compound. **WEN091** dose-dependently lowered NAPE and lyso-NAPE levels up to  $\pm$  50% compared to DMSO-treated cells, whereas **WEN258** did not (Figure 3.6B, C for a cross-sectional selection of lipids and Supplementary Figure S3.5 for the full panel). Of note, levels of some NAPEs were increased after **WEN258** treatment, which might be due to inhibition of a NAPE-metabolizing enzyme. Interestingly, the levels of *N*-

docosahexaenoyl (*N*-22:6)-lyso-NAPEs were not increased upon PLA2G4E overexpression (Supplementary Figure S3.4B), but were by both **WEN091** and **WEN258** treatment (Figure 3.6C and Supplementary Figure S3.6). This may suggest that *N*-22:6 lyso-NAPEs are biosynthesized via a PLA2G4E-independent pathway and/or that these lipids are rapidly metabolized by a common off-target of **WEN091** and **WEN258**. Treatment with the inhibitors showed no significant effect on lyso-pNAPE levels, suggesting these lipids are metabolized independently of PLA2G4E and other targets of the compounds. Furthermore, **WEN091** did not significantly modulate NAE levels, but **WEN258** increased these (Figure 3.6D). This might be explained by inhibition of FAAH by both compounds (Table 3.3 and Figure 3.7), suggesting combined inhibition of PLA2G4E and FAAH by **WEN091** balances NAE levels. Finally, both compounds decreased GP-PEA, FFA and 2-AG levels, confirming PLA2G4E-independent activity of the inhibitors (Supplementary Figure S3.7). To conclude, **WEN091** is an inhibitor of PLA2G4E that lowered intracellular (lyso)-NAPE production, but has several off-targets that modulate other lipid species.

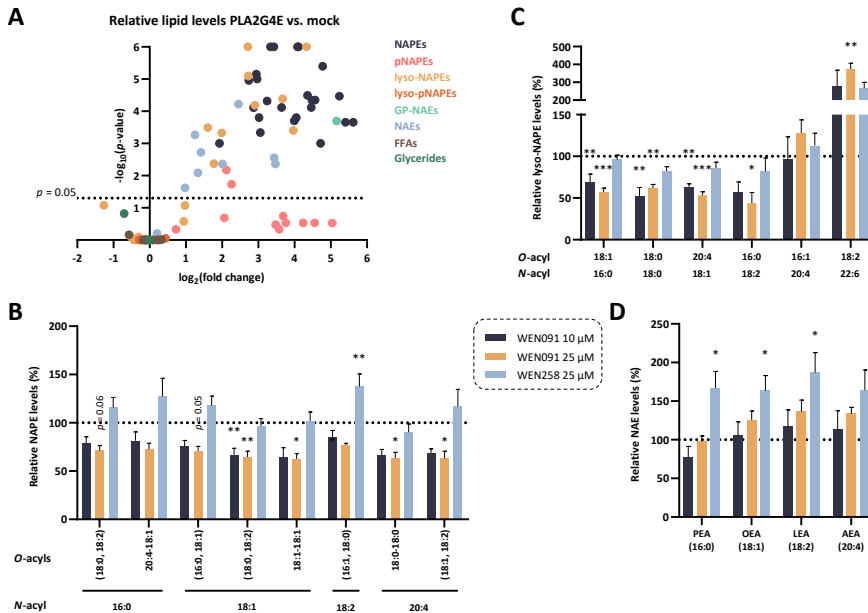


**Figure 3.6.** Lipid levels in Neuro-2a cells overexpressing PLA2G4E and following treatment with WEN091. A) Volcano plot of relative lipid levels in PLA2G4E-transfected vs. mock-transfected Neuro-2a cells (24 h p.t.). Statistical significance calculated for each lipid using a two-tailed *t*-test with Holm-Sidak multiple comparison correction. B-D) Effect of inhibitor or control compound treatment (8 h) on the levels of several NAPEs (B), lyso-NAPEs (C) and NAEs (D) in PLA2G4E-overexpressing Neuro-2a cells (24 h p.t.), expressed as relative levels compared to vehicle-treated cells (mean  $\pm$  SEM,  $N = 5$ ). Statistical significance calculated for each lipid using one-way ANOVA with Dunnett's multiple comparison correction.  $*p < 0.05$ ,  $**p < 0.01$ ,  $***p < 0.001$ .

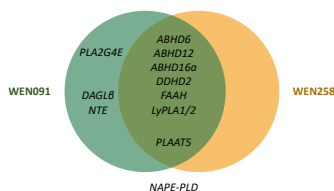


**Figure 3.7. Selectivity profile of WEN091 and WEN258.** Included are serine hydrolases identified in Neuro-2a cells and (human orthologs of) enzymes involved in mouse NAPE metabolism for which inhibition data of both inhibitors was obtained and that are inhibited at least 50% by 10  $\mu$ M of inhibitor. For complete data of **WEN258**, see Chapter 4.

## Discussion and Conclusion

In Chapter 2, **WEN091** was identified as the first potent inhibitor of PLA2G4E. Here, its activity was confirmed on the mouse ortholog, showing high potency in gel-based cABPP and biochemical assays using recombinant mPLA2G4E and endogenous PLA2G4E in mouse brain. **WEN091** was cellular active and inhibited the formation of NAPEs and lyso-NAPEs in PLA2G4E-overexpressing Neuro-2a cells, but did not affect NAE levels. It was selective over the cannabinoid receptors and NAPE-PLD, but unexpectedly inhibited PLAAT2–5, albeit at 10-fold higher concentration. PLA2G4E and PLAATs bear no structural or sequence similarities and belong to different protein classes (serine and cysteine hydrolases, respectively), but they have similar biosynthetic activity. This suggests that the active sites of these two enzyme families have evolved in convergent evolutionary pathways to recognize similar phospholipids as substrates. This may potentially explain why both NAPE-producing enzyme families also interact with **WEN091**. In line, **WEN091** inhibited phospholipase PLAAT3 less effectively than principal acyltransferases PLAAT2, PLAAT4 and PLAAT5.<sup>18</sup> Previously, selective PLAAT inhibitors that do not cross-react with PLA2G4E were reported.<sup>44,50</sup> Combining this tool set with **WEN091** may allow to investigate the activity of PLA2G4E and NAPEs in various tissues under normal and pathological conditions (e.g. ischemia or inflammation).<sup>17,39</sup> This will increase the understanding of the (patho)physiological role of PLA2G4E, PLAATs and their products, which may provide new therapeutic opportunities.<sup>8,40,51</sup>

Overexpression of PLA2G4E in Neuro-2a cells resulted in elevated levels of NAPEs, lyso-NAPEs, GP-NAEs and NAEs, which confirms that the formation of the (lyso)-NAPEs by PLA2G4E is the rate-limiting step in biosynthetic pathways of these signaling lipids. In line with previous findings<sup>6</sup>, PLA2G4E overexpression resulted in increased levels of all NAPE species analyzed. The greater increase in *N*-16:0 and *N*-18:1 species reflects the relative abundance of these lipid chains in PC, suggesting limited substrate preference of PLA2G4E.<sup>52</sup> Treatment with control compound **WEN258** increased the levels of some NAPEs, which could be the result of inhibition of NAPE-metabolizing enzymes (e.g. ABHD4 or FAAH). As **WEN091** and **WEN258** share a similar off-target profile, this could indicate that the effect of **WEN091** on NAPE levels is underestimated due to inhibition of other enzymes.

The elevated levels of lyso-NAPes and GP-PEA in PLA2G4E-overexpressing cells could be the result of ABHD4 activity in these cells, which has been reported before.<sup>53</sup> Treatment with **WEN091** or **WEN258** decreased GP-PEA levels, indicating both compounds inhibited ABHD4, which is in line with **WEN091**'s chemical proteomics results (Supplementary Figure S3.3). In contrast, lyso-NAPE levels were in general lowered by **WEN091**, but not affected by **WEN258**. This suggests the existence of an ABHD4-independent biosynthesis pathway for these lipids. Previously, Ca<sup>2+</sup>-dependent *N*-acylation of lyso-PE in ischemic tissue has been suggested.<sup>54</sup> This activity might be attributed to PLA2G4E, leading to the hypothesis that PLA2G4E is responsible for the direct biosynthesis of both NAPes and lyso-NAPes in these cells (Figure 3.8). *N*-22:6 NAPE levels were elevated by PLA2G4E overexpression, but *N*-22:6 lyso-NAPes were not. Treatment with **WEN091** or **WEN258** increased *N*-22:6 lyso-NAPE levels, possibly through inhibition of their degradation by ABHD4. This might suggest that these specific species are biosynthesized in a PLA2G4E-independent manner. Further research is needed to dissect the specific metabolic pathways of the individual lipid species. Both **WEN091** and **WEN258** lowered the levels of 2-AG and FFAs. The cABPP results showed that **WEN091** inhibited 2-AG-producing enzyme DAGL $\beta$ , but **WEN258** did not. Both compounds, however, inhibited ABHD6, which was previously reported to have diacylglycerol lipase activity in Neuro-2a (see also Chapter 6).<sup>53</sup> Thus, these results may indicate that ABHD6 is responsible for tonic 2-AG levels in these cells. As many enzymes are involved in FFA production (including PLA2G4A, ABHD4, ABHD6 and FAAH), inhibition of one or more of these enzymes by both compounds can account for the observed changes.

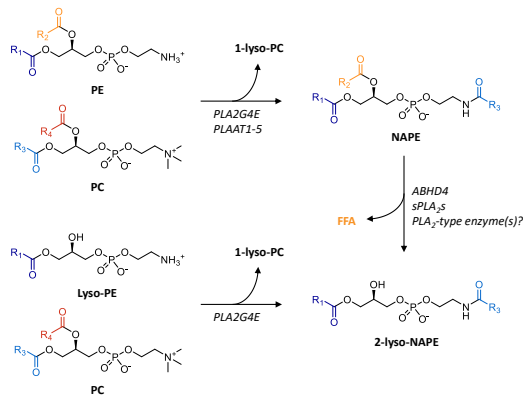


**Figure 3.8. Putative updated overview of lyso-NAPE biosynthesis pathways.** This work suggests the existence of ABHD4-independent NAPE-hydrolytic activity, which could be attributed to secretory PLA<sub>2</sub>s (sPLA<sub>2</sub>s) or other unidentified PLA<sub>2</sub>-type enzymes, or to direct biosynthesis of lyso-NAPes from lyso-PE by PLA2G4E. R = saturated, mono- or polyunsaturated fatty acyl.

Triazole urea-based inhibitors have been leveraged for targeting multiple enzymes within the serine hydrolase superfamily, including ABHD6, DAGL $\alpha$ , DDHD2 and LyPLA1/2.<sup>47,55–58</sup> The cellular selectivity of azole urea-based inhibitors was previously shown to deviate from the biochemical profile<sup>49,59</sup>, as was observed with **WEN091** in this study. Tuning the reactivity of the urea and the interactions of the azole with the active site is likely important to obtain selectivity.<sup>60</sup> Further improvement of the selectivity profile of **WEN091** using these parameters is required to investigate the effects of acute PLA2G4E inhibition in cellular and *in vivo* systems (see Chapter 4).

## Acknowledgements

Michael Schafroth and Benjamin Cravatt are kindly acknowledged for performing NAT assays and chemical proteomics, Xinyu Di, Thomas Hankemeier and Wouter Driever for targeted lipidomics, Wouter Driever and Laura de Paus for selectivity assays. Hans den Dulk and Tom van der Wel are acknowledged for plasmid cloning and purification.

## Experimental procedures

### General remarks

All reagents and chemicals were obtained from Bio-Rad or Thermo Fisher Scientific, solvents from Sigma-Aldrich and used without further purification, unless otherwise noted. Activity-based probes were purchased from Thermo Fisher Scientific (FP-TAMRA) or synthesized in-house (MB064)<sup>61</sup> (Chemical structures shown in Supplementary Figure S3.8). **WEN091** was synthesized as described in Chapter 2.

### Plasmids

The full-length cDNA of wild type human PLA2G4E (GenScript Biotech), murine PLA2G4B, hPLA2G4C, mPLA2G4D (Source BioScience), hPLAAT2–5 and hNAPE-PLD (kindly provided by Prof. Natsuo Ueda) were cloned into pcDNA™3.1(+) expression vectors in-frame with a C-terminal FLAG tag. Plasmids were isolated from transformed *Escherichia coli* XL-10 using a Qiagen Plasmid Midi kit and stored at 4°C in TE buffer (10 mM Tris, 0.1 mM EDTA, pH 8.0). The sequence was determined (Macrogen) and verified using CLC Main Workbench.

### Cell culture

HEK293T (human embryonic kidney) and Neuro-2a (murine neuroblastoma) cells (ATCC) were cultured in Dulbecco's Modified Eagle's Medium (DMEM, Sigma-Aldrich D6546) with additional heat-inactivated newborn calf serum (10% (v/v), Avantor Seradigm), L-Ala-L-Gln (2 mM, Sigma-Aldrich), penicillin and streptomycin (both 200 µg/mL, Duchefa Biochemie) at 37°C, 7% CO<sub>2</sub>. Medium was refreshed every 2–3 days and cells were passaged twice a week at 70–80% confluence by aspirating the medium, thorough pipetting in fresh medium and seeding to appropriate density. Cell cultures were regularly tested for mycoplasma and discarded after 2–3 months.

### Overexpression lysate preparation

One day prior to transfection, 10<sup>7</sup> HEK293T cells were seeded to a 15 cm dish. For transfection, medium was replaced with 13 mL fresh medium. Per 15 cm dish, 20 µg pcDNA™3.1(+) plasmid was dissolved in 1 mL serum-free DMEM and mixed with 1 mL serum-free DMEM containing 60 µg polyethyleneimine (PEI, Polysciences). The mixture was incubated for 15 min and added dropwise to the cells. 24 h p.t., medium was replaced with 25 mL fresh medium. 72 h p.t., medium was aspirated, cells were washed with Dulbecco's PBS (DPBS, Sigma-Aldrich D8537, RT) and harvested in DPBS (RT) by thorough pipetting. Cells were centrifuged (3000 × *g*, 15 min), pellets were flash-frozen in liquid N<sub>2</sub> and stored at –80°C until further use.

Cell pellets were thawed on ice, homogenized in 2 mL ice-cold lysis buffer (50 mM Tris-HCl, 2 mM DTT, 1 mM MgCl<sub>2</sub>, 5 U/mL Benzonase® (Santa Cruz Biotechnology, Inc.), pH 8.0 with additional 3 mM CaCl<sub>2</sub> for hPLA2G4E) per 15 cm cell culture dish using a Sonics® Vibra-Cell VCX 130 probe sonicator equipped with a 2 mm microtip (3 × 10 s on/10 s off, 20% amplitude). After incubation on ice for 30 min, the insoluble ("membrane") fraction was separated from the soluble ("cytosol") fraction by ultracentrifugation (10<sup>5</sup> × *g*, 35 min, 4°C, Beckman-Coulter ultracentrifuge, Ti70.1 rotor). The pellet was resuspended in 1 mL ice-cold storage buffer (50 mM Tris-HCl, 2 mM DTT, pH 8.0 with additional 3 mM CaCl<sub>2</sub> for hPLA2G4E) per 15 cm plate and homogenized by passing through an insulin needle. After determination of the protein concentration using a Quick Start™ Bradford Protein Assay, the samples were diluted to 1.0 mg/mL (hPLA2G4E, mPLA2G4B, hPLA2G4C and mPLA2G4D) or 0.5 mg/mL (mPLA2G4E) in ice-cold storage buffer, aliquoted to single-use volumes, flash-frozen in liquid N<sub>2</sub> and stored at –80°C until use.



mPLA2G4E plasmids were cloned as described before<sup>6</sup>. 48 h p.t., medium was aspirated, cells were washed with PBS and harvested by scraping in PBS. After centrifugation the pellet was resuspended in lysis buffer (50 mM Tris-HCl, 0.5% IGEPAL CA-630, pH 8.0) and sonicated. Insoluble proteins were removed by ultracentrifugation ( $10^5 \times g$ , 15 min), after which the supernatant was aliquoted, flash-frozen in liquid N<sub>2</sub> and stored at  $-80^\circ\text{C}$  until use.

hPLAAT2–5, hNAPE-PLD and CB<sub>1/2</sub> overexpression and lysate preparation was performed as described before.<sup>44,46</sup>

### Mouse brain lysate preparation

For ABPP experiments, mouse brains were harvested from surplus C57Bl/6J mice (8–14 weeks old) that were killed by cervical dislocation, according to guidelines approved by the ethical committee of Leiden University (AVD1060020171144), immediately flash-frozen in liquid N<sub>2</sub> and stored at  $-80^\circ\text{C}$  until use. Upon preparation, intact brains were thawed on ice and homogenized in 6 mL ice-cold lysis buffer (20 mM HEPES, 2 mM DTT, 250 mM sucrose, 1 mM MgCl<sub>2</sub>, 25 U/mL Benzonase®, pH 6.8) using a Wheaton™ dounce homogenizer (DWK Life Sciences) and incubated on ice for 1 h. Cell debris was removed by low-speed centrifugation ( $170 \times g$ , 5 min,  $4^\circ\text{C}$ ), after which the supernatant was subjected to ultracentrifugation to separate insoluble (“membrane”) and soluble (“cytosol”) fractions ( $10^5 \times g$ , 35 min,  $4^\circ\text{C}$ , Beckman-Coulter ultracentrifuge, Ti70.1 rotor). The pellet was resuspended in ice-cold storage buffer (20 mM HEPES, 2 mM DTT, pH 6.8) and homogenized by passing through an insulin needle. The protein concentrations of both fractions were determined using a Quick Start™ Bradford Protein Assay and samples were diluted to 2.0 mg/mL (membrane) or 1.0 mg/mL (cytosol) using ice-cold storage buffer, aliquoted to single-use volumes, flash-frozen in liquid N<sub>2</sub> and stored at  $-80^\circ\text{C}$  until use.

For Ca-NAT activity assays, mouse brains were harvested from male C57Bl/6J mice (10 weeks old) which were anesthetized with isoflurane and killed by cervical dislocation, according to guidelines approved by The Scripps Research Institute-Institutional Animal Care and Use Committee Office, immediately flash-frozen in liquid N<sub>2</sub> and stored at  $-80^\circ\text{C}$  until use. Upon preparation, intact brains were thawed on ice and homogenized in 5 volumes (v/w) ice-cold lysis buffer (50 mM Tris-HCl, 320 mM sucrose, pH 8.0) using a dounce homogenizer. Ultracentrifugation ( $10^5 \times g$ , 15 min) yielded the cytosol fraction as supernatant, after which the pellet was washed with 50 mM Tris-HCl, 1 M NaCl (pH 8.0) and centrifuged again. The resulting pellet was resuspended in 50 mM Tris-HCl (pH 8.0) and used as membrane fraction. Fractions were aliquoted, flash-frozen in liquid N<sub>2</sub> and stored at  $-80^\circ\text{C}$  until use.

### Activity-based protein profiling

HEK293T or mouse brain lysates were thawed on ice. 19.5  $\mu\text{L}$  lysate was incubated with 0.5  $\mu\text{L}$  inhibitor solution in DMSO (Sigma-Aldrich) for 30 min (RT), followed by addition of 0.5  $\mu\text{L}$  probe in DMSO (hPLA2G4E: FP-TAMRA, 50 nM, 5 min; mPLA2G4E: FP-TAMRA, 100 nM, 5 min; mPLA2G4B, hPLA2G4C, mPLA2G4D: FP-TAMRA, 500 nM, 20 min; hPLAAT2, hPLAAT3: MB064, 250 nM, 20 min; hPLAAT4, hPLAAT5: MB064, 500 nM, 20 min; mouse brain: FP-TAMRA, 500 nM, 20 min or MB064, 250 nM, 20 min, RT. Final DMSO concentration 5% (v/v)). The reaction was quenched by addition of 7  $\mu\text{L}$  4 $\times$  Laemmli sample buffer (240 mM Tris, 8% (w/v) SDS, 40% (v/v) glycerol, 5% (v/v)  $\beta$ -mercaptoethanol (Sigma-Aldrich), 0.04% bromophenol blue) and incubation for 15 min at RT. 10  $\mu\text{L}$  sample was resolved on 8% (hPLA2G4E), 10% (mPLA2G4E, mPLA2G4B, hPLA2G4C, mPLA2G4D, mouse brain) or 15% (hPLAAT2–5) acrylamide SDS-PAGE gels (180V, 75 min) and the gel was imaged on a Bio-Rad Chemidoc MP using Cy3/TAMRA settings (ex. 532/12 nm, em. 602/50 nm). Coomassie Brilliant Blue

R250 staining was used for total protein loading correction. Images were analyzed using Bio-Rad Image Lab 6. IC<sub>50</sub> calculations were performed in GraphPad Prism 7.

### ***In vitro* NAPE production assay**

HEK293T overexpression lysate (diluted to 40  $\mu$ L 0.1 mg/mL in assay buffer (50 mM Tris-HCl, 2 mM DTT, 3 mM CaCl<sub>2</sub>, 0.1% IGEPAL CA-630, pH 8.0)) or mouse brain membrane proteome (diluted to 40  $\mu$ L 2.0 mg/mL in assay buffer) were incubated with inhibitor in DMSO (30 min, 37°C), followed by treatment with *sn*-1,2-dipalmitoylphosphatidylcholine (DPPC, Avanti Polar Lipids) and *sn*-1,2-dioleoylphosphatidylethanolamine (DOPE, Cayman Chemicals) (final concentrations 40  $\mu$ M and 75  $\mu$ M, respectively (HEK293T), or 250  $\mu$ M each (mouse brain)) for 30 (HEK293T) or 60 min (mouse brain) at 37°C. Reactions were quenched by addition of 150  $\mu$ L 2:1 MeOH:CHCl<sub>3</sub> containing 10 pmol *N*-C19:1 DOPE internal standard<sup>23</sup>, followed by 50  $\mu$ L CHCl<sub>3</sub> and 50  $\mu$ L 0.9% KCl in water. After centrifugation, layers were separated and 100  $\mu$ L of the organic layer was mixed with 50  $\mu$ L MeOH.

The sample was injected into the LC-MS system consisting of an LC/MSD (Agilent Technologies). Separation was performed in a Phenomenex Gemini C18 analytical column (50 mm  $\times$  4.6 mm  $\times$  5  $\mu$ m) coupled to a Gemini C18 guard column (4  $\times$  3 mm). The mobile phase consisted of 14 mM NH<sub>4</sub>OH in 95:5 (v/v) H<sub>2</sub>O:MeOH (A) and 14 mM NH<sub>4</sub>OH in 60:35:5 *i*PrOH:MeOH:H<sub>2</sub>O (B). The elution method started with 0.1 mL/min 90% A for 5 min, followed by 0.4 mL 100% B for 6.5 min and final equilibration with 0.5 mL/min 90% A for 2 min. Lipids were detected with electrospray ionization (ESI) operating in negative ion mode and MS acquisition in selected ion monitoring mode (*m/z* 980.8 and 1020.8 for *N*-C16:0 DOPE product and *N*-C19:1 DOPE internal standard, respectively).

### **NAPE-PLD activity assay**

The activity of hNAPE-PLD was measured in a fluorogenic surrogate substrate assay based on *N*-((6-(2,4-dinitrophenyl)amino)hexanoyl)-2-(4,4-difluoro-5,7-dimethyl-4-bora-3a,4a-diaza-*s*-indacene-3-pentanoyl)-1-hexadecanoyl-*sn*-glycero-3-phosphoethanolamine, triethylammonium salt (PED6) as described before, with minor alterations.<sup>45</sup> Fluorescence measurements were performed in a BMG LABTECH CLARIOstar® plate reader, scanning every 2 minutes for 1 h (37°C, ex. 485 nm, em. 535 nm, gain 1054). The slope of  $t = 2$  min to  $t = 6$  min was used as the enzymatic rate (RFU/min), which was normalized to generate IC<sub>50</sub> curves in GraphPad Prism 9. All measurements were performed in  $N = 2$ ,  $n = 2$  or  $N = 2$ ,  $n = 4$  for controls and only accepted when  $Z' \geq 0.6$ .

### **CB<sub>1/2</sub> assay**

The [<sup>3</sup>H]CP55,940 displacement assay was performed as described before.<sup>46</sup>

## **Chemical proteomics**

### **Sample preparation**

Mouse brain membrane or cytosol proteome (500  $\mu$ L, 2.0 mg/mL in 50 mM Tris-HCl, 2 mM DTT, 3 mM CaCl<sub>2</sub>, pH 8.0) was incubated with DMSO or 1  $\mu$ M WEN091 in DMSO for 30 min (37°C), followed by labeling of residual enzyme activity with 4  $\mu$ M FP-biotin for 60 min (RT). Labeling of heat-denatured proteome was used as control. Reactions were quenched by protein precipitation in 2.5 mL 4:1 MeOH/CHCl<sub>3</sub>. The mixture was centrifuged (5000  $\times g$ , 15 min, 4°C), after which the pellet was washed with 1:1 MeOH/CHCl<sub>3</sub> (3  $\times$  1 mL) and then probe sonicated in 2.5 mL 4:1 MeOH/CHCl<sub>3</sub> and pelleted again (5000  $\times g$ , 15 min, 4°C). The pellet was redissolved in 500  $\mu$ L 50 mM Tris-HCl, 6 M urea, 2% (w/v) SDS, 10 mM DTT, pH 8.0, reduced using Tris(2-carboxyethyl)phosphine (TCEP) (10 mM, 30 min, 37°C) and methylated with iodoacetamide (20 mM, 30 min, 25°C in the dark). Biotinylated proteins were enriched by sequential addition of 140  $\mu$ L 10% (w/v) SDS, 5.5 mL PBS and 20  $\mu$ L PBS-washed avidin-

agarose beads (Sigma-Aldrich) and shaking (1.5 h, 25°C). Beads were pelleted (1000 × *g*, 2 min), washed sequentially with 0.2% (w/v) SDS in PBS (3 × 10 mL), PBS (3 × 10 mL) and 100 mM triethylammonium bicarbonate (3 × 10 mL) and transferred to an Eppendorf LoBind® tube. On-bead digestion was performed using Promega Sequencing Grade trypsin (500 ng) in 100 mM triethylammonium bicarbonate. Resulting peptides were labeled with either 4% formaldehyde (“light”) or <sup>13</sup>C-labeled deuterated formaldehyde (“heavy”) (0.15% final concentration) in combination with NaBH<sub>3</sub>CN (22.2 mM, 1h, RT). The reaction was quenched by addition of 1% NH<sub>4</sub>OH and 5% formic acid (final concentrations 0.23% and 0.5%, respectively), after which the light and heavy-labeled samples were combined for analysis.

### LC-MS/MS analysis

4 μL was injected into the LC-MS/MS system, consisting of an Agilent 1200 HPLC coupled to an LTQ Orbitrap Velos. Separation was performed on an in-house packed tip column (Phenomenex Gemini 5 μm C18, 150 × 0.1 mm), using a linear gradient of CH<sub>3</sub>CN in 0.1% formic acid with a flow rate of 300 nL/min. Each full-scan mass spectrum (350–2000 *m/z*) was followed by top 20 data-dependent MS/MS scans. Dynamic exclusion was used with an exclusion list of 500 and a repeat time of 20 s.

MS/MS spectra were searched against a FASTA file of serine hydrolases assembled from the mouse UniProt database (retrieved Nov 9, 2012) with the ProLuCID algorithm using a target-decoy approach, in which each protein sequence was reversed and concatenated to the normal database. Search parameters were set to a 50-ppm precursor mass tolerance, with carbamidomethylation of cysteine residues (+57.0215 Da) as a static modification and oxidation of methionine residues (+15.9949 Da) as a variable modification. In addition, methylation of lysine residues and N-termini (light: +28.0313 Da, heavy: +34.06312 Da) was specified as static modification. Search results were filtered with DTASelect 2.0.47, limiting to tryptic peptides and applying a peptide FDR < 1%, and for serine hydrolase annotations (both reviewed and unreviewed). Ratios of peak areas were quantified using CIMAGE software by generating a MS1 chromatogram (± 10 ppm) using a retention time window of ± 10 min centered on the time the peptide was selected for fragmentation. Computation filters included a co-elution correlation score  $R^2 \geq 0.8$  and an isotopic envelope correlation score  $R^2 > 0.8$ . Proteins only detected in either light or heavy-labeled samples were manually given a maximal or minimal ratio of 5 or 0.05, respectively.

### Cellular ABPP assay

Two days prior to the experiment, Neuro-2a cells were seeded to 12-wells plates (~0.25 · 10<sup>6</sup> cells per well). Before the experiment was started, medium was aspirated. Medium with DMSO or inhibitor in DMSO (0.25% (v/v) DMSO) was added and cells were incubated for 30 min at 37°C. Then medium was aspirated and cells were washed with DPBS (RT). Cells were harvested in ice-cold DPBS by thorough pipetting and centrifuged (1000 × *g*, 6 min, RT). Pellets were flash-frozen in liquid N<sub>2</sub> and stored at –80°C until further use.

Cell pellets were thawed on ice and lysed in 50 μL lysis buffer (20 mM HEPES, 2 mM DTT, 250 mM sucrose, 1 mM MgCl<sub>2</sub>, 25 U/mL Benzonase®, pH 6.8). After incubation on ice for 20 min, the protein concentration was determined using Quick Start™ Bradford Protein Assay and the samples were diluted to 2.0 mg/mL using storage buffer (20 mM HEPES, 2 mM DTT, pH 6.8). 19.5 μL of this whole lysate was incubated with FP-TAMRA (500 nM) or MB064 (2 μM) in DMSO (20 min, RT). Reactions were then quenched with 7 μL 4× Laemmli sample buffer and proteins were resolved and images analyzed as described under Activity-based protein profiling.

## Targeted lipidomics

### Sample preparation

One day prior to transfection, Neuro-2a cells were seeded to 6-cm dishes ( $\sim 1.8 \cdot 10^6$  cells per dish). Upon transfection, medium was replaced with 2 mL fresh medium. Per dish, 1  $\mu$ g PLA2G4E or mock plasmid was dissolved in 100  $\mu$ L serum-free DMEM and mixed with 100  $\mu$ L serum-free DMEM containing 5  $\mu$ g polyethyleneimine (PEI, Polysciences). The mixture was incubated for 15 min and added dropwise to the cells. After 24 h, cells were harvested or inhibitor treatment was started. For harvest, medium was removed and cells were washed with 500  $\mu$ L DPBS (RT) and harvested in 1250  $\mu$ L DPBS by thorough pipetting. 1000  $\mu$ L of the cell suspension was centrifuged ( $1000 \times g$ , 5 min) in Eppendorf® Safe-Lock tubes and the pellet was flash-frozen in liquid N<sub>2</sub> and stored at  $-80^\circ\text{C}$  until further use. The remaining 250  $\mu$ L was used for cell count (Trypan Blue). For inhibitor experiments, inhibitor in DMSO was diluted in DMEM (0.25% (v/v) DMSO) to prepare treatment medium. Medium was replaced with 2 mL treatment medium per dish and cells were incubated for 8 h ( $37^\circ\text{C}$ ). Cells were harvested as described above.

### Lipid extraction

Pellets were thawed on ice. To each sample 10  $\mu$ L internal standard mix (reference lipids *N*-heptadecanoyl (17:0)-1,2-dioleoyl (18:1)-*sn*-glycero-3-phosphoethanolamine, *N*-heptadecanoyl-1-oleoyl-2-lyso-*sn*-glycero-3-phosphoethanolamine, *N*-heptadecanoyl-1-(1-enyl-stearoyl) (p18:0)-2-stearoyl (18:0)-*sn*-glycero-3-phosphoethanolamine, *N*-heptadecanoyl-1-(1-enyl-stearoyl)-2-lyso-*sn*-glycero-3-phosphoethanolamine (all synthesized in-house), *N*-palmitoyl (16:0) ethanolamine-d<sub>4</sub>, *N*-stearoyl ethanolamine-d<sub>3</sub>, *N*-oleoyl ethanolamine-d<sub>4</sub>, *N*-linoleoyl (18:2) ethanolamine-d<sub>4</sub>, *N*-arachidonoyl (20:4) ethanolamine-d<sub>8</sub>, *N*-docosahexaenoyl (22:6) ethanolamine-d<sub>4</sub> and 2-arachidonoylglycerol-d<sub>8</sub> (Cayman Chemical Company)) was added, followed by 100  $\mu$ L extraction buffer (0.2 M citric acid, 0.1 M Na<sub>2</sub>HPO<sub>4</sub>, pH 4) and 1000  $\mu$ L extractant (1:1 (v/v) MTBE:BuOH). Samples were mixed in a Next Advance Bullet Blender® Blue tissue homogenizer (5 min, 90% speed, RT) and centrifuged ( $16,000 \times g$ , 10 min,  $4^\circ\text{C}$ ). 950  $\mu$ L of the organic layer was transferred to clean, pre-cooled tubes and concentrated in a SpeedVac Vacuum Concentrator (Thermo Fisher Scientific). 50  $\mu$ L reconstitution solution (1:1 (v/v) BuOH:CH<sub>3</sub>CN) was added and the samples were agitated for 15 min, after which they were centrifuged ( $16,000 \times g$ , 10 min,  $4^\circ\text{C}$ ). 40  $\mu$ L was transferred into autosampler vials with inserts. Samples were kept at  $7^\circ\text{C}$  in the autosampler for less than 24 h before analysis. Quality control (QC) samples were simultaneously prepared using blank cell pellets.

### LC-MS/MS analysis

10  $\mu$ L of sample was analyzed using a Shimadzu LC system hyphenated with a SCIEX QTRAP® 6500+ mass spectrometer. Separation was performed on a Acquity BEH C8 column (2.1  $\times$  50 mm, 1.7  $\mu$ m) (Waters Corporation) maintained at  $40^\circ\text{C}$ , with the eluent flow rate set to 0.4 mL/min. The mobile phase consisted of 2 mM NH<sub>4</sub>HCO<sub>2</sub>, 10 mM formic acid in water (A), CH<sub>3</sub>CN (B) and isopropanol (C). Initial gradient conditions were 20% B, 20% C for 1 min, followed by linear increase to 40% B, 20% C over the course of 1 min, which was held for 5 min. It was then linearly increased to 40% B, 50% C over the course of 1 min, which was held for 2.5 min. The system returned to initial conditions and was re-equilibrated for 1.5 min. Electrospray ionization (ESI)-MS acquisition was carried out in positive and negative mode with the following ESI parameters: source temperature:  $600^\circ\text{C}$ , nebulizer gas: 50 L/min, heater gas: 50 L/min, curtain gas: 30 L/min, collision gas: medium, ion spray voltage:  $\pm 4500$  V. Selected reaction monitoring (SRM) was used for data acquisition. Peak detection and integration were carried out in SCIEX OS software. Relative lipid levels were calculated as the ratio of analyte peak

to corresponding internal standard. QC samples were regularly injected during the measurements to evaluate the quality of the data, including blank effect (BE), retention time shifts and relative standard deviation (RSD) calculated for analyte present in the QC samples. Metabolites with  $BE \leq 40\%$  and  $RSD \leq 30\%$  were included for further analysis. Metabolites with  $15\% \leq RSD \leq 30\%$  were reported, but should be interpreted with caution. Relative lipid levels were corrected for cell count and normalized to mock-transfected cells or DMSO-treated cells. Relative levels were transferred to GraphPad Prism 8 for statistical analysis. Each lipid was tested for equality between treatment and control groups using one-way ANOVA with Dunnett's multiple comparison correction.

## References

1. Leslie, C. C. Cytosolic phospholipase A<sub>2</sub>: Physiological function and role in disease. *J. Lipid Res.* **56**, 1386–1402 (2015).
2. Murakami, M. *et al.* Recent progress in phospholipase A<sub>2</sub> research: From cells to animals to humans. *Prog. Lipid Res.* **50**, 152–192 (2011).
3. Ghomashchi, F. *et al.* Interfacial kinetic and binding properties of mammalian group IVB phospholipase A<sub>2</sub> (cPLA<sub>2</sub>β) and comparison with the other cPLA<sub>2</sub> isoforms. *J. Biol. Chem.* **285**, 36100–36111 (2010).
4. Ohto, T., Uozumi, N., Hirabayashi, T. & Shimizu, T. Identification of novel cytosolic phospholipase A<sub>2</sub>s, murine cPLA<sub>2</sub>δ, ε, and ζ, which form a gene cluster with cPLA<sub>2</sub>β. *J. Biol. Chem.* **280**, 24576–24583 (2005).
5. Ghosh, M., Tucker, D. E., Burchett, S. A. & Leslie, C. C. Properties of the Group IV phospholipase A<sub>2</sub> family. *Prog. Lipid Res.* **45**, 487–510 (2006).
6. Ogura, Y., Parsons, W. H., Kamat, S. S. & Cravatt, B. F. A calcium-dependent acyltransferase that produces *N*-Acyl phosphatidylethanolamines. *Nat. Chem. Biol.* **12**, 669–671 (2016).
7. Hussain, Z. *et al.* Phosphatidylserine-stimulated production of *N*-acyl-phosphatidylethanolamines by Ca<sup>2+</sup>-dependent *N*-acyltransferase. *Biochim. Biophys. Acta - Mol. Cell Biol. Lipids* **1863**, 493–502 (2018).
8. Wellner, N., Diep, T. A., Janfelt, C. & Hansen, H. S. *N*-acylation of phosphatidylethanolamine and its biological functions in mammals. *Biochim. Biophys. Acta - Mol. Cell Biol. Lipids* **1831**, 652–662 (2013).
9. Hansen, H. S., Moesgaard, B., Hansen, H. H., Schousboe, A. & Petersen, G. Formation of *N*-acyl-phosphatidylethanolamine and *N*-acylethanolamine (including anandamide) during glutamate-induced neurotoxicity. *Lipids* **34**, S327–S330 (1999).
10. Swamy, M. J., Tarafdar, P. K. & Kamlekar, R. K. Structure, phase behaviour and membrane interactions of *N*-acylethanolamines and *N*-acylphosphatidylethanolamines. *Chem. Phys. Lipids* **163**, 266–279 (2010).
11. Térová, B., Petersen, G., Hansen, H. S. & Slotte, J. P. *N*-acyl phosphatidylethanolamines affect the lateral distribution of cholesterol in membranes. *Biochim. Biophys. Acta - Biomembr.* **1715**, 49–56 (2005).
12. Shangguan, T., Pak, C. C., Ali, S., Janoff, A. S. & Meers, P. Cation-dependent fusogenicity of an *N*-acyl phosphatidylethanolamine. *Biochim. Biophys. Acta* **1368**, 171–183 (1998).
13. Palese, F., Pontis, S., Realini, N. & Piomelli, D. NAPE-specific phospholipase D regulates LRRK2 association with neuronal membranes. in *Advances in Pharmacology* **90**, 217–238 (Academic Press Inc., 2021).
14. Mileykovskaya, E. & Dowhan, W. Role of membrane lipids in bacterial division-site selection. *Curr. Opin. Microbiol.* **8**, 135–142 (2005).
15. Gillum, M. P. *et al.* *N*-acylphosphatidylethanolamine, a Gut-Derived Circulating Factor Induced by Fat Ingestion, Inhibits Food Intake. *Cell* **135**, 813–824 (2008).
16. Romano, A., Tempesta, B., Provensi, G., Passani, M. B. & Gaetani, S. Central mechanisms mediating the hypophagic effects of oleoylethanolamide and *N*-acylphosphatidylethanolamines: Different lipid signals? *Front. Pharmacol.* **6**, 1–8 (2015).
17. Shiratsuchi, A. *et al.* Inhibitory effect of *N*-palmitoylphosphatidylethanolamine on macrophage phagocytosis through inhibition of Rac1 and Cdc42. *J. Biochem.* **145**, 43–50 (2008).

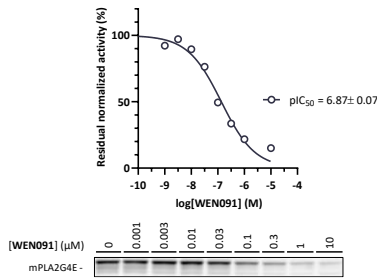
18. Uyama, T. *et al.* Generation of *N*-acylphosphatidylethanolamine by members of the phospholipase A/acyltransferase (PLA/AT) family. *J. Biol. Chem.* **287**, 31905–31919 (2012).
19. Uyama, T., Jin, X. H., Tsuboi, K., Tonai, T. & Ueda, N. Characterization of the human tumor suppressors TIG3 and HRASLS2 as phospholipid-metabolizing enzymes. *Biochim. Biophys. Acta - Mol. Cell Biol. Lipids* **1791**, 1114–1124 (2009).
20. Okamoto, Y., Morishita, J., Tsuboi, K., Tonai, T. & Ueda, N. Molecular Characterization of a Phospholipase D Generating Anandamide and Its Congeners. *J. Biol. Chem.* **279**, 5298–5305 (2004).
21. Tsuboi, K. *et al.* Glycerophosphodiesterase GDE4 as a novel lysophospholipase D: A possible involvement in bioactive *N*-acylethanolamine biosynthesis. *Biochim. Biophys. Acta - Mol. Cell Biol. Lipids* **1851**, 537–548 (2015).
22. Sun, Y. X. *et al.* Biosynthesis of anandamide and *N*-palmitoylethanolamine by sequential actions of phospholipase A2 and lysophospholipase D. *Biochem. J.* **380**, 749–756 (2004).
23. Simon, G. M. & Cravatt, B. F. Endocannabinoid biosynthesis proceeding through glycerophospho-*N*-acyl ethanolamine and a role for  $\alpha/\beta$ -hydrolase 4 in this pathway. *J. Biol. Chem.* **281**, 26465–26472 (2006).
24. Liu, J. *et al.* Multiple pathways involved in the biosynthesis of anandamide. *Neuropharmacology* **54**, 1–7 (2008).
25. Rahman, I. A. S. *et al.* Calcium-dependent generation of *N*-acylethanolamines and lysophosphatidic acids by glycerophosphodiesterase GDE7. *Biochim. Biophys. Acta - Mol. Cell Biol. Lipids* **1861**, 1881–1892 (2016).
26. Simon, G. M. & Cravatt, B. F. Anandamide biosynthesis catalyzed by the phosphodiesterase GDE1 and detection of glycerophospho-*N*-acyl ethanolamine precursors in mouse brain. *J. Biol. Chem.* **283**, 9341–9349 (2008).
27. Liu, J. *et al.* A biosynthetic pathway for anandamide. *Proc. Natl. Acad. Sci. U. S. A.* **103**, 13345–13350 (2006).
28. Mattace Raso, G., Russo, R., Calignano, A. & Meli, R. Palmitoylethanolamide in CNS health and disease. *Pharmacol. Res.* **86**, 32–41 (2014).
29. Petrosino, S. & Di Marzo, V. The pharmacology of palmitoylethanolamide and first data on the therapeutic efficacy of some of its new formulations. *Br. J. Pharmacol.* **174**, 1349–1365 (2017).
30. Dalle Carbonare, M. *et al.* A saturated *N*-acylethanolamine other than *N*-palmitoyl ethanolamine with anti-inflammatory properties: A neglected story... *J. Neuroendocrinol.* **20**, 26–34 (2008).
31. Fu, J. *et al.* Oleylethanolamide regulates feeding and body weight through activation of the nuclear receptor PPAR- $\alpha$ . *Nature* **425**, 90–93 (2003).
32. Tsuboi, K., Uyama, T., Okamoto, Y. & Ueda, N. Endocannabinoids and related *N*-acylethanolamines: biological activities and metabolism. *Inflamm. Regen.* **38**, (2018).
33. Morena, M. *et al.* Upregulation of anandamide hydrolysis in the basolateral complex of amygdala reduces fear memory expression and indices of stress and anxiety. *J. Neurosci.* **39**, 1275–1292 (2019).
34. Devane, W. A. *et al.* Isolation and structure of a brain constituent that binds to the cannabinoid receptor. *Science* **258**, 1946–1949 (1992).
35. Maccarrone, M. *et al.* Anandamide inhibits metabolism and physiological actions of 2-arachidonoylglycerol in the striatum. *Nat. Neurosci.* **11**, 152–159 (2008).
36. Katona, I. & Freund, T. F. Multiple Functions of Endocannabinoid Signaling in the Brain. *Annu. Rev. Neurosci.* **35**, 529–558 (2012).

37. Fotio, Y., Ciccocioppo, R. & Piomelli, D. *N*-acylethanolamine acid amidase (NAAA) inhibition decreases the motivation for alcohol in Marchigian Sardinian alcohol-preferring rats. *Psychopharmacology* **238**, 249–258 (2021).
38. Cravatt, B. F. *et al.* Molecular characterization of an enzyme that degrades neuromodulatory fatty-acid amides. *Nature* **384**, 83–87 (1996).
39. Berger, C. *et al.* Massive accumulation of *N*-acylethanolamines after stroke. Cell signalling in acute cerebral ischemia? *J. Neurochem.* **88**, 1159–1167 (2004).
40. Palese, F., Pontis, S., Realini, N. & Piomelli, D. A protective role for *N*-acylphosphatidylethanolamine phospholipase D in 6-OHDA-induced neurodegeneration. *Sci. Rep.* **9**, 1–16 (2019).
41. Tuo, W. *et al.* Therapeutic Potential of Fatty Acid Amide Hydrolase, Monoacylglycerol Lipase, and *N*-Acylethanolamine Acid Amidase Inhibitors. *J. Med. Chem.* **60**, 4–46 (2016).
42. Cadas, H., Di Tomaso, E. & Piomelli, D. Occurrence and biosynthesis of endogenous cannabinoid precursor, *N*-arachidonoyl phosphatidylethanolamine, in rat brain. *J. Neurosci.* **17**, 1226–1242 (1997).
43. Mock, E. D. *et al.* Discovery of a NAPE-PLD inhibitor that modulates emotional behavior in mice. *Nat. Chem. Biol.* **16**, 667–675 (2020).
44. Zhou, J. *et al.* Structure-Activity Relationship Studies of  $\alpha$ -Ketoamides as Inhibitors of the Phospholipase A and Acyltransferase Enzyme Family. *J. Med. Chem.* **63**, 9340–9359 (2020).
45. Mock, E. D. *et al.* Structure-Activity Relationship Studies of Pyrimidine-4-Carboxamides as Inhibitors of *N*-Acylphosphatidylethanolamine Phospholipase D. *J. Med. Chem.* **64**, 481–515 (2021).
46. Soethoudt, M. *et al.* Cannabinoid CB<sub>2</sub> receptor ligand profiling reveals biased signalling and off-target activity. *Nat. Commun.* **8**, (2017).
47. Hsu, K. L. *et al.* Discovery and optimization of piperidyl-1,2,3-triazole ureas as potent, selective, and *in vivo*-active inhibitors of  $\alpha/\beta$ -hydrolase domain containing 6 (ABHD6). *J. Med. Chem.* **56**, 8270–8279 (2013).
48. Baggelaar, M. P. *et al.* Highly Selective, Reversible Inhibitor Identified by Comparative Chemoproteomics Modulates Diacylglycerol Lipase Activity in Neurons. *J. Am. Chem. Soc.* **137**, 8851–8857 (2015).
49. Janssen, A. P. A. Hit-to-Lead Optimization of Triazole Sulfonamide DAGL- $\alpha$  inhibitors. *Inhibitor Selectivity: Profiling and Prediction* (Leiden University, 2019).
50. Zhou, J. *et al.* Activity-Based Protein Profiling Identifies  $\alpha$ -Ketoamides as Inhibitors for Phospholipase A2 Group XVI. *ACS Chem. Biol.* **14**, 164–169 (2019).
51. Coulon, D., Faure, L., Salmon, M., Watted, V. & Bessoule, J. J. Occurrence, biosynthesis and functions of *N*-acylphosphatidylethanolamines (NAPE): Not just precursors of *N*-acylethanolamines (NAE). *Biochimie* **94**, 75–85 (2012).
52. Sugiura, T. *et al.* Enzymatic synthesis of anandamide, an endogenous cannabinoid receptor ligand, through *N*-Acylphosphatidylethanolamine pathway in testis: Involvement of Ca<sup>2+</sup>-dependent transacylase and phosphodiesterase activities. *Biochem. Biophys. Res. Commun.* **218**, 113–117 (1996).
53. van Esbroeck, A. C. M. *et al.* Identification of  $\alpha,\beta$ -Hydrolase Domain Containing Protein 6 as a Diacylglycerol Lipase in Neuro-2a Cells. *Front. Mol. Neurosci.* **12**, (2019).
54. Natarajan, V., Reddy, P. V., Schmid, P. C. & Schmid, H. H. O. *N*-acylation of ethanolamine phospholipids in canine myocardium. *Biochim. Biophys. Acta - Lipids Lipid Metab.* **712**, 342–355 (1982).

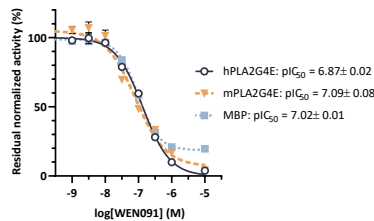


55. Deng, H. *et al.* Triazole Ureas Act as Diacylglycerol Lipase Inhibitors and Prevent Fasting-Induced Refeeding. *J. Med. Chem.* **60**, 428–440 (2017).
56. Inloes, J. M. *et al.* The hereditary spastic paraplegia-related enzyme DDHD2 is a principal brain triglyceride lipase. *Proc. Natl. Acad. Sci. U. S. A.* **111**, 14924–14929 (2014).
57. Hulce, J. J. *et al.* An *in vivo* active carbamate-based dual inhibitor of Lysophospholipase 1 (LyPLA1) and Lysophospholipase 2 (LyPLA2). *Probe Reports From NIH Mol. Libr. Progr.* (2013).
58. Adibekian, A. *et al.* Click-generated triazole ureas as ultrapotent *in vivo*-active serine hydrolase inhibitors. *Nat. Chem. Biol.* **7**, 469–478 (2011).
59. Van Esbroeck, A. C. M. *et al.* Activity-based protein profiling reveals off-target proteins of the FAAH inhibitor BIA 10-2474. *Science* **356**, 1084–1087 (2017).
60. Janssen, A. P. A. *et al.* Structure Kinetics Relationships and Molecular Dynamics Show Crucial Role for Heterocycle Leaving Group in Irreversible Diacylglycerol Lipase Inhibitors. *J. Med. Chem.* **62**, 7910–7922 (2019).
61. Baggelaar, M. P. *et al.* Development of an activity-based probe and *in silico* design reveal highly selective inhibitors for diacylglycerol lipase- $\alpha$  in brain. *Angew. Chemie - Int. Ed.* **52**, 12081–12085 (2013).

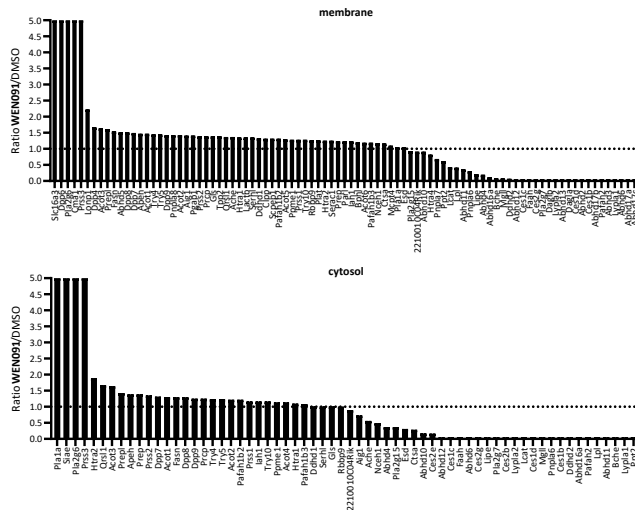
## Supplementary information



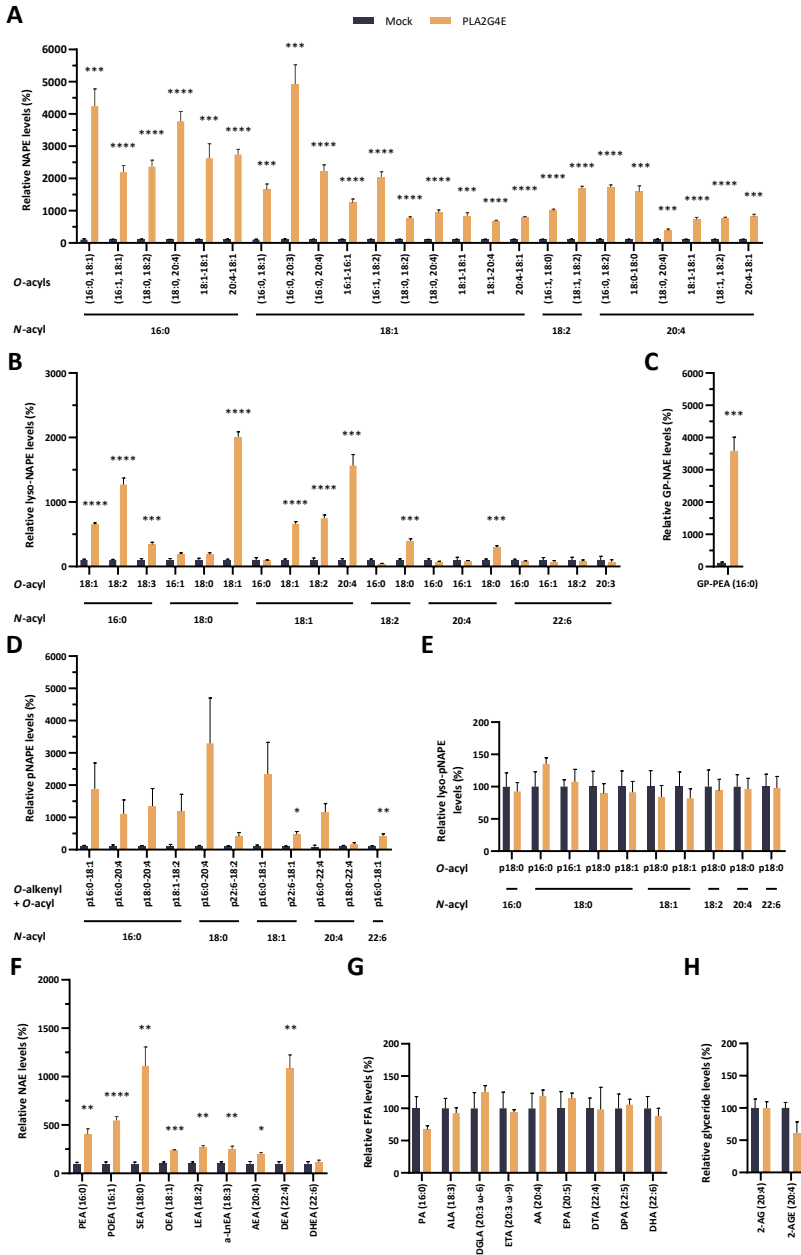
**Supplementary Figure S3.1. Inhibition of mouse PLA2G4E by WEN091.** Excerpt of cABPP gel on mPLA2G4E-overexpressing HEK293T lysate and corresponding inhibition curve and  $pIC_{50}$  value (preliminary,  $N = 1$ ).



**Supplementary Figure S3.2. Inhibition curves of WEN091 in NAPE production assay.** Graph corresponding to Figure 3.2D–F. Curves generated from conversion rates of Ca-NAT activity assay on overexpression lysate and mouse brain proteome (MBP). Data presented as mean  $\pm$  SEM ( $N = 2$ ).

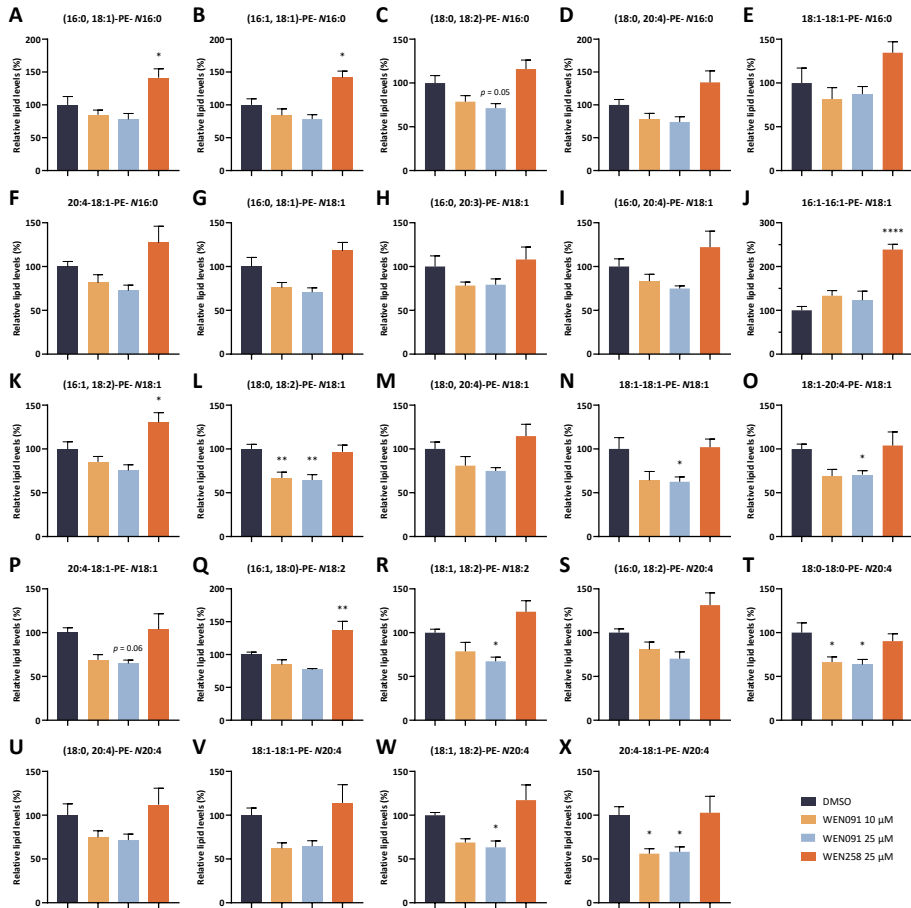


**Supplementary Figure S3.3. Activity of WEN091 in chemical proteomics experiment.** Mouse brain membrane or cytosol enzymes identified by LC-MS/MS in pull-down experiment with FP-biotin (4  $\mu$ M, 60 min, RT) after pretreatment with WEN091 (1  $\mu$ M, 30 min, 37°C). Bars represent ratios of quantified peptides between WEN091 and DMSO-treated samples ( $N = 1$ ). Maximal and minimal ratios were manually set to 5 and 0.05, respectively.

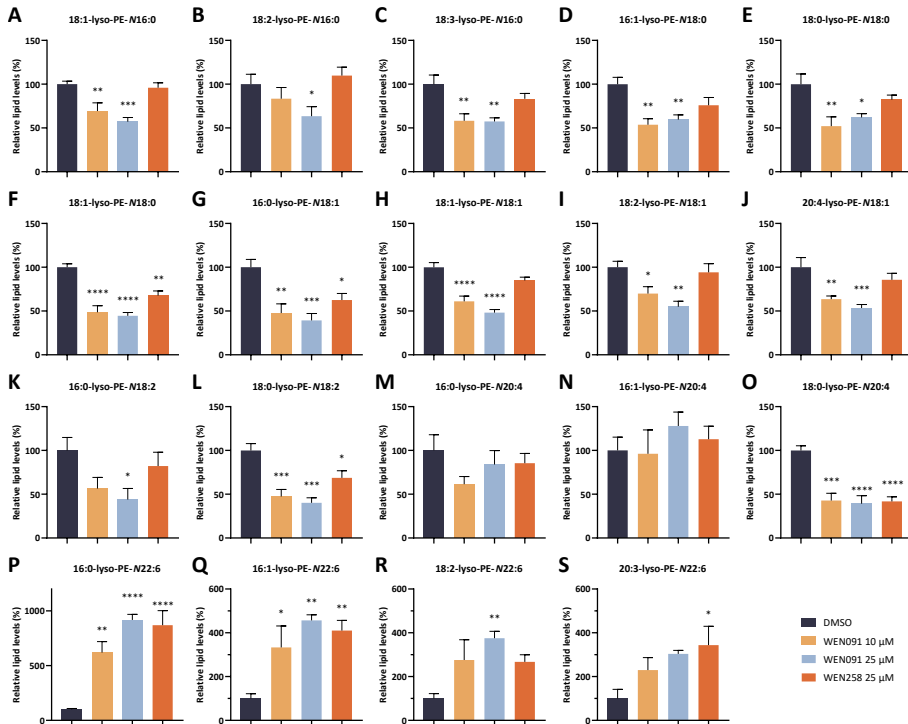


**Supplementary Figure S3.4. Lipid level changes in Neuro-2a cells overexpressing PLA2G4E.** Relative lipid levels in hPLA2G4E-transfected Neuro-2a cells expressed as percentage compared to mock-transfected cells (24 h p.t.). For individual NAPEs (A) parentheses indicate that the absolute *sn* configuration of the *O*-acyls was not determined. Data expressed as mean ± SEM (N = 5). Statistical significance calculated for each lipid using a two-tailed *t*-test with Holm-Sidak multiple comparison correction. \**p* < 0.05, \*\**p* < 0.01, \*\*\**p* < 0.001, \*\*\*\**p* < 0.0001. PEA: *N*-palmitoylethanolamine, POEA: *N*-palmitoleoylethanolamine, SEA: *N*-stearoylethanolamine, OEA: *N*-oleoylethanolamine, LEA: *N*-linoleoylethanolamine, α-LNEA: *N*-α-linolenoylethanolamine, AEA: *N*-arachidonoylethanolamine, DEA: *N*-docosatetraenoyl-

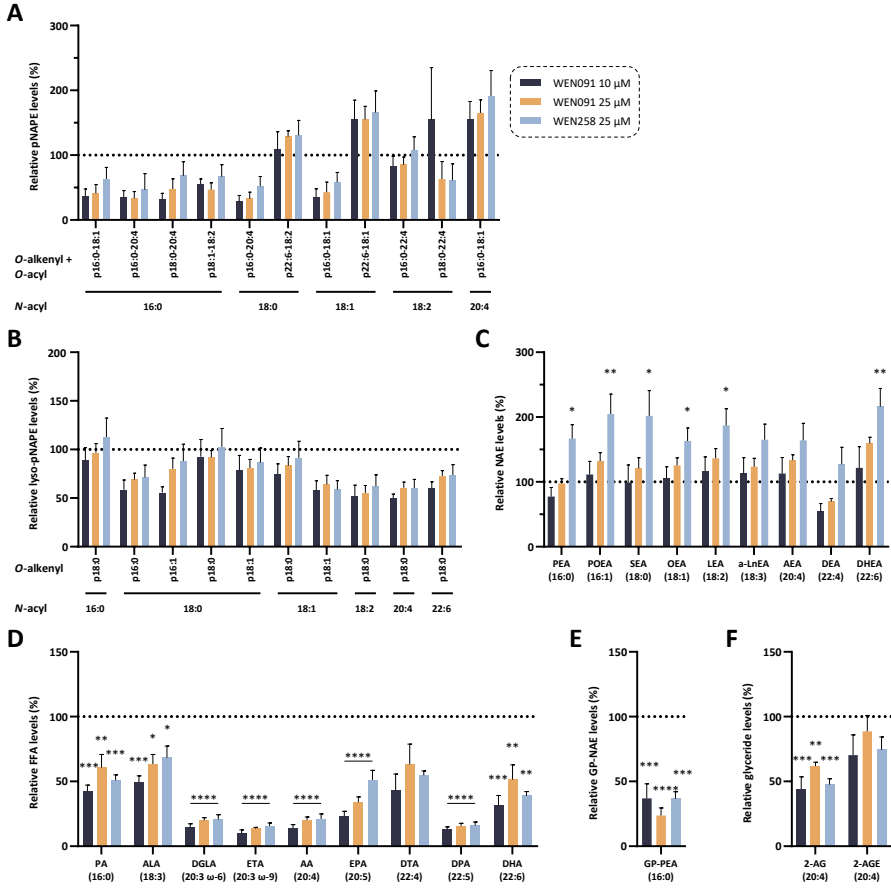
ethanolamine, DHEA: *N*-docosahexaenylethanolamine (synaptamide), PA: palmitic acid, ALA:  $\alpha$ -linolenic acid, DGLA: dihomogamma-linolenic acid, ETA: eicosatrienoic acid (mead acid), AA: arachidonic acid, EPA: eicosapentaenoic acid, DTA: docosatetraenoic acid (adrenic acid), DPA: docosapentaenoic acid, DHA: docosahexaenoic acid, 2-AG: 2-arachidonoyl glycerol, 2-AGE: 2-arachidonyl glyceryl ether (noladin ether).



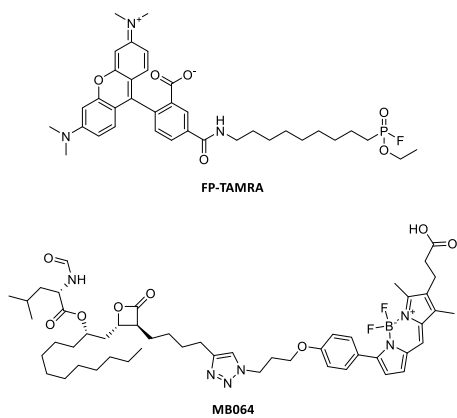
**Supplementary Figure S3.5. Relative levels of NAPE species in Neuro-2a cells following inhibitor treatment.** Levels determined in PLA2G4E-overexpressing Neuro-2a cells (24 h p.t.) treated with **WEN091**, **WEN258** or vehicle (8 h) expressed as percentage compared to DMSO-treated cells (mean  $\pm$  SEM, N = 5). Lipid notation as follows: {sn-1 O-acyl}- {sn-2 O-acyl}-PE-N(N-acyl). Parentheses indicate that the absolute sn configuration of the O-acyls was not determined. Statistical significance calculated for each lipid using one-way ANOVA with Dunnett's multiple comparison correction. \* $p < 0.05$ , \*\* $p < 0.01$ .



**Supplementary Figure S3.6. Relative levels of lyso-NAPE species in Neuro-2a cells following inhibitor treatment.** Levels determined in PLA2G4E-overexpressing Neuro-2a cells (24 h p.t.) treated with WEN091, WEN258 or vehicle (8 h) expressed as percentage compared to DMSO-treated cells (mean  $\pm$  SEM, N = 5). Lipid notation as follows: {O-acyl}-lyso-PE-N{N-acyl}. Statistical significance calculated for each lipid using one-way ANOVA with Dunnett's multiple comparison correction. \* $p < 0.05$ , \*\* $p < 0.01$ , \*\*\* $p < 0.001$ , \*\*\*\* $p < 0.0001$ .



**Supplementary Figure S3.7. Relative levels of lipid species in Neuro-2a cells following inhibitor treatment.** Levels of (A) pNAPes, (B) lyso-pNAPes, (C) NAEs, (D) FFAs, (E) GP-NAEs and (F) glycerides determined in PLA2G4E-overexpressing Neuro-2a cells (24 h p.t.) treated with **WEN091**, **WEN258** or vehicle (8 h) expressed as percentage compared to DMSO-treated cells (mean ± SEM, N = 5). Statistical significance calculated for each lipid using one-way ANOVA with Dunnett's multiple comparison correction. \* $p < 0.05$ , \*\* $p < 0.01$ , \*\*\* $p < 0.001$ , \*\*\*\* $p < 0.0001$ .



**Supplementary Figure S3.8. Chemical structures of the two activity-based probes used in this study.** Commercially available broad-spectrum serine hydrolase probe FP-TAMRA and in-house synthesized tetrahydrolipstatin-based lipase probe MB064.

# 4

**Optimization of WENo91 towards  
selective PLA<sub>2</sub>G<sub>4</sub>E inhibitors**



Phospholipase A<sub>2</sub>ε (PLA2G4E) is a serine hydrolase that belongs to the Group IV or cytosolic phospholipases A<sub>2</sub> (cPLA<sub>2</sub>).<sup>1,2</sup> This family is involved in phospholipid metabolism, with each of the six members (PLA2G4A–F) having specific PLA<sub>1</sub>, PLA<sub>2</sub>, lyso-PLA or acyltransferase activities, calcium-dependency and expression pattern.<sup>1,3</sup> Recently, PLA2G4E was identified as a calcium-dependent *N*-acyltransferase (Ca-NAT) capable of producing *N*-acylphosphatidylethanolamines (NAPEs).<sup>4,5</sup>

In humans, two isoforms of PLA2G4E have been identified. The canonical isoform (868 amino acids, 100 kDa) has an N-terminal C2 domain, which is truncated in the alternative splicing product (834 amino acids, 97 kDa).<sup>5</sup> This C2 domain is characteristic of the PLA2G4 family and functions as a calcium-dependent lipid-binding domain.<sup>6,7</sup> In contrast to other PLA2G4 enzymes, PLA2G4E has an additional C-terminal polybasic (PB) domain which is also involved in lipid-binding.<sup>5,8</sup> These positively charged amino acids (KKKRLK) are able to bind phosphatidylinositide phosphates (PIPs), which localizes the enzymes to the membranes of the clathrin-independent endocytic machinery. Here, PLA2G4E is involved in tubule formation required for major histocompatibility complex (MHC) class I protein recycling.<sup>8</sup> Both the C2 and PB domain are needed for catalytic activity and correct cellular distribution.<sup>5</sup> In the catalytic domain, a Ser-Asp catalytic dyad, characteristic of the PLA2G4 family, is responsible for the *N*-acyltransferase activity.<sup>2,4</sup> The nucleophilic serine of PLA2G4E preferentially cleaves the *sn*-1 ester of phosphatidylcholine (PC), which leads to the release of lyso-PC. The acyl chain is subsequently transferred to the amine of phosphatidylethanolamine (PE), thereby producing NAPEs.

NAPEs are a low-abundant class of phospholipids that have both structural and signaling functions.<sup>9</sup> They control membrane dynamics by supporting their structural integrity and inducing membrane fusion<sup>10–12</sup>, and regulate the localization of intracellular membrane-interacting proteins.<sup>13</sup> They have inhibitory effects on food-intake<sup>14,15</sup> and inflammation<sup>16</sup> and are highly elevated during ischemia and stress, which is suggested to be a cytoprotective mechanism.<sup>17–19</sup> Furthermore, NAPEs are the precursors to *N*-acylethanolamines (NAEs) through the hydrolytic activity of NAPE-specific phospholipase D (NAPE-PLD).<sup>20</sup> NAEs are a class of lipids with highly diverse signaling functions, including satiety, nociception and anxiety.<sup>21–24</sup> Activity of NAEs is terminated by fatty acid amide hydrolase (FAAH) (Figure 4.1).<sup>25</sup>



**Figure 4.1. Schematic overview of biosynthesis and degradation of NAPEs and NAEs.** Alternative pathways are not depicted. PE: phosphatidylethanolamine, PC: phosphatidylcholine, NAPE: *N*-acylphosphatidylethanolamine, NAE: *N*-acylethanolamine, FFA: free fatty acid, PLA2G4E: phospholipase A<sub>2</sub> Group IV E, PLAATs: phospholipase A/acyltransferases, NAPE-PLD: NAPE-specific phospholipase D, FAAH: fatty acid amide hydrolase.

The calcium-dependent activity of PLA2G4E is currently hypothesized to be the major pathway of NAPE biosynthesis.<sup>26,27</sup> Additionally, NAPEs are also synthesized calcium-independently by *N*-acyltransferase activity of phospholipases/acyltransferases (PLAATs) 1–5.<sup>28,29</sup> Acute, selective inhibition of PLA2G4E would help elucidate the physiological roles of these two pathways. In Chapter 3, **WEN091** was identified as a potent inhibitor of PLA2G4E that was able to reduce production of NAPEs in cells overexpressing PLA2G4E. However, biological profiling revealed off-target activity on NAE-degrading enzyme FAAH, which may complicate the interpretation of downstream signaling events. In this chapter, the synthesis and biochemical profiling of novel analogues of **WEN091** are described with a focus on their selectivity profile.

## Results

### Design and synthesis of PLA2G4E inhibitors 1–38

**WEN091** is an irreversible, covalent PLA2G4E inhibitor that belongs to the class of triazole ureas. The electrophilic carbonyl of the urea acts as a warhead by carbamoylating the catalytic serine of PLA2G4E (Chapter 2). The triazole functions as a leaving group, while the amine group that is covalently bound to the enzyme is referred to as the staying group. In this chapter, 38 new analogues of **WEN091** were synthesized to further explore the structure-activity relationships on PLA2G4E and FAAH (Figure 4.2). Previously, it was shown that irreversible inhibitors with high intrinsic reactivity may bind in a non-specific manner to other members of the same enzyme family (e.g. FAAH).<sup>30,31</sup> The reactivity of the triazole urea was, therefore, investigated in compounds **1–3** (Table 4.1) and the steric and electronic properties of the leaving group were modulated in compounds **4–31** (Table 4.1–Table 4.3). In addition, the role of the staying group was further explored in compounds **32–38** (Table 4.4) (Figure 4.2).

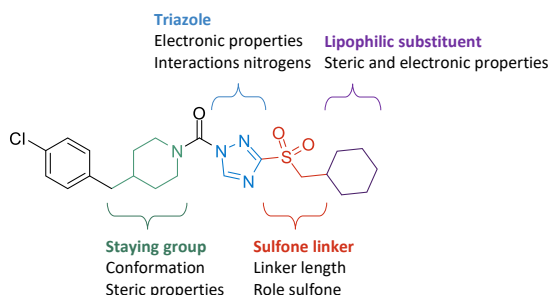


**Figure 4.2. Optimization strategy for improving WEN091's selectivity profile.** The structure of **WEN091** is depicted with parts of the molecule that were investigated in this chapter highlighted.

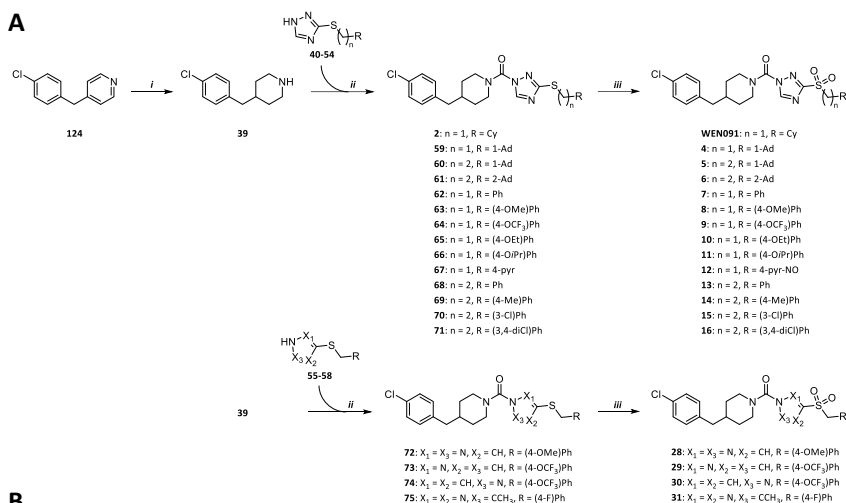
Based on **WEN091**, a similar synthesis plan was deployed for compounds **1–16** and **28–31** (Scheme 4.1A). Briefly, optimized staying group 4-(4-chlorobenzyl)piperidine (**39**, see Chapter 2) was coupled to different substituted triazole or pyrazole leaving groups (**40–**

**58**) using triphosgene, yielding triazole or pyrazole ureas **2**, **3**, **59–75**. Subsequent oxidation of the thioether in compound **2** to sulfoxide afforded compound **1**. Oxidation of the thioether in **59–75** to sulfone afforded inhibitors **4–16** and **28–31** (Scheme 4.1A).

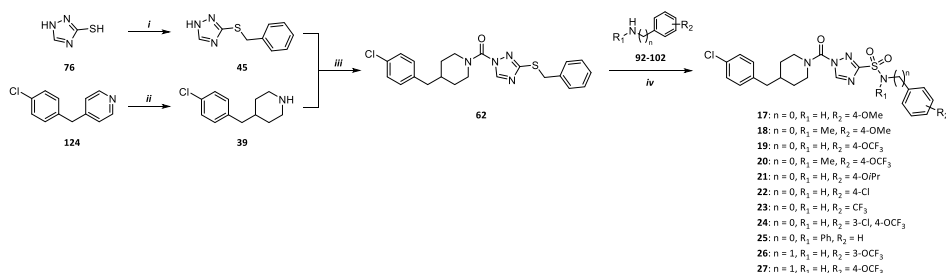
Variations in the triazole leaving group of compounds **1**, **2** and **7–16** were introduced by substitution of 1,2,4-triazole-3-thiol (**76**) with various commercial and tailor-made organohalides, leading to compounds **40** and **45–54** (Supplementary Scheme S4.1). The triazole amide leaving group **41** of inhibitor **3** was synthesized by reacting 1,2,4-triazole-3-carboxylic acid (**77**) with thionyl chloride, followed by substitution with *N*-methylcyclohexylamine (**78**, Supplementary Scheme S4.2). Incorporation of caged hydrocarbons in compounds **4–6** requested a different approach (Scheme 4.1B, see also Chapter 6). Adamantanecarboxylic acid (**79**) and the methyl esters **80** and **81** were reduced with LiAlH<sub>4</sub>. Triflation of the resulting alcohols (**82–84**) and subsequent substitution with potassium thioacetate afforded thioacetates **85–87**. These were reduced using LiAlH<sub>4</sub> and oxidized with molecular bromine, forming disulfides **88–90**. Lithiation of 1-(pyrrolidin-1-ylmethyl)-1*H*-1,2,4-triazole (synthesized according to literature)<sup>32</sup> using *n*-BuLi followed by careful addition of disulfides **88–90** led to the formation of the desired thioethers, while the pyrrolidin-1-ylmethyl protecting groups were removed immediately by the liberated thiols, providing triazole thioether building blocks **42–44**. The byproduct formed in this reaction was easily removed after treatment with NaBH<sub>4</sub> in ethanol. For pyrazole building blocks **56** and **57**, the respective aminopyrazole was diazotized using *in situ*-generated nitrous acid, followed by immediate substitution with 4-(trifluoromethoxy)benzyl mercaptan (**91**, Supplementary Scheme S4.3). Each of these azole building blocks was reacted with staying group **39**, forming **2**, **3** and **59–75**, and oxidized as depicted in Scheme 4.1A.

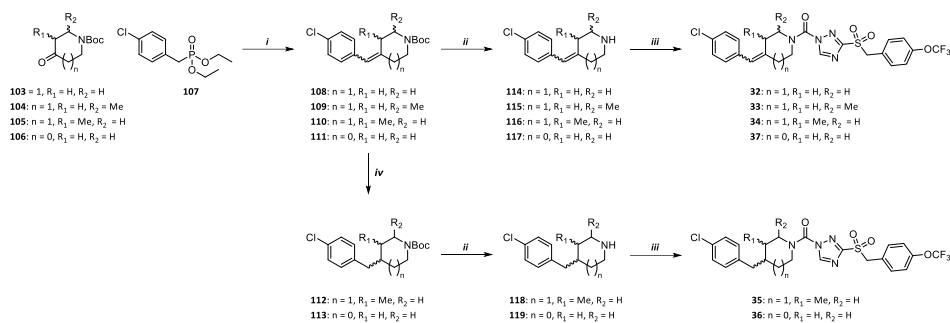
Sulfonamide variants **17–27** were obtained by a one-pot oxidative chlorination-substitution reaction between triazole urea thioether **62** and desired aniline analogues **92–102** (Scheme 4.2, Supplementary Scheme S4.4).

Variations of the 4-(4-chlorobenzyl)piperidine staying group were introduced in inhibitors **32–38**. The staying groups in compounds **32–37** were synthesized by a Horner-Wadsworth-Emmons olefination of piperidinones **103–105** or pyrrolidinone **106** using diethyl (4-chlorobenzyl)phosphonate (**107**), providing **108–111** (Scheme 4.3). Hydrogenation of **110** and **111** over palladium on carbon yielded **112** and **113**. **108–113** were deprotected to yield the amines **114–119**. For compound **38**, Grignard reaction of 4-chlorophenylmagnesium bromide (**120**) with isonipecotic acid ethyl ester **121** and subsequent acidic dehydration afforded amine **122** (Supplementary Scheme S4.5). All amine building blocks were coupled to triazole sulfone leaving group **123** in the triphosgene-mediated urea formation, yielding **32–38**.



**Scheme 4.1. Synthetic routes towards PLA2G4E inhibitors 2, 4–16 and 28–31.** A) General synthetic scheme of **2–16** and **28–31**. Reagents and conditions: *i*) 4 bar  $\text{H}_2$ ,  $\text{PtO}_2$ ,  $\text{HCl}$ ,  $\text{EtOH}$ ,  $o/n$  RT; *ii*) 1. **39**, triphosgene,  $\text{Et}_3\text{N}$  or  $\text{DIPEA}$ , 3 h  $0^\circ\text{C} \rightarrow \text{RT}$ , then 2. **40–58**,  $\text{K}_2\text{CO}_3$ ,  $\text{DMF}$ ,  $o/n$  RT; *iii*)  $\text{AcOOH}$ ,  $\text{DCM}$ , 6 h  $0^\circ\text{C} \rightarrow \text{RT}$ . B) Synthesis of adamantane-containing triazole building blocks for **4–6**. Reagents and conditions: *iv*)  $\text{LiAlH}_4$ ,  $\text{THF}$ , 0.5 h reflux; *v*) 1.  $\text{TiF}_2\text{O}$ ,  $\text{pyr}$ ,  $\text{DCM}$ , 45 min  $-15^\circ\text{C} \rightarrow \text{RT}$ , then 2.  $\text{AcSK}$ , 18-Crown-6,  $\text{CH}_3\text{CN}$ , 72 h RT; *vi*) 1.  $\text{LiAlH}_4$ ,  $\text{THF}$ , 1.5 h RT  $\rightarrow 50^\circ\text{C}$ , then 2.  $\text{Br}_2$ ,  $\text{DCM}/\text{H}_2\text{O}$ , RT; *vii*) 1. 1-(pyrrolydin-1-ylmethyl)-1*H*-1,2,4-triazole, *n*-BuLi,  $\text{THF}$ , 21 h  $-80^\circ\text{C} \rightarrow \text{RT}$ , then 2.  $\text{NaBH}_4$ ,  $\text{EtOH}$ , 5 min RT. **42–44** were treated as described in reaction *ii* and *iii* to generate the final compounds. 1-Ad: adamant-1-yl, 2-Ad: adamant-2-yl.





**Scheme 4.3.** Synthetic routes towards PLA2G4E inhibitors **32–37**. Reagents and conditions: *i*) KOtBu or NaH, THF, o/n  $-10^{\circ}\text{C}$   $\rightarrow$  RT; *ii*) TFA, DCM, o/n RT; *iii*) 1. **114–119**, triphosgene, DIPEA, THF, 3 h  $0^{\circ}\text{C}$   $\rightarrow$  RT, then 2. **123**,  $\text{K}_2\text{CO}_3$ , DMF, o/n RT; *iv*) 1 atm  $\text{H}_2$ , Pd/C, EtOAc, 5 h RT.

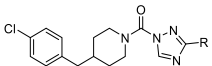
### Biochemical evaluation and structure-activity relationships of **1–38**

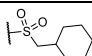
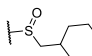
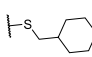
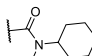
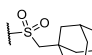
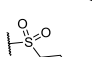

The activity of **1–38** was tested in a gel-based competitive activity-based protein profiling (cABPP) assay. This technique assesses the activity and selectivity of a small molecule on multiple enzymes in a biologically relevant context in one experiment. Fluorophosphonate-tetramethylrhodamine (FP-TAMRA) was used as an activity-based probe to measure PLA2G4E and FAAH activity.<sup>33,34</sup> Briefly, lysate of human embryonic kidney (HEK293T) cells overexpressing recombinant hPLA2G4E was treated with inhibitor at different concentrations or vehicle (30 min) and the remaining enzyme activity was labeled with FP-TAMRA (50 nM, 5 min). The proteins were resolved on molecular weight by sodium dodecyl sulfate–polyacrylamide gel electrophoresis (SDS-PAGE) and in-gel fluorescence scanning allowed the quantification of residual enzyme activity and determination of the apparent half-maximal inhibitory concentration ( $\text{IC}_{50}$ ). The inhibitory potency of the compounds on FAAH was determined in a similar manner by using mouse brain proteome.<sup>35</sup>

#### Sulfone linker and small lipophilic substituents are preferred structural elements for PLA2G4E inhibition

Optimization of the triazole leaving group of **WEN091** was started by investigating the role of the sulfone linker between the triazole and the aliphatic substituent (Table 4.1). The decreased potency of sulfoxide, thioether and amide variants **1–3** demonstrated the important role of the sulfone. In contrast, activity on FAAH was less strongly affected and **1** and **2** showed a slightly increased activity on FAAH. The apparent selectivity (app. sel.) of **1** for PLA2G4E over FAAH, defined as the ratio of the respective apparent  $\text{IC}_{50}$  values, was calculated to be 5-fold, whereas that of **WEN091** was 32-fold (Table 4.1). This suggested that the sulfone improves binding to PLA2G4E either through direct interactions with the active site or through its inductive effect on the triazole. Inhibitors with bulky adamantyl substituents (**4–6**) showed markedly reduced activity on FAAH, but the activity on PLA2G4E was also lower, indicating smaller lipophilic groups were favored in both enzymes.

**Table 4.1. Structure-activity relationships of PLA2G4E inhibitors 1–6.** Activity determined with gel-based cABPP on PLA2G4E-overexpressing HEK293T membranes or mouse brain proteome (N ≥ 2). Apparent selectivity (app. sel.) =  $IC_{50}(\text{PLA2G4E})/IC_{50}(\text{FAAH}) = 10^{pIC_{50}(\text{PLA2G4E}) - pIC_{50}(\text{FAAH})}$ .



ID	R	pIC <sub>50</sub> ± SEM		App. sel.
		PLA2G4E	FAAH	
WEN091		8.01 ± 0.02	6.52 ± 0.04	32
1		7.69 ± 0.01	6.98 ± 0.08	5
2		< 5.0	6.93 ± 0.09	< 1
3		5.15 ± 0.39	6.42 ± 0.04	< 1
4		7.12 ± 0.01	5.26 ± 0.08	72
5		7.40 ± 0.19	< 5.0	> 251
6		7.25 ± 0.20	< 5.0	> 177

### *para*-Substituted benzyl groups provided highest potency and selectivity

Next, the electronic properties of the leaving group were investigated by substituting the cyclohexylmethyl of **WEN091** with various aromatic groups (Table 4.2). **7**, which contains a benzyl group, was a slightly less potent inhibitor than **WEN091**. Compounds with ether substituents on the *para* position of the benzyl group (**8–11**) were tolerated and showed both increasing potency on PLA2G4E and selectivity over FAAH with increasing size and lipophilicity. **12**, which contains a polar 4-pyridine-*N*-oxide, showed decreased activity on PLA2G4E. This suggested that a lipophilic pocket is available in the active site of PLA2G4E, but not in FAAH. Trifluoromethoxy-substituted compound **9** demonstrated over 800-fold higher activity on PLA2G4E ( $pIC_{50} = 8.1$ ) than on FAAH ( $pIC_{50} = 5.2$ ), which makes it the most potent and selective PLA2G4E inhibitor identified in this study. Compound **13**, with an ethylene linker between the sulfone and the phenyl, had slightly lower potency on PLA2G4E, which was similar with *para* (**14**, **16**) and further decreased with *meta* (**15**) substitutions on the phenyl ring. These compounds, however, did not show increased selectivity over FAAH (e.g. **16**: app. sel. 79-fold), indicating they did not have similar PLA2G4E-specific interactions as compounds **9** and **11**.

Compounds **17–27** (Table 4.3), which contain a sulfonamide instead of a sulfone, were synthesized, based on the structures of **8**, **9** and **11**. It was hypothesized that a weaker electron-withdrawing effect of the sulfonamide could decrease the reactivity of the urea,

thereby reducing inhibitory potency on FAAH and improving the selectivity. Sulfonamides **17** and **18** were equally potent on PLA2G4E to **8** ( $pIC_{50} = 7.0$ ). Sulfonamides **19** and **21**, however, showed a 10-fold decrease in potency on PLA2G4E compared to sulfones **9** and **11**, respectively, while methylated sulfonamide **20** showed an even larger reduction ( $pIC_{50} = 6.4$ ). **17**, **19** and **21** had a lower activity on FAAH than their respective sulfone counterparts, but the apparent selectivity window of **19** and **21** was not improved (**19**: app. sel. 148-fold, **21**: 100-fold). Compounds with lipophilic but electron-withdrawing substituents on the *para* position of the phenyl ring (**22**, **23**) had lower potency on PLA2G4E compared to the ones with electron-donating ether groups (**17**, **21**). Inhibitors **24** and **25**, with bulkier substituents, also showed a decreased potency ( $pIC_{50} < 7.0$ ), while **26** and **27**, with a methylene linker between the sulfonamide and the phenyl, were tolerated but did not have an improved selectivity over FAAH (**26**: app. sel. 123-fold, **27**: 60-fold).

**Table 4.2. Structure-activity relationships of PLA2G4E inhibitors 7–16.** Activity determined with gel-based cABPP on PLA2G4E-overexpressing HEK293T membranes or mouse brain proteome ( $N \geq 2$ ). Apparent selectivity (app. sel.) =  $IC_{50}$  (PLA2G4E)/ $IC_{50}$  (FAAH) =  $10^{pIC_{50}(\text{PLA2G4E}) - pIC_{50}(\text{FAAH})}$ .

ID	R	$pIC_{50} \pm SEM$		
		PLA2G4E	FAAH	App. sel.
WEN091		8.01 ± 0.02	6.52 ± 0.04	32
7		7.23 ± 0.04	7.39 ± 0.06	< 1
8		7.06 ± 0.05	6.43 ± 0.05	4
9 (IK015)		8.10 ± 0.02	5.18 ± 0.18	832
10		7.67 ± 0.03	6.49 ± 0.14	15
11		8.03 ± 0.04	5.35 ± 0.05	479
12		5.44 ± 0.07	5.46 ± 0.03	1
13		7.73 ± 0.05	7.06 ± 0.08	5
14		7.76 ± 0.19	5.99 ± 0.04	59
15		7.18 ± 0.05	6.65 ± 0.10	3
16		7.84 ± 0.15	5.94 ± 0.12	79

**Table 4.3. Structure-activity relationships of PLA2G4E inhibitors 17–31.** Activity determined with gel-based cABPP on PLA2G4E-overexpressing HEK293T membranes or mouse brain proteome ( $N \geq 2$ ). Apparent selectivity (app. sel.) =  $IC_{50}(\text{PLA2G4E})/IC_{50}(\text{FAAH}) = 10^{pIC_{50}(\text{PLA2G4E}) - pIC_{50}(\text{FAAH})}$ .

ID	R	pIC <sub>50</sub> ± SEM		
		PLA2G4E	FAAH	App. sel.
8		7.06 ± 0.05	6.43 ± 0.05	4
17		7.01 ± 0.07	5.70 ± 0.15	20
18		7.04 ± 0.07	6.17 ± 0.07	7
9		8.10 ± 0.02	5.18 ± 0.18	832
19 (WEN222)		7.04 ± 0.05	4.87 ± 0.10	148
20		6.38 ± 0.03	6.02 ± 0.07	2
11		8.03 ± 0.04	5.35 ± 0.05	479
21		7.08 ± 0.04	5.08 ± 0.10	100
22		6.58 ± 0.04	4.98 ± 0.36	40
23		6.66 ± 0.05	4.94 ± 0.12	52
24		6.74 ± 0.04	< 5.0	> 54
25		6.21 ± 0.04	< 5.0	> 16
26		7.13 ± 0.03	5.04 ± 0.13	123
27		6.76 ± 0.03	4.98 ± 0.17	60
28		8.07 ± 0.02	6.42 ± 0.09	45
29		5.24 ± 0.06	< 5.0	> 1
30 (WEN258)		< 5.0	< 5.0	NA
31		< 5.0	< 5.0	NA



Next, the role of the triazole in inhibitor binding and reactivity was investigated (Table 4.3). 1,2,3-Triazole urea **28** was a more potent PLA2G4E inhibitor than its 1,2,4-triazole counterpart **8**, but it also had a higher activity on FAAH compared to **9**. Pyrazole ureas **29** and **30** showed greatly diminished activity on both PLA2G4E and FAAH. This might be explained by the higher  $pK_a$  of pyrazole (14.2<sup>36</sup>, compared to 10.1 for 1,2,4-triazole<sup>37</sup>) and corresponding lower leaving group ability, or by loss of interactions between the third nitrogen and residues in the active sites. Compound **31**, which contains a small methyl substituent on the C5 position of the 1,2,4-triazole, had completely abolished activity on both PLA2G4E and FAAH ( $pIC_{50} < 5.0$ ), possibly induced by a detrimental steric clash of the methyl group with the enzymes.

**Table 4.4. Structure-activity relationships of PLA2G4E inhibitors 32–38.** Activity determined with gel-based cABPP on PLA2G4E-overexpressing HEK293T membranes or mouse brain proteome ( $N \geq 2$ ). Apparent selectivity (app. sel.) =  $IC_{50}(\text{PLA2G4E})/IC_{50}(\text{FAAH}) = 10^{pIC_{50}(\text{PLA2G4E}) - pIC_{50}(\text{FAAH})}$ .

ID	R	$pIC_{50} \pm \text{SEM}$		
		PLA2G4E	FAAH	App. sel.
9		8.10 ± 0.02	5.18 ± 0.18	832
32		7.23 ± 0.02	5.03 ± 0.04	158
33		6.35 ± 0.04	6.19 ± 0.04	1
34		5.95 ± 0.06	< 5.0	> 8
35		6.47 ± 0.10	< 5.0	> 29
36		6.30 ± 0.03	5.63 ± 0.02	5
37		6.69 ± 0.04	4.64 ± 0.06	112
38		< 5.0	< 5.0	NA

### Variations of the benzylpiperidine staying group did not improve selectivity

In Chapter 2, a 4-(4-chlorobenzyl)piperidine staying group was found to provide inhibitors with a high potency on PLA2G4E. To improve the selectivity profile of the inhibitors, the conformational and steric properties of this staying group in compound **9** were further explored (Table 4.4). **32**, which has a conformationally restricted staying group, was less potent on PLA2G4E than **9**, while its activity on FAAH was similar. **33–35** showed a further decreased activity ( $pIC_{50} < 6.5$ ), indicating methyl substituents on the 2- or 3-position of the piperidine were not tolerated in PLA2G4E's active site. However, 2-methylpiperidine **33** was a more potent FAAH inhibitor than **32**. Johnson *et al.* have previously described benzylpyrrolidine ureas to be less potent FAAH inhibitors than benzylpiperidine urea analogs.<sup>38</sup> In this study, however, benzylpyrrolidine **36** did not show reduced activity on FAAH compared to benzylpiperidine **9**, while benzylpyrrolidine **37** showed only little reduction. Instead, both **36** and **37** showed a larger decrease in potency on PLA2G4E, leading to an app. sel. of 5-fold and 112-fold, respectively. **38**, which contains an additional phenyl group, was completely inactive on both PLA2G4E and FAAH ( $pIC_{50} < 5.0$ ), indicating both active sites cannot accommodate this bulky structure.

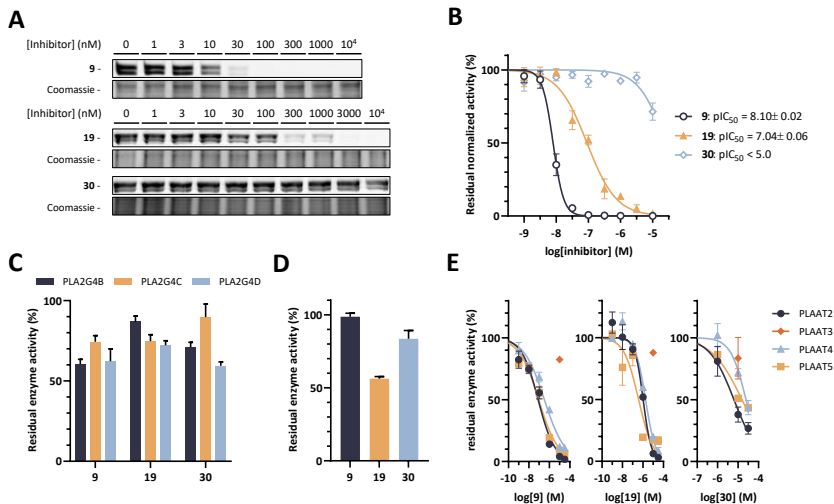


**Figure 4.3. Activity of 9, 19 and 30 on PLA2G4B–E and enzymes involved in NAPE metabolism.** A) Representative gel excerpts of cABPP experiments with **9**, **19** and **30** on PLA2G4E overexpression lysate. B) Corresponding inhibition curves and  $pIC_{50}$  values. Data presented as mean  $\pm$  SEM ( $N \geq 2$ ). C) At 10  $\mu$ M, **9**, **19** and **30** show less than 50% inhibition (compared to vehicle) of other PLA2G4 family members. Data presented as mean  $\pm$  SEM of cABPP experiments on overexpression lysate ( $N = 2$ ). D) At 10  $\mu$ M, **9**, **19** and **30** show less than 50% inhibition (compared to vehicle) of NAPE-PLD. Data presented as mean  $\pm$  SEM of fluorogenic substrate (PED6) assays on overexpression lysate ( $N = 2$ ,  $n = 2$ ). E) Inhibition curves of **9**, **19** and **30** on PLAAT family members. Data presented as mean  $\pm$  SEM of cABPP experiments on overexpression lysate ( $N = 2$ ).

**Table 4.5. Inhibition values of **9**, **19** and **30** on PLA2G4B–E and enzymes involved in NAPE metabolism.** Inhibition values obtained from cABPP experiments (PLA2G4B–E, PLAAT2–5) or PED6 substrate assay (NAPE-PLD) on overexpression lysate, corresponding to Figure 4.3. Data presented as  $pIC_{50} \pm SEM$ . When  $pIC_{50}$  could not be determined within the used concentration range, mean % inhibition  $\pm SEM$  is reported ( $N \geq 2$ ).

	PLA2G4B	PLA2G4C	PLA2G4D	PLAAT2	PLAAT3	PLAAT4	PLAAT5	NAPE-PLD
<b>9</b>	39 $\pm$ 5%	26 $\pm$ 5%	38 $\pm$ 11%	7.10 $\pm$ 0.11	18 $\pm$ 2%	6.49 $\pm$ 0.11	7.05 $\pm$ 0.10	1 $\pm$ 5%
<b>19</b>	13 $\pm$ 5%	25 $\pm$ 6%	28 $\pm$ 4%	5.99 $\pm$ 0.08	12 $\pm$ 3%	5.75 $\pm$ 0.08	6.43 $\pm$ 0.21	44 $\pm$ 3%
<b>30</b>	29 $\pm$ 4%	10 $\pm$ 12%	41 $\pm$ 3%	5.20 $\pm$ 0.11	17 $\pm$ 24%	28 $\pm$ 5%	49 $\pm$ 3%	17 $\pm$ 11%

## Biological profiling of **9**, **19** and **30**

### *In vitro* selectivity over related enzymes

Compounds **9** and **19** were selected for further biological characterization, because **9** was the most potent PLA2G4E inhibitor with the highest selectivity over FAAH and **19** is a close structural analog of **9** with lower lipophilicity (Supplementary Table S4.1). Analog **30** was selected as a potential control compound that would inhibit the off-targets of compound **9**, but not PLA2G4E (Figure 4.3). **9**, **19** and **30** did not bind the CB<sub>1</sub> and CB<sub>2</sub> receptors (Supplementary Table S4.2) and did not inhibit NAPE-PLD, PLA2G4B, PLA2G4C or PLA2G4D (Figure 4.3C–D, Table 4.5). Of note, the activity on PLA2G4A and PLA2G4F could not be determined due to a lack of expression of the proteins in HEK293T cells. Surprisingly, **9** and **19** did inhibit the *N*-acyltransferases PLAAT2, PLAAT4 and PLAAT5 with submicromolar activity, but not phospholipase PLAAT3 (Figure 4.3E, Table 4.5).<sup>29,39,40</sup> **30** only inhibited PLAAT2 with  $IC_{50} < 10 \mu M$ . PLAATs are structurally distinct from PLA2G4E, but their active sites may share common structural features that not only recognize similar endogenous substrates, but also the same synthetic inhibitors.

The selectivity of **9** and **19** and control compound **30** over other serine hydrolases was assessed with cABPP on mouse brain lysate (Figure 4.4). **9** and **19** displayed in general good selectivity (>30-fold) over the other identified hydrolases. Both inhibited one unidentified serine hydrolase (~70–80 kDa) with a similar  $IC_{50}$  value as for PLA2G4E and  $\alpha/\beta$  hydrolase domain-containing protein 6 (ABHD6) at approximately four times higher concentration (**9**:  $pIC_{50}$  (ABHD6) = 7.4, **19**:  $pIC_{50}$  (ABHD6) = 6.5, Table 4.6). ABHD12, monoacylglycerol lipase (MAGL), diacylglycerol lipase  $\alpha$  (DAGL $\alpha$ ) and acyl protein thioesterases 1 and 2 (LyPLA1 and 2) were inhibited at concentrations  $\geq 1 \mu M$ . **30** had a similar off-target profile as **9**, albeit slightly less potent on most enzymes (Table 4.6). In conclusion, **9** and **19** are selective inhibitors of NAPE-producing enzymes regardless whether these proteins can be activated by calcium ions or not.

### Cellular activity on Neuro-2a serine hydrolases

Finally, compounds **9**, **19** and **30** were also assessed on their cellular activity. Briefly, Neuro-2a cells were treated with increasing concentrations of the inhibitors (30 min), harvested and lysed, and the remaining enzyme activity was determined by gel-based cABPP (Figure 4.5). In general, the inhibitors maintained their overall selectivity profile, albeit that ABHD6

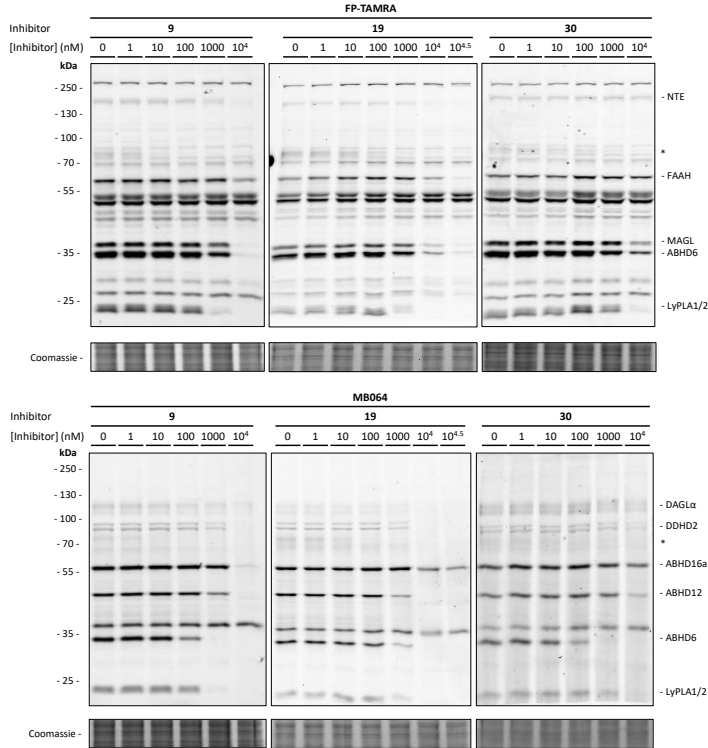


**Figure 4.4.** *In vitro* activity of **9**, **19** and **30** on mouse brain serine hydrolases. Representative gel images of cABPP experiments on mouse brain membrane proteome. Names of identified off-targets of these inhibitors are indicated. Unidentified off-target indicated with \*.

**Table 4.6.** *In vitro* pIC<sub>50</sub> values of **9**, **19** and **30** on mouse brain serine hydrolases. Inhibition values obtained from cABPP experiments on mouse brain membrane proteome using FP-TAMRA and MB064, corresponding to Figure 4.4. When pIC<sub>50</sub> could not be determined within the used concentration range, % inhibition at 10 μM is reported. Data reported as mean ± SEM (N ≥ 2). Inhibition of unidentified ~70-80 kDa protein could not reliably be quantified.

	ABHD6	ABHD12	ABHD16a	DAGLα	DDHD2	FAAH	LyPLA1/2	MAGL	NTE
<b>9</b>	7.43 ± 0.02	6.37 ± 0.06	5.96 ± 0.02	5.98 ± 0.15	6.14 ± 0.03	5.18 ± 0.18	6.73 ± 0.05	5.95 ± 0.04	5.04 ± 0.11
<b>19</b>	6.48 ± 0.05	6.34 ± 0.07	4.65 ± 0.18	5.48 ± 0.10	5.83 ± 0.06	4.87 ± 0.10	5.82 ± 0.21	5.13 ± 0.09	5.30 ± 0.08
<b>30</b>	7.10 ± 0.04	5.41 ± 0.05	4.90 ± 0.23	4.89 ± 0.20	4.98 ± 0.24	0 ± 5%	5.71 ± 0.16	5.24 ± 0.10	9 ± 4%

and FAAH inhibition by **9** and **30** was 10- to 100-fold increased compared to the mouse brain lysate (Table 4.6 and Table 4.7). Interestingly, **19** also showed increased activity on FAAH, but not on ABHD6.

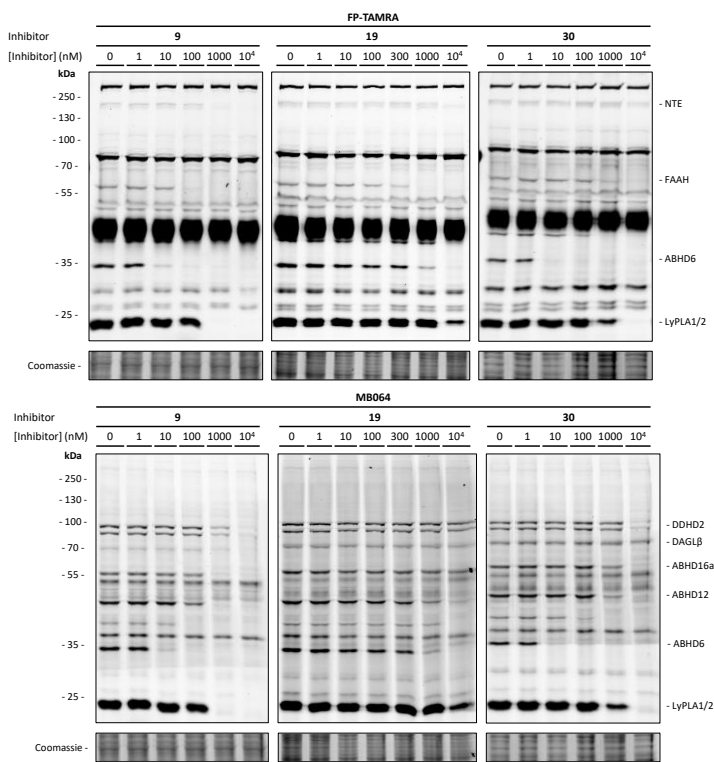


**Figure 4.5.** Cellular activity of **9**, **19** and **30** on Neuro-2a serine hydrolases. Representative gel images of cABPP experiments on Neuro-2a cells. Names of identified off-targets of the inhibitors are indicated.

**Table 4.7.** Cellular  $pIC_{50}$  values of **9**, **19** and **30** on Neuro-2a serine hydrolases. Inhibition values obtained from cABPP experiments on Neuro-2a cells using FP-TAMRA and MB064, corresponding to Figure 4.5. When  $pIC_{50}$  could not be determined within the used concentration range, % inhibition at 10  $\mu$ M is reported. Data reported as mean  $\pm$  SEM ( $N \geq 2$ ).

	ABHD6	ABHD12	ABHD16a	DAGL $\beta$	DDHD2	FAAH	LyPLA1/2	NTE
<b>9</b>	8.40 $\pm$ 0.03	6.97 $\pm$ 0.09	6.43 $\pm$ 0.10	5.96 $\pm$ 0.19	6.08 $\pm$ 0.06	7.29 $\pm$ 0.14	6.91 $\pm$ 0.06	6.44 $\pm$ 0.08
<b>19</b>	6.48 $\pm$ 0.07	6.13 $\pm$ 0.06	3 $\pm$ 14%	8 $\pm$ 9%	22 $\pm$ 10%	6.74 $\pm$ 0.05	5.49 $\pm$ 0.08	5.20 $\pm$ 0.06
<b>30</b>	8.67 $\pm$ 0.05	6.39 $\pm$ 0.10	6.04 $\pm$ 0.03	7 $\pm$ 19%	5.50 $\pm$ 0.07	6.50 $\pm$ 0.14	6.42 $\pm$ 0.07	4.69 $\pm$ 0.18

## Discussion and conclusions

In this study, **9** (**IK015**) and **19** (**WEN222**) were identified by gel-based cABPP as the most potent and selective PLA2G4E inhibitors identified to date. Interestingly, the NAPE-producing enzymes PLAAT2, PLAAT4 and PLAAT5 were also inhibited by **9** and **19**, which suggests that these compounds are general inhibitors of NAPE-biosynthesis. As such, they could be used to study the inhibition of NAPE biosynthesis on membrane integrity<sup>41</sup>, inflammatory responses<sup>16</sup>, NAE production<sup>26</sup> or in response to ischemic stress<sup>42</sup> in an acute

setting. Although **9** and **19** do not specifically inhibit the  $\text{Ca}^{2+}$ -dependent pathway, pan-PLAAT inhibitor **LEI-301** can be used in conjunction to dissect these two pathways.<sup>43</sup> **30** was not active on PLA2G4E *in vitro*, but showed a similar off-target profile to **9** and **19** in both mouse brain proteome and Neuro-2a cells. It is anticipated that **30 (WEN258)** can therefore be used as a control compound in biological experiments to distinguish off-target activities from PLA2G4E mediated effects (see Chapter 3).

In general, compounds loose activity in cellular systems due to restricted membrane permeability.<sup>44</sup> In contrast, **9** showed increased FAAH activity in an intact cellular system compared to lysates. This was previously also observed with the FAAH inhibitor BIA 10-2474.<sup>31</sup> The increased inhibition was also observed for ABHD6, but not for other enzymes, such as ABHD12 and ABHD16a. ABHD12, ABHD16a and FAAH are all reported to be localized in the endoplasmic reticulum<sup>45,46</sup>, suggesting that (subcellular) compound accumulation is not sufficient to explain the increased cellular potency. Further studies are required to explain this phenomenon. While **19** demonstrated activity on several lipases in mouse brain proteome, it was less active on most serine hydrolases in Neuro-2a cells (Table 4.6 and Table 4.7). Its high topological polar surface area (tPSA = 104 Å<sup>2</sup>, Supplementary Table S4.1), which impairs cell permeability, may explain this effect.<sup>47,48</sup> The different cellular activity profiles of compounds **9** and **19** indicate that biochemical activity does not always reflect the cellular activity even within one chemical series. To our knowledge, there is currently no cellular system available that exhibits endogenous PLA2G4E activity. This complicates the evaluation of PLA2G4E inhibitors. A cellular target engagement assay using overexpressed PLA2G4E would be a first step to link the biochemical activity of these inhibitors to their cellular effects (see Chapter 5).

Finally, **9** is a useful first chemical tool compound to study the biological role of PLA2G4E *in vitro*, but a better understanding of its molecular interactions with PLA2G4E and PLAAT2–5, obtained e.g. via co-crystallization or cryo-EM experiments, may lead to the discovery of advanced inhibitors that are specific for  $\text{Ca}^{2+}$ -dependent NAPE biosynthesis. Projecting forward, rapid metabolism of the compound (i.e. hydrolysis of the urea by carboxyl esterases) may pose a problem for *in vivo* studies.<sup>49</sup> Reducing the intrinsic reactivity of the urea or discovery of alternative scaffolds may address this problem. Furthermore, brain-active inhibitors preferentially have tPSA < 90 Å<sup>2</sup> and cLogP 1–3.<sup>48</sup> Therefore, the physico-chemical properties should be taken into careful consideration for the optimization of the next generation of PLA2G4E inhibitors.

## Acknowledgements

Mathijs Wissingh, Ivan Kulyk and Yevhenii Radchenko are kindly acknowledged for performing organic synthesis and cABPP, Wouter Driever and Laura de Paus for selectivity assays, Hans van den Elst for preparative HPLC. Hans den Dulk and Tom van der Wel are acknowledged for plasmid cloning and purification.

## Experimental procedures

### General remarks

All chemicals and reagents were purchased from Thermo Fisher Scientific or Bio-Rad, unless noted otherwise. Activity-based probes were purchased from Thermo Fisher Scientific (FP-TAMRA) or synthesized in-house (MB064) (chemical structures in Chapter 3 Supplementary Figure S3.8). Inhibitors were synthesized in-house as described below.

### Plasmids

The full-length cDNA of wild type human PLA2G4E (GenScript Biotech), murine PLA2G4B, hPLA2G4C, mPLA2G4D (Source BioScience), hPLAAT2, hPLAAT3, hPLAAT4, hPLAAT5 and hNAPE-PLD (kindly provided by Prof. Natsuo Ueda) were cloned into a pcDNA™3.1(+) expression vector in-frame with a C-terminal FLAG tag. Plasmids were isolated from transformed *Escherichia coli* XL-10 using a Qiagen Plasmid Midi kit and stored at 4°C in TE buffer (10 mM Tris, 0.1 mM EDTA, pH 8.0). The sequence was determined (Macrogen) and verified using CLC Main Workbench.

### Cell culture

HEK293T (human embryonic kidney, ATCC) cells were cultured in DMEM (Sigma-Aldrich, D6546) with additional heat-inactivated new-born calf serum (10% (v/v), Avantor Seradigm), L-Ala-L-Gln (2 mM, Sigma-Aldrich), penicillin and streptomycin (both 200 µg/mL, Duchefa Biochemie) at 37°C, 7% CO<sub>2</sub>. Medium was refreshed every 2–3 days and cells were passaged twice a week at 70–80% confluence by aspirating the medium, thorough pipetting in fresh medium and seeding to appropriate density. Cell cultures were regularly tested for mycoplasma and discarded after 2–3 months.

### Transient transfection

One day prior to transfection 10<sup>7</sup> HEK293T cells were seeded to a 15 cm dish. Upon transfection medium was aspirated and replaced by 13 mL fresh medium. Plasmid DNA (20 µg per 15 cm dish) and PEI (60 µg per 15 cm dish) were separately dissolved in 1 mL DMEM without serum, mixed, incubated for 15 min and added dropwise to the cells. 24 h p.t. medium was replaced by 25 mL fresh medium. 72 h p.t. medium was aspirated and the cells were washed with RT Dulbecco's PBS, harvested in PBS and centrifuged (3000 × *g*, 15 min, RT). Cell pellets were flash-frozen in liquid N<sub>2</sub> and stored at –80°C until use.

### Overexpression lysate preparation

PLA2G4B–E overexpression and lysate preparation was performed as described in Chapter 3. Sample preparation of PLAAT2–5, NAPE-PLD and CB<sub>1/2</sub> was performed as described before.<sup>43,50</sup>

### Mouse brain lysate preparation

Mouse brains were harvested and lysate was prepared as described in Chapter 3.

### Activity-based protein profiling

Gel-based ABPP on PLA2G4B–E, PLAAT2–5 and mouse brain proteome was performed as described in Chapter 3.

### NAPE-PLD activity assay

The PED6 assay was performed as described in Chapter 3.

**CB1/2**

The [<sup>3</sup>H]CP55,940 displacement assay was performed as described before.<sup>50</sup>

**Cellular activity assay**

Neuro-2a cellular ABPP was performed as described in Chapter 3.

**Organic synthesis****General remarks**

All reagents were purchased from Sigma-Aldrich, Acros Organics, Merck and Fluorochem and used without further purification. Solvents were purchased from Sigma-Aldrich, VWR Chemicals or Honeywell Riedel-de Haën, common salts from Sigma-Aldrich or Chem-Lab and used without further purification. Moisture-sensitive reactions were carried out in solvents dried over heat-activated molecular sieves (4 Å, Sigma-Aldrich), using flame-dried glassware under an atmosphere of N<sub>2</sub>. TLC analysis was performed on Merck silica gel 60 F<sub>254</sub> aluminum TLC plates, on which compounds were visualized under 254 or 366 nm UV light and using KMnO<sub>4</sub> (30 mM KMnO<sub>4</sub>, 180 mM K<sub>2</sub>CO<sub>3</sub> in water) or ninhydrin (7.5 mM ninhydrin, 10% (v/v) AcOH in EtOH) stains. Flash column chromatography was performed using SiO<sub>2</sub> (Macherey-Nagel, 60 M) as stationary phase.

NMR spectra were recorded on a Bruker AV-400 MHz or AV-500 MHz spectrometer at 400 MHz (<sup>1</sup>H) and 101 MHz (<sup>13</sup>C) or 500 MHz (<sup>1</sup>H) and 126 MHz (<sup>13</sup>C) respectively, using CDCl<sub>3</sub> or MeOD (Eurisotop) as solvent. Chemical shifts are reported in ppm with TMS (<sup>1</sup>H CHCl<sub>3</sub>, δ 0.00) or solvent resonance (<sup>1</sup>H MeOD, δ 3.31; <sup>13</sup>C MeOD, δ 49.00; <sup>13</sup>C CHCl<sub>3</sub>, δ 77.16) as internal standard. Data are reported as follows: chemical shift δ (ppm), multiplicity (s = singlet, d = doublet, t = triplet, p = pentet, dd = doublet of doublets, td = triplet of doublets, qd = quartet of doublets, dt = doublet of triplets, bs = broad singlet (<sup>1</sup>H), br = broad (<sup>13</sup>C), m = multiplet), coupling constants *J* (Hz) and integration. HPLC-MS analysis was performed on a Finnigan Surveyor HPLC system equipped with a Macherey-Nagel NUCLEODUR C<sub>18</sub> Gravity, 5 μm, 50×4.6 mm column followed by a Thermo Scientific LTQ Orbitrap XL spectrometer, using H<sub>2</sub>O/CH<sub>3</sub>CN + 1% TFA as mobile phase. All compounds used for biological experiments were ≥95% pure based on LC-MS UV absorbance.

**General procedure A**

Peracetic acid (5–10 eq, 36–40% in AcOH) was added to a solution of triazole urea thioether (1 eq) in DCM (20–30 mL/mmol) and the mixture was stirred for at least 4 h. Upon reaction completion, the mixture was diluted with DCM, washed with water and brine and concentrated *in vacuo*.

**General procedure B**

4 M HCl in 1,4-dioxane (35 eq) was diluted to 1 M in DCM and cooled to –10°C. To this a 15% NaOCl solution in water (21 eq) was added carefully and the mixture was stirred for 1 h, during which it turned bright yellow. **62** (1 eq) dissolved in DCM (10 mL/mmol) was added dropwise and the mixture was stirred for 1 h. Desired substituted aniline (35 eq) was added dropwise, after which the dark suspension was stirred for 1 h before it was allowed to warm to RT and stirred overnight or until full conversion was confirmed on TLC. The reaction was quenched with 0.1 M aq. HCl, after which the aqueous layer was extracted with EtOAc. The combined organic layers were washed with brine, dried over MgSO<sub>4</sub>, filtrated and concentrated *in vacuo*.

**General procedure C**

Initial steps of the reaction were carried out as described in General procedure B. After addition of **62** the mixture was stirred for 70 min at –10°C followed by 1 h at RT. The reaction was then cooled back



to  $-10^{\circ}\text{C}$  and partially quenched by addition of DIPEA (20 eq, 450  $\mu\text{L}$ ). Desired substituted benzylamine (15 eq) dissolved in 2 mL DCM was added carefully and the mixture was stirred for 1 h, before being allowed to warm to RT and stirred for another 42 h. The mixture was diluted with EtOAc and the reaction was quenched with 0.1 M aq. HCl, after which the layers were separated. The organic layer was washed with 0.1 M aq. HCl and brine, dried over  $\text{MgSO}_4$ , filtrated and concentrated *in vacuo*.

#### General procedure D

To an ice-cold solution of triphosgene (3 eq) and  $\text{Na}_2\text{CO}_3$  or DIPEA (3 eq) in dry THF (5–10 mL) a solution of (substituted) 4-benzylpiperidine (1 eq) in dry THF (5–10 mL) was added dropwise ( $< 1$  mL/min). The mixture was stirred on ice for 1 h, followed by 2 h at RT. The mixture was then diluted with EtOAc and washed with 1 M aq. HCl and brine, dried over  $\text{MgSO}_4$ , filtrated and concentrated *in vacuo*. Water was removed by co-evaporation with toluene. The resulting oil was dissolved in dry DMF (2–5 mL), triazole thioether (1 eq) and  $\text{K}_2\text{CO}_3$  (3 eq) were added and the reaction mixture was stirred overnight. The mixture was diluted with EtOAc, washed with water and brine, dried over  $\text{MgSO}_4$ , filtrated and concentrated *in vacuo*.

#### General procedure E

To an ice-cold solution of  $\text{LiAlH}_4$  (1.5 eq) in dry THF (20 mL/g of thioacetate) a solution of thioacetate (1 eq) in dry THF (10 mL/g of thioacetate) was added dropwise. The reaction mixture was allowed to warm to RT and stirred for 30 min, followed by 1 h at  $50^{\circ}\text{C}$ . The reaction was cooled and quenched by addition of 0.1 M aq. HCl on an ice bath. Solids were removed by filtration and washed with DCM. Combined filtrates were concentrated *in vacuo*. The resulting yellow oil was dissolved in DCM (20 mL/g of thioacetate) and added to a suspension of silica powder (5 g/g of thioacetate) in water (2.5 mL/g of thioacetate). 1 M  $\text{Br}_2$  in DCM was added until the mixture started to color. Solids were removed by filtration. The filtrate was dried over  $\text{Na}_2\text{SO}_4$ , filtrated and concentrated *in vacuo*. Silica plug purification with pentane provided the disulfide.

#### General procedure F

1*H*-1,2,4-Triazole-3-thiol or sodium 1*H*-1,2,3-triazole-4-thiolate (1–1.1 eq), desired organohalide (1 eq) were dissolved in dry DMF (2–10 mL/mmol of triazole). To reactions with 1*H*-1,2,4-triazole-3-thiol  $\text{K}_2\text{CO}_3$  (1–2 eq) was added. The mixture was stirred for at least 3 h. When full conversion was confirmed using TLC analysis EtOAc and water were added and the layers were separated. The aqueous layer was extracted with EtOAc, after which the combined organic layers were washed with brine, dried over  $\text{MgSO}_4$ , filtrated and concentrated *in vacuo*.

#### General procedure G

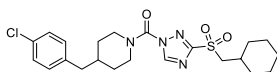
A solution of 1-(pyrrolidin-1-ylmethyl)-1*H*-1,2,4-triazole (2 eq) in dry THF (10 mL/mmol of triazole) was degassed by  $\text{N}_2$  purging and cooled to  $-80^{\circ}\text{C}$ . *n*-BuLi (2.3 M in THF, 2.2 eq) was added portion wise, after which the reaction mixture was stirred at  $-80^{\circ}\text{C}$  for 30 min followed by 90 min at  $-30$  to  $-25^{\circ}\text{C}$  during which a white precipitate formed. The mixture was then cooled to  $-80^{\circ}\text{C}$  and a solution of disulfide (1 eq) in dry THF (3 mL/mmol of disulfide) was added portion wise. The reaction was stirred for  $\geq 3$  h at  $-75^{\circ}\text{C}$ , after which it was allowed to warm to RT and stirred overnight. Volatiles were removed under reduced pressure, after which the concentrate was diluted in DCM and washed with water. The organic layer was concentrated *in vacuo*. The residue was brought onto a silica gel column and washed with pentane and DCM. The product was then eluted using 1:1 DCM:MeOH. The fractions containing product were combined and concentrated *in vacuo*.

The product was treated with NaBH<sub>4</sub> in EtOH (20 eq) and stirred for 5 min. Volatiles were removed under reduced pressure, after which the residue was dissolved in DCM and washed with water and brine. The organic layer was concentrated *in vacuo*. The residue was dispersed in 5 M aq. KOH and extracted with chloroform. The pH of the aqueous layer was lowered to 7 using 12 M aq. HCl, after which it was again extracted with chloroform. The combined organic layers were dried over Na<sub>2</sub>SO<sub>4</sub>, filtrated and concentrated *in vacuo* yielding the triazole thioether, which was used without further purification.

#### General procedure H

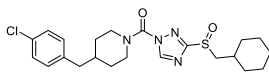
Diethyl 4-chlorobenzylphosphonate (1.2 eq) was dissolved in dry THF (2–3 mL/mmol of ketone) and cooled to –10°C. To this, freshly prepared 1 M KO<sup>t</sup>Bu in dry THF (1.5 eq) was added dropwise over the course of 10 min, upon which the mixture turned yellow and cloudy. The mixture was stirred for 1–3 h keeping the temperature below 5°C. Desired Boc-protected piperidinone or pyrrolidinone (1 eq) was dissolved in dry THF (1–2 mL/mmol) and added dropwise, upon which the color of the mixture slightly changed. The mixture was then allowed to warm to RT and stirred overnight. When full conversion was confirmed using TLC analysis, the reaction mixture was poured into ice-cold water and stirred for 1–2 h. The mixture was then extracted with EtOAc. The combined organic layers were washed with brine, dried over MgSO<sub>4</sub>, filtrated and concentrated *in vacuo*.

#### (4-(4-Chlorobenzyl)piperidin-1-yl)(3-((cyclohexylmethyl)sulfonyl)-1H-1,2,4-triazol-1-yl)-methanone (WEN091)



The title compound was synthesized as described in Chapter 2.

#### (4-(4-Chlorobenzyl)piperidin-1-yl)(3-((cyclohexylmethyl)sulfinyl)-1H-1,2,4-triazol-1-yl)-methanone (1)



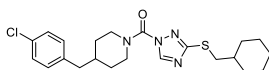
**2** (7 mg, 0.016 mmol) was oxidized according to General procedure A, but only 2 eq of AcOOH were used. Flash column chromatography (40 → 100% EtOAc in pentane) afforded the title compound (2 mg, 4.5 μmol, 28%).

<sup>1</sup>H NMR (500 MHz, CDCl<sub>3</sub>) δ 8.84 (s, 1H), 7.30 – 7.23 (m, 2H), 7.11 – 7.03 (m, 2H), 4.68 – 4.29 (m, 2H), 3.28 (dd, *J* = 13.0, 5.2 Hz, 1H), 3.19 – 2.82 (m, 2H), 2.97 (dd, *J* = 13.0, 8.8 Hz, 1H), 2.56 (d, *J* = 6.8 Hz, 2H), 2.06 – 2.00 (m, 2H), 2.02 – 1.91 (m, 1H), 1.86 – 1.72 (m, 3H), 1.68 (m, 2H), 1.47 – 1.22 (m, 6H), 1.26 – 1.06 (m, 2H).

<sup>13</sup>C NMR (126 MHz, CDCl<sub>3</sub>) δ 147.73, 138.07, 130.51, 128.69, 61.43, 42.17, 37.98, 32.33, 30.46, 29.85, 26.09, 26.03.

HRMS: [M+H]<sup>+</sup> calculated for C<sub>22</sub>H<sub>29</sub>ClN<sub>4</sub>O<sub>2</sub>S+H<sup>+</sup> 449.1773, found 449.1774.

#### (4-(4-Chlorobenzyl)piperidin-1-yl)(3-((cyclohexylmethyl)thio)-1H-1,2,4-triazol-1-yl)-methanone (2)



**39** (1.1 eq, 20 mg, 0.095 mmol) was reacted with **40** (17 mg, 0.086 mmol) according to General procedure D. The residue was purified by flash column chromatography (0 → 30% EtOAc in pentane) yielding

the title compound as a white gum (29 mg, 0.067 mmol, 78%).

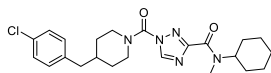
*Analytical data on next page.*

$^1\text{H}$  NMR (400 MHz,  $\text{CDCl}_3$ )  $\delta$  8.67 (s, 1H), 7.30 – 7.22 (m, 2H), 7.11 – 7.03 (m, 2H), 4.85 – 4.27 (m, 2H), 3.02 (d,  $J = 6.9$  Hz, 2H), 2.99 – 2.89 (m, 2H), 2.56 (d,  $J = 7.0$  Hz, 2H), 1.94 – 1.86 (m, 2H), 1.86 – 1.76 (m, 1H), 1.81 – 1.70 (m, 6H), 1.69 – 1.57 (m, 1H), 1.35 (qd,  $J = 12.5, 4.1$  Hz, 2H), 1.24 – 1.08 (m, 2H), 1.00 (qd,  $J = 12.0, 3.4$  Hz, 2H).

$^{13}\text{C}$  NMR (101 MHz,  $\text{CDCl}_3$ )  $\delta$  163.40, 148.36, 147.39, 138.22, 132.08, 130.48, 128.61, 42.28, 38.87, 38.08, 37.90, 32.71, 31.98, 29.82, 26.37, 26.13.

HRMS:  $[\text{M}+\text{H}]^+$  calculated for  $\text{C}_{22}\text{H}_{29}\text{ClN}_4\text{OS}+\text{H}^+$  433.18234, found 433.28218.

### 1-(4-(4-Chlorobenzyl)piperidine-1-carbonyl)-*N*-cyclohexyl-*N*-methyl-1*H*-1,2,4-triazole-3-carboxamide (3)



**39** (1.1 eq, 111 mg, 0.53 mmol) was reacted with **41** (1 eq, 100 mg, 0.48 mmol) according to General procedure D. Flash column chromatography (EtOAc in pentane) yielded two rotationally restricted isomers (ratio ~1.7:1) of the title compound as slightly yellowish oil (127 mg, 0.29 mmol, 60%).

Rotamer 1:

$^1\text{H}$  NMR (400 MHz,  $\text{CDCl}_3$ )  $\delta$  8.78 (s, 1H), 7.30 – 7.23 (m, 2H), 7.11 – 7.04 (m, 2H), 4.79 – 4.31 (m, 2H), 3.68 (tt,  $J = 11.8, 3.6$  Hz, 1H), 3.10 – 2.85 (m, 2H), 3.01 (s, 3H), 2.55 (d,  $J = 6.9$  Hz, 2H), 1.90 – 1.71 (m, 7H), 1.66 – 1.62 (m, 1H), 1.63 – 1.51 (m, 2H), 1.35 (qd,  $J = 12.9, 3.8$  Hz, 2H), 1.24 – 1.01 (m, 3H).

$^{13}\text{C}$  NMR (101 MHz,  $\text{CDCl}_3$ )  $\delta$  161.50, 158.33, 148.26, 148.24, 138.12, 132.12, 130.49, 128.63, 58.12, 42.22, 38.00, 30.95, 27.96, 25.66, 25.60.

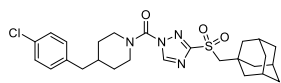
Rotamer 2:

$^1\text{H}$  NMR (400 MHz,  $\text{CDCl}_3$ )  $\delta$  8.76 (s, 1H), 7.30 – 7.23 (m, 2H), 7.11 – 7.04 (m, 2H), 4.79 – 4.31 (m, 2H), 4.60 – 4.49 (m, 1H), 3.10 – 2.85 (m, 2H), 2.95 (s, 3H), 2.55 (d,  $J = 6.9$  Hz, 2H), 1.90 – 1.71 (m, 7H), 1.51 – 1.42 (m, 3H), 1.35 (qd,  $J = 12.9, 3.8$  Hz, 2H), 1.24 – 1.01 (m, 3H).

$^{13}\text{C}$  NMR (101 MHz,  $\text{CDCl}_3$ )  $\delta$  161.14, 158.61, 148.26, 148.24, 138.13, 132.12, 130.49, 128.63, 53.45, 42.18, 38.00, 31.23, 29.57, 25.64, 25.28.

HRMS:  $[\text{M}+\text{H}]^+$  calculated for  $\text{C}_{23}\text{H}_{30}\text{ClN}_5\text{O}_2+\text{H}^+$  444.21608, found 444.21616.

### (3-(((Adamant-1-yl)methyl)sulfonyl)-1*H*-1,2,4-triazol-1-yl)(4-(4-chlorobenzyl)piperidin-1-yl)-methanone (4)



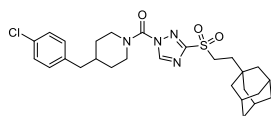
**59** (30 mg, 0.062 mmol) was oxidized according to General procedure A. Flash column chromatography (33% EtOAc in pentane) afforded the title compound as a white solid (25 mg, 0.048 mmol, 81%).

$^1\text{H}$  NMR (500 MHz,  $\text{CDCl}_3$ )  $\delta$  8.82 (s, 1H), 7.29 – 7.24 (m, 2H), 7.10 – 7.06 (m, 2H), 4.55 – 4.34 (bs, 2H), 3.25 (s, 2H), 3.18 – 2.85 (m, 2H), 2.56 (d,  $J = 5.1$  Hz, 2H), 2.01 – 1.96 (m, 3H), 1.88 – 1.61 (m, 15H), 1.37 (qd,  $J = 13.2, 4.3$  Hz, 2H).

$^{13}\text{C}$  NMR (126 MHz,  $\text{CDCl}_3$ )  $\delta$  163.42, 148.01, 147.32, 137.98, 132.17, 130.48, 128.65, 66.22, 47.83 (br), 46.62 (br), 42.07, 42.00, 37.87, 36.40, 34.76, 28.38.

HRMS:  $[\text{M}+\text{H}]^+$  calculated for  $\text{C}_{26}\text{H}_{33}\text{ClN}_4\text{O}_3\text{S}+\text{H}^+$  517.20347, found 517.20322.

### (3-(((2-(Adamant-1-yl)ethyl)sulfonyl)-1*H*-1,2,4-triazol-1-yl)(4-(4-chlorobenzyl)piperidin-1-yl)-methanone (5)



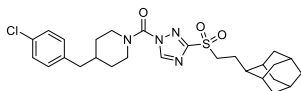
**60** (25 mg, 0.050 mmol) was oxidized according to General procedure A. Flash column chromatography (33% EtOAc in pentane) afforded the title compound as a white solid (25 mg, 0.047 mmol, 94%).

$^1\text{H}$  NMR (500 MHz,  $\text{CDCl}_3$ )  $\delta$  8.85 (s, 1H), 7.29 – 7.24 (m, 2H), 7.11 – 7.05 (m, 2H), 4.56 – 4.36 (m, 2H), 3.41 – 3.32 (m, 2H), 3.20 – 2.86 (m, 2H), 2.57 (d,  $J$  = 6.8 Hz, 2H), 1.97 (p,  $J$  = 3.1 Hz, 3H), 1.87 – 1.52 (m, 9H), 1.47 – 1.43 (m, 6H), 1.37 (qd,  $J$  = 13.1, 4.1 Hz, 2H).

$^{13}\text{C}$  NMR (126 MHz,  $\text{CDCl}_3$ )  $\delta$  161.81, 148.22, 147.25, 137.97, 132.19, 130.47, 128.66, 49.54, 47.77 (br), 46.21 (br), 42.07, 42.00, 37.87, 36.88, 35.33, 32.07, 28.51.

HRMS:  $[\text{M}+\text{H}]^+$  calculated for  $\text{C}_{27}\text{H}_{35}\text{ClN}_4\text{O}_3\text{S}+\text{H}^+$  531.21912, found 531.21895.

**(3-((2-(Adamant-2-yl)ethyl)sulfonyl)-1H-1,2,4-triazol-1-yl)(4-(4-chlorobenzyl)piperidin-1-yl)-methanone (6)**



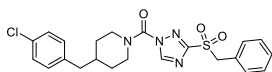
**61** (28 mg, 0.056 mmol) was oxidized according to General procedure A. Flash column chromatography (33% EtOAc in pentane) afforded the title compound as a white solid (29 mg, 0.055 mmol, 97%).

$^1\text{H}$  NMR (500 MHz,  $\text{CDCl}_3$ )  $\delta$  8.85 (s, 1H), 7.29 – 7.25 (m, 2H), 7.11 – 7.04 (m, 2H), 4.53 – 4.36 (m, 2H), 3.41 – 3.34 (m, 2H), 3.20 – 2.87 (m, 2H), 2.61 – 2.52 (m, 2H), 2.02 – 1.92 (m, 2H), 1.91 – 1.60 (m, 16H), 1.55 – 1.48 (m, 2H), 1.37 (qd,  $J$  = 13.1, 4.1 Hz, 2H).

$^{13}\text{C}$  NMR (126 MHz,  $\text{CDCl}_3$ )  $\delta$  161.89, 148.22, 147.23, 137.96, 132.18, 130.47, 128.66, 53.10, 47.98 (br), 46.45 (br), 43.44, 42.06, 38.94, 38.16, 37.87, 31.58, 31.38, 28.07, 27.86, 24.74.

HRMS:  $[\text{M}+\text{H}]^+$  calculated for  $\text{C}_{27}\text{H}_{35}\text{ClN}_4\text{O}_3\text{S}+\text{H}^+$  531.21912, found 531.21893.

**(3-(Benzylsulfonyl)-1H-1,2,4-triazol-1-yl)(4-(4-chlorobenzyl)piperidin-1-yl)methanone (7)**



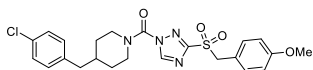
**62** (30 mg, 0.070 mmol) was oxidized according to General procedure A. Flash column chromatography afforded the title compound (28 mg, 0.063 mmol, 90%).

$^1\text{H}$  NMR (400 MHz,  $\text{CDCl}_3$ )  $\delta$  8.82 (s, 1H), 7.33 – 7.24 (m, 7H), 7.10 – 7.02 (m, 2H), 4.63 (s, 2H), 4.44 – 3.99 (m, 2H), 3.08 – 2.78 (m, 2H), 2.68 – 2.40 (m, 2H), 1.87 – 1.70 (m, 1H), 1.86 – 1.53 (m, 2H), 1.39 – 1.15 (m, 2H).

$^{13}\text{C}$  NMR (101 MHz,  $\text{CDCl}_3$ )  $\delta$  160.75, 148.12, 147.12, 137.98, 132.16, 131.12, 130.47, 129.26, 128.97, 128.65, 126.50, 60.76, 47.90, 46.29, 42.03, 37.81, 32.12, 31.32.

HRMS:  $[\text{M}+\text{Na}]^+$  calculated for  $\text{C}_{22}\text{H}_{23}\text{ClN}_4\text{O}_3\text{S}+\text{Na}^+$  481.1072, found 481.1070.

**(4-(4-Chlorobenzyl)piperidin-1-yl)(3-((4-methoxybenzyl)sulfonyl)-1H-1,2,4-triazol-1-yl)-methanone (8)**

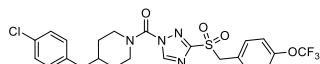


**63** (30 mg, 0.066 mmol) was oxidized according to General procedure A. Flash column chromatography afforded the title compound (29 mg, 0.059 mmol, 90%).

$^1\text{H}$  NMR (400 MHz,  $\text{CDCl}_3$ )  $\delta$  8.82 (s, 1H), 7.30 – 7.24 (m, 2H), 7.21 – 7.15 (m, 2H), 7.10 – 7.04 (m, 2H), 6.84 – 6.78 (m, 2H), 4.56 (s, 2H), 4.45 – 4.22 (m, 1H), 4.19 – 4.00 (m, 1H), 3.72 (s, 3H), 3.04 – 2.80 (m, 2H), 2.54 (d,  $J$  = 7.0 Hz, 2H), 1.86 – 1.70 (m, 2H), 1.70 – 1.52 (m, 1H), 1.38 – 1.29 (m, 2H).

$^{13}\text{C}$  NMR (101 MHz,  $\text{CDCl}_3$ )  $\delta$  160.82, 160.35, 148.10, 147.17, 138.00, 132.34, 132.15, 130.47, 128.65, 118.22, 114.42, 60.18, 55.33, 46.23 (br), 42.04, 37.82, 32.03 (br).

HRMS:  $[\text{M}+\text{Na}]^+$  calculated for  $\text{C}_{23}\text{H}_{25}\text{ClN}_4\text{O}_4\text{S}+\text{Na}^+$  511.1177, found 511.1182.

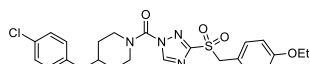
**(4-(4-Chlorobenzyl)piperidin-1-yl)(3-((4-(trifluoromethoxy)benzyl)sulfonyl)-1H-1,2,4-triazol-1-yl)methanone (9, IK015)**

**64** (40 mg, 0.078 mmol) was oxidized according to General procedure A. Flash column chromatography afforded the title compound (40 mg, 0.074 mmol, 94%).

$^1\text{H}$  NMR (400 MHz,  $\text{CDCl}_3$ )  $\delta$  8.85 (s, 1H), 7.39 – 7.31 (m, 2H), 7.30 – 7.21 (m, 2H), 7.21 – 7.13 (m, 2H), 7.10 – 7.02 (m, 2H), 4.64 (s, 2H), 4.44 – 4.10 (m, 2H), 3.09 – 2.82 (m, 2H), 2.54 (d,  $J$  = 6.5 Hz, 2H), 1.86 – 1.72 (m, 1H), 1.72 – 1.58 (m, 2H), 1.38 – 1.20 (m, 2H).

$^{13}\text{C}$  NMR (101 MHz,  $\text{CDCl}_3$ )  $\delta$  160.76, 150.02 (q,  $J$  = 1.8 Hz), 148.28, 147.01, 137.92, 132.77, 132.20, 130.46, 128.67, 125.09, 121.32, 120.42 (q,  $J$  = 258.2 Hz), 59.75, 47.92 (br), 46.49 (br), 42.02, 37.81, 31.43 (br).

HRMS:  $[\text{M}+\text{H}]^+$  calculated for  $\text{C}_{23}\text{H}_{22}\text{ClF}_3\text{N}_4\text{O}_4\text{S}+\text{H}^+$  543.10751, found 543.10753.

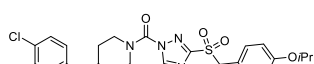
**(4-(4-Chlorobenzyl)piperidin-1-yl)(3-((4-ethoxybenzyl)sulfonyl)-1H-1,2,4-triazol-1-yl)-methanone (10)**

**65** (40 mg, 0.085 mmol) was oxidized according to General procedure A. Flash column chromatography afforded the title compound (35 mg, 0.070 mmol, 82%).

$^1\text{H}$  NMR (400 MHz,  $\text{CDCl}_3$ )  $\delta$  8.82 (s, 1H), 7.29 – 7.23 (m, 2H), 7.20 – 7.12 (m, 2H), 7.10 – 7.03 (m, 2H), 6.83 – 6.75 (m, 2H), 4.56 (s, 2H), 4.42 – 4.26 (m, 1H), 4.16 – 4.01 (m, 1H), 3.94 (q,  $J$  = 7.1 Hz, 2H), 3.03 – 2.79 (m, 2H), 2.53 (d,  $J$  = 7.0 Hz, 2H), 1.85 – 1.69 (m, 1H), 1.83 – 1.56 (m, 2H), 1.36 (t,  $J$  = 7.0 Hz, 3H), 1.33 – 1.18 (m, 2H).

$^{13}\text{C}$  NMR (101 MHz,  $\text{CDCl}_3$ )  $\delta$  160.76, 159.69, 148.06, 147.14, 137.98, 132.28, 132.08, 130.44, 128.59, 117.96, 114.85, 63.52, 60.18, 47.73 (br), 46.22 (br), 41.99, 37.76, 31.99 (br), 31.35 (br), 14.80.

HRMS:  $[\text{M}+\text{H}]^+$  calculated for  $\text{C}_{24}\text{H}_{27}\text{ClN}_4\text{O}_4\text{S}+\text{H}^+$  503.15143, found 503.15122.

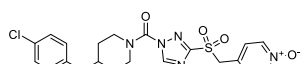
**(4-(4-Chlorobenzyl)piperidin-1-yl)(3-((4-isopropoxybenzyl)sulfonyl)-1H-1,2,4-triazol-1-yl)-methanone (11)**

**66** (40 mg, 0.082 mmol) was oxidized according to General procedure A. Flash column chromatography afforded the title compound (33 mg, 0.064 mmol, 77%).

$^1\text{H}$  NMR (400 MHz,  $\text{CDCl}_3$ )  $\delta$  8.82 (s, 1H), 7.31 – 7.23 (m, 2H), 7.20 – 7.11 (m, 2H), 7.13 – 7.03 (m, 2H), 6.83 – 6.74 (m, 2H), 4.56 (s, 2H), 4.47 (hept,  $J$  = 6.1 Hz, 1H), 4.42 – 4.25 (m, 1H), 4.22 – 4.03 (m, 1H), 3.07 – 2.81 (m, 2H), 2.54 (d,  $J$  = 6.9 Hz, 2H), 1.82 – 1.70 (m, 1H), 1.85 – 1.58 (m, 2H), 1.38 – 1.22 (m, 2H), 1.28 (d,  $J$  = 6.0 Hz, 6H).

$^{13}\text{C}$  NMR (101 MHz,  $\text{CDCl}_3$ )  $\delta$  160.92, 158.79, 148.08, 147.21, 138.00, 132.38, 132.19, 130.49, 128.68, 117.77, 116.07, 70.00, 60.21, 47.67 (br), 42.08, 37.89, 32.28 (br), 31.38 (br), 22.07.

HRMS:  $[\text{M}+\text{H}]^+$  calculated for  $\text{C}_{25}\text{H}_{29}\text{ClN}_4\text{O}_4\text{S}+\text{H}^+$  517.16708, found 517.16687.

**4-(((1-(4-(4-Chlorobenzyl)piperidine-1-carbonyl)-1H-1,2,4-triazol-3-yl)sulfonyl)methyl)-pyridine 1-oxide (12)**

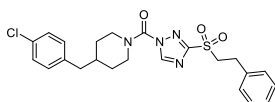
**67** (50 mg, 0.12 mmol) was oxidized according to General procedure A. Flash column chromatography afforded the title compound (53 mg, 0.011 mmol, 95%).

$^1\text{H}$  NMR (400 MHz,  $\text{CDCl}_3$ )  $\delta$  8.87 (s, 1H), 8.19 – 8.11 (m, 2H), 7.31 – 7.21 (m, 4H), 7.11 – 7.03 (m, 2H), 4.61 (s, 2H), 4.42 – 4.26 (m, 2H), 3.15 – 2.85 (m, 2H), 2.65 – 2.46 (m, 2H), 1.87 – 1.71 (m, 3H), 1.41 – 1.28 (m, 2H).

$^{13}\text{C}$  NMR (101 MHz,  $\text{CDCl}_3$ )  $\delta$  160.46, 146.81, 139.68, 137.91, 132.24, 130.50, 128.71, 128.51, 124.52, 58.49, 42.03, 37.82.

HRMS:  $[\text{M}+\text{H}]^+$  calculated for  $\text{C}_{21}\text{H}_{22}\text{ClN}_5\text{O}_4\text{S}+\text{H}^+$  476.11538, found 476.11525.

**(4-(4-Chlorobenzyl)piperidin-1-yl)(3-(phenethylsulfonyl)-1H-1,2,4-triazol-1-yl)methanone (13)**



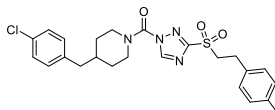
**68** (40 mg, 0.091 mmol) was oxidized according to General procedure A. Flash column chromatography afforded the title compound (16 mg, 0.033 mmol, 36%).

$^1\text{H}$  NMR (400 MHz,  $\text{CDCl}_3$ )  $\delta$  8.82 (s, 1H), 7.32 – 7.24 (m, 5H), 7.19 – 7.14 (m, 2H), 7.10 – 7.04 (m, 2H), 4.54 – 4.33 (m, 2H), 3.80 – 3.57 (m, 2H), 3.27 – 3.13 (m, 2H), 3.13 – 2.83 (m, 2H), 2.57 (d,  $J$  = 6.8 Hz, 2H), 1.94 – 1.68 (m, 3H), 1.37 (qd,  $J$  = 13.3, 4.1 Hz, 2H).

$^{13}\text{C}$  NMR (101 MHz,  $\text{CDCl}_3$ )  $\delta$  161.73, 148.27, 147.15, 137.96, 136.99, 132.21, 130.49, 128.99, 128.69, 128.52, 127.25, 55.62, 46.85 (br), 42.09, 37.90, 28.44.

HRMS:  $[\text{M}+\text{Na}]^+$  calculated for  $\text{C}_{23}\text{H}_{25}\text{ClN}_4\text{O}_3\text{S}+\text{Na}^+$  495.1228, found 473.1232.

**(4-(4-Chlorobenzyl)piperidin-1-yl)(3-((4-methylphenethyl)sulfonyl)-1H-1,2,4-triazol-1-yl)methanone (14)**



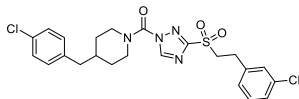
**69** (40 mg, 0.088 mmol) was oxidized according to General procedure A. Flash column chromatography afforded the title compound (22 mg, 0.045 mmol, 51%).

$^1\text{H}$  NMR (400 MHz,  $\text{CDCl}_3$ )  $\delta$  8.82 (s, 1H), 7.32 – 7.22 (m, 2H), 7.14 – 6.99 (m, 6H), 4.60 – 4.27 (m, 2H), 3.76 – 3.58 (m, 2H), 3.22 – 3.09 (m, 2H), 3.09 – 2.84 (m, 2H), 2.57 (d,  $J$  = 6.8 Hz, 2H), 2.31 (s, 3H), 1.94 – 1.68 (m, 3H), 1.36 (qd,  $J$  = 13.2, 4.1 Hz, 2H).

$^{13}\text{C}$  NMR (101 MHz,  $\text{CDCl}_3$ )  $\delta$  161.74, 148.26, 147.15, 137.96, 136.91, 133.87, 132.21, 130.49, 129.63, 128.69, 128.38, 55.74, 47.84 (br), 42.09, 37.89, 28.02, 21.15.

HRMS:  $[\text{M}+\text{Na}]^+$  calculated for  $\text{C}_{24}\text{H}_{27}\text{ClN}_4\text{O}_3\text{S}+\text{Na}^+$  509.1385, found 509.1382.

**(4-(4-Chlorobenzyl)piperidin-1-yl)(3-((3-chlorophenethyl)sulfonyl)-1H-1,2,4-triazol-1-yl)methanone (15)**



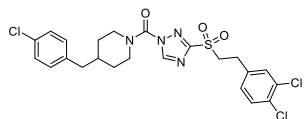
**70** (40 mg, 0.084 mmol) was oxidized according to General procedure A. Flash column chromatography afforded the title compound (32 mg, 0.063 mmol, 75%).

$^1\text{H}$  NMR (400 MHz,  $\text{CDCl}_3$ )  $\delta$  8.82 (s, 1H), 7.30 – 7.24 (m, 2H), 7.23 – 7.19 (m, 2H), 7.18 – 7.16 (m, 1H), 7.12 – 7.01 (m, 3H), 4.51 – 4.35 (m, 2H), 3.73 – 3.61 (m, 2H), 3.20 – 3.13 (m, 2H), 3.11 – 2.87 (m, 2H), 2.57 (d,  $J$  = 6.8 Hz, 2H), 1.89 – 1.71 (m, 3H), 1.37 (qd,  $J$  = 13.2, 4.1 Hz, 2H).

$^{13}\text{C}$  NMR (101 MHz,  $\text{CDCl}_3$ )  $\delta$  161.57, 148.30, 147.05, 138.89, 137.95, 134.64, 132.16, 130.48, 130.22, 128.75, 128.66, 127.46, 126.74, 55.17, 42.05, 37.86, 32.02, 28.18.

HRMS:  $[\text{M}+\text{H}]^+$  calculated for  $\text{C}_{23}\text{H}_{24}\text{Cl}_2\text{N}_4\text{O}_3\text{S}+\text{H}^+$  507.1019, found 507.1016.

**(4-(4-Chlorobenzyl)piperidin-1-yl)(3-((3,4-dichlorophenethyl)sulfonyl)-1H-1,2,4-triazol-1-yl)-methanone (16)**



**71** (28 mg, 0.055 mmol) was oxidized according to General procedure A. Flash column chromatography afforded the title compound (12 mg, 0.023 mmol, 41%).

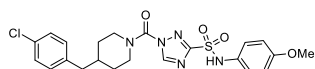
$^1\text{H NMR}$  (500 MHz,  $\text{CDCl}_3$ )  $\delta$  8.83 (s, 1H), 7.35 (d,  $J = 8.2$  Hz, 1H), 7.31 – 7.23 (m, 3H), 7.11 – 7.04 (m, 2H), 7.02 (dd,  $J = 8.2, 2.1$  Hz, 1H),

4.52 – 4.36 (m, 2H), 3.75 – 3.60 (m, 2H), 3.27 – 3.12 (m, 2H), 3.12 – 2.83 (m, 2H), 2.66 – 2.51 (m, 2H), 1.91 – 1.69 (m, 3H), 1.37 (qd,  $J = 13.2, 4.2$  Hz, 2H).

$^{13}\text{C NMR}$  (126 MHz,  $\text{CDCl}_3$ )  $\delta$  161.63, 147.03, 137.95, 137.14, 132.93, 132.24, 131.50, 130.89, 130.64, 130.50, 128.70, 127.99, 55.01, 42.08, 37.88, 27.73.

HRMS:  $[\text{M}+\text{Na}]^+$  calculated for  $\text{C}_{23}\text{H}_{23}\text{Cl}_3\text{N}_4\text{O}_3\text{S}+\text{Na}^+$  563.0449, found 563.0455.

**1-(4-(4-Chlorobenzyl)piperidine-1-carbonyl)-N-(4-methoxyphenyl)-1H-1,2,4-triazole-3-sulfonamide (17)**



**62** (1 eq, 50 mg, 0.12 mmol) was reacted with *p*-anisidine (**92**, 50 eq, 721 mg dissolved in 1.3 mL DCM, 5.86 mmol) according to General procedure B. Flash column chromatography (30 → 60%

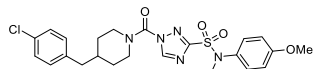
EtOAc in pentane) afforded the title compound as off-white gum (15 mg, 0.031 mmol, 26%).

$^1\text{H NMR}$  (500 MHz,  $\text{CDCl}_3$ )  $\delta$  8.83 (s, 1H), 7.28 – 7.23 (m, 2H), 7.21 – 7.16 (m, 2H), 7.09 – 7.04 (m, 2H), 6.82 – 6.78 (m, 2H), 4.45 – 4.23 (m, 2H), 3.74 (s, 3H), 3.45 (s, 3H), 3.07 – 2.80 (m, 2H), 2.53 (d,  $J = 6.4$  Hz, 2H), 1.82 – 1.55 (m, 3H), 1.39 – 1.16 (m, 2H).

$^{13}\text{C NMR}$  (126 MHz,  $\text{CDCl}_3$ )  $\delta$  160.83, 158.44, 148.06, 147.28, 138.04, 132.17, 130.49, 128.67, 127.80, 125.81, 114.61, 55.50, 47.81 (br), 46.26 (br), 42.07, 37.83, 32.05 (br), 31.39 (br).

HRMS:  $[\text{M}+\text{H}]^+$  calculated for  $\text{C}_{22}\text{H}_{24}\text{ClN}_5\text{O}_4\text{S}+\text{H}^+$  419.13103, found 419.13099.

**1-(4-(4-Chlorobenzyl)piperidine-1-carbonyl)-N-(4-methoxyphenyl)-N-methyl-1H-1,2,4-triazole-3-sulfonamide (18)**



**62** (1 eq, 50 mg, 0.12 mmol) was reacted with *N*-methyl-*p*-anisidine (**93**, 35 eq, 562 mg dissolved in 2 mL DCM, 4.10 mmol) according to General procedure B. Flash column chromatography

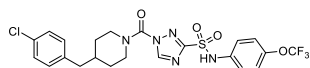
(30 → 55% EtOAc in pentane) afforded the title compound as slightly brown oil (43 mg, 0.085 mmol, 73%).

$^1\text{H NMR}$  (500 MHz,  $\text{CDCl}_3$ )  $\delta$  8.83 (s, 1H), 7.29 – 7.23 (m, 4H), 7.18 (d,  $J = 8.3$  Hz, 2H), 7.06 (d,  $J = 8.0$  Hz, 3H), 6.81 (d,  $J = 8.3$  Hz, 2H), 4.34 (s, 2H), 3.74 (s, 3H), 3.45 (s, 3H), 3.07 – 2.80 (m, 2H), 2.53 (d,  $J = 6.4$  Hz, 2H), 1.82 – 1.55 (m, 3H), 1.39 – 1.16 (m, 1H).

$^{13}\text{C NMR}$  (126 MHz,  $\text{CDCl}_3$ )  $\delta$  161.03, 159.12, 147.82, 147.37, 137.97, 133.01, 132.01, 130.43, 128.60, 128.55, 114.44, 55.49, 47.77 (br), 46.19 (br), 41.97, 40.03, 37.73, 31.95 (br), 31.36 (br).

HRMS:  $[\text{M}+\text{H}]^+$  calculated for  $\text{C}_{23}\text{H}_{26}\text{ClN}_5\text{O}_4\text{S}+\text{H}^+$  504.14668, found 504.14631.

**1-(4-(4-Chlorobenzyl)piperidine-1-carbonyl)-N-(4-(trifluoromethoxy)phenyl)-1H-1,2,4-triazole-3-sulfonamide (19, WEN222)**



**62** (1 eq, 50 mg, 0.12 mmol) was reacted with 4-(trifluoromethoxy)aniline (**94**, 35 eq, 550  $\mu\text{L}$ , 4.10 mmol) according to General procedure B. Flash column chromatography (25 → 40%

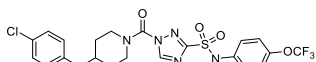
EtOAc in pentane) afforded the title compound as slightly brown oil (33 mg, 0.061 mmol, 52%).

$^1\text{H}$  NMR (400 MHz,  $\text{CDCl}_3$ )  $\delta$  8.94 (s, 1H), 8.89 (s, 1H), 7.37 – 7.31 (m, 2H), 7.32 – 7.22 (m, 2H), 7.14 – 7.08 (m, 2H), 7.09 – 7.03 (m, 2H), 4.47 – 3.95 (m, 2H), 3.03 – 2.80 (m, 2H), 2.53 (d,  $J$  = 6.6 Hz, 2H), 1.85 – 1.49 (m, 3H), 1.38 – 1.15 (m, 2H).

$^{13}\text{C}$  NMR (101 MHz,  $\text{CDCl}_3$ )  $\delta$  160.51, 148.38, 147.08, 146.90 (d,  $J$  = 1.9 Hz), 137.92, 134.33, 132.18, 130.44, 128.65, 123.53, 122.08, 120.43 (q,  $J$  = 257.4 Hz), 47.74 (br), 46.35 (br), 41.99, 37.75, 32.03 (br), 31.33 (br).

HRMS:  $[\text{M}+\text{H}]^+$  calculated for  $\text{C}_{22}\text{H}_{21}\text{ClF}_3\text{N}_5\text{O}_4\text{S}+\text{H}^+$  544.10276, found 544.10268.

#### 1-(4-(4-Chlorobenzyl)piperidine-1-carbonyl)-*N*-methyl-*N*-(4-(trifluoromethoxy)phenyl)-1*H*-1,2,4-triazole-3-sulfonamide (20)



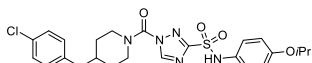
**62** (1 eq, 49 mg, 0.12 mmol) was reacted with *N*-methyl-4-(trifluoromethoxy)aniline (**95**, 10 eq, 175  $\mu\text{L}$ , 1.17 mmol) according to General procedure C. Flash column chromatography (20  $\rightarrow$  50% EtOAc in pentane) afforded the title compound as grayish gum (8 mg, 0.014 mmol, 12%).

$^1\text{H}$  NMR (500 MHz,  $\text{CDCl}_3$ )  $\delta$  8.82 (s, 1H), 7.40 – 7.33 (m, 2H), 7.32 – 7.22 (m, 2H), 7.20 – 7.14 (m, 2H), 7.11 – 7.03 (m, 2H), 4.42 – 4.30 (m, 2H), 3.48 (s, 3H), 3.09 – 2.83 (m, 2H), 2.54 (d,  $J$  = 6.1 Hz, 2H), 1.85 – 1.74 (m, 1H), 1.85 – 1.64 (m, 2H), 1.39 – 1.20 (m, 2H).

$^{13}\text{C}$  NMR (126 MHz,  $\text{CDCl}_3$ )  $\delta$  161.02, 148.40 (q,  $J$  = 1.4 Hz), 147.95, 147.33, 139.08, 137.95, 132.22, 130.47, 128.80, 128.68, 121.74, 120.46 (q,  $J$  = 258.1 Hz), 47.85 (br), 46.35 (br), 42.06, 39.76, 37.87, 32.17 (br), 31.45 (br).

HRMS:  $[\text{M}+\text{H}]^+$  calculated for  $\text{C}_{23}\text{H}_{23}\text{ClF}_3\text{N}_5\text{O}_4\text{S}+\text{H}^+$  558.11841, found 558.11824.

#### 1-(4-(4-Chlorobenzyl)piperidine-1-carbonyl)-*N*-(4-isopropoxyphenyl)-1*H*-1,2,4-triazole-3-sulfonamide (21)



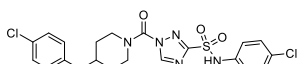
**62** (1 eq, 51 mg, 0.12 mmol) was reacted with **96** (10 eq, 177 mg dissolved in 1 mL DCM, 1.17 mmol) according to General procedure C. Flash column chromatography (20  $\rightarrow$  60% EtOAc in pentane) afforded the title compound as brown oil (3 mg, 6  $\mu\text{mol}$ , 5%).

$^1\text{H}$  NMR (500 MHz,  $\text{CDCl}_3$ )  $\delta$  8.79 (s, 1H), 7.31 (bs, 1H), 7.30 – 7.24 (m, 2H), 7.16 – 7.10 (m, 2H), 7.08 – 7.03 (m, 2H), 6.78 – 6.71 (m, 2H), 4.42 (hept,  $J$  = 6.1 Hz, 1H), 4.39 – 4.09 (m, 2H), 2.91 (s, 2H), 2.53 (d,  $J$  = 6.9 Hz, 2H), 1.82 – 1.71 (m, 1H), 1.82 – 1.56 (m, 2H), 1.36 – 1.20 (m, 2H), 1.27 (d,  $J$  = 6.1 Hz, 6H).

$^{13}\text{C}$  NMR (126 MHz,  $\text{CDCl}_3$ )  $\delta$  161.07, 156.90, 147.30, 138.03, 132.20, 130.49, 128.69, 127.30, 125.92, 116.43, 70.28, 68.13, 47.93 (br), 46.26 (br), 42.11, 37.91, 22.07.

HRMS:  $[\text{M}+\text{H}]^+$  calculated for  $\text{C}_{24}\text{H}_{28}\text{ClN}_5\text{O}_4\text{S}+\text{H}^+$  518.16233, found 518.16209.

#### 1-(4-(4-Chlorobenzyl)piperidine-1-carbonyl)-*N*-(4-chlorophenyl)-1*H*-1,2,4-triazole-3-sulfonamide (22)



**62** (1 eq, 49 mg, 0.12 mmol) was reacted with 4-chloroaniline (**97**, 53 eq, 781 mg dissolved in 1 mL DCM, 4.10 mmol) according to General procedure B. Flash column chromatography (20  $\rightarrow$  40% EtOAc in pentane) afforded the title compound as white solid (10 mg, 0.020 mmol, 18%).

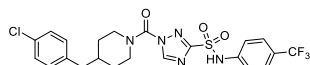
$^1\text{H}$  NMR (500 MHz,  $\text{CDCl}_3$ )  $\delta$  8.81 (s, 1H), 8.10 (s, 1H), 7.31 – 7.24 (m, 2H), 7.24 – 7.20 (m, 4H), 7.10 – 7.05 (m, 2H), 4.43 – 4.02 (m, 2H), 3.00 – 2.81 (m, 2H), 2.54 (d,  $J$  = 7.0 Hz, 2H), 1.84 – 1.73 (m, 1H), 1.85 – 1.53 (m, 2H), 1.36 – 1.17 (m, 2H).

$^{13}\text{C}$  NMR (126 MHz,  $\text{CDCl}_3$ )  $\delta$  160.59, 148.16, 147.08, 137.97, 134.14, 132.24, 131.90, 130.49, 129.60, 128.71, 123.79, 47.80 (br), 46.35 (br), 42.06, 37.82, 32.09 (br), 31.01 (br).

HRMS:  $[\text{M}+\text{H}]^+$  calculated for  $\text{C}_{21}\text{H}_{21}\text{Cl}_2\text{N}_5\text{O}_3\text{S}+\text{H}^+$  494.08149, found 494.08133.



**1-(4-(4-Chlorobenzyl)piperidine-1-carbonyl)-N-(4-(trifluoromethyl)phenyl)-1H-1,2,4-triazole-3-sulfonamide (23)**



**62** (1 eq, 67 mg, 0.16 mmol) was reacted with 4-(trifluoromethyl)aniline (**98**, 35 eq, 650  $\mu$ L diluted to 1 mL with DCM, 5.15 mmol) according to General procedure B. Flash column

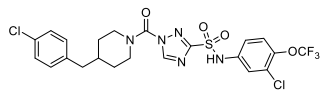
chromatography (20  $\rightarrow$  40% EtOAc in pentane) afforded the title compound as off-white gum (66 mg, 0.13 mmol, 80%).

$^1\text{H}$  NMR (500 MHz,  $\text{CDCl}_3$ )  $\delta$  8.84 (s, 1H), 7.54 – 7.49 (m, 2H), 7.43 – 7.37 (m, 2H), 7.30 – 7.24 (m, 2H), 7.09 – 7.04 (m, 2H), 4.44 – 4.03 (m, 2H), 3.02 – 2.84 (m, 2H), 2.54 (d,  $J$  = 5.7 Hz, 2H), 1.84 – 1.72 (m, 1H), 1.85 – 1.53 (m, 2H), 1.38 – 1.16 (m, 2H).

$^{13}\text{C}$  NMR (126 MHz,  $\text{CDCl}_3$ )  $\delta$  160.58, 148.35, 147.00, 139.11, 137.91, 132.25, 130.46, 128.70, 127.65 (q,  $J$  = 32.9 Hz), 126.75 (q,  $J$  = 3.7 Hz), 123.91 (d,  $J$  = 272.2 Hz), 120.80, 47.83 (br), 46.36 (br), 42.02, 37.79, 32.08 (br).

HRMS:  $[\text{M}+\text{H}]^+$  calculated for  $\text{C}_{22}\text{H}_{21}\text{ClF}_3\text{N}_5\text{O}_3\text{S}+\text{H}^+$  528.10785, found 528.10765.

**N-(3-Chloro-4-(trifluoromethoxy)phenyl)-1-(4-(4-chlorobenzyl)piperidine-1-carbonyl)-1H-1,2,4-triazole-3-sulfonamide (24)**



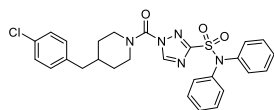
**62** (1 eq, 49 mg, 0.12 mmol) was reacted with 3-chloro-4-(trifluoromethoxy)aniline (**99**, 14 eq, 228  $\mu$ L diluted to 1 mL with DCM, 1.57 mmol) according to General procedure C. Flash column chromatography (20  $\rightarrow$  50% EtOAc in pentane) afforded the title compound as white solid (8 mg, 0.014 mmol, 12%).

$^1\text{H}$  NMR (500 MHz,  $\text{CDCl}_3$ )  $\delta$  8.86 (s, 1H), 8.53 (s, 1H), 7.49 (dd,  $J$  = 2.0, 0.9 Hz, 1H), 7.30 – 7.25 (m, 2H), 7.23 – 7.17 (m, 2H), 7.10 – 7.04 (m, 2H), 4.45 – 4.13 (m, 2H), 3.08 – 2.83 (m, 2H), 2.55 (d,  $J$  = 3.9 Hz, 2H), 1.85 – 1.74 (m, 1H), 1.84 – 1.60 (m, 2H), 1.37 – 1.18 (m, 2H).

$^{13}\text{C}$  NMR (126 MHz,  $\text{CDCl}_3$ )  $\delta$  160.49, 146.95, 142.86 (q,  $J$  = 1.7 Hz), 137.91, 135.18, 132.24, 130.47, 128.69, 128.46, 123.58, 123.53, 120.93, 47.83 (br), 46.43 (br), 42.03, 37.82, 32.07 (br), 41.44 (br).

HRMS:  $[\text{M}+\text{H}]^+$  calculated for  $\text{C}_{22}\text{H}_{20}\text{Cl}_2\text{F}_3\text{N}_5\text{O}_4\text{S}+\text{H}^+$  578.06379, found 578.06321.

**1-(4-(4-Chlorobenzyl)piperidine-1-carbonyl)-N,N-diphenyl-1H-1,2,4-triazole-3-sulfonamide (25)**

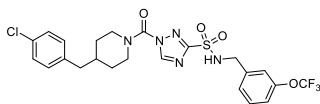


**62** (1 eq, 50 mg, 0.12 mmol) was reacted with diphenylamine (**100**, 35 eq, 578  $\mu$ L dissolved in 2 mL DCM, 4.10 mmol) according to General procedure B. Preparative HPLC afforded the title compound as dark oil (5 mg, 9  $\mu$ mol, 8%).

$^1\text{H}$  NMR (500 MHz,  $\text{CDCl}_3$ )  $\delta$  8.85 (s, 1H), 7.51 – 7.44 (m, 4H), 7.36 – 7.28 (m, 4H), 7.29 – 7.23 (m, 4H), 7.09 – 7.03 (m, 2H), 4.38 – 4.23 (m, 2H), 3.01 – 2.85 (m, 2H), 2.54 (d,  $J$  = 6.9 Hz, 2H), 2.03 – 1.85 (m, 3H), 1.83 – 1.72 (m, 1H), 1.70 – 1.55 (m, 1H).

$^{13}\text{C}$  NMR (126 MHz,  $\text{CDCl}_3$ )  $\delta$  162.11, 147.40, 140.82, 138.02, 132.23, 130.50, 129.49, 128.69, 128.30, 127.80, 77.42, 77.16, 76.91, 42.11, 37.89.

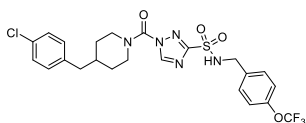
HRMS:  $[\text{M}+\text{H}]^+$  calculated for  $\text{C}_{27}\text{H}_{26}\text{ClN}_5\text{O}_3\text{S}$  536.15176, found 536.15163.

**1-(4-(4-Chlorobenzyl)piperidine-1-carbonyl)-N-(3-(trifluoromethoxy)benzyl)-1H-1,2,4-triazole-3-sulfonamide (26)**

**62** (1 eq, 50 mg, 0.12 mmol) was reacted with 3-(trifluoromethoxy)benzylamine (**101**, 15 eq, 263  $\mu$ L, 1.78 mmol) according to General procedure C. Flash column chromatography (5  $\rightarrow$  50% EtOAc in pentane) afforded the title compound as grayish gum (13 mg, 0.023 mmol, 20%).

$^1\text{H}$  NMR (500 MHz,  $\text{CDCl}_3$ )  $\delta$  8.74 (s, 1H), 7.36 – 7.30 (m, 1H), 7.29 – 7.22 (m, 3H), 7.19 – 7.16 (m, 1H), 7.16 – 7.10 (m, 1H), 7.11 – 7.03 (m, 2H), 5.99 – 5.80 (m, 1H), 4.41 (app. d,  $J$  = 6.2 Hz, 4H), 3.13 – 2.83 (m, 2H), 2.56 (d,  $J$  = 6.9 Hz, 2H), 1.87 – 1.75 (m, 1H), 1.68 (s, 2H), 1.34 (qd,  $J$  = 13.3, 4.1 Hz, 2H).

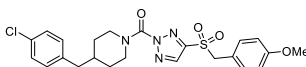
$^{13}\text{C}$  NMR (126 MHz,  $\text{CDCl}_3$ )  $\delta$  162.15, 149.53 (q,  $J$  = 1.9 Hz), 147.28, 138.47, 137.99, 132.19, 130.49, 130.31, 128.68, 126.32, 125.74, 120.63, 120.56, 120.50 (q,  $J$  = 257.4 Hz), 47.15, 44.47, 42.07, 37.88, 31.81. HRMS:  $[\text{M}+\text{H}]^+$  calculated for  $\text{C}_{23}\text{H}_{23}\text{ClF}_3\text{N}_5\text{O}_4\text{S}+\text{H}^+$  558.11841, found 558.11832.

**1-(4-(4-Chlorobenzyl)piperidine-1-carbonyl)-N-(4-(trifluoromethoxy)benzyl)-1H-1,2,4-triazole-3-sulfonamide (27)**

**62** (1 eq, 50 mg, 0.12 mmol) was reacted with 4-(trifluoromethoxy)benzylamine (**102**, 15 eq, 268  $\mu$ L, 1.78 mmol) according to General procedure C. Preparative HPLC afforded the title compound as colorless oil (< 1 mg, < 2  $\mu$ mol, < 2%).

$^1\text{H}$  NMR (500 MHz,  $\text{CDCl}_3$ )  $\delta$  8.79 (s, 1H), 7.38 – 7.31 (m, 2H), 7.30 – 7.26 (m, 2H), 7.21 – 7.15 (m, 2H), 7.11 – 7.04 (m, 2H), 4.50 – 4.34 (m, 2H), 4.40 (d,  $J$  = 6.2 Hz, 2H), 3.16 – 2.85 (m, 2H), 2.57 (d,  $J$  = 6.8 Hz, 2H), 1.87 – 1.71 (m, 3H), 1.36 (qd,  $J$  = 12.4, 4.2 Hz, 2H).

$^{13}\text{C}$  NMR (126 MHz,  $\text{CDCl}_3$ )  $\delta$  147.33, 140.58, 132.24, 130.51, 129.57, 128.71, 121.45, 47.17, 42.12, 37.92. HRMS:  $[\text{M}+\text{H}]^+$  calculated for  $\text{C}_{23}\text{H}_{23}\text{ClF}_3\text{N}_5\text{O}_4\text{S}+\text{H}^+$  558.11841, found 558.11810.

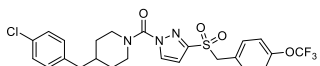
**(4-(4-Chlorobenzyl)piperidin-1-yl)(4-((4-methoxybenzyl)sulfonyl)-2H-1,2,3-triazol-2-yl)-methanone (28)**

**72** (15 mg, 0.033 mmol) was oxidized according to General procedure A. Flash column chromatography afforded the title compound (9.7 mg, 0.020 mmol, 60%).

$^1\text{H}$  NMR (400 MHz,  $\text{CDCl}_3$ )  $\delta$  7.84 (s, 1H), 7.29 – 7.24 (m, 2H), 7.18 – 7.11 (m, 2H), 7.11 – 7.05 (m, 2H), 6.86 – 6.79 (m, 2H), 4.51 (s, 2H), 4.50 – 4.41 (m, 1H), 3.76 (s, 3H), 3.70 – 3.59 (m, 1H), 3.11 – 2.94 (m, 2H), 2.57 (d,  $J$  = 7.0 Hz, 2H), 1.90 – 1.75 (m, 2H), 1.75 – 1.54 (m, 1H), 1.40 – 1.32 (m, 2H).

$^{13}\text{C}$  NMR (101 MHz,  $\text{CDCl}_3$ )  $\delta$  160.48, 147.65, 147.52, 137.98, 136.53, 132.36, 132.22, 130.48, 128.70, 118.32, 114.53, 61.75, 55.40, 48.02, 46.23, 42.09, 37.91, 32.06.

HRMS:  $[\text{M}+\text{Na}]^+$  calculated for  $\text{C}_{23}\text{H}_{25}\text{ClN}_4\text{O}_4\text{S}+\text{Na}^+$  511.1177, found 511.1177.

**(4-(4-Chlorobenzyl)piperidin-1-yl)(3-((4-(trifluoromethoxy)benzyl)sulfonyl)-1H-pyrazol-1-yl)-methanone (29)**

**73** (36 mg, 0.071 mmol) was oxidized according to General procedure A. Flash column chromatography (10  $\rightarrow$  40% EtOAc in pentane) afforded the title compound as gray gum (31 mg, 0.057 mmol, 81%).

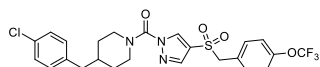
Analytical data on next page.

$^1\text{H}$  NMR (500 MHz,  $\text{CDCl}_3$ )  $\delta$  8.09 (d,  $J = 2.7$  Hz, 1H), 7.31 – 7.22 (m, 4H), 7.20 – 7.13 (m, 2H), 7.11 – 7.05 (m, 2H), 6.64 (d,  $J = 2.8$  Hz, 1H), 4.48 (s, 2H), 4.45 – 4.22 (m, 2H), 3.09 – 2.84 (m, 2H), 2.56 (d,  $J = 7.1$  Hz, 2H), 1.86 – 1.68 (m, 3H), 1.40 – 1.27 (m, 2H).

$^{13}\text{C}$  NMR (126 MHz,  $\text{CDCl}_3$ )  $\delta$  151.11, 149.84 (q,  $J = 1.9$  Hz), 149.47, 138.11, 133.78, 132.60, 132.10, 130.47, 128.62, 126.01, 121.18, 120.42 (q,  $J = 257.8$  Hz), 108.77, 60.99, 42.11, 37.96, 29.80.

HRMS:  $[\text{M}+\text{NH}_4]^+$  calculated for  $\text{C}_{24}\text{H}_{23}\text{ClF}_3\text{N}_3\text{O}_4\text{S}+\text{NH}_4^+$  559.13881, found 559.13867.

**(4-(4-Chlorobenzyl)piperidin-1-yl)(4-((4-(trifluoromethoxy)benzyl)sulfonyl)-1H-pyrazol-1-yl)methanone (30, WEN258)**



**74** (28 mg, 0.055 mmol) was oxidized according to General procedure A. Flash column chromatography (15 → 40% EtOAc in pentane) afforded the title compound as white solid (25 mg,

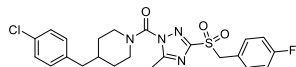
0.046 mmol, 84%).

$^1\text{H}$  NMR (500 MHz,  $\text{CDCl}_3$ )  $\delta$  8.31 (d,  $J = 0.8$  Hz, 1H), 7.50 (d,  $J = 0.8$  Hz, 1H), 7.31 – 7.23 (m, 4H), 7.23 – 7.16 (m, 2H), 7.10 – 7.04 (m, 2H), 4.42 – 4.33 (m, 2H), 4.36 (s, 2H), 3.00 – 2.91 (m, 2H), 2.56 (d,  $J = 7.1$  Hz, 2H), 1.86 – 1.67 (m, 3H), 1.34 (qd,  $J = 12.8, 4.1$  Hz, 2H).

$^{13}\text{C}$  NMR (126 MHz,  $\text{CDCl}_3$ )  $\delta$  149.97 (d,  $J = 1.9$  Hz), 149.28, 140.32, 138.13, 135.45, 132.56, 132.11, 130.48, 128.63, 126.63, 122.07, 121.28, 120.45 (q,  $J = 257.4$  Hz), 62.90, 42.19, 37.99, 31.91 (br).

HRMS:  $[\text{M}+\text{Na}]^+$  calculated for  $\text{C}_{24}\text{H}_{23}\text{ClF}_3\text{N}_3\text{O}_4\text{S}+\text{Na}^+$  564.09421, found 564.09377.

**(4-(4-Chlorobenzyl)piperidin-1-yl)(3-((4-fluorobenzyl)sulfonyl)-5-methyl-1H-1,2,4-triazol-1-yl)methanone (31)**



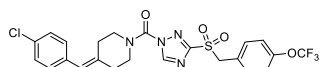
**75** (49 mg, 0.107 mmol) was oxidized according to General procedure A. Flash column chromatography (30 → 80% EtOAc in pentane) afforded the title compound (52 mg, 0.106 mmol, quant.).

$^1\text{H}$  NMR (400 MHz,  $\text{CDCl}_3$ )  $\delta$  7.33 – 7.21 (m, 4H), 7.10 – 7.03 (m, 2H), 7.06 – 6.96 (m, 2H), 4.56 (s, 2H), 4.41 – 4.33 (m, 1H), 3.49 (d,  $J = 13.5$  Hz, 1H), 2.97 – 2.83 (m, 2H), 2.67 (s, 3H), 2.61 – 2.47 (m, 2H), 1.81 – 1.65 (m, 2H), 1.65 – 1.57 (m, 1H), 1.39 – 1.18 (m, 2H).

$^{13}\text{C}$  NMR (101 MHz,  $\text{CDCl}_3$ )  $\delta$  164.56, 160.61 (d,  $J = 296.7$  Hz), 158.54, 147.97, 137.96, 132.99 (d,  $J = 8.5$  Hz), 132.14, 130.45, 128.63, 122.40 (d,  $J = 3.3$  Hz), 116.05 (d,  $J = 21.8$  Hz), 59.86, 47.98, 45.57, 41.96, 37.78, 32.04, 31.29, 13.73.

HRMS:  $[\text{M}+\text{H}]^+$  calculated for  $\text{C}_{24}\text{H}_{24}\text{ClFN}_4\text{O}_3\text{S}$  491.13144, found 491.13150.

**(4-(4-Chlorobenzylidene)piperidin-1-yl)(3-((4-(trifluoromethoxy)benzyl)sulfonyl)-1H-1,2,4-triazol-1-yl)methanone (32)**

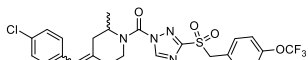


**114** (125 mg, 0.39 mmol) was reacted with **123** (1.2 eq, 143 mg, 0.47 mmol) according to General procedure D. The residue was purified by flash column chromatography (0 → 30% EtOAc in pentane) yielding the title compound as off-white gum (27 mg, 0.050 mmol, 13%).

$^1\text{H}$  NMR (500 MHz,  $\text{CDCl}_3$ )  $\delta$  8.89 (s, 1H), 7.38 – 7.33 (m, 2H), 7.33 – 7.28 (m, 2H), 7.21 – 7.16 (m, 2H), 7.14 – 7.09 (m, 2H), 6.39 (s, 1H), 4.65 (s, 2H), 3.81 – 3.74 (m, 2H), 3.69 – 3.61 (m, 2H), 2.67 – 2.37 (m, 4H).

$^{13}\text{C}$  NMR (126 MHz,  $\text{CDCl}_3$ )  $\delta$  160.95, 150.06, 148.37, 147.09, 136.14, 135.17, 132.80, 132.75, 130.22, 128.65, 125.38, 125.08, 122.17, 121.35, 120.43 (q,  $J = 258.2$  Hz), 77.41, 77.16, 76.91, 59.76.

HRMS:  $[\text{M}+\text{Na}]^+$  calculated for  $\text{C}_{23}\text{H}_{20}\text{ClF}_3\text{N}_4\text{O}_4\text{S}$  563.07381, found 563.07342.

**(4-(4-Chlorobenzylidene)-2-methylpiperidin-1-yl)(3-((4-(trifluoromethoxy)benzyl)sulfonyl)-1H-1,2,4-triazol-1-yl)methanone (33)**

**115** (58 mg, 0.17 mmol) was reacted with **123** (1.2 eq, 65 mg, 0.21 mmol) according to General procedure D. The residue was purified by flash column chromatography (10 → 40% EtOAc in pentane) yielding the title compound as mixture of two *E/Z* isomers (ratio ~4:3) as yellow-gray gum (35 mg, 0.063 mmol, 37%).

Isomer 1:

<sup>1</sup>H NMR (500 MHz, CDCl<sub>3</sub>) δ 8.88 (s, 1H), 7.39 – 7.33 (m, 2H), 7.33 – 7.28 (m, 2H), 7.21 – 7.15 (m, 2H), 7.15 – 7.07 (m, 2H), 6.50 (s, 1H), 4.80 – 4.55 (m, 1H), 4.64 (s, 2H), 4.32 – 4.15 (m, 1H), 3.29 (td, *J* = 13.3, 3.3 Hz, 1H), 2.75 – 2.60 (m, 1H), 2.50 (td, *J* = 13.5, 4.8 Hz, 1H), 2.45 – 2.38 (m, 2H), 1.19 (d, *J* = 5.7 Hz, 3H).

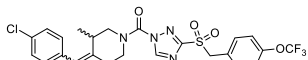
<sup>13</sup>C NMR (126 MHz, CDCl<sub>3</sub>) δ 160.80, 149.98 (q, *J* = 1.4 Hz), 148.36, 147.15, 135.23, 134.04, 132.78, 132.64, 130.02, 128.63, 127.03, 125.10, 121.29, 120.06 (q, *J* = 258.3 Hz), 59.71, 49.95, 42.82, 35.46, 34.26, 16.88.

Isomer 2:

<sup>1</sup>H NMR (500 MHz, CDCl<sub>3</sub>) δ 8.88 (s, 1H), 7.39 – 7.33 (m, 2H), 7.33 – 7.28 (m, 2H), 7.21 – 7.15 (m, 2H), 7.15 – 7.07 (m, 2H), 6.37 (s, 1H), 4.80 – 4.55 (m, 1H), 4.64 (s, 2H), 4.14 – 3.96 (m, 1H), 3.23 – 3.14 (m, 1H), 2.84 – 2.75 (m, 1H), 2.75 – 2.60 (m, 1H), 2.35 – 2.14 (m, 2H), 1.30 (d, *J* = 7.2 Hz, 3H).

<sup>13</sup>C NMR (126 MHz, CDCl<sub>3</sub>) δ 160.80, 149.98 (q, *J* = 1.4 Hz), 148.36, 147.15, 135.27, 133.91, 132.78, 132.66, 130.07, 128.62, 126.83, 125.08, 121.29, 120.06 (q, *J* = 258.3 Hz), 59.71, 50.36, 41.92, 40.63, 29.15, 16.65.

HRMS: [M+Na]<sup>+</sup> calculated for C<sub>24</sub>H<sub>22</sub>ClF<sub>3</sub>N<sub>4</sub>O<sub>4</sub>S+Na<sup>+</sup> 577.08946, found 577.08896.

**(4-(4-Chlorobenzylidene)-3-methylpiperidin-1-yl)(3-((4-(trifluoromethoxy)benzyl)sulfonyl)-1H-1,2,4-triazol-1-yl)methanone (34)**

**116** (80 mg, 0.24 mmol) was reacted with **123** (1.1 eq, 81 mg, 0.26 mmol) according to General procedure D. The residue was purified by flash column chromatography (10 → 50% EtOAc in pentane) yielding a mixture of *E/Z* isomers (ratio ~2:1) of the title compound as colorless oil (79 mg, 0.14 mmol, 60%).

*Analytical data on next page.*

## Isomer 1:

$^1\text{H}$  NMR (400 MHz,  $\text{CDCl}_3$ )  $\delta$  8.91 (s, 1H), 7.38 – 7.33 (m, 2H), 7.33 – 7.28 (m, 2H), 7.20 – 7.14 (m, 2H), 7.13 – 7.06 (m, 2H), 6.37 (s, 1H), 4.65 (s, 2H), 4.01 – 3.90 (m, 1H), 3.78 – 3.67 (m, 1H), 3.63 – 3.46 (m, 1H), 3.38 – 3.28 (m, 1H), 2.84 – 2.69 (m, 1H), 2.66 – 2.58 (m, 1H), 2.40 – 2.24 (m, 1H), 1.32 – 1.18 (m, 3H).

$^{13}\text{C}$  NMR (101 MHz,  $\text{CDCl}_3$ )  $\delta$  160.78, 149.94, 148.42, 147.25, 140.76, 135.41, 132.75, 132.55, 130.26, 128.53, 125.07, 123.14, 121.24, 120.35 (q,  $J = 258.1$  Hz), 59.76, 52.96 (br), 48.26 (br), 37.95 (br), 27.83 (br), 16.32.

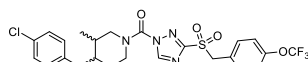
## Isomer 2:

$^1\text{H}$  NMR (400 MHz,  $\text{CDCl}_3$ )  $\delta$  8.91 (s, 1H), 7.38 – 7.33 (m, 2H), 7.33 – 7.28 (m, 2H), 7.20 – 7.14 (m, 2H), 7.13 – 7.06 (m, 2H), 6.29 (s, 1H), 4.65 (s, 2H), 3.90 – 3.80 (m, 1H), 3.78 – 3.67 (m, 1H), 3.63 – 3.46 (m, 1H), 3.44 – 3.37 (m, 1H), 2.84 – 2.69 (m, 1H), 2.59 – 2.50 (m, 1H), 2.51 – 2.41 (m, 1H), 1.13 – 1.03 (m, 3H).

$^{13}\text{C}$  NMR (101 MHz,  $\text{CDCl}_3$ )  $\delta$  160.78, 149.94, 148.42, 147.25, 140.65, 135.15, 132.75, 132.55, 129.82, 128.63, 125.07, 124.33, 121.24, 120.35 (q,  $J = 258.1$  Hz), 59.76, 54.09 (br), 46.94 (br), 38.51 (br), 26.94 (br), 17.11 (br).

HRMS:  $[\text{M}+\text{Na}]^+$  calculated for  $\text{C}_{24}\text{H}_{22}\text{ClF}_3\text{N}_4\text{O}_4\text{S}+\text{Na}^+$  577.08946, found 577.08839.

(4-(4-Chlorobenzyl)-3-methylpiperidin-1-yl)(3-((4-(trifluoromethoxy)benzyl)sulfonyl)-1H-1,2,4-triazol-1-yl)methanone (**35**)



**118** (75 mg, 0.22 mmol) was reacted with **123** (1.1 eq, 75 mg, 0.24 mmol) according to General procedure D. The residue was purified by flash column chromatography (25 → 50% EtOAc in pentane)

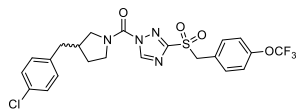
yielding the title compound as colorless oil (88 mg, 0.17 mmol, 71%).

$^1\text{H}$  NMR (400 MHz,  $\text{CDCl}_3$ )  $\delta$  8.87 (s, 1H), 7.38 – 7.29 (m, 2H), 7.31 – 7.22 (m, 2H), 7.20 – 7.13 (m, 2H), 7.12 – 7.02 (m, 2H), 4.64 (s, 2H), 4.35 – 3.95 (m, 2H), 3.16 (s, 2H), 2.62 – 2.42 (m, 2H), 2.06 – 1.70 (m, 2H), 1.66 – 1.48 (m, 2H), 1.04 – 0.73 (m, 3H).

$^{13}\text{C}$  NMR (101 MHz,  $\text{CDCl}_3$ )  $\delta$  160.51, 149.84 (q,  $J = 1.7$  Hz), 148.23, 148.21, 138.22, 132.66, 131.94, 130.22, 128.58, 125.12, 120.30 (q,  $J = 257.9$  Hz), 121.15, 59.66, 53.65 (br), 52.40 (br), 47.64 (br), 46.33 (br), 40.83, 38.10 (br), 31.95 (br), 26.28 (br), 25.28 (br), 11.08 (br).

HRMS:  $[\text{M}+\text{Na}]^+$  calculated for  $\text{C}_{24}\text{H}_{24}\text{ClF}_3\text{N}_4\text{O}_4\text{S}+\text{Na}^+$  579.10511, found 579.10457.

(3-(4-Chlorobenzyl)pyrrolidin-1-yl)(3-((4-(trifluoromethoxy)benzyl)sulfonyl)-1H-1,2,4-triazol-1-yl)methanone (**36**)



**117** (50 mg, 0.16 mmol) was reacted with **123** (1.2 eq, 60 mg, 0.20 mmol) according to General procedure D. The residue was purified by flash column chromatography (30 → 50% EtOAc in pentane) yielding a mixture of two conformationally restricted isomers of the

title compound (ratio ~3:2) as gray gum (31 mg, 0.059 mmol, 36%).

## Conformer 1:

$^1\text{H}$  NMR (500 MHz,  $\text{CDCl}_3$ )  $\delta$  8.98 (s, 1H), 7.36 – 7.31 (m, 2H), 7.31 – 7.22 (m, 2H), 7.20 – 7.13 (m, 2H), 7.13 – 7.06 (m, 2H), 4.63 (s, 2H), 3.85 – 3.78 (m, 1H), 3.81 – 3.70 (m, 1H), 3.64 – 3.55 (m, 1H), 3.35 – 3.28 (m, 1H), 2.73 – 2.69 (m, 2H), 2.53 – 2.39 (m, 1H), 2.09 – 2.02 (m, 1H), 1.73 – 1.57 (m, 1H).

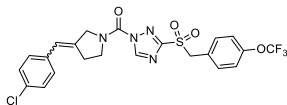
$^{13}\text{C}$  NMR (126 MHz,  $\text{CDCl}_3$ )  $\delta$  161.00, 149.98, 147.70, 145.93 (d,  $J = 2.6$  Hz), 137.85, 132.74, 132.50, 130.07, 128.91, 125.17, 121.30, 120.35 (q,  $J = 257.2$  Hz), 59.70, 53.93, 49.53, 38.71, 38.07, 31.89.

## Conformer 2:

$^1\text{H}$  NMR (500 MHz,  $\text{CDCl}_3$ )  $\delta$  8.97 (s, 1H), 7.36 – 7.31 (m, 2H), 7.31 – 7.22 (m, 2H), 7.20 – 7.13 (m, 2H), 7.13 – 7.06 (m, 2H), 4.63 (s, 2H), 3.93 – 3.86 (m, 2H), 3.81 – 3.70 (m, 1H), 3.55 – 3.48 (m, 1H), 2.79 – 2.66 (m, 1H), 2.61 – 2.53 (m, 1H), 2.53 – 2.39 (m, 1H), 2.02 – 1.95 (m, 1H), 1.73 – 1.57 (m, 1H).

$^{13}\text{C}$  NMR (126 MHz,  $\text{CDCl}_3$ )  $\delta$  161.00, 149.98, 147.64, 145.93 (d,  $J = 2.6$  Hz), 137.90, 132.74, 132.50, 130.07, 128.91, 125.13, 121.30, 120.35 (q,  $J = 257.2$  Hz), 59.70, 54.74, 48.77, 41.61, 38.01, 29.21.

HRMS:  $[\text{M}+\text{Na}]^+$  calculated for  $\text{C}_{22}\text{H}_{20}\text{ClF}_3\text{N}_4\text{O}_4\text{S}+\text{Na}^+$  529.09186, found 529.09164.

**(3-(4-Chlorobenzylidene)pyrrolidin-1-yl)(3-((4-(trifluoromethoxy)benzyl)sulfonyl)-1H-1,2,4-triazol-1-yl)methanone (37)**

**119** (114 mg, 0.37 mmol) was reacted with **123** (1.1 eq, 127 mg, 0.41 mmol) according to General procedure D. The residue was purified by preparative HPLC yielding a mixture of two *E/Z* isomers of the title compound (ratio ~2:1) as white powder (24 mg, 0.046 mmol, 12%).

## Isomer 1:

$^1\text{H}$  NMR (500 MHz,  $\text{CDCl}_3$ )  $\delta$  9.02 (s, 1H), 7.40 – 7.31 (m, 4H), 7.23 – 7.15 (m, 2H), 7.16 – 7.11 (m, 2H), 6.49 (s, 1H), 4.64 (s, 2H), 4.52 – 4.49 (s, 1H), 4.49 – 4.47 (m, 1H), 3.98 – 3.92 (m, 1H), 3.85 – 3.79 (m, 1H), 2.93 – 2.81 (m, 2H).

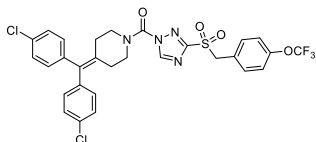
$^{13}\text{C}$  NMR (126 MHz,  $\text{CDCl}_3$ )  $\delta$  161.22, 150.02, 147.81, 145.93, 137.04, 134.58, 133.30, 132.76, 132.69, 129.53, 128.94, 125.11, 123.41, 121.34, 59.72, 54.70, 51.16, 48.08, 47.18, 34.42, 31.58.

## Isomer 2:

$^1\text{H}$  NMR (500 MHz,  $\text{CDCl}_3$ )  $\delta$  9.03 (s, 1H), 7.40 – 7.31 (m, 4H), 7.23 – 7.15 (m, 2H), 7.11 – 7.06 (m, 2H), 6.45 (s, 1H), 4.72 – 4.69 (m, 1H), 4.64 (s, 2H), 4.62 – 4.60 (m, 1H), 4.05 – 4.00 (m, 1H), 3.92 – 3.87 (m, 1H), 2.93 – 2.81 (m, 2H).

$^{13}\text{C}$  NMR (126 MHz,  $\text{CDCl}_3$ )  $\delta$  161.22, 150.02, 147.81, 145.93, 136.88 (br), 134.79 (br), 133.17 (br), 132.69, 129.73, 129.70, 128.84, 128.80, 125.14, 123.07, 121.34, 59.84, 55.10, 52.28, 49.71, 49.10, 29.88, 27.50.

HRMS:  $[\text{M}+\text{Na}]^+$  calculated for  $\text{C}_{22}\text{H}_{18}\text{ClF}_3\text{N}_4\text{O}_4\text{S}+\text{Na}^+$  527.07621, found 527.07611.

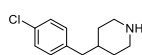
**(4-(Bis(4-chlorophenyl)methylene)piperidin-1-yl)(3-((4-(trifluoromethoxy)benzyl)sulfonyl)-1H-1,2,4-triazol-1-yl)methanone (38)**

**122** (81 mg, 0.19 mmol) was reacted with **123** (1.1 eq, 63 mg, 0.21 mmol) according to General procedure D. The residue was purified by flash column chromatography (10 → 40% EtOAc in pentane) yielding the title compound as white crystalline solid (84 mg, 0.13 mmol, 69%).

$^1\text{H}$  NMR (400 MHz,  $\text{CDCl}_3$ )  $\delta$  8.90 (s, 1H), 7.33 (d,  $J = 8.1$  Hz, 2H), 7.29 (d,  $J = 8.0$  Hz, 4H), 7.14 (d,  $J = 7.7$  Hz, 2H), 7.02 (d,  $J = 6.5$  Hz, 4H), 4.63 (s, 2H), 3.72 – 3.67 (m, 4H), 2.58 – 2.31 (m, 4H).

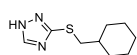
$^{13}\text{C}$  NMR (101 MHz,  $\text{CDCl}_3$ )  $\delta$  160.77, 149.89 (q,  $J = 1.6$  Hz), 148.39, 147.02, 139.45, 136.82, 133.17, 132.87, 132.72, 130.88, 128.66, 125.07, 121.24, 120.22 (q,  $J = 257.1$  Hz), 59.70, 48.26 (br), 46.83 (br), 31.37 (br), 30.83 (br).

HRMS:  $[\text{M}+\text{Na}]^+$  calculated for  $\text{C}_{29}\text{H}_{23}\text{Cl}_2\text{F}_3\text{N}_4\text{O}_4\text{S}+\text{Na}^+$  651.08419, found 651.08416.

**4-(4-Chlorobenzyl)piperidine (39)**

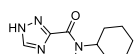
4-(4-Chlorobenzyl)pyridine (**124**, 1 eq, 1.71 mL, 9.82 mmol), PtO<sub>2</sub> (4 mol%, 89 mg, 0.39 mmol) and hydrochloric acid (1 eq, 818 μL 12 M, 9.82 mmol) were added to EtOH (30 mL) and shaken for 24 h under 3 bar H<sub>2</sub> in a Parr reaction vessel. Catalyst was removed by filtration and volatiles under reduced pressure. Flash column chromatography (5 → 15% 7M methanolic ammonia in EtOAc) afforded the title compound as yellow oil (1.79 g, 8.53 mmol, 87%)  
<sup>1</sup>H NMR (400 MHz, CDCl<sub>3</sub>) δ 7.27 – 7.19 (m, 2H), 7.10 – 7.02 (m, 2H), 3.03 (dt, *J* = 12.6, 3.0 Hz, 2H), 2.54 (td, *J* = 12.3, 2.1 Hz, 2H), 2.49 (d, *J* = 6.5 Hz, 2H), 1.66 (bs, 1H), 1.64 – 1.55 (m, 2H), 1.58 – 1.51 (m, 1H), 1.13 (qd, *J* = 13.8, 13.3, 3.8 Hz, 2H).

<sup>13</sup>C NMR (101 MHz, CDCl<sub>3</sub>) δ 139.09, 131.58, 130.55, 128.31, 46.80, 43.22, 38.48, 33.44.

**3-((Cyclohexylmethyl)thio)-1H-1,2,4-triazole (40)**

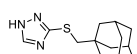
1H-1,2,4-Triazole-3-thiol (**76**, 2.00 g, 19.8 mmol) was dissolved in 70 mL dry DMF and (bromomethyl)cyclohexane (1 eq, 2.76 mL, 19.8 mmol) was added slowly. K<sub>2</sub>CO<sub>3</sub> (0.73 eq, 2.00 g, 14.4 mmol) was added and the mixture was stirred for 6 h, during which it turned light purple and finally white and cloudy. The mixture was diluted with EtOAc and washed with water. The aqueous layer was extracted with EtOAc, after which the combined organic layers were washed with brine, dried over MgSO<sub>4</sub>, filtrated and concentrated *in vacuo*. Flash column chromatography (20 → 40% EtOAc in pentane) afforded the title compound as white crystalline solid (3.43 g, 17.4 mmol, 88%).  
<sup>1</sup>H NMR (400 MHz, CDCl<sub>3</sub>) δ 13.13 (bs, 1H), 8.20 (s, 1H), 3.08 (d, *J* = 7.0 Hz, 2H), 1.91 – 1.80 (m, 2H), 1.76 – 1.61 (m, 3H), 1.69 – 1.52 (m, 1H), 1.31 – 1.05 (m, 3H), 0.98 (qd, *J* = 11.7, 3.4 Hz, 2H).

<sup>13</sup>C NMR (101 MHz, CDCl<sub>3</sub>) δ 157.29, 147.61, 39.96, 37.84, 32.49, 26.22, 25.95.

**N-cyclohexyl-N-methyl-1H-1,2,4-triazole-3-carboxamide (41)**

To a solution of 1H-1,2,4-triazole-3-carboxylic acid (**77**, 1 eq, 100 mg, 0.88 mmol) in dry THF (10 mL) with a few drops of DMF, SOCl<sub>2</sub> (78 eq, 5.0 mL, 68.5 mmol) was added and the mixture was refluxed for 14 h. All volatiles were removed *in vacuo*, after which the residual lime green oil was dissolved in dry DCM (5 mL) and added dropwise to an ice-cold solution of N-methylcyclohexanamine (**78**, 13 eq, 1.5 mL, 11.5 mmol) in dry DCM (5 mL). The mixture was allowed to warm to RT and stirred overnight. Because TLC showed little reaction progress DIPEA (2 eq, 300 μL, 1.72 mmol) was added and stirring was continued for 110 h. All volatiles were removed *in vacuo*. Flash column chromatography of the residue (40 → 70% EtOAc in petroleum ether) afforded the title compound as white solid (129 mg, 0.62 mmol, 70%).

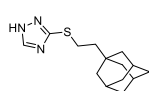
LC-MS: [M+H]<sup>+</sup> calculated for C<sub>10</sub>H<sub>16</sub>N<sub>4</sub>O+H<sup>+</sup> 209.14, found 209.07. RT = 7.78 min (0 → 50% CH<sub>3</sub>CN in H<sub>2</sub>O)

**3-(((Adamant-1-yl)methyl)thio)-1H-1,2,4-triazole (42)**

**88** (405 mg, 1.12 mmol) was treated according to General procedure G to obtain the title compound as a white solid (89 mg, 0.36 mmol, 65%).

<sup>1</sup>H NMR (400 MHz, CDCl<sub>3</sub>) δ 10.80 (bs, 1H), 8.15 (s, 1H), 3.08 (s, 1H), 2.01 – 1.95 (m, 4H), 1.74 – 1.53 (m, 11H).

<sup>13</sup>C NMR (101 MHz, CDCl<sub>3</sub>) δ 157.87, 148.01, 46.99, 41.54, 36.78, 33.89, 28.51.

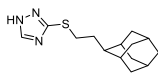
**3-((2-(Adamant-1-yl)ethyl)thio)-1H-1,2,4-triazole (43)**

**89** (462 mg, 1.18 mmol) was treated according to General procedure G to obtain the title compound as a white solid (100 mg, 0.380 mmol, 64%).

$^1\text{H}$  NMR (400 MHz,  $\text{CDCl}_3$ )  $\delta$  11.68 (bs, 1H), 8.12 (s, 1H), 3.19 – 3.10 (m, 2H), 1.96 (p,  $J$  = 3.1 Hz, 3H), 1.75 – 1.57 (m, 6H), 1.54 – 1.44 (m, 8H).

$^{13}\text{C}$  NMR (101 MHz,  $\text{CDCl}_3$ )  $\delta$  44.08, 42.22, 37.15, 33.06, 28.70, 27.47.

### 3-((2-(Adamant-2-yl)ethyl)thio)-1H-1,2,4-triazole (44)

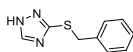


**90** (393 mg, 1.01 mmol) was treated according to General procedure G to obtain the title compound as a white solid (220 mg, 0.835 mmol, 83%).

$^1\text{H}$  NMR (500 MHz,  $\text{CDCl}_3$ )  $\delta$  8.15 (s, 1H), 3.21 – 3.14 (m, 2H), 1.90 – 1.75 (m, 9H), 1.75 – 1.68 (m, 6H), 1.54 – 1.47 (m, 2H).

$^{13}\text{C}$  NMR (126 MHz,  $\text{CDCl}_3$ )  $\delta$  157.19, 148.10, 43.73, 39.16, 38.40, 32.62, 31.76, 31.72, 31.42, 28.30, 28.09, 0.13.

### 3-(Benzylthio)-1H-1,2,4-triazole (45)

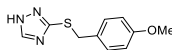


1,2,4-Triazole-3-thiol (**76**, 1.05 eq, 500 mg, 4.94 mmol) was benzylated with benzyl bromide (1 eq, 560  $\mu\text{L}$ , 4.70 mmol) according to General procedure F. Flash column chromatography (40  $\rightarrow$  70% EtOAc in pentane) afforded the title compound as white crystalline solid (669 mg, 3.50 mmol, 74%).

$^1\text{H}$  NMR (500 MHz,  $\text{CDCl}_3$ )  $\delta$  13.49 (bs, 1H), 8.09 (s, 1H), 7.31 – 7.26 (m, 2H), 7.26 – 7.17 (m, 3H), 4.33 (s, 2H).

$^{13}\text{C}$  NMR (126 MHz,  $\text{CDCl}_3$ )  $\delta$  136.82, 128.92, 128.73, 127.72, 37.48.

### 3-((4-Methoxybenzyl)thio)-1H-1,2,4-triazole (46)

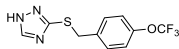


1H-1,2,4-Triazole-3-thiol (**76**, 1.4 eq, 106 mg, 1.05 mmol) was benzylated with 4-methoxybenzyl chloride (1 eq, 105  $\mu\text{L}$ , 0.77 mmol) according to General procedure F. Flash column chromatography afforded the title compound (116 mg, 0.52 mmol, 64%).

$^1\text{H}$  NMR (400 MHz,  $\text{CDCl}_3$ )  $\delta$  10.95 (bs, 1H), 8.12 (s, 1H), 7.26 – 7.17 (m, 2H), 6.82 – 6.74 (m, 2H), 4.30 (s, 2H), 3.74 (s, 3H).

$^{13}\text{C}$  NMR (101 MHz,  $\text{CDCl}_3$ )  $\delta$  159.10, 156.43, 147.53, 130.16, 128.71, 114.11, 55.35, 37.06.

### 3-((4-(Trifluoromethoxy)benzyl)thio)-1H-1,2,4-triazole (47)

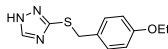


1H-1,2,4-Triazole-3-thiol (**76**, 1.05 eq, 400 mg, 3.96 mmol) was benzylated with 4-(trifluoromethoxy)benzyl bromide (1 eq, 958 mg, 3.76 mmol) according to General procedure F. This afforded the title compound (433 mg, 1.57 mmol, 40%), which was used without further purification.

$^1\text{H}$  NMR (400 MHz,  $\text{CDCl}_3$ )  $\delta$  10.31 (bs, 1H), 8.16 (s, 1H), 7.41 – 7.33 (m, 2H), 7.15 – 7.07 (m, 2H), 4.36 (s, 2H).

$^{13}\text{C}$  NMR (101 MHz,  $\text{CDCl}_3$ )  $\delta$  148.66 (q,  $J$  = 2.1 Hz), 135.93, 130.42, 121.18, 120.53 (q,  $J$  = 257.3 Hz), 36.32.

### 3-((4-Ethoxybenzyl)thio)-1H-1,2,4-triazole (48)

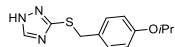


1H-1,2,4-Triazole-3-thiol (**76**, 1 eq, 500 mg, 4.94 mmol) was reacted with **126** (1 eq, 844 mg, 4.94 mmol) according to General procedure F. This afforded the title compound (783 mg, 3.33 mmol, 67%), which was used without further purification.

$^1\text{H}$  NMR (400 MHz,  $\text{CDCl}_3$ )  $\delta$  8.69 (bs, 1H), 8.14 (s, 1H), 7.28 – 7.20 (m, 2H), 6.86 – 6.75 (m, 2H), 4.32 (s, 2H), 3.99 (q,  $J$  = 7.0 Hz, 2H), 1.39 (t,  $J$  = 7.0 Hz, 3H).

$^{13}\text{C}$  NMR (101 MHz,  $\text{CDCl}_3$ )  $\delta$  158.62, 130.19, 128.58, 114.76, 63.60, 37.07, 14.95.



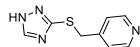
**3-((4-Isopropoxybenzyl)thio)-1H-1,2,4-triazole (49)**

1H-1,2,4-Triazole-3-thiol (**76**, 1 eq, 400 mg, 3.96 mmol) was reacted with **130** (1 eq, 730 mg, 3.96 mmol) according to General procedure F. This afforded the title compound (348 mg, 1.40 mmol, 35%), which was used without further

purification.

$^1\text{H}$  NMR (400 MHz,  $\text{CDCl}_3$ )  $\delta$  8.11 (s, 1H), 7.25 – 7.17 (m, 2H), 6.82 – 6.74 (m, 2H), 4.49 (hept,  $J$  = 6.1 Hz, 1H), 4.31 (s, 2H), 1.30 (d,  $J$  = 6.1 Hz, 6H).

$^{13}\text{C}$  NMR (101 MHz,  $\text{CDCl}_3$ )  $\delta$  157.48, 130.20, 128.48, 116.03, 70.05, 37.07, 22.12.

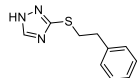
**4-(((1H-1,2,4-triazol-3-yl)thio)methyl)pyridine (50)**

1H-1,2,4-Triazole-3-thiol (**76**, 1 eq, 500 mg, 4.94 mmol) was reacted with 4-

(bromomethyl)pyridine hydrobromide (1 eq, 1.25 g, 4.94 mmol) according to General procedure F. This afforded the title compound (630 mg, 3.28 mmol, 66%), which was used without further purification.

$^1\text{H}$  NMR (400 MHz,  $\text{CDCl}_3$ )  $\delta$  12.93 (bs, 1H), 8.49 – 8.43 (m, 2H), 8.16 (s, 1H), 7.34 – 7.29 (m, 2H), 4.31 (s, 2H).

$^{13}\text{C}$  NMR (101 MHz,  $\text{CDCl}_3$ )  $\delta$  149.24, 147.92, 124.27, 35.76.

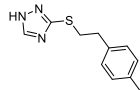
**3-(Phenethylthio)-1H-1,2,4-triazole (51)**

1H-1,2,4-Triazole-3-thiol (**76**, 1.05 eq, 100 mg, 0.99 mmol) was reacted with phenethyl bromide (1 eq, 128  $\mu\text{L}$ , 0.94 mmol) according to General procedure F. Flash column chromatography (30  $\rightarrow$  70% EtOAc in pentane) afforded the title compound

(126 mg, 0.61 mmol, 65%).

$^1\text{H}$  NMR (400 MHz,  $\text{CDCl}_3$ )  $\delta$  11.44 (bs, 1H), 8.17 (s, 1H), 7.31 – 7.23 (m, 2H), 7.23 – 7.14 (m, 3H), 3.43 – 3.33 (m, 2H), 3.05 – 2.96 (m, 2H).

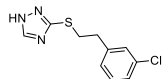
$^{13}\text{C}$  NMR (101 MHz,  $\text{CDCl}_3$ )  $\delta$  156.86, 147.12, 139.66, 128.67, 128.55, 126.61, 35.98, 34.00.

**3-((4-Methylphenethyl)thio)-1H-1,2,4-triazole (52)**

1H-1,2,4-Triazole-3-thiol (**76**, 1.05 eq, 100 mg, 0.99 mmol) was reacted with 4-methylphenethyl bromide (1 eq, 143  $\mu\text{L}$ , 0.94 mmol) according to General procedure F. Flash column chromatography (30  $\rightarrow$  70% EtOAc in pentane) afforded the title compound (181 mg, 0.83 mmol, 88%).

$^1\text{H}$  NMR (400 MHz,  $\text{CDCl}_3$ )  $\delta$  12.35 (bs, 1H), 8.18 (s, 1H), 7.08 – 7.01 (m, 4H), 3.39 – 3.31 (m, 2H), 2.97 – 2.90 (m, 2H), 2.27 (s, 3H).

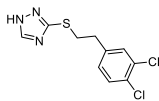
$^{13}\text{C}$  NMR (101 MHz,  $\text{CDCl}_3$ )  $\delta$  156.82, 146.96, 136.43, 136.05, 129.15, 128.41, 35.42, 34.11, 20.99.

**3-((3-Chlorophenethyl)thio)-1H-1,2,4-triazole (53)**

1H-1,2,4-Triazole-3-thiol (**76**, 1.05 eq, 100 mg, 0.99 mmol) was reacted with 3-chlorophenethyl bromide (1 eq, 138  $\mu\text{L}$ , 0.94 mmol) according to General procedure F. Flash column chromatography (30  $\rightarrow$  70% EtOAc in pentane) afforded the title compound (131 mg, 0.55 mmol, 58%).

$^1\text{H}$  NMR (400 MHz,  $\text{CDCl}_3$ )  $\delta$  12.34 (bs, 1H), 8.23 (s, 1H), 7.22 – 7.13 (m, 3H), 7.11 – 7.02 (m, 1H), 3.42 – 3.31 (m, 2H), 3.04 – 2.93 (m, 2H).

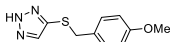
$^{13}\text{C}$  NMR (101 MHz,  $\text{CDCl}_3$ )  $\delta$  157.00, 147.03, 141.60, 134.25, 129.85, 128.81, 126.92, 126.86, 35.68, 33.65.

**3-((3,4-Dichlorophenethyl)thio)-1H-1,2,4-triazole (54)**

1H-1,2,4-Triazole-3-thiol (**76**, 1.05 eq, 100 mg, 0.99 mmol) was reacted with **132** (1 eq, 197 mg, 0.94 mmol) according to General procedure F. Flash column chromatography (30 → 50% EtOAc in pentane) afforded the title compound (160 mg, 0.58 mmol, 62%).

<sup>1</sup>H NMR (400 MHz, CDCl<sub>3</sub>) δ 8.19 (s, 1H), 7.34 (d, *J* = 8.2 Hz, 1H), 7.31 (d, *J* = 2.0 Hz, 1H), 7.05 (dd, *J* = 8.2, 2.1 Hz, 1H), 3.45 – 3.31 (m, 2H), 3.08 – 2.91 (m, 2H).

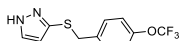
<sup>13</sup>C NMR (101 MHz, CDCl<sub>3</sub>) δ 147.26, 139.93, 132.50, 130.78, 130.75, 130.54, 128.30, 35.28, 33.45.

**4-((4-Methoxybenzyl)thio)-2H-1,2,3-triazole (55)**

Sodium 2H-1,2,3-triazole-4-thiolate (1.05 eq, 100 mg, 0.81 mmol) was benzylated with 4-methoxybenzyl chloride (1 eq, 105 μL, 0.77 mmol) according to General procedure F, with the exception that no base was added. Flash column chromatography (5 → 40% EtOAc in pentane) afforded the title compound (111 mg, 0.50 mmol, 65%).

<sup>1</sup>H NMR (400 MHz, CDCl<sub>3</sub>) δ 10.89 (bs, 1H), 7.48 (s, 1H), 7.19 – 7.08 (m, 2H), 6.83 – 6.74 (m, 2H), 4.06 (s, 2H), 3.75 (s, 3H).

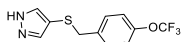
<sup>13</sup>C NMR (101 MHz, CDCl<sub>3</sub>) δ 158.91, 139.43, 133.59, 130.11, 129.22, 113.99, 55.29, 39.00.

**3-((4-(Trifluoromethoxy)benzyl)thio)-1H-pyrazole (56)**

3-Aminopyrazole (**133**, 1.25 eq, 200 mg, 2.41 mmol) was dissolved in 40% H<sub>2</sub>SO<sub>4</sub> in water (10 mL) and cooled on ice. NaNO<sub>2</sub> (1.2 eq, 200 mg, 2.89 mmol) dissolved in water (10 mL) was added dropwise over the course of 15 min. After stirring for 35 min the pH of the yellow mixture was adjusted to 5 with sat. aq. NaOAc. This mixture was then added dropwise to an ice-cold stirring solution of 4-trifluoromethoxybenzyl mercaptan (**91**, 1 eq, 308 μL, 1.93 mmol) in 1 M aq. NaOH (2 mL) over the course of 35 min. Immediately precipitate formed and the mixture turned orange. The mixture was stirred on ice for 1 h. Water and EtOAc were added and the layers were separated. The aqueous layer was extracted with EtOAc until the organic layer remained colorless. The combined organic layers were washed with brine, dried over MgSO<sub>4</sub>, filtrated and concentrated *in vacuo*. Flash column chromatography (10 → 40% EtOAc in pentane) afforded the title compound as yellow oil (131 mg, 0.48 mmol, 25%).

<sup>1</sup>H NMR (400 MHz, CDCl<sub>3</sub>) δ 10.42 (bs, 1H), 7.53 (d, *J* = 2.2 Hz, 1H), 7.28 – 7.19 (m, 2H), 7.08 (d, *J* = 7.9 Hz, 2H), 6.22 (d, *J* = 2.2 Hz, 1H), 4.04 (s, 2H).

<sup>13</sup>C NMR (101 MHz, CDCl<sub>3</sub>) δ 148.44 (q, *J* = 1.9 Hz), 141.51, 136.79, 132.65, 130.29, 121.05, 120.54 (q, *J* = 257.1 Hz), 109.35, 39.23.

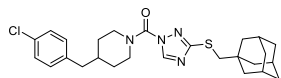
**4-((4-(Trifluoromethoxy)benzyl)thio)-1H-pyrazole (57)**

**135** (1.25 eq, 200 mg, 2.41 mmol) was dissolved in 40% H<sub>2</sub>SO<sub>4</sub> in water (10 mL) and cooled on ice. NaNO<sub>2</sub> (1.2 eq, 200 mg, 2.89 mmol) dissolved in water (10 mL) was added dropwise over the course of 10 min. After stirring for 30 min the pH of the yellow mixture was adjusted to 5 with sat. aq. NaOAc. This mixture was then added dropwise to an ice-cold stirring solution of 4-trifluoromethylbenzyl mercaptan (**91**, 1 eq, 308 μL, 1.93 mmol) in 1 M aq. NaOH (2 mL) over the course of 30 min. Immediately precipitate formed and the mixture turned orange. The mixture was stirred on ice for 1 h. Water and EtOAc were added and the layers were separated. The aqueous layer was extracted with EtOAc until the organic layer remained colorless. The combined organic layers were washed with brine, dried over MgSO<sub>4</sub>, filtrated and concentrated *in vacuo*. Flash column chromatography (15 → 40% EtOAc in pentane) afforded the title compound as yellowish crystalline solid (49 mg, 0.18 mmol, 9%). *Analytical data on next page.*

$^1\text{H}$  NMR (400 MHz,  $\text{CDCl}_3$ )  $\delta$  9.49 (bs, 1H), 7.42 – 7.36 (m, 2H), 7.20 – 7.07 (m, 4H), 3.78 (s, 2H).

$^{13}\text{C}$  NMR (101 MHz,  $\text{CDCl}_3$ )  $\delta$  148.35 (q,  $J = 2.0$  Hz), 138.40, 137.28, 130.44, 120.98, 120.56 (q,  $J = 257.1$  Hz), 41.27.

**(3-(((Adamant-1-yl)methyl)thio)-1H-1,2,4-triazol-1-yl)(4-(4-chlorobenzyl)piperidin-1-yl)-methanone (59)**

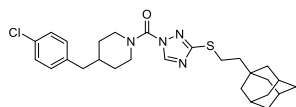


**39** (1.1 eq, 92 mg, 0.44 mmol) and **42** (1 eq, 99 mg, 0.40 mmol) were coupled according to General procedure D to obtain the title compound as a white solid (120 mg, 0.247 mmol, 62%).

$^1\text{H}$  NMR (500 MHz,  $\text{CDCl}_3$ )  $\delta$  8.65 (s, 1H), 7.29 – 7.23 (m, 2H), 7.11 – 7.04 (m, 2H), 4.71 – 4.31 (m, 2H), 3.03 (s, 2H), 2.99 – 2.90 (m, 2H), 2.56 (d,  $J = 7.1$  Hz, 2H), 1.98 (p,  $J = 3.1$  Hz, 3H), 1.88 – 1.76 (m, 1H), 1.76 – 1.54 (m, 14H), 1.36 (qd,  $J = 12.5, 4.2$  Hz, 2H).

$^{13}\text{C}$  NMR (126 MHz,  $\text{CDCl}_3$ )  $\delta$  163.92, 148.42, 138.24, 132.10, 130.49, 128.62, 45.71, 42.29, 41.62, 38.09, 36.85, 33.93, 32.01, 28.56.

**(3-((2-(Adamant-1-yl)ethyl)thio)-1H-1,2,4-triazol-1-yl)(4-(4-chlorobenzyl)piperidin-1-yl)-methanone (60)**

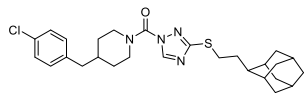


**39** (1.2 eq, 44 mg, 0.21 mmol) and **43** (1 eq, 46 mg, 0.18 mmol) were coupled according to General procedure D to obtain the title compound as a white solid (57 mg, 0.11 mmol, 65%).

$^1\text{H}$  NMR (500 MHz,  $\text{CDCl}_3$ )  $\delta$  8.68 (s, 1H), 7.29 – 7.22 (m, 2H), 7.10 – 7.04 (m, 2H), 4.91 – 4.28 (m, 2H), 3.13 – 3.06 (m, 2H), 3.01 – 2.89 (m, 2H), 2.55 (d,  $J = 7.1$  Hz, 2H), 1.96 (p,  $J = 3.2$  Hz, 3H), 1.86 – 1.68 (m, 6H), 1.66 – 1.58 (m, 3H), 1.55 – 1.48 (m, 8H), 1.36 (qd,  $J = 12.9, 4.2$  Hz, 2H).

$^{13}\text{C}$  NMR (126 MHz,  $\text{CDCl}_3$ )  $\delta$  163.11, 148.36, 138.21, 132.09, 130.42, 128.70, 128.60, 44.27, 44.16, 42.28, 42.25, 38.03, 37.16, 33.02, 32.00, 28.70, 26.22.

**(3-((2-(Adamant-2-yl)ethyl)thio)-1H-1,2,4-triazol-1-yl)(4-(4-chlorobenzyl)piperidin-1-yl)-methanone (61)**



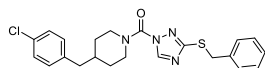
**39** (1.2 eq, 44 mg, 0.21 mmol) and **44** (1 eq, 46 mg, 0.18 mmol) were coupled according to General procedure D to obtain the title compound as a white solid (64 mg, 0.13 mmol, 73%).

*Analytical data on next page.*

$^1\text{H}$  NMR (500 MHz,  $\text{CDCl}_3$ )  $\delta$  8.68 (s, 1H), 7.28 – 7.23 (m, 2H), 7.10 – 7.05 (m, 2H), 4.85 – 4.14 (m, 2H), 3.15 – 3.07 (m, 2H), 2.99 – 2.90 (m, 2H), 2.55 (d,  $J = 7.2$  Hz, 2H), 1.92 – 1.65 (m, 18H), 1.54 – 1.48 (m, 2H), 1.34 (qd,  $J = 12.5, 4.2$  Hz, 2H).

$^{13}\text{C}$  NMR (126 MHz,  $\text{CDCl}_3$ )  $\delta$  163.05, 148.32, 138.18, 132.03, 130.41, 128.55, 43.90, 42.18, 39.13, 38.35, 37.97, 32.72, 31.91, 31.73, 30.26, 28.26, 28.04.

**(3-(Benzylthio)-1H-1,2,4-triazol-1-yl)(4-(4-chlorobenzyl)piperidin-1-yl)methanone (62)**

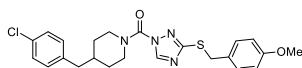


**39** (1 eq, 600 mg, 2.86 mmol) was reacted with **45** (1.1 eq, 602 mg, 3.15 mmol) according to General procedure D. Flash column chromatography (10 → 40% EtOAc in pentane) yielded the title compound as slightly yellowish oil (915 mg, 2.14 mmol, 75%).

$^1\text{H}$  NMR (400 MHz,  $\text{CDCl}_3$ )  $\delta$  8.68 (s, 1H), 7.42 – 7.34 (m, 2H), 7.33 – 7.18 (m, 5H), 7.09 – 7.02 (m, 2H), 4.57 – 4.30 (m, 2H), 4.35 (s, 2H), 2.94 – 2.83 (m, 2H), 2.52 (d,  $J = 7.1$  Hz, 2H), 1.84 – 1.72 (m, 1H), 1.72 – 1.60 (m, 2H), 1.28 (qd,  $J = 13.7, 13.2, 4.2$  Hz, 2H).

$^{13}\text{C}$  NMR (101 MHz,  $\text{CDCl}_3$ )  $\delta$  162.17, 148.11, 147.39, 138.12, 136.94, 131.89, 130.38, 128.79, 128.50, 128.45, 127.42, 42.06, 37.82, 35.96, 31.79 (br).

**(4-(4-Chlorobenzyl)piperidin-1-yl)(3-((4-methoxybenzyl)thio)-1H-1,2,4-triazol-1-yl)methanone (63)**

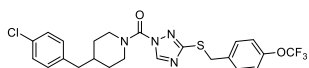


42%).

$^1\text{H}$  NMR (400 MHz,  $\text{CDCl}_3$ )  $\delta$  8.68 (s, 1H), 7.36 – 7.26 (m, 2H), 7.29 – 7.22 (m, 2H), 7.12 – 7.02 (m, 2H), 6.85 – 6.77 (m, 2H), 4.61 – 4.36 (m, 2H), 4.31 (s, 2H), 3.75 (s, 3H), 3.02 – 2.78 (m, 2H), 2.54 (d,  $J = 7.1$  Hz, 2H), 1.86 – 1.74 (m, 1H), 1.70 (m, 2H), 1.31 (qd,  $J = 12.7, 3.9$  Hz, 2H).

$^{13}\text{C}$  NMR (101 MHz,  $\text{CDCl}_3$ )  $\delta$  162.35, 158.98, 148.23, 147.41, 138.17, 131.97, 130.43, 130.06, 128.87, 128.54, 113.95, 55.30, 47.23 (br), 42.15, 37.93, 35.59, 31.93 (br).

**(4-(4-Chlorobenzyl)piperidin-1-yl)(3-((4-(trifluoromethoxy)benzyl)thio)-1H-1,2,4-triazol-1-yl)methanone (64)**

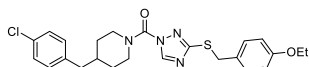


60%).

$^1\text{H}$  NMR (400 MHz,  $\text{CDCl}_3$ )  $\delta$  8.69 (s, 1H), 7.46 – 7.39 (m, 2H), 7.30 – 7.22 (m, 2H), 7.16 – 7.10 (m, 2H), 7.10 – 7.03 (m, 2H), 4.47 – 4.42 (m, 2H), 4.35 (s, 2H), 2.98 – 2.85 (m, 2H), 2.54 (d,  $J = 7.1$  Hz, 2H), 1.86 – 1.74 (m, 1H), 1.74 – 1.66 (m, 2H), 1.29 (qd,  $J = 12.8, 3.5$  Hz, 2H).

$^{13}\text{C}$  NMR (101 MHz,  $\text{CDCl}_3$ )  $\delta$  161.90, 148.56 (q,  $J = 1.8$  Hz), 148.22, 147.61, 138.16, 136.06, 132.14, 130.47, 130.32, 128.64, 121.13, 120.54 (q,  $J = 257.2$  Hz), 42.21, 38.01, 35.23, 31.94 (br).

**(4-(4-Chlorobenzyl)piperidin-1-yl)(3-((4-ethoxybenzyl)thio)-1H-1,2,4-triazol-1-yl)methanone (65)**

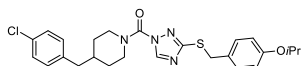


77%).

$^1\text{H}$  NMR (400 MHz,  $\text{CDCl}_3$ )  $\delta$  8.68 (s, 1H), 7.33 – 7.21 (m, 4H), 7.10 – 7.04 (m, 2H), 6.84 – 6.77 (m, 2H), 4.60 – 4.35 (m, 2H), 4.31 (s, 2H), 3.98 (q,  $J = 7.0$  Hz, 2H), 2.97 – 2.86 (m, 2H), 2.54 (d,  $J = 7.0$  Hz, 2H), 1.85 – 1.75 (m, 1H), 1.75 – 1.65 (m, 2H), 1.39 (t,  $J = 7.0$  Hz, 3H), 1.31 (qd,  $J = 12.5, 4.1$  Hz, 2H).

$^{13}\text{C}$  NMR (101 MHz,  $\text{CDCl}_3$ )  $\delta$  162.46, 158.41, 148.30, 147.46, 138.20, 132.04, 130.46, 130.09, 128.73, 128.59, 114.55, 63.53, 47.25 (br), 42.21, 37.99, 35.67, 31.93 (br), 14.92.

**(4-(4-Chlorobenzyl)piperidin-1-yl)(3-((4-isopropoxybenzyl)thio)-1H-1,2,4-triazol-1-yl)methanone (66)**



91%).

Analytical data on next page.

**39** (1 eq, 95 mg, 0.45 mmol) was reacted with **46** (1 eq, 100 mg, 0.45 mmol) according to General procedure D. Flash column chromatography yielded the title compound (86 mg, 0.19 mmol,

**39** (1.1 eq, 126 mg, 0.60 mmol) was reacted with **47** (1 eq, 150 mg, 0.55 mmol) according to General procedure D. Flash column chromatography yielded the title compound (167 mg, 0.33 mmol,

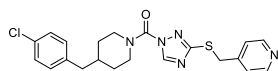
**39** (1.1 eq, 294 mg, 1.40 mmol) was reacted with **48** (1 eq, 300 mg, 1.28 mmol) according to General procedure D. Flash column chromatography yielded the title compound (465 mg, 0.99 mmol,

**39** (1.1 eq, 139 mg, 0.66 mmol) was reacted with **49** (1 eq, 150 mg, 0.60 mmol) according to General procedure D. Flash column chromatography yielded the title compound (267 mg, 0.55 mmol,

$^1\text{H}$  NMR (400 MHz,  $\text{CDCl}_3$ )  $\delta$  8.68 (s, 1H), 7.33 – 7.21 (m, 4H), 7.11 – 7.03 (m, 2H), 6.83 – 6.76 (m, 2H), 4.60 – 4.37 (m, 2H), 4.49 (hept,  $J = 6.1$  Hz, 1H), 4.31 (s, 2H), 2.97 – 2.86 (m, 2H), 2.54 (d,  $J = 7.0$  Hz, 2H), 2.17 (s, 2H), 1.85 – 1.76 (m, 1H), 1.76 – 1.67 (m, 2H), 1.38 – 1.24 (m, 2H), 1.31 (d,  $J = 6.1$  Hz, 6H).

$^{13}\text{C}$  NMR (101 MHz,  $\text{CDCl}_3$ )  $\delta$  162.49, 157.37, 148.31, 147.46, 138.20, 132.05, 130.47, 130.12, 128.63, 128.59, 115.88, 69.95, 42.21, 38.01, 35.67, 31.93 (br), 22.12.

**(4-(4-Chlorobenzyl)piperidin-1-yl)(3-((pyridin-4-ylmethyl)thio)-1H-1,2,4-triazol-1-yl)-methanone (67)**



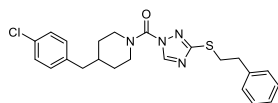
**39** (1.1 eq, 240 mg, 1.14 mmol) was reacted with **50** (1 eq, 200 mg, 1.04 mmol) according to General procedure D. Flash column chromatography yielded the title compound (320 mg, 0.75 mmol,

72%).

$^1\text{H}$  NMR (400 MHz,  $\text{CDCl}_3$ )  $\delta$  8.68 (s, 1H), 8.55 – 8.49 (m, 2H), 7.37 – 7.31 (m, 2H), 7.31 – 7.23 (m, 2H), 7.11 – 7.03 (m, 2H), 4.45 – 4.37 (m, 2H), 4.31 (s, 2H), 2.94 – 2.83 (m, 2H), 2.54 (d,  $J = 7.1$  Hz, 2H), 1.84 – 1.71 (m, 1H), 1.74 – 1.65 (m, 2H), 1.31 – 1.23 (m, 2H).

$^{13}\text{C}$  NMR (101 MHz,  $\text{CDCl}_3$ )  $\delta$  161.37, 149.96, 148.07, 147.65, 146.62, 138.12, 132.10, 130.46, 128.62, 123.78, 46.63 (br), 42.17, 37.94, 34.72, 31.89 (br).

**(4-(4-Chlorobenzyl)piperidin-1-yl)(3-(phenethylthio)-1H-1,2,4-triazol-1-yl)methanone (68)**

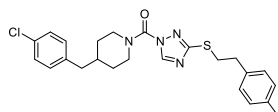


**39** (1 eq, 102 mg, 0.49 mmol) was reacted with **51** (1 eq, 100 mg, 0.49 mmol) according to General procedure D. Flash column chromatography (5 → 30%  $\text{Et}_2\text{O}$  in pentane) yielded the title compound (217 mg, 0.49 mmol, quant.).

$^1\text{H}$  NMR (400 MHz,  $\text{CDCl}_3$ )  $\delta$  8.70 (s, 1H), 7.32 – 7.26 (m, 2H), 7.26 – 7.16 (m, 5H), 7.07 – 7.01 (m, 2H), 4.85 – 4.15 (m, 2H), 3.39 – 3.30 (m, 2H), 3.13 – 3.01 (m, 2H), 3.01 – 2.87 (m, 2H), 2.52 (d,  $J = 7.1$  Hz, 2H), 1.86 – 1.75 (m, 1H), 1.75 – 1.64 (m, 2H), 1.40 – 1.26 (m, 2H).

$^{13}\text{C}$  NMR (101 MHz,  $\text{CDCl}_3$ )  $\delta$  162.45, 148.12, 147.37, 139.86, 138.07, 131.81, 130.33, 128.51, 128.47, 128.41, 126.51, 47.09, 42.02, 37.81, 36.04, 32.81, 31.78.

**(4-(4-Chlorobenzyl)piperidin-1-yl)(3-((4-methylphenethyl)thio)-1H-1,2,4-triazol-1-yl)-methanone (69)**

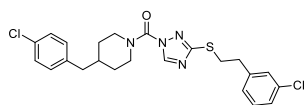


**39** (1 eq, 102 mg, 0.49 mmol) was reacted with **52** (1 eq, 107 mg, 0.49 mmol) according to General procedure D. Flash column chromatography (5 → 30%  $\text{Et}_2\text{O}$  in pentane) yielded the title compound (221 mg, 0.49 mmol, quant.).

$^1\text{H}$  NMR (400 MHz,  $\text{CDCl}_3$ )  $\delta$  8.70 (s, 1H), 7.28 – 7.20 (m, 2H), 7.14 – 7.07 (m, 4H), 7.07 – 7.01 (m, 2H), 4.76 – 4.36 (m, 2H), 3.37 – 3.29 (m, 2H), 3.05 – 2.96 (m, 2H), 2.98 – 2.86 (m, 2H), 2.53 (d,  $J = 7.1$  Hz, 2H), 2.32 (s, 3H), 1.88 – 1.76 (m, 1H), 1.76 – 1.65 (m, 2H), 1.41 – 1.30 (m, 2H).

$^{13}\text{C}$  NMR (101 MHz,  $\text{CDCl}_3$ )  $\delta$  162.52, 148.12, 147.38, 138.08, 136.80, 136.01, 131.82, 130.33, 129.15, 128.40, 128.38, 47.10, 42.04, 37.83, 35.60, 32.95, 31.79, 21.03.

**(4-(4-Chlorobenzyl)piperidin-1-yl)(3-((3-chlorophenethyl)thio)-1H-1,2,4-triazol-1-yl)-methanone (70)**

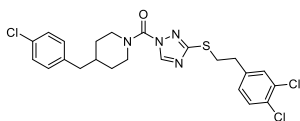


**39** (1 eq, 88 mg, 0.42 mmol) was reacted with **53** (1 eq, 100 mg, 0.42 mmol) according to General procedure D. Flash column chromatography (5 → 30%  $\text{Et}_2\text{O}$  in pentane) yielded the title compound as slightly yellowish oil (130 mg, 0.27 mmol, 66%).

$^1\text{H}$  NMR (400 MHz,  $\text{CDCl}_3$ )  $\delta$  8.70 (s, 1H), 7.29 – 7.17 (m, 5H), 7.12 – 7.08 (m, 1H), 7.05 (d,  $J$  = 8.4 Hz, 2H), 4.90 – 4.14 (m, 2H), 3.38 – 3.29 (m, 2H), 3.10 – 3.00 (m, 2H), 3.00 – 2.84 (m, 2H), 2.54 (d,  $J$  = 7.1 Hz, 2H), 1.89 – 1.77 (m, 1H), 1.77 – 1.68 (m, 2H), 1.34 (qd,  $J$  = 12.9, 4.2 Hz, 2H).

$^{13}\text{C}$  NMR (101 MHz,  $\text{CDCl}_3$ )  $\delta$  162.29, 148.18, 147.48, 141.90, 138.12, 134.22, 131.91, 130.39, 129.81, 128.73, 128.49, 126.85, 126.77, 47.38, 42.08, 37.90, 35.79, 32.54, 31.85.

**(4-(4-Chlorobenzyl)piperidin-1-yl)(3-((3,4-dichlorophenethyl)thio)-1H-1,2,4-triazol-1-yl)-methanone (71)**

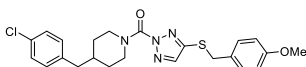


**39** (2 eq, 160 mg, 0.76 mmol) was reacted with **54** (1 eq, 100 mg, 0.37 mmol) according to General procedure D. Flash column chromatography yielded the title compound (56 mg, 0.11 mmol, 30%).

$^1\text{H}$  NMR (400 MHz,  $\text{CDCl}_3$ )  $\delta$  7.83 (s, 1H), 7.40 – 7.32 (m, 2H), 7.30 – 7.22 (m, 2H), 7.13 – 7.04 (m, 3H), 4.46 – 4.33 (m, 2H), 3.50 – 3.37 (m, 2H), 3.10 – 3.01 (m, 2H), 3.01 – 2.84 (m, 2H), 2.55 (d,  $J$  = 7.0 Hz, 2H), 1.85 – 1.77 (m, 1H), 1.77 – 1.69 (m, 2H), 1.36 (qd,  $J$  = 12.7, 4.0 Hz, 2H).

$^{13}\text{C}$  NMR (101 MHz,  $\text{CDCl}_3$ )  $\delta$  158.57, 151.05, 149.60, 140.05, 138.29, 134.31, 132.09, 130.76, 130.58, 130.51, 128.63, 128.27, 42.28, 38.10, 34.67, 33.43, 31.98.

**(4-(4-Chlorobenzyl)piperidin-1-yl)(4-((4-methoxybenzyl)thio)-2H-1,2,3-triazol-2-yl)-methanone (72)**

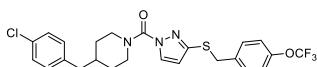


**39** (1 eq, 95 mg, 0.425 mmol) was reacted with **55** (1 eq, 100 mg, 0.425 mmol) according to General procedure D. Flash column chromatography (5 → 30%  $\text{Et}_2\text{O}$  in pentane) yielded the title compound (30 mg, 0.066 mmol, 15%).

$^1\text{H}$  NMR (400 MHz,  $\text{CDCl}_3$ )  $\delta$  7.50 (s, 1H), 7.28 – 7.21 (m, 4H), 7.12 – 7.03 (m, 2H), 6.85 – 6.78 (m, 2H), 4.59 – 4.28 (m, 1H), 4.21 (s, 2H), 4.13 – 3.88 (m, 1H), 3.76 (s, 3H), 3.05 – 2.85 (m, 2H), 2.55 (d,  $J$  = 7.0 Hz, 2H), 1.90 – 1.72 (m, 1H), 1.71 – 1.51 (m, 2H), 1.39 – 1.30 (m, 2H).

$^{13}\text{C}$  NMR (101 MHz,  $\text{CDCl}_3$ )  $\delta$  159.13, 148.88, 145.09, 138.24, 136.42, 132.05, 130.48, 130.21, 128.60, 114.10, 55.36, 42.22, 38.06, 37.30, 32.06.

**(4-(4-Chlorobenzyl)piperidin-1-yl)(3-((4-(trifluoromethoxy)benzyl)thio)-1H-pyrazol-1-yl)-methanone (73)**

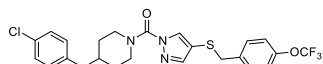


**39** (1 eq, 46 mg, 0.22 mmol) was reacted with **56** (2.2 eq, 131 mg, 0.48 mmol) according to General procedure D. Flash column chromatography (10 → 40%  $\text{EtOAc}$  in pentane) yielded the title compound as slightly yellowish gum (62 mg, 0.12 mmol, 55%).

$^1\text{H}$  NMR (500 MHz,  $\text{CDCl}_3$ )  $\delta$  8.02 (d,  $J$  = 2.7 Hz, 1H), 7.40 – 7.34 (m, 2H), 7.28 – 7.23 (m, 2H), 7.16 – 7.09 (m, 2H), 7.09 – 7.03 (m, 2H), 6.21 (d,  $J$  = 2.7 Hz, 1H), 4.51 – 4.39 (m, 2H), 4.22 (s, 2H), 2.89 (td,  $J$  = 12.9, 2.6 Hz, 2H), 2.52 (d,  $J$  = 7.2 Hz, 2H), 1.83 – 1.70 (m, 1H), 1.69 – 1.60 (m, 2H), 1.29 (qd,  $J$  = 12.7, 4.2 Hz, 2H).

$^{13}\text{C}$  NMR (126 MHz,  $\text{CDCl}_3$ )  $\delta$  150.55, 148.75, 148.38, 138.36, 136.40, 133.43, 131.96, 130.45, 130.19, 128.53, 121.04, 120.51 (q,  $J$  = 257.2 Hz), 108.12, 42.28, 38.11, 36.16, 32.00.

**(4-(4-Chlorobenzyl)piperidin-1-yl)(4-((4-(trifluoromethoxy)benzyl)thio)-1H-pyrazol-1-yl)-methanone (74)**



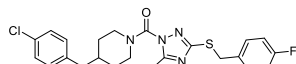
**39** (1.2 eq, 46 mg, 0.22 mmol) was reacted with **57** (1 eq, 49 mg, 0.18 mmol) according to General procedure D. Flash column chromatography (15 → 50% Et<sub>2</sub>O in pentane) yielded the title

compound as yellowish gum (44 mg, 0.086 mmol, 48%).

<sup>1</sup>H NMR (500 MHz, CDCl<sub>3</sub>) δ 7.92 (d, *J* = 0.7 Hz, 1H), 7.33 (d, *J* = 0.7 Hz, 1H), 7.28 – 7.22 (m, 2H), 7.22 – 7.17 (m, 2H), 7.15 – 7.10 (m, 2H), 7.09 – 7.04 (m, 2H), 4.46 – 4.40 (m, 2H), 3.84 (s, 2H), 2.92 (td, *J* = 12.5, 6.3 Hz, 2H), 2.54 (d, *J* = 7.1 Hz, 2H), 1.84 – 1.74 (m, 1H), 1.74 – 1.66 (m, 2H), 1.33 (qd, *J* = 12.8, 4.2 Hz, 2H).

<sup>13</sup>C NMR (126 MHz, CDCl<sub>3</sub>) δ 150.52, 148.45, 145.17, 138.34, 136.73, 135.28, 131.99, 130.49, 130.40, 128.56, 121.06, 120.53 (q, *J* = 257.2 Hz), 112.31, 42.29, 40.56, 38.14, 31.99.

**(4-(4-Chlorobenzyl)piperidin-1-yl)(3-((4-fluorobenzyl)thio)-5-methyl-1H-1,2,4-triazol-1-yl)-methanone (75)**



**39** (1 eq, 65 mg, 0.31 mmol) was reacted with 3-((4-fluorobenzyl)thio)-1H-1,2,4-triazole (**58**, 70 mg, 0.31 mmol, kindly provided by Anthe Janssen) according to General procedure D. The

residue was purified by flash column chromatography (0 → 40% EtOAc in pentane) yielding the title compound as gray gum (84 mg, 0.18 mmol, 59%).

<sup>1</sup>H NMR (400 MHz, CDCl<sub>3</sub>) δ 7.39 – 7.31 (m, 2H), 7.31 – 7.22 (m, 2H), 7.10 – 7.02 (m, 2H), 7.02 – 6.91 (m, 2H), 4.43 – 4.25 (m, 1H), 4.29 (s, 2H), 4.04 – 3.82 (m, 1H), 2.96 – 2.79 (m, 2H), 2.58 (s, 3H), 2.54 (d, *J* = 7.0 Hz, 2H), 1.84 – 1.68 (m, 1H), 1.70 – 1.56 (m, 2H), 1.36 – 1.14 (m, 2H).

<sup>13</sup>C NMR (101 MHz, CDCl<sub>3</sub>) δ 161.55 (d, *J* = 359.9 Hz), 160.89, 157.58, 149.37, 138.16, 132.99 (d, *J* = 3.2 Hz), 132.03, 130.53 (d, *J* = 8.2 Hz), 130.43, 128.56, 115.41 (d, *J* = 21.5 Hz), 47.91 (br), 45.32 (br), 42.13, 37.93, 35.24, 31.97, 13.85.

**1-Adamantanemethanol (82)**

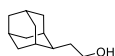


A solution of 1-adamantanecarboxylic acid (**79**, 5.0 g, 28 mmol) in dry THF (10 mL/g) was added dropwise to an ice-cold suspension of LiAlH<sub>4</sub> (2.5 eq, 35 mL 2.0 M in THF, 70 mmol) in dry THF (20 mL/g). The reaction mixture was warmed to RT and stirred for 30 min, followed by reflux for 30 min. The reaction was then quenched by addition of 10% aq. NaOH on an ice bath. Solids were removed by filtration and washed with DCM. Combined filtrates were dried over Na<sub>2</sub>SO<sub>4</sub>, filtrated and concentrated *in vacuo* to obtain the title compound as a white solid (4.7 g, 27 mmol, 99%), which was used without further purification.

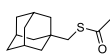
<sup>1</sup>H NMR (500 MHz, CDCl<sub>3</sub>) δ 3.20 (s, 2H), 2.00 (p, *J* = 3.1 Hz, 3H), 1.77 – 1.61 (m, 7H), 1.51 (d, *J* = 2.9 Hz, 6H).

<sup>13</sup>C NMR (126 MHz, CDCl<sub>3</sub>) δ 74.03, 39.17, 37.31, 34.62, 28.31.

**2-Adamantaneethanol (84)**



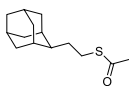
Methyl 2-(adamant-2-yl)acetate (**81**, 32.0 g, 154 mmol) in dry THF (10 mL/g) was added dropwise to an ice-cold suspension of LiAlH<sub>4</sub> (2.5 eq, 193 mL 2.0 M in THF, 385 mmol) in dry THF (20 mL/g). The reaction mixture was warmed to RT and stirred for 30 min, followed by reflux for 30 min. The reaction was then quenched by addition of 10% aq. NaOH on an ice bath. Solids were removed by filtration and washed with DCM. Combined filtrates were dried over Na<sub>2</sub>SO<sub>4</sub>, filtrated and concentrated *in vacuo* to obtain the title compound as a white solid (27.0 g, 150 mmol, 97%) which was used without characterization.

**S-(adamant-1-ylmethyl)thioacetate (85)**

Triflic anhydride (1.05 eq, 8.9 g, 32 mmol) was added portionwise to a solution of **82** (1 eq, 5.0 g, 30 mmol) and pyridine (1.2 eq, 2.9 mL, 36 mmol) in dry DCM (60 mL), while maintaining the temperature between  $-15$  and  $-5^{\circ}\text{C}$ . The mixture was stirred for 15 min followed by 30 min at RT. The mixture was then diluted with hexane (150 mL), cooled to  $0^{\circ}\text{C}$  and ice-cold 1 M aq.  $\text{H}_2\text{SO}_4$  was added until  $\text{pH} < 7$ . The layers were separated, the organic layer was washed with water and brine, dried over  $\text{Na}_2\text{SO}_4$ , filtrated and concentrated *in vacuo*. The resulting brown liquid was dissolved in  $\text{CH}_3\text{CN}$  (50 mL) and cooled to  $0^{\circ}\text{C}$ . AcSK (2 eq, 6.9 g, 60 mmol) and 18-Crown-6 (0.3 eq, 1.9 mL, 9 mmol) were added, the mixture was warmed to RT and stirred for  $\geq 72$  h. Solids were removed by filtration and washed with hexane until they were colorless. Combined filtrates were concentrated *in vacuo*. Flash column chromatography (150:1 hexane:EtOAc) provided the thioacetate as a red solid (4.3 g, 19 mmol, 64%).

$^1\text{H}$  NMR (500 MHz,  $\text{CDCl}_3$ )  $\delta$  2.73 (s, 2H), 2.35 (s, 3H), 1.96 (hept,  $J = 3.0$  Hz, 3H), 1.72 – 1.58 (m, 6H), 1.50 (d,  $J = 2.9$  Hz, 6H).

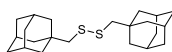
$^{13}\text{C}$  NMR (126 MHz,  $\text{CDCl}_3$ )  $\delta$  196.16, 42.62, 41.56, 36.88, 33.37, 30.89, 28.57.

**S-(2-(adamant-2-yl)ethyl)thioacetate (87)**

Triflic anhydride (1.05 eq, 5.0 g, 18 mmol) was added portionwise to a solution of **84** (1 eq, 3.0 g, 17 mmol) and pyridine (1.2 eq, 1.6 mL, 20 mmol) in dry DCM (34 mL), while maintaining the temperature at  $-70^{\circ}\text{C}$ . The mixture was stirred for 15 min followed by 30 min at RT. The mixture was then diluted with hexane (85 mL), cooled to  $0^{\circ}\text{C}$  and ice-cold 1 M aq.  $\text{H}_2\text{SO}_4$  was added until  $\text{pH} < 7$ . The layers were separated, the organic layer was washed with water and brine, dried over  $\text{Na}_2\text{SO}_4$ , filtrated and concentrated *in vacuo*. The resulting brown liquid was dissolved in  $\text{CH}_3\text{CN}$  (28 mL) and cooled to  $0^{\circ}\text{C}$ . AcSK (2 eq, 3.9 g, 34 mmol) and 18-Crown-6 (0.3 eq, 1.1 mL, 5 mmol) were added, the mixture was warmed to RT and stirred for  $\geq 72$  h. Solids were removed by filtration and washed with hexane until they were colorless. Combined filtrates were concentrated *in vacuo*. Flash column chromatography (150:1 hexane:EtOAc) provided the thioacetate as a red liquid (2.2 g, 9.2 mmol, 56%).

$^1\text{H}$  NMR (400 MHz,  $\text{CDCl}_3$ )  $\delta$  2.89 – 2.81 (m, 2H), 2.32 (s, 3H), 1.92 – 1.64 (m, 15H), 1.57 – 1.47 (m, 2H).

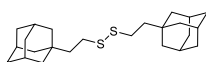
$^{13}\text{C}$  NMR (101 MHz,  $\text{CDCl}_3$ )  $\delta$  195.91, 43.80, 39.07, 38.30, 32.43, 31.60, 31.57, 28.21, 27.98, 27.57.

**Bis(adamant-1-ylmethyl)disulfide (88)**

**85** (1.0 g, 4.5 mmol) was treated according to General procedure E to obtain the title compound as a white solid (790 g, 2.18 mmol, 98%).

$^1\text{H}$  NMR (500 MHz,  $\text{CDCl}_3$ )  $\delta$  2.63 (s, 4H), 1.98 (p,  $J = 3.1$  Hz, 6H), 1.73 – 1.59 (m, 12H), 1.57 (d,  $J = 2.9$  Hz, 12H).

$^{13}\text{C}$  NMR (126 MHz,  $\text{CDCl}_3$ )  $\delta$  56.23, 41.90, 36.97, 34.33, 28.61.

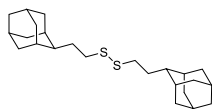
**Bis(2-(Adamant-1-yl)ethyl)disulfide (89)**

S-(2-(adamant-1-yl)ethyl)thioacetate (**86**, 1.5 g, 6.3 mmol, kindly provided by Alexander Pashenko) was treated according to General procedure E to obtain the title compound as a white crystalline solid (800 mg, 2.05 mmol, 65%).

$^1\text{H}$  NMR (500 MHz,  $\text{CDCl}_3$ )  $\delta$  2.70 – 2.63 (m, 4H), 1.96 (p,  $J = 3.1$  Hz, 6H), 1.74 – 1.59 (m, 12H), 1.49 (d,  $J = 2.9$  Hz, 12H), 1.47 – 1.41 (m, 4H).

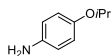
$^{13}\text{C}$  NMR (126 MHz,  $\text{CDCl}_3$ )  $\delta$  44.24, 42.44, 37.23, 33.57, 32.89, 28.78.



**Bis(2-(adamant-2-yl)ethyl)disulfide (90)**

**87** (1.05 g, 4.40 mmol) was treated according to General procedure E to obtain the title compound as a white crystalline solid (430 g, 1.10 mmol, 50%).  
 $^1\text{H NMR}$  (400 MHz,  $\text{CDCl}_3$ )  $\delta$  2.73 – 2.65 (m, 4H), 1.92 – 1.66 (m, 30H), 1.52 (d,  $J$  = 12.6 Hz, 4H).

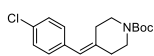
$^{13}\text{C NMR}$  (101 MHz,  $\text{CDCl}_3$ )  $\delta$  43.58, 39.24, 38.46, 37.68, 32.47, 31.86, 31.79, 28.37, 28.16.

**4-Isopropoxyaniline (96)**

**137** (1 eq, 491 mg, 2.71 mmol) was dissolved in MeOH (8 mL), Pd/C (1.7 mol%, 49 mg 10%, 0.046 mmol) was added and the mixture was purged with  $\text{N}_2$ . HCl (1.3 eq, 300  $\mu\text{L}$  12 M, 3.60 mmol) was added and purging was continued. The mixture was then purged with  $\text{H}_2$  and stirred for 5 h. The mixture was purged with  $\text{N}_2$  before it was filtrated over celite, treated with activated charcoal and filtrated over celite again. The filtrate was concentrated *in vacuo*, affording the title compound as brown solid (392 mg, 2.59 mmol, 96%), which was used without further purification.

$^1\text{H NMR}$  (400 MHz, MeOD)  $\delta$  7.32 (m, 2H), 7.03 (m, 2H), 4.63 (p,  $J$  = 6.0 Hz, 1H), 1.30 (d,  $J$  = 5.8 Hz, 6H).

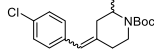
$^{13}\text{C NMR}$  (101 MHz, MeOD)  $\delta$  159.57, 125.22, 125.10, 123.81, 117.93, 71.35, 22.10.

**tert-Butyl 4-(4-chlorobenzylidene)piperidine-1-carboxylate (108)**

*N*-Boc-4-piperidinone (**103**, 500 mg, 2.51 mmol) was reacted with diethyl (4-chlorobenzyl)phosphonate (**107**, 1.1 eq, 609  $\mu\text{L}$ , 2.76 mmol) according to General procedure H. Flash column chromatography (0  $\rightarrow$  10% EtOAc in pentane) yielded the title compound as white crystalline solid (482 mg, 1.57 mmol, 62%).

$^1\text{H NMR}$  (400 MHz,  $\text{CDCl}_3$ )  $\delta$  7.32 – 7.24 (m, 2H), 7.14 – 7.07 (m, 2H), 6.30 (s, 1H), 3.54 – 3.47 (m, 2H), 3.43 – 3.36 (m, 2H), 2.45 – 2.38 (m, 2H), 2.36 – 2.28 (m, 2H), 1.48 (s, 9H).

$^{13}\text{C NMR}$  (101 MHz,  $\text{CDCl}_3$ )  $\delta$  154.82, 139.33, 135.91, 132.12, 130.27, 128.42, 123.48, 79.72, 36.26, 29.24, 28.54.

**tert-Butyl 4-(4-chlorobenzylidene)-2-methylpiperidine-1-carboxylate (109)**

*N*-Boc-2-methyl-4-piperidinone (**104**, 285 mg, 1.34 mmol) was reacted with diethyl (4-chlorobenzyl)phosphonate (**107**, 1.3 eq, 373  $\mu\text{L}$ , 1.69 mmol) according to General procedure H. Flash column chromatography (0  $\rightarrow$  15% Et<sub>2</sub>O in pentane) yielded a mixture of *E/Z* isomers (ratio ~3:2) of the title compound as colorless oil (195 mg, 0.61 mmol, 45%).

Isomer 1:

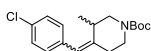
$^1\text{H NMR}$  (400 MHz,  $\text{CDCl}_3$ )  $\delta$  7.30 – 7.21 (m, 2H), 7.16 – 7.04 (m, 2H), 6.41 (s, 1H), 4.54 – 4.41 (m, 1H), 4.12 – 4.03 (m, 1H), 2.98 (td,  $J$  = 12.8, 3.6 Hz, 1H), 2.60 – 2.51 (m, 1H), 2.41 – 2.29 (m, 1H), 2.29 – 2.21 (m, 2H), 1.47 (s, 9H), 1.02 (d,  $J$  = 6.9 Hz, 3H).

$^{13}\text{C NMR}$  (101 MHz,  $\text{CDCl}_3$ )  $\delta$  154.80, 136.95, 135.99, 132.01, 130.01, 128.35, 125.15, 79.48, 47.25 (br), 39.78 (br), 35.96, 33.81, 28.51, 16.94.

Isomer 2:

$^1\text{H NMR}$  (400 MHz,  $\text{CDCl}_3$ )  $\delta$  7.30 – 7.21 (m, 2H), 7.16 – 7.04 (m, 2H), 6.27 (s, 1H), 4.54 – 4.41 (m, 1H), 4.02 – 3.94 (m, 1H), 2.89 (td,  $J$  = 12.8, 3.5 Hz, 1H), 2.70 (dt,  $J$  = 14.4, 3.3 Hz, 1H), 2.64 – 2.57 (m, 1H), 2.20 – 2.07 (m, 2H), 1.47 (s, 9H), 1.13 (d,  $J$  = 6.8 Hz, 3H).

$^{13}\text{C NMR}$  (101 MHz,  $\text{CDCl}_3$ )  $\delta$  154.71, 136.86, 135.94, 132.01, 130.13, 128.35, 124.98, 79.50, 47.83 (br), 41.26, 38.84 (br), 28.95, 28.51, 16.94.

**tert-Butyl 4-(4-chlorobenzylidene)-3-methylpiperidine-1-carboxylate (110)**

NaH (1.6 eq, 300 mg 60% dispersion in mineral oil, 7.50 mmol) was suspended in dry THF (10 mL) and cooled on ice. Diethyl (4-chlorobenzyl)phosphonate (**107**, 1.1 eq, 1.20 mL, 5.16 mmol) dissolved in dry THF (10 mL) was added dropwise and the mixture was stirred for 1.5 h. *N*-Boc-3-methyl-4-piperidinone (**105**, 1 eq, 1.0 g, 4.69 mmol) dissolved in dry THF (10 mL) was added dropwise. The mixture was allowed to warm to RT and stirred for 2 d. The reaction was cooled on ice and quenched with sat. aq.  $\text{NH}_4\text{Cl}$ . The aqueous layer was extracted with EtOAc. The combined organic layers were washed with brine, dried over  $\text{MgSO}_4$ , filtered and concentrated *in vacuo*. Flash column chromatography (0 → 15%  $\text{Et}_2\text{O}$  in pentane) yielded a mixture of *E/Z* isomers (ratio ~2:1) of the title compound as white crystalline solid (900 mg, 2.80 mmol, 60%).

Isomer 1:

$^1\text{H}$  NMR (300 MHz,  $\text{CDCl}_3$ )  $\delta$  7.31 – 7.21 (m, 2H), 7.15 – 7.02 (m, 2H), 6.27 (s, 1H), 3.66 (dd,  $J = 13.0, 3.1$  Hz, 1H), 3.48 (dt,  $J = 11.4, 5.7$  Hz, 1H), 3.31 (d,  $J = 4.4$  Hz, 1H), 3.08 (dd,  $J = 12.6, 7.4$  Hz, 1H), 2.63 – 2.49 (m, 1H), 2.48 – 2.34 (m, 1H), 2.32 – 2.16 (m, 1H), 1.47 (s, 9H), 1.15 (d,  $J = 6.7$  Hz, 3H).

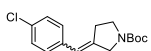
$^{13}\text{C}$  NMR (75 MHz,  $\text{CDCl}_3$ )  $\delta$  155.10, 143.94, 136.47, 132.32, 130.43, 128.48, 121.61, 79.58, 51.62, 45.04, 38.68, 28.64, 27.91, 16.52.

Isomer 2:

$^1\text{H}$  NMR (300 MHz, DMSO)  $\delta$  7.32 – 7.22 (m, 2H), 7.15 – 7.05 (m, 2H), 6.21 (s, 1H), 4.35 – 4.16 (m, 1H), 3.96 – 3.86 (m, 1H), 3.00 – 2.88 (m, 1H), 2.85 – 2.68 (m, 2H), 2.61 (tdd,  $J = 13.0, 5.0, 1.8$  Hz, 1H), 2.05 (dt,  $J = 13.3, 1.9$  Hz, 1H), 1.47 (s, 9H), 1.17 (d,  $J = 6.9$  Hz, 3H).

$^{13}\text{C}$  NMR (75 MHz,  $\text{CDCl}_3$ )  $\delta$  155.44, 144.00, 136.22, 132.44, 130.08, 128.61, 122.91, 79.64, 50.17, 45.83, 32.70, 32.54, 28.67, 17.42.

NB: NMR recorded at 60 °C.

**tert-Butyl 3-(4-chlorobenzylidene)pyrrolidine-1-carboxylate (111)**

Boc-3-pyrrolidinone (**106**, 500 mg, 2.70 mmol) was reacted with diethyl (4-chlorobenzyl)phosphonate (**107**, 1.1 eq, 655  $\mu\text{L}$ , 2.97 mmol) according to General procedure H. Flash column chromatography (0 → 8% EtOAc in pentane) yielded a mixture of *E/Z* isomers (ratio ~3:2) of the title compound as colorless oil (357 mg, 1.22 mmol, 45%).

Isomer 1:

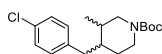
$^1\text{H}$  NMR (400 MHz,  $\text{CDCl}_3$ )  $\delta$  7.35 – 7.22 (m, 2H), 7.21 – 7.14 (m, 2H), 6.37 – 6.31 (m, 1H), 4.24 – 4.06 (m, 2H), 3.50 – 3.39 (m, 2H), 2.81 – 2.68 (m, 2H), 1.49 (s, 9H).

$^{13}\text{C}$  NMR (101 MHz,  $\text{CDCl}_3$ )  $\delta$  154.35, 138.93, 135.70, 135.48 (br), 135.40 (br), 132.34, 129.47, 128.45, 121.47, 79.45, 48.63, 44.27, 43.85, 34.13, 33.39, 28.48.

Isomer 2:

$^1\text{H}$  NMR (400 MHz,  $\text{CDCl}_3$ )  $\delta$  7.35 – 7.22 (m, 2H), 7.13 – 7.05 (m, 2H), 6.37 – 6.31 (m, 1H), 4.24 – 4.06 (m, 2H), 3.61 – 3.49 (m, 2H), 2.81 – 2.68 (m, 2H), 1.48 (s, 9H).

$^{13}\text{C}$  NMR (101 MHz,  $\text{CDCl}_3$ )  $\delta$  154.45, 139.94, 135.40 (br), 132.26, 129.25, 128.53, 120.87 (br), 79.53 (br), 52.08 (br), 51.89 (br), 46.08 (br), 45.74 (br), 29.68, 29.06, 28.48.

**tert-Butyl 4-(4-chlorobenzyl)-3-methylpiperidine-1-carboxylate (112)**

A solution of **110** (200 mg, 0.62 mmol) in EtOAc (1 mL) was purged with N<sub>2</sub> (10 min). Pd/C (5 mol%, 33 mg 10%, 0.031 mmol) was added and purging was continued (10 min). The mixture was purged with H<sub>2</sub> and stirred overnight. Solids were removed by filtration over celite, volatiles *in vacuo*. Flash column chromatography (0 → 20% Et<sub>2</sub>O in pentane) afforded the title compound as mixture of isomers (178 mg, 0.55 mmol, 88%, ratio ~3:1).

Isomer 1:

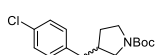
<sup>1</sup>H NMR (400 MHz, CDCl<sub>3</sub>) δ 7.26 – 7.17 (m, 2H), 7.10 – 7.00 (m, 2H), 4.18 – 4.04 (m, 1H), 3.89 – 3.74 (m, 1H), 2.90 – 2.82 (m, 1H), 2.68 – 2.55 (m, 1H), 2.55 – 2.38 (m, 3H), 1.89 – 1.76 (m, 1H), 1.75 – 1.64 (m, 1H), 1.45 (s, 9H), 1.34 – 1.20 (m, 1H), 0.91 (d, *J* = 6.1 Hz, 3H).

<sup>13</sup>C NMR (101 MHz, CDCl<sub>3</sub>) δ 155.01, 138.77, 131.37, 130.09, 128.19, 78.85, 50.69 (br), 43.27 (br), 41.05, 38.71, 38.57 (br), 31.72, 28.26, 10.94.

Isomer 2:

<sup>1</sup>H NMR (400 MHz, CDCl<sub>3</sub>) δ 7.26 – 7.17 (m, 2H), 7.10 – 7.00 (m, 2H), 4.03 – 3.88 (m, 2H), 3.06 – 2.96 (m, 1H), 2.79 – 2.68 (m, 1H), 2.55 – 2.38 (m, 2H), 2.38 – 2.25 (m, 1H), 2.18 – 2.09 (m, 1H), 1.45 (s, 9H), 1.34 – 1.20 (m, 2H), 1.00 (d, *J* = 6.1 Hz, 3H).

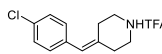
<sup>13</sup>C NMR (101 MHz, CDCl<sub>3</sub>) δ 154.42, 138.67, 131.37, 130.36, 128.11, 78.99, 49.35 (br), 44.17, 43.96 (br), 38.71, 38.07 (br), 35.63, 28.26, 16.67.

**tert-Butyl 3-(4-chlorobenzyl)pyrrolidine-1-carboxylate (113)**

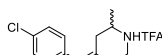
A solution of **111** (51 mg, 0.17 mmol) in EtOAc (4 mL) was purged with N<sub>2</sub> (15 min). Pd/C (5 mol%, 9 mg 10%, 8.5 μmol) was added and purging was continued (15 min). The mixture was purged with H<sub>2</sub> and stirred for 5 h. Solids were removed by filtration over celite, volatiles *in vacuo*, providing the title compound as colorless oil (50 mg, 0.17 mmol, quant.), which was used without further purification.

<sup>1</sup>H NMR (400 MHz, CDCl<sub>3</sub>) δ 7.32 – 7.22 (m, 2H), 7.09 (d, *J* = 8.2 Hz, 2H), 3.57 – 3.36 (m, 2H), 3.32 – 3.16 (m, 1H), 3.05 – 2.87 (m, 1H), 2.76 – 2.54 (m, 2H), 2.44 – 2.29 (m, 1H), 1.97 – 1.85 (m, 1H), 1.73 – 1.37 (m, 10H).

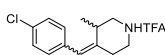
<sup>13</sup>C NMR (101 MHz, CDCl<sub>3</sub>) δ 154.69, 138.86, 132.01, 130.09, 128.77, 128.63, 128.52, 79.19, 51.22, 50.96, 45.66, 45.24, 44.46, 40.74, 40.00, 38.64, 31.44, 30.74, 28.62, 28.11.

**4-(4-Chlorobenzylidene)piperidin-1-ium 2,2,2-trifluoroacetate (114)**

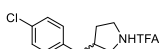
**108** (252 mg, 0.82 mmol) was dissolved in DCM (2 mL) and cooled on ice. To this, TFA (5.6 eq, 350 μL, 4.59 mmol) was added dropwise. The reaction was allowed to warm to RT and stirred for 1 h. Volatiles were removed *in vacuo*. The residual off-white crystalline solid was used immediately in the next reaction.

**4-(4-Chlorobenzylidene)-2-methylpiperidin-1-ium 2,2,2-trifluoroacetate (115)**

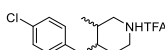
**109** (65 mg, 0.20 mmol) was dissolved in DCM (2 mL). To this, TFA (10 eq, 166 μL, 2.17 mmol) was added carefully, after which the mixture was stirred for 26 h. All volatiles were removed *in vacuo*. The residue was used immediately in the next reaction.

**4-(4-Chlorobenzylidene)-3-methylpiperidin-1-ium 2,2,2-trifluoroacetate (116)**

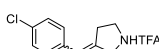
**110** (200 mg, 0.62 mmol) was dissolved in DCM (1 mL). To this, TFA (5.3 eq, 250  $\mu$ L, 3.27 mmol) was added dropwise and the reaction was stirred for 5 h. All volatiles were removed *in vacuo*. The resulting oil was triturated with 9:1 *n*-hexane:EtOAc, yielding the title compound as white crystalline solid, which was used immediately in the next reaction.

**3-(4-Chlorobenzyl)pyrrolidin-1-ium 2,2,2-trifluoroacetate (117)**

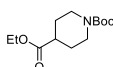
**113** (50 mg, 0.17 mmol) was dissolved in DCM (3 mL). To this, TFA (10 eq, 130  $\mu$ L, 1.70 mmol) was added dropwise and the mixture was stirred for 3 d. Solids were removed by filtration over celite, volatiles *in vacuo*. The residue was used immediately in the next reaction.

**4-(4-Chlorobenzyl)-3-methylpiperidin-1-ium 2,2,2-trifluoroacetate (118)**

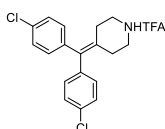
**112** (178 mg, 0.55 mmol) was dissolved in DCM (1 mL). To this, TFA (5 eq, 210  $\mu$ L, 2.75 mmol) was added dropwise and the mixture was stirred for 18 h. All volatiles were removed *in vacuo*. The resulting brown crystalline solid was triturated with 9:1 *n*-hexane:EtOAc, affording the title compound as white crystalline solid (150 mg, 0.44 mmol, 81%), which was used immediately in the next reaction.

**3-(4-Chlorobenzylidene)pyrrolidin-1-ium 2,2,2-trifluoroacetate (119)**

**111** (109 mg, 0.37 mmol) was dissolved in DCM (2.2 mL). To this TFA (6 eq, 163  $\mu$ L, 2.13 mmol) was added dropwise, after which the mixture was stirred for 19 h. All volatiles were removed *in vacuo* and the residual brown solid was used immediately in the next reaction.

**1-(tert-Butyl) 4-ethyl piperidine-1,4-dicarboxylate (121)**

Ethyl isonipecotate (**138**, 1 eq, 500 mg, 3.18 mmol) and Et<sub>3</sub>N (1.5 eq, 665  $\mu$ L, 4.77 mmol) were dissolved in DCM (7 mL) and cooled on ice. Boc<sub>2</sub>O (1.2 eq, 833 mg, 3.82 mmol) was added portionwise. The mixture was stirred on ice for 30 min, after which it was allowed to warm to RT and stirred for 50 h. Water was added and the layers were separated. The organic layer was washed with water and brine, dried over MgSO<sub>4</sub>, filtrated and concentrated *in vacuo*. The residue was used immediately in the next reaction.

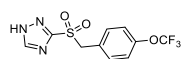
**4-(Bis(4-chlorophenyl)methylene)piperidin-1-ium 2,2,2-trifluoroacetate (122)**

**139** (350 mg, 0.80 mmol) was dissolved in DCM (5 mL). To this, TFA (10 eq, 607  $\mu$ L, 7.93 mmol) was added dropwise, after which the reaction was stirred for 6 d. All volatiles were removed *in vacuo*. The resulting brown oil was mixed with 9:1 *n*-hexane:EtOAc (0.5 mL) causing white precipitation. The brown solution was discarded. This procedure was repeated until no more white precipitate formed.

Solids were isolated by filtration and eluted with MeOH, after which they were concentrated *in vacuo*, affording the title compound as white crystalline solid (285 mg, 0.66 mmol, 82%).

<sup>1</sup>H NMR (400 MHz, MeOD)  $\delta$  7.39 – 7.31 (m, 4H), 7.18 – 7.10 (m, 4H), 3.29 – 3.21 (m, 4H), 2.61 – 2.54 (m, 4H).

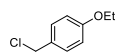
<sup>13</sup>C NMR (101 MHz, MeOD)  $\delta$  140.79, 138.84, 134.35, 132.05, 131.53, 129.69, 49.64, 49.43, 49.21, 49.00, 48.79, 48.57, 48.36, 46.09, 29.26.

**3-((4-(Trifluoromethoxy)benzyl)sulfonyl)-1H-1,2,4-triazole (123)**

**47** (345 mg, 1.25 mmol) was oxidized according General procedure A, affording the title compound as white crystalline solid (347 mg, 1.13 mmol, 90%) of sufficient purity to use in the next reaction.

$^1\text{H}$  NMR (400 MHz, MeOD)  $\delta$  8.69 (s, 1H), 7.40 – 7.33 (m, 2H), 7.25 – 7.19 (m, 2H), 4.76 (s, 2H).

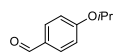
$^{13}\text{C}$  NMR (101 MHz, MeOD)  $\delta$  161.54, 150.93, 147.02, 134.09, 128.00, 122.04, 121.84 (q,  $J$  = 258.6 Hz), 60.65.

**1-(Chloromethyl)-4-ethoxybenzene (126)**

To an ice-cold solution of 4-ethoxybenzyl alcohol (**125**, 1.0 g, 6.57 mmol) in dry Et<sub>2</sub>O with a few drops of DMF, SOCl<sub>2</sub> (2 eq, 953  $\mu\text{L}$ , 13.1 mmol) was added dropwise. The mixture was allowed to warm to RT and stirred overnight. Volatiles were removed *in vacuo*, after which the residue was dissolved in DCM and washed with water and 1 M aq. Na<sub>2</sub>CO<sub>3</sub>. The organic layer was dried over MgSO<sub>4</sub>, filtrated and concentrated *in vacuo*, yielding the title compound (965 mg, 5.66 mmol, 86%) in sufficient purity to be used as such.

$^1\text{H}$  NMR (400 MHz, CDCl<sub>3</sub>)  $\delta$  7.33 – 7.25 (m, 2H), 6.90 – 6.82 (m, 2H), 4.56 (s, 2H), 4.02 (q,  $J$  = 7.0 Hz, 2H), 1.41 (t,  $J$  = 7.0 Hz, 3H).

$^{13}\text{C}$  NMR (101 MHz, CDCl<sub>3</sub>)  $\delta$  159.17, 130.17, 129.63, 114.76, 63.62, 46.49, 14.91.

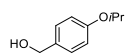
**4-Isopropoxybenzaldehyde (128)**

4-Hydroxybenzaldehyde (**127**, 1 eq, 2.0 g, 16.4 mmol), K<sub>2</sub>CO<sub>3</sub> (1.2 eq, 2.72 g, 19.7 mmol), KI (1.01 eq, 2.75 g, 16.5 mmol) and isopropyl iodide (2.4 eq, 3.92 mL, 39.3 mmol) were dissolved in dry DMF (50 mL), heated to 75°C and stirred overnight. Volatiles were removed *in vacuo*, after which the residue was dissolved in CHCl<sub>3</sub> and washed with water. The aqueous layer was extracted with CHCl<sub>3</sub> and the combined organic layers were dried over MgSO<sub>4</sub>, filtrated and concentrated *in vacuo*. Flash column chromatography (20% EtOAc in pentane) yielded the title compound (1.89 g, 11.5 mmol, 70%).

Analytical data on next page.

$^1\text{H}$  NMR (400 MHz, CDCl<sub>3</sub>)  $\delta$  9.86 (s, 1H), 7.85 – 7.77 (m, 2H), 7.01 – 6.93 (m, 2H), 4.67 (p,  $J$  = 6.1 Hz, 1H), 1.37 (d,  $J$  = 6.1 Hz, 6H).

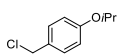
$^{13}\text{C}$  NMR (101 MHz, CDCl<sub>3</sub>)  $\delta$  190.81, 163.23, 132.08, 129.56, 115.63, 70.35, 21.92.

**(4-Isopropoxyphenyl)methanol (129)**

**128** (1.5 g, 9.13 mmol) was dissolved in 1:1 THF:H<sub>2</sub>O (20 mL) and cooled on ice. NaBH<sub>4</sub> (3 eq, 1.0 g, 27.4 mmol) was added portionwise, after which the mixture was allowed to warm to RT and stirred overnight. Volatiles were removed *in vacuo*, EtOAc and water were added to the residue and the layers were separated. The aqueous layer was extracted with EtOAc, after which the organic layer was washed with brine, dried over MgSO<sub>4</sub>, filtrated and concentrated *in vacuo*. Flash column chromatography (EtOAc in pentane) yielded the title compound (1.45 g, 8.72 mmol, 96%).

$^1\text{H}$  NMR (400 MHz, CDCl<sub>3</sub>)  $\delta$  7.30 – 7.23 (m, 2H), 6.91 – 6.83 (m, 2H), 4.60 (s, 2H), 4.54 (hept,  $J$  = 6.1 Hz, 1H), 1.72 (bs, 1H), 1.33 (d,  $J$  = 6.1 Hz, 6H).

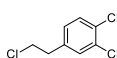
$^{13}\text{C}$  NMR (101 MHz, CDCl<sub>3</sub>)  $\delta$  157.50, 133.03, 128.75, 116.00, 70.03, 64.97, 22.09.

**1-(Chloromethyl)-4-isopropoxybenzene (130)**

To an ice-cold solution of **129** (1.0 g, 6.02 mmol) in dry Et<sub>2</sub>O with a few drops of DMF, SOCl<sub>2</sub> (2 eq, 873 μL, 12.0 mmol) was added dropwise. The mixture was allowed to warm to RT and stirred overnight. Volatiles were removed *in vacuo*, after which the residue was dissolved in DCM and washed with water and 1 M aq. Na<sub>2</sub>CO<sub>3</sub>. The organic layer was dried over MgSO<sub>4</sub>, filtrated and concentrated *in vacuo*, yielding the title compound (647 mg, 3.65 mmol, 61%) in sufficient purity to be used as such.

<sup>1</sup>H NMR (400 MHz, CDCl<sub>3</sub>) δ 7.32 – 7.24 (m, 2H), 6.88 – 6.82 (m, 2H), 4.55 (s, 2H), 4.54 (hept, *J* = 6.0 Hz, 1H), 1.33 (d, *J* = 6.1 Hz, 6H).

<sup>13</sup>C NMR (101 MHz, CDCl<sub>3</sub>) δ 158.14, 130.19, 129.48, 116.00, 70.00, 46.49, 22.10.

**1,2-Dichloro-4-(2-chloroethyl)benzene (132)**

3,4-Dichlorophenethyl alcohol (**131**, 128 μL, 1.05 mmol) was dissolved in dry DCM (11 mL) with a few drops of DMF and cooled on ice. SOCl<sub>2</sub> (9 eq, 684 μL, 9.42 mmol) was added dropwise, after which the mixture was heated to 40°C and stirred for a week. When TLC confirmed full conversion the reaction was quenched with water and the layers were separated. The aqueous layer was extracted with CHCl<sub>3</sub>, after which the combined organic layers were dried over MgSO<sub>4</sub>, filtrated and concentrated *in vacuo*, affording the title compound (179 mg, 0.85 mmol, 81%), which was used without further purification.

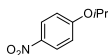
<sup>1</sup>H NMR (400 MHz, CDCl<sub>3</sub>) δ 7.37 (d, *J* = 8.2 Hz, 1H), 7.30 (d, *J* = 2.0 Hz, 1H), 7.05 (dd, *J* = 8.2, 2.1 Hz, 1H), 3.68 (t, *J* = 7.0 Hz, 2H), 3.00 (t, *J* = 7.0 Hz, 2H).

No <sup>13</sup>C NMR recorded.

**1H-Pyrazol-4-amine (135)**

4-Nitropyrazole (**134**, 1 eq, 1.60 g, 14.2 mmol) was dissolved in EtOH (13 mL), Pd/C (2 mol%, 282 mg 10%, 0.27 mmol) was added and the mixture was purged with N<sub>2</sub> for 30 min. The mixture was then purged with H<sub>2</sub> and stirred for 12 h. H<sub>2</sub> was removed by purging with N<sub>2</sub>, solids by filtration over celite and volatiles *in vacuo*. This yielded the title compound as dark red crystalline solid (1.17 g, 14.1 mmol, quant.), which was used without further purification.

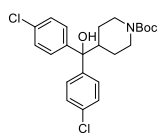
<sup>1</sup>H NMR (400 MHz, MeOD) δ 7.22 (s, 2H).

**1-Isopropoxy-4-nitrobenzene (137)**

In a MW vial 4-nitrophenol (**136**, 1 eq, 1.0 g, 7.19 mmol) was dissolved in dry DMF (2.5 mL), to which then K<sub>2</sub>CO<sub>3</sub> (1.5 eq, 1.5 g, 10.8 mmol) was added. To the stirring suspension then isopropyl bromide (1.5 eq, 1.0 mL, 10.8 mmol) was added carefully. The vial was sealed and heated to 120°C overnight. Upon completion all volatiles were removed *in vacuo*. The residue was dissolved in EtOAc and washed with brine, 1 M aq. NaOH and brine again, dried over MgSO<sub>4</sub>, filtrated and concentrated *in vacuo*, yielding the title compound as yellowish runny oil (1.07 g, 5.89 mmol, 82%), which was used without further purification.

<sup>1</sup>H NMR (400 MHz, CDCl<sub>3</sub>) δ 8.21 – 8.12 (m, 2H), 6.97 – 6.88 (m, 2H), 4.68 (p, *J* = 6.1 Hz, 1H), 1.39 (d, *J* = 6.1 Hz, 6H).

<sup>13</sup>C NMR (101 MHz, CDCl<sub>3</sub>) δ 163.24, 140.90, 125.88, 115.17, 70.95, 21.72.

**tert-Butyl 4-(bis(4-chlorophenyl)(hydroxy)methyl)piperidine-1-carboxylate (139)**

**121** (381 mg, 1.48 mmol) was dissolved in dry THF (16 mL) and cooled on ice. 4-chlorophenylmagnesium bromide (**120**, 6.7 eq, 10 mL 1.0 M in Et<sub>2</sub>O, 10 mmol) was added dropwise to the cloudy mixture over the course of 15 min. The mixture became clear when the ice bath was removed after 20 min, after which it was allowed to warm to RT and stirred for 4 d, during which it became cloudy again.

The reaction was cooled on ice and quenched with sat. aq. NH<sub>4</sub>Cl. EtOAc was added and the layers were separated. The aqueous layer was extracted with EtOAc, after which the combined organic layers were washed with brine, dried over MgSO<sub>4</sub>, filtrated and concentrated *in vacuo*. Flash column chromatography (0 → 15% EtOAc in pentane) afforded the title compound as white crystalline solid (570 mg, 1.31 mmol, 88%).

<sup>1</sup>H NMR (400 MHz, CDCl<sub>3</sub>) δ 7.41 – 7.33 (m, 4H), 7.32 – 7.22 (m, 4H), 4.21 – 4.01 (m, 2H), 2.75 – 2.58 (m, 2H), 2.46 (tt, *J* = 11.8, 3.0 Hz, 1H), 1.50 – 1.37 (m, 2H), 1.41 (s, 9H), 1.29 (qd, *J* = 12.5, 4.2 Hz, 2H).

<sup>13</sup>C NMR (101 MHz, CDCl<sub>3</sub>) δ 154.73, 143.97, 132.80, 128.56, 127.35, 79.64, 79.13, 77.48, 77.36, 77.16, 76.84, 44.30, 43.49 (br), 28.49, 26.38.

## References

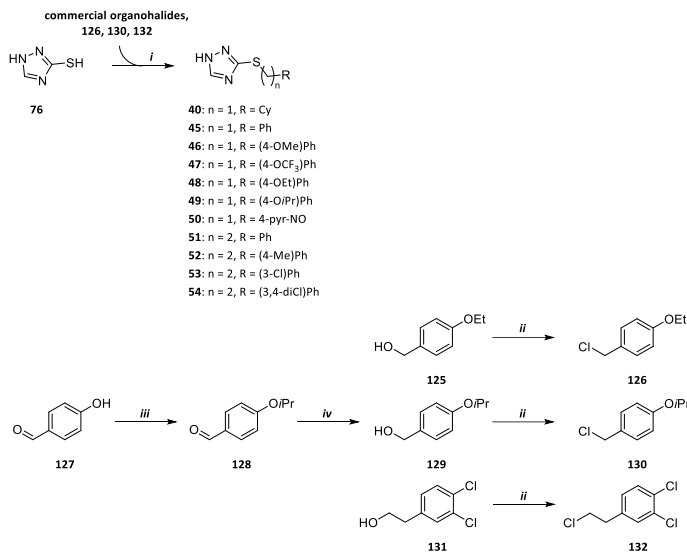
1. Leslie, C. C. Cytosolic phospholipase A2: Physiological function and role in disease. *J. Lipid Res.* **56**, 1386–1402 (2015).
2. Ghosh, M., Tucker, D. E., Burchett, S. A. & Leslie, C. C. Properties of the Group IV phospholipase A<sub>2</sub> family. *Prog. Lipid Res.* **45**, 487–510 (2006).
3. Ohto, T., Uozumi, N., Hirabayashi, T. & Shimizu, T. Identification of novel cytosolic phospholipase A<sub>2</sub>s, murine cPLA<sub>2</sub>δ, ε, and ζ, which form a gene cluster with cPLA<sub>2</sub>β. *J. Biol. Chem.* **280**, 24576–24583 (2005).
4. Ogura, Y., Parsons, W. H., Kamat, S. S. & Cravatt, B. F. A calcium-dependent acyltransferase that produces *N*-Acyl phosphatidylethanolamines. *Nat. Chem. Biol.* **12**, 669–671 (2016).
5. Hussain, Z. *et al.* Phosphatidylserine-stimulated production of *N*-acyl-phosphatidylethanolamines by Ca<sup>2+</sup>-dependent *N*-acyltransferase. *Biochim. Biophys. Acta - Mol. Cell Biol. Lipids* **1863**, 493–502 (2018).
6. Perisic, O., Fong, S., Lynch, D. E., Bycroft, M. & Williams, R. L. Crystal structure of a calcium-phospholipid binding domain from cytosolic phospholipase A<sub>2</sub>. *J. Biol. Chem.* **273**, 1596–1604 (1998).
7. Evans, J. H., Spencer, D. M., Zweifach, A. & Leslie, C. C. Intracellular Calcium Signals Regulating Cytosolic Phospholipase A<sub>2</sub> Translocation to Internal Membranes. *J. Biol. Chem.* **276**, 30150–30160 (2001).
8. Capestrano, M. *et al.* Cytosolic phospholipase A<sub>2</sub>ε drives recycling through the clathrin-independent endocytic route. *J. Cell Sci.* **127**, 977–993 (2014).
9. Basu, A., Prenc, E., Garrett, K., Glew, R. H. & Ellingson, J. S. Comparison of *N*-acyl phosphatidylethanolamines with different *N*-acyl groups as activators of glucocerebrosidase in various forms of Gaucher's disease. *Arch. Biochem. Biophys.* **243**, 28–34 (1985).
10. Domingo, J. C., Mora, M. & Africa de Madariaga, M. Incorporation of *N*-acylethanolamine phospholipids into egg phosphatidylcholine vesicles: characterization and permeability properties of the binary systems. *Biochim. Biophys. Acta - Biomembr.* **1148**, 308–316 (1993).
11. Térová, B., Petersen, G., Hansen, H. S. & Slotte, J. P. *N*-acyl phosphatidylethanolamines affect the lateral distribution of cholesterol in membranes. *Biochim. Biophys. Acta - Biomembr.* **1715**, 49–56 (2005).
12. Shangguan, T., Pak, C. C., Ali, S., Janoff, A. S. & Meers, P. Cation-dependent fusogenicity of an *N*-acyl phosphatidylethanolamine. *Biochim. Biophys. Acta* **1368**, 171–183 (1998).
13. Palese, F., Pontis, S., Realini, N. & Piomelli, D. NAPE-specific phospholipase D regulates LRRK2 association with neuronal membranes. in *Advances in Pharmacology* **90**, 217–238 (Academic Press Inc., 2021).
14. Gillum, M. P. *et al.* *N*-acylphosphatidylethanolamine, a Gut-Derived Circulating Factor Induced by Fat Ingestion, Inhibits Food Intake. *Cell* **135**, 813–824 (2008).
15. Wellner, N. *et al.* Studies on the anorectic effect of *N*-acylphosphatidylethanolamine and phosphatidylethanolamine in mice. *Biochim. Biophys. Acta - Mol. Cell Biol. Lipids* **1811**, 508–512 (2011).
16. Shiratsuchi, A. *et al.* Inhibitory effect of *N*-palmitoylphosphatidylethanolamine on macrophage phagocytosis through inhibition of Rac1 and Cdc42. *J. Biochem.* **145**, 43–50 (2008).
17. Epps, D. E., Natarajan, V., Schmid, P. C. & Schmid, H. H. O. Accumulation of *N*-acylethanolamine glycerophospholipids in infarcted myocardium. *Biochim. Biophys. Acta - Lipids Lipid Metab.* **618**, 420–430 (1980).



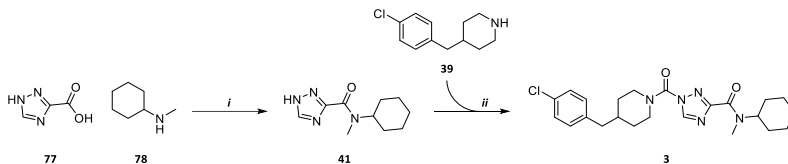
18. Kondo, S. *et al.* Accumulation of various *N*-acylethanolamines including *N*-arachidonylethanolamine (anandamide) in cadmium chloride-administered rat testis. *Arch. Biochem. Biophys.* **354**, 303–310 (1998).
19. Moesgaard, B., Petersen, G., Jaroszewski, J. W. & Hansen, H. S. Age dependent accumulation of *N*-acyl-ethanolamine phospholipids in ischemic rat brain: A  $^{31}\text{P}$  NMR and enzyme activity study. *J. Lipid Res.* **41**, 985–990 (2000).
20. Tsuboi, K. *et al.* Enzymatic formation of *N*-acylethanolamines from *N*-acylethanolamine plasmalogen through *N*-acylphosphatidylethanolamine-hydrolyzing phospholipase D-dependent and -independent pathways. *Biochim. Biophys. Acta - Mol. Cell Biol. Lipids* **1811**, 565–577 (2011).
21. Romano, A., Tempesta, B., Provensi, G., Passani, M. B. & Gaetani, S. Central mechanisms mediating the hypophagic effects of oleoylethanolamide and *N*-acylphosphatidylethanolamines: Different lipid signals? *Front. Pharmacol.* **6**, 1 (2015).
22. Gómez-Boronat, M. *et al.* Diurnal Profiles of *N*-Acylethanolamines in goldfish brain and gastrointestinal tract: Possible role of feeding. *Front. Neurosci.* **13**, 450 (2019).
23. Ahn, K. *et al.* Mechanistic and pharmacological characterization of PF-04457845: A highly potent and selective fatty acid amide hydrolase inhibitor that reduces inflammatory and noninflammatory pain. *J. Pharmacol. Exp. Ther.* **338**, 114–124 (2011).
24. Morena, M. *et al.* Upregulation of anandamide hydrolysis in the basolateral complex of amygdala reduces fear memory expression and indices of stress and anxiety. *J. Neurosci.* **39**, 1275–1292 (2019).
25. Cravatt, B. F. *et al.* Molecular characterization of an enzyme that degrades neuromodulatory fatty acid amides. *Nature* **384**, 83–87 (1996).
26. Hussain, Z., Uyama, T., Tsuboi, K. & Ueda, N. Mammalian enzymes responsible for the biosynthesis of *N*-acylethanolamines. *Biochim. Biophys. Acta - Mol. Cell Biol. Lipids* **1862**, 1546–1561 (2017).
27. Cadas, H., Gaillet, S., Beltramo, M., Venance, L. & Piomelli, D. Biosynthesis of an endogenous cannabinoid precursor in neurons and its control by calcium and cAMP. *J. Neurosci.* **16**, 3934–3942 (1996).
28. Uyama, T., Jin, X. H., Tsuboi, K., Tonai, T. & Ueda, N. Characterization of the human tumor suppressors TIG3 and HRASLS2 as phospholipid-metabolizing enzymes. *Biochim. Biophys. Acta - Mol. Cell Biol. Lipids* **1791**, 1114–1124 (2009).
29. Uyama, T. *et al.* Generation of *N*-acylphosphatidylethanolamine by members of the phospholipase A/acyltransferase (PLA/AT) family. *J. Biol. Chem.* **287**, 31905–31919 (2012).
30. Janssen, A. P. A. *et al.* Structure Kinetics Relationships and Molecular Dynamics Show Crucial Role for Heterocycle Leaving Group in Irreversible Diacylglycerol Lipase Inhibitors. *J. Med. Chem.* **62**, 7910–7922 (2019).
31. Van Esbroeck, A. C. M. *et al.* Activity-based protein profiling reveals off-target proteins of the FAAH inhibitor BIA 10-2474. *Science* **356**, 1084–1087 (2017).
32. Katritzky, A. R., Darabantu, M., Aslan, D. C. & Oniciu, D. C. Selective Reactivity of sp<sup>3</sup> and sp<sup>2</sup> Carbanions of 1-Substituted 1,2,4-Triazoles. A Comparative Approach. *J. Org. Chem.* **63**, 4323–4331 (1998).
33. Zhou, J. Development of a PLA2G4E Assay and Subsequent Application in Hit Identification. *Inhibitor Discovery of Phospholipase and N-Acyltransferase* (Leiden University, 2020).
34. Liu, Y., Patricelli, M. P. & Cravatt, B. F. Activity-based protein profiling: The serine hydrolases. *Proc. Natl. Acad. Sci.* **96**, 14694–14699 (1999).

35. Baggelaar, M. P. *et al.* Development of an activity-based probe and in silico design reveal highly selective inhibitors for diacylglycerol lipase- $\alpha$  in brain. *Angew. Chemie - Int. Ed.* **52**, 12081–12085 (2013).
36. Catalán, J. *et al.* Basicity and Acidity of Azoles: The Annulation Effect in Azoles. *J. Am. Chem. Soc.* **110**, 4105–4111 (1988).
37. Potts, K. T. The Chemistry of 1,2,4-Triazoles. *Chem. Rev.* **61**, 87–127 (1961).
38. Johnson, D. S. *et al.* Discovery of PF-04457845: A Highly Potent, Orally Bioavailable, and Selective Urea FAAH Inhibitor. *Chem. Lett* **2**, 91–96 (2011).
39. Uyama, T. *et al.* The tumor suppressor gene H-Rev107 functions as a novel Ca<sup>2+</sup>-independent cytosolic phospholipase A1/2 of the thiol hydrolase type. *J. Lipid Res.* **50**, 685–693 (2009).
40. Pang, X. Y. *et al.* Structure/function relationships of adipose phospholipase A<sub>2</sub> containing a Cys-His-His catalytic triad. *J. Biol. Chem.* **287**, 35260–35274 (2012).
41. Mercadal, M., Domingo, J. C., Bermudez, M., Mora, M. & De Madariaga, M. A. *N*-Palmitoylphosphatidylethanolamine stabilizes liposomes in the presence of human serum: effect of lipidic composition and system characterization. *Biochim. Biophys. Acta - Biomembr.* **1235**, 281–288 (1995).
42. Berger, C. *et al.* Massive accumulation of *N*-acylethanolamines after stroke. Cell signalling in acute cerebral ischemia? *J. Neurochem.* **88**, 1159–1167 (2004).
43. Zhou, J. *et al.* Structure-Activity Relationship Studies of  $\alpha$ -Ketoamides as Inhibitors of the Phospholipase A and Acyltransferase Enzyme Family. *J. Med. Chem.* **63**, 9340–9359 (2020).
44. Degoe, D. A., Chen, H. J., Cox, P. B. & Wendt, M. D. Beyond the Rule of 5: Lessons Learned from AbbVie's Drugs and Compound Collection. *J. Med. Chem.* **61**, 2636–2651 (2018).
45. Singh, S., Joshi, A. & Kamat, S. S. Mapping the Neuroanatomy of ABHD16A, ABHD12, and Lysophosphatidylserines Provides New Insights into the Pathophysiology of the Human Neurological Disorder PHARC. *Biochemistry* **59**, 2299–2311 (2020).
46. Kaczocha, M., Glaser, S. T. & Deutsch, D. G. Identification of intracellular carriers for the endocannabinoid anandamide. *Proc. Natl. Acad. Sci. U. S. A.* **106**, 6375–6380 (2009).
47. Palm, K., Luthman, K., Ungell, A. L., Strandlund, G. & Artursson, P. Correlation of Drug Absorption with Molecular Surface Properties. *J. Pharm. Sci.* **85**, 32–39 (1996).
48. Hitchcock, S. A. & Pennington, L. D. Structure-brain exposure relationships. *J. Med. Chem.* **49**, 7559–7583 (2006).
49. Laizure, S. C., Herring, V., Hu, Z., Witbrodt, K. & Parker, R. B. The Role of Human Carboxylesterases in Drug Metabolism: Have We Overlooked Their Importance? *Pharmacother. J. Hum. Pharmacol. Drug Ther.* **33**, 210–222 (2013).
50. Soethoudt, M. *et al.* Cannabinoid CB<sub>2</sub> receptor ligand profiling reveals biased signalling and off-target activity. *Nat. Commun.* **8**, (2017).

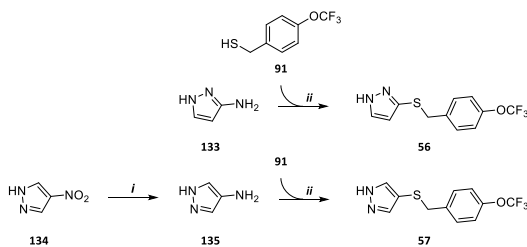
## Supplementary information



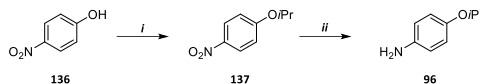
**Supplementary Scheme S4.1. Synthesis of 1,2,4-triazole building blocks 40, 45–54.** Reagents and conditions: i) K<sub>2</sub>CO<sub>3</sub>, DMF, 3 h RT; ii) SOCl<sub>2</sub>, cat. DMF, Et<sub>2</sub>O, 0/n 0°C → RT; iii) Isopropyl iodide, KI, K<sub>2</sub>CO<sub>3</sub>, DMF, 0/n 75°C; iv) NaBH<sub>4</sub>, THF:H<sub>2</sub>O, 0/n 0°C → RT.



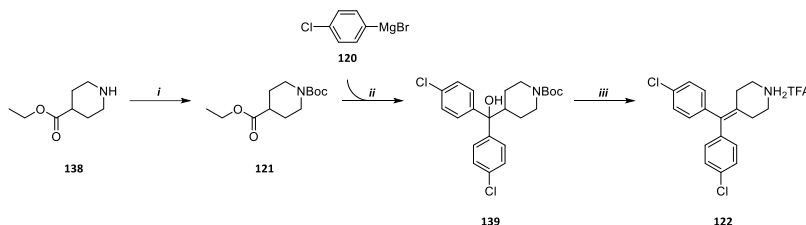
**Supplementary Scheme S4.2. Synthesis of triazole amide inhibitor 3.** Reagents and conditions: i) 1. **77**, SOCl<sub>2</sub>, cat. DMF, THF, 14 h reflux, then 2. **78**, DIPEA, DCM, > 110 h 0°C → RT; ii) 1. **39**, triphosgene, DIPEA, THF, 3 h 0°C → RT, then 2. **41**, K<sub>2</sub>CO<sub>3</sub>, DMF, 0/n RT.



**Supplementary Scheme S4.3. Synthesis of pyrazole building blocks 56 and 57.** Reagents and conditions: i) 1 atm H<sub>2</sub>, Pd/C, EtOH, 12 h RT; ii) 1. **133** or **135**, H<sub>2</sub>SO<sub>4</sub>, NaNO<sub>2</sub>, H<sub>2</sub>O, 30 min 0°C, then 2. **91**, NaOH, H<sub>2</sub>O, 1.5 h 0°C.



**Supplementary Scheme S4.4. Synthesis of aniline building block 96.** Reagents and conditions: *i*) Isopropyl bromide,  $K_2CO_3$ , o/n 120°C; *ii*)  $H_2$  (1 atm), Pd/C, HCl, MeOH, 5 h RT.



**Supplementary Scheme S4.5. Synthesis of amine building block 122.** Reagents and conditions: *i*)  $Et_3N$ , Boc<sub>2</sub>O, DCM, 50 h 0°C → RT; *ii*) THF, 4 d 0°C → RT; *iii*) TFA, DCM, 6 d RT.

**Supplementary Table S4.1. Physicochemical properties of 9, 19 and 30.** Potency on PLA2G4E determined using gel-based cABPP ( $N \geq 2$ ) <sup>a</sup>Molecular weight (MW) and topological polar surface area (tPSA) calculated using ChemDraw Professional 16.0; <sup>b</sup>Partition coefficient (clogP) calculated using DataWarrior 5.0.0; <sup>c</sup>HAC = number of heavy atoms; <sup>d</sup>HBA = number of hydrogen bond acceptors; <sup>e</sup>HBD = number of hydrogen bond donors; <sup>f</sup>RB = number of rotatable bonds; <sup>g</sup>Lipophilic efficiency LipE =  $pIC_{50} - clogP$ ; <sup>h</sup>Ligand efficiency LE =  $1.4pIC_{50}/HAC$ .

	$pIC_{50} \pm SEM$	MW (Da) <sup>a</sup>	tPSA (Å <sup>2</sup> ) <sup>a</sup>	clogP <sup>b</sup>	HAC <sup>c</sup>	HBA <sup>d</sup>	HBD <sup>e</sup>	RB <sup>f</sup>	LipE <sup>g</sup>	LE <sup>h</sup>
9	8.10 ± 0.02	543	92	4.98	36	8	0	8	3.12	0.32
19	7.04 ± 0.05	544	104	4.80	36	9	1	7	2.24	0.27
30	< 5.0	542	79	4.86	36	7	0	8	< 0.14	< 0.19

**Supplementary Table S4.2. CB<sub>1</sub> and CB<sub>2</sub> receptor binding by 9, 19 and 30.** Percentage displacement of [<sup>3</sup>H]CP55,940 by 1 μM of inhibitor expressed as mean ± SEM (N = 2).

	CB <sub>1</sub>	CB <sub>2</sub>
9	18 ± 14%	14 ± 22%
19	31 ± 7%	28 ± 20%
30	33 ± 8%	20 ± 23%



# 5

**Development of an activity-based  
probe that visualizes cellular  
PLA<sub>2</sub>G<sub>4</sub>E activity**

One of the important aspects of molecular biology is acquiring an understanding of the spatiotemporal function of enzymes.<sup>1,2</sup> Genetic abrogation of enzyme expression, such as accomplished with CRISPR-Cas9, is useful to investigate enzyme functions due to its high target specificity<sup>3</sup>, but does not provide temporal control and may disrupt multiple functionalities of the target because it completely removes a protein from the biological system.<sup>4-6</sup> Inhibitors allow acute modulation of enzyme activity, which enables the study of the physiological function of an enzyme in a dynamic fashion.<sup>5,7</sup> Because inhibitors may have multiple cellular targets, evidence of a direct interaction between the inhibitor molecule and the protein of interest, referred to as ‘target engagement’, is critical to assign the phenotypic effects observed to the studied enzyme.<sup>8-10</sup> In drug discovery, proof of target engagement in combination with a desired phenotypic effect is important to validate the protein as a drug target.<sup>8,11,12</sup> In addition, information about the drug concentration needed for full target engagement may help to determine the maximal dose required for efficacy with minimal side-effects.<sup>8,13</sup>

Activity-based protein profiling (ABPP) has become one of the key methodologies to determine enzyme activity in a physiological setting and can be used for target engagement studies.<sup>14,15</sup> ABPP makes use of an activity-based probe (ABP) that covalently engages with the catalytic residue and is equipped with a fluorescent or biotin reporter tag for visualization and identification purposes, respectively (Figure 5.1).<sup>16,17</sup> In a ‘two-step labeling’ approach, selective ligation of the probe to its reporter tag is executed after sample treatment to minimize the interference of a large reporter group with the probe’s activity and cell permeability (Figure 5.1).<sup>18</sup> In competitive ABPP, pre-treatment of samples with an inhibitor prevents the binding of the ABP, leading to a dose-dependent decrease in labeling. This provides evidence of target engagement by the inhibitor in cells and allows to determine its potency and selectivity in a single experiment.<sup>19-21</sup> Competitive ABPP is, therefore, a powerful method to investigate these critical drug properties in early drug discovery.

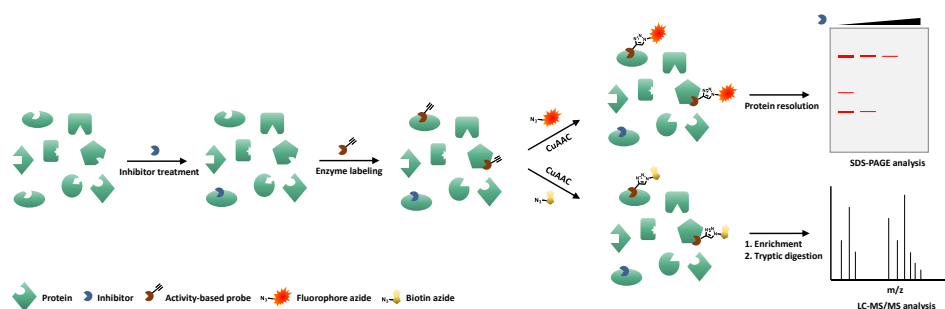


**Figure 5.1. Schematic overview of competitive ABPP workflow.** Cells or lysate are treated with inhibitor, followed by activity-based alkyne probe. After lysis, copper-catalyzed alkyne-azide cycloaddition (CuAAC) is used to attach a reporter group. SDS-PAGE and subsequent in-gel fluorescence scanning or probe target enrichment via biotin-streptavidin pull-down in combination with LC-MS/MS are used to analyze labeled enzymes.

PLA2G4E is a 868 amino acid (100 kDa) serine hydrolase (SH) that is one of the six known members of the group IV phospholipases (PLA2G4A–F).<sup>22,23</sup> These enzymes share common structural characteristics that include an N-terminal calcium-dependent lipid binding domain (C2) and a catalytic Ser-Asp dyad, which are important for their subcellular localization and catalytic activity.<sup>24,25</sup> PLA2G4E has an additional C-terminal polybasic domain (KKKRLK) which is involved in its localization.<sup>26</sup> While PLA2G4A–F all metabolize phospholipids, they have different activities, substrate preferences and expression patterns.<sup>23,24,27</sup> In 2016, PLA2G4E was reported to be an *N*-acyltransferase capable of producing *N*-acylphosphatidylethanolamines (NAPEs) from phosphatidylethanolamine (PE) and phosphatidylcholine (PC) in a calcium-dependent manner.<sup>28</sup> NAPEs are a low-abundant class of lipids that have both signaling and structural functionalities. They are involved in regulation of satiety<sup>29</sup> and have anti-inflammatory properties.<sup>30</sup> In addition, they modulate membrane dynamics by providing stability and stimulating fusion.<sup>31–33</sup> Via several pathways, NAPE hydrolysis leads to the formation of *N*-acylethanolamines (NAEs), a highly diverse family of signaling lipids.<sup>34–39</sup> Depending on the nature of their fatty acid substituent, NAEs are involved in a wide range of bioactivities, including nociception, anxiety, fertility, appetite, inflammation and memory formation.<sup>40–47</sup>

In previous chapters, competitive ABPP was applied to the discovery of inhibitors for PLA2G4E, using broad-spectrum serine hydrolase probe fluorophosphonate-tetramethylrhodamine (FP-TAMRA). **WEN091** was identified as a potent inhibitor of PLA2G4E *in vitro* ( $pC_{50} \pm SEM = 8.01 \pm 0.02$ , Chapter 2), which was able to reduce NAPE levels in a cellular PLA2G4E overexpression system and showed cellular activity on other serine hydrolases (Chapter 3). To confirm the physical, intracellular interaction between **WEN091** and PLA2G4E, a cell-permeable ABP targeting PLA2G4E is required. Here, the design and synthesis of ABP **1** and its application to study the cellular target engagement of **WEN091** is described.

## Results

### Design and synthesis of ABP **1**

The broad reactivity of FP-TAMRA and its charged fluorophore that compromises its cell permeability made this probe not suitable for cellular engagement studies.<sup>48,49</sup> Therefore, a new probe was required to study the cellular target engagement of PLA2G4E inhibitors. It was envisioned that compound **2**, a PLA2G4E inhibitor identified in Chapter 4, could serve as starting point for the design of a cell-permeable probe (Figure 5.2A). The electrophilic carbonyl of **2** is thought to bind to the catalytic serine of PLA2G4E and the triazole functions as a leaving group (Figure 5.2B). The benzylpiperidine acts as a 'staying group' and irreversibly carbamoylates the serine. Modification of the benzylpiperidine with a ligation handle would, therefore, allow visualization of the active enzyme by conjugation to a fluorescent reporter group. A commonly used ligation strategy involves bioorthogonal Huisgen 1,3-dipolar cycloaddition ('click' chemistry) of an azide and an alkyne, often



catalyzed by copper (also referred to as CuAAC).<sup>49</sup> It was envisioned that an alkyne could be incorporated at the *meta* position of the benzyl group, since substitution at this position was tolerated by PLA2G4E (e.g. compound **3**, Figure 5.2A, see also Chapter 2).

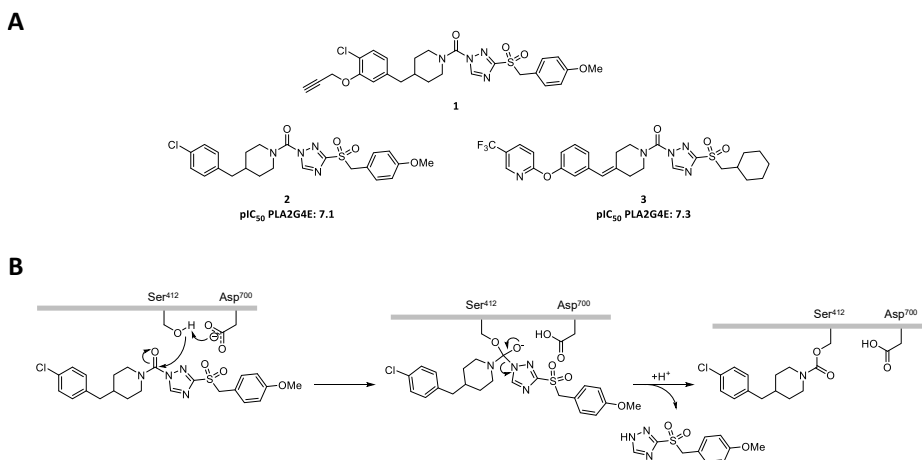


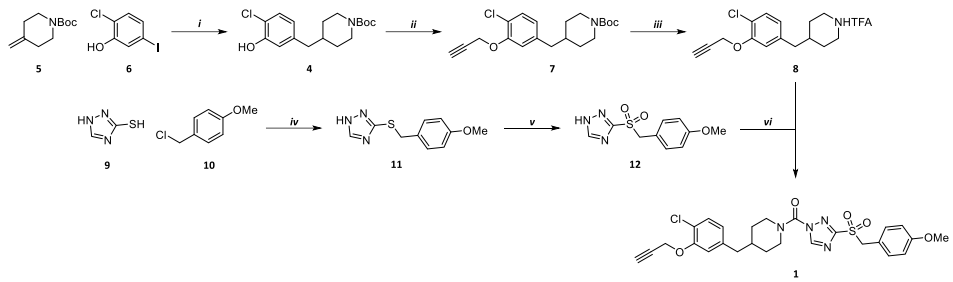
**Figure 5.2. Rationale of the design of PLA2G4E probe 1.** A) The design of **1** was based on the chemical structure of inhibitors **2** and **3**.  $pI_{C_{50}}$  values were determined with gel-based ABPP on PLA2G4E-HEK293T lysate. B) Hypothesized mechanism of PLA2G4E inhibition by **2**. PLA2G4E's nucleophilic residue Ser<sup>412</sup> is activated by Asp<sup>700</sup> and attacks the electrophilic carbonyl of **2**. The triazole moiety leaves, forming a stable adduct of the piperidine moiety on PLA2G4E.

Synthesis of ABP **1** was started with construction of benzylpiperidine **4** from 4-methylenepiperidine **5** and 2-chloro-5-iodophenol (**6**) via Suzuki-Miyaura cross-coupling (Scheme 5.1). Installation of the propargyl group (**7**) and Boc-deprotection yielded the piperidinium salt (**8**). In a parallel route, 1*H*-1,2,4-triazole-3-thiol (**9**) was benzylated with 4-methoxybenzyl chloride (**10**) to form **11** and subsequently oxidated with peracetic acid to sulfone **12**. Triphosgene-mediated urea formation between piperidine **8** and triazole **12** finally afforded ABP **1**.

### Biological characterization of PLA2G4E ABP **1**

#### **1** is an activity-based probe for PLA2G4E

The ability of **1** to inhibit PLA2G4E was assessed in a competitive ABPP experiment using FP-TAMRA. Briefly, PLA2G4E-overexpressing HEK293T cell lysate was treated with **1** at increasing concentrations (30 min), followed by FP-TAMRA (50 nM, 5 min). Sodium dodecyl sulfate-polyacrylamide gel electrophoresis (SDS-PAGE) and in-gel fluorescence scanning enabled determination of the apparent half maximal inhibitory concentration ( $IC_{50}$ ) of **1** to be 54 nM ( $pI_{C_{50}} \pm SEM = 7.27 \pm 0.02$ , Figure 5.3A, B). Of note, **1** did not inhibit overexpressed recombinant PLA2G4B-D up to 1–10  $\mu$ M (Figure 5.3C). To confirm the fluorescent labeling of PLA2G4E by **1**, overexpression lysate was treated with **1** (1  $\mu$ M, 30 min), followed by copper-catalyzed click conjugation of Cy5-azide to **1**. Resolution of the



**Scheme 5.1. Synthesis of 1.** Reagents and conditions: *i*) 1. **5**, 9-BBN, THF, 6 h 0°C → RT, then 2. **6**, K<sub>2</sub>CO<sub>3</sub>, Pd(dppf)Cl<sub>2</sub>, THF:DMF:H<sub>2</sub>O (1:1:0.1), o/n 60°C (84%); *ii*) Propargyl bromide, K<sub>2</sub>CO<sub>3</sub>, DMF, 48 h RT (quant.); *iii*) TFA, DCM, 21 h RT; *iv*) K<sub>2</sub>CO<sub>3</sub>, DMF, 5 h RT; *v*) AcOOH, DCM, o/n 0°C → RT (90%); *vi*) 1. **8**, triphosgene, DIPEA, THF, o/n 0°C → RT, then 2. **12**, K<sub>2</sub>CO<sub>3</sub>, DMF, o/n RT (48%).

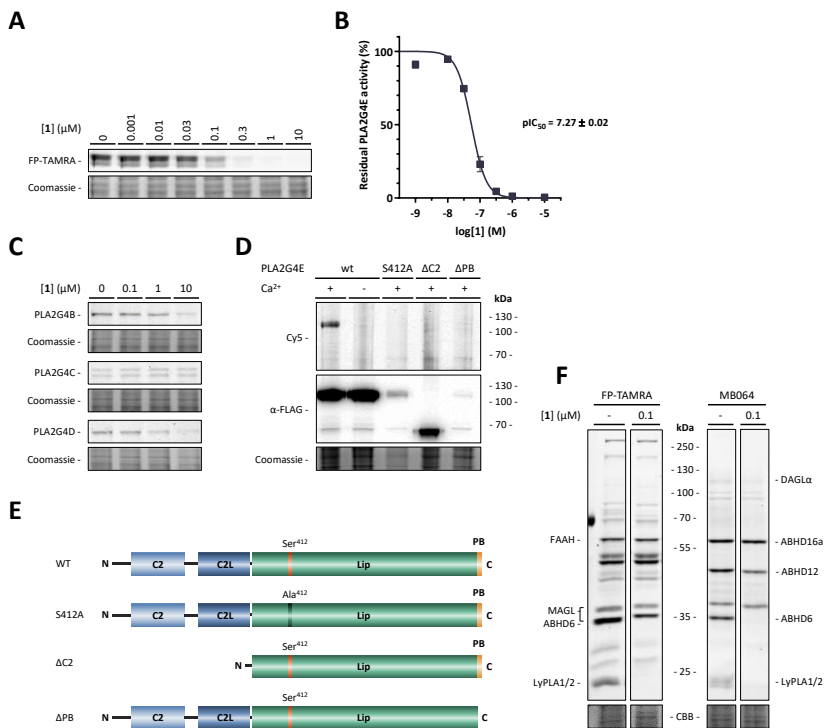


**Figure 5.3. Activity of 1 on PLA2G4E and related enzymes.** A) Representative gel excerpts of ABPP experiments on PLA2G4E overexpression lysate, using FP-TAMRA as ABP. B) Corresponding inhibition curve and pIC<sub>50</sub> value. Data reported as mean ± SEM (N = 3). C) Representative gel excerpts of ABPP experiments on PLA2G4B, PLA2G4C and PLA2G4D overexpression lysate, using FP-TAMRA as ABP. D) Activity-based labeling of recombinantly overexpressed wt and mutant PLA2G4E by **1** (1 μM). Excerpts of fluorescence image after CuAAC conjugation to Cy5, western blot and coomassie loading control. E) Schematic representation of PLA2G4E wt and mutant constructs used in this study, indicating the calcium-dependent lipid binding domain (C2), the C2-like domain (C2L), the lipase domain (Lip) with nucleophilic residue Ser<sup>412</sup> and polybasic stretch (PB). F) Representative gel excerpts of ABPP experiments on mouse brain membrane proteome, using FP-TAMRA and MB064 as ABPs.

proteins by SDS-PAGE and fluorescence scanning showed a fluorescent band at the expected MW of PLA2G4E (Figure 5.3D, first lane). No labeling was observed in the absence of  $\text{Ca}^{2+}$  (Figure 5.3D, second lane) or when the catalytic serine was mutated to an alanine (S412A) (third lane), indicating that labeling of PLA2G4E by **1** is dependent on its catalytic activity. In addition, mutants in which the C2 domain ( $\Delta\text{C2}$ ) or polybasic domain ( $\Delta\text{PB}$ ) were removed were not labeled by **1** (Figure 5.3D, E). This confirms and extends previous reports that these mutants were not active in a substrate-based assay.<sup>50</sup> Altogether, these results demonstrate that **1** can be used as an ABP to visualize the PLA2G4E activity.

The selectivity of **1** over other serine hydrolases was investigated using competitive ABPP on mouse brain membrane proteome as reported in Chapter 3. **1** (100 nM, 30 min) inhibited several other serine hydrolases, including  $\alpha/\beta$ -hydrolase domain-containing protein 6 (ABHD6), diacylglycerol lipase  $\alpha$  (DAGL $\alpha$ ) and protein thioesterases 1 and 2 (LyPLA1/2), while it partially inhibited ABHD12 (Figure 5.3F). NAE-degrading enzyme fatty acid amide hydrolase (FAAH) and monoacylglycerol lipase (MAGL) were not inhibited. Thus, compound **1** is a potent PLA2G4E ABP with limited serine hydrolase off-targets in mouse brain proteome.

#### Cellular activity of probe **1** confirmed *in situ* target engagement of inhibitor WEN091

The activity of **1** in a cellular system was investigated using mouse neuroblastoma cell line Neuro-2a. In brief, Neuro-2a cells were transiently transfected with recombinant human PLA2G4E or mock plasmid. The cells were incubated with **1** at various concentrations for 30 min, harvested and lysed. The resulting homogenate was subjected to CuAAC using Cy5-azide followed by SDS-PAGE to enable visualization of PLA2G4E labeling. With increasing concentration of **1**, a band at the MW of PLA2G4E was fluorescently labeled in overexpressing cells, but not in mock (Figure 5.4A). This indicated **1** was able to engage with and label PLA2G4E in the overexpressing cells. Of note, a second band (~37 kDa) is dose-dependently labeled, but also in mock. This probably indicated engagement of **1** with an off-target protein in Neuro-2a cells. Thus, **1** is a cellular active ABP that can be used to visualize the intracellular activity of PLA2G4E.

Next, Neuro-2a cells overexpressing PLA2G4E were pre-treated with inhibitor **WEN091** (30 min) followed by treatment with **1** (1  $\mu\text{M}$ , 30 min). Cells were then lysed and the resulting homogenate was subjected to CuAAC. **WEN091** dose-dependently inhibited labeling of PLA2G4E by **1** ( $\text{pIC}_{50} = 6.47 \pm 0.19$ , Figure 5.4C, D) achieving full inhibition at 10  $\mu\text{M}$ . These results proved the intracellular engagement of **WEN091** with PLA2G4E.

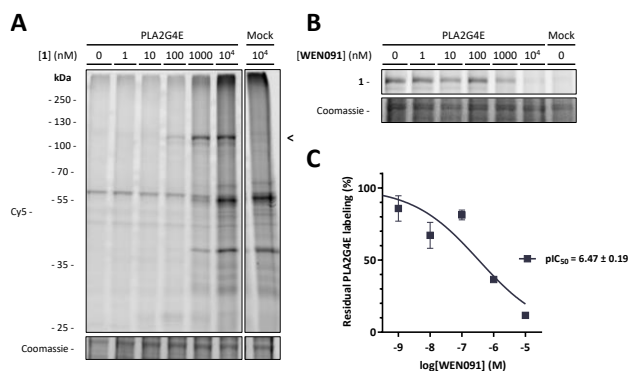


**Figure 5.4. Activity on and labeling of PLA2G4E in Neuro-2a cells by ABP 1.** A) Labeling of PLA2G4E- and mock-transfected Neuro-2a cells by **1** (30 min). **1** was clicked to Cy5-N<sub>3</sub> after cell lysis. Band of PLA2G4E is indicated with an arrow. B) Intracellular PLA2G4E labeling by **1** (1 μM, 30 min) is dose-dependently outcompeted by **WEN091** (30 min). **1** was clicked to Cy5-N<sub>3</sub> after cell lysis. C) Corresponding inhibition curve and pIC<sub>50</sub> value of **WEN091**. Data reported as mean ± SEM (N = 4).

## Discussion and conclusions

In drug discovery, cellular target engagement studies are important to correlate the phenotypic effects of an inhibitor to its presumed mode of action. It helps to validate the protein as a drug target and provides information about the dose required for full target occupancy.<sup>10,12,13</sup> **WEN091** was identified as a nanomolar potent inhibitor of PLA2G4E in biochemical assays (Chapter 2), but lowered (lyso)-NAPE levels in PLA2G4E-overexpressing Neuro-2a cells only at micromolar concentrations (Chapter 3). This discrepancy may suggest that **WEN091** has restricted cell permeability and/or limited engagement with PLA2G4E in a cellular setting. Here, cellular PLA2G4E ABP **1** (**WEN175**) was developed to address this question.

Compound **1** was able to label PLA2G4E in a dose-dependent manner. It did not label PLA2G4E in the absence of calcium, demonstrating the activity-dependent nature of the probe. Furthermore, it did not label PLA2G4E-S412A, confirming Ser<sup>412</sup> to be the catalytic residue.<sup>50</sup> **1** was able to visualize cellular PLA2G4E activity, and using **1**, it was determined that **WEN091** intracellularly engaged with PLA2G4E with pIC<sub>50</sub> = 6.47 ± 0.17. This shows that **WEN091** is cell-permeable, but that it is more than 30-fold less potent in a cellular setting. Full target engagement was achieved at 10 μM, which is in line with the lipidomics measurements that showed (lyso)-NAPE reduction at >10 μM (Chapter 3). High cellular levels of substrates PE and PC that compete for interaction with PLA2G4E may explain this reduced activity of **WEN091** in cells.<sup>51</sup> These results also indicate that biochemical assays *in vitro* may overestimate a compound's activity and emphasize the importance of cellular target engagement assays to guide the development of inhibitors.

Projecting forward, ABP **1** can potentially be used to detect endogenous PLA2G4E activity in cells and tissues and to investigate its activity under (patho)physiological conditions. For example, NAPEs are highly elevated in ischemic tissue, possibly as a cytoprotective mechanism.<sup>52-54</sup> It is envisioned that **1** could be employed to visualize PLA2G4E activity under normal and ischemic conditions using chemical proteomics to investigate the role of PLA2G4E in this process. Calcium-independent NAPE producing enzymes phospholipase A/acyltransferase (PLAAT) 1 and PLAAT5 share a similar expression profile to PLA2G4E.<sup>55,56</sup> Quantification of PLA2G4E activity using ABP **1** will help to elucidate the contribution of PLA2G4E to NAPE production in healthy and ischemic tissue. Visualizing the subcellular localization of active PLA2G4E using **1** and a fluorescent reporter tag may show whether PLA2G4E, similar to PLA2G4A, translocates before activation.<sup>57-59</sup> The C2 domain is thought to regulate the subcellular localization of PLA2G4 family members and to be involved in enzyme activity through interactions with substrate lipids in cellular membranes.<sup>57-60</sup> PLA2G4E's PB domain was previously demonstrated to be involved in the enzyme's localization towards membranes of the endocytic recycling machinery.<sup>26</sup> Here, however, both the C2 and PB domain were needed for probe binding in lysate, indicating a more direct involvement of these domains in PLA2G4E's activity.

A drawback of ABP **1** is that it targets multiple other serine hydrolases, which might hamper the identification of endogenous PLA2G4E using gel-based ABPP or microscopy. Future optimization of this chemical series may lead to more specific probes suitable for microscopy experiments.

In conclusion, we report **1** as the first cell-permeable activity-based probe that was used to confirm the intracellular activity of PLA2G4E in an overexpression system and to prove intracellular target engagement of PLA2G4E inhibitor **WEN091**.

## Acknowledgements

Lian van den Berg, Sanne Uitenbroek, Hans den Dulk and Tom van der Wel are kindly acknowledged for plasmid cloning and purification, Hans van den Elst for HRMS analysis.

## Experimental procedures

### General remarks

All chemicals and reagents for biochemical experiments were purchased from Thermo Fisher Scientific or Bio-Rad, unless noted otherwise. Activity-based probes were purchased from Thermo Fisher Scientific (FP-TAMRA) or synthesized in-house (MB064)<sup>21</sup>.

### Plasmids

The full-length cDNA of wild type human PLA2G4E (GenScript Biotech), murine PLA2G4B, hPLA2G4C and mPLA2G4D (Source BioScience) were cloned into a pcDNA™3.1(+) expression vector in-frame with a C-terminal FLAG tag. PLA2G4E mutants were generated by PCR amplification using the primers listed in Supplementary Table S5.1. Purified PCR products were cloned into pcDNA™3.1(+) in-frame with a C-terminal FLAG tag. Plasmids were isolated from transformed *Escherichia coli* XL-10 using a Qiagen Plasmid Midi kit and stored at 4°C in TE buffer (10 mM Tris, 0.1 mM EDTA, pH 8.0). The sequence was determined (Macrogen) and verified using CLC Main Workbench.

Supplementary Table S5.1. Oligonucleotides used for generating PLA2G4E mutant constructs.

Construct name	Direc.	Sequence	Restriction site used
PLA2G4E-S412A	fw	5'-ATCGTCTCACCGGTATGAGTCTCCAGGCCTCGGAAGGC-3'	Kpn2I
	rev	5'-CATCTCTAGACTACGTACGCTCGAGCTTATCGTCGTCATCCTTGAATC-3'	Pfl23II
PLA2G4E-ΔC2	fw	5'-CATGGTACCGCCACCATGGTGCGGCTGGGCTCAGCCT-3'	Acc65I
	rev	5'-CATCTCTAGACTACGTACGCTCGAGCTTATCGTCGTCATCCTTGAATC-3'	XhoI
PLA2G4E-ΔPB	fw	5'-CTTAAGCTTTACCGGTACCGCCACCATGAGTCTCCAGGCCTCGGAAGGC-3'	Acc65I
	rev	5'-CTACGTACGCTCGAGCTTATCGTCGTCATCCTTGAATCCTCCACTGCGAGCCGACAGGCC-3'	XhoI

### Cell culture

HEK293T (human embryonic kidney) and Neuro-2a (murine neuroblastoma) cells (ATCC) were cultured in Dulbecco's Modified Eagle's Medium (DMEM, Sigma-Aldrich D6546) with additional heat-inactivated new-born calf serum (10% (v/v), Avantor Seradigm), L-Ala-L-Gln (2 mM, Sigma-Aldrich), penicillin and streptomycin (both 200 µg/mL, Duchefa Biochemie) at 37°C, 7% CO<sub>2</sub>. Medium was refreshed every 2–3 days and cells were passaged twice a week at 70–80% confluence by aspirating the medium, thorough pipetting in fresh medium and seeding to appropriate density. Cell cultures were regularly tested for mycoplasma and discarded after 2–3 months.

### HEK293T membrane preparation

One day prior to transfection, 10<sup>7</sup> HEK293T cells were seeded to a 15 cm dish. Upon transfection, medium was aspirated and replaced by 13 mL fresh medium. Plasmid DNA (20 µg per 15 cm dish) and PEI (60 µg per 15 cm dish) were separately dissolved in 1 mL DMEM without serum per dish, combined, incubated for 15 min and added dropwise to the cells. 24 h p.t. medium was replaced by 25 mL fresh medium. 72 h p.t. medium was aspirated and the cells were washed with RT Dulbecco's PBS (DPBS, Sigma-Aldrich D8537), harvested in DPBS and centrifuged (3000 × *g*, 15 min, RT). Cell pellets were flash-frozen in liquid N<sub>2</sub> and stored at –80°C until use.

HEK293T cell pellets were thawed on ice and homogenized in 2 mL ice-cold lysis buffer (50 mM Tris-HCl, 2 mM DTT, 1 mM MgCl<sub>2</sub>, 5 U/mL Benzonase® (Santa Cruz Biotechnology, Inc.), pH 8.0 with additional 3 mM CaCl<sub>2</sub> for PLA2G4E) per 15 cm cell culture dish using a Sonics® Vibra-Cell VXC 130 probe sonicator equipped with a 2 mm microtip (3 × 10 s on/10 s off, 20% amplitude). After incubation on ice for 30 min the insoluble ("membrane") fraction was separated from the soluble ("cytosol") fraction by ultracentrifugation (10<sup>5</sup> × *g*, 35 min, 4°C, Beckman-Coulter ultracentrifuge, Ti70.1 rotor).

The pellet was resuspended in 1 mL ice-cold storage buffer (50 mM Tris-HCl, 2 mM DTT, pH 8.0 with additional 3 mM CaCl<sub>2</sub> for PLA2G4E) per 15 cm plate and homogenized by passing through an insulin needle. After determination of the protein concentration using a Quick Start™ Bradford Protein Assay (Bio-Rad) the samples were diluted to 1.0 mg/mL in ice-cold storage buffer, aliquoted to single-use volumes, flash-frozen in liquid N<sub>2</sub> and stored at –80°C until further use.

### Mouse brain lysate preparation

For ABPP experiments, mouse brains were harvested from surplus C57Bl/6J mice (8–14 weeks old) according to guidelines approved by the ethical committee of Leiden University (AVD1060020171144), immediately flash-frozen in liquid N<sub>2</sub> and stored at –80°C until use. Upon preparation, intact brains were thawed on ice and homogenized in 6 mL ice-cold lysis buffer (20 mM HEPES, 2 mM DTT, 250 mM sucrose, 1 mM MgCl<sub>2</sub>, 25 U/mL Benzonase®, pH 6.8) using a Wheaton™ dounce homogenizer (DWK Life Sciences) and incubated on ice for 1 h. Cell debris was removed by low-speed centrifugation (170 × *g*, 5 min, 4°C), after which the supernatant was subjected to ultracentrifugation to separate membrane and cytosol fractions. The pellet was resuspended in ice-cold storage buffer (20 mM HEPES, 2 mM DTT, pH 6.8) and homogenized by passing through an insulin needle. The protein concentrations of both fractions were determined using a Quick Start™ Bradford Protein Assay and samples were diluted to 2.0 mg/mL (membrane) or 1.0 mg/mL (cytosol) using ice-cold storage buffer, aliquoted to single-use volumes, flash-frozen in liquid N<sub>2</sub> and stored at –80°C until use.

### Activity-based protein profiling

HEK293T or mouse brain lysates were thawed on ice. 19.5 μL lysate was incubated with 0.5 μL inhibitor solution in DMSO (Sigma-Aldrich) for 30 min (RT), followed by addition of 0.5 μL probe in DMSO (PLA2G4E: FP-TAMRA, 50 nM, 5 min; PLA2G4B, PLA2G4C, PLA2G4D: FP-TAMRA, 500 nM, 20 min; mouse brain: FP-TAMRA, 500 nM, 20 min or MB064, 250 nM, 20 min, RT. Final DMSO concentration 5% (v/v)). The reaction was quenched by addition of 7 μL 4× Laemmli sample buffer (240 mM Tris, 8% (w/v) SDS, 40% (v/v) glycerol, 5% (v/v) β-mercaptoethanol (Sigma-Aldrich), 0.04% bromophenol blue) and incubation for 15 min at RT. 10 μL sample was resolved on 8% (PLA2G4E) or 10% (PLA2G4B, PLA2G4C, PLA2G4D, mouse brain) acrylamide SDS-PAGE gels (180 V, 75 min) and the gel was imaged on a Bio-Rad Chemidoc MP using Cy3/TAMRA settings (ex. 532/12 nm, em. 602/50 nm). Coomassie Brilliant Blue (CBB) R250 staining was used for total protein loading correction.

For ABPP on PLA2G4E mutants, 19.5 μL HEK293T overexpression lysate without DTT was treated with 0.5 μL **1** in DMSO for 30 min (RT), followed by addition of 2.2 μL freshly-prepared 'click mix' (i.e. 13 mM CuSO<sub>4</sub>, 2.6 mM tris(3-hydroxypropyl)triazolylmethyl)amine (THPTA), 95 μM Cy5-N<sub>3</sub> and 13 mM tris(2-carboxyethyl)phosphine (TCEP) combined in this order and mixed thoroughly). The ABPP mixture was shaken (800 rpm) for 30 min at 37°C, after which the reaction was quenched and proteins were resolved as described above. After imaging, proteins on the top half of the gel were transferred onto a 0.2 μM polyvinylidene fluoride (PVDF) membrane using a Trans-Blot Turbo Transfer system (Bio-Rad) and subsequently treated with anti-FLAG antibody (mouse, Sigma-Aldrich F3165) and horse radish peroxidase (HRP)-conjugated secondary antibody (m-IgGκ BP-HRP, Santa Cruz Biotechnology, Inc. sc-516102). Blots were developed using Clarity Western ECL Substrate (Bio-Rad). The bottom half of the gel was used for total protein loading correction using CBB. Images were analyzed using Bio-Rad Image Lab 6. IC<sub>50</sub> calculations were performed in GraphPad Prism 7.

## Cellular target engagement assay

Three days prior to the experiment, Neuro-2a cells were seeded to 12-wells plates plates ( $\sim 0.25 \cdot 10^6$  cells per well). One day later, medium was aspirated and replaced by 400  $\mu\text{L}$  fresh medium. PLA2G4E or mock plasmid DNA (1  $\mu\text{g}$  per well) and PEI (5  $\mu\text{g}$  per well) were separately dissolved in 50  $\mu\text{L}$  DMEM without serum per well, combined, incubated for 15 min and added dropwise to the cells. 24 h p.t., medium was replaced by 1 mL fresh medium per well. 48 h p.t., the experiment was started and medium was aspirated and cells were washed with RT DPBS. For competition experiments, 400  $\mu\text{L}$  DMEM without serum with **WEN091** in DMSO (0.25% (v/v) DMSO) was added and cells were incubated for 30 min at 37°C. Medium was aspirated and 400  $\mu\text{L}$  DMEM without serum with **1** in DMSO (0.25% (v/v) DMSO) was added and cells were incubated for 30 min at 37°C. Then medium was aspirated and cells were washed with RT DPBS. Cells were harvested in ice-cold DPBS by thorough pipetting and centrifuged (1000  $\times$  g, 6 min, RT). Pellets were flash-frozen in liquid  $\text{N}_2$  and stored at  $-80^\circ\text{C}$  until further use.

Cell pellets were thawed on ice and lysed in 50  $\mu\text{L}$  lysis buffer (50 mM Tris-HCl, 2 mM DTT, 250 mM sucrose, 3 mM  $\text{CaCl}_2$ , 1 mM  $\text{MgCl}_2$ , 10 U/mL Benzonase®, pH 8.0). After incubation on ice for 20 min, the protein concentration was determined using Quick Start™ Bradford Protein Assay and the samples were diluted to 1.0 mg/mL using lysis buffer. 20  $\mu\text{L}$  of this whole lysate was treated with 2  $\mu\text{L}$  freshly prepared click mix (1.35 mM  $\text{CuSO}_4$ , 8.8 mM sodium ascorbate, 0.14 mM THPTA, 4.9  $\mu\text{M}$  Cy5- $\text{N}_3$ ) and the mixture was incubated for 1 h at 37°C. Reactions were then quenched with 8  $\mu\text{L}$  4 $\times$  Laemmli sample buffer and proteins were resolved and images analyzed as described under Activity-based protein profiling.

## Organic synthesis

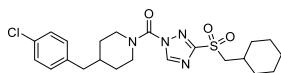
### General remarks

All chemicals were purchased from Sigma-Aldrich, Combi-Blocks, Alfa Aesar or Fluorochem, common salts from Sigma-Aldrich or Chem-Lab and solvents from Sigma-Aldrich or Honeywell Riedel-de Haën and used without further purification. All moisture-sensitive reactions were carried out in solvents dried over heat-activated molecular sieves (4 Å, Sigma-Aldrich), using flame-dried glassware under an atmosphere of  $\text{N}_2$ . TLC analysis was performed on Merck silica gel 60 F<sub>254</sub> aluminum TLC plates, on which compounds were visualized under 254 or 366 nm UV light and using  $\text{KMnO}_4$  (30 mM  $\text{KMnO}_4$ , 180 mM  $\text{K}_2\text{CO}_3$  in water) or ninhydrin (7.5 mM ninhydrin, 10% (v/v) AcOH in EtOH) stain. Flash column chromatography was performed using  $\text{SiO}_2$  (Macherey-Nagel, 60 M) as stationary phase.

NMR spectra were recorded on a Bruker AV-400 MHz spectrometer at 400 MHz ( $^1\text{H}$ ) and 101 MHz ( $^{13}\text{C}$ ), using  $\text{CDCl}_3$  or MeOD (Eurisotop) as solvent. Chemical shifts are reported in ppm with TMS ( $^1\text{H}$   $\text{CHCl}_3$ ,  $\delta$  0.00) or solvent resonance ( $^1\text{H}$  MeOD,  $\delta$  3.31;  $^{13}\text{C}$  MeOD,  $\delta$  49.00;  $^{13}\text{C}$   $\text{CHCl}_3$ ,  $\delta$  77.16) as internal standard. Data are reported as follows: chemical shift  $\delta$  (ppm), multiplicity (s = singlet, d = doublet, t = triplet, dd = doublet of doublets, td = triplet of doublets, qd = quartet of doublets, dt = doublet of triplets, bs = broad singlet ( $^1\text{H}$ ), br = broad ( $^{13}\text{C}$ ), m = multiplet), coupling constants  $J$  (Hz) and integration. HPLC/MS analysis was performed on a Finnigan Surveyor HPLC system equipped with a Macherey-Nagel NUCLEODUR C<sub>18</sub> Gravity, 5  $\mu\text{m}$ , 50  $\times$  4.6 mm column followed by a Thermo Scientific LTQ Orbitrap XL spectrometer, using  $\text{H}_2\text{O}/\text{CH}_3\text{CN}$  + 1% TFA as mobile phase. All compounds used for biological experiments were  $\geq 95\%$  pure based on LC/MS UV absorbance.

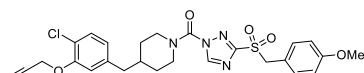


**(4-(4-Chlorobenzyl)piperidin-1-yl)(3-((cyclohexylmethyl)sulfonyl)-1H-1,2,4-triazol-1-yl)methanone (WEN091)**



The title compound was synthesized as described in Chapter 2.

**(4-(4-Chloro-3-(prop-2-yn-1-yloxy)benzyl)piperidin-1-yl)(3-((4-methoxybenzyl)sulfonyl)-1H-1,2,4-triazol-1-yl)methanone (1, WEN175)**



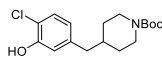
To an ice-cold solution of triphosgene (3 eq, 400 mg, 1.35 mmol) and DIPEA (3 eq, 234  $\mu$ L, 1.34 mmol) in dry THF (5 mL), **9** (1 eq, 169 mg, 0.45 mmol) dissolved in dry THF (10 mL) was added dropwise over the course of 20 min. The mixture was stirred on ice for 1 h before it was allowed to warm to RT and stirred overnight. When TLC analysis confirmed full conversion the mixture was diluted with EtOAc and washed with water and brine. The organic layer was dried over  $MgSO_4$ , filtrated and concentrated *in vacuo*. Water was removed by co-evaporation with toluene, after which the resulting dark green oil was dissolved in dry DMF (6 mL). **13** (1.2 eq, 136 mg, 0.54 mmol) and  $K_2CO_3$  (3 eq, 188 mg, 1.36 mmol) were added and the mixture was stirred overnight. The mixture was diluted with EtOAc and washed with water and brine. The organic layer was dried over  $MgSO_4$ , filtrated and concentrated *in vacuo*. Flash column chromatography (20  $\rightarrow$  60% EtOAc in pentane) afforded the title compound as pale yellow sticky oil (117 mg, 0.22 mmol, 48%).

$^1H$  NMR (400 MHz,  $CDCl_3$ )  $\delta$  8.84 (s, 1H), 7.28 (d,  $J$  = 8.0 Hz, 1H), 7.20 – 7.12 (m, 2H), 6.88 (d,  $J$  = 1.8 Hz, 1H), 6.83 – 6.76 (m, 2H), 6.74 (dd,  $J$  = 8.1, 1.8 Hz, 1H), 4.79 (d,  $J$  = 2.3 Hz, 2H), 4.55 (s, 2H), 4.42 – 4.26 (m, 1H), 4.15 – 3.94 (m, 1H), 3.70 (s, 2H), 2.98 – 2.83 (m, 2H), 2.67 (t,  $J$  = 2.4 Hz, 1H), 2.60 – 2.49 (m, 3H), 1.88 – 1.72 (m, 2H), 1.66 – 1.55 (m, 1H), 1.45 – 1.14 (m, 2H).

$^{13}C$  NMR (101 MHz,  $CDCl_3$ )  $\delta$  160.50, 160.12, 152.62, 148.00, 146.94, 139.44, 132.14, 130.08, 122.83, 120.75, 118.06, 115.29, 114.19, 76.84, 76.60, 59.99, 56.63, 55.12, 47.06 (br), 45.98 (br), 42.20, 37.58, 31.50 (br).

HRMS:  $[M+NH_4]^+$  calculated for  $C_{26}H_{27}ClN_4O_5S + NH_4^+$  560.17289, found 560.17282.

**tert-Butyl 4-(4-chloro-3-hydroxybenzyl)piperidine-1-carboxylate (4)**

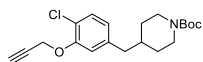


To an ice-cold solution of *N*-Boc 4-methylenepiperidine (**5**, 1 eq, 1.03 mL, 5.06 mmol) in degassed dry THF (20 mL), 9-BBN (1.4 eq, 14 mL 0.5 M in THF, 7.0 mmol) was added dropwise. The reaction was allowed to warm to RT and stirred for 6 h. In the meantime, a three-neck flask equipped with a reflux condenser was charged with  $K_2CO_3$  (1.5 eq, 1.05 g, 7.60 mmol), 2-chloro-5-iodophenol (**6**, 1.6 eq, 2.0 g, 7.86), DMF (20 mL) and water (2 mL) and purged with  $N_2$ . When TLC analysis confirmed full conversion, the reaction mixture was added to the three-neck flask and purging was continued for 30 min.  $Pd(dppf)Cl_2$  (0.01 eq, 37 mg, 0.051 mmol) was added, upon which the mixture turned dark red, and the reaction was stirred overnight at 60°C under continuous  $N_2$  flow. The mixture was allowed to cool to RT, diluted with  $Et_2O$  and washed with 1 M aq. NaOH. The pH of the aqueous layer was neutralized with 12 M hydrochloric acid before the aqueous layer was extracted with  $Et_2O$ . The combined organic layers were washed with brine, dried over  $MgSO_4$ , filtrated and concentrated *in vacuo*. Flash column chromatography (0  $\rightarrow$  35% EtOAc in pentane) afforded the title compound as off-white crystalline solid (1.38 g, 4.25 mmol, 84%).

$^1\text{H}$  NMR (400 MHz,  $\text{CDCl}_3$ )  $\delta$  7.20 (d,  $J$  = 8.1 Hz, 1H), 6.80 (d,  $J$  = 2.0 Hz, 1H), 6.63 (dd,  $J$  = 8.1, 2.0 Hz, 1H), 4.17 – 4.03 (m, 3H), 2.69 – 2.58 (m, 2H), 2.45 (d,  $J$  = 6.9 Hz, 2H), 1.97 – 1.76 (m, 1H), 1.71 – 1.55 (m, 2H), 1.45 (s, 9H), 1.12 (qd,  $J$  = 13.0, 12.5, 3.9 Hz, 2H).

$^{13}\text{C}$  NMR (101 MHz,  $\text{CDCl}_3$ )  $\delta$  155.08, 151.47, 140.99, 128.88, 122.04, 117.62, 116.97, 79.63, 44.03, 42.67, 38.05, 31.97, 28.57.

#### **tert-Butyl 4-(4-chloro-3-(prop-2-yn-1-yloxy)benzyl)piperidine-1-carboxylate (7)**



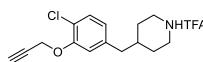
**4** (1 eq, 345 mg, 1.06 mmol) and  $\text{K}_2\text{CO}_3$  (2.2 eq, 321 mg, 2.32 mmol) were dissolved in dry DMF (10 mL) and stirred for 0.5 h. Propargyl bromide (2.2 eq, 248  $\mu\text{L}$ , 2.30 mmol) was added carefully and the mixture was stirred for 48 h.

When TLC analysis confirmed full conversion water and the mixture was extracted with EtOAc. The combined organic layers were washed with water and brine, dried over  $\text{MgSO}_4$ , filtrated and concentrated *in vacuo*. Flash column chromatography (0  $\rightarrow$  30% EtOAc in pentane) afforded the title compound as colorless oil (381 mg, 1.05 mmol, quant.).

$^1\text{H}$  NMR (400 MHz,  $\text{CDCl}_3$ )  $\delta$  7.27 (d,  $J$  = 8.0 Hz, 1H), 6.86 (d,  $J$  = 1.8 Hz, 1H), 6.73 (dd,  $J$  = 8.0, 1.8 Hz, 1H), 4.78 (d,  $J$  = 2.4 Hz, 2H), 4.07 (dt,  $J$  = 13.3, 2.6 Hz, 2H), 2.63 (td,  $J$  = 13.3, 2.2 Hz, 2H), 2.54 (t,  $J$  = 2.4 Hz, 1H), 2.52 (d,  $J$  = 6.9 Hz, 2H), 1.71 – 1.57 (m, 3H), 1.45 (s, 9H), 1.14 (qd,  $J$  = 13.1, 4.6 Hz, 2H).

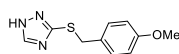
$^{13}\text{C}$  NMR (101 MHz,  $\text{CDCl}_3$ )  $\delta$  154.97, 152.82, 140.32, 130.18, 123.24, 120.92, 115.52, 79.44, 78.21, 76.27, 58.25, 56.89, 44.03, 42.99, 38.26, 32.00, 28.59.

#### **4-(4-Chloro-3-(prop-2-yn-1-yloxy)benzyl)piperidin-1-ium 2,2,2-trifluoroacetate (8)**



Trifluoroacetic acid (10 eq, 445  $\mu\text{L}$ , 4.48 mmol) was added dropwise to an ice-cold solution of **7** (1 eq, 163 mg, 0.45 mmol) in dry DCM (20 mL), after which the mixture was allowed to warm to RT and stirred for 21 h. When TLC analysis confirmed complete conversion, all volatiles were removed under reduced pressure, affording the title compound without further purification.

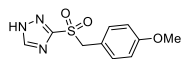
#### **3-((4-Methoxybenzyl)thio)-1H-1,2,4-triazole (11)**



**1H-1,2,4-triazole-3-thiol (9)**, 1.1 eq, 1.01 g, 9.99 mmol) and  $\text{K}_2\text{CO}_3$  (1.1 eq, 1.4 g, 10 mmol) were dissolved in dry DMF (20 mL) and stirred for 0.5 h. 4-Methoxybenzyl chloride (**10**, 1 eq, 1.2 mL, 8.9 mmol) was added dropwise and the mixture was stirred for 5 h. EtOAc and water were added and the layers were separated. The aqueous layer was extracted with EtOAc, after which the combined organic layers were washed with water and brine, dried over  $\text{MgSO}_4$ , filtrated and concentrated *in vacuo*. The residue was dissolved in a small amount of EtOAc and put at  $-30^\circ\text{C}$  for 7 days, affording part of the title compound as white crystals (514 mg, 2.32 mmol, 23%) while the remaining residue was stored.

$^1\text{H}$  NMR (400 MHz,  $\text{CDCl}_3$ )  $\delta$  13.68 (bs, 1H), 8.15 (s, 1H), 7.23 – 7.14 (m, 2H), 6.80 – 6.69 (m, 2H), 4.28 (s, 2H), 3.70 (s, 3H).

$^{13}\text{C}$  NMR (101 MHz,  $\text{CDCl}_3$ )  $\delta$  158.93, 147.07, 130.02, 128.54, 113.96, 55.18, 37.01.

**3-((4-Methoxybenzyl)sulfonyl)-1*H*-1,2,4-triazole (12)**

AcOOH (5 eq, 2.2 mL 35–40% in AcOH, 11.6 mmol) was added dropwise to an ice-cold solution of **11** (1 eq, 514 mg, 2.32 mmol) in dry DCM, after which the mixture was allowed to warm to RT and stirred overnight. When TLC analysis confirmed complete conversion, volatiles were removed under reduced pressure. Flash column chromatography (50 → 100% EtOAc in pentane) afforded the title compound as light brown crystals (532 mg, 2.10 mmol, 90%).

<sup>1</sup>H NMR (400 MHz, MeOD) δ 8.67 (s, 1H), 7.18 – 7.10 (m, 2H), 6.87 – 6.78 (m, 2H), 4.62 (s, 2H), 3.75 (s, 3H).

<sup>13</sup>C NMR (101 MHz, MeOD) δ 161.69, 146.95, 133.43, 120.16, 115.03, 61.05, 55.70.

## References

1. Barglow, K. T. & Cravatt, B. F. Discovering disease-associated enzymes by proteome reactivity profiling. *Chem. Biol.* **11**, 1523–1531 (2004).
2. Satyanarayana, A. & Kaldis, P. Mammalian cell-cycle regulation: Several cdk, numerous cyclins and diverse compensatory mechanisms. *Oncogene* **28**, 2925–2939 (2009).
3. Schuster, A. *et al.* RNAi/CRISPR Screens: from a Pool to a Valid Hit. *Trends Biotechnol.* **37**, 38–55 (2019).
4. Weiss, W. A., Taylor, S. S. & Shokat, K. M. Recognizing and exploiting differences between RNAi and small-molecule inhibitors. *Nat. Chem. Biol.* **3**, 739–744 (2007).
5. Mock, E. D. *et al.* Discovery of a NAPE-PLD inhibitor that modulates emotional behavior in mice. *Nat. Chem. Biol.* **16**, 667–675 (2020).
6. Knight, Z. A. & Shokat, K. M. Chemical Genetics: Where Genetics and Pharmacology Meet. *Cell* **128**, 425–430 (2007).
7. Ogasawara, D. *et al.* Selective blockade of the lyso-PS lipase ABHD12 stimulates immune responses *in vivo*. *Nat. Chem. Biol.* **14**, 1099–1108 (2018).
8. Simon, G. M., Niphakis, M. J. & Cravatt, B. F. Determining target engagement in living systems. *Nature Chemical Biology* **9**, 200–205 (2013).
9. Jost, M. & Weissman, J. S. CRISPR Approaches to Small Molecule Target Identification. *ACS Chemical Biology* **13**, 366–375 (2018).
10. Schürmann, M., Janning, P., Ziegler, S. & Waldmann, H. Small-Molecule Target Engagement in Cells. *Cell Chem. Biol.* **23**, 435–441 (2016).
11. Wagner, J. A. Strategic approach to fit-for-purpose biomarkers in drug development. *Annu. Rev. Pharmacol. Toxicol.* **48**, 631–651 (2008).
12. Durham, T. B. & Blanco, M. J. Target Engagement in Lead Generation. *Bioorg. Med. Chem. Lett.* **25**, 998–1008 (2015).
13. Grimwood, S. & Hartig, P. R. Target site occupancy: Emerging generalizations from clinical and preclinical studies. *Pharmacol. Ther.* **122**, 281–301 (2009).
14. Willems, L. I., Overkleeft, H. S. & Van Kasteren, S. I. Current developments in activity-based protein profiling. *Bioconjug. Chem.* **25**, 1181–1191 (2014).
15. Niphakis, M. J. & Cravatt, B. F. Enzyme Inhibitor Discovery by Activity-Based Protein Profiling. *Annu. Rev. Biochem.* **83**, 341–377 (2014).
16. Adam, G. C., Sorensen, E. J. & Cravatt, B. F. Proteomic profiling of mechanistically distinct enzyme classes using a common chemotype. *Nat. Biotechnol.* **20**, 805–809 (2002).
17. Cravatt, B. F., Wright, A. T. & Kozarich, J. W. Activity-based protein profiling: From enzyme chemistry to proteomic chemistry. *Annu. Rev. Biochem.* **77**, 383–414 (2008).
18. Janssen, A. P. A. *et al.* Development of a Multiplexed Activity-Based Protein Profiling Assay to Evaluate Activity of Endocannabinoid Hydrolase Inhibitors. *ACS Chem. Biol.* **13**, 2406–2413 (2018).
19. Van Esbroeck, A. C. M. *et al.* Activity-based protein profiling reveals off-target proteins of the FAAH inhibitor BIA 10-2474. *Science* **356**, 1084–1087 (2017).
20. Verdoes, M. *et al.* A Fluorescent Broad-Spectrum Proteasome Inhibitor for Labeling Proteasomes *In Vitro* and *In Vivo*. *Chem. Biol.* **13**, 1217–1226 (2006).
21. Baggelaar, M. P. *et al.* Development of an activity-based probe and *in silico* design reveal highly selective inhibitors for diacylglycerol lipase- $\alpha$  in brain. *Angew. Chemie - Int. Ed.* **52**, 12081–12085 (2013).

22. Hussain, Z. *et al.* Phosphatidylserine-stimulated production of *N*-acyl-phosphatidylethanolamines by Ca<sup>2+</sup>-dependent *N*-acyltransferase. *Biochim. Biophys. Acta - Mol. Cell Biol. Lipids* **1863**, 493–502 (2018).
23. Ghosh, M., Tucker, D. E., Burchett, S. A. & Leslie, C. C. Properties of the Group IV phospholipase A2 family. *Prog. Lipid Res.* **45**, 487–510 (2006).
24. Leslie, C. C. Cytosolic phospholipase A2: Physiological function and role in disease. *J. Lipid Res.* **56**, 1386–1402 (2015).
25. Murakami, M. *et al.* Recent progress in phospholipase A2 research: From cells to animals to humans. *Prog. Lipid Res.* **50**, 152–192 (2011).
26. Capestrano, M. *et al.* Cytosolic phospholipase A<sub>2</sub>ε drives recycling through the clathrin-independent endocytic route. *J. Cell Sci.* **127**, 977–993 (2014).
27. Wang, H. *et al.* Structure of Human GIVD Cytosolic Phospholipase A2 Reveals Insights into Substrate Recognition. *J. Mol. Biol.* **428**, 2769–2779 (2016).
28. Ogura, Y., Parsons, W. H., Kamat, S. S. & Cravatt, B. F. A calcium-dependent acyltransferase that produces *N*-Acyl phosphatidylethanolamines. *Nat. Chem. Biol.* **12**, 669–671 (2016).
29. Gillum, M. P. *et al.* *N*-acylphosphatidylethanolamine, a Gut-Derived Circulating Factor Induced by Fat Ingestion, Inhibits Food Intake. *Cell* **135**, 813–824 (2008).
30. Shiratsuchi, A. *et al.* Inhibitory effect of *N*-palmitoylphosphatidylethanolamine on macrophage phagocytosis through inhibition of Rac1 and Cdc42. *J. Biochem.* **145**, 43–50 (2008).
31. Swamy, M. J., Tarafdar, P. K. & Kamlekar, R. K. Structure, phase behaviour and membrane interactions of *N*-acylethanolamines and *N*-acylphosphatidylethanolamines. *Chem. Phys. Lipids* **163**, 266–279 (2010).
32. Domingo, J. C., Mora, M. & Africa de Madariaga, M. Incorporation of *N*-acylethanolamine phospholipids into egg phosphatidylcholine vesicles: characterization and permeability properties of the binary systems. *Biochim. Biophys. Acta - Biomembr.* **1148**, 308–316 (1993).
33. Shangguan, T., Pak, C. C., Ali, S., Janoff, A. S. & Meers, P. Cation-dependent fusogenicity of an *N*-acyl phosphatidylethanolamine. *Biochim. Biophys. Acta* **1368**, 171–183 (1998).
34. Hussain, Z., Uyama, T., Tsuboi, K. & Ueda, N. Mammalian enzymes responsible for the biosynthesis of *N*-acylethanolamines. *Biochimica et Biophysica Acta - Molecular and Cell Biology of Lipids* **1862**, 1546–1561 (2017).
35. Tsuboi, K. *et al.* Enzymatic formation of *N*-acylethanolamines from *N*-acylethanolamine plasmalogen through *N*-acylphosphatidylethanolamine-hydrolyzing phospholipase D-dependent and -independent pathways. *Biochim. Biophys. Acta - Mol. Cell Biol. Lipids* **1811**, 565–577 (2011).
36. Leung, D., Saghatelian, A., Simon, G. M. & Cravatt, B. F. Inactivation of *N*-Acyl phosphatidylethanolamine phospholipase D reveals multiple mechanisms for the biosynthesis of endocannabinoids. *Biochemistry* **45**, 4720–4726 (2006).
37. Sun, Y. X. *et al.* Biosynthesis of anandamide and *N*-palmitoylethanolamine by sequential actions of phospholipase A2 and lysophospholipase D. *Biochem. J.* **380**, 749–756 (2004).
38. Simon, G. M. & Cravatt, B. F. Endocannabinoid biosynthesis proceeding through glycerophospho-*N*-acyl ethanolamine and a role for α/β-hydrolase 4 in this pathway. *J. Biol. Chem.* **281**, 26465–26472 (2006).
39. Simon, G. M. & Cravatt, B. F. Anandamide biosynthesis catalyzed by the phosphodiesterase GDE1 and detection of glycerophospho-*N*-acyl ethanolamine precursors in mouse brain. *J. Biol. Chem.* **283**, 9341–9349 (2008).

40. Tsuboi, K., Uyama, T., Okamoto, Y. & Ueda, N. Endocannabinoids and related *N*-acylethanolamines: biological activities and metabolism. *Inflamm. Regen.* **38**, (2018).
41. Hansen, H. S. & Vana, V. Non-endocannabinoid *N*-acylethanolamines and 2-monoacylglycerols in the intestine. *Br. J. Pharmacol.* **176**, 1443–1454 (2019).
42. Katona, I. & Freund, T. F. Multiple Functions of Endocannabinoid Signaling in the Brain. *Annu. Rev. Neurosci.* **35**, 529–558 (2012).
43. Lutz, B., Marsicano, G., Maldonado, R. & Hillard, C. J. The endocannabinoid system in guarding against fear, anxiety and stress. *Nat. Rev. Neurosci.* **16**, 705–718 (2015).
44. Mattace Raso, G., Russo, R., Calignano, A. & Meli, R. Palmitoylethanolamide in CNS health and disease. *Pharmacol. Res.* **86**, 32–41 (2014).
45. Petrosino, S. & Di Marzo, V. The pharmacology of palmitoylethanolamide and first data on the therapeutic efficacy of some of its new formulations. *Br. J. Pharmacol.* **174**, 1349–1365 (2017).
46. Dalle Carbonare, M. *et al.* A saturated *N*-acylethanolamine other than *N*-palmitoyl ethanolamine with anti-inflammatory properties: A neglected story... *J. Neuroendocrinol.* **20**, 26–34 (2008).
47. Fu, J. *et al.* Oleylethanolamide regulates feeding and body weight through activation of the nuclear receptor PPAR- $\alpha$ . *Nature* **425**, 90–93 (2003).
48. Gillet, L. C. J. *et al.* In-cell selectivity profiling of serine protease inhibitors by activity-based proteomics. *Mol. Cell. Proteomics* **7**, 1241–1253 (2008).
49. Speers, A. E., Adam, G. C. & Cravatt, B. F. Activity-Based Protein Profiling *In Vivo* Using a Copper(I)-Catalyzed Azide-Alkyne [3 + 2] Cycloaddition. *J. Am. Chem. Soc.* **125**, 4686–4687 (2003).
50. Binte Mustafiz, S. S. *et al.* The role of intracellular anionic phospholipids in the production of *N*-acyl-phosphatidylethanolamines by cytosolic phospholipase A<sub>2</sub> $\epsilon$ . *J. Biochem.* **165**, 343–352 (2019).
51. van der Veen, J. N. *et al.* The critical role of phosphatidylcholine and phosphatidylethanolamine metabolism in health and disease. *Biochim. Biophys. Acta - Biomembr.* **1859**, 1558–1572 (2017).
52. Natarajan, V., Schmid, P. C. & Schmid, H. H. O. *N*-Acylethanolamine phospholipid metabolism in normal and ischemic rat brain. *Biochim. Biophys. Acta - Lipids Lipid Metab.* **878**, 32–41 (1986).
53. Epps, D. E., Natarajan, V., Schmid, P. C. & Schmid, H. H. O. Accumulation of *N*-acylethanolamine glycerophospholipids in infarcted myocardium. *Biochim. Biophys. Acta - Lipids Lipid Metab.* **618**, 420–430 (1980).
54. Moesgaard, B., Petersen, G., Jaroszewski, J. W. & Hansen, H. S. Age dependent accumulation of *N*-acyl-ethanolamine phospholipids in ischemic rat brain: A <sup>31</sup>P NMR and enzyme activity study. *J. Lipid Res.* **41**, 985–990 (2000).
55. Jin, X. H. *et al.* cDNA cloning and characterization of human and mouse Ca<sup>2+</sup>-independent phosphatidylethanolamine *N*-acyltransferases. *Biochim. Biophys. Acta - Mol. Cell Biol. Lipids* **1791**, 32–38 (2009).
56. Akiyama, H. *et al.* Molecular cloning and biological activity of a novel Ha-Ras suppressor gene predominantly expressed in skeletal muscle, heart, brain, and bone marrow by differential display using clonal mouse EC cells, ATDC5. *J. Biol. Chem.* **274**, 32192–32197 (1999).
57. Schievella, A. R., Regier, M. K., Smith, W. L. & Lin, L. L. Calcium-mediated translocation of cytosolic phospholipase A<sub>2</sub> to the nuclear envelope and endoplasmic reticulum. *J. Biol. Chem.* **270**, 30749–30754 (1995).
58. Glover, S., Bayburt, T., Jonas, M., Chi, E. & Gelb, M. H. Translocation of the 85-kDa phospholipase A<sub>2</sub> from cytosol to the nuclear envelope in rat basophilic leukemia cells stimulated with calcium ionophore or IgE/antigen. *J. Biol. Chem.* **270**, 15359–15367 (1995).

59. Evans, J. H., Spencer, D. M., Zweifach, A. & Leslie, C. C. Intracellular Calcium Signals Regulating Cytosolic Phospholipase A<sub>2</sub> Translocation to Internal Membranes. *J. Biol. Chem.* **276**, 30150–30160 (2001).
60. Ohto, T., Uozumi, N., Hirabayashi, T. & Shimizu, T. Identification of novel cytosolic phospholipase A<sub>2</sub>s, murine cPLA<sub>2</sub>δ, ε, and ζ, which form a gene cluster with cPLA<sub>2</sub>β. *J. Biol. Chem.* **280**, 24576–24583 (2005).

# 6

**Development of potent and selective ABHD6 inhibitors based on caged hydrocarbon structures**



Since its discovery in 1933<sup>1</sup>, adamantane, an organic compound consisting of three fused cyclohexanes in their chair conformation ((CH)<sub>4</sub>(CH<sub>2</sub>)<sub>6</sub>, **1**, Figure 6.1), has intrigued chemists due to its physicochemical and biological properties.<sup>2,3</sup> Named after the Greek *adamantinos*, meaning diamond-related, it is the simplest member of the family of caged hydrocarbons that have their carbon atoms in a diamond-like lattice arrangement (named diamondoids), which gives them an extraordinarily rigid and almost strain-free structure.<sup>2,4</sup> Initially, adamantane could only be isolated from petroleum, which limited the possibilities for derivatization and its widespread use. The first convenient synthesis published in 1957 opened up the possibilities for its application in medicinal chemistry.<sup>5</sup> Derivatives such as amantadine (**2**), memantine (**3**) and vildagliptin (**4**) have since entered the clinic for the treatment of viral infections, diabetes mellitus and neurodegenerative diseases such as Alzheimer's and Parkinson's disease (Figure 6.1).<sup>3,6–12</sup>

Diamondoids are lipophilic moieties. Inhibitors with an adamantyl group, however, have a lower lipophilicity than their cyclohexyl counterparts, as determined by their octanol–water partition coefficient (logP).<sup>13</sup> Adamantane has therefore been dubbed the 'lipophilic bullet', providing a compact moiety of critical hydrophobicity to a drug.<sup>3</sup> For this reason, adamantane has been used as a fatty acid-mimic in peroxisome proliferator-activated receptor (PPAR) pan-agonists<sup>14</sup> and as cell membrane anchor in glucosylceramidase inhibitors.<sup>15–17</sup> It has also been incorporated in various drug candidates to increase their water solubility<sup>18</sup>, improve brain-penetration<sup>19</sup> or to increase their selectivity.<sup>20</sup> Its hydrophobicity may, however, negatively impact oral bioavailability, but increase the volume of distribution and half-life.<sup>21,22</sup> The rigidity and bulkiness of adamantane may improve the metabolic stability of a drug by inducing steric hindrance.<sup>6,23,24</sup> Importantly, combination of these beneficial properties is not easily obtained by using more conventional structures.<sup>25–27</sup>

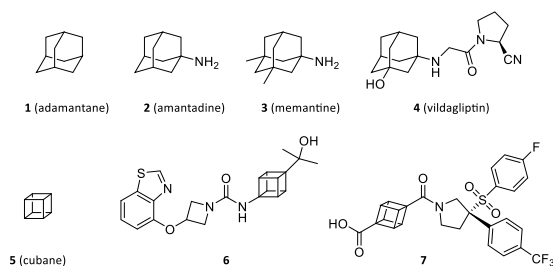


**Figure 6.1. Examples of caged hydrocarbons and their use in published drugs.** Adamantane is the smallest representative of the diamondoid class. Amantadine has been used as antiviral and for the treatment of Parkinson's disease<sup>62</sup>, memantine for the treatment of Alzheimer's disease<sup>7</sup>, vildagliptin is used as anti-diabetic.<sup>12</sup> Cubane is another small caged hydrocarbon that was used in this study. Compound **6** has been published as an inhibitor of prostaglandin D synthase, **7** is a retinoid-related orphan receptor  $\gamma$  ligand.<sup>28</sup>

Following the increased use of adamantane, other caged hydrocarbons such as cubanes have also been leveraged by medicinal chemists (**5–7**, Figure 6.1). The size of a cubyl group (2.72 Å) is almost identical to that of a phenyl (2.79 Å), making it a potential bioisoster for this commonly applied functional group in drug discovery. A clear advantage of cubane is its three-dimensional structure which allows for derivatization in different exit vectors compared to the phenyl ring. In addition, the cubyl group is highly stable towards light, heat and oxidation.<sup>28,29</sup> Its widespread use is, however, hampered by a lack of readily available building blocks.<sup>30</sup>

Serine hydrolases (SHs), a superfamily of enzymes characterized by the presence of a catalytic serine used for substrate hydrolysis, play key roles in multiple (patho)physiological processes, including coagulation, neurotransmission, hypertension, cancer and neuroinflammation.<sup>31–33</sup> They are important drug targets, and currently over ten SH inhibitors have entered the clinic.<sup>32</sup> Several SHs, such as diacylglycerol lipases  $\alpha$  and  $\beta$  (DAGL $\alpha$  and DAGL $\beta$ ) and  $\alpha/\beta$  hydrolase domain-containing proteins 6 and 16a (ABHD6 and ABHD16a), are potential targets for the treatment of neurological diseases associated with neuroinflammation. DAGL $\alpha$  and DAGL $\beta$  hydrolyze diacylglycerols into free fatty acids and monoacylglycerols, including 2-arachidonoyl glycerol (2-AG), an endogenous agonist of the cannabinoid CB<sub>1</sub> and CB<sub>2</sub> receptors.<sup>31,34</sup> It is also an intermediate in the formation of pro-inflammatory lipids, such as prostaglandins and eicosanoids.<sup>34–37</sup> ABHD6 converts di- and monoacylglycerols into free fatty acids and glycerol and participates in both production and degradation of 2-AG.<sup>38</sup> It has recently been suggested as potential drug target in microglial cells that play a fundamental function in the development of neuroinflammation<sup>39–42</sup>, including for the treatment of traumatic brain injury<sup>43</sup> and multiple sclerosis.<sup>44–46</sup> Of note, while several ABHD6 inhibitors have been developed, their off-target effects have hampered this research.<sup>44,47</sup> ABHD16a is a phosphatidyl serine (PS) lipase producing lyso-PS in the brain. This lipid mediator is involved in several pathways of inflammatory responses, and elevated levels caused by attenuated degradation are the hallmark of the neurological disorder polyneuropathy, hearing loss, ataxia, retinitis pigmentosa, cataract (PHARC).<sup>48–50</sup> Inhibition of ABHD16a may therefore provide a treatment opportunity for PHARC patients.

For both DAGL and ABHD6 various inhibitors have been developed and shown to exhibit potent inhibition in cellular and animal models of neuroinflammation (**8–11**, Figure 6.2).<sup>34,51–54</sup> ABHD16a can be inhibited by XGN067 (**12**).<sup>55</sup> These inhibitors belong to the class of triazole ureas and contain an electrophilic carbonyl that covalently binds to the catalytic serine of SHs, with the triazole functioning as leaving group. KT109 (**8**), DH376 (**9**) and AJ126 (**10**) were developed as DAGL inhibitors, but cross-reactivity was observed with ABHD6, whereas XGN067 was shown to target multiple enzymes beside ABHD16a.<sup>54–56</sup> KT182 (**11**) is a highly potent, *in vivo* active ABHD6 inhibitor which has been used to study the role of ABHD6 in neuroinflammation<sup>44,46</sup>, but its off-targets include FAAH, the enzyme responsible for the degradation of anandamide (*N*-arachidonoyl ethanolamine, AEA), the

second major CB receptor agonist.<sup>53,57</sup> Improving the selectivity of these inhibitors would aid in the development of compounds that specifically modulate the desired physiological function of the targeted enzyme. In this chapter, a set of triazole urea-based compounds with caged hydrocarbon substituents were synthesized to investigate their effect on the activity and selectivity of these lipase inhibitors.

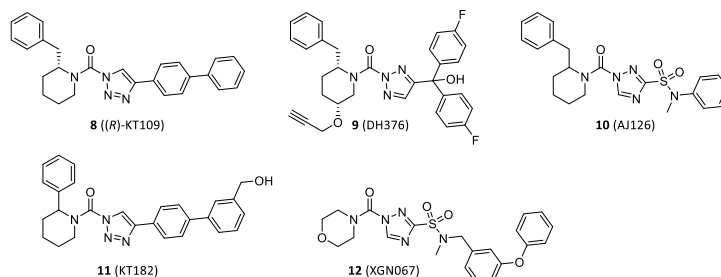


**Figure 6.2. Chemical structures of some previously published DAGL, ABHD6 and ABHD16a inhibitors.** 2-Benzylpiperidine-containing compounds KT109, DH376 and AJ126 were reported as DAGL or dual DAGL/ABHD6 inhibitors<sup>52,54,56,59,63</sup>, 2-phenylpiperidine-containing compound KT182 was reported as ABHD6 inhibitor.<sup>53</sup> Morpholine-containing XGN067 was reported as ABHD16a inhibitor.<sup>55</sup>

## Results and discussion

### Design and synthesis of compounds 13–21

The DAGL, ABHD6 and ABHD16a inhibitors outlined in Figure 6.2 feature lipophilic phenyl moieties in the triazole leaving group. These phenyl groups make important hydrophobic interactions with their respective enzymes<sup>53,56</sup> and were replaced with a caged hydrocarbon as a bioisoster. Nine novel inhibitors (**13–21**) were designed in which a C1- or C2-linked adamantyl or a cubyl group was attached to a 1,2,4-triazole sulfone scaffold (selected for synthetic ease) via either a methylene or ethylene linker (Figure 6.3).

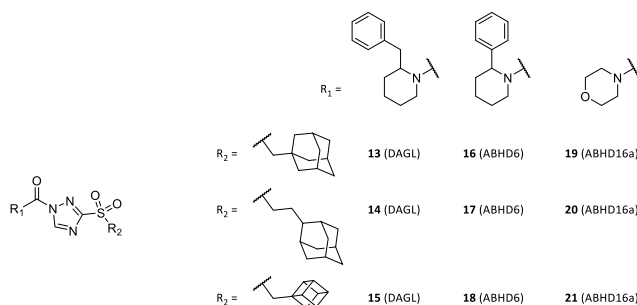
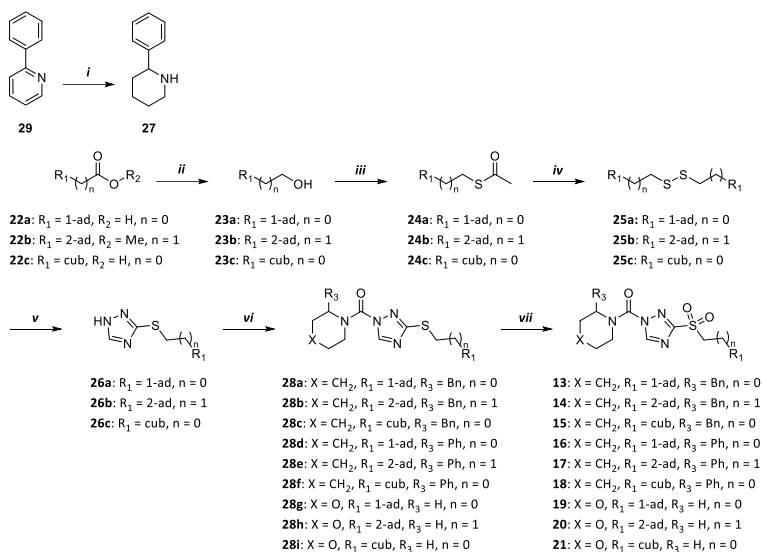


**Figure 6.3. Design of the nine inhibitors synthesized.** Chemical structures of the central sulfonamide triazole urea, the previously developed amines for targeting DAGL, ABHD6 or ABHD16a (R<sub>1</sub>, indicated at compound number) and the selected caged hydrocarbons (R<sub>2</sub>).

Synthesis started with commercially available adamantancarboxylic acid (**22a**) or methyl ester (**22b**) or cubanecarboxylic acid (**22c**), which were reduced to the alcohols **23a–c** using LiAlH<sub>4</sub> (Scheme 6.1). Subsequent triflation provided a suitable substrate for substitution with potassium thioacetate, affording thioacetates **24a–c** in moderate yields (38–64%). Reduction by LiAlH<sub>4</sub> and oxidation using molecular bromine afforded the symmetrical disulfides **25a–c** (49–99% yield). To synthesize the desired thioether, 1-(pyrrolidin-1-ylmethyl)-1*H*-1,2,4-triazole (synthesized according to literature<sup>58</sup>) was lithiated using *n*-BuLi. Careful addition of disulfide **25a–c** led to formation of the thioether, while the pyrrolidin-1-ylmethyl protecting group was removed by the liberated thiol at the same time, providing thioethers **26a–c** (65–83% yield). The byproduct originating from the deprotection was easily removed after reduction with NaBH<sub>4</sub> in ethanol. The resulting triazole thioether was reacted with the desired carbamoyl chloride, which was either commercially available (4-morpholinecarbonyl chloride) or formed by treating the corresponding piperidine (commercially available 2-benzylpiperidine or 2-phenylpiperidine **27**) with triphosgene, affording triazole ureas **28a–i** (62–73% yield). To obtain the desired sulfone, the thioether was oxidized using peracetic acid, yielding final products **13–21** quantitatively. For all inhibitors, an overall yield was achieved of 5 to 29%, which is comparable to or better than previously reported structurally similar inhibitors that do not contain caged hydrocarbon moieties.<sup>53–56,59</sup>



**Scheme 6.1.** General synthesis route of diamondoid-containing DAGL, ABHD6 and ABHD16a inhibitors. Reagents and conditions: *i*) H<sub>2</sub>, PtO<sub>2</sub>, HCl, EtOH, 3 h RT; *ii*) LiAlH<sub>4</sub>, THF, 0.5 h reflux; *iii*) 1. Tf<sub>2</sub>O, pyr, DCM, 45 min -15°C → RT; 2. AcSK, 18-Crown-6, CH<sub>3</sub>CN, 72 h RT; *iv*) 1. LiAlH<sub>4</sub>, THF, 1.5 h RT → 50°C; 2. Br<sub>2</sub>, DCM/H<sub>2</sub>O, RT; *v*) 1. 1-(pyrrolidin-1-ylmethyl)-1*H*-1,2,4-triazole, *n*-BuLi, THF, 21 h -80°C → RT; 2. NaBH<sub>4</sub>, EtOH, 5 min RT; *vi*) 1. 2-benzylpiperidine (**28a–c**) or **27** (**28d–f**), triphosgene, DIPEA, DCM, 3 h 0°C; 2. 4-morpholinecarbonyl chloride (**28g–i**), **26a–i**, K<sub>2</sub>CO<sub>3</sub>, DMF, 2–5 d RT; *vii*) AcOOH, DCM, 4–12 h RT. 1-Ad: adamant-1-yl, 2-ad: adamant-2-yl, cub: cubyl.

## Biological evaluation

### Activity of caged hydrocarbon inhibitors in mouse brain proteome

Inhibitors **13–21** were tested in mouse brain proteome for their activity against DAGL, ABHD6 or ABHD16a using competitive activity-based protein profiling (cABPP), a powerful chemical biology technique that allows to concomitantly assess inhibitor activity and selectivity in biologically relevant samples.<sup>60,61</sup> In brief, mouse brain membrane proteome was incubated with inhibitor in several concentrations (30 min), followed by broad-spectrum SH probes MB064 or FP-TAMRA, which covalently and fluorescently labeled any residual DAGL $\alpha$  (120 kDa), FAAH (63 kDa), ABHD16a (63 kDa) and ABHD6 (38 kDa) activity. Resolution of the proteins by molecular weight using sodium dodecyl sulfate–polyacrylamide gel electrophoresis (SDS-PAGE) and in-gel fluorescence scanning enabled the determination of the half maximal inhibitory concentration ( $IC_{50}$ ) of the inhibitor for each labeled enzyme. Inhibitors **13–21** all inhibited their intended target with  $IC_{50}$  values in the sub-micromolar range (Figure 6.4, Table 6.1). Compounds **13–15** showed preferential inhibition of DAGL $\alpha$ , with  $pIC_{50}$  values between 7.4 and 8.0. It appeared a cubanemethylene moiety yielded the most potent DAGL $\alpha$  inhibitor (**15**), which was also the most selective over ABHD6 (12-fold). **16–18** preferentially inhibited ABHD6 ( $pIC_{50}$  6.3–6.8), with 4 to 10-fold selectivity over DAGL $\alpha$ . **17**, bearing a 2-(adamant-2-yl)ethylene moiety, was the most potent ABHD6 inhibitor of this series, as well as the most selective over DAGL $\alpha$  and FAAH ( $pIC_{50} < 5$ ). **13–18** inhibited both ABHD6 and DAGL $\alpha$  at concentrations up to 10  $\mu$ M, but all but **18** did not inhibit ABHD16a or FAAH. Compounds **19–21** did show activity on ABHD16a, with  $pIC_{50}$  values between 6.4 and 7.6. However, they had no selectivity over ABHD6 ( $pIC_{50}$  7.3–7.8) and **21** also showed activity on FAAH ( $pIC_{50} = 5.6$ ). Because of their superior selectivity profile compounds **15** and **17** were selected for further profiling (Supplementary Figure S6.1).

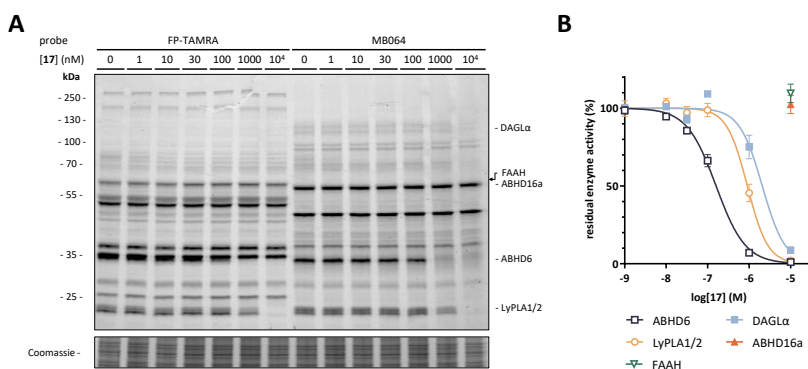


**Figure 6.4. Inhibitory activity of 17 on mouse brain proteome.** A) Representative example gel image of cABPP experiment of **17** on mouse brain proteome. B) Inhibition curves of **17** on mouse brain enzymes as determined by cABPP.

**Table 6.1. *In vitro* activity of 13–21 and reference inhibitors.** pIC<sub>50</sub> values on ABHD6, ABHD16a, DAGL $\alpha$  and FAAH (left column for each enzyme) determined in cABPP experiments on mouse brain proteome using FP-TAMRA and MB064 (8–10, 12–21) or on Neuro-2a lysate using FP-TAMRA (11). If available, data is presented as mean + SEM (N = 3). The right column states the apparent fold selectivity (app. sel.) of that inhibitor on its intended target (indicated with a “–”) over its respective off-targets. NR: data not reported.

	ABHD6		ABHD16a		DAGL $\alpha$		FAAH	
	pIC <sub>50</sub> $\pm$ SEM	App. sel.	pIC <sub>50</sub> $\pm$ SEM	App. sel.	pIC <sub>50</sub> $\pm$ SEM	App. sel.	pIC <sub>50</sub> $\pm$ SEM	App. sel.
8 ((R)-KT109)	7.1 $\pm$ 0.1 <sup>56</sup>	10	< 5.0 <sup>56</sup>	> 1000	8.1 $\pm$ 0.1 <sup>56</sup>	–	< 5.0 <sup>56</sup>	> 1000
9 (DH376)	7.1 $\pm$ 0.1 <sup>56</sup>	126	< 5.0 <sup>56</sup>	> 10,000	9.2 $\pm$ 0.1 <sup>56</sup>	–	NR	NR
10 (AJ126)	6.1 $\pm$ 0.1 <sup>54</sup>	100	NR	NR	8.1 $\pm$ 0.1 <sup>54</sup>	–	NR	NR
13	6.49 $\pm$ 0.07	17	< 5.0	> 537	7.73 $\pm$ 0.08	–	< 5.0	> 537
14	7.05 $\pm$ 0.03	3.4	< 5.0	> 380	7.58 $\pm$ 0.09	–	< 5.0	> 380
15	6.84 $\pm$ 0.06	14	< 5.0	> 1000	8.00 $\pm$ 0.06	–	< 5.0	> 1000
11 (KT182)	8.8 <sup>53</sup>	–	NR	NR	NR	NR	< 6.0 <sup>53</sup>	> 631
16	6.49 $\pm$ 0.05	–	< 5.0	> 30	5.60 $\pm$ 0.08	7.8	< 5.0	> 30
17 (RED353)	6.80 $\pm$ 0.03	–	< 5.0	> 63	5.68 $\pm$ 0.07	13	< 5.0	> 63
18	6.61 $\pm$ 0.05	–	< 5.0	> 40	6.00 $\pm$ 0.07	4.1	5.59 $\pm$ 0.06	10
12 (XGN067)	8.18 $\pm$ 0.08 <sup>55</sup>	< 1	8.10 $\pm$ 0.13 <sup>55</sup>	–	5.46 $\pm$ 0.11 <sup>55</sup>	437	6.14 $\pm$ 0.10 <sup>55</sup>	91
19	7.53 $\pm$ 0.05	< 1	7.03 $\pm$ 0.07	–	5.44 $\pm$ 0.19	39	< 5.0	> 107
20	7.82 $\pm$ 0.03	< 1	7.55 $\pm$ 0.04	–	5.75 $\pm$ 0.13	63	< 5.0	> 354
21	7.26 $\pm$ 0.07	< 1	6.36 $\pm$ 0.07	–	4.91 $\pm$ 0.24	28	5.64 $\pm$ 0.04	5.2

### Profiling of caged hydrocarbon inhibitors as ABHD6 inhibitors in neuronal cells

The cellular activity of **15** and **17** was investigated in a widely used mouse neuroblastoma cell line (Neuro-2a) that expresses both DAGL $\beta$  and ABHD6. In brief, Neuro-2a cells were treated with inhibitor at increasing concentrations (1 h), harvested, lysed and the resulting homogenate was incubated with FP-TAMRA and MB064 to fluorescently label any remaining SH activity. KT182 was taken along for comparison of the results (*in vitro* activity in Supplementary Table S6.1). Both **15** and **17** exhibited a more than 10-fold increased potency at inhibiting ABHD6 (pIC<sub>50</sub> = 8.1 and 8.4, respectively, Table 6.2) compared to their activity measured in mouse brain lysate (Table 6.1). Their inhibitory activity on other SHs, such as DDHD2, FAAH and LyPLA1 and 2, was also increased (Table 6.2 and Supplementary Table S6.1). Compound **15**'s activity on DAGL $\beta$  (pIC<sub>50</sub> = 6.7) was lower than the activity on DAGL $\alpha$  *in vitro* (pIC<sub>50</sub> = 8.0), giving it a poor cellular selectivity profile. ABHD6 inhibitor **17** demonstrated an increased selectivity to almost 300-fold over DAGL and 90-fold over LyPLA1/2. Its selectivity over FAAH was more than 60-fold, whereas KT182 showed less than 30-fold selectivity (Table 6.2, Figure 6.5A).

**Table 6.2. Cellular inhibition values of 15, 17 and KT182 on Neuro-2a enzymes.** pIC<sub>50</sub> values determined from cABPP experiments with probes FP-TAMRA and MB064. Data presented as mean ± SEM (N = 3). For each inhibitor the apparent fold selectivity (app. sel.) on its intended target (indicated with “–”) over its respective off-targets is stated in the right column.

	15		17		KT182	
	pIC <sub>50</sub> ± SEM	App. sel.	pIC <sub>50</sub> ± SEM	App. sel.	pIC <sub>50</sub> ± SEM	App. sel.
ABHD6	8.10 ± 0.05	< 1	8.39 ± 0.03	–	8.87 ± 0.03	–
ABHD12	< 5.0	> 50	< 5.0	> 1000	< 5.0	> 1000
ABHD16a	< 5.0	> 50	< 5.0	> 1000	< 5.0	> 1000
DAGLβ	6.74 ± 0.09	–	5.92 ± 0.04	295	< 5.0	> 1000
DDHD2	5.49 ± 0.08	18	< 5.0	> 1000	< 5.0	> 1000
FAAH	6.59 ± 0.09	1.4	6.58 ± 0.07	65	7.41 ± 0.06	29
KIAA1363	< 5.0	> 50	< 5.0	> 1000	< 5.0	> 1000
LyPLA1/2	5.88 ± 0.06	7.2	6.44 ± 0.08	89	5.99 ± 0.03	759
NTE	< 5.0	> 50	< 5.0	> 1000	6.07 ± 0.15	631

Since compound **17** showed the most promising ABHD6 inhibitor profile in both cABPP assays, its inhibitory activity was investigated in an orthogonal fluorogenic substrate assay. **17** and KT182 were tested on hABHD6-overexpressing HEK293T cells for their ability to block the hydrolysis of 4-methylumbelliferyl heptanoate (4-MUH). Both **17** and KT182 inhibited the conversion of 4-MUH hydrolysis by ABHD6 with pIC<sub>50</sub>s of 8.8 and 7.9, respectively (Figure 6.5B). Of note, substrate conversion by wild type HEK293T lysate was virtually unaffected even at high concentrations, demonstrating the selectivity of **17**.

Finally, the activity of **17** and KT182 in Neuro-2a was measured with quantifying changes in select lipids using HPLC-MS/MS. Neuro-2a cells were treated with each inhibitor at 100 nM (1 h), a concentration that fully inhibits ABHD6 without affecting DAGLβ, according to the cABPP results (Table 6.2). Although KT182 fully inhibited ABHD6, this treatment did not influence 2-AG levels, whereas **17** substantially lowered these (Figure 6.5C). In addition, KT182 increased AEA levels, whereas **17** did not affect the levels of this second endocannabinoid. These data agree with the recent observation that ABHD6 also possesses DAG lipase activity, thereby contributing to the generation of 2-AG in Neuro-2a cells.<sup>38</sup> The lack of effect on 2-AG levels by KT182 may suggest that FAAH-inhibition and increased NAE-levels indirectly modulate 2-AG biosynthesis. These results show that **17** is a highly potent and one of the most selective inhibitors of ABHD6 identified to date.

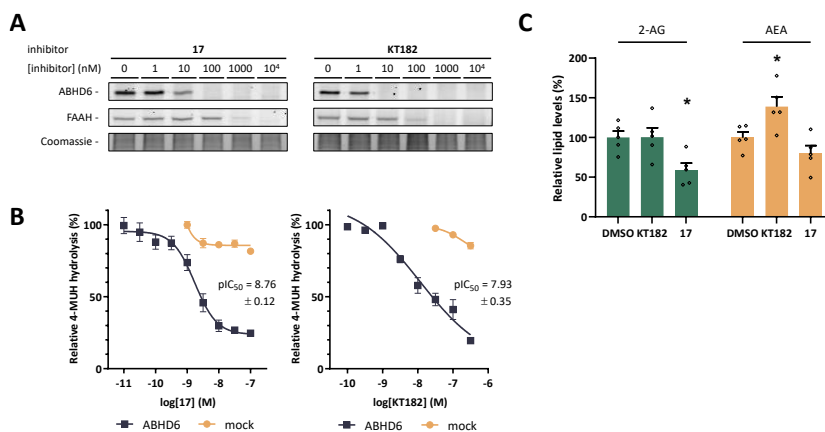


**Figure 6.5. Cellular activity of 17 and KT182.** A) Dose-dependent inhibition of ABHD6 and FAAH in Neuro-2a cells by **17** and KT182. Representative gel image excerpts of cABPP experiments with probes FP-TAMRA and MB064 (full images in Supplementary Figure S6.1). B) Dose-dependent inhibition by **17** and KT182 of 4-MUH hydrolysis on ABHD6-overexpressing or mock HEK293T membrane preparations. Corresponding  $pIC_{50}$  values on ABHD6 are indicated. Data presented as mean  $\pm$  SEM ( $N \geq 3$ ). C) Levels of 2-AG (combined with 1-AG) and AEA measured in Neuro-2a by targeted lipidomics analysis after treatment with **17** or KT182 (1h, 100 nM), expressed as relative levels compared to those measured in DMSO-treated cells. Individual measurements are shown, as well as means  $\pm$  SEM ( $N = 5$ ). Data were tested for equality by one-way ANOVA with Dunnett's multiple comparison correction. \*: adjusted  $p < 0.05$ .

## Conclusion

In conclusion, caged hydrocarbons were successfully leveraged to develop novel inhibitors of DAGL, ABHD6 and ABHD16a. A bulky 2-(adamant-2-yl)ethylene moiety likely favored the cellular activity of **17** (**RED353**), the most potent and selective ABHD6 inhibitor in this series. This case study shows the first example of caged hydrocarbon structures incorporated in triazole urea-based inhibitors and the first application in lipase inhibitors, providing a new chemical tool for the investigation of the physiological functions of ABHD6. The synthesis and results presented here could expand the medicinal chemists' toolbox with new chemical properties, leading to new possibilities for inhibitor design.

## Acknowledgements

Yevhenii Radchenko is kindly acknowledged for performing organic synthesis and ABPP, Simar Singh and Nephi Stella for 4-MUH assays, Floor Stevens for targeted lipidomics, Hans van den Elst for HRMS analysis. Hans den Dulk is acknowledged for plasmid cloning and purification.



## Experimental procedures

### General remarks

All chemicals and reagents were purchased from Thermo Fisher Scientific or Bio-Rad and used without further purification, unless noted otherwise. Solvents were obtained from Biosolve Chemicals or Merck, salts from Chem-Lab, and used as such. Activity-based probes were purchased from Thermo Fisher Scientific (FP-TAMRA) or synthesized in-house (MB064) (chemical structures in Chapter 3 Supplementary Figure S3.8). Inhibitors were synthesized in-house as described below.

### Cell culture

Neuro-2a (mouse neuroblastoma, ATCC) cells were cultured in DMEM (Sigma-Aldrich, D6546) with additional heat-inactivated new-born calf serum (10% (v/v), Avantor Seradigm), L-Ala-L-Gln (2 mM, Sigma-Aldrich), penicillin and streptomycin (both 200 µg/mL, Duchefa Biochemie) at 37°C, 7% CO<sub>2</sub>. Medium was refreshed every 2–3 days and cells were passaged twice a week at 70–80% confluence by aspirating the medium, thorough pipetting in fresh medium and seeding to appropriate density. Cell cultures were regularly tested for mycoplasma and discarded after 2–3 months.

### ABHD6 overexpression lysate preparation

HEK293T (human embryonic kidney) cells, seeded to 50% confluence, were transfected with hABHD6 plasmid using polyethylenimine (PEI, Polysciences). 24 h p.t. medium was aspirated and cells were washed twice with ice-cold PBS. Cells were harvested in ice-cold PBS by scraping or thorough pipetting and centrifuged (4 °C, 1150 × *g*, 10 min). Pellets were flash-frozen in liquid N<sub>2</sub> and stored at –80°C until further use.

Cell pellets were thawed on ice and lysed by dounce homogenization in 500 µL TE buffer (50 mM Tris-HCl, 1 mM EDTA, pH 7.4) and subsequent sonication (30 s, 10% amplitude). Protein concentration was determined using Bio-Rad *DC* Protein Assay and aliquots were flash-frozen in liquid N<sub>2</sub> and stored at –80°C until further use.

### Mouse brain lysate preparation

Mouse brains were harvested from surplus C57Bl/6J mice (8–14 weeks old) according to guidelines approved by the ethical committee of Leiden University (AVD1060020171144), flash-frozen in liquid N<sub>2</sub> and stored at –80°C until use. Upon preparation, intact brains were thawed on ice and homogenized in 6 mL ice-cold lysis buffer (20 mM HEPES, 2 mM DTT, 250 mM sucrose, 1 mM MgCl<sub>2</sub>, 25 U/mL Benzonase®, pH 6.8) using a Wheaton™ dounce homogenizer (DWK Life Sciences) and incubated on ice for 1 h. Cell debris was removed by low-speed centrifugation (170 × *g*, 5 min, 4°C), after which the supernatant was subjected to ultracentrifugation to separate membrane and cytosol fractions. The pellet was resuspended in ice-cold storage buffer (20 mM HEPES, 2 mM DTT, pH 6.8) and homogenized by passing through an insulin needle. The protein concentrations of both fractions were determined using a Quick Start™ Bradford Protein Assay and samples were diluted to 2.0 mg/mL (membrane) or 1.0 mg/mL (cytosol) using ice-cold storage buffer, aliquoted to single-use volumes, flash-frozen in liquid N<sub>2</sub> and stored at –80°C until further use.

### Activity-based protein profiling

Mouse brain lysates were thawed on ice. 19.5 µL lysate was incubated with 0.5 µL inhibitor in DMSO (30 min, RT), followed by 0.5 µL activity-based probe (final concentration 500 nM FP-TAMRA or 250 nM MB064) in DMSO (20 min, RT, final DMSO concentration 5%). The reactions were quenched by

addition of 7  $\mu$ L 4 $\times$  Laemmli buffer (240 mM Tris, 8% (w/v) SDS, 40% (v/v) glycerol, 5% (v/v)  $\beta$ -mercaptoethanol (Sigma-Aldrich), 0.04% bromophenol blue). 10  $\mu$ L sample was resolved on 10% acrylamide SDS-PAGE gel (180 V, 70 min) and afterwards imaged on a Bio-Rad Chemidoc MP using Cy3/TAMRA settings (ex. 532/12 nm, em. 602/50 nm). Coomassie Brilliant Blue R250 staining was used for total protein loading correction. Images were analyzed using Bio-Rad Image Lab 6. IC<sub>50</sub> calculations were performed in GraphPad Prism 7.

### ABPP of *in situ* treatments

Two days prior to treatment, Neuro-2a cells were seeded to 12-wells plates ( $\sim 0.25 \cdot 10^6$  cells per well). Before the experiment was started medium was aspirated. Medium with DMSO or inhibitor in DMSO (0.25% (v/v) DMSO) was added and cells were incubated for 1 h at 37°C. Then medium was aspirated and cells were washed with RT Dulbecco's PBS (Sigma-Aldrich). Cells were harvested in ice-cold PBS by thorough pipetting and centrifuged (1000  $\times g$ , 6 min, RT). Pellets were flash-frozen in liquid N<sub>2</sub> and stored at  $-80^\circ\text{C}$  until further use.

Cell pellets were thawed on ice and lysed in 50  $\mu$ L lysis buffer. After incubation on ice for 1 h, the protein concentration was determined using Quick Start™ Bradford Protein Assay and the samples were diluted to 1.0 or 2.0 mg/mL using storage buffer. 19.5  $\mu$ L of this whole lysate was incubated with 0.5  $\mu$ L FP-TAMRA (500 nM) or MB064 (2  $\mu$ M) in DMSO (20 min, RT). Reactions were then quenched, proteins resolved and images analyzed as described under Activity-based protein profiling.

### Biochemical fluorogenic substrate assay

Lysate was thawed on ice and diluted to 0.024 mg/mL in TE buffer. To each well of a Greiner Bio-One black 96-wells plate with clear, flat bottom, 10  $\mu$ L inhibitor (or DMSO) solution in TE buffer was added. After short vortex, 85  $\mu$ L lysate (2  $\mu$ g total protein) was added and the plate was incubated for 30 min at 37°C. 5  $\mu$ L 1 mM 4-methylumbelliferyl heptanoate in EtOH was added (final concentration 50  $\mu$ M) and fluorescence was measured immediately every 1–2 minutes for 120 min (ex. 355 nm, em. 460 nm, 37 °C). IC<sub>50</sub> calculations were performed in GraphPad Prism 7.

### Targeted lipidomics

#### Sample preparation

One or two days prior to treatment, Neuro-2a cells were seeded to 6 cm dishes ( $\sim 2.5 \cdot 10^6$  cells per dish). Before the experiment was started medium was aspirated and cells were washed with RT PBS. Treatment medium with DMSO or inhibitor in DMSO (0.25% (v/v) DMSO) was added and cells were incubated for 1 h at 37°C. Then medium was removed and cells were washed with RT PBS. Cells were harvested in 1250  $\mu$ L RT PBS by thorough pipetting. 1000  $\mu$ L was centrifuged (1000  $\times g$ , 6 min, RT) in Eppendorf® Safe-Lock tubes. Cell count was performed on the remaining 250  $\mu$ L, after which this was centrifuged as well. Pellets were flash-frozen in liquid N<sub>2</sub> and stored at  $-80^\circ\text{C}$  until further use.

The 250- $\mu$ L pellets were thawed on ice and lysed in 50  $\mu$ L lysis buffer. After incubation on ice for 30 min, the protein concentration was determined using Quick Start™ Bradford Protein Assay.

#### Lipid extraction

Pellets were thawed on ice. To each 1000- $\mu$ L pellet, 10  $\mu$ L internal standard mix (deuterated reference lipids 2-arachidonoyl glycerol-d<sub>8</sub>, *N*-arachidonoyl ethanolamine-d<sub>8</sub>, *N*-docosahexaenoyl ethanolamine-d<sub>4</sub>, *N*-linoleoyl ethanolamine-d<sub>4</sub>, *N*-oleoyl ethanolamine-d<sub>4</sub>, *N*-palmitoyl ethanolamine-d<sub>5</sub>, *N*-stearoyl ethanolamine-d<sub>3</sub>, *N*-eicosapentaenoyl ethanolamine-d<sub>4</sub> and arachidonic acid-d<sub>8</sub>, Cayman Chemical Company) was added, followed by 100  $\mu$ L extraction buffer (100 mM NH<sub>4</sub>OAc, 0.5% (m/v) NaCl, pH 4). After short mixing, 1000  $\mu$ L MTBE was added and lipids were

extracted in a Next Advance Bullet Blender® Blue tissue homogenizer (7 min, 80% speed, RT) followed by centrifugation ( $16,000 \times g$ , 11 min,  $4^{\circ}\text{C}$ ). 925  $\mu\text{L}$  of the organic layer was transferred into clean, pre-cooled tubes and concentrated in an Eppendorf® Concentrator Plus (40 min,  $30^{\circ}\text{C}$ ). The lipid residue was reconstituted in 30  $\mu\text{L}$  9:1 (v/v)  $\text{CH}_3\text{CN}:\text{H}_2\text{O}$  by thorough mixing, centrifuged ( $10,000 \times g$ , 4 min,  $4^{\circ}\text{C}$ ) and 25  $\mu\text{L}$  was transferred to LC-MS vials (KG 09 0188, Screening Devices) with insert (ME 06 0232, Screening Devices).

### LC-MS/MS analysis

10  $\mu\text{L}$  of sample was injected into the system, consisting of an Acquity UPLC I class binary solvent manager pump in conjugation with a tandem quadrupole mass spectrometer (Waters Corporation). The separation was performed in an Acquity HSS T3 column ( $2.1 \times 100$  mm,  $1.8 \mu\text{m}$ ) maintained at  $45^{\circ}\text{C}$ , with the eluent flow rate set to 0.55 mL/min. The mobile phase consisted of 2 mM  $\text{NH}_4\text{HCO}_2$ , 10 mM formic acid in water (A) and  $\text{CH}_3\text{CN}$  (B). Initial gradient conditions were 55% B for 0.5 min, then linearly increased to 60% over 1.5 min. The gradient was then linearly ramped up to 100% B over 5 min and then held for 2 min. After 10 s the system returned to the initial conditions, which were held for 2 min before the next injection. For lipid quantification ESI-MS and a selective multiple reaction mode (sMRM) were used, with individually optimized MRM transitions for target compounds using synthetic standards and internal standards (see Lipid extraction protocol for composition). Peak area integration was performed manually with MassLynx 4.1 (Waters Corporation). Absolute values of lipid levels were calculated by correction for internal standard peak area and comparison to the calibration curve of the respective synthetic standard. In case of 2-AG, combined levels of 1-AG and 2-AG were calculated and compared to combined internal standard.

Lipid levels were corrected for cell count or protein concentration. Statistical analysis was performed using GraphPad Prism 8. For each lipid, one-way ANOVA was performed between treatment and control groups, with Dunnett's multiple comparison correction for using one control group for both treatment groups.

## Organic synthesis

### General remarks

All reagents were purchased from Sigma-Aldrich, Acros Organics, Merck or Fluorochem and used without further purification. Solvents were purchased from Sigma-Aldrich, VWR Chemicals, Honeywell Riedel-de Haën or Biosolve Chemicals, common salts from Sigma-Aldrich or Chem-Lab, and used without further purification. Moisture-sensitive reactions were carried out in solvents dried over heat-activated molecular sieves ( $4 \text{ \AA}$ , Sigma-Aldrich), using flame-dried glassware under an atmosphere of  $\text{N}_2$ . TLC analysis was performed on Merck silica gel 60  $\text{F}_{254}$  aluminum TLC plates, on which compounds were visualized under 254 or 366 nm UV light and using  $\text{KMnO}_4$  (30 mM  $\text{KMnO}_4$ , 180 mM  $\text{K}_2\text{CO}_3$  in water) or ninhydrin (7.5 mM ninhydrin, 10% (v/v)  $\text{AcOH}$  in  $\text{EtOH}$ ) stain. Flash column chromatography was performed using  $\text{SiO}_2$  (Macherey-Nagel, 60 M) as stationary phase.

NMR spectra were recorded on a Bruker AV-400 MHz or AV-500 MHz spectrometer at 400 MHz ( $^1\text{H}$ ) and 101 MHz ( $^{13}\text{C}$ ) or 500 MHz ( $^1\text{H}$ ) and 126 MHz ( $^{13}\text{C}$ ) respectively, using  $\text{CDCl}_3$  (Eurisotop) as solvent. Chemical shifts are reported in ppm with TMS ( $^1\text{H}$ ,  $\delta$  0.00) or solvent resonance ( $^{13}\text{C}$ ,  $\delta$  77.16) as internal standard. Data are reported as follows: chemical shift  $\delta$  (ppm), multiplicity (s = singlet, d = doublet, t = triplet, p = pentet, dd = doublet of doublets, td = triplet of doublets, qd = quartet of doublets, dt = doublet of triplets, bs = broad singlet ( $^1\text{H}$ ), br = broad ( $^{13}\text{C}$ ), m = multiplet), coupling constants  $J$  (Hz) and integration. HPLC-MS analysis was performed on a Finnigan Surveyor HPLC system equipped with a Macherey-Nagel NUCLEODUR  $\text{C}_{18}$  Gravity,  $5 \mu\text{m}$ ,  $50 \times 4.6$  mm column followed

by a Thermo Scientific LTQ Orbitrap XL spectrometer, using H<sub>2</sub>O/CH<sub>3</sub>CN + 1% TFA as mobile phase. All compounds used for biological experiments were ≥95% pure based on LC-MS UV absorbance.

#### General procedure A

Peracetic acid (10–15 eq, 36–40% in AcOH) was added to a solution of triazole urea thioether (1 eq) in DCM (150 mL/mmol) and the mixture was stirred for 4–12 h. Upon completion the reaction mixture was diluted with DCM, washed with water and brine and concentrated *in vacuo*. Flash column chromatography yielded the sulfone final product.

#### General procedure B

A solution of adamantanecarboxylic acid or ester (1 eq) in dry THF (10 mL/g) was added dropwise to an ice-cold suspension of LiAlH<sub>4</sub> (2.5 eq) in dry THF (20 mL/g). The reaction mixture was warmed to RT and stirred for 30 min, followed by reflux for 30 min. The reaction was then quenched by addition of 10% aq. NaOH on an ice bath. Solids were removed by filtration and washed with DCM. Combined filtrates were dried over Na<sub>2</sub>SO<sub>4</sub>, filtrated and concentrated *in vacuo*. The product was used without further purification.

#### General procedure C

Triflic anhydride (1.05 eq) was added portionwise to a solution of alcohol (1 eq) and pyridine (1.2 eq) in dry DCM (15 mL/g), while maintaining the temperature between –15 and –5°C. The mixture was stirred for 15 min followed by 30 min at RT. The mixture was then diluted with hexane (30 mL/g), cooled to 0°C and ice-cold 1 M aq. H<sub>2</sub>SO<sub>4</sub> was added until pH < 7. The layers were separated, the organic layer was washed with water and brine, dried over Na<sub>2</sub>SO<sub>4</sub>, filtrated and concentrated *in vacuo*. The resulting brown liquid was dissolved in CH<sub>3</sub>CN (10 mL/g) and cooled to 0°C. AcSK (2 eq) and 18-Crown-6 (0.3 eq) were added, the mixture was warmed to RT and stirred for ≥72 h. Solids were removed by filtration and washed with hexane until they were colorless. Combined filtrates were concentrated *in vacuo*. Flash column chromatography (150:1 hexane:EtOAc) provided the thioacetate.

#### General procedure D

To an ice-cold solution of LiAlH<sub>4</sub> (1.5 eq) in dry THF (20 mL/g), a solution of thioacetate (1 eq) in dry THF (10 mL/g) was added dropwise. The reaction mixture was allowed to warm to RT and stirred for 30 min, followed by 1 h at 50°C. The reaction was cooled and quenched by addition of 0.1 M aq. HCl on an ice bath. Solids were removed by filtration and washed with DCM. Combined filtrates were concentrated *in vacuo*. The resulting yellow oil was dissolved in DCM (20 mL/g) and added to a suspension of silica powder (5 g/g) in water (2.5 mL/g). 1 M Br<sub>2</sub> in DCM was added until the mixture started to color. Solids were removed by filtration. The filtrate was dried over Na<sub>2</sub>SO<sub>4</sub>, filtrated and concentrated *in vacuo*. Silica plug purification with pentane provided the disulfide.

#### General procedure E

A solution of 1-(pyrrolidin-1-ylmethyl)-1*H*-1,2,4-triazole (2 eq)<sup>58</sup> in dry THF (10 mL/mmol) was degassed by N<sub>2</sub> purging and cooled to –80°C. *n*-BuLi (2.3 M in THF, 2.2 eq) was added portionwise, after which the reaction mixture was stirred at –80°C for 30 min followed by 90 min at –30 to –25°C during which a white precipitate formed. The mixture was then cooled to –80°C and a solution of disulfide (1 eq) in dry THF (3 mL/mmol) was added portionwise. The reaction was stirred for ≥3 h at –75°C, after which it was allowed to warm to RT and stirred overnight. Volatiles were removed under reduced pressure, after which the concentrate was diluted in DCM and washed with water. The organic layer was concentrated *in vacuo*. The residue was brought onto a silica gel column and washed with

pentane and DCM. The product was then eluted using 1:1 DCM:MeOH. The fractions containing product were combined and concentrated *in vacuo*.

The product was treated with NaBH<sub>4</sub> in EtOH (20 eq, 20 mL/mmol) and stirred for 5 min. Volatiles were removed under reduced pressure, after which the residue was dissolved in DCM and washed with water and brine. The organic layer was concentrated *in vacuo*. The residue was dispersed in 5 M aq. KOH and extracted with CHCl<sub>3</sub>. The pH of the aqueous layer was lowered to 7, after which it was again extracted with CHCl<sub>3</sub>. The combined organic layers were dried over Na<sub>2</sub>SO<sub>4</sub>, filtrated and concentrated *in vacuo* yielding the triazole thioether, which was used without further purification.

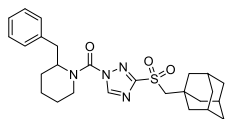
#### General procedure F

To an ice-cold solution of triphosgene (1 eq) dry DCM (25 mL/mmol), 2-phenylpiperidine or 2-benzylpiperidine (1 eq) and DIPEA (3 eq) were added. The mixture was stirred on ice for 90 min. When TLC analysis confirmed full conversion the mixture was diluted with DCM and washed with 1 M aq. HCl and brine, dried over Na<sub>2</sub>SO<sub>4</sub>, filtrated and concentrated *in vacuo*. Water was removed by co-evaporation with toluene. The resulting oil was dissolved in dry DMF (150 mL/mmol), triazole thioether (1 eq) and K<sub>2</sub>CO<sub>3</sub> (3 eq) were added and the reaction mixture was stirred for 2–5 days. The mixture was diluted with DCM, washed with water and brine, dried over Na<sub>2</sub>SO<sub>4</sub>, filtrated and concentrated *in vacuo*. Flash column chromatography afforded the triazole urea thioether.

#### General procedure G

4-Morpholinecarbonyl chloride (2 eq), K<sub>2</sub>CO<sub>3</sub> (3.5 eq) and triazole thioether (1 eq) were dissolved in dry DMF (175 mL/mmol) and stirred for 48 h. The mixture was then concentrated *in vacuo* and dissolved in DCM, washed with water and brine, dried over Na<sub>2</sub>SO<sub>4</sub>, filtrated and concentrated *in vacuo*. Flash column chromatography afforded the triazole urea thioether.

#### (3-(((Adamant-1-yl)methyl)sulfonyl)-1H-1,2,4-triazol-1-yl)(2-benzylpiperidin-1-yl)methanone (13)



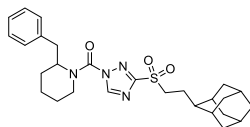
**28a** (13 mg, 0.029 mmol) was oxidized according to General procedure A to obtain the title compound as a white solid (14 mg, 0.029 mmol, quant.).

<sup>1</sup>H NMR (500 MHz, CDCl<sub>3</sub>) δ 7.87 (bs, 1H), 7.35 – 6.94 (m, 5H), 4.81 – 4.71 (m, 1H), 4.33 – 4.18 (m, 1H), 3.41 – 3.26 (m, 1H), 3.26 – 3.12 (m, 3H), 2.81 – 2.60 (m, 1H), 1.99 (p, *J* = 3.1 Hz, 3H), 1.96 – 1.57 (m, 18H).

<sup>13</sup>C NMR (126 MHz, CDCl<sub>3</sub>) δ 162.88, 147.20, 137.70, 129.16, 128.98, 127.07, 66.26, 56.87, 41.99, 41.26, 36.70, 36.42, 34.71, 28.73, 28.39, 25.30, 18.83.

HRMS: [M+Na]<sup>+</sup> calculated for C<sub>26</sub>H<sub>34</sub>N<sub>4</sub>NaO<sub>3</sub>S 505.22438, found 505.22396.

#### (3-(((Adamant-2-yl)ethyl)sulfonyl)-1H-1,2,4-triazol-1-yl)(2-benzylpiperidin-1-yl)methanone (14)



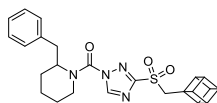
**28b** (8 mg, 0.02 mmol) was oxidized according to General procedure A to obtain the title compound as a white solid (12 mg, 0.025 mmol, quant.).

<sup>1</sup>H NMR (500 MHz, CDCl<sub>3</sub>) δ 7.89 (bs, 1H), 7.27 – 6.94 (m, 5H), 4.87 – 4.73 (m, 1H), 4.33 – 4.20 (m, 1H), 3.42 – 3.27 (m, 3H), 3.26 – 3.12 (m, 1H), 2.74

– 2.63 (m, 1H), 2.04 – 1.48 (m, 23H).

<sup>13</sup>C NMR (126 MHz, CDCl<sub>3</sub>) δ 161.24, 147.48, 137.69, 129.12, 128.99, 127.10, 56.87, 53.15, 43.48, 41.29, 38.96, 38.18, 36.73, 31.61, 31.40, 28.77, 28.09, 27.88, 25.33, 24.77, 18.84.

HRMS: [M+Na]<sup>+</sup> calculated for C<sub>27</sub>H<sub>36</sub>N<sub>4</sub>NaO<sub>3</sub>S 519.24003, found 519.23964.

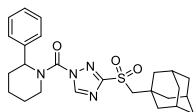
**(2-Benzylpiperidin-1-yl)(3-((cuban-1-ylmethyl)sulfonyl)-1H-1,2,4-triazol-1-yl)methanone (15)**

**28c** (10 mg, 0.024 mmol) was oxidized according to General procedure A to obtain the title compound as a white solid (13 mg, 0.029 mmol, quant.).

<sup>1</sup>H NMR (500 MHz, CDCl<sub>3</sub>) δ 7.93 (bs, 1H), 7.27 – 6.93 (m, 5H), 4.83 – 4.73 (m, 1H), 4.34 – 4.21 (m, 1H), 3.99 – 3.94 (m, 1H), 3.94 – 3.88 (m, 6H), 3.73 (s, 2H), 3.40 – 3.26 (m, 1H), 3.26 – 3.14 (m, 1H), 2.78 – 2.64 (m, 1H), 2.03 – 1.52 (m, 7H).

<sup>13</sup>C NMR (126 MHz, CDCl<sub>3</sub>) δ 162.14, 147.47, 137.67, 129.19, 128.98, 127.10, 57.56, 56.84, 49.30, 48.11, 45.03, 41.29, 36.68, 28.76, 25.42, 18.82.

HRMS: [M+Na]<sup>+</sup> calculated for C<sub>24</sub>H<sub>26</sub>N<sub>4</sub>O<sub>3</sub>S 473.16178, found 473.16153.

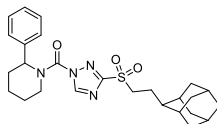
**(3-(((Adamant-1-yl)methyl)sulfonyl)-1H-1,2,4-triazol-1-yl)(2-phenylpiperidin-1-yl)-methanone (16)**

**28d** (12 mg, 0.027 mmol) was oxidized according to General procedure A to obtain the title compound as a white solid (11 mg, 0.023 mmol, 85%).

<sup>1</sup>H NMR (500 MHz, CDCl<sub>3</sub>) δ 8.88 (s, 1H), 7.44 – 7.36 (m, 2H), 7.34 – 7.27 (m, 3H), 5.83 – 5.77 (m, 1H), 4.32 – 4.25 (m, 1H), 3.21 (s, 2H), 3.15 (td, *J* = 13.7, 3.1 Hz, 1H), 2.54 – 2.44 (m, 1H), 2.15 – 2.05 (m, 1H), 1.97 (p, *J* = 3.1 Hz, 3H), 1.87 – 1.61 (m, 16H).

<sup>13</sup>C NMR (126 MHz, CDCl<sub>3</sub>) δ 163.57, 148.67, 148.15, 137.73, 129.18, 127.53, 126.59, 66.18, 56.67 (br), 43.71 (br), 42.01, 36.44, 28.42, 28.02, 25.63, 19.23.

HRMS: [M+Na]<sup>+</sup> calculated for C<sub>25</sub>H<sub>32</sub>N<sub>4</sub>NaO<sub>3</sub>S 491.20873, found 491.20830.

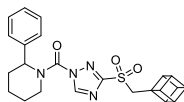
**(3-((2-(Adamant-2-yl)ethyl)sulfonyl)-1H-1,2,4-triazol-1-yl)(2-phenylpiperidin-1-yl)methanone (17, RED353)**

**28e** (12 mg, 0.027 mmol) was oxidized according to General procedure A to obtain the title compound as a white solid (9 mg, 0.02 mmol, 70%).

<sup>1</sup>H NMR (500 MHz, CDCl<sub>3</sub>) δ 8.91 (s, 1H), 7.42 – 7.37 (m, 2H), 7.34 – 7.28 (m, 3H), 5.83 – 5.77 (m, 1H), 4.33 – 4.25 (m, 1H), 3.40 – 3.27 (m, 2H), 3.20 – 3.10 (m, 1H), 2.53 – 2.45 (m, 1H), 2.15 – 2.05 (m, 1H), 2.00 – 1.92 (m, 2H), 1.91 – 1.61 (m, 17H), 1.55 – 1.47 (m, 2H).

<sup>13</sup>C NMR (126 MHz, CDCl<sub>3</sub>) δ 162.08, 148.59, 148.34, 137.67, 129.18, 127.54, 126.58, 56.70 (br), 53.06, 43.73 (br), 43.47, 38.99, 38.21, 31.61, 31.42, 28.12, 27.99, 27.90, 25.66, 24.70, 19.22.

HRMS: [M+Na]<sup>+</sup> calculated for C<sub>26</sub>H<sub>34</sub>N<sub>4</sub>O<sub>3</sub>S 505.22438, found 505.22407.

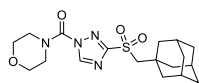
**(2-Phenylpiperidin-1-yl)(3-((cuban-1-ylmethyl)sulfonyl)-1H-1,2,4-triazol-1-yl)methanone (18)**

**28f** (16 mg, 0.030 mmol) was oxidized according to General procedure A to obtain the title compound as a white solid (8 mg, 0.017 mmol, 58%).

<sup>1</sup>H NMR (500 MHz, CDCl<sub>3</sub>) δ 8.90 (s, 1H), 7.43 – 7.37 (m, 2H), 7.33 – 7.27 (m, 3H), 5.85 – 5.76 (m, 1H), 4.33 – 4.25 (m, 1H), 4.00 – 3.95 (m, 1H), 3.94 – 3.89 (m, 6H), 3.73 (s, 2H), 3.16 (td, *J* = 13.9, 3.4 Hz, 1H), 2.54 – 2.45 (m, 1H), 2.15 – 2.05 (m, 1H), 1.88 – 1.64 (m, 4H).

<sup>13</sup>C NMR (126 MHz, CDCl<sub>3</sub>) δ 162.80, 148.59, 148.33, 137.73, 129.18, 127.54, 126.58, 57.45, 56.65 (br), 51.12, 49.37, 48.15, 45.06, 43.80 (br), 28.03, 25.66, 19.23.

HRMS: [M+Na]<sup>+</sup> calculated for C<sub>23</sub>H<sub>24</sub>N<sub>4</sub>O<sub>3</sub>S 459.14613, found 459.14559.

**(3-(((Adamant-1-yl)methyl)sulfonyl)-1H-1,2,4-triazol-1-yl)(morpholino)methanone (19)**

**28g** (5 mg, 0.01 mmol) was oxidized according to General procedure A to obtain the title compound as a white solid (5 mg, 0.01 mmol, 92%).

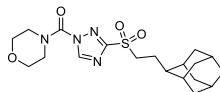
*Analytical data on next page.*

$^1\text{H}$  NMR (500 MHz,  $\text{CDCl}_3$ )  $\delta$  8.88 (s, 1H), 4.10 – 3.64 (m, 8H), 3.25 (s, 2H), 2.03 – 1.96 (m, 3H), 1.87 – 1.81 (m, 6H), 1.77 – 1.64 (m, 6H).

$^{13}\text{C}$  NMR (126 MHz,  $\text{CDCl}_3$ )  $\delta$  163.76, 148.33, 147.35, 66.58, 66.25, 48.19 (br), 45.97 (br), 42.07, 36.44, 28.43.

HRMS:  $[\text{M}+\text{Na}]^+$  calculated for  $\text{C}_{18}\text{H}_{26}\text{N}_4\text{NaO}_4\text{S}$  417.15670, found 417.15615.

### (3-((2-(Adamant-2-yl)ethyl)sulfonyl)-1H-1,2,4-triazol-1-yl)(morpholino)methanone (20)

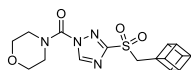


**28h** (9 mg, 0.02 mmol) was oxidized according to General procedure A to obtain the title compound as a white solid (9 mg, 0.02 mmol, 92%).

$^1\text{H}$  NMR (500 MHz,  $\text{CDCl}_3$ )  $\delta$  8.91 (s, 1H), 4.14 – 3.61 (m, 8H), 3.44 – 3.35 (m, 2H), 2.01 – 1.94 (m, 2H), 1.92 – 1.66 (m, 13H), 1.56 – 1.49 (m, 2H).

$^{13}\text{C}$  NMR (126 MHz,  $\text{CDCl}_3$ )  $\delta$  162.27, 148.51, 147.26, 66.56, 53.10, 48.08 (br), 45.97 (br), 43.50, 38.98, 38.19, 31.63, 31.43, 28.10, 27.90, 24.73.

### (3-((Cuban-1-ylmethyl)sulfonyl)-1H-1,2,4-triazol-1-yl)(morpholino)methanone (21)



**28i** (13 mg, 0.038 mmol) was oxidized according to General procedure A to obtain the title compound as a white solid (13 mg, 0.034 mmol, 91%).

$^1\text{H}$  NMR (500 MHz,  $\text{CDCl}_3$ )  $\delta$  8.91 (s, 1H), 4.02 – 3.96 (m, 2H), 3.95 – 3.91 (m, 8H), 3.90 – 3.71 (m, 4H), 3.77 (s, 3H).

$^{13}\text{C}$  NMR (126 MHz,  $\text{CDCl}_3$ )  $\delta$  162.99, 148.46, 147.23, 66.56, 57.49, 49.35, 48.15, 46.02 (br), 45.06.

HRMS:  $[\text{M}+\text{Na}]^+$  calculated for  $\text{C}_{16}\text{H}_{18}\text{N}_4\text{O}_4\text{S}$  385.09410, found 385.09299.

### 1-Adamantanemethanol (23a)

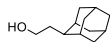


1-Adamantanecarboxylic acid **22a** (5.0 g, 28 mmol) was reduced according to General procedure B to obtain the title compound as a white solid (4.7 g, 27 mmol, 99%).

$^1\text{H}$  NMR (500 MHz,  $\text{CDCl}_3$ )  $\delta$  3.20 (s, 2H), 2.00 (p,  $J$  = 3.1 Hz, 3H), 1.77 – 1.61 (m, 7H), 1.51 (d,  $J$  = 2.9 Hz, 6H).

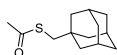
$^{13}\text{C}$  NMR (126 MHz,  $\text{CDCl}_3$ )  $\delta$  77.41, 77.16, 76.91, 74.03, 39.17, 37.31, 34.62, 28.31.

### 2-Adamantaneethanol (23b)



Methyl 2-(adamant-2-yl)acetate **22b** (32.0 g, 154 mmol)<sup>64</sup> was reduced according to General procedure B to obtain the title compound as a white solid (27.0 g, 150 mmol, 97%) which was used without characterization.

### S-(adamant-1-ylmethyl)thioacetate (24a)

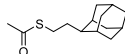


**23a** (5.0 g, 30 mmol) was treated according to General procedure C to obtain the title compound as a red solid (4.3 g, 19 mmol, 64%).

$^1\text{H}$  NMR (500 MHz,  $\text{CDCl}_3$ )  $\delta$  2.73 (s, 2H), 2.35 (s, 3H), 1.96 (p,  $J$  = 3.0 Hz, 3H), 1.72 – 1.54 (m, 10H), 1.50 (d,  $J$  = 2.9 Hz, 6H).

$^{13}\text{C}$  NMR (126 MHz,  $\text{CDCl}_3$ )  $\delta$  196.16, 42.62, 41.56, 36.88, 33.37, 30.89, 28.57.

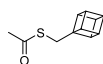
### S-(2-(adamant-2-yl)ethyl)thioacetate (24b)



**23b** (3.0 g, 17 mmol) was treated according to General procedure C (with the exception that in the first step the mixture was stirred at  $-70^\circ\text{C}$  instead of  $-15$  to  $-5^\circ\text{C}$ ) to obtain the title compound as a red liquid (2.2 g, 9.2 mmol, 56%).

$^1\text{H}$  NMR (400 MHz,  $\text{CDCl}_3$ )  $\delta$  2.89 – 2.81 (m, 2H), 2.32 (s, 3H), 1.92 – 1.64 (m, 11H), 1.57 – 1.47 (m, 3H).

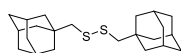
$^{13}\text{C}$  NMR (101 MHz,  $\text{CDCl}_3$ )  $\delta$  195.91, 43.80, 39.07, 38.30, 32.43, 31.60, 31.57, 28.21, 27.98, 27.57.

**S-(cuban-1-ylmethyl)thioacetate (24c)**

DIAD (2 eq, 2.28 mL, 11.6 mmol) was added dropwise to a solution of PPh<sub>3</sub> (2 eq, 3.05 g, 11.6 mmol) in dry THF (15 mL) while keeping the temperature between -5°C and 0°C. The mixture was warmed to RT, stirred for 15 min and cooled back to -5°C. To this, a solution of (cuban-1-yl)methanol (1 eq, 780 mg, 5.81 mmol)<sup>30</sup> and thioacetic acid (2 eq, 820 μL, 11.6 mmol) in dry THF (15 mL) was added dropwise while keeping the temperature below 0°C. The reaction mixture was stirred for 1 h at 0°C followed by 30 min at RT, resulting in a yellow solution. This was poured into 90 mL of 10:1 hexane:EtOAc and concentrated under reduced pressure to 25 mL. Solids were removed by filtration and the filtrate was concentrated *in vacuo*. Flash column chromatography (150:1 hexane:EtOAc) afforded the title compound as a brown oil with an intense odor (420 mg, 2.18 mmol, 38%).

<sup>1</sup>H NMR (500 MHz, CDCl<sub>3</sub>) δ 4.04 – 3.98 (m, 1H), 3.88 – 3.82 (m, 3H), 3.78 – 3.72 (m, 3H), 3.20 (s, 2H), 2.36 (s, 3H).

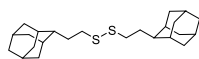
<sup>13</sup>C NMR (126 MHz, CDCl<sub>3</sub>) δ 196.13, 56.67, 48.84, 48.55, 43.94, 32.54, 30.85.

**Bis(adamant-1-ylmethyl)disulfide (25a)**

**24a** (1.0 g, 4.5 mmol) was treated according to General procedure D to obtain the title compound as a white solid (790 g, 2.18 mmol, 98%).

<sup>1</sup>H NMR (500 MHz, CDCl<sub>3</sub>) δ 2.63 (s, 4H), 1.98 (p, *J* = 3.1 Hz, 6H), 1.73 – 1.59 (m, 12H), 1.57 (d, *J* = 2.9 Hz, 12H).

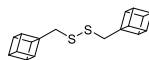
<sup>13</sup>C NMR (126 MHz, CDCl<sub>3</sub>) δ 56.23, 41.90, 36.97, 34.33, 28.61.

**Bis(2-(adamant-2-yl)ethyl)disulfide (25b)**

**24b** (1.05 g, 4.40 mmol) was treated according to General procedure D to obtain the title compound as a white crystalline solid (430 g, 1.10 mmol, 50%).

<sup>1</sup>H NMR (400 MHz, CDCl<sub>3</sub>) δ 2.73 – 2.65 (m, 4H), 1.92 – 1.66 (m, 30H), 1.52 (d, *J* = 12.6 Hz, 4H).

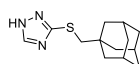
<sup>13</sup>C NMR (101 MHz, CDCl<sub>3</sub>) δ 77.48, 77.16, 76.84, 43.58, 39.24, 38.46, 37.68, 32.47, 31.86, 31.79, 28.37, 28.16.

**Bis(cuban-1-ylmethyl)disulfide (25c)**

**24c** (420 mg, 2.18 mmol) was treated according to General procedure D to obtain the title compound as a white solid (0.16 g, 0.54 mmol, 49%).

<sup>1</sup>H NMR (500 MHz, CDCl<sub>3</sub>) δ 4.08 – 3.99 (m, 2H), 3.95 – 3.85 (m, 12H), 3.05 (s, 4H).

<sup>13</sup>C NMR (126 MHz, CDCl<sub>3</sub>) δ 77.41, 77.16, 76.91, 57.47, 48.96, 48.72, 44.34, 43.81, 30.46.

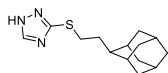
**3-(((Adamant-1-yl)methyl)thio)-1H-1,2,4-triazole (26a)**

**25a** (405 mg, 1.12 mmol) was treated according to General procedure E to obtain the title compound as a white solid (89 mg, 0.36 mmol, 65%).

<sup>1</sup>H NMR (400 MHz, CDCl<sub>3</sub>) δ 10.80 (bs, 1H), 8.15 (s, 1H), 3.08 (s, 1H), 2.01 – 1.95 (m, 4H), 1.74 – 1.53 (m, 11H).

<sup>13</sup>C NMR (101 MHz, CDCl<sub>3</sub>) δ 157.87, 148.01, 46.99, 41.54, 36.78, 33.89, 28.51.

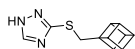


**3-((2-(Adamant-2-yl)ethyl)thio)-1H-1,2,4-triazole (26b)**

**25b** (393 mg, 1.01 mmol) was treated according to General procedure E to obtain the title compound as a white solid (220 mg, 0.835 mmol, 83%).

$^1\text{H NMR}$  (500 MHz,  $\text{CDCl}_3$ )  $\delta$  8.15 (s, 1H), 3.21 – 3.14 (m, 2H), 1.90 – 1.75 (m, 9H), 1.75 – 1.68 (m, 6H), 1.54 – 1.47 (m, 2H).

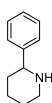
$^{13}\text{C NMR}$  (126 MHz,  $\text{CDCl}_3$ )  $\delta$  157.19, 148.10, 43.73, 39.16, 38.40, 32.62, 31.76, 31.72, 31.42, 28.30, 28.09, 0.13.

**3-((Cuban-1-ylmethyl)thio)-1H-1,2,4-triazole (26c)**

**25c** (150 mg, 0.503 mmol) was treated according to General procedure E to obtain the title compound as a white solid (75 mg, 0.35 mmol, 69%).

$^1\text{H NMR}$  (500 MHz,  $\text{CDCl}_3$ )  $\delta$  12.60 (bs, 1H), 8.15 (s, 1H), 4.02 – 3.96 (m, 1H), 3.90 – 3.81 (m, 3H), 3.81 – 3.74 (m, 3H), 3.52 (s, 2H).

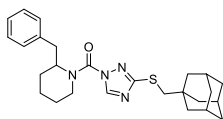
$^{13}\text{C NMR}$  (126 MHz,  $\text{CDCl}_3$ )  $\delta$  148.23, 57.14, 48.71, 48.62, 44.09, 36.64.

**2-Phenylpiperidine (27)**

2-Phenylpiperidine **29** (1.0 g, 6.4 mmol) was dissolved in EtOH (25 mL) and degassed by  $\text{N}_2$  purging with a balloon. 1 mL 12 M HCl and  $\text{PtO}_2$  (8 mol%, 117 mg, 0.515 mmol) were added and the mixture was stirred for 3 h under continuous  $\text{H}_2$  purging with a balloon. The reaction was quenched by  $\text{N}_2$  purging with a balloon, after which the catalyst was removed by filtration over celite. The filtrate was concentrated *in vacuo*. Flash column chromatography (7:3 EtOAc:10%  $\text{NH}_4\text{OH}$  in MeOH) afforded the title compound as a yellow oil (85 mg, 0.53 mmol, 7.9%).

$^1\text{H NMR}$  (500 MHz,  $\text{CDCl}_3$ )  $\delta$  7.39 – 7.34 (m, 2H), 7.34 – 7.28 (m, 2H), 7.26 – 7.21 (m, 1H), 3.59 (dd,  $J$  = 10.6, 2.6 Hz, 1H), 3.24 – 3.16 (m, 1H), 2.80 (td,  $J$  = 11.6, 2.8 Hz, 1H), 1.92 – 1.85 (m, 1H), 1.83 – 1.73 (m, 1H), 1.71 – 1.62 (m, 1H), 1.62 – 1.42 (m, 3H).

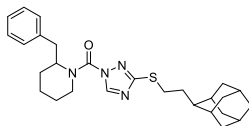
$^{13}\text{C NMR}$  (126 MHz,  $\text{CDCl}_3$ )  $\delta$  145.56, 128.50, 127.17, 126.78, 62.47, 47.91, 35.03, 26.47, 25.97, 25.55.

**(3-(((Adamant-1-yl)methyl)thio)-1H-1,2,4-triazol-1-yl)(2-benzylpiperidin-1-yl)methanone (28a)**

2-Benzylpiperidine (1.5 eq, 11 mg, 0.060 mmol) and **26a** (1 eq, 10 mg, 0.040 mmol) were coupled according to General procedure F to obtain the title compound as a white solid (13 mg, 0.029 mmol, 73%).

$^1\text{H NMR}$  (500 MHz,  $\text{CDCl}_3$ )  $\delta$  8.05 (bs, 1H), 7.27 – 7.17 (m, 3H), 7.11 – 7.05 (m, 2H), 5.01 – 4.79 (m, 1H), 4.39 – 4.18 (m, 1H), 3.24 (td,  $J$  = 13.3, 2.8 Hz, 1H), 3.19 – 3.11 (m, 1H), 3.09 – 2.96 (m, 2H), 2.91 – 2.67 (m, 1H), 1.99 (p,  $J$  = 3.1 Hz, 3H), 1.86 – 1.54 (m, 15H), 1.35 – 1.19 (m, 7H).

$^{13}\text{C NMR}$  (126 MHz,  $\text{CDCl}_3$ )  $\delta$  163.23, 149.30, 146.65, 138.04, 129.10, 128.73, 126.81, 45.66, 41.57, 36.84, 36.40, 33.98, 32.02, 31.53, 29.79, 28.54, 25.50, 18.92, 0.09.

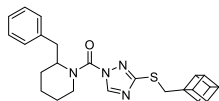
**(3-((2-(Adamant-2-yl)ethyl)thio)-1H-1,2,4-triazol-1-yl)(2-benzylpiperidin-1-yl)methanone (28b)**

2-Benzylpiperidine (1.5 eq, 10 mg, 0.057 mmol) and **26b** (1 eq, 10 mg, 0.038 mmol) were coupled according to General procedure F to obtain the title compound as a white solid (11 mg, 0.024 mmol, 62%).

$^1\text{H NMR}$  (500 MHz,  $\text{CDCl}_3$ )  $\delta$  8.12 (bs, 1H), 7.27 – 7.16 (m, 3H), 7.16 – 7.02 (m, 2H), 5.02 – 4.81 (m, 1H), 4.42 – 4.18 (m, 1H), 3.24 (td,  $J$  = 13.4, 2.8 Hz, 1H), 3.18 – 3.05 (m, 3H), 2.90 – 2.70 (m, 1H), 1.93 – 1.48 (m, 18H), 1.32 – 1.21 (m, 7H).

$^{13}\text{C}$  NMR (126 MHz,  $\text{CDCl}_3$ )  $\delta$  162.41, 149.33, 146.98, 138.06, 129.15, 128.78, 126.87, 55.81 (br), 43.89 (br), 41.23, 39.19, 38.42, 36.44, 32.77, 31.85, 31.81, 31.79, 31.70, 30.37, 29.84, 28.32, 28.10, 25.55, 18.97, 14.27.

**(2-Benzylpiperidin-1-yl)(3-((cuban-1-ylmethyl)thio)-1H-1,2,4-triazol-1-yl)methanone (28c)**

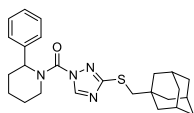


2-Benzylpiperidine (1.5 eq, 12 mg, 0.069 mmol) and **26c** (1 eq, 10 mg, 0.046 mmol) were coupled according to General procedure F to obtain the title compound as a white solid (12 mg, 0.029 mmol, 62%).

$^1\text{H}$  NMR (500 MHz,  $\text{CDCl}_3$ )  $\delta$  8.08 (bs, 1H), 7.26 – 7.01 (m, 5H), 4.96 – 4.82 (m, 1H), 4.38 – 4.22 (m, 1H), 4.05 – 3.99 (m, 1H), 3.90 – 3.80 (m, 6H), 3.49 (d,  $J$  = 2.0 Hz, 2H), 3.24 (td,  $J$  = 13.3, 2.8 Hz, 1H), 3.20 – 3.10 (m, 1H), 2.88 – 2.73 (m, 1H), 1.86 – 1.51 (m, 3H), 1.28 – 1.23 (m, 4H).

$^{13}\text{C}$  NMR (126 MHz,  $\text{CDCl}_3$ )  $\delta$  162.57, 149.28, 146.83, 138.09, 129.18, 128.77, 126.87, 55.57 (br), 48.79, 48.69, 44.07, 41.48 (br), 36.42, 35.36, 29.84, 27.30, 25.55, 22.84, 18.96.

**(3-(((Adamant-1-yl)methyl)thio)-1H-1,2,4-triazol-1-yl)(2-phenylpiperidin-1-yl)methanone (28d)**

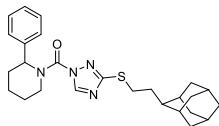


**27** (1.5 eq, 10 mg, 0.060 mmol) and **26a** (1 eq, 10 mg, 0.040 mmol) were coupled according to General procedure F to obtain the title compound as a white solid (12 mg, 0.027 mmol, 69%).

$^1\text{H}$  NMR (500 MHz,  $\text{CDCl}_3$ )  $\delta$  8.74 (s, 1H), 7.43 – 7.32 (m, 4H), 7.32 – 7.27 (m, 1H), 5.97 – 5.87 (m, 1H), 4.42 – 4.32 (m, 1H), 3.02 (td,  $J$  = 13.3, 3.0 Hz, 1H), 2.88 (s, 2H), 2.52 – 2.44 (m, 1H), 2.09 – 1.98 (m, 1H), 1.96 – 1.91 (m, 3H), 1.82 – 1.54 (m, 11H), 1.52 – 1.45 (m, 6H).

$^{13}\text{C}$  NMR (126 MHz,  $\text{CDCl}_3$ )  $\delta$  164.05, 149.64, 147.51, 138.20, 128.98, 127.18, 126.85, 56.41 (br), 45.45, 42.93 (br), 41.45, 36.83, 33.83, 28.52, 28.10, 25.77, 19.52.

**(3-((2-Adamant-2-yl)ethyl)thio)-1H-1,2,4-triazol-1-yl)(2-phenylpiperidin-1-yl)methanone (28e)**

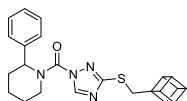


**27** (1.6 eq, 9 mg, 0.06 mmol) and **26b** (1 eq, 10 mg, 0.038 mmol) were coupled according to General procedure F to obtain the title compound as a white solid (12 mg, 0.027 mmol, 70%).

$^1\text{H}$  NMR (500 MHz,  $\text{CDCl}_3$ )  $\delta$  8.76 (s, 1H), 7.41 – 7.32 (m, 4H), 7.31 – 7.27 (m, 1H), 6.00 – 5.84 (m, 1H), 4.46 – 4.33 (m, 1H), 3.10 – 2.92 (m, 3H), 2.52 – 2.44 (m, 1H), 2.10 – 1.98 (m, 1H), 1.90 – 1.58 (m, 19H), 1.53 – 1.45 (m, 2H).

$^{13}\text{C}$  NMR (126 MHz,  $\text{CDCl}_3$ )  $\delta$  163.23, 149.62, 147.67, 138.21, 128.94, 127.17, 126.81, 56.27 (br), 43.75 (br), 43.05, 39.16, 38.40, 32.45, 31.75, 31.71, 31.67, 30.20, 28.31, 28.07, 28.00, 25.78, 19.50.

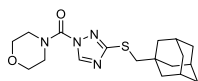
**(2-Phenylpiperidin-1-yl)(3-((cuban-1-ylmethyl)thio)-1H-1,2,4-triazol-1-yl)methanone (28f)**



**27** (1.5 eq, 11 mg, 0.069 mmol) and **26c** (1 eq, 10 mg, 0.046 mmol) were coupled according to General procedure F to obtain the title compound as a white solid (16 mg, 0.030 mmol, 64%).

$^1\text{H}$  NMR (500 MHz,  $\text{CDCl}_3$ )  $\delta$  8.75 (s, 1H), 7.41 – 7.32 (m, 4H), 7.31 – 7.27 (m, 1H), 5.94 – 5.84 (m, 1H), 4.43 – 4.32 (m, 1H), 4.03 – 3.96 (m, 1H), 3.86 – 3.80 (m, 3H), 3.80 – 3.73 (m, 3H), 3.36 (s, 2H), 3.03 (td,  $J$  = 13.4, 2.8 Hz, 1H), 2.52 – 2.44 (m, 1H), 2.10 – 1.99 (m, 1H), 1.81 – 1.59 (m, 4H).

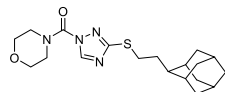
$^{13}\text{C}$  NMR (126 MHz,  $\text{CDCl}_3$ )  $\delta$  163.35, 149.60, 147.58, 138.23, 128.93, 127.15, 126.81, 56.34 (br), 48.75, 48.65, 44.01, 43.06 (br), 35.13, 28.03, 25.75, 19.49.

**(3-(((Adamant-1-yl)methyl)thio)-1H-1,2,4-triazol-1-yl)(morpholino)methanone (28g)**

4-Morpholinecarbonyl chloride (2 eq, 12 mg, 0.080 mmol) and **26a** (1 eq, 10 mg, 0.040 mmol) were coupled according to General procedure G to obtain the title compound as a white solid (5 mg, 0.01 mmol, 34%).

$^1\text{H}$  NMR (500 MHz,  $\text{CDCl}_3$ )  $\delta$  8.71 (s, 1H), 4.10 – 3.67 (m, 4H), 3.82 – 3.76 (m, 4H), 3.03 (s, 2H), 1.99 (p,  $J$  = 3.1 Hz, 3H), 1.75 – 1.55 (m, 12H).

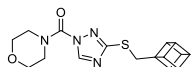
$^{13}\text{C}$  NMR (126 MHz,  $\text{CDCl}_3$ )  $\delta$  164.37, 148.41, 147.40, 66.74, 46.77 (br), 45.74, 41.66, 36.85, 33.93, 29.85, 28.55.

**(3-(((2-Adamant-2-yl)ethyl)thio)-1H-1,2,4-triazol-1-yl)(morpholino)methanone (28h)**

4-Morpholinecarbonyl chloride (2 eq, 11 mg, 0.076 mmol) and **26b** (1 eq, 10 mg, 0.038 mmol) were coupled according to General procedure G to obtain the title compound as a white solid (9 mg, 0.02 mmol, 55%).

$^1\text{H}$  NMR (500 MHz,  $\text{CDCl}_3$ )  $\delta$  8.73 (s, 1H), 4.18 – 3.58 (m, 4H), 3.81 – 3.76 (m, 4H), 3.15 – 3.09 (m, 2H), 1.92 – 1.69 (m, 17H), 1.56 – 1.49 (m, 2H).

$^{13}\text{C}$  NMR (126 MHz,  $\text{CDCl}_3$ )  $\delta$  163.59, 148.37, 147.67, 66.73, 46.75 (br), 43.93, 39.17, 38.38, 32.75, 31.78, 30.30, 28.29, 28.07.

**(3-(((Cuban-1-yl)methyl)thio)-1H-1,2,4-triazol-1-yl)(morpholino)methanone (28i)**

4-Morpholinecarbonyl chloride (14 mg, 0.092 mmol) and **26c** were coupled according to General procedure G to obtain the title compound as a white solid (13 mg, 0.038 mmol, 41%).

$^1\text{H}$  NMR (500 MHz,  $\text{CDCl}_3$ )  $\delta$  8.73 (s, 1H), 4.06 – 3.99 (m, 1H), 4.08 – 3.70 (m, 4H), 3.90 – 3.85 (m, 3H), 3.85 – 3.81 (m, 3H), 3.81 – 3.76 (m, 4H), 3.49 (s, 2H).

$^{13}\text{C}$  NMR (126 MHz,  $\text{CDCl}_3$ )  $\delta$  163.68, 148.32, 147.52, 66.72, 57.02, 48.78, 48.66, 46.98 (br), 44.06, 35.34.

## References

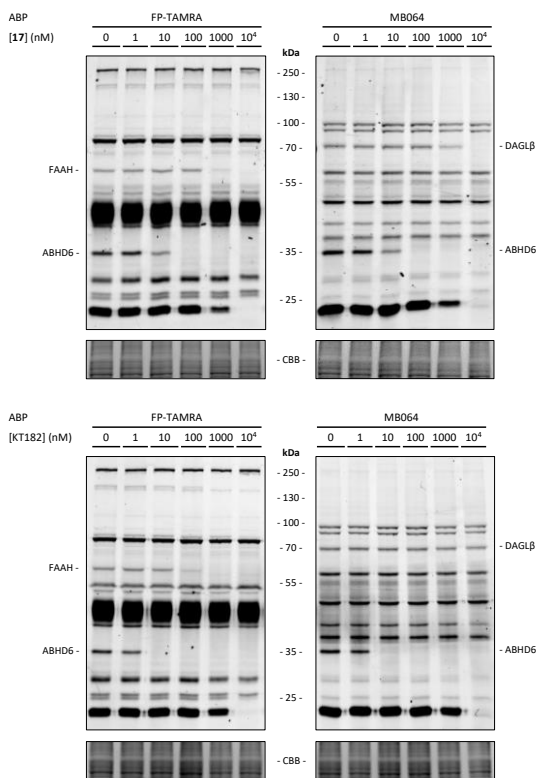
1. Landa, S. & Macháček, V. Sur l'adamantane, nouvel hydrocarbure extrait du naphthe. *Collect. Czechoslov. Chem. Commun.* **5**, 1–5 (1933).
2. Lamoureux, G. & Artavia, G. Use of the Adamantane Structure in Medicinal Chemistry. *Curr. Med. Chem.* **17**, 2967–2978 (2010).
3. Wanka, L., Iqbal, K. & Schreiner, P. R. The lipophilic bullet hits the targets: Medicinal chemistry of adamantane derivatives. *Chem. Rev.* **113**, 3516–3604 (2013).
4. Dahl, J. E., Liu, S. G. & Carlson, R. M. K. Isolation and structure of higher diamondoids, nanometer-sized diamond molecules. *Science (80-. )*. **299**, 96–99 (2003).
5. Schleyer, P. V. R. A Simple Preparation of Adamantane. *J. Am. Chem. Soc.* **79**, 3292 (1957).
6. Liu, J., Obando, D., Liao, V., Lifa, T. & Codd, R. The many faces of the adamantyl group in drug design. *Eur. J. Med. Chem.* **46**, 1949–1963 (2011).
7. Reisberg, B. *et al.* Memantine in Moderate-to-Severe Alzheimer's Disease. *N. Engl. J. Med.* **348**, 1333–1341 (2003).
8. Rosenthal, K. S., Sokol, M. S., Ingram, R. L., Subramanian, R. & Fort, R. C. Tromantadine: inhibitor of early and late events in herpes simplex virus replication. *Antimicrob. Agents Chemother.* **22**, 1031–1036 (1982).
9. Ickes, D. E., Venetta, T. M., Phonphok, Y. & Rosenthal, K. S. Tromantadine inhibits a late step in herpes simplex virus type 1 replication and syncytium formation. *Antiviral Res.* **14**, 75–85 (1990).
10. Balzarini, J., Orzeszko-Krzesińska, B., Maurin, J. K. & Orzeszko, A. Synthesis and anti-HIV studies of 2- and 3-adamantyl-substituted thiazolidin-4-ones. *Eur. J. Med. Chem.* **44**, 303–311 (2009).
11. Balzarini, J., Orzeszko, B., Maurin, J. K. & Orzeszko, A. Synthesis and anti-HIV studies of 2-adamantyl-substituted thiazolidin-4-ones. *Eur. J. Med. Chem.* **42**, 993–1003 (2007).
12. Barnett, A. DPP-4 inhibitors and their potential role in the management of type 2 diabetes. *Int. J. Clin. Pract.* **60**, 1454–1470 (2006).
13. Kim, I. H., Morisseau, C., Watanabe, T. & Hammock, B. D. Design, Synthesis, and Biological Activity of 1,3-Disubstituted Ureas as Potent Inhibitors of the Soluble Epoxide Hydrolase of Increased Water Solubility. *J. Med. Chem.* **47**, 2110–2122 (2004).
14. Kasuga, J. *et al.* SAR-oriented discovery of peroxisome proliferator-activated receptor pan agonist with a 4-adamantylphenyl group as a hydrophobic tail. *Bioorg. Med. Chem. Lett.* **18**, 1110–1115 (2008).
15. Wennekes, T. *et al.* Synthesis and evaluation of dimeric lipophilic iminosugars as inhibitors of glucosylceramide metabolism. *Tetrahedron: Asymmetry* **20**, 836–846 (2009).
16. Wennekes, T. *et al.* Development of adamantan-1-yl-methoxy-functionalized 1-deoxynojirimycin derivatives as selective inhibitors of glucosylceramide metabolism in man. *J. Org. Chem.* **72**, 1088–1097 (2007).
17. Overkleeft, H. S. *et al.* Generation of Specific Deoxynojirimycin-type Inhibitors of the Non-lysosomal Glucosylceramidase. *J. Biol. Chem.* **273**, 26522–26527 (1998).
18. Mylvaganam, M. & Lingwood, C. A. Adamantyl Globotriaosyl Ceramide: A Monovalent Soluble Mimic Which Inhibits Verotoxin Binding to Its Glycolipid Receptor. *Biochem. Biophys. Res. Commun.* **257**, 391–394 (1999).
19. Tsuzuki, N. *et al.* Adamantane as a Brain-Directed Drug Carrier for Poorly Absorbed Drug. 2. AZT Derivatives Conjugated with the 1-Adamantane Moiety. *J. Pharm. Sci.* **83**, 481–484 (1994).
20. Lu, D. *et al.* Adamantyl cannabinoids: A novel class of cannabinergic ligands. *J. Med. Chem.* **48**, 4576–4585 (2005).

21. Jia, L. *et al.* Pharmacodynamics and pharmacokinetics of SQ109, a new diamine-based antitubercular drug. *Br. J. Pharmacol.* **144**, 80–87 (2005).
22. Kaur, G. *et al.* Synthesis, structure–activity relationship, and p210bcr-abl protein tyrosine kinase activity of novel AG 957 analogs. *Bioorg. Med. Chem.* **13**, 1749–1761 (2005).
23. Bodor, N., El-Koussi, A. A., Khalifa, M. M. & Kano, M. Soft Drugs. 7. Soft  $\beta$ -Blockers for Systemic and Ophthalmic Use. *J. Med. Chem.* **31**, 1651–1656 (1988).
24. Rapala, R. T., Kraay, R. J. & Gerzon, K. The Adamantyl Group in Medicinal Agents. II. Anabolic Steroid 17 $\beta$ -Adamantoates. *J. Med. Chem.* **8**, 580–583 (1965).
25. Gerzon, I. & Kau, D. The Adamantyl Group in Medicinal Agents. III. Nucleoside 5'-Adamantoates. The Adamantoyl Function as a Protecting Group<sup>1</sup>. *J. Med. Chem.* **10**, 189–199 (1967).
26. Masereel, B., Rolin, S., Abbate, F., Scozzafava, A. & Supuran, C. T. Carbonic anhydrase inhibitors: Anticonvulsant sulfonamides incorporating valproyl and other lipophilic moieties. *J. Med. Chem.* **45**, 312–320 (2002).
27. Gerzon, K., Krumkalns, E. V., Brindle, R. L., Marshall, F. J. & Root, M. A. The Adamantyl Group in Medicinal Agents. I. Hypoglycemic *N*-Arylsulfonyl-*N'*-adamantylureas. *J. Med. Chem.* **6**, 760–763 (1963).
28. Reekie, T. A., Williams, C. M., Rendina, L. M. & Kassiou, M. Cubanes in Medicinal Chemistry. *J. Med. Chem.* **62**, 1078–1095 (2019).
29. Auberson, Y. P. *et al.* Improving Nonspecific Binding and Solubility: Bicycloalkyl Groups and Cubanes as para-Phenyl Bioisosteres. *ChemMedChem* **12**, 590–598 (2017).
30. Wlochaj, J., Davies, R. D. M. & Burton, J. Cubanes in medicinal chemistry: Synthesis of functionalized building blocks. *Org. Lett.* **16**, 4094–4097 (2014).
31. Long, J. Z. & Cravatt, B. F. The Metabolic Serine Hydrolases and Their Functions in Mammalian Physiology and Disease. *Chem. Rev.* **111**, 6022–6063 (2011).
32. Bachovchin, D. A. & Cravatt, B. F. The pharmacological landscape and therapeutic potential of serine hydrolases. *Nat. Rev. Drug Discov.* **11**, 52–68 (2012).
33. Faucher, F., Bennett, J. M., Bogoy, M. & Lovell, S. Strategies for Tuning the Selectivity of Chemical Probes that Target Serine Hydrolases. *Cell Chem. Biol.* **27**, 937–952 (2020).
34. Baggelaar, M. P., Maccarrone, M. & van der Stelt, M. 2-Arachidonoylglycerol: A signaling lipid with manifold actions in the brain. *Prog. Lipid Res.* **71**, 1–17 (2018).
35. Kozak, K. R. & Marnett, L. J. Oxidative metabolism of endocannabinoids. *Prostaglandins Leukot. Essent. Fat. Acids* **66**, 211–220 (2002).
36. Hu, S. S. J., Bradshaw, H. B., Chen, J. S. C., Tan, B. & Walker, J. M. Prostaglandin E<sub>2</sub> glycerol ester, an endogenous COX-2 metabolite of 2-arachidonoylglycerol, induces hyperalgesia and modulates NF $\kappa$ B activity. *Br. J. Pharmacol.* **153**, 1538–1549 (2008).
37. Murataeva, N., Straiker, A. & MacKie, K. Parsing the players: 2-arachidonoylglycerol synthesis and degradation in the CNS. *Br. J. Pharmacol.* **171**, 1379–1391 (2014).
38. van Esbroeck, A. C. M. *et al.* Identification of  $\alpha$ , $\beta$ -Hydrolase Domain Containing Protein 6 as a Diacylglycerol Lipase in Neuro-2a Cells. *Front. Mol. Neurosci.* **12**, (2019).
39. Straiker, A. *et al.* COX-2 and fatty acid amide hydrolase can regulate the time course of depolarization-induced suppression of excitation. *Br. J. Pharmacol.* **164**, 1672–1683 (2011).
40. Buisseret, B., Alhouayek, M., Guillemot-Legris, O. & Muccioli, G. G. Endocannabinoid and Prostanoid Crosstalk in Pain. *Trends Mol. Med.* **25**, 882–896 (2019).
41. Marrs, W. R. *et al.* The serine hydrolase ABHD6 controls the accumulation and efficacy of 2-AG at cannabinoid receptors. *Nat. Neurosci.* **13**, 951–957 (2010).

42. Alhouayek, M., Masquelier, J., Cani, P. D., Lambert, D. M. & Muccioli, G. G. Implication of the anti-inflammatory bioactive lipid prostaglandin D<sub>2</sub>-glycerol ester in the control of macrophage activation and inflammation by ABHD6. *Proc. Natl. Acad. Sci.* **110**, 17558–17563 (2013).
43. Tchanchou, F. & Zhang, Y. Selective inhibition of alpha/beta-hydrolase domain 6 attenuates neurodegeneration, alleviates blood brain barrier breakdown, and improves functional recovery in a mouse model of traumatic brain injury. *J. Neurotrauma* **30**, 565–579 (2013).
44. Manterola, A. *et al.* Re-examining the potential of targeting ABHD6 in multiple sclerosis: Efficacy of systemic and peripherally restricted inhibitors in experimental autoimmune encephalomyelitis. *Neuropharmacology* **141**, 181–191 (2018).
45. Wen, J., Ribeiro, R., Tanaka, M. & Zhang, Y. Activation of CB<sub>2</sub> receptor is required for the therapeutic effect of ABHD6 inhibition in experimental autoimmune encephalomyelitis. *Neuropharmacology* **99**, 196–209 (2015).
46. Manterola, A. *et al.* Deregulation of the endocannabinoid system and therapeutic potential of ABHD6 blockade in the cuprizone model of demyelination. *Biochem. Pharmacol.* **157**, 189–201 (2018).
47. Tanaka, M. *et al.* WWL70 attenuates PGE<sub>2</sub> production derived from 2-arachidonoylglycerol in microglia by ABHD6-independent mechanism. *J. Neuroinflammation* **14**, 7 (2017).
48. Blankman, J. L., Long, J. Z., Trauger, S. A., Siuzdak, G. & Cravatt, B. F. ABHD12 controls brain lysophosphatidylserine pathways that are deregulated in a murine model of the neurodegenerative disease PHARC. *Proc. Natl. Acad. Sci.* **110**, 1500–1505 (2013).
49. Kamat, S. S. *et al.* Immunomodulatory lysophosphatidylserines are regulated by ABHD16A and ABHD12 interplay. *Nat. Chem. Biol.* **11**, 164–171 (2015).
50. Singh, S., Joshi, A. & Kamat, S. S. Mapping the Neuroanatomy of ABHD16A, ABHD12, and Lysophosphatidylserines Provides New Insights into the Pathophysiology of the Human Neurological Disorder PHARC. *Biochemistry* **59**, 2299–2311 (2020).
51. Deng, H. & Li, W. Therapeutic potential of targeting  $\alpha/\beta$ -Hydrolase domain-containing 6 (ABHD6). *Eur. J. Med. Chem.* **198**, (2020).
52. Ogasawara, D. *et al.* Rapid and profound rewiring of brain lipid signaling networks by acute diacylglycerol lipase inhibition. *Proc. Natl. Acad. Sci.* **113**, 26–33 (2016).
53. Hsu, K. L. *et al.* Discovery and optimization of piperidyl-1,2,3-triazole ureas as potent, selective, and in vivo-active inhibitors of  $\alpha/\beta$ -hydrolase domain containing 6 (ABHD6). *J. Med. Chem.* **56**, 8270–8279 (2013).
54. Janssen, A. P. A. Hit-to-Lead Optimization of Triazole Sulfonamide DAGL- $\alpha$  inhibitors. *Inhibitor Selectivity: Profiling and Prediction* (Leiden University, 2019).
55. Janssen, F. J. Discovery of 1,2,4-triazole sulfonamide ureas as in vivo active  $\alpha/\beta$  hydrolase domain type 16A inhibitors. *Discovery of novel inhibitors to investigate diacylglycerol lipases and  $\alpha/\beta$  hydrolase domain 16A* (Leiden University, 2016).
56. Deng, H. *et al.* Triazole Ureas Act as Diacylglycerol Lipase Inhibitors and Prevent Fasting-Induced Refeeding. *J. Med. Chem.* **60**, 428–440 (2017).
57. Cravatt, B. F. *et al.* Molecular characterization of an enzyme that degrades neuromodulatory fatty-acid amides. *Nature* **384**, 83–87 (1996).
58. Katritzky, A. R., Darabantu, M., Aslan, D. C. & Oniciu, D. C. Selective Reactivity of sp<sup>3</sup> and sp<sup>2</sup> Carbanions of 1-Substituted 1,2,4-Triazoles. A Comparative Approach. *J. Org. Chem.* **63**, 4323–4331 (1998).
59. Hsu, K. L. *et al.* DAGL $\beta$  inhibition perturbs a lipid network involved in macrophage inflammatory responses. *Nat. Chem. Biol.* **8**, 999–1007 (2012).

60. Van Esbroeck, A. C. M. *et al.* Activity-based protein profiling reveals off-target proteins of the FAAH inhibitor BIA 10-2474. *Science* **356**, 1084–1087 (2017).
61. Liu, Y., Patricelli, M. P. & Cravatt, B. F. Activity-based protein profiling: The serine hydrolases. *Proc. Natl. Acad. Sci.* **96**, 14694–14699 (1999).
62. Pfeiffer, R. F., Wszolek, Z. K. & Ebadi, M. *Parkinson's disease, second edition. Parkinson's Disease, Second Edition* (CRC Press, 2012). doi:10.1201/b12948.
63. Hsu, K. L. *et al.* Development and optimization of piperidyl-1,2,3-triazole ureas as selective chemical probes of endocannabinoid biosynthesis. *J. Med. Chem.* **56**, 8257–8269 (2013).
64. Gopalan, B. *et al.* Discovery of adamantane based highly potent HDAC inhibitors. *Bioorganic Med. Chem. Lett.* **23**, 2532–2537 (2013).

## Supplementary information



**Supplementary Figure S6.1. Full gel images of cellular cABPP assays.** Representative fluorescence images and coomassie protein loading controls of cABPP experiments on Neuro-2a cells, shown for compound **17** (A) and KT182 (B). Activity-based probes (ABPs) used are indicated, as well as intended inhibitor target and most relevant off-targets.



**Supplementary Table S6.1. *In vitro* inhibitory activity of 13–21 and KT182 on mouse brain enzymes.** pIC<sub>50</sub> values (left column for each inhibitor) determined from cABPP experiments on mouse brain proteome with probes FP-TAMRA and MB064. Data presented as mean ± SEM (N = 3). For each inhibitor the apparent fold selectivity (app. sel.) on its intended target (indicated with “–”) over its respective off-targets is stated in the right column.

	13	14	15	16	17	18	KT182	19	20	21									
	pIC <sub>50</sub> ± SEM	App. sel.	pIC <sub>50</sub> ± SEM	App. sel.	pIC <sub>50</sub> ± SEM	App. sel.	pIC <sub>50</sub> ± SEM	App. sel.	pIC <sub>50</sub> ± SEM	App. sel.	pIC <sub>50</sub> ± SEM	App. sel.							
ABHD6	6.49 ± 0.07	17 > 537	7.05 ± 0.03	3.4 > 380	6.84 ± 0.06	14 > 1000	6.49 ± 0.05	–	6.80 ± 0.03	–	6.61 ± 0.05	–	7.40 ± 0.04	7.53 ± 0.05	< 1	7.82 ± 0.03	< 1	7.26 ± 0.07	< 1
ABHD12	< 5.0	> 537	< 5.0	> 380	< 5.0	> 1000	< 5.0	> 30	< 5.0	> 63	< 5.0	> 40	< 5.0	> 251	5.44 ± 0.19	6.29 ± 0.11	18	5.47 ± 0.14	7.8
ABHD16a	< 5.0	> 537	< 5.0	> 380	< 5.0	> 1000	< 5.0	> 30	< 5.0	> 63	< 5.0	> 40	< 5.0	> 251	7.03 ± 0.07	7.55 ± 0.04	–	6.36 ± 0.07	–
DAGLα	7.73 ± 0.08	–	7.58 ± 0.09	–	8.00 ± 0.06	–	5.60 ± 0.08	7.8	5.68 ± 0.06	13	6.00 ± 0.07	4.1	< 5.0	> 251	5.44 ± 0.19	5.75 ± 0.13	63	4.91 ± 0.24	28
DDHD2	< 5.0	> 537	< 5.0	> 380	< 5.0	> 1000	< 5.0	> 30	< 5.0	> 63	< 5.0	> 40	< 5.0	> 251	5.81 ± 0.08	5.64 ± 0.11	81	< 5.0	> 22
FAAH	< 5.0	> 537	< 5.0	> 380	< 5.0	> 1000	< 5.0	> 30	< 5.0	> 63	5.59 ± 0.06	10	< 5.0	> 251	< 5.0	< 5.0	> 354	5.64 ± 0.04	5.2
KIAA1363	< 5.0	> 537	< 5.0	> 380	< 5.0	> 1000	< 5.0	> 30	< 5.0	> 63	< 5.0	> 40	< 5.0	> 251	< 5.0	< 5.0	> 354	< 5.0	> 22
LYPLA1/2	5.20 ± 0.06	339	< 5.0	> 380	6.86 ± 0.03	< 5.0	> 1000	< 1	6.04 ± 0.04	5.8	6.84 ± 0.02	< 1	5.13 ± 0.05	186	7.03 ± 0.10	6.83 ± 0.08	5.2	6.42 ± 0.06	< 1
MAGL	< 5.0	> 537	< 5.0	> 380	< 5.0	> 1000	< 5.0	> 30	< 5.0	> 63	< 5.0	> 40	< 5.0	> 251	< 5.0	< 5.0	> 354	< 5.0	> 22
NTE	< 5.0	> 537	< 5.0	> 380	< 5.0	> 1000	< 5.0	> 30	< 5.0	> 63	< 5.0	> 40	5.46 ± 0.15	87	5.03 ± 0.10	5.62 ± 0.15	85	5.27 ± 0.09	12

# 7

**Summary and future prospects**

*N*-acylphosphatidylethanolamines (NAPEs) are a diverse family of lipids with multifaceted biological functions, but they are relatively underexplored.<sup>1,2</sup> Recently, Phospholipase A2 Group IV E (PLA2G4E) was shown to be capable of calcium-dependent production of NAPEs in cells.<sup>3,4</sup> PLA2G4E is a member of the PLA2G4 family, which consists of six serine hydrolases (PLA2G4A–F).<sup>5</sup> These enzymes are characterized by a Ser-Asp catalytic dyad and an N-terminal calcium-dependent lipid binding C2 domain.<sup>5,6</sup> PLA2G4E has an additional C-terminal polybasic stretch which is involved in its subcellular localization.<sup>7</sup> It was reported to be a principal *N*-acyltransferase that is able to synthesize NAPEs in a calcium-dependent fashion.<sup>3</sup> It is mainly expressed in brain, testes, heart and skeletal muscle, and expression levels were linked to Alzheimer's disease and panic disorder.<sup>3,8,9</sup> In addition, it appeared to be involved in recycling cargo from the clathrin-independent endocytic machinery back to the plasma membrane.<sup>7</sup> Whether NAPEs are involved in these functions is unclear.

No inhibitors of PLA2G4E have been published to date. PLA2G4E inhibitors would be instrumental in elucidating the physiological role of this enzyme in NAPE biology in an acute and time-dependent manner. Selective inhibitors are also required to establish the therapeutic potential of targeting PLA2G4E. Therefore, the overarching aim of this thesis was to develop cellular active inhibitors of PLA2G4E.

**Chapter 1** gives a comprehensive overview of the current understanding of NAPE biology and PLA2G4E. NAPEs are glycerophospholipids with three fatty acyl groups. When these are embedded in lipid membranes, NAPEs may be involved in regulation of membrane dynamics, including membrane curvature, fusion and interactions with membrane-associated proteins.<sup>10–14</sup> NAPEs may also serve as signaling molecules. Hypophagic functions have been attributed to them, though it is disputed whether the effects reported are truly NAPE-specific.<sup>15,16</sup> Their levels are markedly increased in degenerating tissue, an effect observed in e.g. infarcted heart, ischemic brain and inflamed testes.<sup>17–19</sup> In addition, NAPE levels are elevated in models of neurodegeneration, and a protective role has been proposed in Parkinson's disease.<sup>14,20–22</sup> Furthermore, biosynthesis and metabolism of NAPEs plays an important role in the homeostasis of other structural and signaling lipids. They are produced from phosphatidylethanolamine (PE) and phosphatidylcholine (PC)<sup>3,23</sup>, levels of which have also been linked to neurodegenerative diseases.<sup>24–26</sup> Four pathways for the metabolism of NAPEs to *N*-acylethanolamines (NAEs) have been reported, generating various classes of important metabolites, including phosphatidic acid (PA), lysophosphatidic acid (LPA) and free fatty acids (FFAs).<sup>27</sup> Depending on their structure, NAEs exert diverse signaling functionalities through the activation of various receptors, which leads to satietal, anti-inflammatory, analgesic, anti-addictive or anxiolytic effects, among others.<sup>28–34</sup> NAEs are metabolized by the enzyme fatty acid amide hydrolase (FAAH), terminating their biological actions.

In **Chapter 2**, the development of novel PLA2G4E inhibitors is reported. Previously, a competitive activity-based protein profiling (ABPP) assay was developed to measure the

activity of PLA2G4E.<sup>35</sup> Screening of a focused library of lipase inhibitors identified 1,2,4-triazole ureas as inhibitors of PLA2G4E. Compound **1** was selected as starting point for hit optimization, based on its potency, lipophilic efficiency (LipE) and ligand efficiency (LE) (Figure 7.1A). 26 analogs were synthesized and tested for inhibitory activity with the aim of deducing structure-activity relationships (SAR) and improving the potency. Increasing the distance between the phenyl in the amine group and the reactive urea and increasing steric bulk resulted in improved potency, leading to the identification of a 4-benzylpiperidine group providing 10-fold potency improvement. *Ortho* and *meta* substitutions on this benzyl ring were tolerated, but *para* substitutions were preferred. 4-(4-Chlorobenzyl)piperidine-containing compound **WEN091** was identified as the most potent PLA2G4E inhibitor ( $pIC_{50} = 8.01 \pm 0.02$ ). **WEN091** demonstrated ~100-fold potency increase compared to **1** and improved LipE and LE (Figure 7.1A).

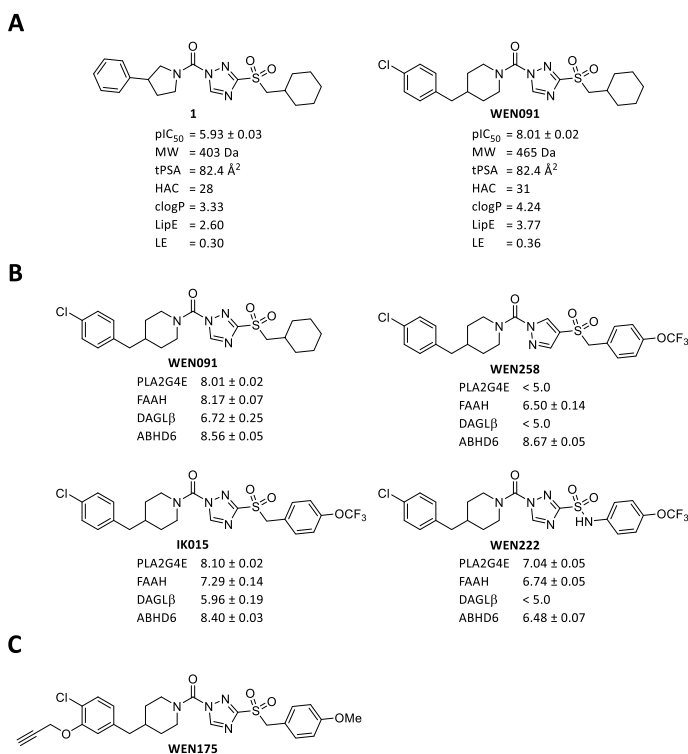


**Figure 7.1. Structures and properties of PLA2G4E inhibitors 1–WEN175.** A) Potency and physicochemical properties of hit **1** and inhibitor **WEN091**. Potency on PLA2G4E determined using gel-based ABPP on HEK293T overexpression lysate ( $pIC_{50} \pm SEM$ ,  $N \geq 2$ ). Molecular weight (MW) and topological polar surface area (tPSA) calculated using ChemDraw Professional 16.0; HAC = heavy atom count; Lipophilic efficiency LipE =  $pIC_{50} - clogP$  (DataWarrior 5.0.0); Ligand efficiency LE =  $1.4pIC_{50}/HAC$ . B) Inhibitory activity of inhibitors **WEN091–WEN258** ( $pIC_{50} \pm SEM$ ) determined using gel-based ABPP on overexpression lysate (PLA2G4E) or Neuro-2a cells (FAAH, DAGLβ, ABHD6) ( $N \geq 2$ ). C) Chemical structure of PLA2G4E probe **WEN175**.

**WEN091** was further biochemically profiled in **Chapter 3**. The activity on PLA2G4E was tested in a natural substrate conversion assay based on liquid chromatography-mass spectrometry (LC-MS) analysis. **WEN091** dose-dependently inhibited the formation of NAPE from exogenous PC and PE in human and mouse PLA2G4E overexpression lysate as well as in mouse brain homogenate ( $pIC_{50} = 6.9-7.1$ ). The compound was more than 20-fold selective over PLA2G4B-D and at least ten-fold over the calcium-independent NAPE biosynthetic enzymes phospholipase A/acyltransferase (PLAAT) 2-5. The compound was not active on NAPE phospholipase D (NAPE-PLD) or the cannabinoid (CB<sub>1/2</sub>) receptors. ABPP profiling of its selectivity on mouse brain proteome and living cells showed inhibition of several serine hydrolases, such as ABHD6, DAGL $\alpha$  and FAAH. **WEN091**, but not its negative control analog **WEN258** (see below), reduced endogenous cellular levels of NAPEs, lyso-NAPEs and glycerophospho-palmitoylethanolamine. Both compounds showed cellular activity on FAAH, but only treatment with **WEN258** affected the NAE levels, suggesting that steady state NAE levels in these cells are controlled by PLA2G4E and FAAH. *N*-22:6 lyso-NAPE levels were not elevated in overexpressing cells, but were after treatment with **WEN091** or **WEN258**, leading to the hypothesis that these lipids are biosynthesized in a PLA2G4E and ABHD4-independent fashion. Both inhibitors lowered levels of the endocannabinoid 2-arachidonoylglycerol (2-AG), but only **WEN091** showed inhibition of its biosynthetic enzyme DAGL $\beta$ . This suggested ABHD6 might be responsible for tonic 2-AG production in these cells, which is in line with previous findings.<sup>36</sup> In conclusion, **WEN091** is a potent PLA2G4E inhibitor with selectivity for calcium-dependent NAPE biosynthesis *in vitro* that was able to reduce PLA2G4E-mediated NAPE production in Neuro-2a cells.

In **Chapter 4**, the SAR study of PLA2G4E inhibitors was expanded with 38 analogs of **WEN091** to improve its selectivity over FAAH. It was concluded that the sulfone was important for activity on PLA2G4E, but not on FAAH. Converting this to a sulfonamide decreased activity on both enzymes and led to lower selectivity. Bulky substituents on the triazolyl leaving group provided higher selectivity over FAAH, leading to the identification of 4-trifluoromethoxybenzyl-containing compound **IK015** as potent PLA2G4E inhibitor ( $pIC_{50} = 8.10 \pm 0.02$ ) with over 800-fold selectivity over FAAH *in vitro* (Figure 7.1B). Further investigation of the steric and electronic properties of this benzyl group did not improve the potency or selectivity. Analogs of the piperidine moiety lowered activity on PLA2G4E.

**IK015** and sulfonamide analog **WEN222** (Figure 7.1B) were selected for further biological characterization. The compounds were selective over PLA2G4B-D, NAPE-PLD and CB<sub>1</sub> and CB<sub>2</sub> receptors. In addition, **IK015** and **WEN222** showed at least 10-fold selectivity over PLAAT2-5 and more than 30-fold selectivity over most serine hydrolases characterized in mouse brain proteome, but selectivity over ABHD6 was limited (~4-fold). In Neuro-2a cells, **IK015** inhibited several enzymes at 1  $\mu$ M, including ABHD6, ABHD12 and FAAH. **WEN222** was less active on most enzymes, which might indicate restricted membrane permeability. Similar to **WEN091**, the compounds showed increased activity

on FAAH in the cellular assay. Altogether, **IK015** and **WEN222** are potent and selective PLA2G4E inhibitors *in vitro* with an improved selectivity profile compared to **IK015**, but showed activity on several serine hydrolases at higher concentrations. Pyrazole urea **WEN258** was identified as structural analog with a similar off-target profile to **WEN091**, **IK015** and **WEN222** but no activity on PLA2G4E (Figure 7.1B).

To support the evidence of **WEN091**'s cellular activity on PLA2G4E, in **Chapter 5**, an activity-based probe (ABP) was developed to visualize intracellular target engagement. The design of probe **WEN175** (Figure 7.1C) was based on PLA2G4E inhibitors identified in **Chapters 2** and **4**. The triazole ureas are hypothesized to covalently modify the catalytic serine of PLA2G4E by the formation of a carbamoyl adduct, which should allow to irreversibly label active enzyme. Therefore, the carbamoylating 'staying group' of **WEN175** was equipped with an alkyne handle to which a fluorophore could be conjugated after cell lysis using copper-catalyzed alkyne-azide cycloaddition (CuAAC). This 'two-step labeling' approach circumvented cell permeability issues associated with bulky, charged fluorophores.<sup>37,38</sup> Probe **WEN175** was able to dose-dependently label PLA2G4E overexpressed in Neuro-2a cells, demonstrating its applicability as cellular active PLA2G4E probe. **WEN175** did not label PLA2G4E mutants in which the catalytic serine was substituted for an alanine (S412A) or the C2 domain ( $\Delta$ C2) or polybasic domain ( $\Delta$ PB) were removed, thereby illustrating the importance of this amino acid and motifs for the catalytic activity.<sup>39</sup> Importantly, pre-treatment with **WEN091** dose-dependently inhibited fluorescent labeling of PLA2G4E by **WEN175**, demonstrating cellular target engagement of **WEN091**. Despite **WEN091**'s low nanomolar  $IC_{50}$  *in vitro*, high concentrations (10  $\mu$ M) were needed to obtain complete *in situ* target engagement, which is in line with the results from the targeted lipidomics experiments in **Chapter 3**. Limited cell penetration and/or high levels of competing substrates are likely to explain the need for high cellular concentrations of inhibitor **WEN091**. The tailored ABP **WEN175** is a useful chemical tool to guide the design of novel PLA2G4E inhibitors with improved cellular activity.

Caged hydrocarbons are polycyclic chemical structures with unique physicochemical properties, but they are not commonly applied in medicinal chemistry. In **Chapter 6**, nine 1,2,4-triazole ureas substituted with caged hydrocarbons were synthesized and tested as inhibitors of ABHD6, ABHD16a and DAGL $\alpha/\beta$  to investigate the effect of caged hydrocarbons on the activity of the inhibitors. All compounds inhibited their primary target with sub-micromolar  $IC_{50}$  values in an ABPP assay on mouse brain proteome. Adamant-2-ylethylene-containing ABHD6 inhibitor **RED353** and cubanemethylene-containing DAGL inhibitor **2** were further profiled in cellular assays (Figure 7.2). **2**'s activity on DAGL $\beta$  in Neuro-2a cells was lower than its activity on DAGL $\alpha$  *in vitro*, but **RED353** inhibited ABHD6 with  $pIC_{50} = 8.39 \pm 0.03$  and showed almost 300-fold selectivity over DAGL $\beta$  and 90-fold over FAAH. **RED353** also inhibited ABHD6-mediated fluorogenic substrate conversion in an orthogonal assay and lowered cellular 2-AG, but not anandamide, levels, outperforming

widely used ABHD6 inhibitor KT182.<sup>40</sup> These results confirm and extend the previous observation that ABHD6 is responsible for the tonic production of 2-AG in Neuro-2a cells.<sup>36</sup>

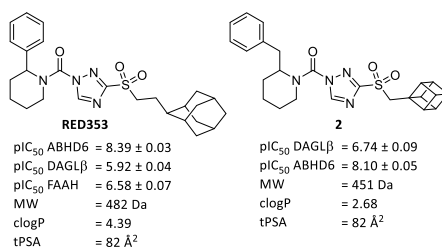


**Figure 7.2. Structure and properties of ABHD6 inhibitors RED353 and 2.** Activity determined using gel-based ABPP on Neuro-2a cells ( $pIC_{50} \pm$  SEM, N = 3). Molecular weight (MW) and topological polar surface area (tPSA) calculated using ChemDraw Professional 16.0, octanol/water partition coefficient (clogP) calculated using DataWarrior 5.0.0.

## Future directions

### Towards improved PLA2G4E and ABHD6 inhibitors

Previously, triazole ureas have been successfully leveraged as tool compounds to study several brain serine hydrolases *in vivo*, e.g. ABHD6, ABHD16a and DAGL $\alpha/\beta$ <sup>40–43</sup>, thereby showing the future potential for the PLA2G4E inhibitors reported in this thesis. PLA2G4E inhibitor **WEN091** showed high potency, cellular target engagement and efficacy in lowering cellular NAPE levels, but inhibited several additional serine hydrolases in Neuro-2a cells. **IK015** has an improved *in vitro* selectivity profile compared to **WEN091** and lower off-target activity in Neuro-2a cells. Further characterization of this inhibitor by investigating *in situ* target engagement, inhibition of NAPE formation and activity on other enzymes involved in NAPE metabolism (ABHD4, PLAAT1–5) will be necessary to determine whether **IK015** is a better lead candidate for *in vivo* PLA2G4E inhibition than **WEN091**. Of note, **IK015** did show inhibition of FAAH and ABHD6 at concentrations below 1  $\mu$ M in a cellular setting and a relatively high topological polar surface area, which may limit brain penetration. Further optimization of the selectivity and physicochemical properties of this chemotype might, therefore, be required.

Structure-based drug design could guide the design of the next series of PLA2G4E inhibitors. Currently, there are no crystal structures available of PLA2G4E. **IK015** was, therefore, docked into a homology model of hPLA2G4E built based on the crystal structure of hPLA2G4D.<sup>44</sup> The predicted binding pose suggests the existence of a narrow pocket lined with hydrophobic residues, limited space around the chlorine atom and a larger pocket around the trifluoromethoxy substituent, in line with the SAR results from **Chapters 2 and 4** (Figure 7.3). The SAR suggest that substituents that create new interactions with the active site may be introduced on the *ortho* or *meta* position of the piperidyl benzyl or *para* position of the sulfonyl benzyl. These substituents might be able to increase the inhibitor's affinity for PLA2G4E and selectivity over other targets. Improving the inhibitor's

potency may potentially allow to remove heteroatoms to reduce the tPSA. One should, however, always take into consideration the effect modifications have on other physico-chemical properties, such as the lipophilicity and molecular weight. A combination of modifications might be required to obtain the optimal balance. Characterization of the pharmacokinetic properties of the inhibitors will be necessary to assess their *in vivo* applicability. Results of these studies may demand further optimization of e.g. metabolic stability, plasma protein binding or brain penetration.

The broad reactivity of triazole ureas towards serine hydrolases makes it challenging to obtain high selectivity, and many previously published triazole urea-based inhibitors have shown cross-reactivity with off-targets at elevated concentrations.<sup>40,41,43</sup> In addition to (adverse) off-target effects, this could lead to limited metabolic stability of the compound due to rapid enzymatic hydrolysis.<sup>45,46</sup> Increasing the non-covalent binding

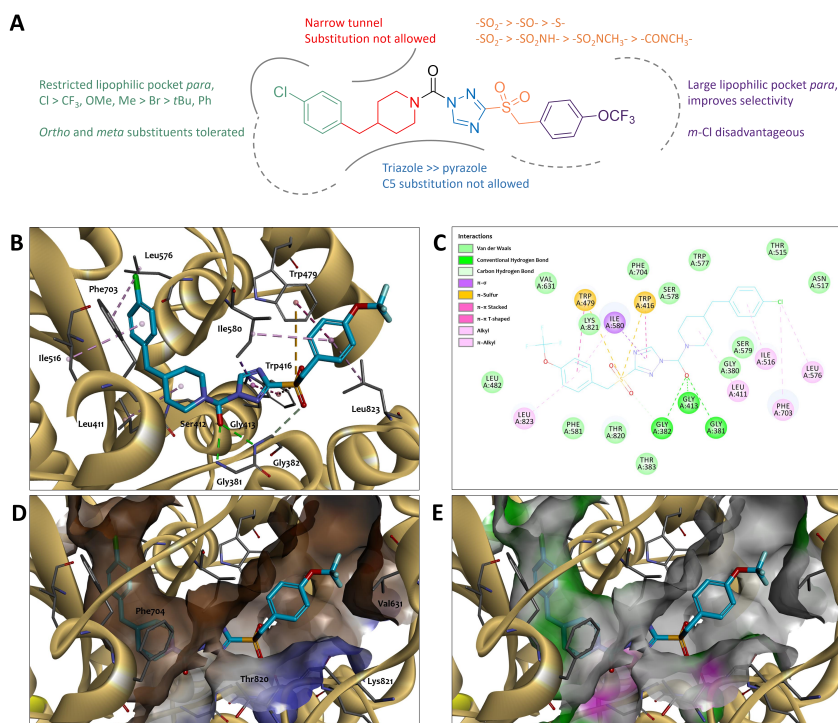


**Figure 7.3. SAR overview and docking results of IK015.** A) Summary of observations regarding the potency and selectivity of synthesized PLA2G4E inhibitors from the SAR studies in Chapters 2 and 4. B–E) **IK015** (cyan carbon atoms) was covalently docked to Ser<sup>412</sup> (bond not shown) in a homology model of hPLA2G4E (sand ribbon) based on hPLA2G4D.<sup>44</sup> Several amino acids interacting with **IK015** are displayed in element color. B) Highest-scored **IK015** docking pose in hPLA2G4E model with predicted enzyme–inhibitor interactions indicated. Interacting amino acids are annotated. C) 2D representation of predicted interactions of **IK015** with hPLA2G4E, corresponding to the docking pose in (B). D) Docking pose with pocket surface shown. Hydrophobic surface is indicated in brown, hydrophilic in blue. E) Docking pose with pocket surface indicating predicted hydrogen bond donating (magenta) and accepting (green) character.



affinity of the PLA2G4E inhibitors for PLA2G4E may allow to reduce the intrinsic reactivity of the urea warhead, which might lead to improved selectivity over other serine hydrolases. However, less promiscuous chemotypes might be better suited for specific PLA2G4E inhibition and high *in vivo* stability.

ABHD6 inhibitor **RED353** displayed high potency and a favorable selectivity profile in Neuro-2a cells. It showed lower activity on FAAH than KT182, but was more active on DAGL $\alpha$  and  $\beta$ . Previous studies on DAGL and ABHD6 inhibitors have shown increased selectivity for ABHD6 when polar groups were introduced on the piperidine or leaving group substituent.<sup>40,47,48</sup> Hence, new derivatives of **RED353** with polar substituents could be explored that might improve the ABHD6 selectivity. These can be used to study the contribution of ABHD6 to 2-AG production in other cell types and under different conditions.

### **PLA2G4E inhibitors may elucidate PLA2G4E and NAPE biology**

PLA2G4A has been extensively exploited for the development of drugs against inflammatory conditions, and several PLA2G4A inhibitors have advanced into clinical trials.<sup>49,50</sup> Similarly, multiple inhibitors of enzymes involved in the endocannabinoid system have been developed to study the therapeutic potential of their targets in inflammatory pain, anxiety or metabolic syndrome.<sup>51–54</sup> *In vivo* active and selective PLA2G4E inhibitors would be valuable tools to study the role of PLA2G4E and NAPes in (patho)physiological processes. They can be used to confirm the role of this enzyme in the homeostasis of NAPes and its precursors PE and PC. Acute inhibition of PLA2G4E will allow to investigate its importance in the development of neurodegenerative diseases<sup>8,14,24</sup> and may illuminate the functions of NAPes during ischemia, cytotoxicity and inflammation.<sup>17,19,21</sup> Furthermore, inhibition of NAPE biosynthesis may aid in clarifying the putative role of NAPes as feeding hormones.<sup>15,16</sup> As PLA2G4E was reported to be localized to the endocytic machinery<sup>7</sup>, inhibitors could be used to elucidate the function of PLA2G4E in endocytic recycling, and the role of NAPes or other products and substrates of PLA2G4E in this process. This might also increase our knowledge on the involvement of the endocannabinoid system in intercellular signaling. In these studies, previously reported NAPE-PLD inhibitors can be used to distinguish the effects of NAPes from that of NAEs.<sup>54</sup> In addition, PLAAT inhibitors can be used in conjunction with PLA2G4E inhibitors to investigate the regulation of the two pathways of NAPE biosynthesis, including their substrate preference and spatiotemporal activity.<sup>55,56</sup>

A PLA2G4E probe that is able to visualize endogenous activity could be used to investigate the relation between the enzymatic activity and subcellular localization of PLA2G4E. Furthermore, it may show PLA2G4E activity and localization in different cell types or brain regions. Expression of (lyso)-NAPE hydrolase ABHD4 was recently shown to be tightly regulated in developing neurons.<sup>57</sup> Visualization of PLA2G4E activity in neuronal

cells in different developmental states could help to elucidate which metabolites are associated with neuronal maturation, differentiation and fate.

### **Closing remarks**

Selective and cellular active inhibitors are instrumental to study the (patho)physiological functions of enzymes. In this work, compounds **WEN091**, **WEN222**, **WEN258**, **IK015** and **WEN175** are presented as the first-in-class tool compounds to study the biology of PLA2G4E. These inhibitors and activity-based probe will be valuable to elucidate the importance of PLA2G4E in NAPE biosynthesis in different cells, tissues and conditions. In conjunction with previously reported inhibitors of PLAAT1–5 and NAPE-PLD, these compounds can be used to study the functionalities and roles of NAPes in homeostasis and disease. The chemical tools developed in this thesis may help to uncover new therapeutic possibilities to treat conditions involving neurodegeneration, inflammation or feeding.

### **Acknowledgements**

Olivier Béquignon and Gerard van Westen are kindly acknowledged for building the homology model and performing docking experiments.

## Experimental procedures

### Computational chemistry

The homology structure model of human PLA2G4E was generated from the X-ray structure of hPLA2G4D (5IXC<sup>44</sup>, obtained from The Protein Data Bank), which shared 47% sequence identity with hPLA2G4E, using SWISS-MODEL. The obtained structure was pre-processed with Schrödinger Protein Preparation Wizard using default parameters. **IK015** was pre-processed with Schrödinger LigPrep using default parameters. **IK015** was subsequently docked to the PLA2G4E model using CovDock, selecting Ser<sup>412</sup> as the reactive residue performing nucleophilic attack on a double bond in thorough sampling mode. Docking results were visually analyzed and images created in BIOVIA Discovery Studio 2016, during which the covalent bond between the protein and ligand was removed for practical purposes.

## References

1. Coulon, D., Faure, L., Salmon, M., Wattelet, V. & Bessoule, J. J. Occurrence, biosynthesis and functions of *N*-acylphosphatidylethanolamines (NAPE): Not just precursors of *N*-acylethanolamines (NAE). *Biochimie* **94**, 75–85 (2012).
2. Wellner, N., Diep, T. A., Janfelt, C. & Hansen, H. S. *N*-acylation of phosphatidylethanolamine and its biological functions in mammals. *Biochim. Biophys. Acta - Mol. Cell Biol. Lipids* **1831**, 652–662 (2013).
3. Ogura, Y., Parsons, W. H., Kamat, S. S. & Cravatt, B. F. A calcium-dependent acyltransferase that produces *N*-Acyl phosphatidylethanolamines. *Nat. Chem. Biol.* **12**, 669–671 (2016).
4. Hussain, Z. *et al.* Phosphatidylserine-stimulated production of *N*-acyl-phosphatidylethanolamines by  $\text{Ca}^{2+}$ -dependent *N*-acyltransferase. *Biochim. Biophys. Acta - Mol. Cell Biol. Lipids* **1863**, 493–502 (2018).
5. Leslie, C. C. Cytosolic phospholipase  $A_2$ : Physiological function and role in disease. *J. Lipid Res.* **56**, 1386–1402 (2015).
6. Ghosh, M., Tucker, D. E., Burchett, S. A. & Leslie, C. C. Properties of the Group IV phospholipase  $A_2$  family. *Prog. Lipid Res.* **45**, 487–510 (2006).
7. Capestrano, M. *et al.* Cytosolic phospholipase  $A_{2\varepsilon}$  drives recycling through the clathrin-independent endocytic route. *J. Cell Sci.* **127**, 977–993 (2014).
8. Pérez-González, M. *et al.* PLA2G4E, a candidate gene for resilience in Alzheimer's disease and a new target for dementia treatment. *Prog. Neurobiol.* **191**, (2020).
9. Morimoto, Y. *et al.* Whole-exome sequencing and gene-based rare variant association tests suggest that PLA2G4E might be a risk gene for panic disorder. *Transl. Psychiatry* **8**, (2018).
10. Lee, Y. C., Zheng, Y. O., Taraschi, T. F. & Janes, N. Hydrophobic alkyl headgroups strongly promote membrane curvature and violate the headgroup volume correlation due to 'headgroup' insertion. *Biochemistry* **35**, 3677–3684 (1996).
11. Domingo, J. C., Mora, M. & de Madariaga, M. A. The influence of *N*-acyl chain length on the phase behaviour of natural and synthetic *N*-acylethanolamine phospholipids. *Chem. Phys. Lipids* **75**, 15–25 (1995).
12. Shangguan, T., Pak, C. C., Ali, S., Janoff, A. S. & Meers, P. Cation-dependent fusogenicity of an *N*-acyl phosphatidylethanolamine. *Biochim. Biophys. Acta* **1368**, 171–183 (1998).
13. Mora, M., Mir, F., Madariaga, M. A. de & Sagrista, M. L. Aggregation and fusion of vesicles composed of *N*-palmitoyl derivatives of membrane phospholipids. *Lipids* **35**, 513–524 (2000).
14. Palese, F., Pontis, S., Realini, N. & Piomelli, D. NAPE-specific phospholipase D regulates LRRK2 association with neuronal membranes. in *Advances in Pharmacology* **90**, 217–238 (Academic Press Inc., 2021).
15. Wellner, N. *et al.* Studies on the anorectic effect of *N*-acylphosphatidylethanolamine and phosphatidylethanolamine in mice. *Biochim. Biophys. Acta - Mol. Cell Biol. Lipids* **1811**, 508–512 (2011).
16. Gillum, M. P. *et al.* *N*-acylphosphatidylethanolamine, a Gut-Derived Circulating Factor Induced by Fat Ingestion, Inhibits Food Intake. *Cell* **135**, 813–824 (2008).
17. Epps, D. E., Natarajan, V., Schmid, P. C. & Schmid, H. H. O. Accumulation of *N*-acylethanolamine glycerophospholipids in infarcted myocardium. *Biochim. Biophys. Acta - Lipids Lipid Metab.* **618**, 420–430 (1980).

18. Hansen, H. H., Hansen, S. H., Schousboe, A. & Hansen, H. S. Determination of the phospholipid precursor of anandamide and other *N*-acylethanolamine phospholipids before and after sodium azide-induced toxicity in cultured neocortical neurons. *J. Neurochem.* **75**, 861–871 (2000).
19. Kondo, S. *et al.* Accumulation of various *N*-acylethanolamines including *N*-arachidonoyl ethanolamine (anandamide) in cadmium chloride-administered rat testis. *Arch. Biochem. Biophys.* **354**, 303–310 (1998).
20. Hansen, H. S., Lauritzen, L., Strand, A. M., Moesgaard, B. & Frandsen, A. Glutamate stimulates the formation of *N*-acylphosphatidylethanolamine and *N*-acylphosphatidylethanolamine in cortical neurons in culture. *Biochim. Biophys. Acta - Lipids Lipid Metab.* **1258**, 303–308 (1995).
21. Palese, F., Pontis, S., Realini, N. & Piomelli, D. A protective role for *N*-acylphosphatidylethanolamine phospholipase D in 6-OHDA-induced neurodegeneration. *Sci. Rep.* **9**, 1–16 (2019).
22. Basit, A., Pontis, S., Piomelli, D. & Armirotti, A. Ion mobility mass spectrometry enhances low-abundance species detection in untargeted lipidomics. *Metabolomics* **12**, 1–10 (2016).
23. Uyama, T. *et al.* Generation of *N*-acylphosphatidylethanolamine by members of the phospholipase A/acyltransferase (PLA/AT) family. *J. Biol. Chem.* **287**, 31905–31919 (2012).
24. Vaz, F. M. *et al.* Mutations in PCYT2 disrupt etherlipid biosynthesis and cause a complex hereditary spastic paraplegia. *Brain* **142**, 3382–3397 (2019).
25. Ross, B. M., Mamalias, N., Moszczynska, A., Rajput, A. H. & Kish, S. J. Elevated activity of phospholipid biosynthetic enzymes in substantia nigra of patients with Parkinson's disease. *Neuroscience* **102**, 899–904 (2001).
26. Wang, S. *et al.* Phosphatidylethanolamine deficiency disrupts  $\alpha$ -synuclein homeostasis in yeast and worm models of Parkinson disease. *Proc. Natl. Acad. Sci.* **111**, E3976–E3985 (2014).
27. Hussain, Z., Uyama, T., Tsuboi, K. & Ueda, N. Mammalian enzymes responsible for the biosynthesis of *N*-acylethanolamines. *Biochim. Biophys. Acta - Mol. Cell Biol. Lipids* **1862**, 1546–1561 (2017).
28. Fu, J., Kim, J., Oveisi, F., Astarita, G. & Piomelli, D. Targeted enhancement of oleoylethanolamide production in proximal small intestine induces across-meal satiety in rats. *Am. J. Physiol. - Regul. Integr. Comp. Physiol.* **295**, 45–50 (2008).
29. Provensi, G. *et al.* Satiety factor oleoylethanolamide recruits the brain histaminergic system to inhibit food intake. *Proc. Natl. Acad. Sci.* **111**, 11527–11532 (2014).
30. González-Aparicio, R. & Moratalla, R. Oleoylethanolamide reduces L-DOPA-induced dyskinesia via TRPV1 receptor in a mouse model of Parkinson's disease. *Neurobiol. Dis.* **62**, 416–425 (2014).
31. Hohmann, A. G. *et al.* An endocannabinoid mechanism for stress-induced analgesia. *Nature* **435**, 1108–1112 (2005).
32. Lutz, B., Marsicano, G., Maldonado, R. & Hillard, C. J. The endocannabinoid system in guarding against fear, anxiety and stress. *Nat. Rev. Neurosci.* **16**, 705–718 (2015).
33. Walter, L. & Stella, N. Cannabinoids and neuroinflammation. *Br. J. Pharmacol.* **141**, 775–785 (2004).
34. Meijerink, J. *et al.* Inhibition of COX-2-mediated eicosanoid production plays a major role in the anti-inflammatory effects of the endocannabinoid *N*-docosahexaenoyl ethanolamine (DHEA) in macrophages. *Br. J. Pharmacol.* **172**, 24–37 (2015).
35. Zhou, J. Development of a PLA2G4E Assay and Subsequent Application in Hit Identification. *Inhibitor Discovery of Phospholipase and N-Acyltransferase* (Leiden University, 2020).
36. van Esbroeck, A. C. M. *et al.* Identification of  $\alpha$ , $\beta$ -Hydrolase Domain Containing Protein 6 as a Diacylglycerol Lipase in Neuro-2a Cells. *Front. Mol. Neurosci.* **12**, (2019).

37. Speers, A. E., Adam, G. C. & Cravatt, B. F. Activity-Based Protein Profiling *in Vivo* Using a Copper(I)-Catalyzed Azide-Alkyne [3 + 2] Cycloaddition. *J. Am. Chem. Soc.* **125**, 4686–4687 (2003).
38. Gillet, L. C. J. *et al.* In-cell selectivity profiling of serine protease inhibitors by activity-based proteomics. *Mol. Cell. Proteomics* **7**, 1241–1253 (2008).
39. Binte Mustafiz, S. S. *et al.* The role of intracellular anionic phospholipids in the production of N-acyl-phosphatidylethanolamines by cytosolic phospholipase A<sub>2</sub>ε. *J. Biochem.* **165**, 343–352 (2019).
40. Hsu, K. L. *et al.* Discovery and optimization of piperidyl-1,2,3-triazole ureas as potent, selective, and *in vivo*-active inhibitors of α/β-hydrolase domain containing 6 (ABHD6). *J. Med. Chem.* **56**, 8270–8279 (2013).
41. Deng, H. *et al.* Triazole Ureas Act as Diacylglycerol Lipase Inhibitors and Prevent Fasting-Induced Refeeding. *J. Med. Chem.* **60**, 428–440 (2017).
42. Hsu, K. L. *et al.* Development and optimization of piperidyl-1,2,3-triazole ureas as selective chemical probes of endocannabinoid biosynthesis. *J. Med. Chem.* **56**, 8257–8269 (2013).
43. Janssen, F. J. Discovery of 1,2,4-triazole sulfonamide ureas as *in vivo* active α/β hydrolase domain type 16A inhibitors. *Discovery of novel inhibitors to investigate diacylglycerol lipases and α/β hydrolase domain 16A* (Leiden University, 2016).
44. Wang, H. *et al.* Structure of Human GIVD Cytosolic Phospholipase A<sub>2</sub> Reveals Insights into Substrate Recognition. *J. Mol. Biol.* **428**, 2769–2779 (2016).
45. Kaur, G. *et al.* Synthesis, structure–activity relationship, and p210bcr-abl protein tyrosine kinase activity of novel AG 957 analogs. *Bioorg. Med. Chem.* **13**, 1749–1761 (2005).
46. Gehringer, M. & Laufer, S. A. Emerging and Re-Emerging Warheads for Targeted Covalent Inhibitors: Applications in Medicinal Chemistry and Chemical Biology. *Journal of Medicinal Chemistry* **62**, 5673–5724 (2019).
47. Deng, H. *et al.* Chiral disubstituted piperidiny ureas: a class of dual diacylglycerol lipase-α and ABHD6 inhibitors. *Medchemcomm* **8**, 982–988 (2017).
48. Janssen, A. P. A. Hit-to-Lead Optimization of Triazole Sulfonamide DAGL-α inhibitors. *Inhibitor Selectivity: Profiling and Prediction* (Leiden University, 2019).
49. Duvernay, M. T., Matafonov, A., Lindsley, C. W. & Hamm, H. E. Platelet Lipidomic Profiling: Novel Insight into Cytosolic Phospholipase A<sub>2</sub>α Activity and Its Role in Human Platelet Activation. *Biochemistry* **54**, 5578–5588 (2015).
50. Lee, K. L. *et al.* Discovery of ecopladib, an indole inhibitor of cytosolic phospholipase A<sub>2</sub>α. *J. Med. Chem.* **50**, 1380–1400 (2007).
51. Ogasawara, D. *et al.* Selective blockade of the lyso-PS lipase ABHD12 stimulates immune responses *in vivo*. *Nat. Chem. Biol.* **14**, 1099–1108 (2018).
52. Johnson, D. S. *et al.* Discovery of PF-04457845: A Highly Potent, Orally Bioavailable, and Selective Urea FAAH Inhibitor. *Chem. Lett* **2**, 91–96 (2011).
53. Baggelaar, M. P. *et al.* Highly Selective, Reversible Inhibitor Identified by Comparative Chemoproteomics Modulates Diacylglycerol Lipase Activity in Neurons. *J. Am. Chem. Soc.* **137**, 8851–8857 (2015).
54. Mock, E. D. *et al.* Discovery of a NAPE-PLD inhibitor that modulates emotional behavior in mice. *Nat. Chem. Biol.* **16**, 667–675 (2020).
55. Zhou, J. *et al.* Activity-Based Protein Profiling Identifies α-Ketoamides as Inhibitors for Phospholipase A<sub>2</sub> Group XVI. *ACS Chem. Biol.* **14**, 164–169 (2019).
56. Zhou, J. *et al.* Structure-Activity Relationship Studies of α-Ketoamides as Inhibitors of the Phospholipase A and Acyltransferase Enzyme Family. *J. Med. Chem.* **63**, 9340–9359 (2020).

57. László, Z. I. *et al.* ABHD4-dependent developmental anoikis safeguards the embryonic brain. *Nat. Commun.* **11**, 1–16 (2020).

## **Samenvatting**



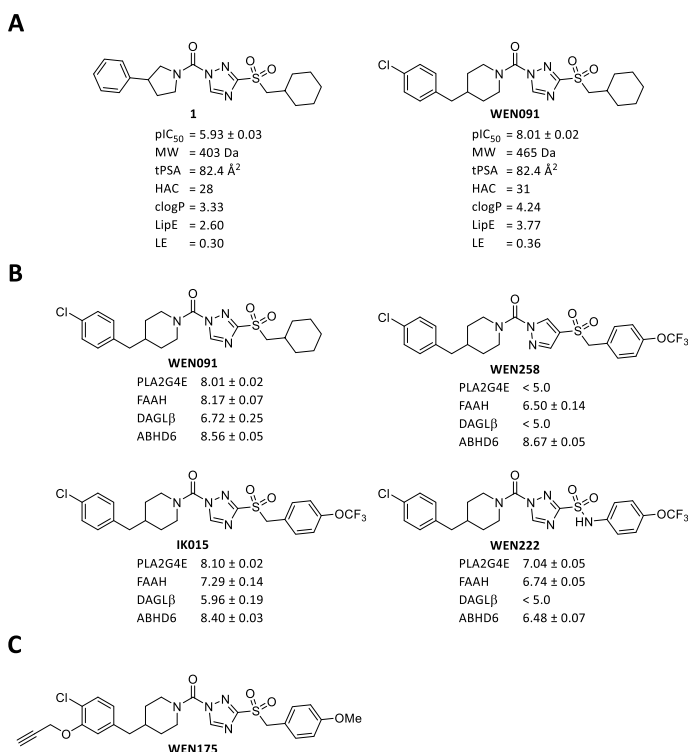
*N*-acylphosphatidylethanolamines (NAPE's) zijn een veelzijdige lipidenfamilie met uiteenlopende biologische functies, maar ze zijn relatief weinig onderzocht.<sup>1,2</sup> Van Fosfolipase A2 Groep IV E (PLA2G4E) is recentelijk aangetoond dat het in staat is tot calcium-afhankelijke productie van NAPE's in cellen.<sup>3,4</sup> PLA2G4E is lid van de PLA2G4-familie, die uit zes serinehydrolases bestaat (PLA2G4A-F).<sup>5</sup> Deze enzymen worden gekenmerkt door een Ser-Asp katalytische dyade en een N-terminaal, calcium-afhankelijk lipidenbindend C2-domein.<sup>5,6</sup> PLA2G4E heeft daarnaast een C-terminaal, polybasisch gebied dat betrokken is bij de subcellulaire lokalisatie.<sup>7</sup> Er is gerapporteerd dat het voornamelijk een *N*-acyltransferase is die in staat is op een calcium-afhankelijke manier NAPE's te synthetiseren.<sup>3</sup> Het komt voornamelijk tot expressie in de hersenen, testikelen, skeletspieren en het hart, en er zijn verbanden gelegd tussen het expressieniveau en de ziekte van Alzheimer en paniekstoornissen.<sup>3,8,9</sup> Daarnaast is gebleken dat het betrokken is bij het terugvoeren van vracht vanuit het clathrine-onafhankelijke endocytosesysteem naar de plasmamembraan.<sup>7</sup> Het is nog onduidelijk of NAPE's betrokken zijn bij deze functies.

Vooralsnog zijn er geen remmers van PLA2G4E gepubliceerd. PLA2G4E-remmers zouden van pas kunnen komen om de fysiologische rol van dit enzym in NAPE-biologie op te helderen door middel van acute modulatie. Selectieve remmers zijn ook vereist om het therapeutisch potentieel van PLA2G4E-remming vast te stellen. Het overkoepelende doel van dit proefschrift was daarom het ontwikkelen van cellulair actieve remmers van PLA2G4E.

**Hoofdstuk 1** geeft een bondig overzicht van de huidige kennis over de biologie van NAPE's en PLA2G4E. NAPE's zijn glycerofosfolipiden met drie vetzuurstaarten. Wanneer die ingebed zitten in lipidenmembranen, kunnen NAPE's betrokken zijn bij de regulatie van membraandynamiek, zoals membraanbuiging, -fusie en interacties met membraan-geassocieerde eiwitten.<sup>10-14</sup> NAPE's kunnen ook dienen als signaalmoleculen. Er zijn hypofage werkingen aan ze toegeschreven, hoewel betwist wordt dat de gerapporteerde effecten daadwerkelijk specifiek voor NAPE's zijn.<sup>15,16</sup> Hun niveaus zijn opvallend verhoogd in beschadigd weefsel, een effect dat gezien is in bijvoorbeeld hartinfarcten, ischemisch hersenweefsel en ontstoken testikelen.<sup>17-19</sup> Ook zijn ze verhoogd in modellen van neurodegeneratie en is een beschermende rol tegen de ziekte van Parkinson gesuggereerd.<sup>14,20-22</sup> Daarnaast spelen de biosynthese en het metabolisme van NAPE's een belangrijke rol in de homeostase van andere structuur- en signallipiden. Ze worden geproduceerd uit fosfatidylethanolamine (PE) en fosfatidylcholine (PC)<sup>3,23</sup>, lipiden waarvan de niveaus ook gerelateerd zijn aan neurodegeneratieve ziekten.<sup>24-26</sup> Er zijn vier routes beschreven voor de omzetting van NAPE's in *N*-acylethanolamines (NAE's), waarbij verschillende klassen van belangrijke metabolieten vrijkomen, waaronder fosfatidezuur (PA), lysofosfatidezuur (LPA) en vrije vetzuren (FFA's).<sup>27</sup> Afhankelijk van hun structuur oefenen NAE's verschillende signaalfuncties uit door middel van activatie van verscheidene receptoren, wat leidt tot onder meer verzadigings-, anti-inflammatoire, pijnstillende,

antiverslavings- of angstverlagende effecten.<sup>28–34</sup> NAE's worden afgebroken door *fatty acid amide hydrolase* (FAAH), wat hun biologische activiteit stopt.

In **Hoofdstuk 2** wordt de ontwikkeling van nieuwe PLA2G4E-remmers besproken. Eerder is er een competitieve *activity-based protein profiling* ("op activiteit gebaseerde eiwitprofielering", ABPP)-assay ontwikkeld om de activiteit van PLA2G4E te meten.<sup>35</sup> Het screenen van een gerichte bibliotheek van lipaseremmers heeft geleid tot de identificatie van 1,2,4-triazoolurea als remmers van PLA2G4E. Verbinding **1** is geselecteerd als startpunt voor hitoptimalisatie, vanwege haar potentie, lipofiele efficiëntie (LipE) en ligandefficiëntie (LE) (Figuur 7.1A). Er zijn 26 analogen gesynthetiseerd en getest op hun remmende activiteit, met als doel structuur-activiteitsrelaties (SAR's) te bepalen en de potentie te verbeteren. Het vergroten van het sterisch volume en het vergroten van de afstand tussen



**Figuur 7.1. Structuren en eigenschappen van PLA2G4E-remmers 1–WEN175.** A) Potentie en fysicochemische eigenschappen van hit **1** en remmer **WEN091**. Potentie op PLA2G4E bepaald met behulp van gel-gebaseerde ABPP op HEK293T-overexpressiecellysaat (pIC<sub>50</sub> ± SEM, N ≥ 2). Moleculair gewicht (MW) en topologische polaire oppervlakte (tPSA) berekend met ChemDraw Professional 16.0; HAC = aantal zware atomen; Lipofiele efficiëntie LipE = pIC<sub>50</sub> – clogP (DataWarrior 5.0.0); Ligandefficiëntie LE = 1.4pIC<sub>50</sub>/HAC. B) Remmende activiteit van remmers **WEN091–WEN222** (pIC<sub>50</sub> ± SEM) bepaald met behulp van gel-gebaseerde ABPP op overexpressiecellysaat (PLA2G4E) of Neuro-2a-cellen (FAAH, DAGLβ, ABHD6) (N ≥ 2). C) Chemische structuur van PLA2G4E-probe **WEN175**.

de fenyl in de aminegroep en het reactieve ureum resulteerden in verhoogde potentie, wat leidde tot de identificatie van een 4-benzylpiperidinegroep die een potentieverbetering van tien keer veroorzaakte. *Ortho*- en *meta*-substituties op deze benzylring waren toegestaan, maar *para*-substituties hadden de voorkeur. 4-(4-Chlorobenzyl)piperidine-bevattende verbinding **WEN091** is geïdentificeerd als de meest potente PLA2G4E-remmer ( $pIC_{50} = 8.01 \pm 0.02$ ). **WEN091** liet zo'n honderdvoud potentietoename zien ten opzichte van **1** en een verbeterde LipE en LE (Figuur 7.1A).

**WEN091** is verder biochemisch gekarakteriseerd in **Hoofdstuk 3**. De activiteit op PLA2G4E is getest in een natuurlijksubstraatconversieassay gebaseerd op vloeistofchromatografie-massaspectrometrieanalyse (LC-MS). **WEN091** remde dosisafhankelijk de vorming van NAPE uit exogeen PC en PE, zowel in overexpressie lysaat van humaan en muizen-PLA2G4E als in muizenbrein homogenaat ( $pIC_{50} = 6.9-7.1$ ). De verbinding had een selectiviteit van meer dan twintigvoud over PLA2G4B-D en minstens tienvoud over de calciumafhankelijke NAPE-biosynthetiserende enzymen fosfolipase A/acyltransferase (PLAAT) 2-5. De verbinding was niet actief op NAPE-specifieke fosfolipase D (NAPE-PLD) of de cannabinoïdenreceptoren ( $CB_{1/2}$ ). ABPP-profilering van de selectiviteit in muizenbrein proteoom en levende cellen liet remming van verschillende serinehydrolases zien, waaronder ABHD6, DAGL $\alpha$  en FAAH. **WEN091** verlaagde endogene cellulaire niveaus van NAPE's, lyso-NAPE's en glycerofosfo-palmitoylethanolamine, maar de negatievecontroleanalogue **WEN258** (zie hieronder) deed dit niet. Beide verbindingen lieten cellulaire activiteit op FAAH zien, maar alleen behandeling met **WEN258** had effect op de NAE-niveaus, wat suggereert dat *steady-state* NAE-niveaus in deze cellen gereguleerd worden door PLA2G4E en FAAH. *N*-22:6 lyso-NAPE-niveaus waren niet verhoogd door overexpressie, maar wel na behandeling met **WEN091** of **WEN258**, wat tot de hypothese heeft geleid dat deze lipiden op een PLA2G4E- en ABHD4-onafhankelijke manier gesynthetiseerd worden. Beide remmers verlaagden de niveaus van endocannabinoïde 2-arachidonoylglycerol (2-AG), maar alleen **WEN091** liet remming zien van het biosynthetische enzym DAGL $\beta$ . Dit suggereert dat ABHD6 mogelijk verantwoordelijk is voor de tonische productie van 2-AG in deze cellen, wat in lijn is met eerdere bevindingen.<sup>36</sup> Concluderend, **WEN091** is een potente PLA2G4E-remmer met selectiviteit voor de calciumafhankelijke NAPE-biosynthese *in vitro* die in staat was PLA2G4E-gemedieerde NAPE-vorming te verminderen in Neuro-2a-cellen.

In **Hoofdstuk 4** is de SAR-studie van PLA2G4E-remmers uitgebreid met 38 analogen van **WEN091** om hun selectiviteit over FAAH te verbeteren. Geconcludeerd werd dat de sulfon belangrijk was voor de activiteit op PLA2G4E, maar niet op FAAH. Deze sulfon veranderen in een sulfonamide verlaagde de activiteit op beide enzymen en leidde tot lagere selectiviteit. Grote substituenten op de vertrekkende triazolylgroep zorgden voor hogere selectiviteit over FAAH, wat leidde tot de identificatie van 4-trifluoromethoxybenzyl-bevattende verbinding **IK015** als potente PLA2G4E-remmer ( $pIC_{50} = 8.01 \pm 0.02$ ) met meer

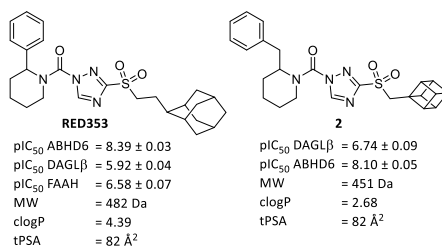
dan 800-voud selectiviteit over FAAH *in vitro* (Figuur 7.1B). Verder onderzoek naar de sterische en elektronische eigenschappen van deze benzylgroep verhoogde de potentie of selectiviteit niet. Analogen van het piperidinedeel verlaagden de activiteit op PLA2G4E.

**IK015** en sulfonamideanaloog **WEN222** (Figuur 7.1B) zijn geselecteerd voor verdere biologische karakterisatie. De verbindingen waren selectief over PLA2G4B-D, NAPE-PLD en de CB<sub>1</sub>- en CB<sub>2</sub>-receptoren. Daarnaast lieten **IK015** en **WEN222** minstens tienvoud selectiviteit zien over PLAAT2-5 en meer dan dertigvoud selectiviteit over de meeste serinehydrolases die in muizenbreinproteoom gekarakteriseerd konden worden, maar de selectiviteit over ABHD6 was beperkt (viervoud). In Neuro-2a-cellen remde **IK015** enkele enzymen op 1  $\mu$ M, waaronder ABHD6, ABHD12 en FAAH. **WEN222** was minder actief op de meeste enzymen, wat zou kunnen duiden op beperkte membraanpermeabiliteit. Net als **WEN091** lieten deze verbindingen verhoogde activiteit zien op FAAH in de cellulaire assay. Alles tezamen zijn **IK015** en **WEN222** potente en selectieve PLA2G4E-remmers *in vitro* met een verbeterd selectiviteitsprofiel ten opzichte van **WEN091**, maar lieten ze remming van andere serinehydrolases zien bij hogere concentraties. Pyrazoolureum **WEN258** is geïdentificeerd als structuuranaloog met een vergelijkbaar off-targetprofiel met **WEN091**, **IK015** en **WEN222**, maar zonder activiteit op PLA2G4E (Figuur 7.1B).

Om het bewijs van de cellulaire activiteit van **WEN091** op PLA2G4E te ondersteunen, is in **Hoofdstuk 5** een *activity-based probe* ("activiteitsgebaseerde sonde", ABP) ontwikkeld om intracellulaire *target engagement* ("doelwitbinding") te visualiseren. Het ontwerp van *probe WEN175* (Figuur 7.1C) was gebaseerd op PLA2G4E-remmers die geïdentificeerd waren in **Hoofdstukken 2** en **4**. Er wordt verondersteld dat de triazoolurea de katalytische serine van PLA2G4E covalent modificeren door de vorming van een carbamoyladduct, wat het mogelijk zou moeten maken actief enzym irreversibel te labelen. Daarom werd de carbamoylerende "blijvende groep" uitgerust met een alkyn, waaraan na cellyse een fluorofoor geconjugeerd kan worden door middel van koper-gekatalyseerde alkyn-azide cycloadditie (CuAAC). Deze tweestapslabelingbenadering omzeilde de celpermeabiliteitsproblemen waarmee grote, geladen fluoroforen gepaard gaan.<sup>37,38</sup> *Probe WEN175* was in staat PLA2G4E die tot overexpressie gebracht was in Neuro-2a-cellen dosisafhankelijk te labelen, wat zijn toepasbaarheid als cellulair actieve PLA2G4E-*probe* aantoonde. **WEN175** labelde geen PLA2G4E-mutanten waarin de katalytische serine vervangen was voor een alanine (S412A) of waarin het C2-domein ( $\Delta$ C2) of polybasisch domein ( $\Delta$ PB) verwijderd was, waarmee het belang van dit aminozuur en deze motieven onderstreept werd.<sup>39</sup> Voorbehandeling met **WEN091** remde de labeling van PLA2G4E door **WEN175** op een dosisafhankelijke manier, wat de cellulaire *target engagement* van **WEN091** met PLA2G4E aantoonde. Ondanks de laag-nanomolair IC<sub>50</sub> van **WEN091** *in vitro* waren hoge concentraties (10  $\mu$ M) nodig om volledige *in situ target engagement* te bewerkstelligen, wat overeenkomt met de resultaten uit de gerichte lipidomicsexperimenten van **Hoofdstuk 3**. Dat deze hoge cellulaire concentraties van **WEN091** nodig waren, kan waarschijnlijk verklaard worden door beperkte celpermeabiliteit en/of hoge niveaus van

competerende substraten. De gespecialiseerde ABP **WEN175** is een waardevol chemisch hulpmiddel om het ontwerp van nieuwe PLA2G4E-remmers met verbeterde cellulaire activiteit te sturen.

Gekooide koolwaterstoffen zijn polycyclische chemische structuren met unieke fysicochemische eigenschappen, maar worden niet algemeen toegepast in medicinale chemie. In **Hoofdstuk 6** zijn negen 1,2,4-triazoolurea gesubstitueerd met gekooide koolwaterstoffen en getest als remmers van ABHD6, ABHD16a en DAGL $\alpha/\beta$  om het effect van gekooide koolwaterstoffen op de activiteit van de remmers te onderzoeken. Alle verbindingen remden hun primaire doelwit met submicromolaire IC<sub>50</sub>-waarden in een ABPP-assay op muizenbreinproteoom. Adamant-2-ylethyleenbevattende ABHD6-remmer **RED353** en cubaanmethyleenbevattende DAGL-remmer **2** zijn verder geprofileerd in cellulaire experimenten (Figuur 7.2). De activiteit van **2** op DAGL $\beta$  in Neuro-2a-cellen was lager dan haar activiteit op DAGL $\alpha$  *in vitro*, maar **RED353** remde ABHD6 met pIC<sub>50</sub> = 8.39 ± 0.03 en liet bijna 300-voud selectiviteit zien over DAGL $\beta$  en 60-voud over FAAH. **RED353** remde ook de ABHD6-gemedieerde omzetting van fluorogeen substraat in een orthogonale assay en verlaagde de cellulaire niveaus van 2-AG, maar niet van anandamide, waarmee het de veelgebruikte ABHD6-remmer KT182 overtrof.<sup>40</sup> Deze resultaten bevestigen en borduren voort op de eerdere observatie dat ABHD6 verantwoordelijk is voor de tonische productie van 2-AG in Neuro-2a-cellen.<sup>36</sup>



**Figuur 7.2. Structuur en eigenschappen van ABHD6-remmers RED353 en 2.** Activiteit bepaald met behulp van gelgebaseerde ABPP op Neuro-2a-cellen (pIC<sub>50</sub> ± SEM, N = 3). Moleculair gewicht (MW) en topologische polaire oppervlakte (tPSA) berekend met ChemDraw Professional 16.0, octanol/water-partitiecöefficient (clogP) berekend met DataWarrior 5.0.0.

## Vervolgstudies

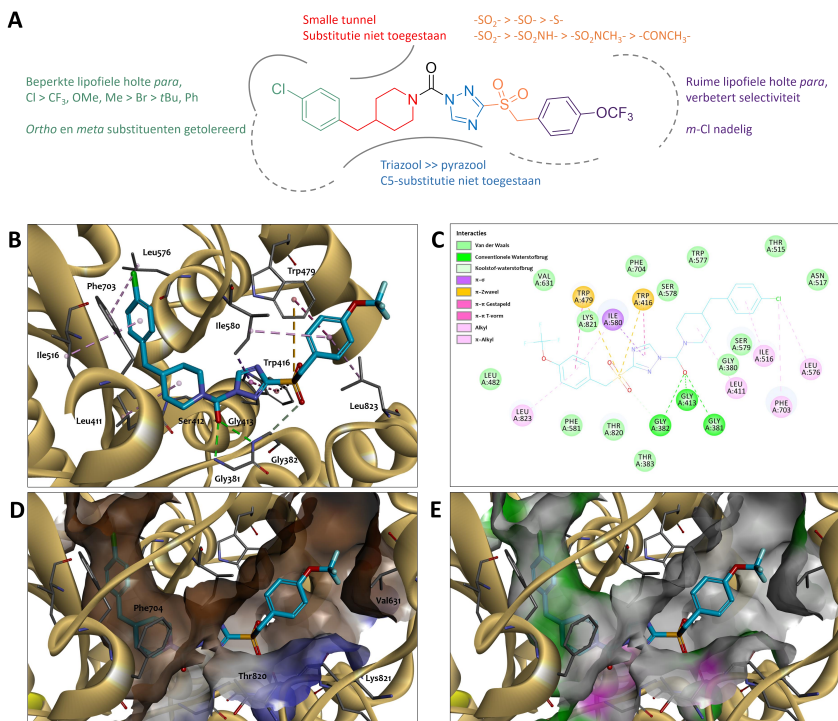
### Richting verbeterde PLA2G4E- en ABHD6-remmers

Triazoolurea zijn eerder succesvol toegepast als chemisch hulpmiddel om meerdere serinehydrolases in de hersenen, zoals ABHD6, ABHD16a en DAGL $\alpha/\beta$ , *in vivo* te bestuderen<sup>40–43</sup>, wat het toekomstig potentieel van de PLA2G4E-remmers beschreven in dit proefschrift schetst. PLA2G4E-remmer **WEN091** heeft hoge potentie, cellulaire *target engagement* en werkzaamheid in het verlagen van cellulaire NAPE-niveaus laten zien, maar remde daarnaast enkele serinehydrolases in Neuro-2a-cellen. **IK015** heeft een verbeterd

*in vitro*-selectiviteitsprofiel ten opzichte van **WEN091** en lagere off-targetactiviteit in Neuro-2a-cellen. Verdere karakterisatie van deze remmer door het onderzoeken van *in situ target engagement*, inhibitie van NAPE-vorming en activiteit op andere enzymen die betrokken zijn bij NAPE-metabolisme (ABHD4, PLAAT1–5) is nodig om te bepalen of **IK015** een betere *lead*-kandidaat is voor *in vivo* PLA2G4E-remming dan **WEN091**. **IK015** liet wel remming van FAAH en ABHD6 zien bij concentraties onder de 1  $\mu\text{M}$  in een cellulaire omgeving en heeft een relatief grote topische polaire oppervlakte (tPSA), wat de hersenpenetratie kan beperken. Verdere optimalisatie van de selectiviteit en fysicochemische eigenschappen van dit chemotype zouden daarom nodig kunnen zijn.

Structuurgebaseerd medicijnontwerp zou het ontwerp van de volgende serie PLA2G4E-remmers kunnen sturen. Op dit moment zijn er geen kristalstructuren van PLA2G4E beschikbaar. **IK015** is daarom geplaatst in een digitaal homologiemodel van PLA2G4E dat gebouwd is op basis van de kristalstructuur van PLA2G4D.<sup>44</sup> De voorspelde bindingspose lijkt te duiden op de aanwezigheid van een nauwe holte die bekleed is met hydrofobe residuen, beperkte ruimte rondom het chlooratoom en een grotere holte rondom de trifluoromethoxysubstituent, in overeenstemming met de SAR-resultaten uit **Hoofdstukken 2 en 4** (Figuur 7.3). De SAR suggereert dat substituenten die nieuwe interacties met de *active site* aan kunnen gaan, geïntroduceerd zouden kunnen worden op de *ortho*- of *meta*-positie van de piperidylbenzylgroep of op de *para*-positie van de sulfonylbenzylgroep. Deze substituenten kunnen mogelijk de affiniteit van de remmer voor PLA2G4E en zijn selectiviteit over andere doelwitten verhogen. Het verbeteren van de potentie van de remmer zou de mogelijkheid kunnen bieden heteroatomen te verwijderen om de tPSA te verlagen. Men moet echter altijd de gevolgen die modificaties hebben op andere fysicochemische eigenschappen, zoals de lipofiliciteit en moleculair gewicht, in ogenschouw nemen. Mogelijk is een combinatie van modificaties vereist om een optimale balans te verkrijgen. Het in kaart brengen van de farmacokinetische eigenschappen van de remmers zal nodig zijn om hun *in vivo*-toepasbaarheid te bepalen. Resultaten uit deze studies nopen mogelijk tot verdere optimalisatie van bijvoorbeeld metabole stabiliteit, plasmaeiwitbinding of hersenpenetratie.

De brede reactiviteit van triazoolurea ten opzichte van serinehydrolases maakt het uitdagend om hoge selectiviteit te verkrijgen, en veel eerder gepubliceerde triazoolureum-gebaseerde remmers hebben dan ook kruisreactiviteit laten zien met *off-targets* bij hogere concentraties.<sup>40,41,43</sup> Naast (nadelige) off-targeteffecten kan dit leiden tot beperkte metabole stabiliteit van de verbinding door snelle enzymatische hydrolyse.<sup>45,46</sup> Het verhogen van de niet-covalente bindingsaffiniteit van de PLA2G4E-remmers voor PLA2G4E zou de mogelijkheid kunnen bieden de intrinsieke reactiviteit van de ureumwarhead te verlagen, wat zou kunnen leiden tot verbeterde selectiviteit over ander serinehydrolases. Echter, minder promiscue chemotypen zijn wellicht meer geschikt voor specifieke PLA2G4E-remming en hoge *in vivo*-stabiliteit.



**Figuur 7.3. SAR-overzicht en dockingsresultaten van IK015.** A) Samenvatting van observaties betreffende de potentie en selectiviteit van gesynthetiseerde PLA2G4E-remmers uit de SAR-studies in Hoofdstukken 2 en 4. B–E) **IK015** (cyan- en groenkleurige koolstofatomen) is covalent gedockt aan Ser<sup>412</sup> (binding niet getoond) in een homologiemodel van hPLA2G4E (zandkleurig lint), gebaseerd op hPLA2G4D.<sup>44</sup> Enkele aminozuren die interageren met **IK015** zijn weergegeven in elementkleuren. B) Hoogstgerangschikte dockingspose van **IK015** in het hPLA2G4E-model met voorspelde enzym-remmerinteracties aangegeven. Interagerende aminozuren zijn geannoteerd. C) 2D-weergave van de voorspelde interacties van **IK015** met hPLA2G4E, corresponderend met de dockingspose in (B). D) Dockingspose met holteoppervlak weergegeven. Hydrofoob oppervlak is weergegeven in het bruin, hydrofiel in blauw. E) Dockingspose met holteoppervlak dat gekleurd is naar voorspeld waterstofdonerend (magenta) en -accepterend (groen) karakter.

ABHD6-remmer **RED353** toonde hoge potentie en een gunstig selectiviteitsprofiel in Neuro-2a-cellen. Hij liet lagere activiteit zien op FAAH dan KT182, maar was actiever op DAGL $\alpha$  en  $\beta$ . Eerdere studies naar DAGL- en ABHD6-remmers hebben verbeterde selectiviteit voor ABHD6 aangetoond wanneer polaire groepen geïntroduceerd werden op de piperidine of de vertrekkendegroeps substituent.<sup>40,47,48</sup> Nieuwe derivaten van **RED353** met polaire substituenten die de selectiviteit voor ABHD6 zouden kunnen verbeteren, zouden daarom onderzocht kunnen worden. Deze kunnen gebruikt worden om de bijdrage van ABHD6 aan 2-AG-productie te onderzoeken in andere celtypen en onder andere omstandigheden.

### PLA2G4E-remmers kunnen mogelijk PLA2G4E- en NAPE-biologie ophelderen

PLA2G4A is uitgebreid geëxploiteerd voor de ontwikkeling van medicijnen tegen inflammatoire aandoeningen, en enkele PLA2G4A-remmers zijn tot in klinische tests onderzocht.<sup>49,50</sup> Ook zijn er meerdere remmers van enzymen die betrokken zijn bij het endocannabinoïdensysteem ontwikkeld om het therapeutisch potentieel van hun doelwitten in ontstekingspijn, angst of metabool syndroom te bestuderen.<sup>51-54</sup> *In vivo*-actieve en selectieve PLA2G4E-remmers zouden waardevolle hulpmiddelen zijn om de rol van PLA2G4E en NAPE's in (patho)fysiologische processen te bestuderen. Ze kunnen gebruikt worden om de rol van dit enzym te bestuderen in de homeostase van NAPE's en hun precursors PE en PC. Acute inhibitie van PLA2G4E maakt het mogelijk zijn belang in de ontwikkeling van neurodegeneratieve ziekten te onderzoeken<sup>8,14,24</sup> en kan de functies van NAPE's tijdens ischemie, cytotoxiciteit en ontsteking belichten.<sup>17,19,21</sup> Bovendien zou remming van NAPE-biosynthese kunnen helpen bij het verduidelijken van de mogelijke rol van NAPE's als verzadigingshormoon.<sup>15,16</sup> Omdat gerapporteerd is dat PLA2G4E gelokaliseerd is bij het endocytosesysteem<sup>7</sup>, zouden remmers gebruikt kunnen worden om de functie van PLA2G4E in endocytische recycling op te helderen, alsmede de rol van NAPE's of andere substraten en producten van PLA2G4E in dit proces. Dit kan ook onze kennis uitbreiden over de betrokkenheid van het endocannabinoïdensysteem bij intercellulaire signaaltransductie. In deze studies kunnen eerder gepubliceerde NAPE-PLD-remmers gebruikt worden om onderscheid te maken tussen de effecten van NAPE's en NAE's.<sup>54</sup> Daarnaast kunnen PLAAT-remmers in combinatie met PLA2G4E-remmers gebruikt worden om de regulatie van de twee routes voor NAPE-biosynthese te bestuderen, waaronder hun substraatvoorkeuren en spatiotemporele activiteit.<sup>55,56</sup>

Een PLA2G4E-probe die in staat is endogene activiteit zichtbaar te maken, zou gebruikt kunnen worden om de relatie tussen de enzymatische activiteit en subcellulaire lokalisatie te onderzoeken. Bovendien zou deze de PLA2G4E-activiteit en -lokalisatie in verschillende celtypen en hersenregio's kunnen laten zien. Onlangs is aangetoond dat de expressie van (lyso)-NAPE-hydrolase ABHD4 strak gereguleerd is in ontwikkelende neuronen.<sup>57</sup> Het zichtbaar maken van PLA2G4E-activiteit in neuronale cellen in verschillende stadia van ontwikkeling kan helpen op te helderen welke metaboliëten betrokken zijn bij neuronale maturatie, differentiatie en bestemming.

### Tot slot

Selectieve en cellulair actieve remmers zijn nuttig om de (patho)fysiologische functies van enzymen te bestuderen. In dit proefschrift zijn verbindingen **WEN091–WEN222** gepresenteerd als de eerste chemische instrumenten in hun klasse om de biologie van PLA2G4E te bestuderen. Deze remmers en *activity-based probe* zullen waardevol zijn in het ophelderen van het belang van PLA2G4E in NAPE-biosynthese in verschillende cellen, weefsels en onder verschillende omstandigheden. In combinatie met eerder gerapporteerde remmers van PLAAT1–5 en NAPE-PLD kunnen deze verbindingen gebruikt



worden om de functies en rollen van NAFÉ's in homeostase en ziekte te bestuderen. De chemische hulpmiddelen die in dit proefschrift ontwikkeld zijn, kunnen mogelijk helpen bij het ontdekken van nieuwe therapeutische mogelijkheden om aandoeningen waarbij neurodegeneratie, ontstekingen en voeding betrokken zijn te behandelen.

## **Dankwoord**

Olivier Béquignon en Gerard van Westen worden hartelijk bedankt voor het bouwen van het homologiemodel en het uitvoeren van de computationele experimenten.

## Experimentele procedures

### Computationale chemie

Het homologiestructuurmodel van humaan PLA2G4E is met behulp van SWISS-MODEL gegenereerd uit de röntgenstructuur van hPLA2G4D (5IXC<sup>44</sup>, verkregen uit The Protein Data Bank), die 47% sequentie-identiteit deelt met hPLA2G4E. De verkregen structuur is voorbehandeld met Schrödinger Protein Preparation Wizard met standaardparameters. **IK015** is voorbehandeld met Schrödinger LigPrep met standaardparameters. **IK015** is vervolgens in het PLA2G4E-model geplaatst met behulp van CovDock, waarbij Ser<sup>412</sup> geselecteerd is als het reactieve residu dat een nucleofiele aanval uitvoert op een dubbele band, in *thorough sampling mode*. Dockingsresultaten zijn visueel geanalyseerd en afbeeldingen zijn gecreëerd in BIOVIA Discovery Studio 2016, waarbij de covalente binding tussen het eiwit en ligand verwijderd is om praktische redenen.

## Referenties

1. Coulon, D., Faure, L., Salmon, M., Wattelet, V. & Bessoule, J. J. Occurrence, biosynthesis and functions of *N*-acylphosphatidylethanolamines (NAPE): Not just precursors of *N*-acylethanolamines (NAE). *Biochimie* **94**, 75–85 (2012).
2. Wellner, N., Diep, T. A., Janfelt, C. & Hansen, H. S. *N*-acylation of phosphatidylethanolamine and its biological functions in mammals. *Biochim. Biophys. Acta - Mol. Cell Biol. Lipids* **1831**, 652–662 (2013).
3. Ogura, Y., Parsons, W. H., Kamat, S. S. & Cravatt, B. F. A calcium-dependent acyltransferase that produces *N*-Acyl phosphatidylethanolamines. *Nat. Chem. Biol.* **12**, 669–671 (2016).
4. Hussain, Z. *et al.* Phosphatidylserine-stimulated production of *N*-acyl-phosphatidylethanolamines by Ca<sup>2+</sup>-dependent *N*-acyltransferase. *Biochim. Biophys. Acta - Mol. Cell Biol. Lipids* **1863**, 493–502 (2018).
5. Leslie, C. C. Cytosolic phospholipase A<sub>2</sub>: Physiological function and role in disease. *J. Lipid Res.* **56**, 1386–1402 (2015).
6. Ghosh, M., Tucker, D. E., Burchett, S. A. & Leslie, C. C. Properties of the Group IV phospholipase A<sub>2</sub> family. *Prog. Lipid Res.* **45**, 487–510 (2006).
7. Capestrano, M. *et al.* Cytosolic phospholipase A<sub>2</sub>ε drives recycling through the clathrin-independent endocytic route. *J. Cell Sci.* **127**, 977–993 (2014).
8. Pérez-González, M. *et al.* PLA2G4E, a candidate gene for resilience in Alzheimer's disease and a new target for dementia treatment. *Prog. Neurobiol.* **191**, (2020).
9. Morimoto, Y. *et al.* Whole-exome sequencing and gene-based rare variant association tests suggest that PLA2G4E might be a risk gene for panic disorder. *Transl. Psychiatry* **8**, (2018).
10. Lee, Y. C., Zheng, Y. O., Taraschi, T. F. & Janes, N. Hydrophobic alkyl headgroups strongly promote membrane curvature and violate the headgroup volume correlation due to 'headgroup' insertion. *Biochemistry* **35**, 3677–3684 (1996).
11. Domingo, J. C., Mora, M. & de Madariaga, M. A. The influence of *N*-acyl chain length on the phase behaviour of natural and synthetic *N*-acylethanolamine phospholipids. *Chem. Phys. Lipids* **75**, 15–25 (1995).
12. Shangguan, T., Pak, C. C., Ali, S., Janoff, A. S. & Meers, P. Cation-dependent fusogenicity of an *N*-acyl phosphatidylethanolamine. *Biochim. Biophys. Acta* **1368**, 171–183 (1998).
13. Mora, M., Mir, F., Madariaga, M. A. de & Sagrista, M. L. Aggregation and fusion of vesicles composed of *N*-palmitoyl derivatives of membrane phospholipids. *Lipids* **35**, 513–524 (2000).
14. Palese, F., Pontis, S., Realini, N. & Piomelli, D. NAPE-specific phospholipase D regulates LRRK2 association with neuronal membranes. in *Advances in Pharmacology* **90**, 217–238 (Academic Press Inc., 2021).
15. Wellner, N. *et al.* Studies on the anorectic effect of *N*-acylphosphatidylethanolamine and phosphatidylethanolamine in mice. *Biochim. Biophys. Acta - Mol. Cell Biol. Lipids* **1811**, 508–512 (2011).
16. Gillum, M. P. *et al.* *N*-acylphosphatidylethanolamine, a Gut-Derived Circulating Factor Induced by Fat Ingestion, Inhibits Food Intake. *Cell* **135**, 813–824 (2008).
17. Epps, D. E., Natarajan, V., Schmid, P. C. & Schmid, H. H. O. Accumulation of *N*-acylethanolamine glycerophospholipids in infarcted myocardium. *Biochim. Biophys. Acta - Lipids Lipid Metab.* **618**, 420–430 (1980).

18. Hansen, H. H., Hansen, S. H., Schousboe, A. & Hansen, H. S. Determination of the phospholipid precursor of anandamide and other *N*-acylethanolamine phospholipids before and after sodium azide-induced toxicity in cultured neocortical neurons. *J. Neurochem.* **75**, 861–871 (2000).
19. Kondo, S. *et al.* Accumulation of various *N*-acylethanolamines including *N*-arachidonylethanolamine (anandamide) in cadmium chloride-administered rat testis. *Arch. Biochem. Biophys.* **354**, 303–310 (1998).
20. Hansen, H. S., Lauritzen, L., Strand, A. M., Moesgaard, B. & Frandsen, A. Glutamate stimulates the formation of *N*-acylphosphatidylethanolamine and *N*-acylphosphatidylethanolamine in cortical neurons in culture. *Biochim. Biophys. Acta - Lipids Lipid Metab.* **1258**, 303–308 (1995).
21. Palese, F., Pontis, S., Realini, N. & Piomelli, D. A protective role for *N*-acylphosphatidylethanolamine phospholipase D in 6-OHDA-induced neurodegeneration. *Sci. Rep.* **9**, 1–16 (2019).
22. Basit, A., Pontis, S., Piomelli, D. & Armirotti, A. Ion mobility mass spectrometry enhances low-abundance species detection in untargeted lipidomics. *Metabolomics* **12**, 1–10 (2016).
23. Uyama, T. *et al.* Generation of *N*-acylphosphatidylethanolamine by members of the phospholipase A/acyltransferase (PLA/AT) family. *J. Biol. Chem.* **287**, 31905–31919 (2012).
24. Vaz, F. M. *et al.* Mutations in PCYT2 disrupt etherlipid biosynthesis and cause a complex hereditary spastic paraplegia. *Brain* **142**, 3382–3397 (2019).
25. Ross, B. M., Mamalias, N., Moszczynska, A., Rajput, A. H. & Kish, S. J. Elevated activity of phospholipid biosynthetic enzymes in substantia nigra of patients with Parkinson's disease. *Neuroscience* **102**, 899–904 (2001).
26. Wang, S. *et al.* Phosphatidylethanolamine deficiency disrupts  $\alpha$ -synuclein homeostasis in yeast and worm models of Parkinson disease. *Proc. Natl. Acad. Sci.* **111**, E3976–E3985 (2014).
27. Hussain, Z., Uyama, T., Tsuboi, K. & Ueda, N. Mammalian enzymes responsible for the biosynthesis of *N*-acylethanolamines. *Biochim. Biophys. Acta - Mol. Cell Biol. Lipids* **1862**, 1546–1561 (2017).
28. Fu, J., Kim, J., Oveisi, F., Astarita, G. & Piomelli, D. Targeted enhancement of oleoylethanolamide production in proximal small intestine induces across-meal satiety in rats. *Am. J. Physiol. - Regul. Integr. Comp. Physiol.* **295**, 45–50 (2008).
29. Provensi, G. *et al.* Satiety factor oleoylethanolamide recruits the brain histaminergic system to inhibit food intake. *Proc. Natl. Acad. Sci.* **111**, 11527–11532 (2014).
30. González-Aparicio, R. & Moratalla, R. Oleoylethanolamide reduces L-DOPA-induced dyskinesia via TRPV1 receptor in a mouse model of Parkinson's disease. *Neurobiol. Dis.* **62**, 416–425 (2014).
31. Hohmann, A. G. *et al.* An endocannabinoid mechanism for stress-induced analgesia. *Nature* **435**, 1108–1112 (2005).
32. Lutz, B., Marsicano, G., Maldonado, R. & Hillard, C. J. The endocannabinoid system in guarding against fear, anxiety and stress. *Nat. Rev. Neurosci.* **16**, 705–718 (2015).
33. Walter, L. & Stella, N. Cannabinoids and neuroinflammation. *Br. J. Pharmacol.* **141**, 775–785 (2004).
34. Meijerink, J. *et al.* Inhibition of COX-2-mediated eicosanoid production plays a major role in the anti-inflammatory effects of the endocannabinoid *N*-docosahexaenylethanolamine (DHEA) in macrophages. *Br. J. Pharmacol.* **172**, 24–37 (2015).
35. Zhou, J. Development of a PLA2G4E Assay and Subsequent Application in Hit Identification. *Inhibitor Discovery of Phospholipase and N-Acyltransferase* (Leiden University, 2020).
36. van Esbroeck, A. C. M. *et al.* Identification of  $\alpha$ , $\beta$ -Hydrolase Domain Containing Protein 6 as a Diacylglycerol Lipase in Neuro-2a Cells. *Front. Mol. Neurosci.* **12**, (2019).

37. Speers, A. E., Adam, G. C. & Cravatt, B. F. Activity-Based Protein Profiling *in Vivo* Using a Copper(I)-Catalyzed Azide-Alkyne [3 + 2] Cycloaddition. *J. Am. Chem. Soc.* **125**, 4686–4687 (2003).
38. Gillet, L. C. J. *et al.* In-cell selectivity profiling of serine protease inhibitors by activity-based proteomics. *Mol. Cell. Proteomics* **7**, 1241–1253 (2008).
39. Binte Mustafiz, S. S. *et al.* The role of intracellular anionic phospholipids in the production of *N*-acyl-phosphatidylethanolamines by cytosolic phospholipase A2 $\epsilon$ . *J. Biochem.* **165**, 343–352 (2019).
40. Hsu, K. L. *et al.* Discovery and optimization of piperidyl-1,2,3-triazole ureas as potent, selective, and *in vivo*-active inhibitors of  $\alpha/\beta$ -hydrolase domain containing 6 (ABHD6). *J. Med. Chem.* **56**, 8270–8279 (2013).
41. Deng, H. *et al.* Triazole Ureas Act as Diacylglycerol Lipase Inhibitors and Prevent Fasting-Induced Refeeding. *J. Med. Chem.* **60**, 428–440 (2017).
42. Hsu, K. L. *et al.* Development and optimization of piperidyl-1,2,3-triazole ureas as selective chemical probes of endocannabinoid biosynthesis. *J. Med. Chem.* **56**, 8257–8269 (2013).
43. Janssen, F. J. Discovery of 1,2,4-triazole sulfonamide ureas as *in vivo* active  $\alpha/\beta$  hydrolase domain type 16A inhibitors. *Discovery of novel inhibitors to investigate diacylglycerol lipases and  $\alpha/\beta$  hydrolase domain 16A* (Leiden University, 2016).
44. Wang, H. *et al.* Structure of Human GIVD Cytosolic Phospholipase A $_2$  Reveals Insights into Substrate Recognition. *J. Mol. Biol.* **428**, 2769–2779 (2016).
45. Kaur, G. *et al.* Synthesis, structure–activity relationship, and p210bcr-abl protein tyrosine kinase activity of novel AG 957 analogs. *Bioorg. Med. Chem.* **13**, 1749–1761 (2005).
46. Gehringer, M. & Laufer, S. A. Emerging and Re-Emerging Warheads for Targeted Covalent Inhibitors: Applications in Medicinal Chemistry and Chemical Biology. *Journal of Medicinal Chemistry* **62**, 5673–5724 (2019).
47. Deng, H. *et al.* Chiral disubstituted piperidinyl ureas: a class of dual diacylglycerol lipase- $\alpha$  and ABHD6 inhibitors. *Medchemcomm* **8**, 982–988 (2017).
48. Janssen, A. P. A. Hit-to-Lead Optimization of Triazole Sulfonamide DAGL- $\alpha$  inhibitors. *Inhibitor Selectivity: Profiling and Prediction* (Leiden University, 2019).
49. Duvernavy, M. T., Matafonov, A., Lindsley, C. W. & Hamm, H. E. Platelet Lipidomic Profiling: Novel Insight into Cytosolic Phospholipase A $_2\alpha$  Activity and Its Role in Human Platelet Activation. *Biochemistry* **54**, 5578–5588 (2015).
50. Lee, K. L. *et al.* Discovery of ecopladib, an indole inhibitor of cytosolic phospholipase A $_2\alpha$ . *J. Med. Chem.* **50**, 1380–1400 (2007).
51. Ogasawara, D. *et al.* Selective blockade of the lyso-PS lipase ABHD12 stimulates immune responses *in vivo*. *Nat. Chem. Biol.* **14**, 1099–1108 (2018).
52. Johnson, D. S. *et al.* Discovery of PF-04457845: A Highly Potent, Orally Bioavailable, and Selective Urea FAAH Inhibitor. *Chem. Lett* **2**, 91–96 (2011).
53. Baggelaar, M. P. *et al.* Highly Selective, Reversible Inhibitor Identified by Comparative Chemoproteomics Modulates Diacylglycerol Lipase Activity in Neurons. *J. Am. Chem. Soc.* **137**, 8851–8857 (2015).
54. Mock, E. D. *et al.* Discovery of a NAPE-PLD inhibitor that modulates emotional behavior in mice. *Nat. Chem. Biol.* **16**, 667–675 (2020).
55. Zhou, J. *et al.* Activity-Based Protein Profiling Identifies  $\alpha$ -Ketoamides as Inhibitors for Phospholipase A2 Group XVI. *ACS Chem. Biol.* **14**, 164–169 (2019).
56. Zhou, J. *et al.* Structure-Activity Relationship Studies of  $\alpha$ -Ketoamides as Inhibitors of the Phospholipase A and Acyltransferase Enzyme Family. *J. Med. Chem.* **63**, 9340–9359 (2020).

57. László, Z. I. *et al.* ABHD4-dependent developmental anoikis safeguards the embryonic brain. *Nat. Commun.* **11**, 1–16 (2020).

## List of publications

### Discovery of 1,2,4-triazole ureas as potent and cellular active inhibitors of Ca<sup>2+</sup>-dependent *N*-acyltransferase PLA<sub>2</sub>G<sub>4</sub>E

T.J. Wendel, X. Di, J. Zhou, M.F. Wissingh, P. ten Bras, F. Schutter, W.P.F. Driever, L.V. de Paus, L. van den Berg, S. Uitenbroek, T. van der Wel, C.A.A. van Boeckel, M.A. Schafroth, B.F. Cravatt, T. Hankemeier, M. van der Stelt  
*Manuscript in preparation*

### Potent and selective ABHD6 inhibitors based on caged hydrocarbon structures

T.J. Wendel, Y.D. Radchenko, A.F. Stevens, S. Singh, A.E. Pashenko, A.A. Fokin, N. Stella, M. van der Stelt  
*Manuscript in preparation*

### Roles of *N*-acylphosphatidylethanolamines in homeostasis and disease

T.J. Wendel, M. van der Stelt  
*Manuscript in preparation*

### Discovery of a NAPE-PLD inhibitor that modulates emotional behavior in mice

E.D. Mock, M. Mustafa, O. Gunduz-Cinar, R. Cinar, G.N. Petrie, V. Kantae, X. Di, D. Ogasawara, Z.V. Varga, J. Paloczi, C. Miliano, G. Donvito, A.C.M. van Esbroeck, A.M.F. van der Gracht, I. Kotsogianni, J.K. Park, A. Martella, T. van der Wel, M. Soethoudt, M. Jiang, T.J. Wendel, A.P.A. Janssen, A.T. Bakker, C.M. Donovan, L.I. Castillo, B.I. Florea, J. Wat, H. van den Hurk, M. Wittwer, U. Grether, A. Holmes, C.A.A. van Boeckel, T. Hankemeier, B.F. Cravatt, M.W. Buczynski, M.N. Hill, P. Pacher, A.H. Lichtman, M. van der Stelt  
*Nature Chemical Biology* **16** 667–675 (2020)

### Structure–Activity Relationship Studies of $\alpha$ -Ketoamides as Inhibitors of the Phospholipase A and Acyltransferase Enzyme Family

J. Zhou, E.D. Mock, K. Al Ayed, X. Di, V. Kantae, L. Burggraaff, A.F. Stevens, A. Martella, F. Mohr, M. Jiang, T. van der Wel, T.J. Wendel, T.P. Ofman, Y. Tran, N. de Koster, G.J.P. van Westen, T. Hankemeier, M. van der Stelt  
*Journal of Medicinal Chemistry* **63** 9340–9359 (2020)

## Curriculum vitae

Tiemen Josse Wendel was born on a cold Wednesday morning, July 21<sup>st</sup>, 1993, in Delft. After graduating from the *gymnasium* (pre-university education with classical languages) at Stanislascollege Westplantsoen in Delft, he started the Bachelor Life Science & Technology at Leiden University and Delft University of Technology in 2011. He finished this in 2014 with a research internship titled 'DNA encapsulation in neutrally charged liposomes', which was performed at the Leiden Institute of Chemistry, department of Supramolecular & Biomaterials Chemistry, under the supervision of Dr. René Olsthoorn and Prof. Dr. Alexander Kros. Subsequently, he started the Master Life Science & Technology at Leiden University, from which he graduated in 2016 (*cum laude*). As part of the master's program, a research internship was performed under the supervision of Dr. Mario van der Stelt at the department of Bio-Organic Synthesis, Leiden Institute of Chemistry. This project, titled 'Design, synthesis and characterization of DAGL $\alpha$ -specific inhibitors', aimed to develop inhibitor molecules that could discriminate between DAGL $\alpha$  and DAGL $\beta$  using a covalent complementarity approach.

Later that year, he started as a PhD student in the same group. In 2017, he joined the newly formed department of Molecular Physiology of (now) Prof. Dr. Van der Stelt to continue his PhD research, which eventually led to the publication of this thesis. The work described in Chapter 3 was performed in collaboration with Prof. Dr. Thomas Hankemeier of Analytical Biosciences (Leiden Academic Centre for Drug Research) and Prof. Dr. Benjamin Cravatt of Chemical Physiology (The Scripps Institute, La Jolla, CA, USA) and the work described in Chapter 6 was performed in collaboration with Prof. Dr. Hankemeier and Prof. Dr. Nephi Stella of Pharmacology and Psychiatry (University of Washington, Seattle, WA, USA). Parts of the work described herein have been presented on posters at CHAINS (Veldhoven, 2017, 2018, 2019), International Cannabinoid Research Conference (Leiden, 2018), Activity-Based Protein Profiling meeting (Leuven, 2018), Ficon Dutch Medicines Days (Leiden, 2019) and Reedijk Symposium (Leiden, 2019).

In 2022, Timo started working as a post-doctoral researcher in the department of Human Genetics at the Leiden University Medical Center under the supervision of Dr. Sylvie Noordermeer.



## Dankwoord

Het is al vaak gezegd en geschreven: een promotieonderzoek doe je niet in afzondering. Er prijkt maar een naam op de voorkant, maar dit proefschrift was er niet geweest zonder de hulp van enkele mensen.

Allereerst en bovenal Mario. Jij hebt mij in 2016 na mijn stage de kans gegeven dit te vervolgen met een promotieproject, waardoor ik nog jaren met plezier chemisch-biologisch onderzoek heb mogen doen. Ik heb je feedback tijdens werkbesprekingen en doelgerichte visie op het project als geheel altijd gewaardeerd. Ik was het niet altijd meteen met je eens, maar je had eigenlijk wel altijd gelijk. Daarnaast wil ik Stan en co-promotor Richard hartelijk bedanken voor jullie waardevolle en gedetailleerde commentaar en suggesties gedurende het traject.

Several parts of the work described have been performed by or in collaboration with other research groups. I thank Michael, Ben, Xinyu and Thomas for their important experiments regarding the selectivity and activity profiles of WEN091, Olivier and Gerard for shedding light on the binding mode of WEN091 to PLA2G4E and Simar and Nephi for their collaboration on the biological evaluation of RED353.

In ons eigen lab hebben Hans den Dulk, Hans van den Elst, Rian, Nico, Bobby, Fons, Karthick, Hellen, Annelies en Sebastiaan ervoor gezorgd dat alle faciliteiten als vanzelfsprekend worden ervaren. Dit is een luxe die niet altijd onderkend wordt. Dank (en chapeau) daarvoor. I want to thank all current and former members of MolPhys, Freek, Marc, Marjolein, Hui, Sebastian, Juan, Eva, Elliot, Anthe, Sebastiaan, Annelot, Tom, Berend, Ming, Rob, Alexander, Florian, Vasu, Andrea, Bing, Laura, Floor, Hedwich, Wouter, Verena, Noëlle, Na, Joel, Daan, Frans, Marnix, Julia, Kim, Annemarieke en Jessica, as well as lab mates from CC and BioSyn for all help, advice, distraction, coffee, good vibes and gezelligheid within and outside of the lab. Mijn paranimfen Rob en Floor, dagelijkse lab-en kantoorgenoot, in het bijzonder bedankt voor het inkleuren van de dagen.

Een mens kan maar zoveel, dus de waardevolle hulp van stagestudenten mag niet worden onderschat. Daiva, Mathijs, Sanne, Paul, Yevhenii, Ivan, Lian, Danique and Dominique, many of you may find parts of your work in this thesis, but even if they have not made the final cut, your valuable contributions have led to new insights and are highly appreciated.

Tot slot is het leven buiten werk ook belangrijk geweest. Vrienden van de scouting en daarbuiten, pap, mam, Lotus, Steven, opa en Jenny, jullie hebben mijn gedachten altijd weten te verzetten. Natascha, jij bent er al heel lang altijd voor mij en hebt me ook hierin altijd gesteund. Je weet inmiddels dat tijdschattingen niet mijn sterkste kant zijn, maar ik hoop dat ik goed inschat dat we nog een lange toekomst samen hebben.



